



HAL
open science

Elaboration de phases stationnaires originales pour la Chromatographie Liquide Haute Performance : Synthèse, caractérisation, et évaluation des propriétés chromatographiques des colonnes.

Mélanie Mignot

► **To cite this version:**

Mélanie Mignot. Elaboration de phases stationnaires originales pour la Chromatographie Liquide Haute Performance : Synthèse, caractérisation, et évaluation des propriétés chromatographiques des colonnes.. Chimie analytique. Université de Rouen, France, 2016. Français. NNT : . tel-01674550

HAL Id: tel-01674550

<https://theses.hal.science/tel-01674550>

Submitted on 3 Jan 2018

HAL is a multi-disciplinary open access archive for the deposit and dissemination of scientific research documents, whether they are published or not. The documents may come from teaching and research institutions in France or abroad, or from public or private research centers.

L'archive ouverte pluridisciplinaire **HAL**, est destinée au dépôt et à la diffusion de documents scientifiques de niveau recherche, publiés ou non, émanant des établissements d'enseignement et de recherche français ou étrangers, des laboratoires publics ou privés.



Normandie Université

THÈSE

Pour obtenir le diplôme de doctorat

Spécialité Chimie

Préparée au sein de l'Université de Rouen Normandie

Elaboration de phases stationnaires originales pour la Chromatographie Liquide Haute Performance : Synthèse, caractérisation, et évaluation des propriétés chromatographiques des colonnes

Présentée et soutenue par

Mélanie MIGNOT

**Thèse soutenue publiquement le 1^{er} décembre 2016
devant le jury composé de**

Mme Sabine HEINISCH	Dr, HDR / Ingénieure de recherche Université de Lyon	Rapporteuse
Mme Deirdre CABOOTER	Dr, HDR / Maître de conférences Université de Leuven	Rapporteuse
M. Jean-Luc VEUTHEY	Pr / Université de Genève	Examinateur
M. Alain TCHAPLA	Pr / Université de Paris-Sud	Examinateur
Mme Valérie PEULON-AGASSE	Dr, HDR / Maître de conférences Université de Rouen Normandie	Directrice de thèse
M. Pascal CARDINAEL	Pr / Université de Rouen Normandie	Codirecteur de thèse
M. Vincent TOGNETTI	Dr, HDR / Maître de conférences Université de Rouen Normandie	Membre invité

Thèse dirigée par Valérie PEULON-AGASSE et Pascal CARDINAEL, laboratoire SMS, EA 3233





Normandie Université

PhD THESIS

In view to obtain the degree of Doctor of Philosophy in Science

Specialty: Chemistry

Submitted to the Faculty of Science-University of Rouen Normandie

Elaboration of original stationary phases for high-performance liquid chromatography: Synthesis, characterization, and evaluation of the chromatographic properties

**Presented and defended by
Mélanie MIGNOT**

**Defended the December, 1st 2016
in front of the dissertation committee composed of**

Mme Sabine HEINISCH	Dr. HDR / Research engineer University of Lyon	Reviewer
Mme Deirdre CABOOTER	Dr. HDR / Associate Professor University of Leuven	Reviewer
M. Jean-Luc VEUTHEY	Prof. / University of Geneva	Examiner
M. Alain TCHAPLA	Prof. / University of Paris-South	Examiner
Mme Valérie PEULON-AGASSE	Dr. HDR / Assistant Professor University of Rouen Normandie	Advisor
M. Pascal CARDINAEL	Prof. / University of Rouen Normandie	Co-advisor
M. Vincent TOGNETTI	Dr. HDR / Assistant Professor University of Rouen Normandie	Invited Member

Supervised by Valérie PEULON-AGASSE and Pascal CARDINAEL, SMS laboratory, EA 3233



Table of Contents

ACKNOWLEDGMENTS

ABREVIATION LIST

PUBLICATIONS AND SCIENTIFIC COMMUNICATIONS

INTRODUCTION..... 1

CHAPTER I - GENERALITIES AND STATE OF THE ART 5

I-1. THROUGHPUT ANALYSES IN LIQUID CHROMATOGRAPHY: SENSITIVITY, SPEED, RESOLUTION COMPROMISE 7

I-1-1. CHROMATOGRAPHIC FUNDAMENTAL BACKGROUND..... 7

I-1-1-1. RETENTION FACTOR 7

I-1-1-2. SELECTIVITY FACTOR..... 8

I-1-1-3. EFFICIENCY 8

I-1-1-4. RESOLUTION 10

I-1-1-5. PEAK ASYMMETRY 11

I-1-2. MODERN INSTRUMENTATION..... 12

I-1-2-1. LAST EVOLUTIONS IN LC SYSTEMS 13

I-1-2-2. EXTRA-COLUMN VOLUME EVALUATION..... 13

I-1-3. KINETIC PERFORMANCE EVALUATION 15

I-1-3-1. VAN DEEMTER EQUATION 15

I-1-3-2. KINETIC PLOTS 16

I-1-4. TECHNOLOGY STRATEGIES: FASTER, HOTTER, SMALLER..... 19

I-1-4-1. MONOLITHIC SUPPORTS 19

I-1-4-2. HIGH-TEMPERATURE LIQUID CHROMATOGRAPHY (HTLC)..... 21

I-1-4-3. SUB-2 μ M AND UHPLC..... 25

I-1-4-4. CORE-SHELL TECHNOLOGY 27

CONCLUSION 31

I-2. LIQUID CHROMATOGRAPHY MODES..... 33

I-2-1. NORMAL PHASE LIQUID CHROMATOGRAPHY (NPLC) 33

I-2-2. REVERSED-PHASE LIQUID CHROMATOGRAPHY (RPLC)..... 34

I-2-3. ION EXCHANGE CHROMATOGRAPHY (IEC)..... 35

I-2-4. HYDROPHILIC INTERACTION LIQUID CHROMATOGRAPHY (HILIC) 36

I-2-5. MIXED MODE CHROMATOGRAPHY (MMC)..... 40

CONCLUSION 43

<u>I-3. STATIONARY PHASE SYNTHESIS: FROM BARE SILICA TO FUNCTIONALIZED SILICA</u>	<u>45</u>
I-3-1. SILICA AS CHROMATOGRAPHIC SUPPORT	45
I-3-2. SYNTHETIC PROCEDURES	46
I-3-2-1. ETHERIFICATION	47
I-3-2-2. CHLORINATION REACTION AND ORGANOMETALLIC COMPOUNDS	47
I-3-2-3. SILANIZATION AND HYDROSILATION	47
I-3-2-4. ORGANOSILANIZATION	48
I-3-3. TYPES OF BONDED STATIONARY PHASES	49
I-3-3-1. MONOMERIC PHASES "BRUSH-TYPE"	50
I-3-3-2. OLIGOMERIC-TYPE AND BULK-PHASE TYPE	51
I-3-3-3. MONOMERIC PHASE: CHLORINATION AND ORGANOMETALLIC METHYLATION LIGAND	52
I-3-4. DEALING WITH RESIDUAL SILANOLS	53
I-3-4-1. SILICA PRETREATMENT	53
I-3-4-2. SILICA POST-TREATMENT	54
I-3-4-3. MOBILE PHASE ADDITIVES	55
I-3-4-4. STABILITY UNDER EXTREME PHS	56
<u>CONCLUSION</u>	<u>57</u>
<u>I-4. SILICA CHARACTERIZATION</u>	<u>59</u>
I-4-1. MORPHOLOGICAL STRUCTURE	59
I-4-1-1. SCANNING ELECTRON MICROSCOPY (SEM)	59
I-4-1-2. SPECIFIC SURFACE AREA	59
I-4-2. LIGAND GRAFTING ANALYSIS	61
I-4-2-1. ELEMENTAL ANALYSIS	61
I-4-2-2. THERMOGRAVIMETRIC ANALYSIS (TGA)	61
I-4-3. SPECTROSCOPIC METHODS	62
I-4-3-1. INFRARED SPECTROSCOPY	62
I-4-3-2. NUCLEAR MAGNETIC RESONANCE	63
<u>CONCLUSION</u>	<u>65</u>
<u>I-5. MOLECULAR MODELING BY FUNCTIONAL DENSITY THEORY (DFT)</u>	<u>67</u>
I-5-1. PRINCIPLE	68
I-5-1-1. BORN-OPPENHEIMER SEPARATION	68
I-5-1-2. KOHN-SHAM METHOD	69
I-5-1-3. DFT IN PRACTICE	69
I-5-2. OWN N-LAYERED INTEGRATED MOLECULAR ORBITAL AND MOLECULAR MECHANICS (ONIOM) METHOD	71
I-5-3. SOLVATION EFFECTS	72
I-5-3-1. IMPLICIT SOLVATION	73

I-5-3-2. EXPLICIT SOLVATION	74
CONCLUSION	75
<u>I-6. CHROMATOGRAPHIC EVALUATION AND DATA PROCESSING BY CHEMOMETRIC METHODS.....</u>	<u>77</u>
I-6-1. CHROMATOGRAPHIC EVALUATION OF THERMODYNAMIC PROPERTIES	77
I-6-1-1. HYDROPHOBIC SUBTRACTION MODEL	78
I-6-1-2. ENGELHARDT TEST.....	79
I-6-1-3. TANAKA TEST	80
I-6-1-4. CAROTENOID TEST.....	81
I-6-1-5. OTHER TESTS AND EXTENSIONS	81
I-6-1-6. LINEAR SOLVATION ENERGY RELATIONSHIP (LSER).....	82
I-6-2. CHEMOMETRIC METHODS	84
I-6-2-1. PRINCIPAL COMPONENT ANALYSIS (PCA)	84
I-6-2-2. HIERARCHICAL COMPONENT ANALYSIS (HCA)	87
CONCLUSION	89
<u>I-7. REFERENCES</u>	<u>91</u>
<u>CHAPTER II - CONVENTIONAL REVERSED-PHASE STATIONARY PHASES</u>	<u>99</u>
<u>INTRODUCTION.....</u>	<u>101</u>
<u>II-1. MICROWAVE ORGANOSILANIZATION OF SILICA.....</u>	<u>103</u>
II-1-1. ARTICLE 1: AROUND THE DEVELOPMENT OF A FAST, EFFICIENT, AND REPRODUCIBLE GRAFTING METHOD FOR C18 FUNCTIONALIZATION OF BARE SILICA SPP.	104
<u>II-2. THERMAL PRETREATMENTS OF SILICA</u>	<u>117</u>
II-2-1. ARTICLE 2: TOWARDS A WIDE RANGE OF C18 STATIONARY PHASES FROM THE SAME SPP SILICA BATCH FUNCTIONALIZED WITH THE SAME MICROWAVE PROCEDURE	117
II-2-2. ARTICLE 3: USE OF A HIGH TEMPERATURE PRETREATED C18 SILICA FOR THE SEPARATION OF PHENANTHRENE/ANTHRACENE IN A PHENANTHRENE BATCH	133
II-2-3. ARTICLE 4: USE OF SUPERFICIALLY POROUS SILICA PARTICLES PRETREATED AT DIFFERENT TEMPERATURES IN HILIC	144
<u>CHAPER III - NON-CONVENTIONAL MULTIMODAL STATIONARY PHASES</u>	<u>155</u>
<u>INTRODUCTION.....</u>	<u>157</u>

III-1. ARTICLE 5: NEW POLAR EMBEDDED AROMATIC STATIONARY PHASES.....	159
III-2. CALIX[6]ARENE DERIVATIVE SYNTHESIS.....	201
III-2-1. CALIX[N]ARENE DERIVATIVE OVERVIEW	201
III-2-1-1. CAVITY SIZE EFFECT	202
III-2-1-2. SIZE EFFECT	203
III-2-1-3. <i>P</i> -TBUTYL- AND CARBOXYLIC ACID SUBSTITUTED CALIX[6]ARENE DERIVATIVES	204
III-2-1-4. EVALUATION OF COMMERCIAL CALIX[N]ARENE DERIVATIVES	204
III-2-2. CALIX[6]ARENE DERIVATIVE SYNTHESIS	205
III-2-3. GRAFTING RATES OF THE CALIX[6]ARENE DERIVATIVES.....	207
III-2-4. EVALUATION OF STATIONARY PHASES BASED ON CALIX[6]ARENE DERIVATIVES.....	208
III-2-4-1. LSER MODEL.....	208
III-2-4-2. SYMMETRY EVALUATION	215
III-3. REFERENCES	219
CONCLUSIONS AND PROSPECTS.....	221
APPENDICES.....	227

Acknowledgments

Bien que cette thèse soit européenne et requiert donc une rédaction en anglais, je me permettrais d'apposer ici mes remerciements dans ma langue natale, probablement plus propice à l'expression directe de mes sentiments les plus sincères envers tous ceux qui ont pu contribuer au démarrage, au déroulement, puis à l'aboutissement de ce travail de recherche. Préparer un doctorat ne se résume pas à un intitulé. Réaliser un doctorat, c'est piloter un projet, gérer l'inconnu, s'adapter, et mettre en place des collaborations. Et plus encore, probablement. Cela requiert beaucoup d'énergie et d'implication. C'est à ce prix qu'est cette expérience autant professionnelle que personnelle, dont les contributeurs ci-dessous ont une part significative et profondément respectable.

Je tiens tout d'abord à remercier le Professeur Gérard Coquerel pour m'avoir accueillie au sein du Laboratoire SMS, et ce depuis mon premier stage de découverte en L2. Mon entrée au laboratoire m'aura permis de m'épanouir scientifiquement et humainement les années suivantes, bien encadrée par ceux qui m'ont guidée jusque-là : Valérie et Pascal.

Mes sincères remerciements s'adressent donc au Docteur Valérie Peulon-Agasse, ma directrice et mentor des premiers instants, qui a su croire en moi et me fournir autant d'opportunités d'exprimer un potentiel que je ne soupçonnais pas. Jamais je n'aurais suffisamment de mots pour te remercier pour ton soutien indéfectible, ton optimisme à toute épreuve, et ta bonne humeur contagieuse. Pardon pour les virées nocturnes à Salzburg, et pour toutes les frayeurs que j'ai pu te faire en congrès avec mes mésaventures et ma poisse légendaire. Mais grâce à moi, tu sais désormais que tu disposes d'un certain sens de l'orientation, comparé au mien bien loin d'être certain !



Véritable génératrice de bonnes idées, ta disponibilité, ta réactivité, ton efficacité et ta pédagogie m'ont fait aimer la chimie analytique dès mes prémices universitaires, et ont par la suite grandement contribué au bon déroulement de cette thèse. Merci pour ta confiance, ton

écoute et ton soutien, même non scientifique. Tu es au-delà de l'encadrante, une femme forte et sensible de qui j'ai beaucoup appris.

Ma profonde gratitude va également au Professeur Pascal Cardinael, mon co-directeur de thèse. Top Chef aussi bien scientifique que culinaire, je te dédie mon macaron d'or du chef de labo ! Bien que majoritairement GC-iste, j'ai beaucoup apprécié que tu participes à mon projet LC et échanger avec toi m'a beaucoup appris sur le plan scientifique ... Et sur la complexité de gestion d'une équipe pour laquelle tu t'investis pleinement ;) Merci de m'avoir donné ma chance au sein de ton équipe, et de m'avoir convaincu qu'une thèse était une bonne idée, pour aller au bout de mes rêves. Merci pour la playlist Jean-Jacques-Zaz-Zazie jusque Montluçon, et plus sérieusement pour la mise à disposition des ressources et des compétences de ton laboratoire.



Valérie et Pascal, un binôme de choc dont les conseils avisés, la perspicacité, et l'encadrement m'ont permis de venir au labo avec motivation et plaisir chaque jour, pour mener cette thèse à son terme. Merci également pour votre soutien et vos encouragements dans mes moments de doute, et merci pour la place que vous m'avez accordée et les initiatives que vous m'avez laissée prendre, me permettant ainsi de gagner en autonomie.

Je tiens à vivement remercier le Docteur Deirdre Cabooter et le Docteur Sabine Heinisch de rapporter mon travail de thèse. Un grand merci aux Professeurs Jean-Luc Veuthey et Alain Tchapla pour avoir accepté de faire partie de mon jury pour examiner mon travail. Merci également au Docteur Vincent Tognetti, membre invité de mon jury, et au Docteur Davy Guillaume pour s'être déplacé jusque qu'ici.

C'est un réel plaisir que de soutenir devant vous tous, et un réel challenge aussi !

Je suis également très reconnaissante envers la société Interchim, et plus particulièrement Didier, Olivier, et François pour leur collaboration, leur support, leurs conseils, la mise à disposition des consommables et le remplissage efficace des colonnes ! Merci, au-delà de l'aspect commercial inhérent à une entreprise, d'avoir considéré mon travail scientifique dans son ensemble. Alors que je suis dans l'avion de retour pour Paris, je me remémore cette semaine à HPLC San Francisco qui vient de s'écouler. Une grande aventure pour moi, et un grand plaisir de l'avoir partagée avec vous, tant pour l'aspect scientifique de la semaine de congrès, que sur le plan humain pour le week-end la précédant.

Ma gratitude va également au Professeur Alain Tchaplà, puit de connaissance intarissable, pour sa considération et ses conseils avisés. Votre soutien et vos remarques constructives auront beaucoup apporté à la structure de cette thèse, un grand merci.

J'adresse ensuite mes vifs remerciements à l'équipe du LCAP de l'Université de Genève, au sein de laquelle j'ai effectué une partie de mon échange doctoral. J'y ai découvert un laboratoire efficace, convivial, dont le seul regret que je puisse avoir est de n'y être resté qu'un mois. Mais un mois riche en expérience scientifique intra-labo, et en découvertes extra-labo !

Merci également au Professeur Ivan Jabin du laboratoire LCO de l'Université Libre de Bruxelles pour m'avoir accueillie et à Roy pour m'avoir fait part de son expertise en synthèse de calixarènes.

Je tiens également à remercier les Docteurs Muriel Sebban et Vincent Tognetti pour avoir accepté de collaborer dans une partie de mon projet de thèse. Votre expertise m'a permis de tirer d'importantes informations structurales des analyses RMN du solide, et de modéliser tout le ligand de la phase aromatique à groupement polaire intercalé. Merci également à la joviale et rigoureuse Emilie Petit pour les analyses élémentaires (girl power !) et au Professeur Jean-Philippe Bouillon, pour avoir accepté d'être mon référent de thèse et avoir effectué chaque année les entretiens d'avancement de thèse avec rigueur et intérêt.

Et puis merci à mes collègues de l'IUT Chimie et Mesures Physiques et en particulier à Séverine de m'accueillir dans la famille IUT-ienne pour un an en ATER ;)

Je tiens à exprimer toute ma reconnaissance à tous mes collègues du laboratoire SMS pour leur accueil ainsi que pour tous les excellents moments partagés au labo mais aussi à l'extérieur. Merci pour la bonne ambiance de travail qu'ils font régner dans le laboratoire, qui facilite clairement le long et parfois difficile challenge du travail de thèse. Morgane, fournisseur officiel de cacahuète au wasabi, merci d'avoir mis du piquant dans ma thèse !

Un merci particulier à Marie à qui aucun appareil ne résiste, et à Framboise pour sa disponibilité et sa bonne volonté. Ta rigueur et ta motivation font de toi une collègue scientifique de qualité, et ta bienveillance à nous bichonner font de toi une amie précieuse au grand cœur : ta Ninie t'en remercie ;)



Un grand merci à mes collègues doctorants, post-doctorants et stagiaires, passés et présents : Curataur, JC, Clément, Simon, Florent, Julien, Grace, FX, Lina, Bassam, Manon et James.

Clément DSJ, tes blagues (parfois merdiques !!) n'entachent en rien mon respect pour ta curiosité scientifique, ta bonne volonté, et ta sympathie. Tes abdos naissants me remercieront de te le faire payer au full-contact ;) Emeline, mon acolyte de la pinte partagée, sans quoi tu rentres à pied ! C'est un plaisir que de t'avoir eu au bureau, même avec Evanescence au volume max dans les écouteurs ! Ton écoute, ta bienveillance, et tes bons conseils m'ont beaucoup éclairée dans les moments difficiles, merci. Je suis ravie de te voir désormais épanouie en assumant les choix que tu fais, parce que tu peux en être fière, et que tu le mérites.

Antoine, notre Monsieur grognon et ronchon par principe, dans le doute, parce qu'on sait jamais. Tes qualités scientifiques font de toi une personne de confiance avec qui il est fort plaisant de discuter et travailler. Outre cet aspect, ta sympathie et ta bonne volonté font de toi un collègue très appréciable. Peut-être un peu moins pour ton « Mélanie, ton truc en plus, c'est ta case en moins » ☺



Emilie, Quentin et Ben, avec qui j'ai partagé ma première virée aux States, et avec qui j'ai noué une solide complicité au long de ces 3 années de thèse. Emilie, femme sensible mais de caractère, bonne continuation dans ce qui t'épanouira, je ne doute pas que tu obtiennes ce que tu vises !!

Quentin, le bou(bou)t-en-train toujours de bonne humeur, comme la HILIC, t'es fantastique ! La vie réserve parfois de bonnes surprises aux personnes dignes de les recevoir ... Et capables de les percevoir ;) Je n'aurais jamais pu imaginer les évolutions professionnelles, et personnelles de cette thèse ... Mais ta déclinaison polymorphique plutôt figurative m'a subjuguée, c'était pourtant pas gagné !

Plus sérieusement, merci d'avoir su trouver avec délicatesse les mots justes pour susciter en moi ce déclic sous-jacent, salvateur mais profondément difficile. Et s'il paraît, selon Cocteau, que le verbe *aimer* est le plus compliqué de la langue française ; parce que son passé n'est jamais simple, son présent n'est qu'imparfait et son futur toujours conditionnel ... Je crois pour ma part qu'il faut le faire vivre, tout simplement.

Je finirais par toi Ben, sans qui cette thèse au quotidien n'aurait pas été ce qu'elle est. Tu as su m'écouter et m'aider, me valoriser lorsque je doutais. Ta grande sensibilité, ta maturité, ton sens juste du partage, et ta rigueur scientifique font de toi quelqu'un d'exceptionnel. Merci pour tous tes gentils mots à mon égard, et pour les méchantes droites amicalement infligées au full-contact. Je ne sais pas si j'irai où tu iras, mais j'espère que mon pays ne sera pas loin de toi et Ana. Ce petit rayon de soleil et de bonne humeur te complète si bien, et gère Word comme personne ! Merci beaucoup pour ton aide précieuse Ana ;)

Un grand merci à mes nombreux stagiaires de tous horizons, pour avoir significativement contribué à l'avancée des différents projets qui composent cette thèse et pour m'avoir aidé à explorer de nouvelles voies : Faustine, Dimitri, Enguerrand, Marie-Catherine, Anaïs, Matthieu, Gwendal. Un merci particulier à Evelyne et Adeline, suffisamment motivées (ou inconscientes !!!) pour faire 2 stages sous ma supervision. Votre rigueur, votre intérêt, et votre sympathie font de vous des stagiaires de premier choix ! Je vous souhaite le meilleur pour votre thèse, et espère que vous aurez l'occasion d'encadrer des stagiaires comme vous.

Merci du fond du cœur à ma famille pour leur soutien sans faille depuis le début de mes études. En tant que pionnière de famille en étude supérieure, je vous souhaite à tous, frère et sœur, cousins et cousines, de trouver votre voie et prendre autant plaisir à étudier que j'ai pu en avoir. J'espère que vous aussi aurez des personnes clefs qui vous ouvrent les bonnes portes et vous incitent à poursuivre. A tous, et particulièrement mon frère, pardon pour ma présence bien moins régulière, qui ne traduit en rien l'attachement que j'ai pour toi et le lien indéfectible qui nous unit. Un arbre ne pousse jamais sans ses racines.

Théo, merci pour ton soutien et ton écoute, à ta façon, même lorsque pour toi aussi c'était dur. Tes valeurs profondes font de toi un être sensible, juste et respectueux. Et si tes maladresses peuvent être parfois difficiles à comprendre et gérer, tes qualités te rendent finalement attachant.

Nos chemins se sont séparés là, pour des raisons qui nous sont propres. Mais tu auras laissé dans ma vie une empreinte indélébile, témoin et acteur de ma construction personnelle durant nos années de fac. Bonne route à toi, là où tu voudras t'investir, tu mérites le meilleur, et je sais que tu as désormais les atouts pour y parvenir.

A toi, Maman, je te dédis cette thèse. Une décennie cette année, et toute pile en ce jour d'écriture. Tu rendais nos journées plus belles, et répandais partout sur ton passage bonne humeur et écoute, partage et valeurs profondes. Merci pour ce que tu as eu le temps de me transmettre, et pour ce que tu continues de faire, différemment. Ce challenge, c'en est un bien plat comparé à ceux que tu as pu relever, et au courage sans faille dont tu as fait preuve jusqu'à ton dernier souffle. Mon admiration est sans borne pour la femme, l'amie, la mère, que tu resteras à jamais dans mon cœur.

Cette thèse, c'est finalement un peu la vôtre aussi ... De par votre contribution, d'une façon ou d'une autre, et à partir de toutes mes hypoThèses ... Nous avons pu, sur certains aspects en tout cas, en faire une hyperThèse.

Alors, aussi simplement que sincèrement :



ABBREVIATION LIST

As	Asymmetry factor
ACN	Acetonitrile
BET	Brunauer, Emmett, Teller theory
CAD	Corona Charged aerosol detector
C18	Column with particles functionalized with octadecyl ligands
CP/MAS	Cross Polarization/Magic Angle Spinning
D	Distribution coefficient
DFT	Density Functional Theory
D_m	Molecular diffusion coefficient (m^2/s)
dp	Particle diameter (μm)
DMSO	Dimethylsulfoxide
DRIFT	Diffuse Reflectance Infrared Fourier Transform
E	Separation impedance
ELSD	Evaporative Light Scattering Detector
E_r	Restituted efficiency
FPP	Fully Porous Particle
GC	Gas Chromatography
HEPT	High Equivalent to a Theoretical Plate (μm)
H	Hamiltonian operator
h	Reduced high equivalent to a theoretical plate
HCA	Hierarchical Component Analysis
HILIC	Hydrophilic Interaction Liquid Chromatography
HPLC	High Performance Liquid Chromatography
HTLC	High Temperature Liquid Chromatography
IEC	Ion Exchange Chromatography
I.D.	Internal Diameter
IR	Infrared spectroscopy
k	Retention factor
K_v	Column permeability (mm^2)
L	Column length (mm)
LC	Liquid Chromatography

LSER	Linear Solvation Energy Relationship
MeOH	Methanol
MMC	Mixed Mode c+Chromatography
MS	Mass Spectrometry
MM	Molecular Mechanics
MP	Mobile Phase
N	Theoretical plate number (plates)
NMR	Nuclear Magnetic Resonance
NPLC	Normal Phase Liquid Chromatography
n_c	Peak capacity
NMR	Nuclear Magnetic Resonance
NPLC	Normal Phase Liquid Chromatography
ONIOM	Own N-layered Integrated Molecular Orbital and Molecular Mechanics
P	Partition coefficient
PCA	Principal Component Analysis
PCM	Polarization Continuum Model
pH	Hydrogen potential
QM	Quantum Molecular
QSPR	Quantitative Structure Energy Relationship
R_s	Resolution
RPLC	Reversed-Phase Liquid Chromatography
SCF	Self-Consistent Field
SFC	Supercritical Fluid Chromatography
SP	Stationary Phase
SPE	Solid Phase Extraction
SPP	Superficially Porous Particle (core-shell)
T	Temperature
TF	Tailing Factor
TGA	Thermogravimetry Analysis
TFA	Trifluoroacetic acid
t_d	Delay time (min)
t_r	Retention time (min)
t_0	Dead time (min)

u	Linear mobile phase velocity (mm/s)
u_{opt}	Optimal linear mobile phase velocity (mm/s)
UHPLC	Ultra High Performance/Pressure Liquid Chromatography
UV	Ultraviolet
V_0	Dead column volume (μL)
V_d	Delay volume (μL)
$W_{1/2}$	Peak width at half height
ϵ	Dielectric constant
Φ	Resistance flow factor
μ	Dipolar moment (D)
η	Viscosity (cP)
Γ	Grafting rate ($\mu\text{mol}/\text{m}^2$)
α	Selectivity factor
σ_{ec}^2	Extra column variance (μl^2)
σ_{col}^2	Column variance (μl^2)
σ_{tot}^2	Total variance (μl^2)
ΔP	Backpressure (bar)
ΔH	Enthalpy variation (kcal/mol)
ΔS	Entropy variation (kcal/mol)

PUBLICATIONS AND SCIENTIFIC COMMUNICATIONS

This work led to various publications in peer-reviewed journals, and was presented as oral and/or poster communications in different national and international congresses thanks to various grants from the Doctoral School (ED508 Chimie), French Separation Science Association (AFSEP and C CVS), and Chemical French Society (SCF).

Peer-reviewed articles:

- I. High-density octadecyl chemically bonded core-shell silica phases for high-performance liquid chromatography: comparison of microwave-assisted and classical synthetic routes, structural characterization and chromatographic evaluation.**
Mignot, M.; Tchapla, A.; Mercier, O.; Couvrat, N.; Tisse, S.; Cardinael, P.; Peulon-Agasse, V. *Chromatographia* 2014, 77, 1577-1588.

- II. Thermal pretreatments of superficially porous silica particles for high-performance liquid chromatography: Surface control, structural characterization and chromatographic evaluation.**
Mignot, M.; Sebban, M.; Tchapla, A.; Mercier, O.; Cardinael, P.; Peulon-Agasse, V. *J. Chromatogr. A* 2015, 1419, 45–57.

- III. Evaluation of thermally pretreated silica stationary phases under hydrophilic interaction chromatography conditions.**
Mignot, M.; Périat, A.; Peulon-Agasse, V.; Cardinael, P.; Veuthey, J.-L.; Guillarme, D. *J. Sep. Sci.* 2016, 39, 1611–1618.

- IV. New anthracenyl polar embedded stationary phases with enhanced aromatic selectivity: a combined experimental and theoretical study.**
Mignot, M.; Schammé, B.; Tognetti, V.; Joubert, L.; Tchapla, A.; Mercier, O.; Cardinael, P.; Peulon-Agasse, V. Submitted to *J. Chromatogr. A*, manuscript number JCA-16-1827.

Collaboration articles:

- V. Phenanthrene Purification: Comparison of Zone Melting and Co-Crystallization.**
Burel, A.; Brugman, S.J.T.; Mignot, M.; Cartigny, Y.; Tisse, S.; Couvrat, N.; Peulon-Agasse, V.; Cardinael, P.; Coquerel, G. Chem. Eng. Technol. 2016, 39, 1317-1325
- VI. Molecular Relaxations in Supercooled liquid and Glassy States of Amorphous Quinidine: Dielectric Spectroscopy and Density Functional Theory (DFT) Investigations.**
Schammé, B.; Mignot, M.; Couvrat, N.; Tognetti, V.; Joubert, L.; Dupray, V.; Delbreilh, L.; Dargent, E.; Coquerel, G. J. Phys. Chem. B. 2016, 120, 7579-7592

Oral communications:

- 1. Using DFT approaches to investigate the enhanced aromatic selectivity of new antracenylic polar embedded stationary phases for Liquid Chromatography**
Mignot, M.; Schammé, B.; Tognetti, V.; Joubert, L.; Tchapla, A.; Mercier, O.; Cardinael, P.; Peulon-Agasse, V. ESCB1, Rouen, August 29th-September 2nd
- 2. Same core-shell silica batch, same microwave grafting procedure leading to various C18 stationary phases? Insight in thermal pretreatments**
Mignot, M.; Sebban, M.; Tchapla, A.; Mercier, O.; Cardinael, P.; Peulon-Agasse, V. HPLC 2016, San Francisco, 2016, June, 19-24th
§Finalists for Consideration of the 2016 Csaba Horváth Young Scientist Award
- 3. New insights for the development of polar-embedded aromatic stationary phases**
Mignot, M.; Schammé, B.; Tognetti, V.; Joubert, L.; Tchapla, A.; Mercier, O.; Cardinael, P.; Peulon-Agasse, V. Journées Nord-Ouest Européennes des Jeunes Chercheurs, Lille, 2016, June, 9-10th
- 4. New polar-embedded aromatic stationary phases for HPLC**
Mignot, M.; Schammé, B.; Tognetti, V.; Joubert, L.; Tchapla, A.; Mercier, O.; Cardinael, P.; Peulon-Agasse, V. IX^{èmes} journées scientifiques du Club Jeunes de l'AFSEP, Rouen, 2016, April, 18-19th

5. Microwave preparation, characterization, and evaluation of a new polar-embedded aromatic core-shell stationary phase for high-performance liquid chromatography

Mignot, M.; Schammé, B.; Tognetti, V.; Joubert, L.; Tchapla, A.; Mercier, O.; Cardinael, P.; Peulon-Agasse, V. Euroanalysis, Bordeaux, 2015, September, 6-10th

6. How thermal treatments could impact C18 stationary phases made of core-shell particles?

Mignot, M.; Sebban, M.; Tchapla, A.; Mercier, O.; Cardinael, P.; Peulon-Agasse, V. Journées Nord-Ouest Européennes des Jeunes Chercheurs, Rouen, 2015, May, 11-12th

gAward of the Best Oral conference

7. Dans quelle mesure les prétraitements thermiques impactent-ils les phases stationnaires C18 à base de particules de silice partiellement poreuses?

Mignot, M.; Sebban, M.; Tchapla, A.; Mercier, O.; Cardinael, P.; Peulon-Agasse, V. 11^{ème} congrès francophone de l'AFSEP sur les Sciences séparatives et les couplages, Versailles, 2015, March, 31th-April, 2nd

8. Core-shell silica particles: Functionalization, characterization, and evaluation of the stationary phases

Mignot, M.; Tchapla, A.; Mercier, O.; Couvrat, N.; Tisse, S.; Cardinael, P.; Peulon-Agasse, V. VII^{èmes} journées scientifiques du Club Jeunes de l'AFSEP, Paris, 2014, July, 7-8th

gAward of the best Oral conference

9. Octadecyl-chemically bonded core-shell silica phases for liquid chromatography: comparison of microwave-assisted and classical synthetic routes, structural characterization and chromatographic evaluation of the stationary phases

Mignot, M.; Tchapla, A.; Mercier, O.; Couvrat, N.; Tisse, S.; Cardinael, P.; Peulon-Agasse, V. Journées Nord-Ouest Européennes des Jeunes Chercheurs, Lille, 2014, June, 23-24th

10. Rapidité, résolution, efficacité : Apport des particules semi-poreuses en chromatographie

Mignot, M. Journées du club de chromatographie, Rouen, 2014, April, 3rd

Poster communications

1. New polar-embedded aromatic core-shell stationary phases for high-performance liquid chromatography

Mignot, M.; Schammé, B.; Tognetti, V.; Joubert, L.; Tchapla, A.; Mercier, O.; Cardinael, P.; Peulon-Agasse, V. HPLC 2016, San Francisco, 2016, June, 19-24th

2. Microwave preparation, characterization, and evaluation of a new polar-embedded aromatic core-shell stationary phase for high-performance liquid chromatography

Mignot, M.; Schammé, B.; Tognetti, V.; Joubert, L.; Tchapla, A.; Mercier, O.; Cardinael, P.; Peulon-Agasse, V. HPLC 2015, Geneva, 2015, June, 21-25th

3. Could the same core-shell silica batch functionalized with the same microwave procedure lead to various C18 stationary phases? Insight in thermal pretreatments

Mignot, M.; Sebban, M.; Tchapla, A.; Mercier, O.; Cardinael, P.; Peulon-Agasse, V. HPLC 2015, Geneva, 2015, June, 21-25th

4. Diviser par 10 le temps de fonctionnalisation de particules de silice partiellement poreuses ? Micro-ondes versus chauffage à reflux

Mignot, M.; Tchapla, A.; Mercier, O.; Couvrat, N.; Tisse, S.; Cardinael, P.; Peulon-Agasse, V. 11^{ème} congrès francophone de l'AFSEP sur les Sciences séparatives et les couplages, Versailles, 2015, March, 31th-April, 2nd

5. Core-shell silica particles: Functionalization, characterization and evaluation of the stationary phases. Around the microwave heating silica grafting

Mignot, M.; Tchapla, A.; Mercier, O.; Couvrat, N.; Tisse, S.; Cardinael, P.; Peulon-Agasse, V. 30th International Symposium on Chromatography (ISC 2014), Salzburg, 2014, September, 14-18th

6. Core-shell silica particles: Octadecyl silica particles by hydrosilylation and organosilanization

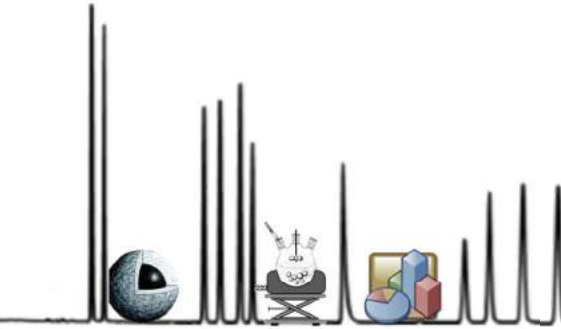
Mignot, M.; Tchapla, A.; Mercier, O.; Couvrat, N.; Tisse, S.; Cardinael, P.; Peulon-Agasse, V. 30th International Symposium on Chromatography (ISC 2014), Salzburg, 2014, September, 14-18th

7. Core-shell silica particles: Octadecyl silica particles by hydrosilylation and organosilanization

Mignot, M.; Tchaplal, A.; Mercier, O.; Couvrat, N.; Tisse, S.; Cardinael, P.; Peulon-Agasse, V. Journée de l'école doctorale normande de chimie (EDNC 508), Le Havre, 2014, May, 27th

Additional involvements:

- First-aid worker (SST)
- Elected member of the Scientific Research Commission for 2 years
- Elected PhD students representative at the laboratory council
- Professional membership of Club Jeunes AFSEP (Communication Manager in 2015/ treasurer in 2016)
- Organization of the 8 and 9th Scientific Days of the AFSEP Young researcher society
- Member of the staff organization for the ESCB1 congress in 2016



INTRODUCTION

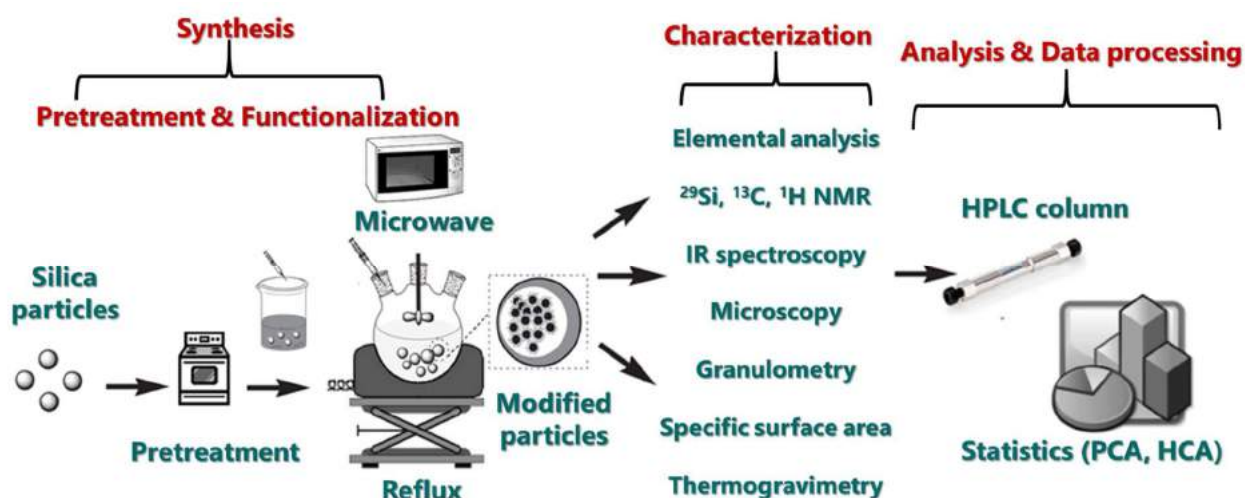


In the past four decades, high-performance liquid chromatography has gained universal acceptance in numerous fields (e.g. pharmaceutical, biological, environmental and food analysis). In the early 1970s, the first commercial packings became available (μ Bondapak C18, 30 cm \times 3.9 mm \times 10 μ m) and John Knox proved the theoretical benefits of using columns packed with small particles. Twenty years later, James Jorgenson provided the proof-of-concept of extending the HPLC performances by using systems capable of working at higher pressures with sub-2 μ m particle columns. Their commercial introduction came in 2004 with short narrow-bore columns packed with sub-2 μ m fully porous particles and chromatographic systems capable of supporting pressures up to 1000 bar. This technology is referred as Ultra-High-Performance Liquid Chromatography (UHPLC) and provides faster analyses while maintaining the chromatographic performance, or higher resolution with a reasonable analytical throughput. Another efficient approach is High-Temperature Liquid Chromatography (HTLC), but as UHPLC it requires a costly dedicated instrumentation. An alternative way allowing to work with a conventional HPLC instrumentation is the use of core-shell particles (i.e. superficially porous particles). This technology is of crucial interest as it combines low-pressure with high efficiency. These particles consist in a solid core surrounded by a porous shell, and the columns packed with them allow for working faster with performances equivalent to those obtained with smaller particles.

One of the main axis of the SMS laboratory concerns the development of original stationary phases based on fully porous particles. This PhD work was devoted to the transfer and the development of this expertise in functionalization and characterization. The main goal was to extend the range of stationary phases based on superficially porous particles. As the column packing is an important step that directly impacts the efficiency, this PhD work was achieved in collaboration with Interchim R&D, which provided the bare silica material and managed the column packing.

This thesis presents a multidisciplinary character that is summarized in the scheme below. Indeed, the strategy followed during this work encompasses the silica pretreatment and the functionalization step (i.e. Synthesis), the characterization of the modified particles through various and complementary techniques (i.e. Characterization); and finally the chromatographic study by selecting the adapted test (Tanaka, Veuthey) for the properties to be evaluated and the surface chemistry of the stationary phases. Those tests were also conducted on the commercial ones, which generated an important amount of data. Consequently, chemometric

approaches (Principal Component Analysis (PCA) and Hierarchical Cluster Analysis (HCA)) were used to process the data and to place the home-made stationary phases among the commercial ones (i.e. Analysis & Data processing).



Representation of the three main steps for the development of new stationary phases: synthesis, characterization, and data processing

The present thesis is divided into four parts:

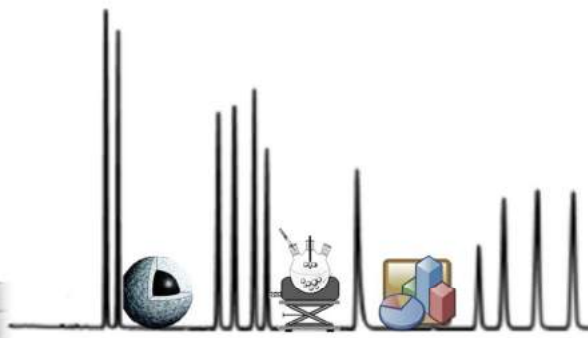
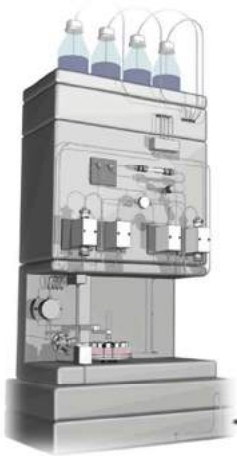
Chapter 1 introduces the theoretical bases and the concepts that will be used in this manuscript. A brief review of the recent technology developments is proposed, and among them the core-shell technology (I.1). The different chromatographic modes are presented (I.2) with a particular emphasis on the silica functionalization (I.3) and the techniques available to characterize the grafting (I.4), including the precise molecular modeling (I.5). The chromatographic evaluation, both kinetic and thermodynamic aspects, are then covered and the data processing by chemometric approaches is finally presented (I.6).

Chapter 2 gathers the four articles published corresponding to the development of stationary phases, from the silica pretreatment and the grafting, to the stationary phase characterization. The first study is focused on the experimental conditions to graft efficiently silica, whatever the organosilane chosen (II.1.1). The second study presents the impact of the silica thermal pretreatment on the silanol population and finally on the chromatographic properties (II.2.1). Additionally, a high temperature pretreated C18 silica was used in the context of phenanthrene ultra-purification (II.2.2). The last study of thermally pretreated silica has been conducted during an internship with Prof. Jean-Luc Veuthey and Dr. Davy Guillarme, LCAP, Université de Genève. The kinetic performances and the applications of the different pretreated

silicas were particularly investigated in Hydrophilic Interaction Chromatography mode (HILIC mode, in II.2.3).

Chapter 3 is devoted to the development of non-conventional stationary phases from the grafting to the stationary phase characterization, and the ligand modeling by Density Functional Theory (DFT). The last article pointed out the potential of DFT to help understanding the chromatographic properties of some original stationary phases capable of developing multiple interactions. This is the case of the polar-embedded aromatic stationary phase that have been developed in the mono- and tri-functional version (III.1). Also, the second part of my internship has been achieved under the supervision of Prof. Ivan Jabin (LCO, Université Libre de Bruxelles) to synthesize calix[6]arene derivatives, and characterize them for further grafting onto silica particles (III.2).

Finally, the Appendices report the collaborative works that have been achieved during this thesis.



CHAPTER I

GENERALITIES AND STATE OF THE ART

I-1. Throughput analyses in Liquid Chromatography: Sensitivity, speed, resolution compromise

I-1-1. Chromatographic fundamental background

Before enter into details, it seems adequate to specify some fundamentals that will highlight the last developments in terms of instrumentation and chromatography developments.

I-1-1-1. Retention factor

The retention factor (k) described in Equation 1 and 1' is a thermodynamic parameter, independent of some key variable factors including flow rate variations and column dimensions. It is a useful parameter when comparing the retention of various solutes obtained using different HPLC systems in isocratic mode (Figure 1).

$$k_A = \frac{t_{R_A} - t_0}{t_i} \text{ with } t_0 = t_e + t_i \quad \text{Equation 1}$$

$$\text{So that } k_A = \frac{t_{R_A} - t_0}{t_0} \text{ with } t_e \ll t_i \quad \text{Equation 1'}$$

With t_{R_A} the retention time of the solute A, t_e and t_i the mobile phase time outside and inside the column, respectively ; and t_0 the dead time.

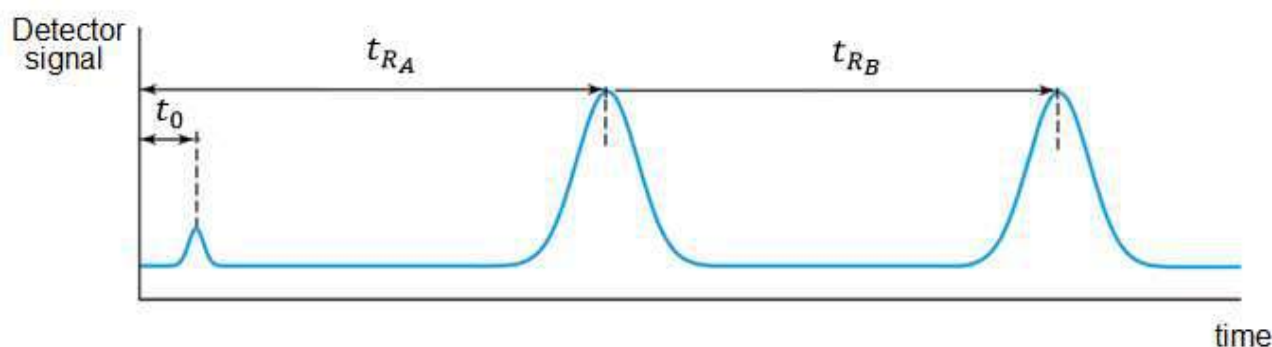


Figure 1: Standard chromatogram of two solutes

Chromatographers like keeping retention factor values between 2 and 10 for optimized separations. The most effective and convenient way to alter the retention factor is to adjust the solvent strength of the mobile phase, typically by modifying the amount of organic modifier in the mobile phase mixture.

I-1-1-2. Selectivity factor

The selectivity factor (α) described in Equation 2 is another thermodynamic parameter, and corresponds to the ability of the chromatographic system to distinguish two successive eluted components.

$$\alpha_{A,B} = \frac{k_B}{k_A} \quad \text{Equation 2}$$

With k_A and k_B the retention factors of the solute A and B, respectively (and B the later eluting compound)

The selectivity is equal to one for co-eluted compounds, and then a higher value indicates better separation. This factor depends on the system solute- Mobile Phase- Stationary Phase (MP-SP) for a given analysis temperature; and may be modified to optimize or change the HPLC separation. Altering the system selectivity is a good strategy to optimize the resolution since small changes in selectivity can lead to large changes in resolution.

For a specific application with a specific column, various changes in the mobile phase can be envisaged to change the selectivity:

- Nature and amount of organic modifier that impact the solvent strength and change the type of interactions
- pH value as the degree of ionization of some solutes affects their hydrophobicity

The temperature has also to be considered as it alters drastically the selectivity for some pairs of solutes.

Last but not least: one of the most efficient way to change the selectivity is to change the stationary phase for another chemistry.

I-1-1-3. Efficiency

The efficiency is a kinetic parameter measuring the dispersion of the solute band during the path through the HPLC system and column. This dispersion depends on the system solute- mobile phase- stationary phase for a given analysis temperature. The chromatographic parameter reflecting the column performance is the number of theoretical plates (N) and is calculated using the following Equation 3, provided a Gaussian peak:

$$N = 5.54 \times \left(\frac{t_R}{W_{1/2}} \right)^2 = \frac{L}{H} \quad \text{Equation 3}$$

With $w_{1/2}$ the half-height peak width, H the height equivalent to a theoretical plate, and L the column length.

Martin and Synge¹, by analogy to distillation, introduced the concept of height equivalent to a theoretical plate (H, or H.E.T.P.,) as a measure of the chromatographic efficiency and as a means to compare column performances. Each plate represents the distance over which the solute achieves one equilibration between the stationary phase and the mobile phase. Measuring the separation efficiency is answering at the question: How many times is the Analyte_{MP} → Analyte_{SP} equilibrium achieved? Consequently, the higher the number of plates available is, the more important the possible equilibria are, and so the better the quality of the separation is. Martin and Synge recognized that a homogeneous bed packed with the smallest possible particle size (requiring higher pressure) was a key to achieve the maximum efficiency. The relation between column and separation system parameters affecting bandspreading was later described by van Deemter².

Many factors contribute to the peak broadening, but considering an optimized system with negligible extra-column volumes; the biggest contribution comes from the column itself. The quality of the column packing, the length of the column, but also both the particle size dispersion and dimension, play an important role in the overall efficiency.

The diffusion of solutes through the column is represented by the 3 terms explained in Equation 4, with the dependence of the diffusion coefficient D_m in the MP, the retention factor k , and the particle diameter d_p , on the height equivalent to a theoretical plate (H):

$$H = A + \frac{B}{u} + C \times u = 2\lambda d_p + 2\gamma \frac{D_m}{u} + f(k) \frac{d_p^2}{D_m} u \quad \text{Equation 4}$$

With A, B, C the coefficients as described below, u the linear velocity, λ the packed bed structural uniformity factor, γ the tortuosity factor.

A schematic representation of the contribution of those diffusion terms is presented in Figure 2.

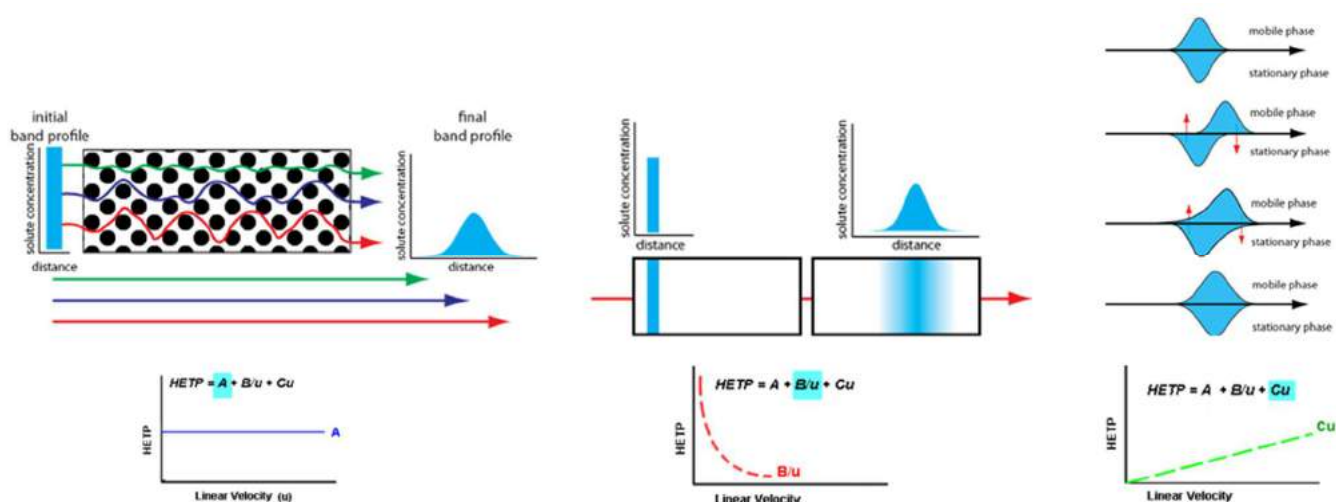


Figure 2: Schematic representation of the van Deemter terms. Adapted from³

In general, the nature and the size of the particles impact the efficiency: Efficiency is improved when using Superficially Porous Particles (SPP) instead of Fully Porous Particles (FPP), and also the smaller the particles are, the higher the efficiency is.

A-term is the convective dispersion or streamline-splitting (eddy-diffusion) parameter, related to channeling through a non-ideal packing. It can be minimized by packing columns homogeneously with silica particles of small and controlled particle size.

B-term is the longitudinal molecular diffusion coefficient of the eluting solutes in the longitudinal direction. It can be minimized by working at high flow rates and using organic modifier of lower viscosity (by reduction of D_m)

C-term is the resistance to the mass transfer of the solute in the stagnant mobile phase and in the stationary phase. It can be minimized by working with a lower flow rate and finally at a higher temperature.

I-1-1-4. Resolution

Obtaining an optimal resolution in a minimum of time is a challenge for chromatographers. Indeed, a value of 1.5 between two consecutive peaks of approximately same magnitude ensures a convenient baseline separation. Assuming that the two adjacent peaks of solutes A and B that have equivalent half-height peak widths, the fundamental Purnell equation can be expressed (Equation 5). The resolution (R_s) is affected by three important parameters: selectivity, efficiency, and retention, and their importance is illustrated in Figure 3.

$$R_{s,A,B} = \frac{\sqrt{N_B}}{4} \times \frac{\alpha_{A,B} - 1}{\alpha_{A,B}} \times \frac{k_B}{k_B + 1} \quad \text{Equation 5}$$

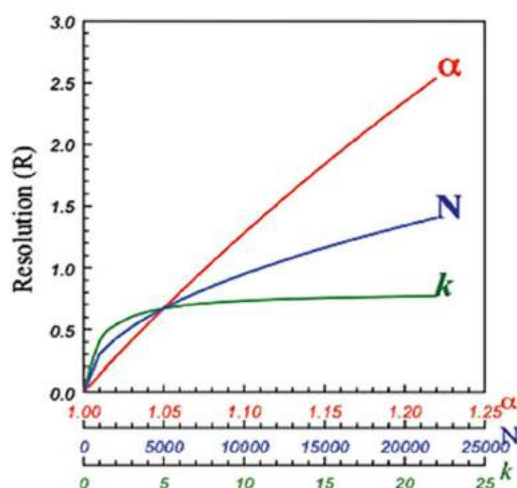


Figure 3: Incidence of selectivity, efficiency, and retention on resolution, adapted from⁴

I-1-1-5. Peak asymmetry

Ideally, all chromatographic peaks would be symmetrical (Gaussian). However, due to the effects of extra-column volumes, adsorptive effects of the stationary phase and the quality of the column packing, peaks can be distorted. Asymmetrical peaks lead to a loss of resolution making the quantification imprecise, and to poor retention reproducibility. The asymmetry factor is estimated at 10% of the peak height. The tailing factor is estimated at 5% of the peak height. These two parameters are calculated according to the Equation 6 and represented in Figure 4.

$$As = \frac{BC}{AC} \text{ and } TF = \frac{AB}{2AC} \quad \text{Equation 6}$$

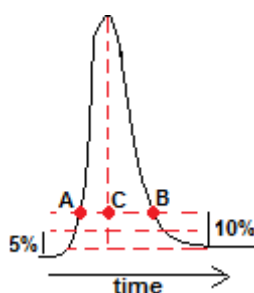


Figure 4: Representation of peak asymmetry and peak tailing factors

Standard limits are set for peak asymmetry. An As value between 1.00-1.05 ($1.00 < TF < 1.03$) is considered as excellent.

Some standard values have been proposed, as by the Food and Drug Administration (FDA) that deemed acceptable the chromatographic values listed below (Table 1).

Parameter	Limit
Retention factor	$k \geq 2$
Resolution	$R_s > 2$
Tailing factor	$TF \leq 2$
Efficiency	$N > 2000$

Table 1: The current FDA values for the validation of chromatographic methods⁵

I-1-2. Modern instrumentation

In the past four decades, High-Performance Liquid Chromatography (HPLC) has been largely used and there is no doubt that it has now gained universal acceptance in industrial as in academic laboratories. This is the method of choice for various fields such as pharmaceutical, biological, environmental and food analysis.

The main evolutions are presented in Figure 5.

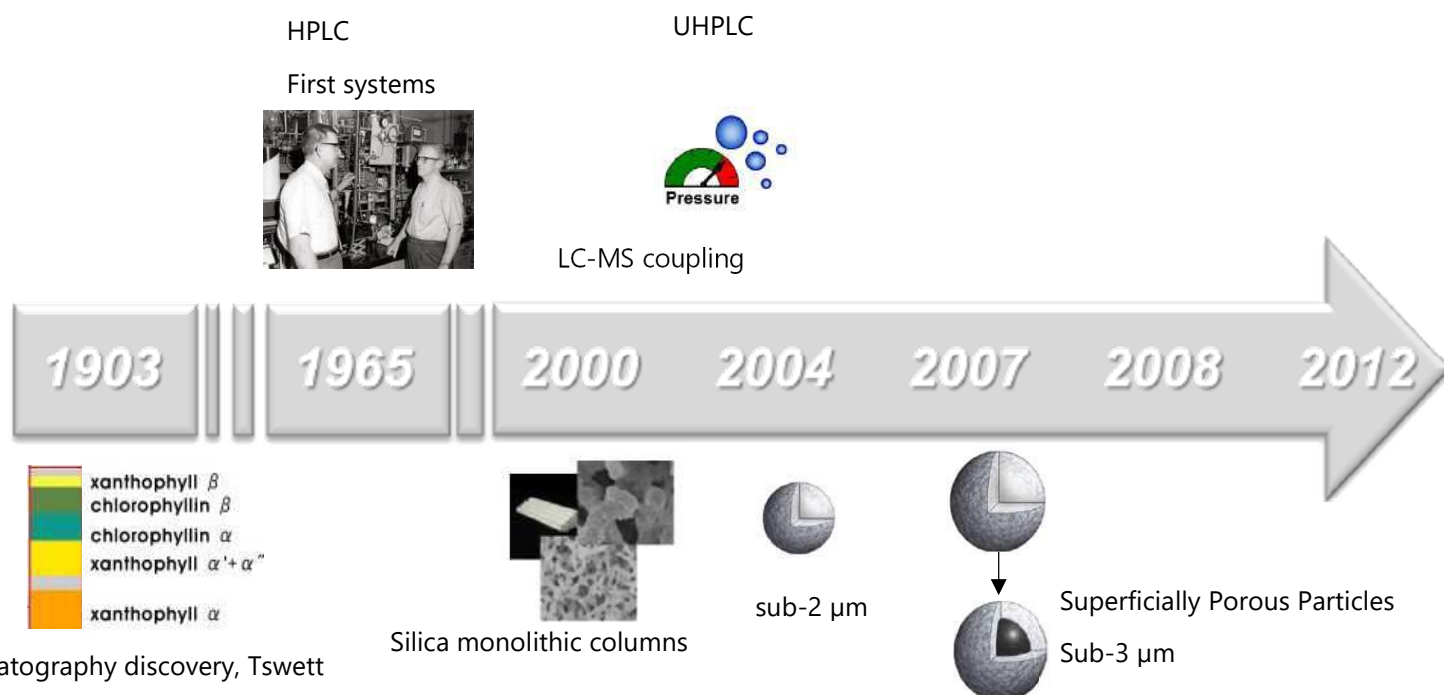


Figure 5: Schematic representation of the main technology developments over the years

Many improvements have been done in terms of instrumentation but also in terms of chromatographic supports, and the following part is dedicated to the strategies allowing to increase the throughput of HPLC.

I-1-2-1. Last evolutions in LC systems

Last years, important improvements have been done in LC systems to fit with the new column generation⁶⁻⁸.

Indeed, due to the lower peak width obtained in UHPLC (<5 s), the UV detector acquisition rate (v_{acq}) has to be high enough to ensure a sufficient number of acquisition points per peak. As analysis time is a big deal, the delay volume (V_d) and injection cycle time (t_{inj}) have to be reduced to ensure fast analysis.

The evolutions on those parameters are listed in the Table 2, adapted from the Fekete *et al.* publication⁶.

LC systems	V_d (mL)	t_{inj} (s)	P_{max} (bar)	v_{acq} (Hz)	σ_{ec}^2 (μL^2)
HPLC	0.5 – 5.0	60	400	10 - 20	> 50
UHPLC	0.1 – 1.0	8 – 60	600 – 1,300	40 - 200	1 – 25

Table 2: Technical values for the modern UHPLC instrument and HPLC instrument, adapted from⁶. Values ranged from the worst and the best commercial instrument.

Another critical point is the extra-column volumes, as they directly impact the global efficiency. Indeed, the peak width depends on the column itself, but also the ability of the instrument to preserve it by reducing the dispersion sources that contribute to peak broadening⁷. It is especially important when using short and/or small I.D. columns⁸.

I-1-2-2. Extra-column volume evaluation

Such volumes came from injector, tubing, and detector cell. To evaluate their contribution, different methods have been developed and allowed for the determination of extra-column variance (σ_{ec}^2) in μL^2 . Such evaluation is not trivial because it is influenced by many parameters: mobile phase viscosity, flow rate, molecular diffusion coefficient of the solute, temperature, and injection volume.

Gritti *et al.* proposed to measure σ_{ec}^2 without the column^{9,10} considering the half height peak width, or using the method of moments. It is also possible to measure it with column, by subtraction of the column variance (σ_{col}^2) to the global variance (σ_{tot}^2) for a solute which extrapolated retention is equal to zero ($k = 0$)¹¹.

This determination is possible considering that the experimental value σ_{tot}^2 corresponds to the sum of σ_{col}^2 and σ_{ec}^2 as represented in Figure 6.

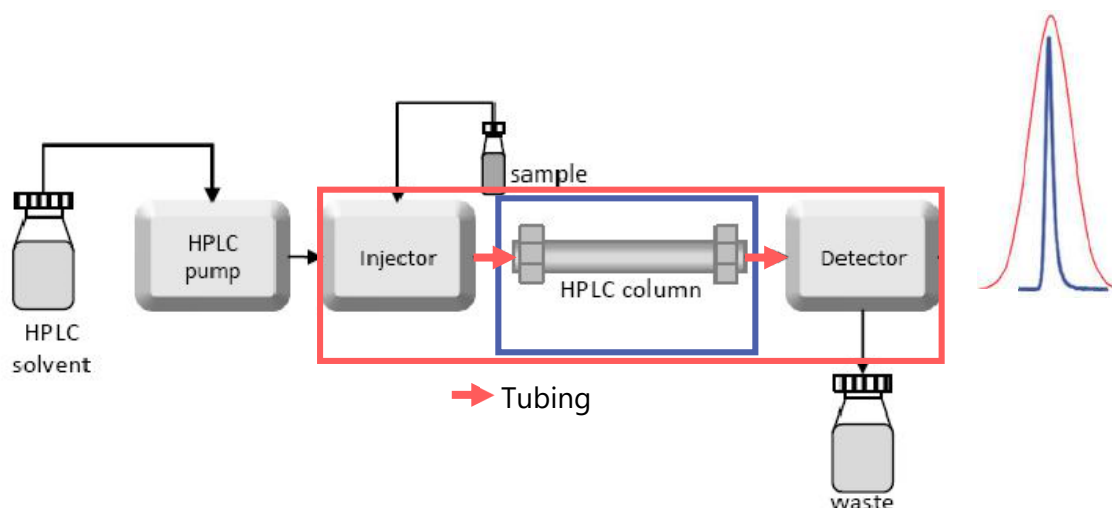


Figure 6: Representation of the contributions to peak width $\sigma_{tot}^2 = \sigma_{col}^2 + \sigma_{ec}^2$

The total variance σ_{tot}^2 depends on the column dead volume, efficiency and retention factor of the solute (Equation 7)

$$\sigma_{tot}^2 = \sigma_{ec}^2 + \sigma_{col}^2 = \sigma_{ec}^2 + \frac{V_r^2}{N_{col}} = \sigma_{ec}^2 + \frac{V_0^2 \times (k+1)^2}{N_{col}} \quad \text{Equation 7}$$

With σ^2 the variance, V_0 the column dead volume, and V_r the retention volume.

Considering this equation, it is important to reduce σ_{ec}^2 , by reducing the detector cell volume, the injection volume, and the tubing dimensions^{7,12}. Modern "zero dead volume" connectors are commercially available, but reducing the I.D. generates backpressure that has to be considered during the optimization of the system.

The final efficiency (called the restituted efficiency, E_r) is necessary less important than what it should be, and this loss of efficiency could be expressed as a percentage of the "real" column efficiency (Equation 8)

$$E_r = 100 \times \frac{N_{tot}}{N_{col}} = 100 \times \frac{\sigma_{col}^2}{\sigma_{ext}^2 + \sigma_{col}^2} \quad \text{Equation 8}$$

With σ^2 the variance and N the efficiency.

The absolute importance of reducing extra-column variance has been highlighted by Fekete *et al.*⁶ who calculated that with a HPLC system ($\sigma_{ec}^2 > 100 \mu\text{L}^2$), a 2.1 mm I.D. x 50 mm, 1.7 μm column and for a solute of $k = 5$, only 30% of the column efficiency could be restituted. As a comparison, on a UHPLC system with only 10 μL^2 of extra-column variance, 80% of the column efficiency could be restituted.

This performance loss could be minimized by using the gradient mode that allows to compensate the peak broadening pre-column contribution by the elution band compression that occurs for separation in gradient mode^{13,14}. The post-column contributions (detector cell and tubings) are nevertheless remaining so there is a need to evaluate precisely the chromatographic system, especially the extra-column volumes, to select the most adapted column dimensions and avoid important loss of efficiency.

Also, it has to be noticed that even with reduced extra-column volumes such as those of modern UHPLC instrument, the columns used on it are also extremely minimized (2.1 mm I.D. x 50 mm), justifying continuous effort to benefit of the best performances of such column technology.

I-1-3. Kinetic performance evaluation

I-1-3-1. Van Deemter equation

To evaluate the kinetic performances of columns, the van Deemter curve is often plotted, recording the efficiency N (inversely proportional to H , as expressed in Equation 3) at different mobile phase linear velocity u . This curve allows for determining the optimal linear velocity u_{opt} at which the efficiency is maximal (H_{min})^{15,16}.

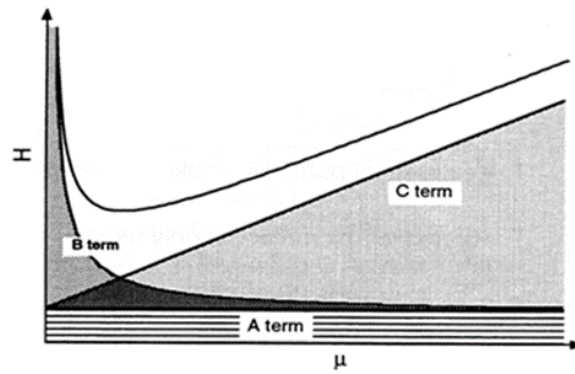


Figure 7: Predominant terms in the van Deemter curve depending on the mobile phase linear velocity

As can be noticed in Figure 7, the A-term that depends on the particle diameter and expresses the packing quality is constant. The B-term ($f(D_m, k)$) is predominant at low linear velocity, contrary to the C-term ($f\left(\frac{d_p^2}{D_m}, k\right)$) that is the most important at high linear velocity. Consequently, the most flat and low, the most efficient at high flow rate is the column. However, the van Deemter curve does not provide information about the permeability and the backpressure¹⁵.

When evaluating different columns of different geometries, another equation proposed by Knox uses the reduced parameters that are dimensionless quantities. The reduced plate height (h) is defined in Equation 9 and the reduced velocity (v) in Equation 10, for the Knox equation in Equation 11.

$$h = \frac{H}{d_p} \quad \text{Equation 9}$$

$$v = \frac{u \times d_p}{D_m} \quad \text{Equation 10}$$

$$h = av^{1/3} + \frac{b}{v} + cv \quad \text{Equation 11}$$

For well-packed columns of varying particle size and differing conditions, the coefficients a , b and c will be roughly constant (e.g. $a = 1$, $b = 2$, and $c = 0.05$ for porous particles).

I-1-3-2. Kinetic plots

Instead of considering the experimental plate number, the kinetic plot methodology considers an extrapolated value, namely the pressure drop limited plate number, which can be easily calculated and combine both efficiency and permeability (K_v) (Equation 12, 13 and 13')¹⁷.

$$\Delta P = \frac{u \times L \times \eta}{K_v} = \frac{L \times \eta}{K_v} \times u \quad \text{Equation 12}$$

With η the viscosity.

Recording the backpressure at different mobile phase velocities give access to the column permeability that is the slope of the plot $\Delta P = f(u)$ (provided that the instrument backpressure is subtracted at each u)

$$K_v = \frac{L \times \eta}{S} \quad \text{Equation 13}$$

$$K_{vi} = \frac{d_p^2}{\phi_i} \quad \text{Equation 14'}$$

With, S the slope of the plot $\Delta P = f(u)$, and ϕ_i the resistance flow factor.

The impedance parameter (E_i in Equation 14 and 14') is a dimensionless value that describes the overall separation power (i.e. the ability to produce high efficiency with short retention time and low pressure drop). So the lower the value is, the most efficient the column is for a low backpressure¹⁸.

$$E_i = \frac{t_i}{N^2} \times \frac{\Delta P}{\eta} = \frac{H^2}{K_{vi}} \quad \text{Equation 15}$$

With ΔP the backpressure.

$$E_i = h^2 \times \phi_i \quad \text{Equation 16'}$$

In the early 70's, Knox and Saleem already noticed that a compromise has to be found between efficiency and analysis time¹⁹. It was the beginning of the particle diameter decrease for faster analysis, as it was later confirmed by Poppe²⁰. Then, Desmet proposed a refined simplified model of the Poppe developments that led to the so-called kinetic plots. Those plots allow for knowing the required time to reach a desired theoretical plates^{20,21}. Basically, instead of considering the theoretical N , this theory takes into account an extrapolated value of N , for a column length and a mobile phase velocity generating a backpressure that corresponds to the instrumentation maximal backpressure. The two fundamental equations (Equation 15 and 16) are used to generate such data, by adding the experimental values of u and H ²².

$$u = \frac{\Delta P}{\eta} \times \frac{K_{vi}}{L} \quad \text{and} \quad L = N \times H \rightarrow N = \frac{K_{vi}}{u \times H} \times \frac{\Delta P}{\eta} \quad \text{Equation 17}$$

$$u = \frac{\Delta P}{\eta} \times \frac{K_{vi}}{L} \quad \text{and} \quad t_i = \frac{L}{u} \rightarrow t_i = \frac{K_{vi}}{u^2} \times \frac{\Delta P}{\eta} \quad \text{Equation 18}$$

The advantage of using the kinetic plot theory is the possibility to directly compare different columns or different technologies (e.g. monolithic vs particulate columns). Indeed, the theory takes into account both the column and instrumentation characteristics, allowing, for a given efficiency, to select the most adapted support to reach this efficiency as fast as possible on the given LC instrument.

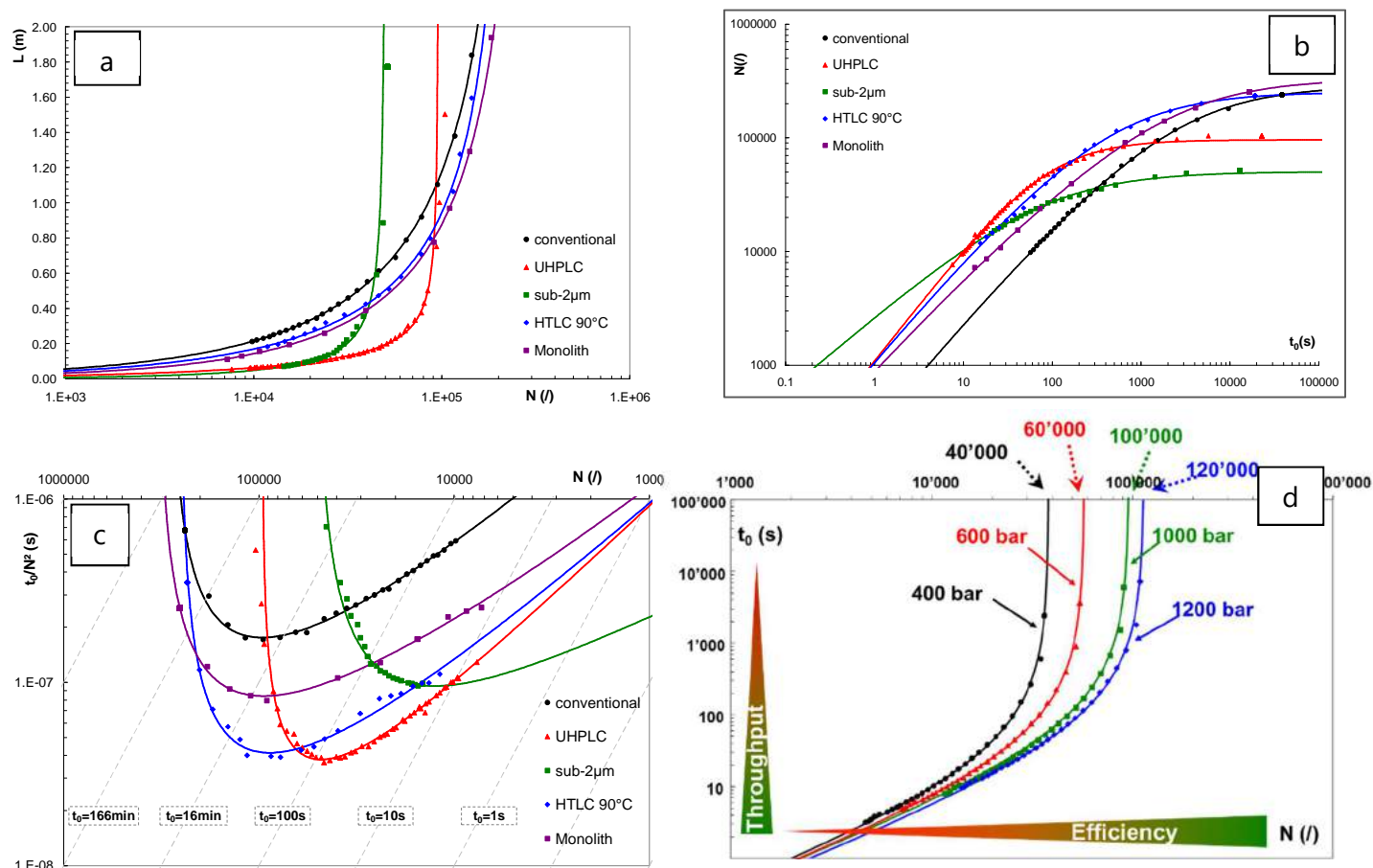


Figure 8: Kinetic performances of different HPLC technologies with the kinetic plot approach. (a) $L=f(N)$, (b) $N=f(t_0)$, (c) $t_0/N^2=f(N)$, (d) $t_0=f(N)$. (d) corresponding to kinetic plots constructed for Waters Acquity BEH C18, 1.7 μ m, considering $\eta= 0.85cp$. Adapted from²³

In the example illustrated in Figure 8, the kinetic performances of different technologies were compared. The Figure 8a ($L=f(N)$) presents which column reaches a certain number of plates on the shortest column length. For example, the best solution to obtain faster 10,000 plates is doing UHPLC or using the sub-2 μ m particles. Also, it proved that in UHPLC, having a column length higher than 60 cm is not interesting as efficiency cannot be higher (due to the backpressure restriction). The Figure 8b ($N=f(t_0)$) gives insight on the time analysis, especially, the dead time necessary to obtain the 10,000 plates. Then the Figure 8c allows for conserving the van Deemter curve shape, and by tracing the time lines, having directly the time necessary to obtain the required efficiency. With this representation, the most to the bottom left it is, the best is the ability to generate quickly high efficiency. For a given plate numbers (x-axis), the lower curve is the technology allowing to reach it as fast as possible, changing both the column length and the mobile phase velocity to maintain a specific maximal backpressure. For instance, if we focus on the particle diameter importance, for fast analysis with an efficiency lower than

50,000, sub-2 μm columns (Figure 8c in green) are recommended. However, when very high efficiency is required, columns packed with larger particles (Figure 8c in black) are more adapted. As they generate lower backpressure, longer columns that improve efficiency can be used, without exceeding the maximal pressure. Increasing the fixed value of backpressure would shift the curves towards higher efficiency, which could extend the range of use of sub-2 μm columns. This feature is illustrated in Figure 8d, in which the fixed data is the column dimensions and no more the backpressure. High-throughput and high-efficiency experiments can be done in LC by increasing the backpressure available.

This discussion applies for k being constant, so adapting the mobile phase conditions from a column to another one. If the data presented here were obtained in isocratic mode, such representations can also be done in gradient mode. In this condition, instead of efficiency, the peak capacity (n_c) is considered²³ with the maximal backpressure during the gradient¹⁵.

I-1-4. Technology strategies: faster, hotter, smaller

Previously achieved with conventional LC columns (4.6 mm (I.D.) \times 150 to 250 mm length) packed with Fully Porous Particles (FPP) of 3.5 to 5 μm as particle diameter (d_p), and with analysis time ranged from approximately 10 minutes to one hour, HPLC encountered limitations due to new analytical challenges. Among them, the number of samples and their constant complexity (e.g. metabolomics) led to new LC instruments, allowing to reduce the analysis time and to reach better resolution as presented previously.

The following part of this manuscript is focused on the different technology strategies that could be set up to achieve high efficient separation, in a continuously reduced time, and increased sensitivity.

Among them, the core-shell technology (i.e. use of SPP) is a very performant one that allows for working faster, achieving high efficient separation without generating pressure incompatible with conventional HPLC equipment. Before deeply presenting this technology, some others are also of interest such as monolithic columns²⁴, sub-2 μm columns of FPP^{15,25}, and High-Temperature Liquid Chromatography (HTLC).

I-1-4-1. Monolithic supports

Increasing the mobile phase velocity is a direct way to ensure fast analysis. However, it impacts efficiency and generates excessive backpressure due to the resistance of the liquid mobile

phase passing through the particle packed bed. The permeability of the column can be improved by increasing the column porosity.

First developments of monolithic columns were reported in the 90's²⁶⁻³⁰ and led in 2000 to a commercialization by Merck (Darmstadt, Germany).

In this technology, a porous one-piece stationary phase is trapped into a PolyEtherEtherKetone (PEEK) tube. The stationary phase can be based on polymer or on silica, the latter being more adapted to the analysis of low molecular mass solutes and providing better performance in HPLC. The interest of monoliths is essentially due to the bimodal structure made of macropores (1 to 5 μm) and mesopores (10 to 30 nm). Macropores provide good permeability and allow for working at high flow rate without excessive pressure drop, and mesopores provide a large surface area in which retention occurs³¹.

Many advantages result from this monolithic structure:

- High mobile phase velocity: It was shown that this parameter could be increased by 5-fold compared to columns packed with 5 μm silica FPP at equivalent dimensions, at pressure compatible with HPLC systems^{24,32}.
- High kinetic performances: The reduction of the C-term of the van Deemter curve allowed for reaching comparable kinetic performances for monolithic silica and columns of the same length packed with 3-4 μm FPP silica particles³³.
- High-resolution analysis: For very high efficiency, monoliths are of prime interest, due to the possible connection of monoliths in serie. Plate count higher than 100,000 have been reached in such configuration^{34,35}.

Also, a second generation appeared in 2011³⁶ and provided efficiency comparable to sub-2 μm particles, but backpressure 3-fold higher than the first generation. Concerning efficiency, Gritti and Guiochon³⁷⁻³⁹ published a study in three parts devoted to the Eddy diffusion coefficient determination.

Nevertheless, some limitations associated with monoliths have to be noticed and counterbalance such advantages. First, couple many monolithic columns is costly, and not compatible with high throughput separations. Also, silica-based monoliths present some disadvantages such as low mechanical (Pressure < 200 bar due to PEEK bursting), thermal (temperature < 60°C) and chemical resistances (2 < pH < 8); and the loss of chromatographic performances due to inhomogeneity of the silica network.

Also, there is a limited number of providers of such technology (mainly Merck and Phenomenex), offering narrow range of surface chemistries (essentially C8 and C18) and column geometries (essentially 2 or 3 or 4.6 mm I.D. × 100 mm maximum). Moreover, bleeding is encountered when using Mass Spectrometry (MS) detection.

I-1-4-2. High-Temperature Liquid Chromatography (HTLC)

Many parameters can be considered during method developments: those concerning the mobile phase (composition, pH, and ionic strength), those concerning the stationary phase (type, particle, pore size and column dimensions). In addition to the liquid chromatography parameters, temperature has gained greater attention as another important variable in HPLC during the last decades.

Some good reasons led the researchers to investigate methods at elevated temperature due to some theoretical analytical benefits. Nevertheless, some practical issues must be considered in developing High Temperature Liquid Chromatography (HTLC) approaches.

Major advantages of HTLC include shortened separation time, improved peak shape and increased efficiency (on a larger flow rate range), and reduction of organic solvent amount. Indeed, working at high temperature allows for increasing the optimal linear velocity and improves the mass transfer. The Wilke/Chang equation takes into account the effect of temperature for the diffusion coefficient D_m (Equation 17), explaining why at higher flow rates the C-term is lower and u_{opt} is improved (Equation 18 and 19)⁴⁰. Also, the lower backpressure (Equation 20) due to the decrease of viscosity of the mobile phase when using HTLC allows for working at higher flow rates to reduce run times.

$$D_m \propto \frac{T}{\eta} \quad \text{Equation 19}$$

With T the temperature.

$$u = \frac{v \times D_m}{d_p} \quad \text{Equation 20}$$

$$C = f\left(\frac{d_p^2}{D_m}\right) \quad \text{Equation 21}$$

Also, the Darcy's law specifies the effect of viscosity in backpressure in Equation 20.

$$\Delta P = \frac{u \times L \times \eta \times \phi}{d_p^2} \quad \text{Equation 22}$$

With ϕ the resistance flow factor.

First, regarding efficiency (Figure 9), temperature is a useful parameter to be considered when optimizing methods. While the A-term could be considered independent of temperature, the remaining B and C-terms are both temperature-dependent. Indeed, the B-term is directly proportional to the diffusion coefficient D_m , which is also a function of the temperature.

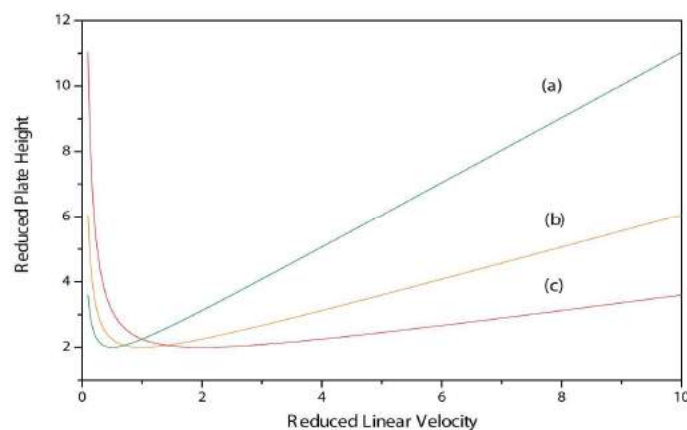


Figure 9: Representation of the van Deemter curves as a function of the isothermal separation temperature (a) $T = 75^{\circ}\text{C}$, (b) $T = 125^{\circ}\text{C}$, (c) $T = 175^{\circ}\text{C}$, adapted from⁴¹

From this representation, it can be deduced that the minimum plate height obtained is relatively independent of the temperature employed. Moreover, when the temperature is increased, the profile of this curve changes. At elevated temperatures, the minimum of the curve is shifted to higher linear velocities. In addition, at flow rates higher than the optimal, the increase is more moderate. This means that if a separation is carried out with a mobile phase flow rate which is much higher than the optimal flow rate, the loss of efficiency at higher temperatures is less pronounced than at lower temperatures. So there is a significant advantage of applying higher temperature when working at flow rates above the optimal value due to the lower C-term.

More viscous organic modifiers such as 2-propanol can be employed to tune selectivity⁴². If high efficiency is required, smaller particles or longer columns can be employed, and at above optimal flow rate to obtain fast efficient separations. The decrease of retention leads to a lower organic solvent consumption, which presents financial benefits. Also, less expensive and/or toxic solvent such as ethanol can be used as mobile phase, even pure water⁴³.

Then, the temperature impacts also the retention and selectivity as described in the Van't Hoff equation (Equation 21)⁴⁴.

$$\ln k = \frac{\Delta H}{RT} + \frac{\Delta S}{R} + \ln \beta \quad \text{Equation 23}$$

With R the universal gas constant, ΔH and ΔS the enthalpy and entropy of transfer, respectively, and β the phase ratio (i.e. the ratio of the volume of mobile phase to that of the stationary phase).

As a function of variations of the temperature, changes in retention can be caused either by changes in enthalpy or entropy. However, deviations from linearity derived from different desorption kinetics of functional groups (e.g. ionizable groups), dual retention mechanisms, or temperature-related changes of the mobile phase (e.g. pH)⁴⁵.

Despite those advantages derived from using HTLC, some considerations have to be taken into account such as the suitability of instrumentation to operate at high temperature, the thermal stability of solutes and stationary phases used, and the suitability of the detection method employed.

When operating at high temperatures, radial temperature gradients across the chromatographic column can lead to thermal mismatch band broadening which is a major drawback for HTLC systems⁴⁶. Preheating the mobile phase or using capillary columns can minimize this effect.

Considering instrumentation, if the majority of the conventional HPLC components can be used, dedicated oven enables to work up to 200°C⁴⁷. Also, compatibility with high temperatures is necessary for a number of instrumental components inside the oven and post-column. Efficient heating and precise temperature control are critical in HTLC. Ideal HTLC temperature control systems should ensure effective homogeneous heating efficiency for both the mobile and the stationary phases throughout the separation column to eliminate thermal mismatch. Indeed, because the analytical column is heated in HTLC at a temperature higher than that of the mobile phase in the reservoir, the low temperature of the incoming mobile phase does not match the high temperature of the separation column if the eluent is not preheated efficiently. This thermal mismatch causes poor reproducibility and other separation problems. Some instrumental strategies were developed as the addition of a preheating coil inside the oven or a heating unit can be added to heat the mobile phase before entering into the column⁴⁸. The extra tubing void volume has to be minimized to reduce additional peak broadening.

The major drawback is the degradation of the SP^{49,50}. Some stationary phases were investigated in HTLC^{51,52} and in general, some silica-bonded packings showed good long-term stability at temperatures around 100°C, although many of them cannot tolerate such temperatures. Zirconia- and other metal oxide-based columns normally can be used at temperatures ranging

from 100°C to 150°C for several thousand column volumes without significant degradation of the stationary phase. Among all existing LC packing materials, polymer stationary phases (e.g. poly(styrene-co-divinylbenzene)) are very stable ones, and can be used reliably at high temperatures, typically at 150°C or higher. However, the efficiency of polymer columns is poorer than that of silica- and zirconia-based columns. Other stationary phases tested in HTLC included Porous Graphitized Carbon (PGC) up to 200°C, and monolithic, encapsulated silica and ethylene-bridged hybrids are stable above 180°C under aqueous conditions⁴³. Specially designed HPLC chips columns also were used for LC separations at various temperatures⁵³. In addition, microbore columns, packed capillary and open tubular columns also have been used in HTLC, and they are more appropriate for separations with programmed temperature.

HTLC separation shortens the solute exposure time to high temperature, which minimizes the solute degradation⁵⁴. Even some pharmaceuticals can withstand high temperatures on the time scale of fast HTLC separation⁵⁴. For separation and analysis of biomolecules, sub-ambient or low temperature can be more appropriate to avoid degradation. If HTLC is used for analysis of biomolecules, ultrafast separation conditions should be considered to minimize the solute exposure time to the harsh high-temperature conditions.

Concerning detection, the most attractive option is to use Mass Spectrometry (MS), but UV-visible can also be used with some considerations. The temperature of the UV flow cell should be constant even during temperature-programmed elution. Moreover, the oven has to contain a post-column cooling to avoid damage of UV cell. Also, the risk of bubbles formation can be countered by adding a pressure restrictor post-detector. Some other detectors such as Evaporative Light Scattering Detector (ELSD) and Corona Charged Aerosol Detector (CAD) can be used without post-column cooling⁵⁵. Also, flame ionization detection is practicable but is limited to non-organic mobile phases⁵⁶.

The combined effects of high temperature and low pressure make it possible for HTLC to use very high flow rates to achieve fast separations, which make HTLC a performant technology to deal with applications requiring high efficiency at elevated flow rates, and for selectivity optimization or increased eluent strength for complex matrices. More robust columns are still needed to cope with long-term operation at high temperatures.

I-1-4-3. Sub-2 μm and UHPLC

At the same time of improving and diversifying the stationary phase chemistry, the silica particle itself evolved with the trend of reducing particle diameter (d_p) to reach better chromatographic performances⁵⁷. The theoretical benefits for columns packed with small particles (sub-2 μm) were demonstrated in the 70's by Knox *et al.*¹⁹.

The main reports dealt with lab-made ultrahigh pressure instrumentation usually connected with capillary columns, with a special study of the injection and pumping devices. The main papers were published by MacNair *et al.*^{58,59}, Halász *et al.*⁶⁰ and many others⁶¹⁻⁶⁴. Even chiral separations were done, Lee *et al.* used a UHPLC system capable to reach 3600 bar and allows for the separation of a 6 racemic herbicides in less than 1 minute in 1999⁶⁵. In 2003, Jorgenson *et al.* succeeded in reaching 300,000 plates on a 430 mm x 50 mm, 1.0 μm column but with a pressure of 7200 bar⁶⁶. At the same time, Xiang *et al.*⁶⁷ discussed about safety aspects in ultrahigh pressure capillary chromatography. They provided the proof-of-concept that working with columns packed with sub-2 μm particles on systems able to support very high pressures was a good combination to extend significantly the HPLC performances.

The breakthrough came in 2004 with the commercial introduction of short narrow-bore columns packed with FPP of 1.7-1.9 μm diameter (sub-2 μm) and chromatographic systems capable to support pressures up to 1000 bar.

Compare to FPP of 5 μm , the size reduction increased significantly the efficiency (N) as described by Equation 22.

$$N = \frac{L}{H} = \frac{L}{h \times d_p} \quad \text{Equation 24}$$

With UHPLC, three strategies are of interest depending on what has to be favored:

- High throughput: To ensure fast analyses, it is possible to reduce the column and particle dimensions (from 150 mm x 5 μm to 50 mm x 1.7 μm) with preservation of efficiency, provided that low dispersion systems are used.
- High efficiency: By maintaining the column length and using 1.7 μm particle instead of 5 μm particles, efficiency can be increased by 3-fold.
- High resolution: If very high efficiency is required, working with 150 mm length column packed with 1.7 μm particles instead of 5 μm , it is possible to couple the columns to increase peak capacity while maintaining an equivalent time of analysis.

Moreover, when d_p is reduced, the optimal linear velocity is higher as illustrated by Equation 18.

Sub-2 μm particles are even more advantageous when working at $u > u_{\text{opt}}$ because the C-term of the van Deemter equation-the most important term in those conditions- is reduced as illustrated in Equation 19.

Also, the Darcy relation links the diameter particle with the backpressure generated in Equation 20.

The use of sub-2 μm particles requires UHPLC systems because of the generation of backpressure not compatible with conventional HPLC instruments limited at 400 bar^{68,69}. Some limitations or precautions have to be underlined when using such technology to benefit of its advantages over the long-term.

First, the mechanical resistance of sub-2 μm particles has to be very important to support packing pressures that are higher than those used during UHPLC analysis. It is a necessary condition to avoid the formation of preferential ways during packing that are deleterious for efficiency. Moreover, cracks of the silica particles may lead to frit clogging that have smaller porosity than those used in HPLC (0.2 - 0.5 μm in UHPLC vs. 2 μm in HPLC). Due to the higher risk of column frits clogging, it is necessary to use only high grade for solvents and salts, and to filter the mobile phase through 0.22 μm membrane filters.

To increase the column lifetime, the chemical resistance can be improved by the Bridged Ethylene Hybrid (BEH) technology, which corresponds to a hybrid silica particle containing ethane bridges between two adjacent silicon atoms^{68,70}.

All in all, to extend column and instrument lifetimes, it is recommended to work at 70-80% of ΔP_{max} .

Another phenomenon that negatively impacts efficiency is the frictional heating that occurs when the pressure exceeds 400 bar⁵⁸. The mobile phase percolation through the sub-2 μm particle packed column induces overheating that, if not dissipated, leads to gradient temperatures (both radial and longitudinal) inside the column^{66,71}. In particular, longitudinal gradients change the mobile phase viscosity and so the retention; and radial gradients cause a deformation of the elution band in which the solutes at the center are faster than those near the column walls. The elution band being wider, a loss of efficiency is noted⁷²⁻⁷⁴. This phenomenon can be attenuated by using smaller column geometries (50 \times 2.1 mm I.D. instead of 150 \times 4.6 mm I.D.)⁷⁵.

Despite those possible complications that are intrinsically due to the use of ultra-high pressure, the combination of sub-2 μm /UHPLC dedicated system is a very effective strategy to quickly generate important plate numbers. Many investigations were done on theoretical aspects and applications (mainly small and biomolecules). Nowadays, this technology is still in progress, both concerning columns with particles down to 1.3 μm , and UHPLC systems operating at pressure up to 1500 bar⁷⁶⁻⁷⁸. The interest of UHPLC in 2D-LC has also been recently highlighted and seemed a reliable way to plenary benefit of the UHPLC advantages⁷⁹. On UHPLC instrument, higher flow rates can be employed if ultra-fast separations are required; or higher column length can be used if ultra-high efficiency is necessary^{80,81}.

I-1-4-4. Core-shell technology

This technology was originally developed by Horvath⁸² who proposed 30-50 μm particles surrounded by a 1-2 μm polymer, but with limited specific surface area and non-uniform and instable surface. Then, in the early 70's, Kirkland proposed a solid core of 10 μm surrounded by a layer of spherical nanoparticles⁸³.

The first commercialization by Agilent took place in the 90's under the trademark Poroshell, and corresponded to a 5 μm particle with a shell of 0.25 μm . The particles presented a better mass transfer allowing for good performances for macromolecules (peptides/proteins)⁸⁴, and afterward for small solutes.

This technology was further updated and widespread since 2007 with the commercialization of 2.6-2.7 μm Superficially Porous Particles (SPP) made of a solid core with a shell thickness of 0.35-0.50 μm . It was rapidly used as an alternative to sub-2 μm particles as they preserve around 80% of Fully Porous Particles (FPP) sub-2 μm efficiency with a backpressure 2-fold lower^{80,85,86}. Such sub-3 μm SPP can be used with a conventional HPLC instrument provided that the extra-column volumes are minimized.

SPPs allow for higher efficiency than the porous ones, as a result of the reduction of the diffusion phenomena. Many studies and papers were done to explain the higher chromatographic performances⁸⁷⁻⁹⁷.

Actually, the narrow particle size distribution combined with a higher roughness allow for a reduction of the A term of the van Deemter curve. Moreover, no longitudinal diffusion can take place in the solid inner core, minimizing the B term. Finally, the global mass transfer resistance

is slightly lower with SPP, so the C term is also reduced. Moreover, a study conducted by Gritti and Guiochon showed that SPP had a higher thermal conductivity that decrease the radial gradient temperature in the column and allows for working at higher mobile phase velocity without increasing too much H^{98} .

If only Agilent provided the Poroshell particle (4.50 μm core-0.25 μm shell) in the 90's, several morphologies (diameter, porous shell thickness, porosity) are now available. Since 2007, the real trend is the 2.6-2.7 μm SPP. If there are many providers of columns based on SPP, few are manufacturers. Consequently, the solid core is mainly 1.6-1.7 μm surrounded by a porous shell, further functionalized and commercialized on their own trademark.

The morphology impacts the kinetic performances and especially the shell thickness that constitutes the active exchange surface for solutes^{99,100}. As the layer is thin, the efficiency is higher but the retention capacity and the loadability are limited, the latter being especially deleterious for ionizable solutes¹⁰¹.

Some factors may limit the application of SPP for method scale up. First, few manufacturers offer a preparative column format, making difficult the transposition from low quantitative methods to preparative scale chromatography. Also, the loading capacity is lower due to limited surface area (170-210 m^2/g). It seems, at least for the moment, that a method has to be run at the analytical scale (Quality and Control) and one at the preparative scale (production).

A good compromise between efficiency, retention and loading capacity has to be found, but this technology is now widely used for ultra-fast analysis¹⁰² and/or high-resolution analysis¹⁰³.

Nowadays, two opposite trends are noticed in terms of SPP size. The use of sub-2 μm SPP launch in 2009 (Kinetex 1.3 and 1.7 μm by Phenomenex, and Cortecs 1.6 μm by Waters) allowed for reaching up to 500,000 plates/meter and pushed the chromatographic performance limits^{104,105}. On the contrary, 4-5 μm SPP launch in 2012 were developed for pharmaceutical purposes to avoid the revalidation of methods already developed on FPP. Halo and Ascentis Express 5 μm SPP are available from Advanced Material Technologies and Sigma, respectively; Kinetex 4.6 μm from Phenomenex and Accucore 4 μm from Thermofisher Scientific. Additionally, developments were proposed in terms of pore size, for instance, widepore SPP

(300-400 Å), launch in 2011, are available from Advanced Material Technologies (Halo 400 Å) and Phenomenex Aeris (300 Å). Even with those improvements, there is still a lack scalability, so it is still important that manufacturers develop a wide range of stationary phases with scaling options to improve lab-productivity. Especially, preparative SPP columns (21.2 mm I.D. launch in 2013) and chiral columns are not very widespread.

As UHPLC, the SPP technology offers high efficiency with reduced run times, and require low dispersion LC systems to provide the vaunted efficiencies.

Conclusion

In the past four decades, many evolutions were done on HPLC that is nowadays, considered as the technique of choice in numerous fields, including pharmaceutical, forensic, biological, environmental and food analysis. Those evolutions encompassed the modern instrumentation with continuously lower extra-column volumes to minimize the diffusion phenomena and to obtain the highest possible efficiency.

To evaluate such kinetic performances, the van Deemter plots are widely used, and can be completed by using the kinetic plot theory. In recent years, kinetic plots have become the tool by which different LC columns, particle types, and particle sizes have been compared with each other. Also, questions about performance, column length, and the merits of different technologies (UHPLC, monoliths, SPP, HTLC) have been tackled using the same tools.

Some conclusions about those technologies and the modern instrumentation can be drawn and are summarized in Table 3. Some assumptions for the future also have been highlighted in a review of Guilleme *et al.*¹⁰⁶



Technology		
Monoliths	<ul style="list-style-type: none"> - Low backpressure (high permeability) - HPLC system compatibility 	<ul style="list-style-type: none"> - Lack of chemistries, providers and long columns (150-250mm) - Undirect method transfer from HPLC to monolith - Resistance ($P < 200$ bar) and pH ($2 < \text{pH} < 8$)
HTLC	<ul style="list-style-type: none"> - Lower organic modifier consumption - Better peak shape for basic and large molecules - Ultra-fast analysis and high-resolution in combination with UHPLC 	<ul style="list-style-type: none"> - Thermal stability of SP and solutes at $T > 100^\circ\text{C}$ - Dedicated instrumentation (preheating + cooling devices, backpressure regulator) - Method transfer difficult as α depends on T
UHPLC	<ul style="list-style-type: none"> - Easy method transfer from HPLC to UHPLC - Fast analysis - Availability of many sub-2 μm columns 	<ul style="list-style-type: none"> - Dedicated instrumentation ((low σ_{ext}^2, elevated acquisition rate, fast injection, pumps) - Consumable costs - Frictional heating, solvent compressibility around 1000 bar - Need of UHPLC columns for biomolecule analysis such as large proteins
Core-shell (SPP)	<ul style="list-style-type: none"> - Lower diffusion than in FPP (especially for large molecules) - Better packing quality - HPLC system compatibility 	<ul style="list-style-type: none"> - Need of widepore SPP for large protein analysis - Lower retention and loading capacity than FPP - Lower backpressure resistance (< 600 bar) than FPP sub-2 μm and pH ($1 < \text{pH} < 11$ for some surface chemistries)

Table 3: Advantages and drawbacks of approaches for high-throughput and high-resolution analysis in liquid chromatography

I-2. Liquid chromatography modes

Liquid chromatography is one of the most used separation techniques in many fields (e.g. environment, pharmaceutical and food industries, chemistry, toxicology). The chromatographic modes employed have to be adapted depending on the physico-chemical properties of solutes. The partition coefficient ($\log P$) is the ratio of the concentration of the compound in octanol to its concentration in water (Equation 23). The distribution coefficient ($\log D$) is the ratio of the sum of the concentrations of all species of the compound in octanol to the sum of the concentrations of all species of the compound in water (Equation 24).

$$\log P_{oct/wat} = \log \left(\frac{[solute]_{octanol}^{un-ionized}}{[solute]_{water}^{un-ionized}} \right) \quad \text{Equation 25}$$

$$\log D_{oct/wat} = \log \left(\frac{[solute]_{octanol}^{un-ionized} + [solute]_{octanol}^{ionized}}{[solute]_{water}^{un-ionized} + [solute]_{water}^{ionized}} \right) \quad \text{Equation 26}$$

In general, three primary characteristics of chemical compounds can be used to monitor HPLC separations: polarity, charge, and molecular size. The following sections are devoted to the presentation of the different achiral LC modes that can be set up depending on the solutes.

I-2-1. Normal Phase Liquid Chromatography (NPLC)

Normal Phase Liquid Chromatography (NPLC) was, chronologically, the first Liquid Chromatographic technique. In the separations of plant extracts, Tswett used a polar stationary phase of chalk in a glass column with a much less polar mobile phase. This classical mode of chromatography became known as normal phase.

This mode is especially used for purification purposes, for example, the separation by class of polarity of the lipid polar groups.

The stationary phase is mainly silica (pH stability 2-8) or alumina (pH stability 2 - 12) and the retention of the compounds is governed by an adsorption mechanism of solutes on the polar, weakly acidic surface of silica gel¹⁰⁷. Also, bonded SP such as cyano, diol or amino groups have been developed. In such case, the mechanism involved is similar to partitioning.

The mobile phase usually consists of an organic solvent mixture of a very nonpolar with a slightly more polar solvent such as heptane/ethyl acetate or heptane/isopropanol. Therefore polar compounds are retained longer than the nonpolar ones.

However, this mode has some limitations: the solvents used are pollutant and/or toxic, unsuitable with ESI-MS¹⁰⁸, and sometimes the solubility of the solute is not good with the solvents. Also, this mode is extremely sensitive to water leading to repeatability troubles (especially when adsorption mechanism), the equilibration time is long and often peaks are broadened.

I-2-2. Reversed-Phase Liquid Chromatography (RPLC)

The Reversed-Phase Liquid Chromatography (RPLC) is the most LC mode employed in chromatography. The mobile phase usually consists of a mixture of water with organic solvent (e.g. methanol, acetonitrile, ethanol, isopropanol, tetrahydrofuran...). The stationary phase is commonly based on silica particles, functionalized with hydrophobic ligand such as alkyl chains. The universal ligand ($\approx 90\%$ of the separations) is the octadecylsilane group (C18), but some other short alkyl chains (octylsilane group: C8, butylsilane: C4) can be used, especially in case of the separation of highly hydrophobic solute that are too retained on C18. The popularity of RPLC and its wide application range is explained by its robustness, MS compatibility, and its versatility. Solutes from a middle to a low polarity are well separated by hydrophobic interactions. But hydrophobic stationary phases have some disadvantages: they can be incompatible with a high aqueous content, the polar solutes retention can be too low, and important peak tailing for such solutes (i.e. basic solutes) leads to poor resolution. The introduction of a polar group into the structure of the ligand, often alkyl stationary phases¹⁰⁹⁻¹¹⁶, led to what is now called polar-embedded stationary phases. Embedding a polar functional group (e.g. amide, carbamate¹¹⁷) into a bonded alkyl chain reduced the peak tailing for basic analytes and showed unique selectivity for certain classes of analytes such as phenols. Also, when high aqueous content in the mobile phase is necessary to achieve the baseline resolution or for solubility purposes, a polar end-capping can be achieved enhancing the wetting of the C18 stationary phase, and/or protect from the residual silanols, and/or tune selectivity^{111,118-121}. Also, original stationary phases such as pentafluorophenyl (PFP) were developed and gave rise to orthogonal retention and selectivity for the analysis of polar/ionisable solutes with conditions of RPLC mode^{122,123}.

Ionisable solute can be analyzed by RP-mode by adjusting the pH of the mobile phase as they are more retained in their neutral form^{124,125}. Caution has to be taken to ensure a pH in the stability range of the stationary phase, which can be for the most stables from 1 to 12.

I-2-3. Ion Exchange Chromatography (IEC)

Ion Exchange Chromatography (IEC) is widely used in industrial processes (e.g. separation of inorganic ions, biomolecules, and oligosaccharides). The resin matrix has generally quite high binding capacities and is usually relatively inexpensive when compared with other types of stationary phase. Ion exchange chromatography is probably the most widely used large-scale chromatographic process but is limited to ionizable water soluble molecules.

Stationary phases for ion-exchange separations are characterized by the nature and strength of the acidic or basic functions on their surfaces and the types of ions that they attract and retain. Positively charged ions are retained and separated on a cation exchange possessing a negative surface. On the contrary, negatively charged ions are analyzed on an anion exchange having positively charged ligands at the surface. The rate of migration and hence the separation depends on the charge, polarizability, and size of solvated ions. Two categories of exchangers can be distinguished: strong and weak ion exchangers.

➤ Strong ion exchangers:

The functional groups (e.g. quaternary ammonium or sodium sulfonate) are always ionized and allow for retaining and separating weak ions. The elution comes from displacement by ions of the mobile phase that are more strongly attracted to the stationary phase.

➤ Weak ion exchangers:

Depending on the pH, the functional groups (e.g. with secondary-amine or carboxylic-acid functions) are charged and retain strong ions. The ions are eluted by displacement or, if not possible, the exchange sites can be neutralized, losing their ability to retain ions by charge. In their neutral form, weak ion exchangers could retain and separate solutes by hydrophobic or hydrophilic interactions. Then, elution strength is determined by the polarity of the mobile phase, so weak ion exchangers may be used for mixed-mode separations (separations based on both polarity and charge). Also, it is possible to change the mobile phase pH to tune the selectivity. Nowadays, new SPs for IEC allow for adjusting the retention and the elution order depending on the polarizability of the ions. Such new SPs developed by Thermo Scientific™ rely on secondary interactions, depending on the functional group inserted in the structure of the SP.

The most widely used type of stationary phase is a synthetic copolymer of styrene and divinyl benzene (PS-DVB), produced as very small beads in the micrometer range. Careful control over

the amount of DVB added dictates the degree of cross-linking, the porosity of the resinous structure, and its stability.

To optimize binding of all charged molecules, the mobile phase is generally a low to medium conductivity (i.e. low to medium salt concentration) solution. By increasing the salt concentration (generally by using a linear salt gradient) the molecules with the weakest ionic interactions start to elute from the column first. Molecules that have a stronger ionic interaction require a higher salt concentration and elute later in the gradient. Some precautions have to be taken, especially if using a strong-cation exchanger to retain a strong base, which leads to strong attraction as they both remain charged. The elution can only be achieved by swamping the strong cation exchanger with a competing ion that exhibits even stronger interactions with the active exchange sites than the solute does.

However, IEC suffers from some limitations: the low kinetic leads to lower efficiency, the MS compatibility¹²⁶ is still difficult, a specific instrumentation is required to support aggressive pH conditions.

I-2-4. Hydrophilic Interaction Liquid Chromatography (HILIC)

Initially described by Alpert in 1990¹²⁷, it is really since 2006 with the studies of McCalley, Hemstroem and Irgum^{128,129} that HILIC-mode became largely used. The main applications are for polar solutes, but the HILIC mode is also applicable for lower polar solutes, allowing for orthogonal separations to RPLC¹³⁰. The stationary phases are polar (e.g. bare silica, polar modified silica such as amide, amine or diol) and the mobile phase is composed of water ($\geq 3\%$), with a high percentage of organic modifier ($\geq 60\%$, mainly acetonitrile). The retention mechanisms are influenced by the SP chemistry, the MP composition (pH, ionic strength, organic modifier), and the solute. The retention mechanisms are multimodal and not completely well-understood¹³¹ and can be summarized^{130,132,133} as represented in Figure 10:

- Hydrophilic partition between the ACN enriched mobile phase and the water layer adsorbed through hydrogen bonds to the silica surface
- Adsorption at the SP surface through hydrogen bonds with silanols, diols or amides groups onto the silica surface

- Electrostatic interactions between ionic or ionizable solutes, and the charged silica surface (negatively from the silanols, positively from amino groups, or both in case of zwitterionic ligand).

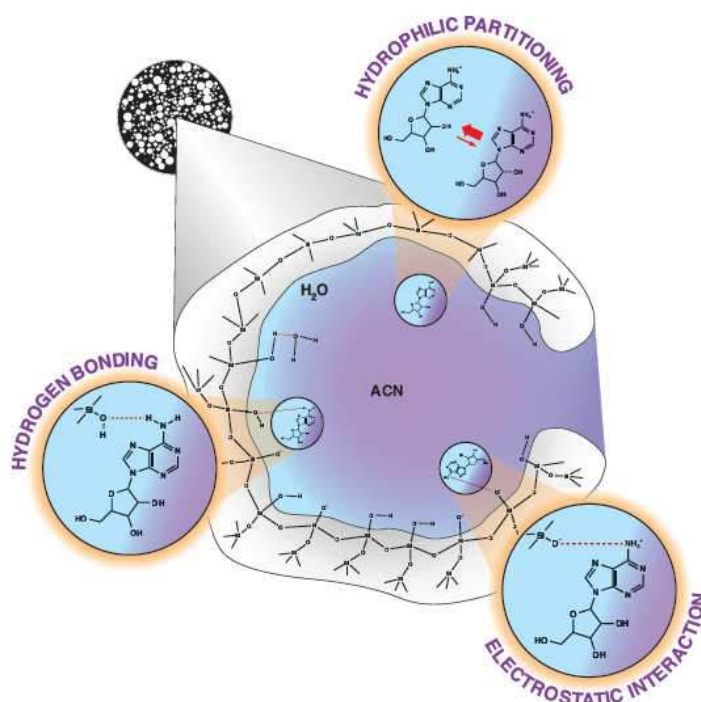


Figure 10: Schematic representation of the HILIC mechanisms¹³⁴

The elution order prediction is tricky as it depends on the polarity, hydrogen bonds capacity, and ionization state of solutes, which is difficult to predict because of the high content of ACN that influences pH of the mobile phase and pK_a of the solute^{135–137}. Even if there is no standard SP such as C18 in RPLC, many stationary phases devoted to HILIC are available, mainly on silica support or polymeric material^{130,138} as presented in Figure 11.

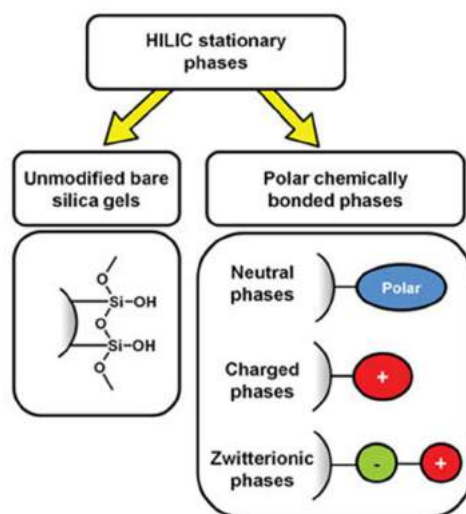


Figure 11: Stationary phase chemistries for HILIC mode and their representation, based on^{130,138}

The bare silica material is the main used as it represents 35% of the applications published¹³⁹. This SP presents good retention of polar solutes and positively charged solutes by electrostatic interactions with the deprotonated silanols at the surface. The second most used SP is the zwitterionic support (25%), with the sulfoalkylbetaine and the phosphocholine-type. The sulfoalkylbetaine contains a sulfonic acid and a quaternary ammonium linked by an alkyl chain. The phosphocholine material possesses both negatively charged phosphoric acid and positively charged quaternary ammonium groups. The positively and/or negatively charged solutes can both be retained by hydrophilic partition and electrostatic interactions. Finally, neutral stationary phases are also used and ionic interactions are only due to residual silanols in those SP. The diol SP is a good one in this category and even more the amide SP, particularly useful for peptides, glucans and oligosaccharides analysis. Then, SP containing a basic function are also available and the most common is aminopropyle, This SP is mainly used for saccharide analyses, as it improves the mutarotation of saccharides anomers, avoiding the double peak formation¹⁴⁰. Indeed, the amine functionality on the bonded phase creates a local high pH environment that is advantageous for collapsing the sugar anomers by increasing the kinetics of interconversion between α and β forms. Some other ligands can be employed in HILIC mode such as cyanopropyle, fluorophenyl, cyclodextrins, polysuccinimide, often for specific applications¹⁴¹.

The MP choice is important as it impacts the retention mechanisms. Buffers are used as they improve the peak shape of ionic compounds^{128,142}. Also, the water layer is probably thinner without buffers, which decreases the neutral solutes retention^{143,144}. Two requirements have to be fulfilled: to be MS compatible, the buffers have to be volatile; also they have to be soluble in high ACN content mixtures such as ammonium acetate or ammonium formate¹⁴².

Ionic interactions are dependent of the salt concentration: the most ionic strength, the less ionic interactions involved in retention. With negatively charged SP (as silica above pH 3), basic solutes are less retained when the salt concentration increases. Conversely, the negatively charged solutes are more retained due to a reduction of electrostatic repulsion. Ionic strength generally improve the shape and peak width, but is detrimental to MS detection.

Concerning the organic modifier, a classification has been done depending on their elution strength as presented in Figure 12.

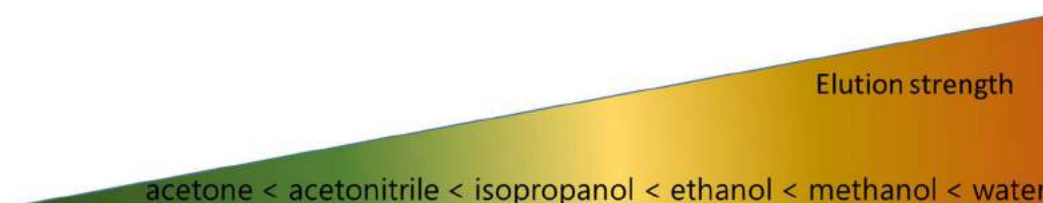


Figure 12: Elution strength evolution in HILIC-mode

ACN is largely favored as it is aprotic, and has a low cut-off compared to acetone that absorbs between 220 and 330 nm. Alcohols are protic, so they may disturb the water layer at the SP surface and decrease the hydrophilic partition. Temperature is also a parameter to consider as it influences diffusivity, viscosity, and transfer enthalpy of the solute between the two phases¹⁴⁵. However, the effect is solute-dependent, for highly polar compounds mainly separated through hydrophilic partition, the increase of temperature may lead to a decrease of retention. Another crucial parameter is the injection solvent that has to be as close as possible to the initial conditions of the MP. A minimum of 80% (v/v) of ACN is a good value, but has to be adapted depending on the solute and its solubility. For highly hydrophilic solutes, IPA, DMSO, EtOH, and in last alternative MeOH, or water can be used, mixed with ACN^{146,147}. It has also to be noticed that the injection volume has to be minimized, between 0.5 and 1.5% of the column volume to avoid losing efficiency¹⁴⁶.

In conclusion, HILIC mode allows the separation of hydrophilic and/or ionizable solutes with MS compatibility. The high organic content favors desolvation of solutes for MS detection^{148,149}, and reduces the mobile phase viscosity, decreasing the backpressure up to 3-folds. This approach is highly compatible with sub-2 μm packed columns, and/or with the use of longer columns for fast and/or high resolution analyses¹⁵⁰. HILIC mode can be seen as a complementary techniques to RPLC due to the variety of mechanisms involved that offers different selectivities.

The main drawback is the use of high content of ACN, which may suffer from high cost depending on the plastic market. Also, the mechanisms being various, HILIC mode is not as predictable as RPLC. As they are dependent of pH, ionic strength, pKa solute, and that all those parameters depends on the organic content, the results can be complicated to rationalize^{128,137}. Another aspect that has to be taken into account is the equilibration time up to 2-4 times longer than in RPLC. Also, the efficiency is generally lower than those obtained under RPLC conditions. It has to be noticed that the sample solvent and the salt concentration are critical parameters that strongly affect efficiency (peak width and peak shape)^{142,146}.

I-2-5. Mixed Mode Chromatography (MMC)

The development of this approach is linked to the need of simultaneous analysis of polar and non-polar, ionizable and neutral, and organic and inorganic compounds. Mixed-Mode Chromatography (MMC) is a powerful tool in separation of various molecules as it presents at least two modes of interactions simultaneously that could be modulated by mobile phase selection. Multiple mechanisms of interactions allow the use of one stationary phase for a wide range of applications compared to RPLC or IEC¹⁵¹. Many LC modes can be combined, like RPLC-IEC, HILIC-IEC, RPLC-HILIC, IEC-RPLC-HILIC^{152,153}. Those modes being orthogonal and complementary, they allow simultaneous separations that could not be achieved in a single mode. For example, for a sample containing apolar and ionized polar molecules, RPLC-IEC avoid using Ion Pairing Reagent (IPR) or high amount of salts, such that MS detection is possible¹⁵⁴.

In the last few years, several companies have introduced new mixed-mode columns with different stationary phases (SIELC, Dionex, Imtakt, Sepax, Agela, *etc.*). The first generation of mixed-mode columns corresponded to low coverage C18 stationary phases. Residual silanol groups that have acidic properties with pKa of 5 provide additional ionic interactions. But contaminations in silica gel (i.e. metallic impurities...) can affect the silanol acidity, leading to variability of the ionic sites. Other problems include the reproducibility of partial coverage, and the narrow range of mobile phase pH to provide the silanol ionization.

Second-generation mixed-mode columns combine one of the ion-exchange groups as a part of hydrophobic ligand attached to the surface. These columns show better reproducibility and retention control for neutral and ionic compounds¹⁵⁵. In case of dual interactions, ions opposite to the stationary phase are retained by ion-exchange interactions¹⁵⁶.

Third-generation mixed-mode columns have an increased capacity and retention control. Ionic compounds can be retained by cation and anion-exchange mechanisms, and the hydrophobic compounds by reversed-phase mechanism. The main advantage of this stationary phase configuration is an ability to retain both cations and anions at the same time with low buffer concentration in the mobile phase. Ionization state of stationary phase and ratio between cation-exchange and anion-exchange sites can be adjusted by changing the pH of the mobile phase.

Modern mixed-mode SPs offer various benefits: great flexibility, reproducibility, and loadability for separation of a wide range of compounds and often, symmetrical peak shape for basic molecules. Multiple controllable interactions on a column allow for a better control of retention for various solutes that can be separated in a single run. In mixed-mode chromatography, the same column can be used either in a single mode (cation-exchange, anion-exchange, reversed-phase), or in combination of modes. Complex interaction of mixed-mode SPs with solutes often produce superior selectivity as compared to single mode SP. The selectivity of separation can be controlled by varying the amounts of organic component, buffer pH, and buffer concentration. Buffer pH will affect both solutes and SP ionization state, because the ionic strength of the column can be modulated based on the pH of the mobile phase.

All modern mixed-mode SPs are compatible with LC/MS and preparative chromatography, and can be used to successfully develop methods in various sectors (e.g. pharmaceutical, chemical, food, and environmental industry). Method development in mixed-mode chromatography is based on understanding of individual interactions (i.e. hydrophobic, HILIC and ion exchange).

However, MMC suffers from a lower efficiency resulting from the multiple interaction types. Also, there are still few mixed-mode columns available in FPP sub-2 μm commercial columns (for UHPLC) and SPP columns (for HPLC).

Conclusion

As the SPs developed during this thesis are usable in different LC-mode (essentially RPLC, JILIC, and MMC), this part was devoted to the presentation of the main LC-modes. Depending on the physico-chemical properties of the solutes to be analyzed, the chromatographic mode have to be adapted. The chromatographic mode choice mainly depends on the polarity of the sample and its solubility in the chromatographic conditions.

The Figure 13 summarizes which LC mode has to be selected depending on the balance hydrophobicity/hydrophilicity.

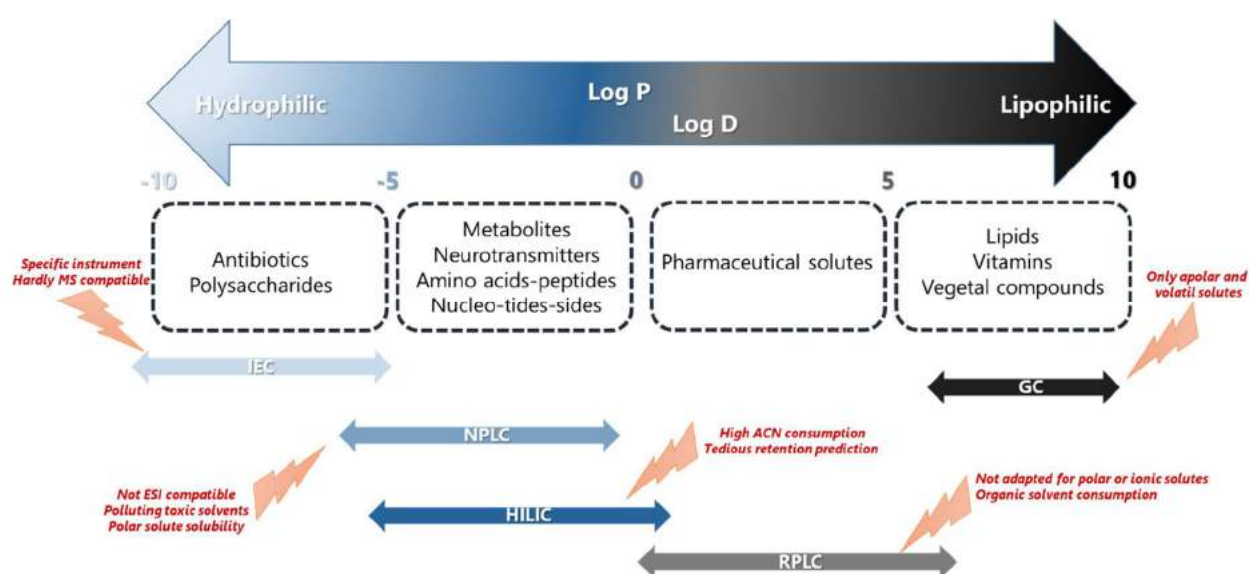


Figure 13: Representation of the chromatographic modes used depending on the log P/log D range. Here the SFC is not represented, but by modulation of the additives, a wide range of polarity can be covered.

Each mode has its own advantages and drawbacks, and some of them can be combined in order to increase orthogonality and have a diversity of interactions allowing for better resolution of complex mixtures. Such attempt is the challenge of 2D-LC using two different SP chemistries.

I-3. Stationary phase synthesis: From bare silica to functionalized silica

The solid supports that can be used for surface modification are polymers, titania, alumina, zirconia, thoria, and silica. Silica is the most widely used solid support in liquid chromatography because it is inexpensive and is commercially available in many particle sizes and in different pore sizes, which make it possible to modify at ease. Moreover, it has a very high mechanical stability and provides high efficiency.

Although silica has been one of the dominant choices as a solid support for stationary phases, numerous attempts have been made to find an alternative material to overcome some of its drawbacks. The major issues of using silica as support are the pH instability and the strong affinity of basic compounds for the silanols at the silica surface. At a pH less than 2, the stationary phase undergoes ligand cleavage, while at pH greater than 8 silica begins to dissolve. However, it is possible to operate columns at a higher pH, provided the silica support is densely bonded, extensively end-capped, or has a longer chain column packing that allows the use of organic buffers as part of the mobile phase.

The following part is dedicated to the pathways developed to functionalize the bare silica material and the different types of bonded phases that could be obtained. Also, the major issues related to the use of silica as bare material, and the way to overcome it are highlighted.

I-3-1. Silica as chromatographic support

The synthetic process for producing very pure starting silica with very controllable particle and pore sizes has enhanced chromatography immensely. Silica gel, SiO_2 , is a partially hydrated and a highly porous form of silica, which is made from the most abundant elements in the earth's crust. Since the 1970s, silica gel has been the most widely used support for RPLC.

There are two main types of silica gel referred to as Type A and B forms, and a specific Type C that corresponds to hydride silica. Type A silica gels are made by aggregating silica-sol particles. This type of silica has a low surface area ($< 200 \text{ m}^2/\text{g}$), a low porosity, and regular pore sizes. Gelling soluble silicates produce type B silica, called xerogel and silgel, or coalescing

fumed silica. This process leads to high surface area ($200 \text{ m}^2/\text{g}$), higher porosities, and irregular pore volumes. The walls of silgels have variable wall thickness leading to a less rigid surface¹⁵⁷. The silica surface has different kinds of active groups presented in Figure 14. It consists of three distinct silanol groups: free or isolated, vicinal, and geminal, along with physio-adsorbed water and siloxanes. All three types of silanols can play important roles during a chromatographic experiment and have different activity levels (Table 4). Acidic silanol groups interact with basic analytes which leads to poor resolution, and peak tailing. Metals such as Fe, Al, and Zn which are found in silica can also contribute to peak tailing and retention properties during separation. As the quantity of metal impurities is largely reduced for the Type B silica, it is nowadays the most commonly used.

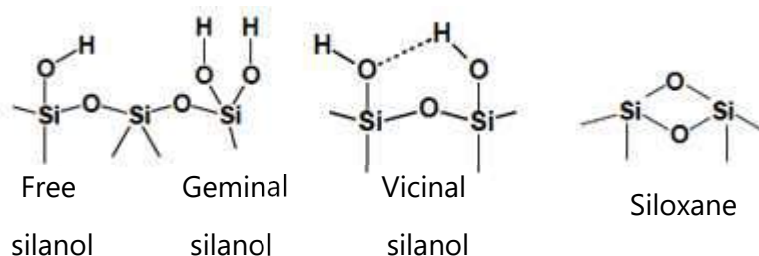


Figure 14: Active groups onto the silica surface

Surface site	Activity level
Internal metal activated	Most
Free or isolated	
Geminal	
Vicinal	
Siloxane	Least

Table 4: Activity level of the silica surface sites

Despite the physical characteristics of the bare silica material, the surface chemistry is similar and corresponds to silanol groups that can be modified through various synthetic routes presented in the following part.

I-3-2. Synthetic procedures

The nature of the starting silica is of major concern. Column-to-column reproducibility is based on the batch-to-batch reproducibility of the manufacturer's silica. Problems can lie in poor particle size, poor control of pore volume and size, and metal impurities that change the acidity of the silanols on the surface. There have been numerous studies looking at the impurity effects on the properties of the SP¹⁵⁸⁻¹⁶¹. Barrett and coworkers¹⁶⁰ showed that rehydroxylation with dilute hydrofluoric acid gives less metal contamination than hydrochloric acid or nitric acid treatments. The metals on the surface are very high energy adsorption sites for basic solutes

and metal complexation can occur. Also, the newer types of base silica have less metal contamination (Type B) and do not require specific pretreatment before grafting.

Bare silica has limited pH stability and may lead to peak tailing when analyzing basic compounds due to interactions with the silanol groups. Making modification can be advantageous in terms of pH stability, as well as peak tailing, and allows the silica to be used with aqueous solutions for a longer period of time. Silanol groups onto the silica surface react with bonding groups to form the bonded phase. Different methods have been developed to modify the silica surface and are presented in the following part.

I-3-2-1. Etherification

The reaction is achieved between a silanol and an alcohol group: $\text{Si-OH} + \text{R-OH} \rightarrow \text{Si-OR} + \text{H}_2\text{O}$

This method is simple and the bonded phase is thermally stable. The drawback of this modification is the instability of the linkage (Si-O-C) in the presence of water. Therefore it is not possible to use stationary phases based on this modification for many HPLC applications with aqueous mobile phases.

I-3-2-2. Chlorination reaction and organometallic compounds

The first step of this procedure consists in a reaction between silica and thionyl chloride to form an unstable chlorinated intermediate. In the second step the chlorinated intermediate reacts with an organometallic compound (i.e. Grignard reagent or organolithium) leading to the formation of a Si-C linkage.

The reaction can be written as: $\text{Si-OH} + \text{SOCl}_2 \rightarrow \text{Si-Cl} + \text{SO}_2 + \text{HCl}$

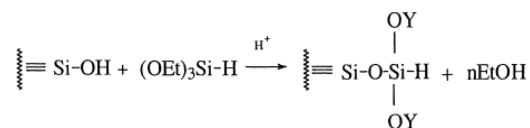
And then $\text{Si-Cl} + \text{BrMgR} \rightarrow \text{Si-R} + \text{MgClBr}$ or $\text{Si-Cl} + \text{Li-R} \rightarrow \text{Si-R} + \text{Li-Cl}$

The disadvantages of this reaction are the elimination of the metal salt byproduct. Also, the chlorinated intermediate is very unstable, hence the reaction has to be carried out in dry solvent^{162,163}, which can lead to reproducibility troubles.

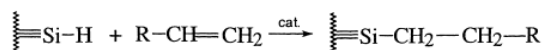
I-3-2-3. Silanization and hydrosilation

Another approach developed by Pesek *et al.*^{162,163} consisted in modifying the silica surface in two steps: first, a silanization with triethoxysilane (TEOS) and then, a hydrosilation reaction to attach an alkyl group onto the silica surface (Figure 15). The silanization reaction involves the

formation of a stable hydride monolayer in the presence of an acid catalyst. The hydride intermediate formed can be stored for longer periods of time, as it is stable in air or water without degradation. A very good yield, up to 95% surface coverage with a nonpolar Si-H monolayer has been reported¹⁶⁴.



where $n = 1-3$ and $Y = \text{H}$ or $\text{Si}(\text{OSi})_2\text{R}$ depending on the extent of crosslinking



where cat = catalyst, metal complex such as hexachloroplatinic acid or free radical initiator such as *t*-butyl peroxide

*Figure 15: Silanization followed by hydrosilation to functionalize the silica surface, based on*¹⁶⁵

The linkage grafting of the organic group at the silica hydride surface occurs in the hydrosilation step and forms the Si-C linkage. The reaction is facilitated by the presence of a transition metal complex catalyst, usually Speier's catalyst: a 2-propanol solution of hexachloroplatinic acid. However, the transition step while attaching an olefin to the silica hydride forms a complex with the catalyst. The latter being a transition metal complex catalyst, the large size of the intermediate generate steric hindrance, which might result in a lower rate of organic group on the surface. Also, the catalyst can undergo reduction by itself. The silica hydride and metal complex catalyst react together and form Pt (0) deposition on the surface, deleterious for the chromatographic performances. The use of free radical initiation instead of a transition metal complex might solve the problem, but limited studies have been done¹⁶⁶. The formation of the Si-C bond at the surface seems to be more stable than the commercially available stationary phases that are formed after an organosilation reaction. An important advantage of hydrosilation method is that the silica hydride intermediate can be used by itself as a stationary phase in reversed-phase conditions, organic normal phase conditions, and aqueous normal phase condition.

I-3-2-4. Organosilanization

Most of commercially available columns result from the silica modification by organosilanization. The reaction involves an organosilane reagent with a leaving group that can be a halide, a dimethylamino group, a methoxy, or an ethoxy group, and the silanol groups at the silica surface. The reactivity is represented in Figure 16, based on the study of Unger *et*

*al.*¹⁶⁷ The highest grafting rate they obtained was 4.1 mol/m² using an organosilane with dimethylamino as leaving group.

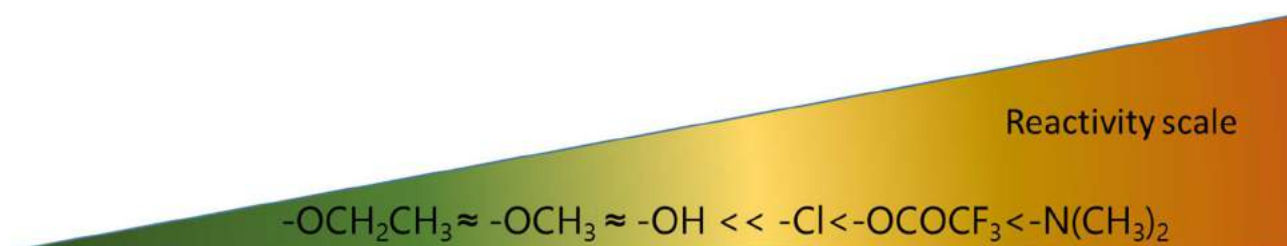


Figure 16: Scale of the silane reactivity

The organosilanization reaction can be written as: $\text{Si-OH} + \text{X-Si R'R} \rightarrow \text{Si-O-Si R'R} + \text{HX}$ with X the leaving group, R and R' the ligand groups. Due to the low cost and commercial availability, chlorosilanes are often used.

The general disadvantage of organosilanization is that an acid by-product is formed during the reaction which can hydrolyze the Si-O-Si-C bonds already formed. Monomeric organosilane stationary phases have poorer hydrolytic stability under acidic and basic conditions than those obtained through hydrosilation procedure^{163,168}, but some approaches discussed later can improve it.

The organosilane reagent is covalently bonded onto the silica surface and depending on the functionality of the reagent, monomeric or polymeric stationary phases are produced. Nevertheless, the one-step organosilanization procedure being relatively easy, reproducible, and thanks to the diversity of commercially available organosilanes, this method is actually the most used to functionalize silica.

I-3-3. Types of bonded stationary phases

Usually, three types are distinguished: the brush phase, the oligomeric phase, and the bulk phase.

They differ by the number of leaving groups, mono, di, or tri substituted¹⁶⁹.

Unfortunately, the orientation of the alkyl chains on the surface is not known as silanols can be evenly or randomly distributed at the silica surface, and inside the pores. Also, steric hindrance has to be considered when large organosilanes (e.g. octadecyldimethylsilane) have to be attached onto the silica surface. Despite those difficulties intrinsically due to the diversity of the bare silica material, some procedures have been developed and allow, on average, to obtain reproducible and efficient supports.

I-3-3-1. Monomeric phases "brush-type"

The first type of bonded phase is the brush-type phase that requires a silane reagent containing only one leaving group. The bonding can only be done through one linkage resulting from the reaction with the silanol functions onto the silica surface. This type of phase is also called monomeric phase. Since the end of 70's, some studies were done to develop such functionalization, that is still largely used today^{170,171}.

Monomeric phases using organosilane chemistry are mainly dimethyl substituted, but sterically protected monomeric SPs can be synthesized if the ligand contains hindering group. Kirkland and Henderson showed that using phases with diisobutyl and diisopropyl side chains led to lower surface coverage but better peak shapes, leading to higher column efficiency for basic drugs at pH 7¹⁷².

A major advantage of the monomeric reaction is the reproducibility and the single layer coverage¹⁷³. The amount of surface coverage or bonding density is very important to the chromatographer. The maximal surface coverage was estimated around $8 \pm 1 \mu\text{mol}/\text{m}^2$. However, only about one-half of the silanols can react due to steric hindrance of the side chains on the ligand. Commercially available columns usually have a bonding density range to 3.0 - 3.5 $\mu\text{mol}/\text{m}^2$.

Generally, five main variables can alter the reaction: the solvent, the base, the leaving group, and the reaction temperature and time. The amount of starting materials in the reaction and the amount of water onto the silica surface is also of concern for reproducible high density^{167,174}. The schematic representation of monofunctionalization using *n*-octadecyltrimethylchlorosilane presented in Figure 17.

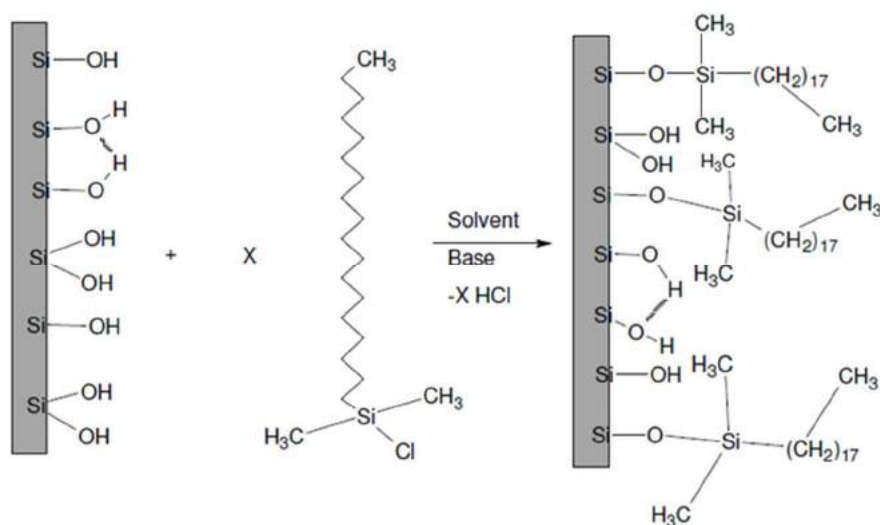


Figure 17: Schematic representation of monofunctionalization using *n*-octadecyltrimethylchlorosilane, from¹⁷⁵

Often, dipolar aprotic solvent such as dichloromethane, tetrahydrofuran, ether, acetonitrile, or *N,N*-dimethylformamide are used. Also, a base (imidazole, pyridine, 2,6-lutidine, quinuclidine, or 4-dimethylaminopyridine) is used to react with the silane and form an intermediate¹⁷⁶. Until 1988, almost all bonding reactions were done under refluxing condition. Sentell *et al.* used sonication to drive reactions at low temperatures¹⁷⁷ and observed a higher bonding. It was previously explained that reactions occurring at a liquid-solid interface are enhanced by ultrasound.

Monochlorosilanes used for monomeric phases have a relatively low reactivity. The role of the leaving group was investigated^{167,176,178-180} and the reactivity scale is represented in Figure 16.

I-3-3-2. Oligomeric-type and bulk-phase type

The second and third types of stationary phases are called the oligomeric-type phase and the bulk-phase type. The oligomeric phase uses a disubstituted silane reagent, and the bulk phase uses a trisubstituted silane one, leading to covalent bonding onto the silica surface with more than one bond possible (the case of monomeric phases)¹⁷². With these phases, vertical polymerization or horizontal polymerization can occur as presented in Figure 18.

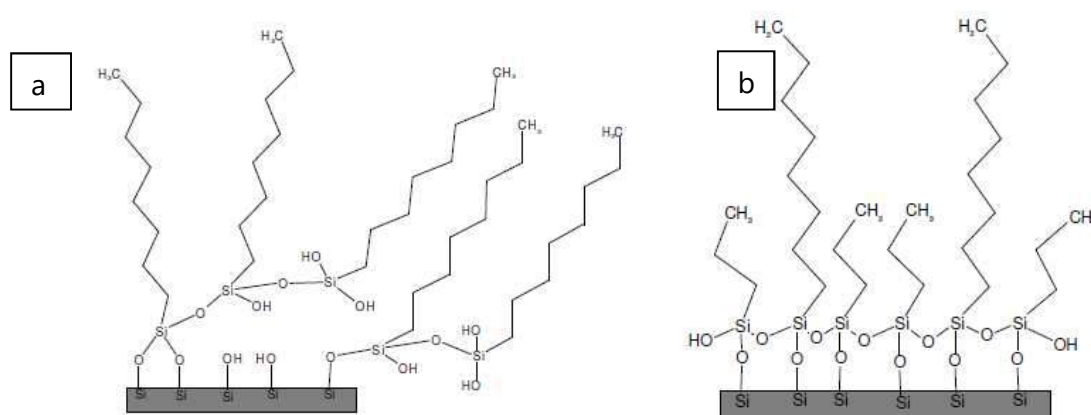


Figure 18: Representation of vertical (a) and horizontal (b) polymerization when using polysubstituted silane reagents, from¹⁷⁵

The vertical polymerized phase shows a very high carbon content, however some of the alkyl chains can be hidden from analyte interaction. There is also a problem with any unreacted functional silane groups that will be hydrolyzed in aqueous mobile phase conditions to form silanols. Moreover, these phases are more difficult to reproduce because the degree of polymerization is due to the amount of water added to the reaction medium.

The horizontal polymerized phases have a very strong connection between short and long chain silanes. In Figure 18b, the short chain is a C3, and the long chain silane is a C8. The main advantage of this type of phase is its ability to support extreme pH¹⁸¹.

For oligomeric phases it is necessary to stop the reaction at the last step by capping, to avoid deleterious effects due to reactive final functions of the oligomer. Also, for the bulk-type bonded phase, water is required onto the surface to allow for the polymerization. Also, it was noticed that polymerized phases have poor peak shape and poor mass transfer compare to monomeric ones¹⁷³. The use of organosilanes with two or three reactive groups results in bonding to the surface and crosslinking among adjacent bonded moieties, which enhance the stability, but is less reproducible than monomeric stationary phases.

I-3-3-3. Monomeric phase: chlorination and organometallic methylation ligand

Finally, another type of SP of interest is that obtained through first chlorination onto the silica surface, followed by attachment of an organometallic methylating agent. The major advantage of such strategy is that the direct Si-C linkage is very strong. Moreover, due to the bulky size of the alkyldimethylsilane used for monomeric phase synthesis, the coverage of the silica surface is incomplete. By chlorinating the surface, prior to covalently bound the methylating agents in a second step, avoid side group steric constraints. With this strategy, Deuel *et al.* obtained 5.3 $\mu\text{mol}/\text{m}^2$ of chlorines to the surface of Aerosil, approaching the maximum silanol concentration of it¹⁸². Almost complete coverage was obtained on porous silica (i.e. 7 $\mu\text{mol}/\text{m}^2$ of chlorine) by Unger and coworkers¹⁸³. It has to be noticed that Aerosil has a much lower silanol concentration than porous silica. There are numerous reagents that can be used to chlorinate the silica surface such as S_2Cl_2 , Cl_2CO , CCl_4 , CH_3COCl , and SOCl_2 ¹⁸⁴.

Finally, due to the ease of preparation and reproducibility, monomeric phases are the most commonly used. Very good coverage could be obtained with by prior chlorination and organometallic coupling, but due to the disadvantages explained in part I.3.2.2, organosilanization is the method of choice. Commercially available column syntheses are proprietary and are not disclosed. Therefore, exact surface chemistry of commercial stationary phases is difficult to obtain.

I-3-4. Dealing with residual silanols

As discussed previously, the main stationary phases used are monomeric and synthesized by organosilanization, meaning that the silica surface has been derivatized with monofunctional silanes. However, this reaction is incomplete due to the spatial requirements or steric hindrance of the silanes. Consequently, the silica surface still contains silanol groups (called residual silanols) that are usually weakly acidic. They are responsible for peak tailing of basic solutes that reduces resolution and column efficiency; and in the worst case, can lead to irreversible adsorption¹⁸⁵.

The density of coverage is important to limit or suppress the silanol activity¹⁸⁵. However, even with densely covered silicas, the residual silanols still play an important role in retention^{186,187}. Different strategies can be proposed to eliminate silanol interactions: higher bonding densities, ligand chemistry, silica pretreatment, silica post-treatment (i.e. end-capping), or adjusting the mobile phase pH or modifiers.

I-3-4-1. Silica pretreatment

It is possible to reduce silanol amount by dehydroxylation of the native silica. The silanols are not only on the surface but also exist throughout the entire porous particle. Many researchers have determined the concentration of silanols onto the silica surface using a variety of techniques that will be highlighted here: chemical methods, physical methods and theoretical calculations.

Dehydroxylation have been used in the past, followed by rehydroxylation of the silica surface to homogenize it. It was believed that if silica was heated above 400°C only partial rehydroxylation can occur¹⁸⁸ and can be fully rehydroxylated if treated with water, and if the water is heated, the process is expedited¹⁸⁹. It was observed that a silica dehydroxylated at 900°C can be rehydroxylated by treatment in boiling water for 60 hours. Also, Kohler *et al.*¹⁹⁰ obtained a much more homogeneous and chemically stable phase by pretreating the Zorbax PSM-60 at 650°C before derivatization with trimethylsilyl enolate¹⁹¹. Then, Boudreau and Cooper studied more deeply the dehydroxylation at different pretreatment temperatures¹⁹¹. They noticed that the 400°C thermally treated surface was more homogeneous and contained fewer residual silanols than the silica treated at 180°C. It was also noted that increasing the

temperature of pretreatment (above 840°C) decreases the specific surface area, until shrinkage and sintering of the silica matrix, making it difficult to pack homogeneously.

There are two other major dehydroxylation techniques besides thermal dehydroxylation. The ultraviolet radiation can be compared to thermal treatment at 1000°C with the major advantage of being specific to eliminate silanols¹⁹².

The other technique to effectively dehydroxylate the silica surface is plasmachemical dehydroxylation at room temperature¹⁹³, which is fast and consume lower energy.

I-3-4-2. Silica post-treatment

Applying a treatment on the derivatized silica is called end-capping and refers to the bonding of a small silane reagent to a derivatized silica¹⁹⁴. This secondary derivatization reaction is used to shield and reduce silanol groups on a modified silica surface^{163,173,195}. Indeed, the organosilane reagent reacts with approximately 50% of the available silanols and the remaining groups can interact with the solutes. These strongly adsorption sites on the surface of silica are the targets of the end-capping¹⁹⁶, which aim is to convert Si-OH groups to Si-O-Si-C groups. The residual silanols can be not accessible for the long alkyl chain silanes but still accessible by a short chain silane such as the trimethylsilyl group¹⁵⁹. A representation of an end-capped C8 phase is shown in Figure 19.

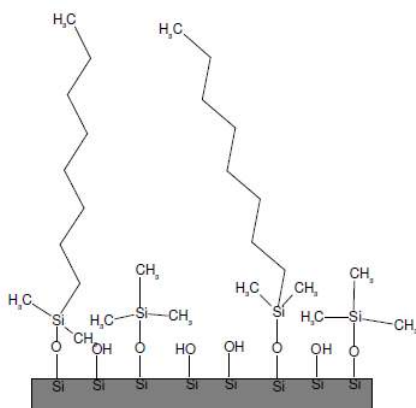


Figure 19: Representation of an end-capped C8 stationary phase, from ¹⁷⁵ It has to be specified that the arrangement of the end-capping and the C8 groups is not known.

End-capping can be done using polar reagents with an amide group or an alcohol group, or using nonpolar reagents with a methyl group depending on the type of separation that needs to be achieved. The two main end-capping reagents are trimethylchlorosilane and hexamethyldisilazane¹⁹⁷. Some authors investigated the efficiency of other end-capping reagents such as trimethylimidazole¹⁹⁸, trimethylsilylphosphine¹⁹⁹, *N,O*-

bis(trimethylsilyl)acetamide^{200,201}, and hexamethylcyclotrisiloxane²⁰². Pesek and coworkers studied the use of a silica hydride intermediate for end-capping^{196,203}. As shown in part I.3.2.4, the reactivity depends on the leaving group, so *N,N*-dimethyltrimethylsilylamine was selected as end-capping ligand during this thesis work.

However, it was pointed out that the total residual silanol concentration can be reduced but not eliminated¹⁵⁹ by such strategy.

I-3-4-3. Mobile phase additives

Other ways to mask the residual silanols onto the silica surface is to use mobile phase modifiers²⁰⁴ or to change the pH acidic mobile phases²⁰⁵. However, mobile phases at the pH extremes is not possible due to stability of the silica matrix and of the grafting^{107,205,206}. At the intermediate pHs (pH 3-8), large percentage of the silica surface is ionized so the protonated bases yield high silanol-base ionic interactions²⁰⁷. To overcome this problem, mobile phase additives (i.e. masking agents) can be used such as quaternary ammonium salts with a long alkyl chain¹⁰⁷. As quaternary ammonium are aggressive towards silica-based stationary phases²⁰⁸, tertiary amines such as trimethylamine or long hydrocarbon amines like hexylamine and *N,N* dimethyloctylamine can be employed to suppress silanol activity at low and neutral pHs²⁰⁹. However, under certain conditions, poor efficiency and high peak asymmetry²¹⁰ were noticed, and those masking agents can be very difficult to remove from the column when switching to other mobile phases²¹¹. The use of cyclohexylamine was reported as efficient masking agent²¹² that presented reduced UV-background compare to triethylamine and did not require purification before use. Also, different alkaline earth metal cations including calcium, magnesium, and barium²¹³ seemed also of interest to act as chelating agents of silanols.

The use of modifiers for the masking of silanols has been shown to be successful in many cases, but it still has many problems that must be overcome. First, the background is higher, especially at low wavelength detection. Then, re-equilibration time is significantly higher, and washing column also needs time. Finally, it is not suitable with LC-MS detection and if the fractions have to be collected, the removal can be challenging²⁰².

I-3-4-4. Stability under extreme pHs

The second major problem with silica stationary phases is the pH stability of silica. Operating above pH 8 for reversed-phase separations on silica stationary phases can lead to early degradation of the column because of dissolution of the silica^{214,215}. It was shown that using densely bonded dimethyl-C18 ligands was preferable to the bulky diisopropyl- and diisobutyl-C18 ligands¹⁸¹. Other interesting SPs have been developed such as polar embedded SPs or hybrid silicas covered by a polymer.

At low pH, the problem comes from the ligand cleavage, which lead to column degradation due to progressive removal of the graft (e.g. TMS end-capping group, C8, C18...). Another interesting feature is that there is no significant influence of the column degradation whether a monomeric or polymeric stationary phase is used, but the type of base silica played an important role in the rate of dissolution. One of the most interesting conclusions was that Type A silica always had better stability towards pH than Type B silica.

Then, the effect of the type of buffer was studied^{216,217} and it was concluded that at pH 7 - 10, carbonate and phosphate buffers alter columns faster than organic (i.e. glycine and TRIS) and borane buffers. Also, the temperature is a factor that decrease the column life.

Kirkland *et al.* studied effects of pH 7 and 11 on end-capped silica based columns¹⁵⁷. The use of mobile phases at pH 11 with organic buffers, such as pyrrolidine, is feasible with certain silica based columns at temperatures below 40°C.

Using untreated silica pre-columns has to be considered as a good solution to greatly extend the lifetime of a column²¹⁸.

Conclusion

Silica remains the mainstay of SP because of its unique properties, including its high surface area, high-mechanical stability and controllable pore structure. Different synthetic strategies have been proposed to functionalize the silica surface as presented previously (etherification, chlorination, hydrosilation, organosilanization). Among them, the most employed is organosilanization with monofunctional reagents to avoid the polymerization or the formation of a complex architecture when using polyfunctional reagents. Because the ligands (e.g. C8, C18), generate steric hindrance, the functionalization is not complete and some silanols are still accessible. Many strategies were developed to hinder the silanol accessibility either by treating directly the silica surface before or after attachment of the ligand, or by adding additives in the mobile phase, or by adjusting the ligand structure. In this work, thermal pretreatment was further considered and led to modification of the silanol rate and nature. Depending on the type of silanols, their reaction with an organosilane is different and led to more or less homogeneous grafted silicas depending on the nature and number of those silanols. Such study is presented in II.2.1. The Figure 20 based on²¹⁹ summarizes the important parameters that have to be considered when functionalizing the silica surface.

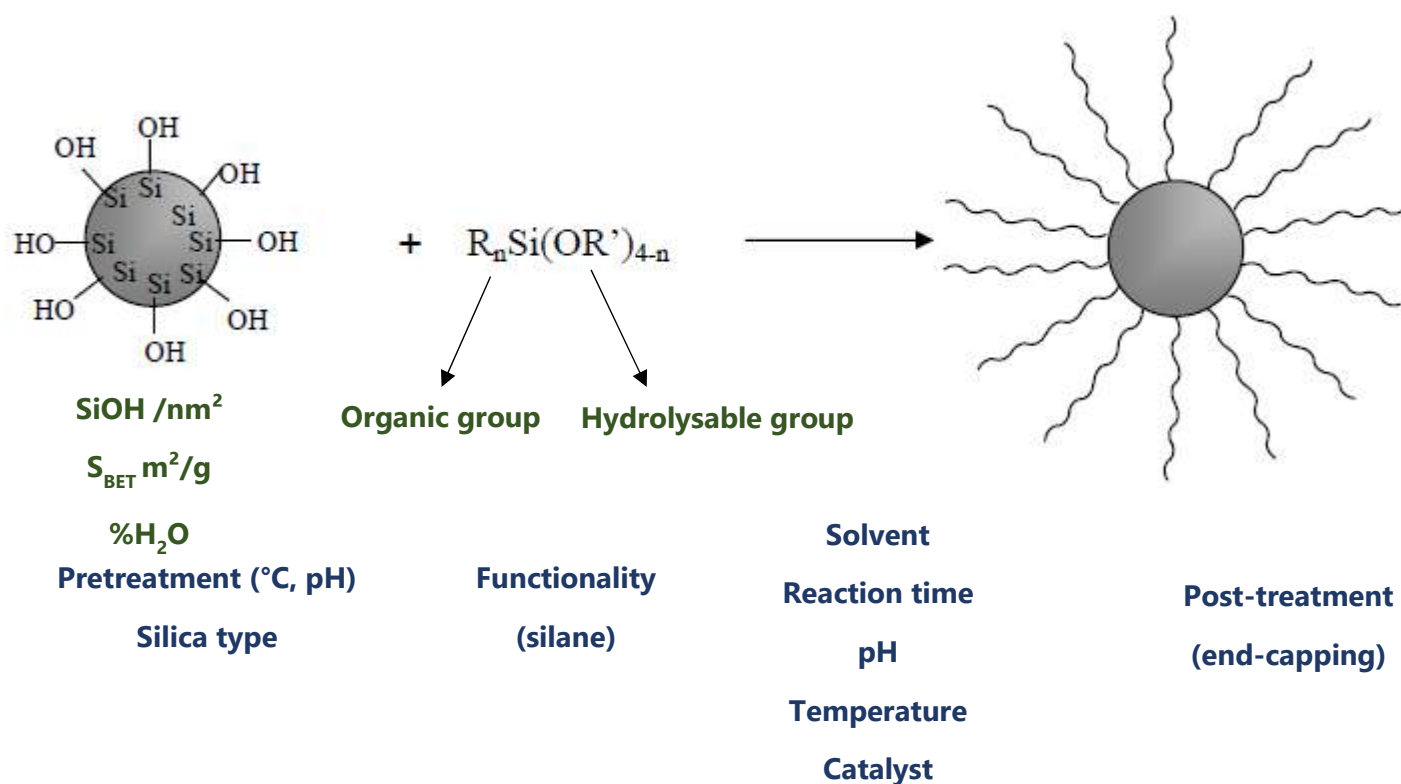


Figure 20: Important parameters for silica functionalization by organosilanization

I-4. Silica characterization

Many techniques are available to characterize both bare silica and modified silica. It encompasses physical and chemical characterization through various and complementary techniques. Some allow for the qualitative determination of the species at the silica surface, other quantitative approaches allow for obtaining the amount of those species.

I-4-1. Morphological structure

I-4-1-1. Scanning Electron Microscopy (SEM)

Scanning Electron Microscopy (SEM) is a reliable technique to have a view of the silica surface and estimate the homogeneity of the sample. This microscope produces images thanks to a focused beam of electrons, which interact with atoms in the sample giving access to the sample's surface topography. The presence of aggregates (Figure 21a) or damaged (Figure 21b) particles can be detected, which is of primary concern for packing homogeneity of the resulting column and to avoid frits clogging. The silica bed being the most homogeneous and stable with particles such as those presented in Figure 21c.

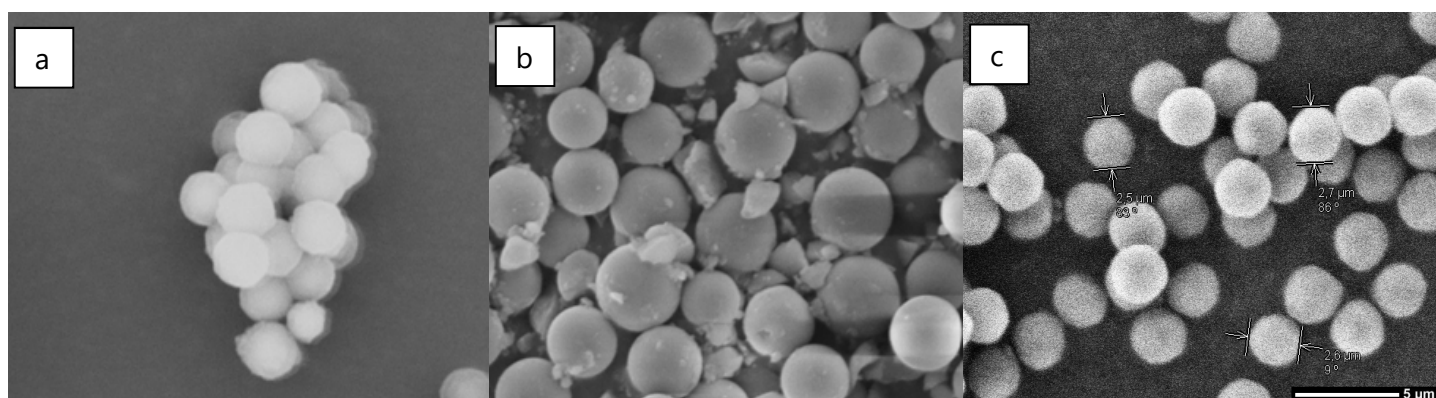


Figure 21: SEM pictures of (a) aggregates, (b) damaged particles, (c) homogeneous and entire particles. The same scale applies for all pictures.

I-4-1-2. Specific surface area

The specific surface area is determined by physical adsorption of a gas on the surface of the solid and by calculating the amount of gas adsorbate corresponding to a monomolecular layer on the surface. Physical adsorption results from van der Waals forces between the adsorbate gas molecules and the adsorbent surface area of silica. Usually, the Brunauer, Emmett, Teller

theory (BET) is used with nitrogen as gas²²⁰, and the values correspond to bare silicas and not grafted ones. The internal surface of silica is irregular and disordered, providing good adsorption properties. The higher the specific surface area, the higher the retention of a solute. Using a support of high specific surface area can allow for decreasing the column length while maintaining the column capacity, or improving the resolution. But the higher the specific surface area, the lower the pore diameters that can lead to size exclusion of some molecules. Also, it was shown that the number of free silanols per surface unit decreases when the specific surface area increases^{221,222}. As the number of OH per nm² is constant and close to 4.6, it signifies that the proportion of linked OH sites is higher, and those silanols are less active²²³.

I.4.1.3 Particle size distribution

Measurement of the particle size and particle size distribution is an extremely important tool for research and development, as the quality of the final stationary phase also depends on the quality of the bare silica material. Indeed, damaged particles and large range of sizes can lead to frits clogging, and decrease the column efficiency due to the inhomogeneity of the silica bed. Such silica is called polydisperse, meaning that the particles in a particular batch vary in size. To adequately characterize it, the simple determination of a particle size by SEM is not sufficient. We must instead determine the system's particle size distribution, which is the purpose of such technique.

Moreover, as the silica particles are spherical, the theory allowing to obtain the Gaussian distribution from the raw data is very well adapted. As can be seen in Figure 22a, the Gaussian distribution is typical for a monodisperse sample, with a narrow peak centered on the average particle size previously determined by SEM (2.6 μm , Figure 21c).

On the contrary, the Figure 22b represents the Gaussian distribution of a polydisperse silica batch, which presents a large proportion of silica particles at the average value, but the peak is broader and presents some seconds population at the lower (0.4 μm) and higher particle sizes (30 μm).

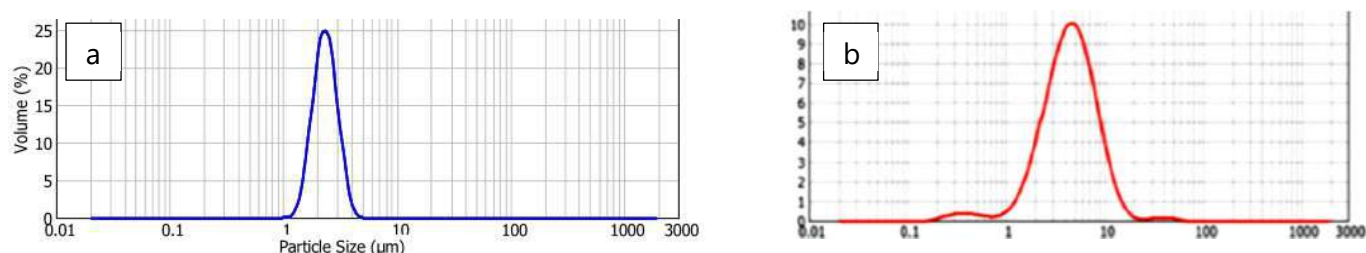


Figure 22: Gaussian distribution of homogeneous silica particles (a) and large size range silica particles (b)

I-4-2. Ligand grafting analysis

I-4-2-1. Elemental analysis

The carbon elemental analysis allows for the quantitative characterization of monofunctional grafting, as only the grafted species contain carbon. The grafting rate (Γ) can be expressed as followed (Equation 25).

$$\Gamma = \frac{10^6 \times p_c}{[10^2 \times M_c \times n_c - p_c \times (M_w - 1)] \times S_{\text{BET}}} \quad \text{Equation 27}$$

With p_c the carbon percentage by weight of the bonded material, M_c the atomic weight of carbon, M_w the molecular weight of the grafted molecule, n_c is the total number of carbon atoms of the bonded organic group and S_{BET} the specific surface area. It is also possible to obtain the grafting rate from the sulfur and/or nitrogen percentage.

However, it is required that no species containing carbon (included the silane reagent and solvents) are adsorbed onto the silica surface to avoid overestimation. It demonstrates the interest of coupling this technique with others to be sure that those requirements are fulfilled.

I-4-2-2. Thermogravimetric Analysis (TGA)

Thermogravimetric Analysis (TGA) is also a good technique to determine the silica surface groups. It was shown that the number of silanols onto the silica surface could be estimated by the mass loss during a heating at 5°C/min until 1250°C²²⁴. The main difficulty lies in the differentiation of dehydration phenomenon (from physically adsorbed water onto the silica surface) and dehydroxylation (from silanol species). It is generally considered that upon 200°C, the mass loss is due to the removal of physio-sorbed water, but it can vary depending on the heating rate used²²⁴.

After silica functionalization, the mass loss measured in TGA allows the calculation of the grafted silane percentage defined in Equation 26.

$$\tau = \frac{100 \times (w_i - w_f)}{w_f} \quad \text{Equation 28}$$

With τ the grafted silane percentage, w_i and w_f the initial and final mass of silica, respectively.

Caution must be taken for the interpretation of the dehydroxylation of the silanols formed after removal of the organic chains. Also, the calculation details are not often furnished, which makes

comparisons difficult. Also, it does not give structural indications of the grafting, which is the purpose of the next spectroscopic methods.

I-4-3. Spectroscopic methods

In order to characterize the silica surface and to follow the grafting, two spectroscopic approaches have been widely used: Infrared spectroscopy (IR) and Nuclear Resonance Magnetic spectroscopy (NMR). Concerning the silanols, those two techniques are complementary as IR²²⁵⁻²³⁰ allows for the determination of free and geminal silanols, and NMR allows to differentiate the geminal silanols but also the free and vicinal ones²³¹⁻²³⁴. Also, they give indications of the nature and structure of the ligand at the silica surface.

I-4-3-1. Infrared spectroscopy

Infrared spectroscopy has been widely used to characterize the bare silica surface (adsorption study^{235,236}, influence of thermal treatment and rehydroxylation²³⁷⁻²³⁹, or study of the modified surface²⁴⁰⁻²⁴⁵).

The region 3660-3750 cm⁻¹ concerns the vibrational stretching bands of silanols. Depending on the silanol type and its environment, the vibration band are different. Below 1200 cm⁻¹, the siloxane bridge vibration bands can be distinguished. The near-IR region²³⁰ has not been done in this study, but is also of interest as it allows for the differentiation of free and vicinal silanols. The main vibrational bands of silanols^{225,226} and siloxane bridges²²⁷⁻²²⁹ are summarized in Table 5. In the 3690-3750 cm⁻¹ region, the interpretation can be difficult, especially if water is adsorbed onto the silica surface, which leads to superimposition to the bands of interest.

Silanol	Geminal	Free	Vicinal	Siloxane
IR	$\sigma_{\text{OH}} \approx 3740 \text{ cm}^{-1}$	$\sigma_{\text{OH}} \approx 3747 \text{ cm}^{-1}$	$\sigma_{\text{OH}} \approx 3500 \text{ cm}^{-1}$	$\delta_{\text{SiO}} \approx 470 \text{ cm}^{-1}$ $\sigma_{\text{SiO}} \approx 810 \text{ cm}^{-1}$ $\sigma_{\text{SiO}} \approx 1110 \text{ cm}^{-1}$ $\sigma_{\text{SiO}} \approx 1050-1085 \text{ cm}^{-1}$ $\sigma_{\text{SiOSi}} \approx 1870 \text{ cm}^{-1}$
NMR ²⁹ Si	Q ² ≈ -90 ppm	Q ³ ≈ -100 ppm	Q ³ ≈ -100 ppm	Q ⁴ ≈ -110 ppm

Table 5: Main vibrational bands and chemical shifts of silanols and siloxane bridges

When silica is derivatized, some other vibrational bands appeared. A review is focused on the comparison by IR, for different modification procedures, of the species onto the silica surface (Si-OR, Si-O-Si(CH₃)₃, Si-R)²⁴⁶.

It can be noticed that IR allows for differentiating the geminal and free silanols from the vicinal silanols that have almost the same chemical shift in NMR. Nevertheless, those results gave preliminary insights but are not sufficient to describe accurately the silica surface because the differentiation of free and geminal silanols is not gained, as well as the difficult differentiation of "internal" silanols (i.e. those that cannot be exchanged into SiOD in presence of deuterium in NMR) and "external" silanols.

IR spectroscopy is a good tool to characterize silica, but is often used in combination with other techniques as it does not furnish direct quantitative results. Many researchers have studied silica surfaces and stationary phases using both IR and NMR^{245,247,248}, this second technique is presented on the following part.

I-4-3-2. Nuclear Magnetic Resonance

Some interactions (dipolar-quadrupolar interactions) that are averaged at the liquid state due to brownian movement, are not at the solid state, leading to broader signals. By rotation of the sample at a specific angle (54.7°), it is possible to average those interactions and obtain narrower signals. Also, using cross-polarization allow the amplification of the signal of scarce spin such as ²⁹Si. Consequently, Cross Polarization at the Magic Angle Spinning (CP/MAS) has proved to be a good tool to characterize the silica species.

Different species can be distinguished by NMR: Q², Q³ and Q⁴ presented in Table 5 and in Figure 23. After derivatization, for example in the case of the grafting of trimethylsilane units, an additional band is noticed at around 14 ppm^{190,233,234,236,238,249-251}.

Q² are converted into Q³ (or Q⁴) and M, Q³ are converted into Q⁴ and M. The grafting rate can be defined as the ratio between the number of modified sites over the total number of sites (Equation 27)

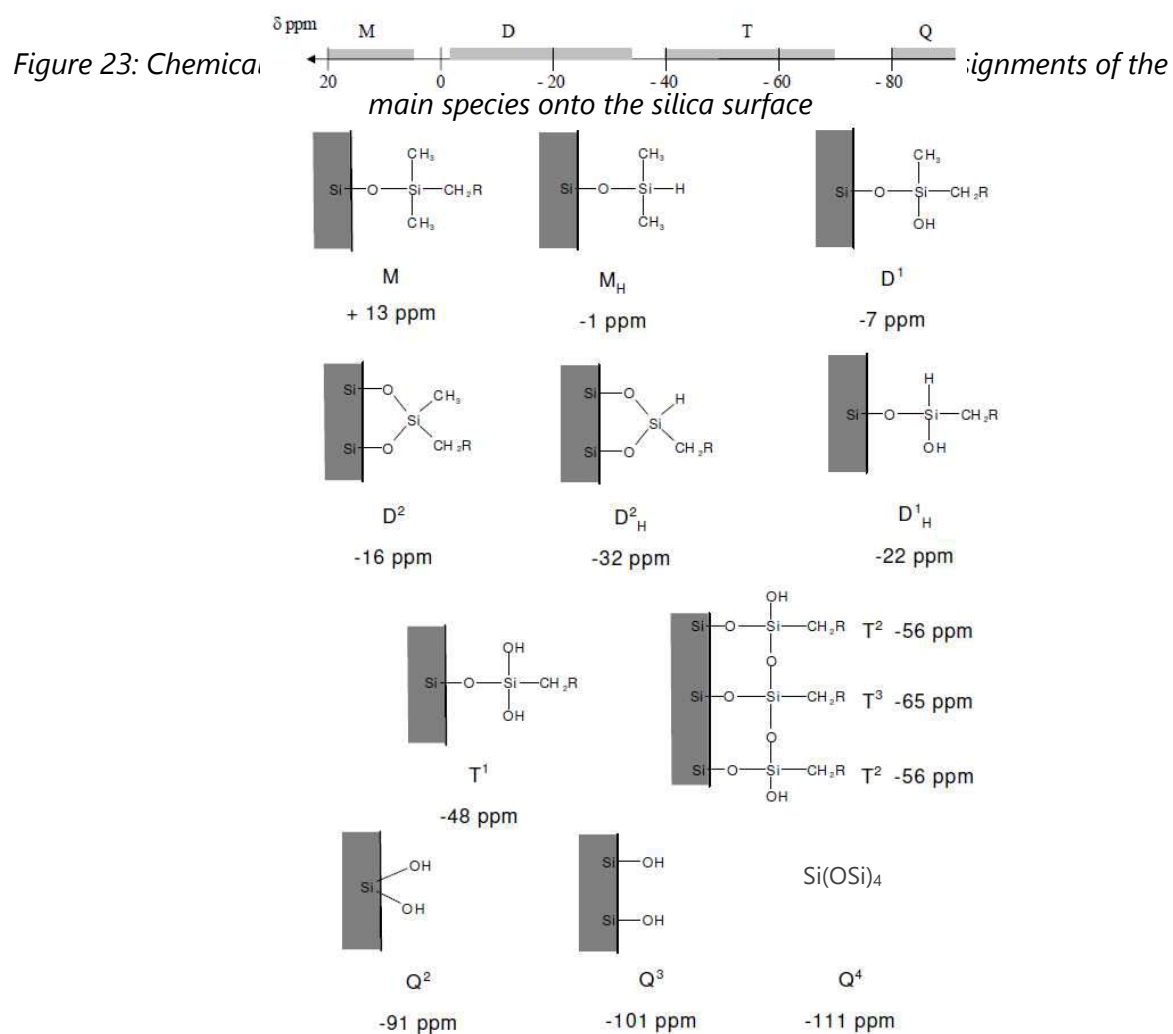
$$\tau = \frac{I_M}{I_M + I_{Q^2} + I_{Q^3}} \quad \text{Equation 29}$$

with I_M, I_{Q²}, I_{Q³} the integrations of the species M, Q², Q³

This determination is semi-quantitative as it only gives the proportion of grafted groups over the total number of silanols, which is a relative value instead of an absolute value. To obtain such amount, it is necessary to multiply the relative value by the total number of silanols.

Moreover, to have quantitative NMR measures, it is necessary to take into account only the species onto the silica surface (and not the silica volume), and so use contact time appropriated^{233,252}.

When the silica surface is functionalized with polyfunctional organosilanes, different structures can be observed: M^n , D^n , or T^n respectively for a reagent mono- $R_3Si(OR')$, di- $R_2Si(OR')_2$ or tri-functional $RSi(OR')_3$ (n being the number of bridging oxygens linked to the central atom). The chemical shifts of such species are represented in Figure 23.



Conclusion

The combination of the methods presented above and used during this work allows for a full characterization of the bare, as well as the modified silica materials (Figure 24).

The silica modification and the surface coverage can be characterized quantitatively and qualitatively. The structure of the modified silicas and the species at the surface can be elucidated by various chemical, spectroscopic and physical techniques.

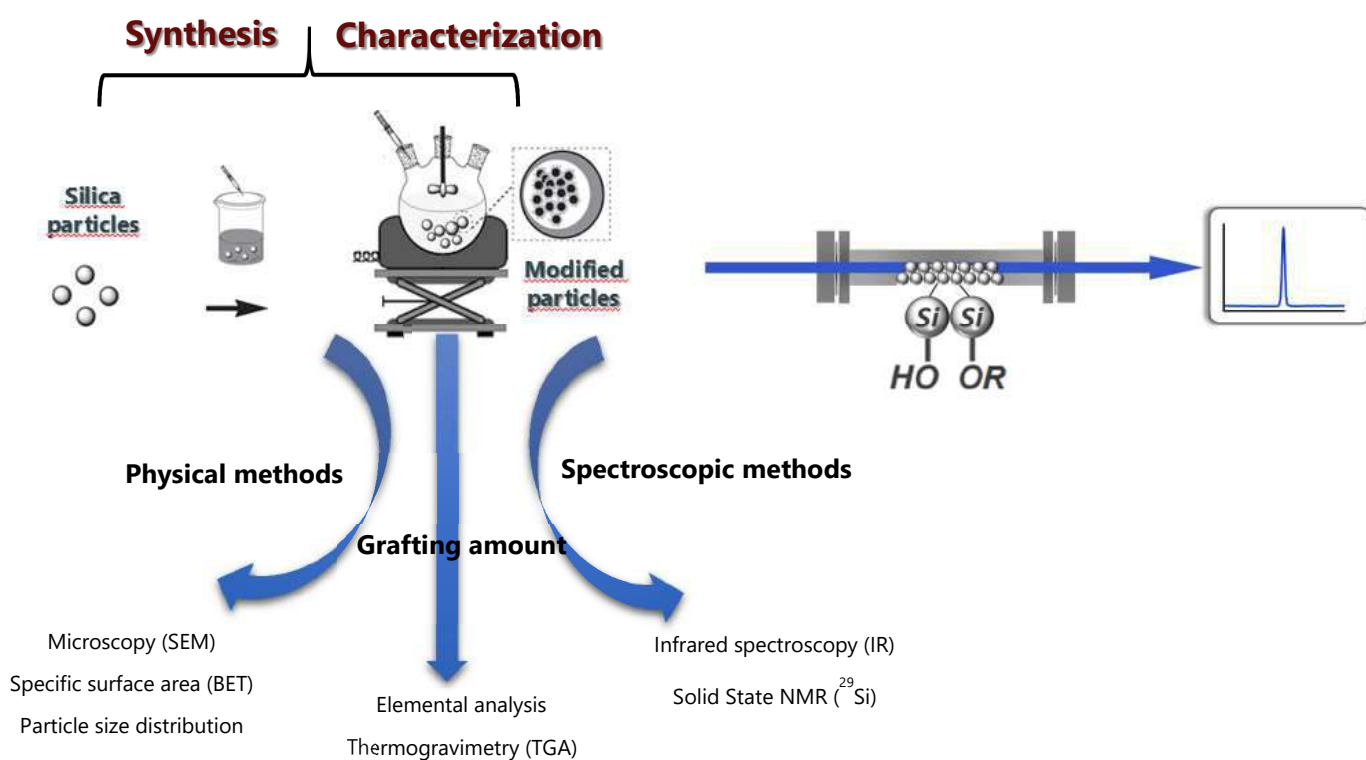


Figure 24: General summary of the techniques available to characterize the bare and the modified silica particles

I-5. Molecular modeling by Functional Density Theory (DFT)

Different methods exist to compute the energy of a structure, allowing for an increase accuracy of the description of the system, but also a higher calculation time. First, force-fields/molecular mechanics correspond to the “ball-and-spring” approach can be employed and give rapidly some insights on the system. Nevertheless, it neglects the electronic structure and is not convenient for accurate description of the intermolecular interactions for example. Then, semi-empirical molecular orbital methods allow for better description by using quantum methods with an approximate/parameterized Hamiltonian. Finally, *ab initio* methods are the most accurate, and consist in a fully quantum mechanical treatment of the electronic wavefunction. For instance, Density Functional Theory (DFT) method takes into account the electronic structure.

DFT is presently the most successful approach to compute the electronic structure of matter. It is especially adapted to chemistry as a predictive method for many molecular properties (e.g. molecular structures, vibrational frequencies, electric and magnetic properties, reaction paths, etc.) In the last years, there have been a growing interest of theoretical conformational calculations or molecular dynamic simulations, sometimes in combination with experimental studies. DFT and its implementation are arguably the most significant developments in the field in the last 40 years. A brief history of DFT is presented here in Figure 25.

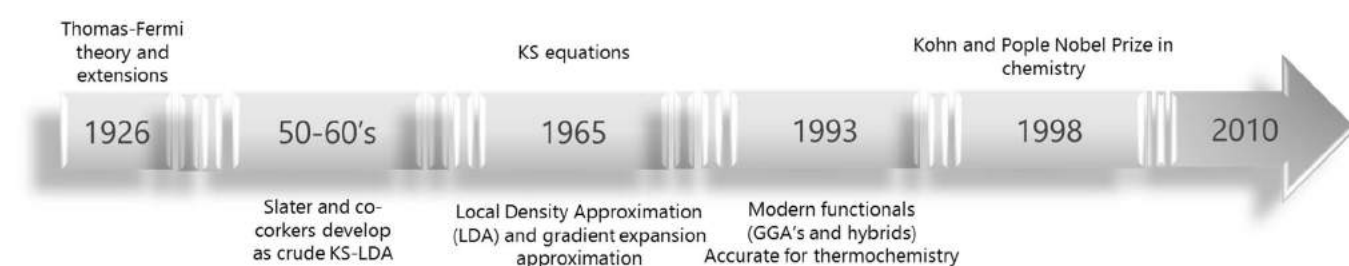


Figure 25: History of DFT developments

I-5-1. Principle

The ultimate goal in quantum chemistry is to solve the time-independent, non-relativistic Schrödinger equation (Equation 28):

$$H\Psi_n = E\Psi_n \quad \text{Equation 30}$$

With H the Hamiltonian operator corresponding to the total energy and Ψ a set of solutions of the Hamiltonian. Methods differ in how H and Ψ are described.

The quantum mechanical wavefunction contains, in principle, all the information about a given system. For the hydrogen atom we can solve the Schrödinger equation exactly in order to get the wavefunction. The big deal is how to solve such equation for many particles (electrons + nuclei) interacting together. This is the many-body problem (N-component system), and some fundamental approximations have to be made. DFT can be defined as method of obtaining an approximate solution to the Schrödinger equation for systems larger than the hydrogen atom.

I-5-1-1. Born-Oppenheimer separation

The aim is to reduce as far as possible the number of degrees of freedom of the system. It refers to the adiabatic approximation, the nuclei can be frozen in their equilibrium positions. Then, the Hamiltonian only contains terms referring to electrons.

In DFT the functional is the electron density which is a function of space and time. Contrary to the Hartree-Fock theory that deals with the N-component wavefunction, DFT uses the electron density as the fundamental property.

Whereas the N-component electronic wavefunction is a function of $3N$ variables (the coordinates of all N atoms in the system independently from the spin), the electron density is only a function of three variables (x, y, z), which speeds up the calculation.

Especially, Hohenberg and Kohn²⁵³ stated a theorem telling that the density of any system determines all ground-state properties of the system. In this case the total ground state energy of a many-electron system is a functional of the density. Knowing the electron density functional, gives access to the total energy of the system, which means that the basic variable is no more the many-body wavefunction $\Psi(\{r\})$ but the electron density $\rho(r)$. The original proof is valid for local, spin-independent external potential, non-degenerate ground state, but there exist extensions to degenerate ground states, spin-dependent, magnetic systems, *etc.*

I-5-1-2. Kohn-Sham method

Now the need is to compute these functionals with the Kohn-Sham method²⁵⁴, in atomic units (Equation 29).

$$\varepsilon_i \varphi_i(\vec{r}) = -\frac{1}{2} \nabla^2 \varphi_i(\vec{r}) + v_{\text{eff}}(\vec{r}) \varphi_i(\vec{r}) \quad \text{Equation 31}$$

Instead of the many-body system of interacting electrons, we define a set of 'KS-orbitals' (φ_i) of fictitious, non-interacting electrons moving in an effective potential (v_{eff}). Then the orbitals satisfying the KS equations give the same density as the interacting system. All the electron-electron interactions are included in the exchange-correlation potential.

It has to be noticed that effective potential depends on the density, which depends on the potential. The use of Self-Consistent Field (SCF) approach (KS-DFT Algorithm) represented in Figure 26 allows for solving it.

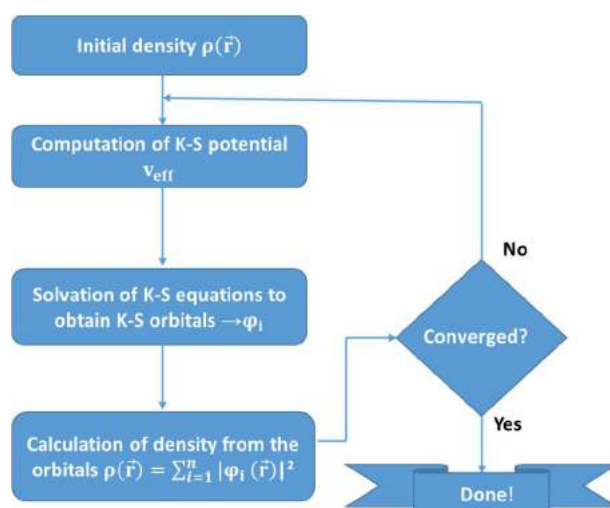


Figure 26: Schematic representation of the SCF used to solve the KS equations

I-5-1-3. DFT in practice

In DFT, electrons are delocalized. The distribution has to be characterized and that is the purpose of the electron density (ρ) defined in Equation 30.

$$\rho(\vec{r}) = \sum_i \Psi_i(\vec{r})^2 \quad \text{Equation 32}$$

The knowledge of the density is all that is necessary for a complete determination of all molecular properties. The quality of the description of the system is dependent on the method

selected (i.e. the functional and basis set). Within the framework of this thesis, this part was in collaboration with a quantum chemist specialized in DFT, Dr. Vincent Tognetti (COBRA, Université de Rouen) for the right selection of the method.

The functional describes the total energy of the system. The lower level of theory takes only into account local density (LDA) while the higher level of theory also consider explicit dependence of unoccupied orbitals. Different functionals have been developed for each level of theory, and have to be used adequately regarding the compromise calculation time-accuracy of description-system to be studied. The Figure 27 presents the Jacob and Perdew scale, with some functionals and examples for each type.

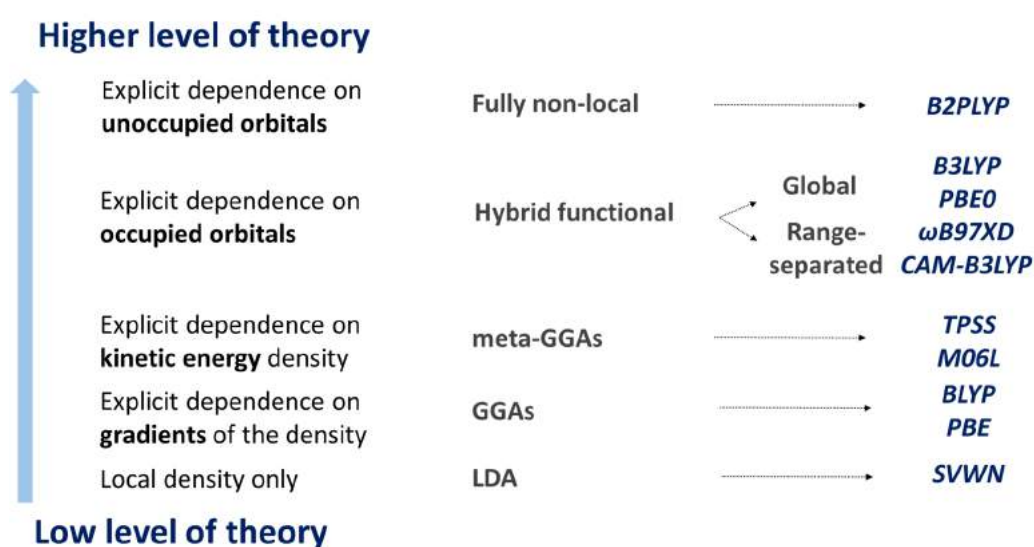


Figure 27: Description of some functionals developed, according to the level of theory

The basis describes the molecular orbitals, the following description ranges the basis from the lower to the higher electronic description (Figure 28).

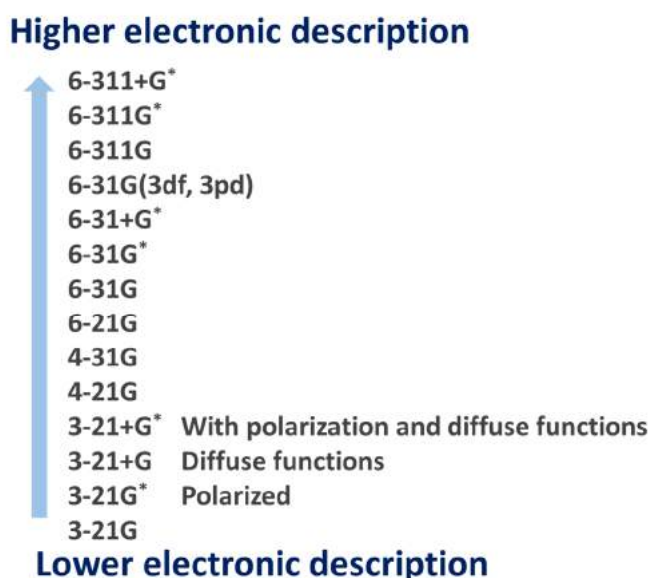


Figure 28: Description of some basis depending on the electronic description

I-5-2. Own N-layered Integrated molecular Orbital and molecular Mechanics (ONIOM) method

IMOMM is a “subtractive” or “extrapolative” method: the total energy of the whole (“real”) system is evaluated as the MO (or QM) energy of the model system ($E_{\text{QM, model}}$) plus the MM energy of the real system ($E_{\text{MM, real}}$), and minus the MM energy of the model system ($E_{\text{MM, model}}$). The subtractive operation removes the “double-counted” MM contributions (Equation 31).

$$E_{\text{IMOMM}} = E_{\text{ONIOM2(QM:MM)}} = E_{\text{QM, model}} + E_{\text{MM, real}} - E_{\text{MM, model}} \quad \text{Equation 33}$$

As shown in Figure 29, subtraction of the MM energy of the real system from that of the model system (i.e. $E_{\text{MM, real}} - E_{\text{MM, model}}$) is used to obtain the effect of the environment on the model system with an inexpensive MM method. Therefore, the IMOMM method can be considered as a size extrapolation from the accurate QM calculation of the small model system ($E_{\text{QM, model}}$) to the large real system (E_{real}), by adding the approximate environmental effect evaluated by the inexpensive MM method. From an alternative viewpoint, the IMOMM method can also be considered as the extrapolation of the method (i.e., $E_{\text{QM, model}} - E_{\text{MM, model}}$) from the MM level to the high accuracy QM level starting from the MM energy of the real system, $E_{\text{MM, real}}$.

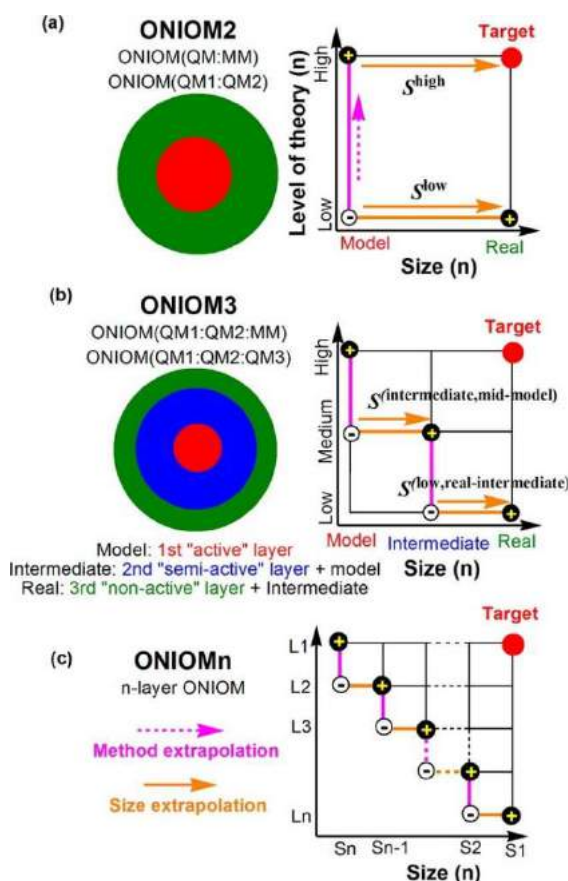


Figure 29: Schematic partitions of the whole system by the ONIOM methods: (a) two-layer ONIOM, (b) three-layer ONIOM, and (c) n -layer ONIOM, from²⁵⁵

The ONIOM method (including IMOMM and IMOMO methods) can be considered as a hybrid method based on a somewhat different concept from the “generic” two-layer QM/MM method. Although ONIOM can be used as a two-layer QM/MM method, it can also, uniquely, combine different QM and QM methods, and can easily be extended to multiple layers.

I-5-3. Solvation effects

Many calculations are performed at the gas state, but some models have been developed to take account for solvation effects. Two approaches are possible: the implicit model and the explicit model, depending on the system, the accuracy needed, and the calculation time available. Explicit solvent modelling consists in explicitly adding the solvent molecules, which is intuitive but very costly. In the implicit solvent modelling approach, the solvent is represented as a Polarizable Continuum Model (PCM), and free energies of solvation are computed, which is less intuitive, but feasible.

I-5-3-1. Implicit solvation

In this approach, the solvent is represented by a uniform polarizable medium with a dielectric constant ϵ . The solute is a molecule in a suitably shaped cavity in the medium (Figure 30). Finally, the solute-solvent interactions are electrostatic interactions between the solute charge distribution and the solvent. This is calculated through a SCF approach as the solute and the solvent polarize each other, inducing charge redistribution until self-consistency.

The solvation free energy is calculated according to Equation 32:

$$\Delta G_{\text{solv}} = \Delta G_{\text{cav}} + \Delta G_{\text{disp}} + \Delta G_{\text{elec}} \quad \text{Equation 34}$$

With ΔG_{cav} the free-energy for the creation of the excluded volume for the solvent S around the solute M, ΔG_{el} the free energy related to the formation of electrostatic interactions between M and S, and ΔG_{disp} a short-range free-energy containing the repulsive and attractive van der Waals-like interactions between M and S.

Three contributions determine the solvation free energy: creating a cavity in the medium costs energy, dispersion interactions between solute and solvent lower the energy, and polarization between solute and solvent induces charge redistribution until self-consistency.

It needs to solve the Poisson equation for discrete or continuous charge distribution of the solute depending on the electrostatic potential (ρ) (Equation 33):

$$\nabla^2 \phi(r) = -\frac{4\pi\rho(r)}{\epsilon} \quad \text{Equation 35}$$

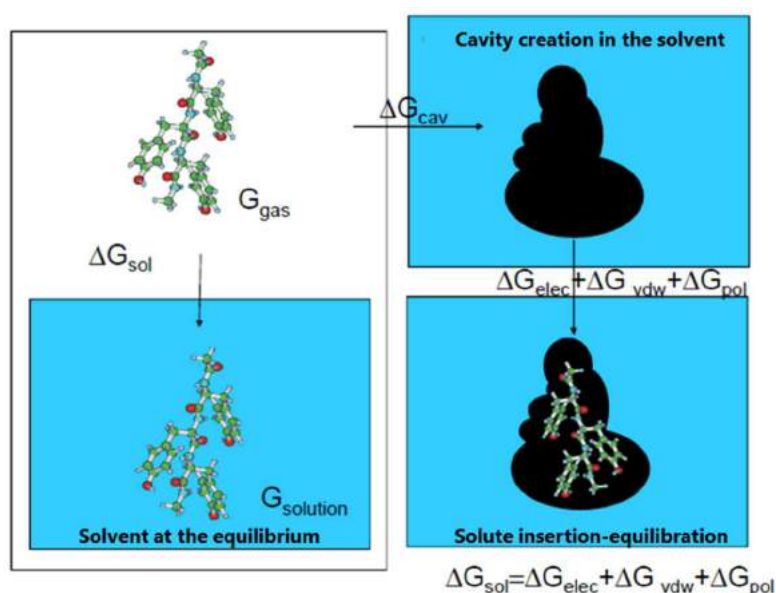


Figure 30: Schematic representation of the implicit solvation method

I-5-3-2. Explicit solvation

In this approach, all the system is described accurately, giving access to the full details on the molecular structure. But treating both solute and solvent at the quantum molecular level is very time-consuming. Some strategies have been proposed, such as treating the solvent at lower quantum molecular level, or at the molecular level, but that is not always possible. Also, Car-Parrinello *ab initio* molecular dynamic approach can be used. Another trick is to use periodic boxes to limit the system size, with Ewald sums for electrostatics. The following table (Table 6) summarizes the main advantages and drawbacks of using one approach instead of the other.



Solvation model		
Explicit (all-atoms description)	<ul style="list-style-type: none"> - Full details on the molecular structure - Realistic physical picture of the system 	<ul style="list-style-type: none"> - Many atoms: costly - Multiple minima: difficulties in equilibrating solvent and solute
Implicit (continuum description)	<ul style="list-style-type: none"> - No explicit solvent atoms: faster - Treatment of solvent effects at QM level possible 	<ul style="list-style-type: none"> - All solvent structural information is lost: No modelling of specific interactions such as H-bonds - Need to define an artificial boundary between solute and solvent

Table 6: Advantages and drawbacks of each solvation model

Conclusion

DFT can be defined as method of obtaining an approximate solution to the Schrödinger equation for systems larger than the hydrogen atom.

The ultimate goal in quantum chemistry is to solve the time-independent, non-relativistic Schrödinger equation, which is analytically only possible for the hydrogen atom. The many-body problem can be solved by using some fundamental approximations

The electron density is the key-variable to study ground-state properties of an interacting electron system. The ground state expectation value of any physical observable of a many-electron system is a unique functional of the electron density ρ .

The total energy functional $E_{\text{HK}(\rho)}$ has a minimum, the ground state energy E_0 , in correspondence to the ground state density ρ_0 . The universal functional $F_{\text{HK}(\rho)}$ is hard to approximate.

The Kohn-Sham scheme proposed a reformulation in terms of one-particle orbitals that allowed for a solvation through the SCF approach. Caution must be taken to rigorously choose a functional/basis set that is suitable for the system studied.

Larger systems can be analyzed with the ONIOM method, allowing to divide the system in different layers with their own level of theory. Also, those calculations are done in the gas phase, but solvation effects can be taken into account by using explicit or implicit methods, depending on the system, the accuracy needed, and the calculation time available.

I-6. Chromatographic evaluation and data processing by chemometric methods

I-6-1. Chromatographic evaluation of thermodynamic properties

The characterization of stationary phases is of primary concern as it aims to obtain a quantitative understanding of the properties influencing the retention. Considering the properties, the researcher can select the appropriate one that fits with its needs.

Over the years, several methods have been established to study the interactions between the stationary-phase and the solutes. As it was discussed earlier (I.4), the silica particles can be analyzed right after the functionalization by different techniques (e.g. spectroscopic techniques, morphological study, ligand grafting analysis...). In addition, the stationary phase can be characterized after being packed into a column using chromatographic test methods. The chromatographic tests can be further divided into the determination of physico-chemical properties and the model based tests. Finally, chemometric methods allows to compare test results and to classify columns as similar or dissimilar^{111,256,257}.

Although the test procedures seek to evaluate similar SP characteristics, different methodologies have been proposed²⁵⁸⁻²⁶¹. Snyder *et al.*²⁶¹ defined a hydrophobic subtraction model and Abraham *et al.*²⁶² adapted the solvatochromic parameters from Taft *et al.*²⁶³ to linear solvation energy relationship. At the same time, Engelhardt²⁶⁴ and Kimata *et al.*²⁶⁵ proposed a procedure (the so-called Tanaka test) that has now relatively widespread acceptance and least recognition. Also, some specific tests have been developed, for instance the Veuthey test for basic compounds²⁶⁶⁻²⁶⁸.

In many tests proposed, experimental retention data of a set of compounds are modelled as a function of a number of their structural properties (e.g. $\log k$ or $\log (k/k_{\text{ref}})$ where k_{ref} is the k value of a non-polar reference solute). Different properties can be estimated such as column efficiency, hydrophobicity, silanol activity, ion-exchange capacity, steric selectivity and presence of metal impurities. The solute probes have to be adequately chosen to reflect given stationary phase properties, considering their retention/separation information. It has also to be diverse enough to account for the diversity of the physical interactions involved in chromatography. The model coefficients provide information on the properties of the column (e.g. hydrophobicity, hydrogen-bonding, steric selectivity).

Some key reviews have been proposed regarding the different characterization methods and techniques. Lesellier and West^{269,270} presented general tests, their extensions, and data treatment to highlight factors that are important when comparing and classifying different stationary phases. The Tanaka and Engelhardt tests are presented as well as the hydrophobic subtraction model, the linear solvation energy relationship model, and the carotenoid test¹²¹. Also, Neue²⁷¹ highlighted the impact of different parameters (e.g. column hydrophobicity, hydrogen-bonding properties, mobile-phase solvent strength, and column temperature) that lead to various selectivities. Finally, Galea *et al.*²⁷² proposed a review concerning the characterization and classification of stationary phases in HPLC and SFC.

I-6-1-1. Hydrophobic subtraction model

The conditions and calculations described in the hydrophobic-subtraction model of Snyder *et al.*²⁶¹ help defining a basis for stationary phase and silica contributions to selectivity, as well as a qualitative approach to column equivalency. The Equation 34 defines the model and the Table 7 the parameters, respectively.

$$\log \alpha = \log \left(\frac{k}{k_{EB}} \right) = (\eta' H) - (\sigma' S^*) + (\beta' A) + (\alpha' B) + k' C \quad \text{Equation 36}$$

Here k is the retention factor of a given solute, k_{EB} the value of k for a non-polar reference solute (ethylbenzene in the present treatment) on the same column under the same conditions, and the remaining selectivity-related symbols represent either empirical, eluent- and temperature-dependent properties of the solute (η' , σ' , β' , α' , κ'), or eluent- and temperature-independent properties of the column (H , S^* , A , B , C). Thus, the various column parameters measure the following column properties: H the hydrophobicity (hydrophobic retention), S^* the steric resistance (resistance to penetration of molecules into stationary phase), A and B the column hydrogen-bond acidity and basicity (with free silanol/siloxanes), respectively and finally C the column cation-exchange activity (ionized silanols – charge measure, pH dependent).

Phase-Solute Interaction	Solute Retention Characteristic	Description	Term in the hydrophobic subtraction model
Dispersion	Hydrophobic	Van der Waals interactions in organic molecules	H
Charge Transfer π -Acidity	Aromatic	Electron deficient solutes interacting with Lewis base phases	$k_{\text{Anisole}} / k_{\text{Ethylbenzene}}$
Hydrogen Bonding	Acidic	Proton donor solute interacting with proton acceptor group embedded in the SP	B
Induced Dipole or π -Basicity	Basic	Electron rich solutes interacting with Lewis acid phases or phases with an induced dipole	C

Table 7: Phase-solute interactions contributing to reversed-phase selectivity

The mobile phase is acetonitrile–0.06M potassium phosphate buffer 50:50 (v/v); the pH is set at 2.8 and the temperature at 35°C. It requires the analysis of a wide range of compounds (at the beginning 67, later reduced to 16) to set up a link between the retention and the properties of these solutes.

I-6-1-2. Engelhardt test

The test has become a standard procedure for the evaluation of hydrophobicity and silanol activity. It is carried out with a non-buffered methanol–water 55:45 (v/v) mobile phase, with a temperature set at 40°C. The test solutes used are toluene and ethylbenzene to evaluate hydrophobicity, phenol, benzoic acid and ethylbenzoate to evaluate the polar interactions, *N,N*-dimethylaniline, aniline and *o*-, *m*- and *p*-toluidine for the silanophilic interactions or the electrostatic interactions. If the stationary phase presents a low silanol activity, aniline should be eluted before phenol with a good peak shape, and the ethylaniline isomers should be co-eluted. The composition of the mobile phase was chosen for its capacity to discriminate C8 and C18 phases, thanks to the reversal in the elution order of ethylbenzoate and toluene²⁶⁴. However, the test is not done at different pHs, so the silanol activity is not completely evaluated.

I-6-1-3. Tanaka test

Kimata *et al.*²⁶⁵ developed their test at the same time as Engelhardt *et al.* The parameters as well as the chromatographic conditions are summarized in Table 8. The tests solutes used are pentylbenzene, butylbenzene, caffeine, benzylamine, phenol, triphenylene and *o*-terphenyl. data are normalized and presented through radar plots, allowing for a visualization of the properties of any studied phase.

Property of stationary phase	Chromatographic parameters	Mobile phases (v/v)	Property evaluated
Hydrophobicity	$\alpha_{PB/BB}$	80% CH ₃ OH 20%H ₂ O	Comparison of the molecular interaction mechanisms (for 2 SPs considered)
Amount of alkyl chains	k_{PB}	80% CH ₃ OH 20%H ₂ O	Surface area of silica, surface coverage
Steric selectivity	$\alpha_{T/O}$	80% CH ₃ OH 20%H ₂ O	Functionality of silane, surface coverage
Hydrogen bonding capacity	$\alpha_{C/P}$	30% CH ₃ OH 70%H ₂ O	Amount of silanols, end-capping, surface coverage
Ion exchange capacity (pH 7.6)	$\alpha_{B/P}$	30% CH ₃ OH 70% phosphate buffer (0.02M)	Amount of silanols and ion exchange sites
Ion exchange capacity (pH 2.7)	$\alpha_{B/P}$	30% CH ₃ OH 70% phosphate buffer (0.02M)	Amount of ion exchange sites at pH 3, silica pretreatment

Table 8: Chromatographic conditions and parameters of the test

Compared to Engelhardt's test, Tanaka's test introduced additional evaluations such as the hydrogen bonding due to the residual silanol groups, evaluated through the caffeine/phenol selectivity. The separation factor decreases with the bonding density and with end-capping treatments, as the retention of caffeine reduces with the proportion of silanol groups. Also, the ion exchange capacity is studied through the benzylamine/phenol selectivity, at two pHs. This test also evaluates the shape selectivity: while the hydrophobicity of triphenylene (planar) and *o*-terphenyl (twisted) is identical, they do not penetrate in the stationary phase to the same extent because of their different volumes.

Finally, the probes are commercially available and cheap, which makes this test a good compromise for fast *versus* complete evaluation.

I-6-1-4. Carotenoid test

The carotenoid test¹²¹ especially used in SFC investigates the hydrophobicity, polar surface area and shape selectivity by analyzing carotene pigments. The retention factor of all-trans- β -carotene, the separation factor of all-trans- β -carotene and zeaxanthin, and the separation 13-cis and all-trans isomers of β -carotene are the parameters needed to study the hydrophobicity, silanophilic interactions and the steric selectivity, respectively.

The carotenoid method allows for the characterization and classification of aromatic ligand and classical C18 bonded phases. The results can be visualized in a classification diagram based on the accessibility of polar sites on the stationary surface, the polar surface area, α (all-trans- β -carotene/zeaxanthin), the hydrophobicity of the stationary phase and the shape selectivity α (13-cis-/all trans- β -carotene). However, the solutes are not necessarily easily available.

I-6-1-5. Other tests and extensions

Sander and Wise shape test is focused on the evaluation of the shape selectivity and is based on the separation of solutes having a different spatial arrangement^{173,273}. The national institute of standards and technology uses it as a column selectivity test to certify the performance characteristics of C18-type phases.

Following the Tanaka and Engelhardt tests, several teams proposed modifications of the tests, and/or extensions to other types of phase. Also, Neue *et al.*^{274,275} developed a test based on the Engelhardt test, Cruz *et al.*²⁵⁹ have followed the Tanaka method and added an efficiency criterion based on a ratio of two theoretical plate numbers measured for two positional isomers of dihydroxynaphthalene (2.3 and 2.7). This evaluation is not only thermodynamic but also kinetic as it takes into account the packing column quality.

Still on the basis of the Tanaka test, Layne²⁷⁶ suggested a test to estimate the properties of polar-embedded and polar-end-capped phases. Also, Sándi *et al.*²⁷⁷ measured the retention of thirteen solutes, for a large part of them, in the Engelhardt and Tanaka tests. Finally, some insights in data treatments were presented to deal with results for a large number of tested columns.

For the specific case of basic solutes, the Veuthey test²⁶⁶⁻²⁶⁸ proposed the analysis of 14 compounds, later reduced to seven basic solutes, with various pKa values and molecular

weights. The retention and asymmetry factors were studied at pH 3 and 7, and the authors used chemometric methods to define clusters of stationary phases.

I-6-1-6. Linear Solvation Energy Relationship (LSER)

LSER model is known as a Quantitative Structure Property Relationship (QSPR), in which the property is modelled as a function of a number of molecular descriptors, representing physico-chemical properties of the analytes. Considering retention as the property investigated, we talk of Quantitative Structure Retention Relationship (QSRR). The goals of applying such approach encompass the prediction of a new solute retention, the understanding of the system molecular separation, or the evaluation of the stationary phase properties²⁷⁸⁻²⁸⁰. This approach was used extensively to study columns in HPLC, GC and SFC²⁸¹⁻²⁸⁵, making comparisons of the same columns in the different chromatographic systems.

The most widely applied representation of the LSER model was presented by Abraham *et al.*²⁶² and is given in Equation 35.

$$\log k = c + eE + sS + aA + bB + vV \quad \text{Equation 37}$$

E is the excess molar refraction (calculated from the refractive index of the molecule) and expresses polarizability contributions from n and p electrons; S is the solute dipolarity/polarizability; A and B are the solute overall hydrogen-bond acidity (donating ability) and basicity (accepting ability); and V is the McGowan characteristic volume. Model coefficient c is a system constant or the model intercept term.

In the equation, the retention is the dependent variable, usually a measure related to solute partitioning (e.g. log k). The terms E, S, A, B, and V are solute-dependent molecular descriptors. Each descriptor is deliberately included in the LSER equation to account for a specific intermolecular interaction. Lower case letters represent the coefficients of the model or system constants, related to the complementary effect of the phases (solute, SP, MP) on these interactions. The different solute interactions incorporated in the LSER model for chromatographic retention are illustrated in Figure 31.

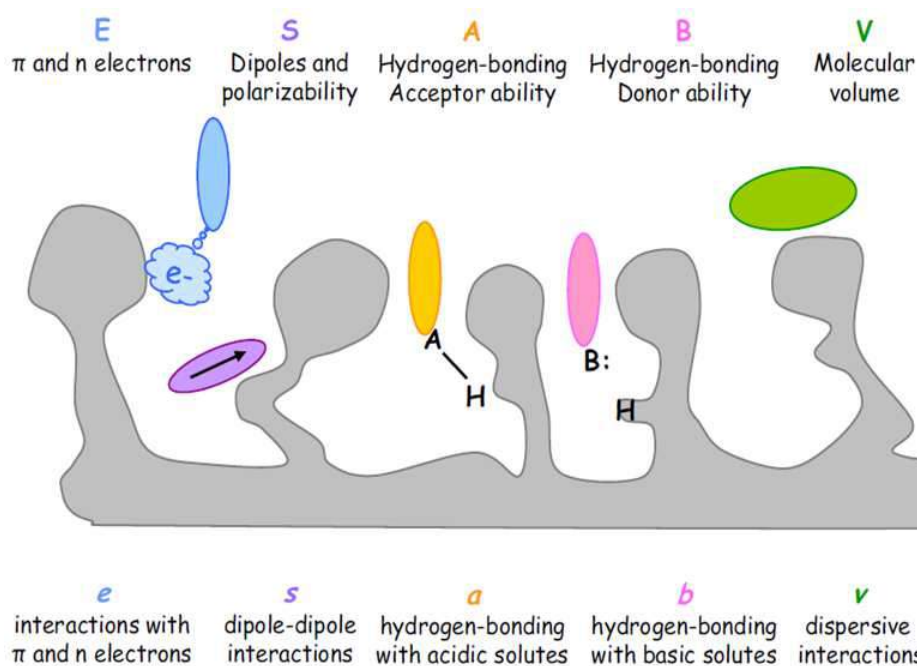


Figure 31: Schematic representation of the LSER parameters, adapted from²⁸⁶

A minimum of 20 carefully chosen solutes need to be included to have a relevant model²⁶⁹. The descriptors of the chosen solutes should be evenly distributed over the interactions. Frequently, the test solutes chosen are simple aromatic compounds, like benzene or naphthalenic derivatives, with different polar and non-polar substituents to represent the diversity of organic groups encountered in chromatography²⁸⁷. The system constants (e , s , a , b and v) are estimated through a multiple linear regression analysis of the retention data for a range of solutes with known descriptors. These system constants mirror the magnitude of difference for that particular interaction between the stationary and mobile phases. A positive sign of a coefficient indicates that the respective molecular interaction is stronger in the stationary phase than in the mobile phase, thus increasing retention.

By conducting LSER studies, different stationary phases can be compared to gain important chemical insight. An important point is that the mobile-phase composition has to be kept constant for all stationary phases being studied. Indeed, modification of the stationary phase by the mobile-phase components varies with the type of bonded functional groups onto the silica support²⁸⁸.



I-6-2. Chemometric methods

Chemometric methods have been used to evaluate or visualize given chromatographic data. It is a rational way to handle and interpret data sets that can be huge. Two approaches can be distinguished as represented in Figure 32.

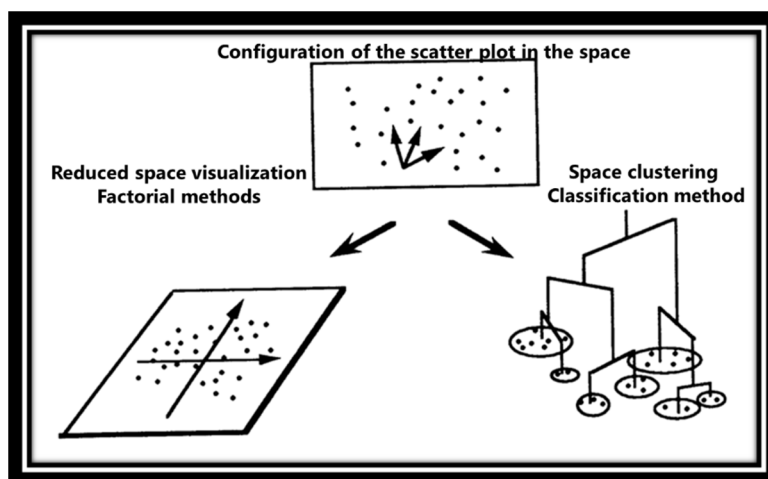


Figure 32: Schematic representation of data classification

Such methods include Principal Component Analysis (PCA) as exploratory data analysis combined with Hierarchical Component Analysis (HCA) to order the data. The following section is dedicated to the presentation of those two methods.

I-6-2-1. Principal Component Analysis (PCA)

PCA is a descriptive statistical method introduced by K. Pearson in 1901²⁸⁹ that allows to represent in one graph a big amount of the information contained in a data table. Various algorithms for the PCA calculation have been developed such as NIPALS (Nonlinear Iterative Partial Least Squares) or SVD (Singular Value Decomposition).

Due to the large number of data generated during the SP characterization through the different tests presented previously (I.6.1), the issue is to represent those n dimensions and summarize the data set by choosing the best projection axes. The aim is to transform p initial variables inter-correlated in p new variables non-correlated called Principal Components (PC) (Figure 33).

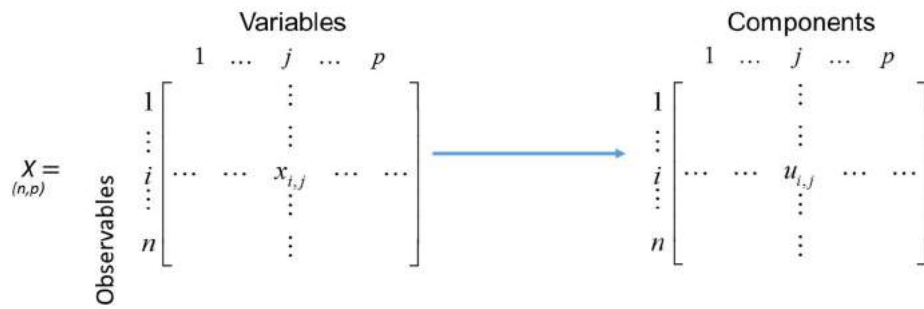


Figure 33: Schematic representation of the transformation of the p initial variables inter-correlated in p new variables non-correlated

The first step is the data standardization (Equation 36) to ensure equal importance of each variables in the final representation.

$$\frac{x_{ik} - \bar{x}_k}{s_k} \quad \text{Equation 38}$$

With x_{ik} the value, \bar{x}_k the average value and s_k the standard deviation.

Then, the variance-covariance (or the correlation matrix) is constructed and PC weights (i.e. eigenvalues) are calculated by the determinant of the matrix in Equation 37.

$$\det(A - \lambda I) = 0 \quad \text{Equation 39}$$

With λ the matrix of eigenvalues and I the identity matrix of order n .

After calculation of the coefficients of the 2 CPs (i.e. eigenvectors) associated to the eigenvalues, the scores of individuals are obtained by linear combination of the initial variables (Equation 38).

$$F_{i,j} = \lambda_1 X_1 + \dots + \lambda_p X_p \quad \text{Equation 40}$$

With X_1, \dots, X_p the initial variables.

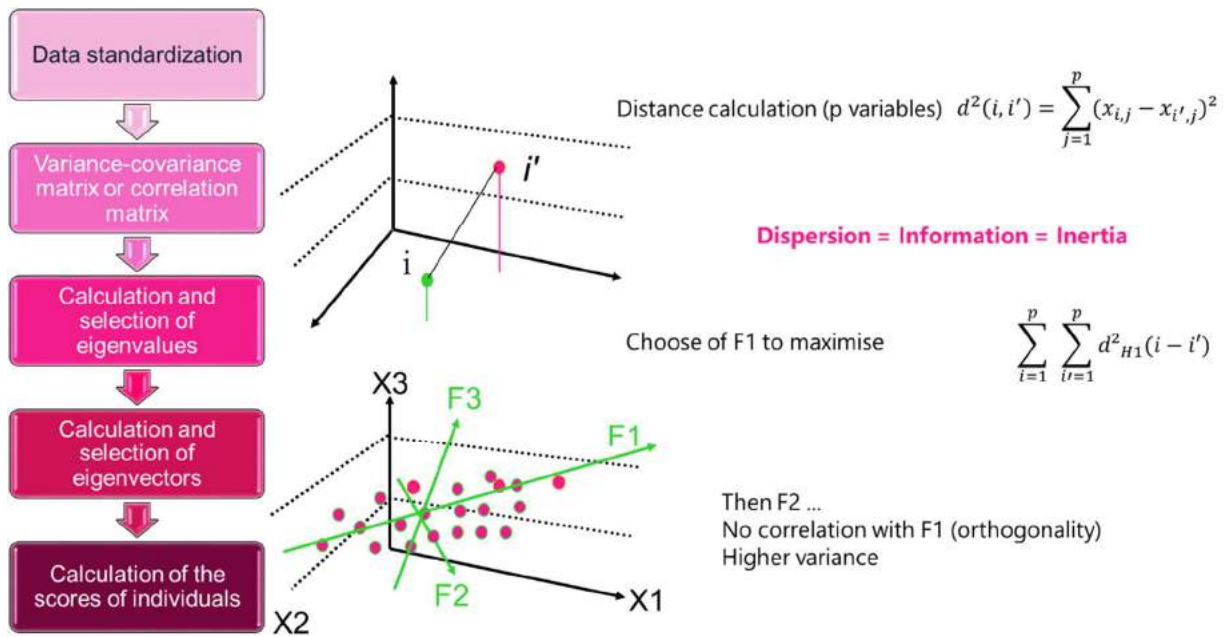


Figure 34: Summary of the PCA procedure

At the end of the procedure, two plots are generated by the software (in our case, XLStat, Addinsoft): score plots for the observables and loading plots for the variables. Those two representations are complementary and can be superimposed to generate the biplot. The score plot is a representation of the projections of observables, and the loading plot is useful to visualize the correlation between variables and PCs.

A tricky point is the choice of the number of factorial axes, some rules help defining it:

- Kaiser limit in normalized PCA: Preserve all the principal components associated to eigenvalues $\lambda > 1$ on the eigenvalues histogram (scree plot in Figure 35).
- Minimal inertia rule: Preserve 50-70% of the cumulated variance
- Common sense: Keep interpretable axes

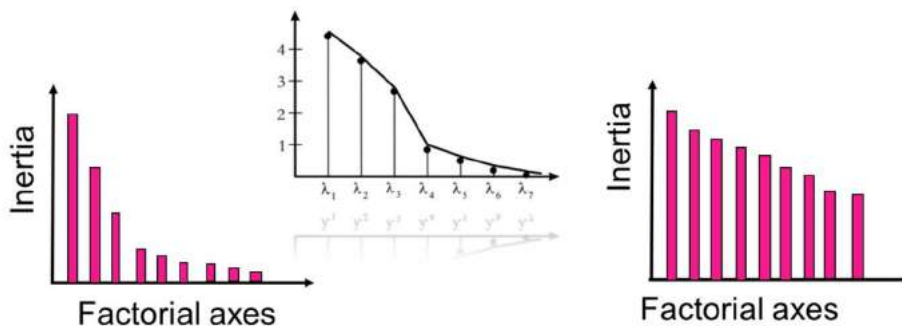


Figure 35: Representation of the inertia cases that can be encountered

Also, the representation quality has to be checked to ensure reliable (amenable) interpretation. Inertia calculation can be used, and the $\cos^2 \theta$ can be calculated as represented in Figure 36. A value close to 1 ensures a good quality of the representation. In the loading plot, it signifies that variables close to the circle are well represented, while those close to the origin are not.

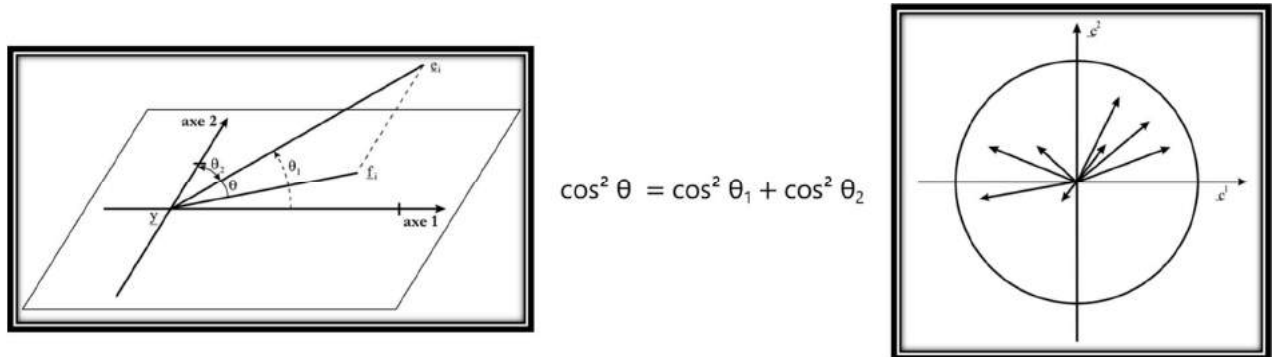


Figure 36: Global quality representation

I-6-2-2. Hierarchical Component Analysis (HCA)

The Cluster Analysis is an explorative analysis that tries to identify structures within the data. Especially, it tries to identify homogenous groups of cases (i.e. observations, participants...). Because it is explorative it does not make any distinction between dependent and independent variables. The cluster analysis is often part of the sequence of analyses of factor analysis, cluster analysis, and finally, discriminant analysis. First, a factor analysis that reduces the dimensions and therefore the number of variables makes it easier to run the cluster analysis. Also, the factor analysis minimizes multicollinearity effects. The next analysis is the cluster analysis, which identifies the grouping. Lastly, a discriminant analysis checks the goodness of fit of the model that the cluster analysis found and profiles the clusters.

In almost all analyses, a discriminant analysis follows a cluster analysis because the cluster analysis does not have any goodness of fit measures or tests of significance. The cluster analysis relies on the discriminant analysis to check if the groups are statistically significant and if the variables significantly discriminate between the groups. However, this does not ensure that the groups are actually meaningful; interpretation and choosing the right clustering requires know-how. It is up to the understanding of the researcher and how well he makes sense of his data. Furthermore, the discriminant analysis builds a predictive model that allows us to plug in the numbers of new cases and to predict the cluster membership.

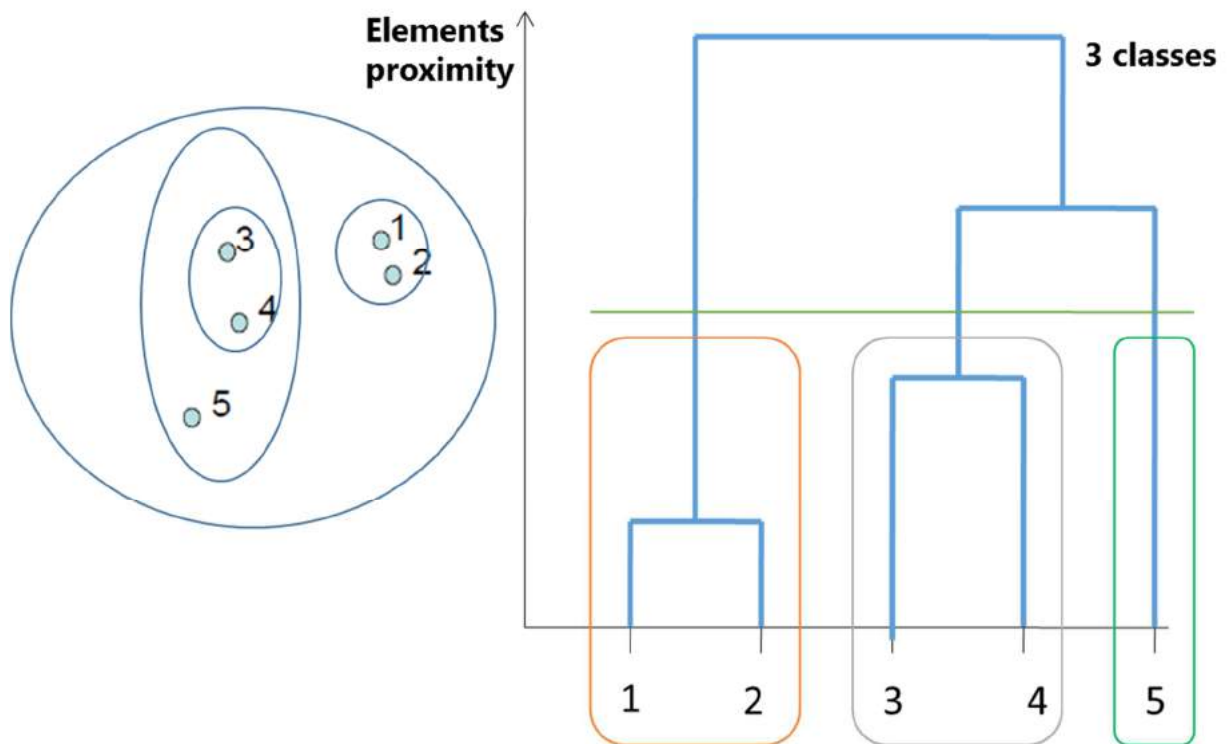


Figure 37: Representation of a HCA analysis

The first step in the hierarchical clustering process is to look for the two elements that are the most similar, that is are the closest in the sense of having the lowest dissimilarity (e.g. elements 1 and 2, and 3 and 4). These two elements are then joined at in the first step of the dendrogram, or clustering tree, this cluster becoming a new element submitted to the same procedure until all elements have been clustered (Figure 37). The distance measure is mostly defined as the Euclidean distance, and different choices are available to define the "between-groups" linkage (distance between clusters is the average distance of all data points within these clusters): nearest neighbor (single linkage: distance between clusters is the smallest distance between two data points), furthest neighbor (complete linkage: distance is the largest distance between two data points), and Ward's method (distance is the distance of all clusters to the grand average of the sample). The usual recommendation is to use single linkage first. Although single linkage tends to create chains of clusters, it helps in identifying outliers. After excluding these outliers, we can move onto Ward's method. Ward's method uses the F value (like an ANOVA) to maximize the significance of differences between cluster, which gives it the highest statistical power of all methods. The downside is that it is prone to outliers and creates small clusters.

Conclusion

Stationary phases are continuously improved and some new ones are introduced each year, on different supports (monolith, sub-2 μm particles, SPP...). The lack of information from manufacturers regarding the exact functionality of their stationary phases highlight the need of classification. Also, it is essential to be able to identify columns possessing similar selectivity for use as replacement/back-up columns. Alternatively, for method development purposes, phases possessing differing selectivities are a prerequisite.

Many authors developed chromatographic tests to evaluate some key properties of the stationary phases. The main strategies are summarized in Figure 38.

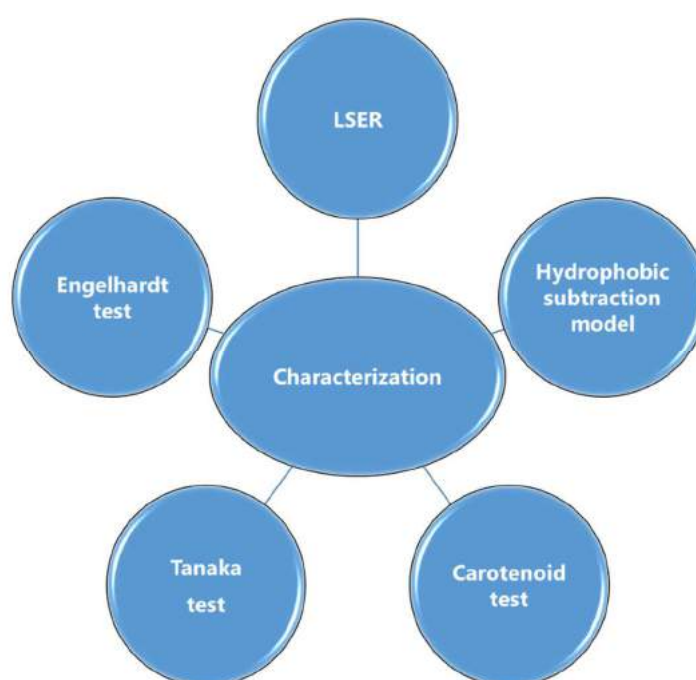


Figure 38: Schematic representation of the main chromatographic tests, from²⁷²

Chemometric methods are also used, such as HCA to measure the proximity between stationary phases. Also, PCA is of interest to identify the criteria affecting retention and the correlations, and to group the stationary phases in a two- or three-dimensional space based on the data initially spread in a multi-dimensional space.

More complex models are also used, based on quantitative structure–retention relationships like the LSER model of Abraham *et al.* or the hydrophobic subtraction model proposed by Snyder *et al.* These thermodynamic approaches necessitate the analysis of a wide range of compounds, properties of which are well known, then setting up of a link between the retention and the properties of these solutes in order to identify the interactions taking place between the solutes and the stationary phase.

I-7. References

- (1) Martin, A. J. P.; Synge, R. L. M. *Biochem. J.* **1941**, *35* (12), 1358–1368.
- (2) van Deemter, J. J.; Zuiderweg, F. J.; Klinkenberg, A. *Chem. Eng. Sci.* **1956**, *5* (6), 271–289.
- (3) The Theory of HPLC
http://www.chromacademy.com/lms/sco3/Theory_Of_HPLC_Band_Broadening.pdf
(05/28/2016)
- (4) Woodruff, M. *Chromatogr. Today* **2014**, 8–10.
- (5) Setting HPLC Chromatographic Parameters
<http://www.chromacademy.com/chromatography-Setting-HPLC-Chromatographic-Parameters.html>.
- (6) Fekete, S.; Kohler, I.; Rudaz, S.; Guillarme, D. *J. Pharm. Biomed. Anal.* **2014**, *87*, 105–119.
- (7) Gritti, F.; Sanchez, C. A.; Farkas, T.; Guiochon, G. *J. Chromatogr. A* **2010**, *1217* (18), 3000–3012.
- (8) Fountain, K. J.; Neue, U. D.; Grumbach, E. S.; Diehl, D. M. *J. Chromatogr. A* **2009**, *1216* (32), 5979–5988.
- (9) Gritti, F.; Felinger, A.; Guiochon, G. *J. Chromatogr. A* **2006**, *1136* (1), 57–72.
- (10) Gritti, F.; Guiochon, G. *J. Chromatogr. A* **2011**, *1218* (28), 4452–4461.
- (11) Gritti, F.; Guiochon, G. *J. Chromatogr. A* **2014**, *1327*, 49–56.
- (12) Wu, N.; Bradley, A. C. *J. Chromatogr. A* **2012**, *1261*, 113–120.
- (13) Gritti, F.; Guiochon, G. *J. Chromatogr. A* **2012**, *1238*, 77–90.
- (14) Spaggiari, D.; Fekete, S.; Eugster, P. J.; Veuthey, J.-L.; Geiser, L.; Rudaz, S.; Guillarme, D. *J. Chromatogr. A* **2013**, *1310*, 45–55.
- (15) *UHPLC in life sciences*; Guillarme, D., Veuthey, J.-L., Eds.; RSC chromatography monographs; RSC Publ., Royal Soc. of Chemistry: Cambridge, 2012.
- (16) Rosset, R.; Caude, M.; Jardy, A. *Chromatographies en phases liquide et supercritique*, Masson.; Paris, 1991.
- (17) Bristow, P. A.; Knox, J. H. *Chromatographia* **1977**, *10* (6), 279–289.
- (18) Desmet, G.; Clicq, D.; Gzil, P. *Anal. Chem.* **2005**, *77* (13), 4058–4070.
- (19) Knox, J. H.; Saleem, M. *J. Chromatogr. Sci.* **1969**, *7* (10), 614–622.
- (20) Poppe, H. *J. Chromatogr. A* **1997**, *778*, 3–21.
- (21) Desmet, G.; Clicq, D.; Gzil, P. *LCGC Eur.* **2005**, *18*, 403–409.
- (22) Gzil, P.; Vervoort, N.; Baron, G. V.; Desmet, G. *Anal. Chem.* **2004**, *76* (22), 6707–6718.
- (23) Neue, U. D. *J. Chromatogr. A* **2005**, *1079* (1–2), 153–161.
- (24) Cabrera, K. *J. Sep. Sci.* **2004**, *27* (10–11), 843–852.
- (25) Nguyen, D. T.-T. *Analyses rapides et ultra-rapides en chromatographie liquide: application aux composés pharmaceutiques*, Genève.
- (26) Svec, F.; Fréchet, J. M. *Anal. Chem.* **1992**, *64* (7), 820–822.
- (27) Tennikova, T. B.; Horák, D.; Švec, F.; Tennikov, M. B.; Kever, E. E.; Belenkii, B. G. *J. Chromatogr. A* **1989**, *475*, 187–194.
- (28) Hjerten, S.; Liao, J.-L.; Zhang, R. *J. Chromatogr. A* **1989**, *473*, 273–275.
- (29) Minakuchi, H.; Nakanishi, K.; Soga, N.; Ishizuka, N.; Tanaka, N. *J. Chromatogr. A* **1998**, *797* (1), 121–131.
- (30) Minakuchi, H.; Nakanishi, K.; Soga, N.; Ishizuka, N.; Tanaka, N. *J. Chromatogr. A* **1997**, *762*, 135–146.
- (31) Lubda, D.; Cabrera, K.; Krass, W.; Schaefer, C.; Cunningham, D. *LC-GC Eur.* **2001**, 2–5.
- (32) Guiochon, G. *J. Chromatogr. A* **2007**, *1168* (1–2), 101–168.
- (33) Leinweber, F. C.; Tallarek, U. *J. Chromatogr. A* **2003**, *1006* (1), 207–228.

- (34) Miyamoto, K.; Hara, T.; Kobayashi, H.; Morisaka, H.; Tokuda, D.; Horie, K.; Koduki, K.; Makino, S.; Núñez, O.; Yang, C.; Kawabe, T.; Ikegami, T.; Takubo, H.; Ishihama, Y.; Tanaka, N. *Anal. Chem.* **2008**, *80* (22), 8741–8750.
- (35) Ikegami, T.; Dicks, E.; Kobayashi, H.; Morisaka, H.; Tokuda, D.; Cabrera, K.; Hosoya, K.; Tanaka, N. *J. Sep. Sci.* **2004**, *27* (15–16), 1292–1302.
- (36) Hormann, K.; Müllner, T.; Bruns, S.; Hölzel, A.; Tallarek, U. *J. Chromatogr. A* **2012**, *1222*, 46–58.
- (37) Gritti, F.; Guiochon, G. *J. Chromatogr. A* **2011**, *1218* (31), 5216–5227.
- (38) Gritti, F.; Guiochon, G. *J. Chromatogr. A* **2012**, *1227*, 82–95.
- (39) Gritti, F.; Guiochon, G. *J. Chromatogr. A* **2012**, *1225*, 79–90.
- (40) Guillarme, D.; Heinisch, S.; Rocca, J. L. *J. Chromatogr. A* **2004**, *1052* (1–2), 39–51.
- (41) Antia, F. D.; Horváth, C. *J. Chromatogr. A* **1988**, *435*, 1–15.
- (42) Teutenberg, T.; Wiese, S.; Wagner, P.; Gmehling, J. *J. Chromatogr. A* **2009**, *1216* (48), 8470–8479.
- (43) Smith, R. M. *J. Chromatogr. A* **2008**, *1184* (1–2), 441–455.
- (44) Vanhoenacker, G.; Sandra, P. *J. Sep. Sci.* **2006**, *29* (12), 1822–1835.
- (45) Greibrokk, T.; Andersen, T. *J. Chromatogr. A* **2003**, *1000* (1–2), 743–755.
- (46) Guillarme, D.; Heinisch, S. *Sep. Purif. Rev.* **2005**, *34* (2), 181–216.
- (47) Heinisch, S.; Rocca, J.-L. *J. Chromatogr. A* **2009**, *1216* (4), 642–658.
- (48) Teutenberg, T.; Goetze, H.-J.; Tuerk, J.; Ploeger, J.; Kiffmeyer, T. K.; Schmidt, K. G.; Kohorst, W. gr.; Rohe, T.; Jansen, H.-D.; Weber, H. *J. Chromatogr. A* **2006**, *1114* (1), 89–96.
- (49) Teutenberg, T. *Anal. Chim. Acta* **2009**, *643* (1–2), 1–12.
- (50) Teutenberg, T.; Tuerk, J.; Holzhauser, M.; Giegold, S. *J. Sep. Sci.* **2007**, *30* (8), 1101–1114.
- (51) Yang, Y. *LC GC Mag.-N. Am.-Solut. Sep. Sci.* **2006**, *29*, 53–57.
- (52) Yang, Y. *J. Sep. Sci.* **2007**, *30* (8), 1131–1140.
- (53) Shih, C.-Y.; Chen, Y.; Xie, J.; He, Q.; Tai, Y.-C. *J. Chromatogr. A* **2006**, *1111* (2), 272–278.
- (54) Thompson, J. D.; Carr, P. W. *Anal. Chem.* **2002**, *74* (5), 1017–1023.
- (55) Hazotte, A.; Libong, D.; Matoga, M.; Chaminade, P. *J. Chromatogr. A* **2007**, *1170* (1–2), 52–61.
- (56) Guillarme, D.; Heinisch, S.; Gauthier, J. Y.; Lanteri, P.; Rocca, J. L. *J. Chromatogr. A* **2005**, *1078* (1–2), 22–27.
- (57) Majors, R. E.; America, L. N. **2005**.
- (58) MacNair, J. E.; Lewis, K. C.; Jorgenson, J. W. *Anal. Chem.* **1997**, *69*, 983–989.
- (59) MacNair, J. E.; Patel, K. D.; Jorgenson, J. W. *Anal. Chem.* **1999**, *71* (3), 700–708.
- (60) Halasz, I.; Endeke, R.; Asshauer, J. *J. Chromatogr. A* **1975**, *112*, 37–60.
- (61) Jorgenson, J. W.; Lukacs, K. D. *Anal. Chem.* **1981**, *53* (8), 1298–1302.
- (62) Wu, N.; Lippert, J. A.; Lee, M. L. *J. Chromatogr. A* **2001**, *911*, 1–12.
- (63) Tolley, L.; Jorgenson, J. W.; Moseley, M. A. *Anal. Chem.* **2001**, *73* (13), 2985–2991.
- (64) Xiang, Y.; Wu, N.; Lippert, J. A.; Lee, M. L. *Chromatographia* **2002**, *55* (7–8), 399–403.
- (65) Lippert, J. A.; Xin, B.; Wu, N.; Lee, M. L. *J. Microcolumn Sep.* **1999**, *11* (9), 631–643.
- (66) Jerkovich, A. D.; Mellors, J. S.; Jorgenson, J. W. *LC-GC N. Am.* **2003**, *21* (7), 600–611.
- (67) Xiang, Y.; Maynes, D. R.; Lee, M. L. *J. Chromatogr. A* **2003**, *991* (2), 189–196.
- (68) Mazzeo, J. R.; Neue, U. D.; Kele, M.; Plumb, R. S. *Anal. Chem.* **2005**, 460–467.
- (69) Swartz, M. E. *Sep. Sci. Re-Defin. LCGC Suppl.* **2005**, *8*, 8–15.
- (70) Wyndham, K. D.; O’Gara, J. E.; Walter, T. H.; Glose, K. H.; Lawrence, N. L.; Alden, B. A.; Izzo, G. S.; Hudalla, C. J.; Iraneta, P. C. *Anal. Chem.* **2003**, *75* (24), 6781–6788.
- (71) Horvath, C. G.; Lin, H.-J. *J. Chromatogr. A* **1978**, *149*, 43–70.

- (72) de Villiers, A.; Lauer, H.; Szucs, R.; Goodall, S.; Sandra, P. *J. Chromatogr. A* **2006**, *1113* (1–2), 84–91.
- (73) Gritti, F.; Guiochon, G. *Anal. Chem.* **2008**, *80* (13), 5009–5020.
- (74) McCalley, D. V. *TrAC Trends Anal. Chem.* **2014**, *63*, 31–43.
- (75) Nováková, L.; Veuthey, J. L.; Guillarme, D. *J. Chromatogr. A* **2011**, *1218* (44), 7971–7981.
- (76) Fekete, S.; Schappler, J.; Veuthey, J.-L.; Guillarme, D. *TrAC Trends Anal. Chem.* **2014**, *63*, 2–13.
- (77) Walter, T. H.; Andrews, R. W. *TrAC Trends Anal. Chem.* **2014**, *63*, 14–20.
- (78) Broeckhoven, K.; Desmet, G. *TrAC Trends Anal. Chem.* **2014**, *63*, 65–75.
- (79) Sarrut, M.; Crétier, G.; Heinisch, S. *TrAC Trends Anal. Chem.* **2014**, *63*, 104–112.
- (80) Gritti, F.; Cavazzini, A.; Marchetti, N.; Guiochon, G. *J. Chromatogr. A* **2007**, *1157* (1–2), 289–303.
- (81) Ali, I.; AL-Othman, Z. A.; Al-Za'abi, M. *Biomed. Chromatogr.* **2012**, 1001–1008.
- (82) Horvath, C. G.; Preiss, B. A.; Lipsky, S. R. *Anal. Chem.* **1967**, *39* (12), 1422–1428.
- (83) Kirkland, J. J. *Anal. Chem.* **1969**, *41*, 218–220.
- (84) Kirkland, J. J.; Truszkowski, F. A.; Dilks Jr., C. H.; Engel, G. S. *J. Chromatogr. A* **2000**, *890*, 3–13.
- (85) Ruta, J.; Zurlino, D.; Grivel, C.; Heinisch, S.; Veuthey, J.-L.; Guillarme, D. *J. Chromatogr. A* **2012**, *1228*, 221–231.
- (86) Fekete, S.; Fekete, J.; Ganzler, K. *J. Pharm. Biomed. Anal.* **2009**, *49* (1), 64–71.
- (87) Gritti, F.; Leonardis, I.; Abia, J.; Guiochon, G. *J. Chromatogr. A* **2010**, *1217* (24), 3819–3843.
- (88) Fekete, S.; Olh, E.; Fekete, J. *J. Chromatogr. A* **2012**, *1228*, 57–71.
- (89) Guiochon, G.; Gritti, F. *J. Chromatogr. A* **2011**, *1218* (15), 1915–1938.
- (90) Hayes, R.; Ahmed, A.; Edge, T.; Zhang, H. *J. Chromatogr. A* **2014**, *1357*, 36–52.
- (91) Kirkland, J. J.; Schuster, S. A.; Johnson, W. L.; Boyes, B. E. *J. Pharm. Anal.* **2013**, *3* (5), 303–312.
- (92) DeStefano, J. J.; Schuster, S. A.; Lawhorn, J. M.; Kirkland, J. J. *J. Chromatogr. A* **2012**, *1258*, 76–83.
- (93) Gritti, F.; Guiochon, G. *J. Chromatogr. A* **2010**, *1217* (52), 8167–8180.
- (94) Gritti, F.; Guiochon, G. *J. Chromatogr. A* **2011**, *1218* (7), 907–921.
- (95) Gritti, F.; Guiochon, G. *J. Chromatogr. A* **2012**, *1252*, 31–44.
- (96) Gritti, F.; Guiochon, G. *J. Chromatogr. A* **2012**, *1252*, 45–55.
- (97) Gritti, F.; Guiochon, G. *J. Chromatogr. A* **2012**, *1252*, 56–66.
- (98) Gritti, F.; Guiochon, G. *J. Chromatogr. A* **2010**, *1217* (31), 5069–5083.
- (99) Horváth, K.; Gritti, F.; Fairchild, J. N.; Guiochon, G. *J. Chromatogr. A* **2010**, *1217* (41), 6373–6381.
- (100) Omamogho, J. O.; Hanrahan, J. P.; Tobin, J.; Glennon, J. D. *J. Chromatogr. A* **2011**, *1218* (15), 1942–1953.
- (101) Poppe, H.; Kraak, J. C. *J. Chromatogr. A* **1983**, *255*, 395–414.
- (102) DeStefano, J. J.; Langlois, T. J.; Kirkland, J. J. *J. Chromatogr. Sci.* **2008**, *46* (3), 254–260.
- (103) Cabooter, D.; Lestremau, F.; Lynen, F.; Sandra, P.; Desmet, G. *J. Chromatogr. A* **2008**, *1212* (1–2), 23–34.
- (104) Fekete, S.; Guillarme, D. *J. Chromatogr. A* **2013**, *1308*, 104–113.
- (105) Sanchez, A. C.; Friedlander, G.; Fekete, S.; Anspach, J.; Guillarme, D.; Chitty, M.; Farkas, T. *J. Chromatogr. A* **2013**, *1311*, 90–97.
- (106) Guillarme, D.; Ruta, J.; Rudaz, S.; Veuthey, J.-L. *Anal. Bioanal. Chem.* **2010**, *397* (3), 1069–1082.

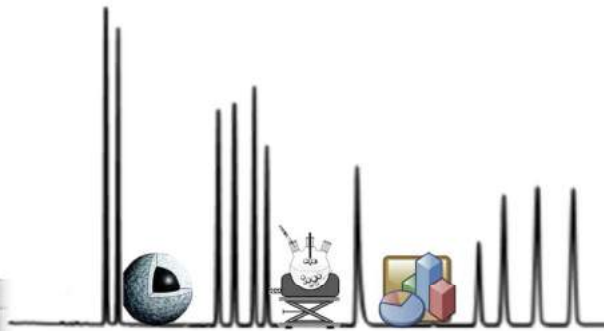
- (107) Snyder, L. R.; Kirkland, J. J.; Glajch, J. L. *Practical HPLC Method Development*, Wiley-Interscience.; New York, 1997.
- (108) Cai, S.-S.; Hanold, K. A.; Syage, J. A. *Anal. Chem.* **2007**, *79* (6), 2491–2498.
- (109) Zhang, M.; Chen, J.; Mallik, A. K.; Qiu, H.; Jiang, S.; Ihara, H. *Anal. Chim. Acta* **2014**, *833*, 48–55.
- (110) Li, Y.; Xu, L.; Chen, T.; Liu, X.; Xu, Z.; Zhang, H. *Anal. Chim. Acta* **2012**, *726*, 102–108.
- (111) Wilson, N. S.; Gilroy, J.; Dolan, J. W.; Snyder, L. R. *J. Chromatogr. A* **2004**, *1026* (1–2), 91–100.
- (112) Liu, X.; Bordunov, A. V.; Pohl, C. A. *J. Chromatogr. A* **2006**, *1119* (1–2), 128–134.
- (113) Rahman, M. M.; Takafuji, M.; Ansarian, H. R.; Ihara, H. *Anal. Chem.* **2005**, *77* (20), 6671–6681.
- (114) Omamogho, J. O.; Stack, E. M.; Santalad, A.; Srijaranai, S.; Glennon, J. D.; Yamen, H.; Albert, K. *Anal. Bioanal. Chem.* **2010**, *397* (6), 2513–2524.
- (115) Silva, C. R.; Jardim, I. C. S. F.; Airoidi, C. *J. Chromatogr. A* **2003**, *987* (1), 127–138.
- (116) Zhang, M.; Liang, X.; Jiang, S.; Qiu, H. *TrAC Trends Anal. Chem.* **2014**, *53*, 60–72.
- (117) O’Gara, J. E.; Alden, B. A.; Walter, T. H.; Petersen, J. S.; Niederlaender, C. L.; Neue, U. D. *Anal. Chem.* **1995**, *67* (20), 3809–3813.
- (118) Callahan, D. L.; Souza, D. D.; Basic, A.; Roessner, U. *J. Sep. Sci.* **2009**, *32* (13), 2273–2280.
- (119) Euerby, M. R.; Petersson, P. *J. Chromatogr. A* **2005**, *1088* (1–2), 1–15.
- (120) McCalley, D. V. *J. Chromatogr. A* **1999**, *844* (1), 23–38.
- (121) Lesellier, E.; West, C.; Tchaplal, A. *J. Chromatogr. A* **2006**, *1111* (1), 62–70.
- (122) Przybyciel, M. *LCGC Eur.* **2006**, *19–20*, 22–27.
- (123) Kloos, D.-P.; Lingeman, H.; Niessen, W. M. A.; Deelder, A. M.; Giera, M.; Mayboroda, O. *J. Chromatogr. B* **2013**, *927*, 90–96.
- (124) Schappler, J.; Nicoli, R.; Nguyen, D.; Rudaz, S.; Veuthey, J.-L.; Guilleme, D. *Talanta* **2009**, *78* (2), 377–387.
- (125) Peng, L.; Farkas, T. *J. Chromatogr. A* **2008**, *1179* (2), 131–144.
- (126) Karu, N.; Dicoski, G. W.; Haddad, P. R. *TrAC Trends Anal. Chem.* **2012**, *40*, 119–132.
- (127) Alpert, A. J. *J. Chromatogr. A* **1990**, *499*, 177–196.
- (128) McCalley, D. V. *J. Chromatogr. A* **2007**, *1171* (1–2), 46–55.
- (129) Hemström, P.; Irgum, K. *J. Sep. Sci.* **2006**, *29* (12), 1784–1821.
- (130) Buszewski, B.; Noga, S. *Anal. Bioanal. Chem.* **2012**, *402* (1), 231–247.
- (131) Tyteca, E.; Périat, A.; Rudaz, S.; Desmet, G.; Guilleme, D. *J. Chromatogr. A* **2014**, *1337*, 116–127.
- (132) Gama, M. R.; da Costa Silva, R. G.; Collins, C. H.; Bottoli, C. B. G. *TrAC Trends Anal. Chem.* **2012**, *37*, 48–60.
- (133) Guo, Y. *The Analyst* **2015**, *140* (19), 6452–6466.
- (134) *A Practical Guide to HILIC Mechanisms, Method Development and Troubleshooting*.
- (135) Espinosa, S.; Bosch, E.; Rosés, M. *J. Chromatogr. A* **2002**, *964*, 55–66.
- (136) Subirats, X.; Bosch, E.; Rosés, M. *J. Chromatogr. A* **2009**, *1216* (12), 2491–2498.
- (137) McCalley, D. V. *J. Chromatogr. A* **2015**, *1411*, 41–49.
- (138) Jandera, P. *Anal. Chim. Acta* **2011**, *692* (1–2), 1–25.
- (139) Kohler, I.; Periat, A. C.; Guilleme, D.; Veuthey, J.-L. *LC-GC Eur.* **2013**, 17–23.
- (140) Moni, L.; Ciogli, A.; D’Acquarica, I.; Dondoni, A.; Gasparrini, F.; Marra, A. *Chem. - Eur. J.* **2010**, *16* (19), 5712–5722.
- (141) Guo, Y.; Gaiki, S. *J. Chromatogr. A* **2011**, *1218* (35), 5920–5938.
- (142) Heaton, J. C.; Russell, J. J.; Underwood, T.; Boughtflower, R.; McCalley, D. V. *J. Chromatogr. A* **2014**, *1347*, 39–48.
- (143) Dinh, N. P.; Jonsson, T.; Irgum, K. *J. Chromatogr. A* **2011**, *1218* (35), 5880–5891.

- (144) Greco, G.; Letzel, T. *J. Chromatogr. Sci.* **2013**, 51 (7), 684–693.
- (145) Hao, Z.; Xiao, B.; Weng, N. *J. Sep. Sci.* **2008**, 31 (9), 1449–1464.
- (146) Ruta, J.; Rudaz, S.; McCalley, D. V.; Veuthey, J.-L.; Guillaume, D. *J. Chromatogr. A* **2010**, 1217 (52), 8230–8240.
- (147) Grumbach, E. S.; Wagrowski-Diehl, D. M.; Mazzeo, J. R.; Alden, B.; Iraneta, P. C. *LC GC Mag.-N. Am.-Solut. Sep. Sci.* **2005**, 20, 89–96.
- (148) Nguyen, H. P.; Schug, K. A. *J. Sep. Sci.* **2008**, 31 (9), 1465–1480.
- (149) Periat, A.; Boccard, J.; Veuthey, J.-L.; Rudaz, S.; Guillaume, D. *J. Chromatogr. A* **2013**, 1312, 49–57.
- (150) McCalley, D. V. *J. Chromatogr. A* **2008**, 1193 (1–2), 85–91.
- (151) Orlovsky, V.; Zelecbonok, Y. *Chromatogr. Today* **2011**, 24–28.
- (152) Wang, Q.; Ye, M.; Xu, L.; Shi, Z. *Anal. Chim. Acta* **2015**, 888, 182–190.
- (153) Qiao, X.; Zhang, L.; Zhang, N.; Wang, X.; Qin, X.; Yan, H.; Liu, H. *J. Chromatogr. A* **2015**, 1400, 107–116.
- (154) Bicker, W.; Lämmerhofer, M.; Lindner, W. *Anal. Bioanal. Chem.* **2008**, 390 (1), 263–266.
- (155) Lämmerhofer, M.; Richter, M.; Wu, J.; Nogueira, R.; Bicker, W.; Lindner, W. *J. Sep. Sci.* **2008**, 31 (14), 2572–2588.
- (156) Liu, X.; Pohl, C. *Am. Lab.* **2007**, 39, 2572–2588.
- (157) Kirkland, J. J.; Henderson, J. W.; DeStefano, J. J.; van Straten, M. A.; Claessens, H. A. *J. Chromatogr. A* **1997**, 762 (1–2), 97–112.
- (158) Sander, L. C.; Wise, S. A. *J. Chromatogr. A* **1984**, 316, 163–181.
- (159) Cox, G. B. *J. Chromatogr. A* **1993**, 656 (1), 353–367.
- (160) Barrett, D. A.; Brown, V. A.; Watson, R. C.; Davies, M. C.; Shaw, P. N.; Ritchie, H. J.; Ross, P. *J. Chromatogr. A* **2001**, 905 (1–2), 69–83.
- (161) Grossmann, F.; Ehwald, V.; von Hohenesche, C. du F.; Unger, K. K. *J. Chromatogr. A* **2001**, 910 (2), 223–236.
- (162) Pesek, J. J.; Matyska, M. T.; Sandoval, J. E.; Williamsen, E. J. *J. Liq. Chromatogr. Relat. Technol.* **1996**, 19 (17–18), 2843–2865.
- (163) Sandoval, J. E.; Pesek, J. J. *Anal. Chem.* **1991**, 63 (22), 2634–2641.
- (164) Chu, C. H.; Jonsson, E.; Auvinen, M.; Pesek, J. J.; Sandoval, J. E. *Anal. Chem.* **1993**, 65 (6), 808–816.
- (165) Matyska, M. T.; Pesek, J. J. *J. Chromatogr. A* **2005**, 1079 (1–2), 366–371.
- (166) Pesek, J. J.; Matyska, M. T.; Williamsen, E. J.; Evanchic, M.; Hazari, V.; Konjuh, K.; Takhar, S.; Tranchina, R. *J. Chromatogr. A* **1997**, 786 (2), 219–228.
- (167) Lork, K. D.; Unger, K. K.; Kinkel, J. N. *J. Chromatogr. A* **1986**, 352, 199–211.
- (168) Kirkland, J. J.; Glajch, J. L.; Farlee, R. D. *Anal. Chem.* **1989**, 61 (1), 2–11.
- (169) Scott, R. P. W. *Silica gel and bonded phases: their production, properties and use in LC*; John Wiley and Sons: England, 1993.
- (170) Unger, K. K.; Becker, N.; Roumeliotis, P. *J. Chromatogr. A* **1976**, 125 (1), 115–127.
- (171) Berendsen, G. E.; Pikaart, K. A.; Galan, L. de. *J. Liq. Chromatogr.* **1980**, 3 (10), 1437–1464.
- (172) Kirkland, J. J.; Henderson, J. W. *J. Chromatogr. Sci.* **1994**, 32 (11), 473–480.
- (173) Sander, L. C.; Wise, S. A.; Lochmüller, C. H. *C R C Crit. Rev. Anal. Chem.* **1987**, 18 (4), 299–417.
- (174) Engelhardt, H.; Dreyer, B.; Schmidt, H. *Chromatographia* **1982**, 16 (1), 11–17.
- (175) Sunseri, J. D. *Synthetic Strategies to Improve Silica-Based Stationary Phases for Reversed-Phase Liquid Chromatography*, Florida State University, 2003.
- (176) Kinkel, J. N.; Unger, K. K. *J. Chromatogr. A* **1984**, 316, 193–200.
- (177) Sentell, K. B.; Barnes, K. W.; Dorsey, J. G. *J. Chromatogr. A* **1988**, 455, 95–104.
- (178) Corey, E. J.; Cho, H.; Rücker, C.; Hua, D. H. *Tetrahedron Lett.* **1981**, 22 (36), 3455–3458.

- (179) Erard, J.-F.; Nagy, L.; Kovats, E. sz. *Colloids Surf.* **1984**, 9 (2), 109–132.
- (180) Schomburg, G.; Deege, A.; Köhler, J.; Bien-Vogelsang, U. *J. Chromatogr. A* **1983**, 282, 27–39.
- (181) Kirkland, J. J.; van Straten, M. A.; Claessens, H. A. *J. Chromatogr. A* **1995**, 691 (1–2), 3–19.
- (182) Deuel, H.; Wartmann, J.; Hutschneker, K.; Schobinger, U.; Güdel, C. *Helv. Chim. Acta* **1959**, 42 (4), 1160–1165.
- (183) Unger, K. K.; Thomas, W.; Adrian, P. *Kolloid ZZ Polym* **1973**, No. 251, 45.
- (184) Unger, K. K.; Gallei, E. *Kolloid-Z Z Polym* **1970**, 237, 358.
- (185) Colin, H.; Guiochon, G. *J. Chromatogr. A* **1977**, 141 (3), 289–312.
- (186) Nahum, A.; Horváth, C. *J. Chromatogr. A* **1981**, 203, 53–63.
- (187) Bij, K. E.; Horváth, C.; Melander, W. R.; Nahum, A. *J. Chromatogr. A* **1981**, 203, 65–84.
- (188) Peri, J. B.; Hensley, A. L. *J. Phys. Chem.* **1968**, 72 (8), 2926–2933.
- (189) Zhuravlev, L. T. *Colloids Surf. Physicochem. Eng. Asp.* **2000**, 173 (1), 1–38.
- (190) Köhler, J.; Chase, D. B.; Farlee, R. D.; Vega, A. J.; Kirkland, J. J. *J. Chromatogr. A* **1986**, 352, 275–305.
- (191) Boudreau, S. P.; Cooper, W. T. *Anal. Chem.* **1989**, 61 (1), 41–47.
- (192) Halfpenny, D. R.; Kane, D. M.; Lamb, R. N.; Gong, B. *Appl. Phys. A* **2000**, 71 (2), 147–151.
- (193) Godfrey, S. P.; Badyal, J. P. S.; Little, I. R. *J. Phys. Chem. B* **2001**, 105 (13), 2572–2577.
- (194) Welsch, T.; Frank, H.; Vigh, G. *J. Chromatogr. A* **1990**, 506, 97–108.
- (195) Akapo, S. O.; Dimandja, J.-M. D.; Matyska, M. T.; Pesek, J. J. *Anal. Chem.* **1996**, 68 (11), 1954–1959.
- (196) Pesek, J. J.; Matyska, M. T.; Yu, R. J. *J. Chromatogr. A* **2002**, 947 (2), 195–203.
- (197) Pryde, A. *J. Chromatogr. Sci.* **1974**, 12 (9), 486–498.
- (198) Murtrey, K. D. M. *J. Liq. Chromatogr.* **1988**, 11 (16), 3375–3384.
- (199) Marshall, D. B.; Cole, C. L.; Norman, A. D. *J. Chromatogr. Sci.* **1987**, 25 (6), 262–266.
- (200) Engelhardt, H.; Müller, H. *Chromatographia* **1984**, 19 (1), 77–84.
- (201) Karch, K.; Sebestian, I.; Halász, I. *J. Chromatogr. A* **1976**, 122, 3–16.
- (202) Sudo, Y. *J. Chromatogr. A* **1996**, 737 (2), 139–147.
- (203) Pesek, J. J.; Matyska, M. T. *J. Chromatogr. A* **2002**, 952 (1–2), 1–11.
- (204) Duez, P.; Chamart, S.; Hanocq, M.; Molle, L.; Vanhaelen, M.; Vanhaelen-Fastré, R. *J. Chromatogr. A* **1985**, 329, 415–421.
- (205) Leach, D. C.; Stadalius, M. A.; Berrus, J. S.; Snyder, L. R. *LC GC* **1988**, 1, 22–30.
- (206) Neue, U. D.; Van Tran, K.; Iraneta, P. C.; Alden, B. A. *J. Sep. Sci.* **2003**, 26 (3–4), 174–186.
- (207) Nawrocki, J. *J. Chromatogr. A* **1997**, 779 (1–2), 29–71.
- (208) Vervoort, R. J. M.; Maris, F. A.; Hindriks, H. *J. Chromatogr. A* **1992**, 623 (2), 207–220.
- (209) Vervoort, R. J. M.; Derksen, M. W. J.; Debets, A. J. *J. Chromatogr. A* **1997**, 765 (2), 157–168.
- (210) McCalley, D. V. *J. Chromatogr. A* **1993**, 636 (2), 213–220.
- (211) McCalley, D. V. *Analyst* **1990**, 115 (10), 1355–1358.
- (212) Cole, S. R.; Dorsey, J. G. *Biomed. Chromatogr.* **1997**, 11 (3), 167–171.
- (213) Reta, M.; Carr, P. W. *J. Chromatogr. A* **1999**, 855 (1), 121–127.
- (214) Horvath, C.; Melander, W.; Molnar, I. *Anal. Chem.* **1977**, 49 (1), 142–154.
- (215) Wehrli, A.; Hildenbrand, J. C.; Keller, H. P.; Stampfli, R.; Frei, R. W. *J. Chromatogr. A* **1978**, 149, 199–210.
- (216) Claessens, H. A.; van Straten, M. A.; Kirkland, J. J. *J. Chromatogr. A* **1996**, 728 (1–2), 259–270.
- (217) Tindall, G. W.; Perry, R. L. *J. Chromatogr. A* **2003**, 988 (2), 309–312.

- (218) Kirkland, J. J.; van Straten, M. A.; Claessens, H. A. *J. Chromatogr. A* **1998**, 797 (1–2), 111–120.
- (219) de Monredon, S. Interaction Organosilanes/Silice de précipitation. Du milieu hydro-alcoolique au milieu aqueux, Paris VI, 2004.
- (220) Brunauer, S.; Emmett, P. H.; Teller, E. *J. Am. Chem. Soc.* **1938**, 60 (2), 309–319.
- (221) Souteyrand, C.; Thibert, M.; Caude, M.; Rosset, R. *J. Chromatogr. A* **1983**, 262, 1–18.
- (222) Souteyrand, C.; Thibert, M.; Caude, M.; Rosset, R. *J. Chromatogr. A* **1984**, 316, 373–388.
- (223) Bather, J. M.; Gray, R. A. C. *J. Chromatogr. A* **1976**, 122, 159–169.
- (224) Ek, S.; Root, A.; Peussa, M.; Niinistö, L. *Thermochim. Acta* **2001**, 379 (1–2), 201–212.
- (225) Blitz, J. P.; Murthy, R. S. S.; Leyden, D. E. *J. Am. Chem. Soc.* **1987**, 109 (23), 7141–7145.
- (226) Zhao, X. S.; Lu, G. Q. *J. Phys. Chem. B* **1998**, 102 (9), 1556–1561.
- (227) Gonzalez-Benito, J.; Cabanelas, J. C.; Aznar, A. J.; Vigil, M. R.; Bravo, J.; Baselga, J. *J. Appl. Polym. Sci.* **1996**, 62 (2), 375–384.
- (228) Ramos, M. A.; Gil, M. H.; Schacht, E.; Matthys, G.; Mondelaers, W.; Figueiredo, M. M. *Powder Technol.* **1998**, 99 (1), 79–85.
- (229) Xu, D.; Sun, L.; Li, H.; Zhang, L.; Guo, G.; Zhao, X.; Gui, L. *New J. Chem.* **2003**, 27 (2), 300–306.
- (230) Zettlemoyer, A. C.; Hsing, H. H. *J. Colloid Interface Sci.* **1977**, 58 (2), 263–274.
- (231) Maciel, G. E.; Sindorf, D. W. *J. Am. Chem. Soc.* **1980**, 102 (25), 7606–7607.
- (232) Sindorf, D. W.; Maciel, G. E. *J. Am. Chem. Soc.* **1983**, 105 (6), 1487–1493.
- (233) Sindorf, D. W.; Maciel, G. E. *J. Phys. Chem.* **1982**, 86 (26), 5208–5219.
- (234) Sindorf, D. W.; Maciel, G. E. *J. Phys. Chem.* **1983**, 87 (26), 5516–5521.
- (235) Bermudez, V. M. *J. Phys. Chem.* **1971**, 75 (21), 3249–3257.
- (236) Haukka, S.; Lakomaa, E. L.; Root, A. *J. Phys. Chem.* **1993**, 97 (19), 5085–5094.
- (237) Morrow, B. A.; McFarlan, A. J. *Langmuir* **1991**, 7 (8), 1695–1701.
- (238) Zhao, X. S.; Lu, G. Q.; Whittaker, A. K.; Millar, G. J.; Zhu, H. Y. *J. Phys. Chem. B* **1997**, 101 (33), 6525–6531.
- (239) Dugas, V.; Chevalier, Y. *J. Colloid Interface Sci.* **2003**, 264 (2), 354–361.
- (240) Tripp, C. P.; Hair, M. L. *Langmuir* **1992**, 8 (4), 1120–1126.
- (241) Tripp, C. P.; Hair, M. L. *Langmuir* **1995**, 11 (4), 1215–1219.
- (242) Bjelopavlic, M.; Singh, P. K.; El-Shall, H.; Moudgil, B. M. *J. Colloid Interface Sci.* **2000**, 226 (1), 159–165.
- (243) Gun'ko, V. M.; Vedamuthu, M. S.; Henderson, G. L.; Blitz, J. P. *J. Colloid Interface Sci.* **2000**, 228 (1), 157–170.
- (244) Snyder, L. R.; Ward, J. W. *J. Phys. Chem.* **1966**, 70 (12), 3941–3952.
- (245) Haukka, S.; Root, A. *J. Phys. Chem.* **1994**, 98 (6), 1695–1703.
- (246) Chmielowiec, J.; Morrow, B. A. *J. Colloid Interface Sci.* **1983**, 94 (2), 319–327.
- (247) Garbassi, F.; Balducci, L.; Chiurlo, P.; Deiana, L. *Appl. Surf. Sci.* **1995**, 84 (2), 145–151.
- (248) Ghanbari-Siahkali, A.; Philippou, A.; Dwyer, J.; Anderson, M. W. *Appl. Catal. Gen.* **2000**, 192 (1), 57–69.
- (249) Huang, W.; Huang, Y.; Zunzhao, Y. *Chin. J. Polym. Sci.* **2000**, 18, 51–55.
- (250) Suratwala, T. I.; Hanna, M. L.; Miller, E. L.; Whitman, P. K.; Thomas, I. M.; Ehrmann, P. R.; Maxwell, R. S.; Burnham, A. K. *J. Non-Cryst. Solids* **2003**, 316 (2–3), 349–363.
- (251) Sutra, P.; Fajula, F.; Brunel, D.; Lentz, P.; Daelen, G.; Nagy, J. B. *Colloids Surf. Physicochem. Eng. Asp.* **1999**, 158 (1–2), 21–27.
- (252) Bauer, F.; Freyer, A.; Ernst, H.; Gläsel, H.-J.; Mehnert, R. *Appl. Surf. Sci.* **2001**, 179 (1–4), 118–121.
- (253) Hohenberg, P.; Kohn, W. *Phys. Rev.* **1964**, 136 (3B), B864–B871.
- (254) Kohn, W.; Sham, L. J. *Phys. Rev.* **1965**, 140 (4A), A1133–A1138.

- (255) Chung, L. W.; Sameera, W. M. C.; Ramozzi, R.; Page, A. J.; Hatanaka, M.; Petrova, G. P.; Harris, T. V.; Li, X.; Ke, Z.; Liu, F.; Li, H.-B.; Ding, L.; Morokuma, K. *Chem. Rev.* **2015**, *115* (12), 5678–5796.
- (256) Jimidar, M.; Bourguignon, B.; Massart, D. L. *J. Chromatogr. A* **1996**, *740* (1), 109–117.
- (257) Dolan, J. W.; Snyder, L. R. *J. Chromatogr. A* **2009**, *1216* (16), 3467–3472.
- (258) Claessens, H. A. *TrAC Trends Anal. Chem.* **2001**, *20* (10), 563–583.
- (259) Cruz, E.; Euerby, M. R.; Johnson, C. M.; Hackett, C. A. *Chromatographia* **1997**, *44* (3–4), 151–161.
- (260) Visky, D.; Vander Heyden, Y.; Iványi, T.; Baten, P.; De Beer, J.; Kovács, Z.; Noszál, B.; Dehouck, P.; Roets, E.; Massart, D. L.; Hoogmartens, J. *J. Chromatogr. A* **2003**, *1012* (1), 11–29.
- (261) Snyder, L. R.; Dolan, J. W.; Carr, P. W. *J. Chromatogr. A* **2004**, *1060* (1–2), 77–116.
- (262) Abraham, M. H.; Ibrahim, A.; Zissimos, A. M. *J. Chromatogr. A* **2004**, *1037* (1–2), 29–47.
- (263) Taft, R. W.; Abboud, J.-L. M.; Kamlet, M. J.; Abraham, M. H. *J. Solut. Chem.* **1985**, *14* (3), 153–186.
- (264) Engelhardt, H.; Jungheim, M. *Chromatographia* **1990**, *29* (1–2), 59–68.
- (265) Kimata, K.; Iwaguchi, K.; Onishi, S.; Jinno, K.; Eksteen, R.; Hosoya, K.; Araki, M.; Tanaka, N. *J. Chromatogr. Sci.* **1989**, *27*, 721–728.
- (266) Stella, C.; Rudaz, S.; Veuthey, J.-L.; Tchaplá, A. *Chromatographia* **2001**, *53* (1), S113–S131.
- (267) Stella, C.; Rudaz, S.; Veuthey, J.-L.; Tchaplá, A. *Chromatographia* *53* (1), S132–S140.
- (268) Stella, C.; Seuret, P.; Rudaz, S.; Tchaplá, A.; Gauthier, J.-Y.; Lanteri, P.; Veuthey, J.-L. *Chromatographia* **2002**, *56* (11–12), 665–671.
- (269) Lesellier, E.; West, C. *J. Chromatogr. A* **2007**, *1158* (1–2), 329–360.
- (270) Lesellier, E.; West, C. *J. Chromatogr. A* **2008**, *1181* (1–2), 166.
- (271) Neue, U. D. *J. Sep. Sci.* **2007**, *30* (11), 1611–1627.
- (272) Galea, C.; Mangelings, D.; Vander Heyden, Y. *Anal. Chim. Acta* **2015**, *886*, 1–15.
- (273) Sander, L. C.; Wise, S. A. *J. High Resolut. Chromatogr.* **1988**, *11* (5), 383–387.
- (274) Neue, U. D.; Alden, B. A.; Walter, T. H. *J. Chromatogr. A* **1999**, *849* (1), 101–116.
- (275) Neue, U. D.; Serowik, E.; Iraneta, P.; Alden, B. A.; Walter, T. H. *J. Chromatogr. A* **1999**, *849* (1), 87–100.
- (276) Layne, J. *J. Chromatogr. A* **2002**, *957* (2), 149–164.
- (277) Sándi, Á.; Bede, Á.; Szepes, L.; Rippel, G. *Chromatographia* **1997**, *45* (1), 206–214.
- (278) Bączek, T.; Kaliszan, R.; Novotná, K.; Jandera, P. *J. Chromatogr. A* **2005**, *1075* (1–2), 109–115.
- (279) Kaliszan, R.; van Straten, M. A.; Markuszewski, M.; Cramers, C. A.; Claessens, H. A. *J. Chromatogr. A* **1999**, *855* (2), 455–486.
- (280) Héberger, K. *J. Chromatogr. A* **2007**, *1158* (1–2), 273–305.
- (281) West, C.; Lesellier, E. *J. Chromatogr. A* **2008**, *1191* (1–2), 21–39.
- (282) Oumada, F. Z.; Rosés, M.; Bosch, E.; Abraham, M. H. *Anal. Chim. Acta* **1999**, *382* (3), 301–308.
- (283) Tan, L. C.; Carr, P. W.; Abraham, M. H. *J. Chromatogr. A* **1996**, *752* (1–2), 1–18.
- (284) Mitchell, C. R.; Benz, N. J.; Zhang, S. *J. Sep. Sci.* **2010**, *33* (19), 3060–3067.
- (285) Li, J.; Dallas, A. J.; Carr, P. W. *J. Chromatogr. A* **1990**, *517*, 103–121.
- (286) West, C.; Zhang, Y.; Morin-Allory, L. *J. Chromatogr. A* **2011**, *1218* (15), 2019–2032.
- (287) Lesellier, E. *J. Sep. Sci.* **2008**, *31* (8), 1238–1251.
- (288) Park, J. H.; Yoon, M. H.; Ryu, Y. K.; Kim, B. E.; Ryu, J. W.; Jang, M. D. *J. Chromatogr. A* **1998**, *796* (2), 249–258.
- (289) Pearson, K. *Philos. Mag. Ser. 6* **1901**, *2* (11), 559–572.



CHAPTER II

Conventional reversed-phase stationary phases

Introduction

This second chapter gathers the results obtained during my thesis concerning the silica surface pretreatment, the grafting of silica particles, especially superficially porous particles. Also, for each new stationary phase, the full characterization of the modified silica particles have been done through different and complementary physico-chemical methods. The packing step is one of the critical stages that directly impacts the efficiency. This step was achieved by Interchim as the company mastered the column packing. We could then estimate that the chromatographic properties of the new stationary phases were independent of the packing quality.

The first study is focused on the development of an efficient route to graft superficially porous silica particles, to successfully obtain various surface chemistries and so different stationary phase selectivities (II.1.1). The choice of the organosilane, and the advantages of using microwave irradiations were particularly highlighted. This methodologic approach was published in *Chromatographia* in 2014.

Then, the impact of thermal pretreatment on silica particles was investigated and led to three publications. The first study published in *Journal of Chromatography, A* in 2015 presents the potential of thermal pretreatment of silica to select the silanol population and finally give access, after organosilanization, a new range of C18 stationary phases starting from the same silica batch (II.2.1). Chemometric approaches allowed for differentiating the C18 pool, and highlighted the specificity of the high temperature pretreated C18 silica.

A concrete application of its unique selectivity is presented, in the context of phenanthrene ultra-purification (II.2.2). This stationary phase presented unique chromatographic properties that allowed baseline resolution of the critical pair phenanthrene/anthracene in a matrix constituted of phenanthrene 98% with some impurities to be quantified at very low level. This study was published in *Chemical Engineering and Technologies* in 2016.

Finally, starting from the same silica batch and without any further grafting, the different pretreatment temperatures applied on silica led to various stationary phases that could be used in HILIC mode. The kinetic performances and the applications of the different pretreated silicas

(II.2.3) were investigated during an internship with Prof. Jean-Luc Veuthey and Dr. Davy Guillarme, LCAP, Université de Genève. The results were published in Journal of Separation Science in 2016.

II-1. Microwave organosilanization of silica

The first part of this work was devoted to the development of a fast, efficient, and reproducible grafting method that could be transposed at the industrial scale. First, we focused on the grafting of an alkyl chain containing 18 carbons (C18) onto the silica surface. As it is the common SP used in RP-mode, C18 is a reference and can be considered as the flagship product of any SP range.

Two pathways were tested: the first one, reported in the literature relied on silanization followed by hydrosilation, as presented in section I.3.2.4. It was compared to the second one, established in collaboration with the company Interchim, as referred to organosilanization (I.3.2.2). Also, two grafting modes were evaluated: under conventional heating and microwave irradiation procedure.

Grafted silicas were fully characterized by several techniques presented in section I.4: elemental analysis, DRIFT, solid state CP/MAS NMR, microscopy, and the chromatographic properties were evaluated by mean of the Tanaka test presented in section I.6.1.3.

Such studies and evaluation led to the first article entitled "High-Density Octadecyl Chemically Bonded Core–Shell Silica Phases for HPLC: Comparison of Microwave-Assisted and Classical Synthetic Routes, Structural Characterization and Chromatographic Evaluation" published in *Chromatographia* in 2014.

II-1-1. Article 1: Around the development of a fast, efficient, and reproducible grafting method for C18 functionalization of bare silica SPP.

Chromatographia (2014) 77:1577–1588
DOI 10.1007/s10337-014-2802-x

ORIGINAL

High-Density Octadecyl Chemically Bonded Core–Shell Silica Phases for HPLC: Comparison of Microwave-Assisted and Classical Synthetic Routes, Structural Characterization and Chromatographic Evaluation

Mélanie Mignot · Alain Tchaplà · Olivier Mercier ·
Nicolas Couvrat · Séverine Tisse · Pascal Cardinael ·
Valérie Peulon-Agasse

Received: 4 July 2014 / Revised: 5 September 2014 / Accepted: 25 September 2014 / Published online: 14 November 2014
© Springer-Verlag Berlin Heidelberg 2014

Abstract In this study, different grafting methods were examined to develop high-density chemically modified octadecyl core–shell silica particles for HPLC applications. The influence of the reagents and the experimental conditions were evaluated, either through conventional heating or by microwave irradiation. For both experimental synthetic processes, chemically bonded phases were prepared by grafting the functionalized silane (octadecyldimethylchlorosilane or octadecyldimethyl(dimethylamino)silane) and, on the other hand, using a hydrosilylation procedure. The bonded silica phases were fully characterized by elemental analysis, diffuse-reflectance infrared Fourier transform (DRIFT) spectroscopy, ^{29}Si cross-polarization magic angle spinning NMR and ^1H magic angle spinning NMR; and the granulometric distribution was evaluated by SEM. The maximum grafting rate ($4.4 \mu\text{mol m}^{-2}$) was determined by direct silylation with hexamethyldisilazane. The best grafting rate ($3.8 \mu\text{mol m}^{-2}$) for octadecyl functionalization was obtained

using octadecyldimethyl(dimethylamino)silane. The Tanaka test was used to estimate the chromatographic behavior of the overall set of synthesized bonded stationary phases, and their chromatographic performances were compared with similar columns available on the market. In this article, we used microwave irradiation methods to drastically reduce the reaction time for a comparable grafting rate and equivalent chromatographic performances.

Keywords High-performance liquid chromatography · Core–shell silica · C18 chemically bonded phase · Microwave irradiation · Octadecylsilane · Stationary phase

Introduction

Various silica-based columns packed with chemically bonded phases (CBPs) have been developed to improve the chromatographic selectivity and enhance the analytical capability of reversed-phase liquid chromatography (RP-HPLC). The packing materials in liquid chromatography can be divided into three groups: polymeric, inorganic and hybrid materials. However, silica remains the mainstay of CBPs because of its unique properties, including its high surface area, high mechanical stability and controllable pore structure. Nevertheless, this inorganic material presents some drawbacks, such as poor pH stability, which can limit its applications. Fully porous spherical silica is widely used as a support in the preparation of CBPs. Pellicular silica particles named, i.e., core–shell or fused core or superficially porous particles, were developed in the late 1960s to improve column efficiency and to reduce band dispersion in the column [1].

According to Guiochon et al. [2], the success of this type of particles can be explained by the resulting low minimum-reduced plate height of their packed columns, which

Electronic supplementary material The online version of this article (doi:10.1007/s10337-014-2802-x) contains supplementary material, which is available to authorized users.

M. Mignot · N. Couvrat · S. Tisse · P. Cardinael ·
V. Peulon-Agasse (✉)
UR, EA3233, Sciences et Méthodes Séparatives,
FR3038, IRCOF, Normandie Univ, rue Tesnières,
76821 Mont-Saint-Aignan Cedex, France
e-mail: valerie.agasse@univ-rouen.fr

A. Tchaplà
Univ Paris-Sud Groupe de Chimie Analytique de Paris-Sud-
LETIAM-EA 4041-IUT d'Orsay- Plateau de Moulon-Orsay,
91400 Orsay, France

O. Mercier
Interchim R & D, 211 bis avenue JF Kennedy, BP 1140,
03100 Montluçon, France

are in the range of 1.2–1.5 instead of near 2.0 for the same columns packed with fully porous particles. Consequently, this type of material is the best solution to improve the sensitivity, the resolution and to decrease the analysis time with high efficiency for a conventional HPLC instrument [3, 5].

The bondage efficiency of silica using different silanization reagents to chemically modify core-shell silica particles under conventional heating or microwave irradiation has not yet been compared.

In the literature, monofunctional reagents have been used to avoid the polymerization or the formation of a complex architecture resulting in a partial silanization of the silanol groups on the surface [6–8]. In this study, two monofunctional octadecylsilanes with different reactive groups were investigated. *n*-octadecyldimethylchlorosilane (ODMCS) was compared to *n*-octadecyldimethyl(dimethyl amino)silane (ODMAS), which was the most efficient reagent [9, 10] for the preparation of well-defined and densely covered silica particles [11]. Another method described by Pesek et al. [12] involved bonding hydrocarbon chains onto silica through a direct silicon-carbon linkage via hydrosilylation using the Speier catalyst.

The use of microwave activation was motivated by the specific absorption of microwave energy by silicon. As a result of an intrinsic property, this absorption leads to confined heating near the surface of the material. The selective heating of the substrate was expected to influence the course and the rate of the silanization reaction at the surface. For a large-scale batch, there are several large laboratory microwave systems available, which use a variety of approaches to achieve kilogram scale; parallel vessels, stopped-flow and continuous-flow, large vessel content, for example, although some of them have inherent limitations and the choice depends on the application. An additional key point in processing comparatively large volumes under pressure in a microwave field is the safety aspect, as any malfunction or rupture of a large pressurized reaction vessel will have a significant impact. Many efforts are still in progress to achieve large-scale reactors with good batch to batch reproducibility, in safety [13].

There are only few reports on the use of microwave irradiation to graft organic functional groups onto silica surfaces [14–16]. For the hydrosilylation procedure, microwave-assisted chemical functionalization was previously used for undecene grafting [17] onto hydride-modified porous silica without the platinum catalyst. In this study, the three synthetic routes (ODMAS grafting, ODMCS grafting, hydrosilylation) were applied using conventional heating and microwave irradiation. Previous surface activation [18] by acid treatment and the influence of an end-capping reaction were also evaluated following the grafting rate and the chromatographic properties.

The primary goal of this study was to compare the functionalization of core-shell silica particles into C18-bonded silica using conventional heating and a microwave irradiation method for RP-HPLC applications. The starting core-shell particles and the bonded particles were investigated by SEM. The degree of coverage was determined by elemental analysis. The presence of the specific vibrational bands of the organic moiety linked to the surface was followed by diffuse-reflectance infrared Fourier transform (DRIFT) spectroscopy. The confirmation of covalent bonding onto the silica surface and the distribution of the C18 chain linked to the different silicon atoms were obtained by ^{29}Si cross-polarization magic angle spinning (CP/MAS) NMR and by ^1H magic angle spinning (MAS) NMR. Finally, the chromatographic properties of the columns packed with the C18-core-shell silica particles were studied via the Tanaka test [19].

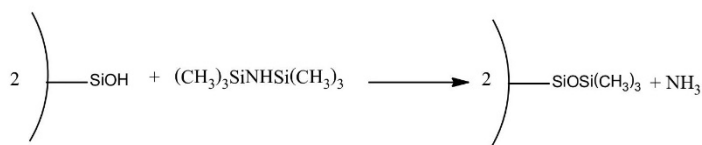
Experimental

Chemicals

The core-shell silica particles were provided by Interchim (Montluçon, France); their specific surface area, nominal particle diameter and pore diameter were $126\text{ m}^2\text{ g}^{-1}$, $2.6\text{ }\mu\text{m}$ and $90\text{ }\text{Å}$, respectively. Dichloromethane was purchased from VWR (Fontenay-sous-Bois, France) and was distilled with phosphorus pentoxide. Aminotriethoxysilane was purchased from Lancaster (WI, USA), and chloroplatinic acid hexahydrate was acquired from Strem Chemicals (Bischheim, France). *n*-octadecyldimethyl(dimethylamino)silane (ODMAS), *n*-octadecyldimethylchlorosilane (ODMCS), bis(dimethylamino)dimethylsilane (BMMS), imidazole and hexamethyldisilazane (HMDS) were obtained from ABCR (Karlsruhe, Germany). Toluene, benzylamine (B), phenol (P), caffeine (C), octadecene and uracil were supplied by Sigma-Aldrich (Saint-Quentin Fallavier, France). Butylbenzene (BB), triphenylene (T) and *o*-terphenyl (O) were purchased from Alfa Aesar (Schiltigheim, France). Methanol, toluene, tetrahydrofuran, acetonitrile, pentylbenzene (PB) and ether were purchased from VWR (Fontenay-sous-Bois, France). All of the solvents were of HPLC quality.

Materials

The columns ($4.6\text{ mm} \times 50\text{ mm}$) were packed by Interchim and were compared to various commercial columns, including a Halo C18 column from Advanced Materials Technology (Wilmington, DE, USA), a Poroshell ES-C18 column from Agilent-Technologies-France (Courtaboeuf, France) and an Accucore C18 column from Thermo Fisher Scientific-France (Courtaboeuf, France).

Scheme 1 Silanization with HMDS**Apparatus**

Carbon analysis by the conventional combustion method was performed using a Flash 2,000 organic elemental analyzer from Thermo Scientific.

The DRIFT spectra were obtained using a PerkinElmer (Norwalk, CT, USA) Spectrum 100. The sample consisted of a mixture of silica with potassium bromide [10 % (m/m) in KBr] placed in a 2-mm-diameter cup. The spectra, which consisted of 64 scans, were acquired at a resolution of 2 cm^{-1} and were referenced against pure KBr over the range $4,000\text{--}450 \text{ cm}^{-1}$.

SEM images were obtained using a JEOL JCM 5,000 NeoScope (München, Germany) operated at an accelerating voltage of 15 kV. The magnification was approximately $440\times$ and $20,000\times$. The powder samples were stabilized on analyzing plots using conductive adhesives; they were subsequently coated with gold using a NeoCoater MP-19020NCTR to reduce charge accumulation during the observations.

The ^{29}Si CP/MAS NMR measurements were performed with a Bruker (Wissembourg, France) DSX 400 spectrometer equipped with a 4-mm MAS probe. The magic angle spinning was performed at 10 kHz, and 12,288 scans were collected for each sample. The ^1H 90° pulses and contact times were 3.05 s and 5 ms, respectively, with a repetition time of 5 s. High-speed ^1H MAS NMR measurements were performed with a Bruker DSX 400 spectrometer equipped with a 2.5-mm probe. The sample spinning rate was 30 kHz, the 90° pulse length was 3.25 s, the repetition time was 5 s and 128 scans were collected for each sample. All chemical shifts were referenced to tetramethylsilane (TMS).

The syntheses were performed in a CEM (Buckingham, UK) Discover microwave at 2,450 MHz. The power delivery system was adjusted during the reaction with a maximum of 300 W. The instrument was monitored with a touch-screen control panel.

The chromatographic measurements were performed with a liquid chromatograph from Thermo-Fisher-Scientific, which consisted of a P680 pump, an injection valve (ASI-100 automated sample injector) equipped with a 20- μL injection loop, and a model UVD 340U diode array detector (DAD). The column temperature was controlled with a TCC-100 thermostated column compartment. The data were collected in a computer using the Chromeleon software.

Chemical Bonding Procedures

Each bonding procedure was performed three times. Two columns were packed for each bonding procedure, except for the HMDS grafting. As the results were similar, the chromatographic performances of one column for each bonding procedure were presented.

Activation of Silanols

In a 1-L three-necked round-bottom flask equipped with a condenser and a mechanical stirrer, 10 g of core-shell silica and 500 mL of a solution $\text{H}_2\text{O}/\text{HNO}_3/\text{H}_2\text{SO}_4$ 7/2/1 (v/v/v) were added. The mixture was heated at 100°C for 24 h. After being rinsed with H_2O until neutral, the silica was filtered and dried at 110°C for 12 h under vacuum.

Conventional HMDS Grafting (Scheme 1)

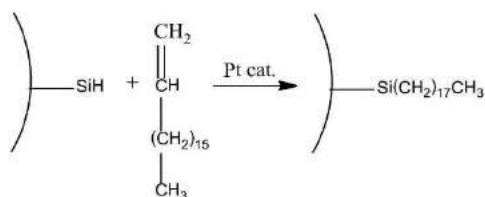
In a 500-mL three-necked round-bottom flask equipped with a mechanical stirrer, 2.5 g of the activated silica was mixed with 50 mL of toluene. A solution of 11.7 mL of HMDS in 26 mL of toluene was added dropwise. The mixture was reacted for 16 h at 110°C . The silica was then washed with 50 mL of toluene, 50 mL of tetrahydrofuran and 50 mL of acetonitrile to remove the excess reagent. After filtration, the silica was dried at 110°C for at least 12 h under vacuum.

Microwave HMDS Grafting

A mass of 500 mg silica, 10 mL of toluene and 2.3 mL of HMDS were placed in a 25 mL Pyrex vessel, and the mixture was reacted for 30 min. The reactor was cooled to room temperature, and the excess reagent was subsequently removed by rinsing with 10 mL of toluene, 10 mL of tetrahydrofuran and 10 mL of acetonitrile. After filtration, the silica was dried at 110°C for 12 h under vacuum.

C18 Grafting by the Pesek Method (Scheme 2)

The C18 grafting was performed by hydrosilylation between the hydride-modified silica surface and octadecene using a procedure previously described [12]. The grafting was followed by an end-capping step with HMDS.

**Scheme 2** Hydrosilylation**Hydrosilylation under Microwave Irradiation**

The triethoxysilane-modified silica (500 mg), 10 mL of toluene and 1.2 mL octadecene were mixed in a 25 mL Pyrex vessel, and the mixture was reacted for 30 min. The reactor was cooled to room temperature, and the excess reagent was removed by rinsing with 10 mL of toluene, 10 mL of tetrahydrofuran and 10 mL of acetonitrile. After filtration, the silica was dried at 110 °C for 12 h under vacuum.

Conventional ODMAS Grafting (Scheme 3)

The ODMAS grafting was performed according to the procedure described by Szabó et al. [20].

Microwave ODMAS Grafting

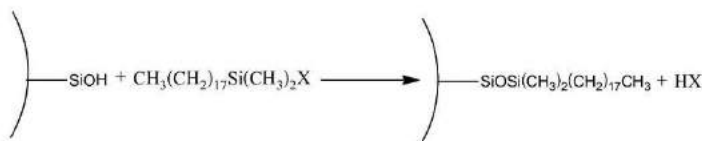
A mass of 500 mg of activated silica, 10 mL of toluene and 1.15 g of ODMAS were placed in a 25-mL Pyrex vessel, and the mixture was reacted for 30 min. The reactor was cooled to room temperature, and the excess reagent was removed by rinsing with 10 mL of toluene, 10 mL of tetrahydrofuran and 10 mL of acetonitrile. After filtration, the silica was dried at 110 °C for 12 h under vacuum.

Conventional ODMCS Grafting (Scheme 3)

The same procedure previously described was used with ODMCS reagent instead of ODMAS.

Microwave ODMCS grafting

In total, 500 mg of the activated silica, 1 g of imidazole, 10 mL of toluene and 1.12 g of ODMCS were placed in a

Scheme 3 Silanization of silica particles with ODMAS (X = N(CH₃)₂) and ODMCS (X = Cl)

25-mL Pyrex vessel, and the mixture was reacted for 30 min. The reactor was cooled to room temperature, and the excess reagent was removed by rinsing with 10 mL of toluene, 10 mL of tetrahydrofuran and 10 mL of acetonitrile. After filtration, the silica was dried at 110 °C for 12 h under vacuum.

Tanaka Test Procedure

The Tanaka test procedures were performed as described in the literature [19], except for the flow rate, which was reduced to 0.5 mL/min because of the column dimensions (50 × 4.6 mm). The oven temperature was set at 30 °C without pre-heating of the mobile phase. The solutes were detected at 254 nm, and the injection volume was 5 μL.

The retention factors (*k*) were calculated using Eq. 1:

$$k = \frac{t_r - t_m}{t_m} \quad (1)$$

where *t_r* is the retention time for the solute and *t_m* is the retention time of uracil taken as the unretained component. The selectivity factors (*α*) were calculated using Eq. 2:

$$\alpha = \frac{k_2}{k_1} \quad (2)$$

where *k₁* and *k₂* are the retention factors for solutes 1 and 2, respectively.

The six parameters considered in the Tanaka test and the mobile phases used are described in Online Resource, Table 1. To estimate the influence of the acid pretreatment, the end-capping step, and the grafting methods on the chromatographic properties, six columns were prepared and evaluated using the Tanaka test (see Table 1). In addition, three commercially available columns packed with core-shell C18 silica from different manufacturers (Poroshell ES-C18, Halo C18, Accucore C18) were also tested for comparison. Each target compound was injected three times. The results are presented in radar plots to magnify the small differences between some parameters and to differentiate each modified silica material.

Results and Discussion**Elemental Analysis**

The carbon content was determined by elemental analysis, and the results were obtained from the amount of organic moieties

Table 1 Summary of all synthesis performed with conditions of heating and the corresponding columns packing

Acid pretreatment	Silanization reagent	Heating	End capping	Column name (4.6 × 50 mm)	Efficiency (N) ^a
No	HMDS	Conventional	No	–	–
No	HMDS	Microwave	No	–	–
H ₂ O/HNO ₃ /H ₂ SO ₄	ODMAS	Conventional	BMMS, concentrated	Number 1	12,730
H ₂ O/HNO ₃ /H ₂ SO ₄	ODMAS	Conventional	BMMS	Number 2	11,360
No	ODMAS	Conventional	BMMS	Number 3	11,470
No	Octadecene	Conventional	HMDS	Number 4	10,840
No	Octadecene	Microwave	No	–	–
No	ODMAS	Conventional	No	Number 5	10,910
No	ODMAS	Microwave	No	Number 6	12,630
No	ODMCS	Conventional	No	–	–
No	ODMCS	Microwave	No	–	–

– No column packed

^a Calculated with fluorene 70 % CH₃CN 30 % H₂O (v/v) $N = 5.54 \times \left[\frac{t_r}{w_b} \right]^2$ with t_r and w_b the total retention time and the peak width at half height respectively

bonded to the silica. The grafting rate (τ) was calculated using Eq. 3, where p_c is the carbon percentage by weight of the bonded material, M_c is the atomic weight of carbon, M_w is the molecular weight of the grafted molecule, n_c is the total number of carbon atoms of the bonded organic group and S_{BET} is the specific surface area ($\text{m}^2 \text{g}^{-1}$ of native silica).

$$\tau (\mu \text{ mol m}^{-2}) = \frac{10^6 \times p_c}{[10^2 \times M_c \times n_c - p_c \times (M_w - 1)] \times S_{\text{BET}}} \quad (3)$$

Table 2 summarizes the average results obtained using the different methods. The maximum coverage obtainable with an octadecyldimethylsilane ligand was approximately 4.0–4.7 $\mu\text{mol m}^{-2}$. The typical bonding densities of monomeric synthesis of C18 materials were between 2.5 and 3 $\mu\text{mol m}^{-2}$ [18]. The reported value (3.8 $\mu\text{mol m}^{-2}$) corresponds to an efficient bonding process.

As expected, the alkyl chain length of the ligands influenced the grafting rate [21]; thus, smaller chain lengths resulted in greater surface coverage. The maximum grafting rate was obtained for HMDS, which was previously used as a probe [22] because of its high reactivity and its ability to access the maximum amount of silanols. The maximum value reported for a trimethylsilane was 5.43 $\mu\text{mol m}^{-2}$ [18].

The grafting rates obtained with ODMAS and with ODMCS were similar; however, the ODMCS grafting method required a basic molecule like imidazole able to capture the byproduct (hydrochloric acid), which had to be removed by rinsing with solvents of various polarities (toluene, tetrahydrofuran, acetonitrile).

The use of microwave irradiation for these reactions did not improve the grafting rate (except for HMDS grafting). The polar components of the reaction mixtures directly

absorbed microwaves to efficiently supply energy to the reactants. Thus, microwave heating was quicker and so increased the productivity compared to that achieved with conventional methods. In this process, the enhancement of the grafting amount by microwave irradiation was strongly dependent on the length of the alkyl side chain [15], which explains the efficiency of HMDS grafting compared to that of the ODMAS or ODMCS silanization reagent. For the conventional grafting process, we performed kinetic studies (see Online Resource, Fig. 1) by modulating the reaction time (between 30 min and 16 h); a minimum time of 5 h was required to maintain the grafting rate. For the microwave grafting procedure, different experiments were done at 30, 45, and 60 min, and the grafting rate was similar. Consequently, we decided to set the time at 30 min for the further reaction.

The grafting rate was clearly lower for the C18 functionalization by hydrosilylation. Moreover, the procedure was longer and required the Speier catalyst, which could adhere to the silica surface. A catalyst was still necessary when the microwave irradiation method was used because the grafting rate was lower (1.4 versus 1.7 $\mu\text{mol m}^{-2}$ for the hydrosilylation step). However, chromatographic evaluation of the grafted silica packed into a column was necessary to determine if replacement of the silanol groups with silane groups was beneficial despite the lower-density coverage. In addition, pretreatment with an acid solution of H₂O/HNO₃/H₂SO₄ 7/2/1 (v/v/v) was performed to activate the silica surface to maximize the number of silanol groups. However, the grafting rate was not modified (data not shown).

Finally, an end-capping reaction with BMMS was performed to eliminate the residual silanol groups. As expected, the grafting rate did not increase because of the high degree of coverage of the bonded phases.

Table 2 Grafting rates of C18 modified core-shell silica particles for the different methods

Type of synthesis	%C (± 0.4)	Anchored group	n_c	M_w (g mol^{-1})	Grafting rate ($\mu\text{mol m}^{-2}$)
Conventional	1.6	$-\text{Si}(\text{CH}_3)_3$	3	73.19	3.6
HMDS	1.5				3.4
Grafting	1.6				3.6
Microwave	1.9	$-\text{Si}(\text{CH}_3)_3$	3	73.19	4.4
HMDS grafting	1.8				4.1
	1.7				3.9
Conventional	4.4	$-\text{C}_{18}\text{H}_{37}$	18	253.49	1.7
Hydrosilylation	4.3				1.7
	4.2				1.6
Microwave	3.7	$-\text{C}_{18}\text{H}_{37}$	18	253.49	1.4
Hydrosilylation	3.6				1.4
	3.6				1.4
Conventional	10.1	$-\text{Si}(\text{CH}_3)_2\text{C}_{18}\text{H}_{37}$	20	311.65	3.8
ODMAS grafting	10.0				3.8
	9.9				3.8
Microwave	9.5	$-\text{Si}(\text{CH}_3)_2\text{C}_{18}\text{H}_{37}$	20	311.65	3.6
ODMAS grafting	9.0				3.4
	8.9				3.3
Conventional	9.9	$-\text{Si}(\text{CH}_3)_2\text{C}_{18}\text{H}_{37}$	20	311.65	3.8
ODMCS grafting	9.8				3.8
	9.7				3.7
Microwave	8.4	$-\text{Si}(\text{CH}_3)_2\text{C}_{18}\text{H}_{37}$	20	311.65	3.1
ODMCS grafting	8.3				3.1
	8.3				3.1

DRIFT

DRIFT spectroscopy is a useful tool for investigating chemically modified surfaces and provides valuable information about the structure of the chemically bonded phases. The substantial structural changes that occur on the silica surface allow for the characterization of the organic moiety. The primary vibration bands are specified in Online Resource, Table 2.

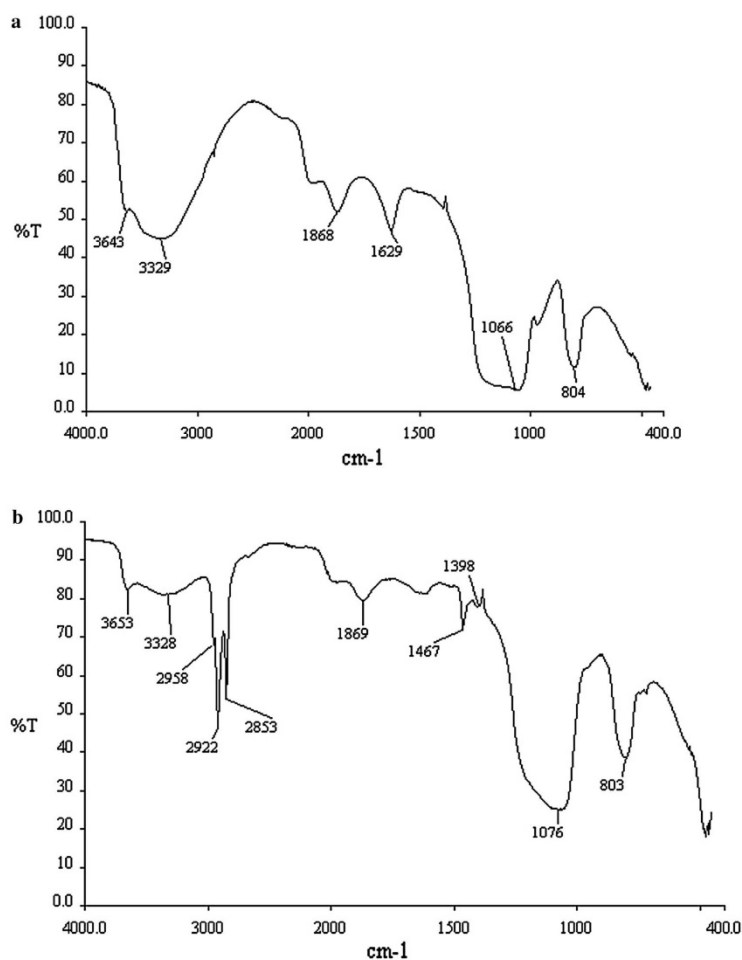
Compared to the spectrum of the native silica (Fig. 1a), the presence of the strong stretching bands in the $3,000\text{--}2,800\text{ cm}^{-1}$ region as well as weak deformation bands in the $1,370\text{--}1,470\text{ cm}^{-1}$ region of the modified silica corresponded with the decrease in intensity of the Si–OH bands at approximately $3,600$ and $3,300\text{ cm}^{-1}$, which clearly indicated the bonding of the alkyl chain (see Fig. 1b). Specifically, the stretching band near $3,653\text{ cm}^{-1}$ (Fig. 1b) was attributed to the internal hydroxyl groups and the band near $3,328\text{ cm}^{-1}$ was attributed to the hydrogen-bonded hydroxyl groups. Absorption bands were not observed at $3,747\text{ cm}^{-1}$, which would correspond to isolated hydroxyl groups; absorption bands were also not observed at $3,535\text{ cm}^{-1}$, which would correspond to vicinal hydroxyl groups [8]. The specific carbon-hydrogen vibration bands indicated successful bonding of the organic moiety at $2,958$ and $2,853\text{ cm}^{-1}$, representing

the anti-symmetrical stretching band of methyl groups and the symmetrical stretching band of methylene groups, respectively; in addition, the symmetrical stretching band of methyl groups and the anti-symmetrical stretching band of methylene groups were observed at approximately $2,870\text{--}2,930\text{ cm}^{-1}$. The relative intensity between the aliphatic chain stretching bands and the silanol stretching bands suggested that an important part of the silanols was grafted during the reaction with ODMAS, which was confirmed by the carbon content (10.1 % C). The primary feature of the silica hydride for the Pesek grafting procedure was the presence of the silicon-hydrogen stretching band at $2,258\text{ cm}^{-1}$ (online resource, Fig. 2a, b after the end-capping procedure). After hydrosilylation, this band decreased in intensity compared to that in the spectrum of the original silica hydride material and different carbon-hydrogen bands appeared. All precise vibration bands are detailed in online resource, Table 2.

SEM

According to the SEM images in Fig. 2, the sphericity was considerable and the distribution was homogeneous with an average value of $2.6\text{ }\mu\text{m}$, and no aggregate was observed. Each particle was well-defined, which confirmed that the

Fig. 1 DRIFT spectra of silica (a) and silica grafted by ODMAS under microwave irradiation (b)



silica particles were not damaged by the mechanical stirring. Similarly, the SEM pictures confirmed that the magnetic stirring did not damage the silica particles as the grafting time of the microwave procedure was shorter.

²⁹Si CP/MAS NMR

According to the literature [23–25], the spectrum of the native silica has a primary resonance centered at 100 ppm because the silicon atoms are linked to a hydroxyl group ((Si–O)₃Si–OH, Q₃, single silanol). In addition, the spectrum of our sample also exhibited two peaks attributed to siloxane atoms close to the surface, (Si (O–Si)₄, Q₄) at

approximately 110 ppm and to silicon atoms linked to two hydroxyl groups ((Si–O)₂Si(OH)₂, Q₂, geminal silanols) at approximately 90 ppm.

The spectrum of C18 grafted silica with ODMAS after microwave irradiation and the spectrum of C18 grafted silica with ODMCS after microwave irradiation are presented in Fig. 3 and Online Resource, Fig. 3, respectively. All of the chemical shifts are shown in Online Resource, Table 3.

The peak observed at 13.1 ppm in Fig. 3 corresponds to the chemical shift for the species resulting from the reaction of the ODMAS on the silica surface. The Q₃ and Q₄ resonances were still present, and no Q₂ signal was detected. As expected, no polymerization occurred on the silica surface;

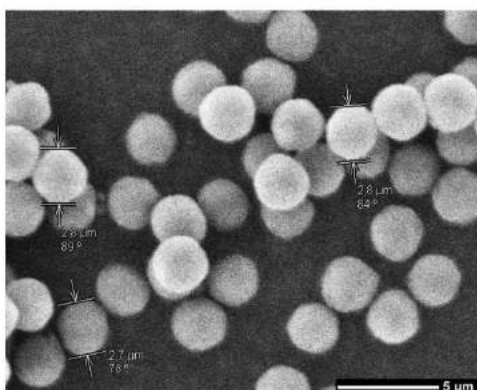


Fig. 2 SEM pictures of silica core-shell particles after the grafting procedure

the peak for the organic moiety was unique and confirmed that the ODMAS reagent was a monofunctional silane.

CP experiments primarily reveal signals of silicon atoms that are close to a hydrogen atom (Q_2 and Q_3) and/or dipolar coupling (siloxane Q_4 close to the surface); however, analysis of the spectra led to other considerations. For example, the Q_4 and the M signals were predominant as a consequence of the dense coverage of the silanol groups. The intensity of Q_4 could also be explained by the different proton density at the silica surface. Under CP conditions, the moiety grafted onto the silica surface is a proton source

and magnetization may be transferred to siloxane nuclei close to the surface [24].

Q_2 signal was at the limit of detection, because of the high grafting rate. They were converted into Q_4 and/or Q_3 if only one of the two SiOH was grafted. After the single-silanol groups were grafted, the Q_3 signal was converted into Q_4 .

Finally, these two spectra (Fig. 3 and Online Resource, Fig. 3) were very similar, which indicates that the structure of the grafted silica surface was not dependent on the silane reactive group (chloro or dimethylamino).

The high-speed ^1H MAS NMR spectra of the various phases were all similar to those presented in Online Resource, Fig. 4. The resolution at 30 kHz spinning was sufficient to clearly distinguish the different signals of the (CH_2) units (1.2 ppm) and the methyl groups (0.7 ppm). The starting reagent contained 5–10 % C18 isomers because the precursor for the product did not contain only alpha-isomers; thus, hydrogen linked to carbon (CH type) was present and was confirmed by the signal at 0.1 ppm.

The spectra were very similar to those previously presented, irrespective of the heating condition (conventional or microwave irradiation). This similarity is consistent with the DRIFT characterization and the elemental analysis measurements that showed the functionalization of silica particles by an alkyl chain at similar grafting rates. In the case of the ODMCS grafting procedure (conventional and microwave), hydrochloric acid was trapped and the resulting imidazole hydrochloride was partially adsorbed onto the silica surface. The presence of imidazole was confirmed on the hydrogen spectrum in Online Resource, Fig. 4; with the appearance of proton signals in the region 8–9 ppm.

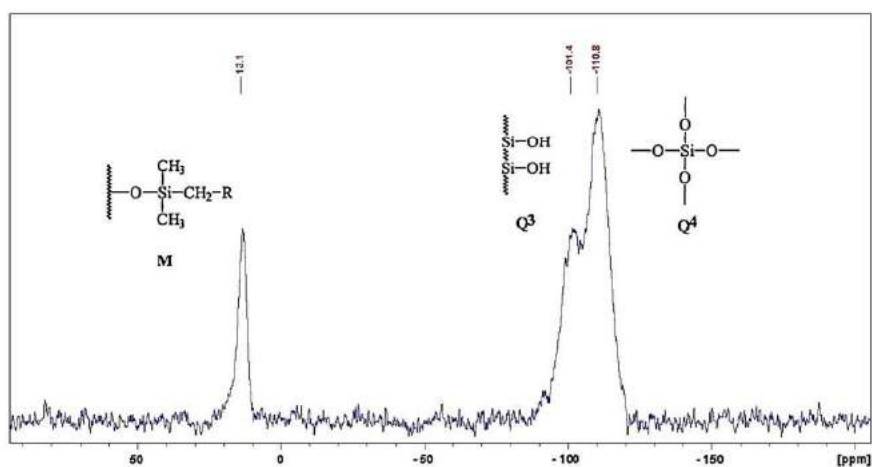
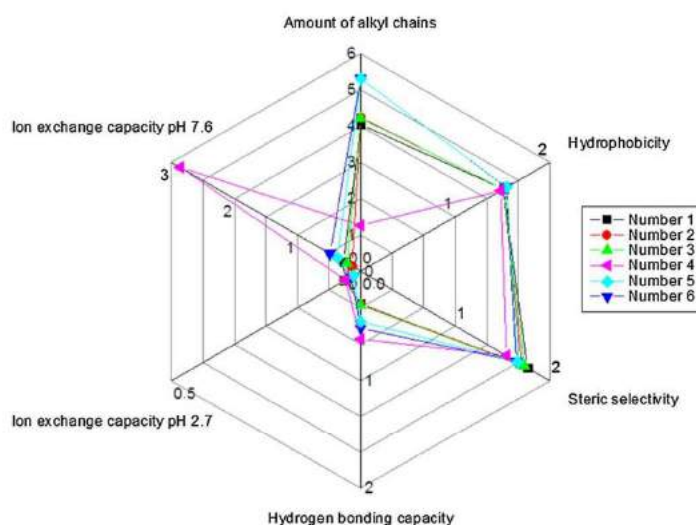


Fig. 3 ^{29}Si CP/MAS NMR spectra of core-shell silica grafted with ODMAS under microwave irradiation

Fig. 4 Chromatographic properties of the different packing materials synthesized



Tanaka Test

The radar plots in Fig. 4 were constructed by plotting the results of the chromatographic characterization. The data were used to describe the predominant properties of the chemically bonded phases synthesized. Table 3 summarizes the results of the Tanaka tests for the different tested packing materials. Greater values of k_{PB} , $\alpha_{PB/BB}$ and $\alpha_{T/O}$ indicate greater retention of hydrocarbons, greater hydrophobicity and greater shape selectivities (steric constraint selectivities), respectively. Conversely, smaller values of $\alpha_{C/P}$, $^{2,7}\alpha_{B/P}$ and $^{7,6}\alpha_{B/P}$ indicate smaller amounts of available silanol or fewer ion-exchange sites.

An excess of silanol was present in the case of the silica C18 grafted by the Pesek method (column 4), which was reflected in the most important ion-exchange capacity at pH 7.6 ($^{7,6}\alpha_{B/P} = 2.86$) and in the value of the hydrogen bonding capacity and peak asymmetry (see Table 3). This excess silanol may be correlated with the small value for the amount of alkyl chain, which was indicated by a lower degree of coverage, as determined by elemental analysis.

Each of the parameters for the three packing materials synthesized by the ODMAS grafting method with an end-capping step (columns 1, 2 and 3) was very similar. The predominant characteristics of the stationary phases were hydrophobicity and the amount of alkyl chains, which was in agreement with the grafting of an organic moiety containing a long alkyl chain and with the high surface coverage determined by elemental analysis. The two columns synthesized by the ODMAS grafting method using conventional heating (column 5)

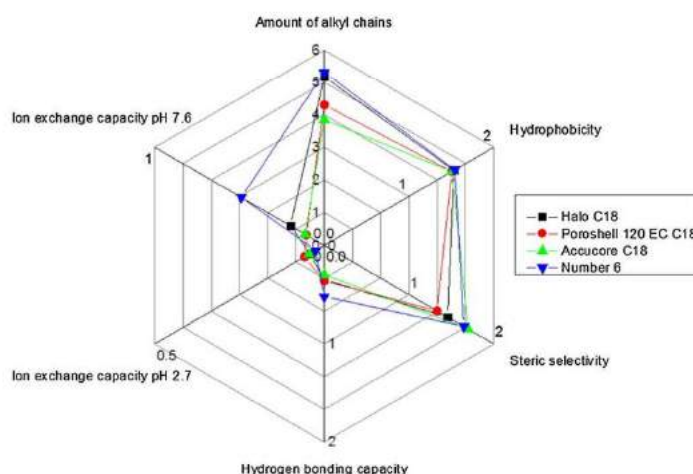
and microwave irradiation (column 6) without an end-capping step had similar profiles. However, the amount of alkyl chain ($k_{PB} = 5.3$) and the hydrophobicity ($\alpha_{PB/BB} = 1.54$) were higher as a result of better surface coverage by the C18 chains. The corresponding end-capped phase (column 3) exhibited a lower k_{PB} as the grafting rate was lower. Moreover, even if the carbon percentage was not improved by the end-capping step, it appeared to influence the chromatographic performances. Indeed, the hydrogen bonding capacity and the total ion exchange were higher compared to column 3 ($\alpha_{C/P} = 0.46$, $^{7,6}\alpha_{B/P} = 0.37$ for column 5 and $\alpha_{C/P} = 0.52$, $^{7,6}\alpha_{B/P} = 0.49$ for column 6). The peak asymmetry of the caffeine and the phenol are detailed in Table 3. All the end-capped grafted silicas (columns 1, 2, 3) presented values similar to those obtained for the commercial columns. For the end-capped grafted silicas, the peak asymmetry of the caffeine presented values lower than those of the non-end-capped ones (columns 5, 6). But for the peak asymmetry of the phenol, non-end-capped columns give lower values than the end-capped grafted ones.

All the packing materials (except the silica modified via the Pesek procedure) exhibited results (see Fig. 5) similar to those obtained for the three tested commercial columns (for column specifications, see Online Resource, Table 4).

The hydrophobicity and the amount of alkyl chain for columns 1, 2 and 3 are similar to those for the Poroshell ES-C18 column. The values for columns 5, 6 and the Halo C18 column were the highest as a consequence of their greater retention (Fig. 6, blue), whereas the Accucore C18 column exhibited lower retention (Fig. 6, pink).

Table 3 Values for the Tanaka test

Parameter	k_{PB}	$\alpha_{PB/BB}$	$\alpha_{T/O}$	$\alpha_{C/P}$	$^{7.6}\alpha_{B/P}$	$^{2.7}\alpha_{B/P}$	A_s (caffeine)	A_s (phenol)	Carbon load (%)
Number 1	4.04	1.51	1.76	0.30	0.27	0.04	1.66	1.37	8.8
Number 2	4.23	1.51	1.70	0.30	0.14	0.04	1.65	1.50	8.6
Number 3	4.21	1.51	1.73	0.31	0.22	0.04	1.69	1.45	8.6
Number 4	1.26	1.48	1.54	0.62	2.86	0.02	1.53	2.15	4.6
Number 5	5.30	1.54	1.66	0.46	0.37	0.02	1.79	1.29	10.1
Number 6	5.31	1.54	1.65	0.52	0.49	0.03	1.80	1.30	9.5
Halo C18	5.16	1.53	1.46	0.35	0.20	0.04	1.61	1.34	7.7
Poroshell ES-C18	4.30	1.51	1.33	0.36	0.11	0.06	1.62	1.30	9.0
Accucore C18	3.85	1.51	1.70	0.30	0.11	0.04	1.74	1.45	8.0

Fig. 5 Chromatographic properties of the different commercial packing materials compared to the ODMAS microwave grafted packing

The silanol activity measured by $\alpha_{B/P}$ at pH 2.7 is a measure of the acidic activity of the silanol groups and provides information related to the presence of metal impurities. At pH 2.7, the silanol moieties were mostly uncharged. Higher values were obtained for silica-containing metal contaminants, which increased the silanol acidity. The total silanol activity was estimated on the basis of $\alpha_{B/P}$ at pH 7.6 and reflected the greater accessibility to residual silanol as a result of a lower coverage or density. In this study, the contribution of ion-exchange sites at pH 2.7 was low for all of the columns tested because the bonded phases were prepared from pure silica, Type B. The small values for ion-exchange sites at pH 7.6 (columns 1, 2 and 3) suggest that few silanol groups remained, which is consistent with the low hydrogen bonding capacity indicated by the $\alpha_{C/P}$ value.

The acid pretreatment was not useful in our case, most likely because of the high purity and the homogeneity of the silica starting material. Moreover, the concentration of the end-capping reagent did not appear to affect the amount

of ion-exchange sites at pH 7.6 because the values were similar for columns 1, 2 and 3. However, in the case of the columns synthesized by the ODMAS grafting method without end capping, the ion-exchange site values at pH 7.6 (columns 5 and 6) suggested that some silanol groups were still accessible to small solutes. As previously reported [7], the end-capping step can affect the chromatographic properties, even if the carbon percentage is not affected.

Lastly, the C18 core-shell columns were tested and compared to commercial columns (Halo C18, Poroshell ES-C18, Accucore C18). The highest values were obtained for the hydrophobic selectivity and the amount of alkyl chains; few silanols remained. The steric selectivity values for our columns were in the range of the most important values for a C18 grafting with a monofunctional reagent. These phases can be considered high-density (HD) monomeric phases that combine the advantages of the HD phases (i.e., restricted accessibility to silanols, high hydrophobicity and steric selectivity) while avoiding the high retention of the

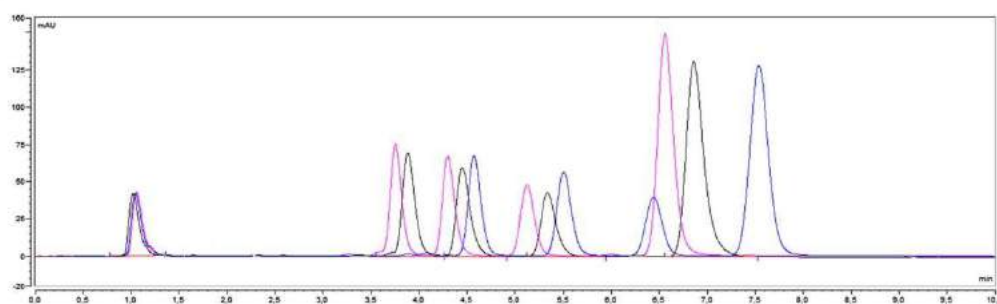


Fig. 6 Chromatogram of Tanaka 1: CH₃OH-H₂O (80:20, v/v) for column Number 2 (black), Halo C18 column (blue) and Accucore C18 column (pink). In order of retention: uracil, butylbenzene, o-terphenyl, pentylbenzene, triphenylene

totally porous HD silica phases. However, if the steric constraint selectivity value is high for a monomeric phase, it remains below the steric constraint selectivity determined for phases that lead to a separation of PAHs, carotenoids or steroid isomers (i.e., parameters such as the numerical value of $\alpha_{T/O}$ are greater than three).

Finally, the microwave process resulted in similar separation performance compared to the high-boiling solvent synthesis process. However, the microwave process provided a final CBP with a synthesis reaction time reduced to 30 min.

Concluding Remarks

The best strategy in terms of grafting rate ($3.8 \mu\text{mol m}^{-2}$) was to perform the C18 grafting procedure using ODMAS, which did not require imidazole for the synthesis process.

The hydrosilylation process resulted in the lowest grafting rate ($1.7 \mu\text{mol m}^{-2}$) among the tested processes. In the Pesek method, the major disadvantage was the use of the platinum catalyst that may adhere to the silica surface. And this catalyst was necessary; also when the procedure was performed under microwave irradiation as the grafting rate was lower ($1.4 \mu\text{mol m}^{-2}$ for the hydrosilylation under microwave without catalyst versus $1.7 \mu\text{mol m}^{-2}$ for the hydrosilylation with catalyst). However, the enhanced grafting induced by the microwave irradiation was strongly dependent on the length of the alkyl side chain; in this study, a long non-polar chain of 18 aliphatic carbons was used.

The Tanaka test was performed to determine the principal chromatographic properties. The highest values were obtained for hydrophobicity and the amount of alkyl chains, which was consistent with the high degree of coverage for the different C18 bonded phases. The low ion-exchange capacity at pH 7.6 suggested that few silanol

groups were accessible to solutes, which was confirmed by the low hydrogen bonding capacity. The pretreatment was not useful, most likely because of the high purity of the silica starting material. The end-capping reaction influenced the chromatographic properties because the greater ion-exchange capacity at pH 7.6 suggested that some silanol groups were accessible to solutes, which was confirmed by the higher hydrogen bonding capacity for the phases without an end-capping step.

The microwave synthetic process was very advantageous to perform the previously described synthetic processes for preparing CBPs. Nowadays, with a large-scale reactor; a batch of 20 g of silica can be grafted with good reproducibility, which is partly due to using multimode microwave reactors more efficient at transferring the microwave energy to a larger reaction mass. This amount of grafted silica allows packing about one hundred columns (50×2.1 mm). This method allows obtaining stationary phases exhibiting as good chromatographic performances than those prepared in conventional synthetic process, but ten times faster.

Acknowledgments The authors would like to acknowledge Emilie Petit and Françoise Ringot for the elemental analysis measurements and Anais Lesur for some of the chromatographic measurements.

Conflict of interest The authors declare no competing financial interest.

References

1. Horvath CG, Lipsky SR (1966) *Nature* 211:748–749
2. Guiochon G, Gritti F (2011) *J Chromatogr A* 1218:1915–1938
3. Qiu H, Liang X, Sun M, Jiang S (2011) *Anal Bioanal Chem* 399:3307–3322
4. Chester T (2013) *Anal Chem* 85:579–589
5. Buszewski B, Jezierska M, Welniak M, Berek D (1998) *J High Resolut Chromatogr* 21:267–281

6. Wirth MJ, Fatunmbi HO (1993) *Anal Chem* 65:822–826
7. Kirkland JJ, Glajch JL, Farlee RD (1989) *Anal Chem* 61:2–11
8. Scott RPW (1993) Chaps 7 and 8. In: Scott RPW, Simpson CF (eds) *An introduction to bonded phases the synthesis of bonded phases*, J. Wiley & sons Chichester West Sussex, England
9. Buszewski B, Suprynowicz Z (1988) *Anal Chim Acta* 208:263–273
10. Lork KD, Unger KK, Kinkel JN (1986) *J Chromatogr* 352:199–211
11. Gaget C, Morel D, Serpinet J (1982) *J Chromatogr A* 244:209–216
12. Sandoval JE, Pesek JJ (1991) *Anal Chem* 63:2634–2641
13. Kremsner JM, Stadler A, Kappe CO (2006) *Top Curr Chem* 266:233–278
14. Procopio A, Das G, Nardi M, Oliverio M, Pasqua L (2008) *Chem Sus Chem* 1:916–919
15. García N, Benito E, Guzmán J, De Francisco R, Tiemblo P (2010) *Langmuir* 26:5499–5506
16. Fukaya N (2011) *J Organomet Chem* 696:825–828
17. Boukherroub R, Petit A, Ozanam AF (2003) *J Phys Chem B* 107:13459–13462
18. Doyle CA, Dorsey JG (1998) Chap 8. In: Katz E, Eksteen R, Schoenmakers P, Miller N (eds) *Handbook of HPLC Chromatogr SCX Series vol 78*, M. Dekker, New York
19. Kimata K, Iwaguchi K, Onishi S, Jinno K, Eksteen R, Hosoya K, Araki M, Tanaka N (1989) *J Chromatogr Sci* 27:721–728
20. Szabo K, Ha NL, Schneider P, Zeltner P, Kovitts E (1984) *Helv Chim Acta* 67:2128–2142
21. Berendsen GE, Galan LD (1980) *J Chromatogr* 196:21–37
22. Sindorf DW, Maciel E (1982) *J Phys Chem B* 86:5208–5219
23. Pursch M, Sander LC, Albert K (1996) *Anal Chem* 68:4107–4113
24. Avolio R, Gentile G, Avella M, Capitani D, Errico ME (2010) *J Polym Sci Part A Polym Chem* 48:5618–5629
25. Léonardelli S, Facchini L, Fretigny C, Tougne P, Legrand AP (1992) *J Am Chem Soc* 114:6412–6418

This first study allowed for establishing a robust protocol, in this case for C18 functionalization of SPP. The best strategy in terms of grafting rate ($3.8 \mu\text{mol}/\text{m}^2$) was to functionalize the silica particles through organosilanization, with n-octadecyldimethyl(dimethylamino)silane.

The hydrosilation process was also tested, but resulted in a lower grafting rate ($1.7 \mu\text{mol}/\text{m}^2$). Moreover, in the Pesek pathway method, the major disadvantage was the use of the platinum catalyst that may adhere to the silica surface. The use of microwave irradiation instead of conventional heating was very advantageous in terms of synthesis time and reproducibility for a similar surface coverage. Finally, the protocol selected was to functionalize the silica particles by organosilanization with n-octadecyldimethyl(dimethylamino)silane, under microwave irradiations, and with an end-capping step. It allowed to obtain stationary phases exhibiting as good chromatographic performances than those prepared with conventional synthetic process, but ten times faster. The Tanaka test was performed to determine the principal chromatographic properties of the C18 stationary phases synthesized through different pathways (organosilanization *versus* hydrosilation, conventional heating *versus* microwave irradiation) or with different organosilanes (chlorosilane *versus* dimethylaminosilane) and compare them to commercial ones. The highest values of our C18 home-made stationary phases were obtained for the hydrophobicity and the amount of alkyl chains, which was consistent with the high degree of coverage for the different C18 bonded phases. The low ion-exchange capacity at pH 7.6 suggested that few silanol groups were accessible to solutes, which was confirmed by the low hydrogen bonding capacity. This parameter being higher when no end-capping step has been performed, justifying the importance of this post-treatment.

The next step was to investigate the influence of the silica thermal pretreatment. Especially the effect of temperature on the silanol population was studied to evaluate the possibility of obtaining different stationary phases, from the same silica batch functionalized with the same procedure.

II-2. Thermal pretreatments of silica

II-2-1. Article 2: Towards a wide range of C18 stationary phases from the same SPP silica batch functionalized with the same microwave procedure

After the development of a robust C18 grafting method on bare silica, the influence of thermal pretreatment of silica was investigated. Especially, the possibility to modify the silica surface by applying different thermal pretreatments was studied in order to obtain a range of various C18 SPs from the same silica batch functionalized with the same grafting procedure.

Both bare and C18 silicas pretreated at different key temperatures were characterized by microscopy and BET measurements to check the morphological structure at the different temperatures. Also, infrared spectroscopy and solid state CP/MAS NMR were used to characterize the silanol types at the silica surface depending on the temperature applied, and the vibrational bands of the ligand grafted. Finally, the chromatographic properties and especially the performances towards basic solute analysis were evaluated by mean of the Veuthey test. All the data generated were treated through chemometric approaches: PCA and HCA presented in section I.6.2.

Such study and evaluation led to the second article entitled "Thermal pretreatments of superficially porous silica particles for high-performance liquid chromatography: Surface control, structural characterization and chromatographic evaluation" published in *Journal of Chromatography, A* in 2015.

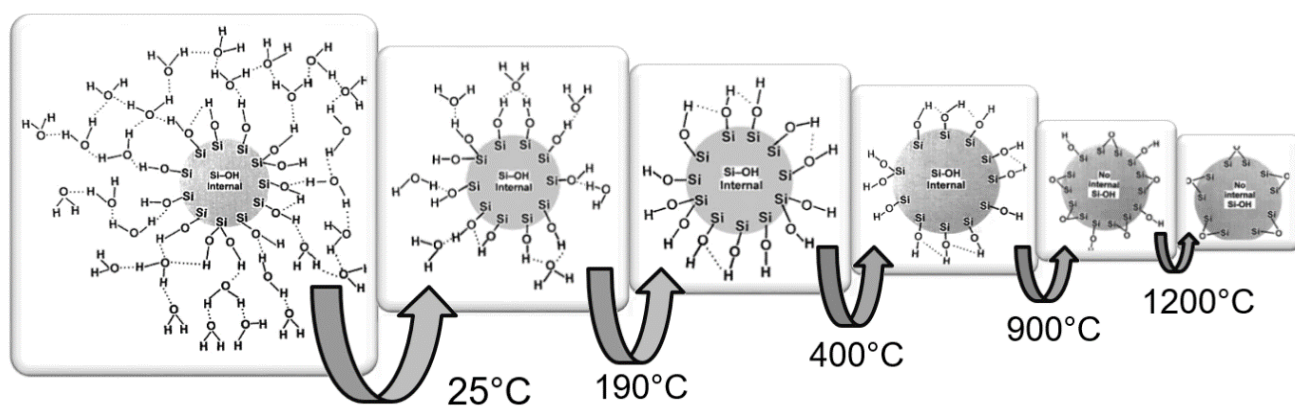


Figure 1: Temperature effect on the silanol population at the silica surface. Inspired from¹

¹ Zhuravlev, L. T. Colloids Surf. Physicochem. Eng. Asp. 2000, 173 (1), 1–38.



Thermal pretreatments of superficially porous silica particles for high-performance liquid chromatography: Surface control, structural characterization and chromatographic evaluation[☆]



Mélanie Mignot^a, Muriel Sebban^b, Alain Tchaplac^c, Olivier Mercier^d, Pascal Cardinael^a, Valérie Peulon-Agasse^{a,*}

^a Normandie Univ, EA3233, Sciences et Méthodes Séparatives, FR3038, IRCOF, 1 rue Tesnière, 76821 Mont Saint-Aignan Cedex, France

^b Normandie Univ, UMR 6014, Chimie Organique, Bioorganique: Réactivité et Analyse, FR3038, IRCOF, 1 rue Tesnière, 76821 Mont Saint-Aignan Cedex, France

^c Lip(Sys)² – LETIAM (FKA EA4041 Groupe de Chimie Analytique de Paris-Sud), Univ Paris-Sud, Université Paris-Saclay, IUT d'Orsay, Plateau de Moulon, F-91400 Orsay, France

^d Interchim R&D, 211 bis avenue JF Kennedy, BP 1140, 03100 Montluçon, France

ARTICLE INFO

Article history:

Received 27 July 2015

Received in revised form

18 September 2015

Accepted 22 September 2015

Available online 26 September 2015

Keywords:

High-performance-liquid-chromatography

Superficially porous silica particles

Octadecylsilane stationary phases

Silica thermal treatment

Principal component analysis

Microwave irradiation

ABSTRACT

This study reports the impact of thermal pretreatment between 400 and 1100 °C on superficially porous silica particles (e.g. core-shell, fused-core; here abbreviated as SPP silica). The different thermally pretreated SPP silica (400 °C, 900 °C and 1100 °C) were chemically bonded with an octadecyl chain under microwave irradiation.

The bare SPP silica, thermally untreated and pretreated, as well as the chemically bonded phases (CBPs) were fully characterized by elemental analysis, diffuse reflectance infrared Fourier transform spectroscopy (DRIFT), and solid state cross polarization magic angle spinning (CP-MAS) ²⁹Si NMR. The chromatographic properties of the overall set of C₁₈-thermally pretreated SPP silica stationary phases were determined using the Tanaka test. Complementary, the simplified Veuthey test was used to deeply study the silanol activity, considering a set of 7 basic solutes with various physicochemical properties. Both tests were also performed on different commercial SPP silica columns and different types of bonding chemistry (C₁₈, Phenyl-hexyl, RP-amide, C30, aQ). Multivariate data analyses (hierarchical cluster analysis and principal component analysis) were carried out to define groups of stationary phases with similar chromatographic properties and situate them in relation to those commercially available. These different C₁₈-thermally pretreated SPP silicas represented a wide range of stationary phases as they were spread out along the score plot. Moreover, this study highlighted that the thermal pretreatment improved the chemical stability of the SPP silica compare to untreated SPP silica and untreated porous silica. Consequently, higher thermal pretreatment can be applied (up to 900 °C) before functionalization without destruction of the silica matrix. Indeed, a significantly lower dissolution of the thermally pretreated SPP silica under aggressive conditions could allow the use of the corresponding functionalized stationary phases at high temperature (60 °C) with good lifetime of the columns.

© 2015 Elsevier B.V. All rights reserved.

1. Introduction

Silica is largely used as a support of the stationary phase in High-Performance Liquid Chromatography (HPLC) because of its numerous advantages, including its large specific surface area and its mechanical stability. The particles can be manufactured as small

spheres with a narrow size distribution and a controlled pore size, which makes a good starting material for preparing efficient HPLC stationary phases.

To increase the chromatographic efficiency and improve the productivity, several methods are currently used such as Ultra-High-Performance Liquid Chromatography (UHPLC) with fully porous sub-2 μm particles, which may or may not be coupled with High-Temperature Liquid Chromatography (HTLC), or the use of monolithic stationary phases. Among these methods, the use of superficially porous silica particles (SPP silica) is another alternative requiring neither specific apparatus nor complicated transfer

[☆] Selected paper from 42nd International Symposium on High Performance Liquid Phase Separations and Related Techniques, 21–25 June 2015, Geneva, Switzerland.

* Corresponding author.

E-mail address: valerie.agasse@univ-rouen.fr (V. Peulon-Agasse).

<http://dx.doi.org/10.1016/j.chroma.2015.09.072>

0021-9673/© 2015 Elsevier B.V. All rights reserved.

methods [1]. Moreover, various chemistries of superficially porous silica particles are commercially available, which is not currently the case for the monolithic stationary phases.

Generally, the analysis of basic molecules is still a challenge in HPLC because of the peak tailing resulting from the strong interactions between these molecules and the different residual silanols present onto the silica surface (hydrogen bonding, ion interactions). Because the ligands (e.g., commonly: C₈, C₁₈), generate steric hindrance, the functionalization is not complete. As a result, some silanols are still accessible, leading to a non-univocal molecular mechanism of retention, which affects the efficiency by peak tailing. Many strategies were developed to hinder the silanol accessibility of the porous stationary phases, such as vertical and horizontal polymerization [2–6], applying a polymer coating [7–11], and the use of lateral bulky chains [12–14] or propylene bridges for bidentate phases [15,16]. The silanols can also be blocked by the addition of a polar embedded group (PEG phases), such as an amide, carbamate, urea, sulfonamide, quaternary ammonium, or an ether group, to the alkyl structure [17–21]. Recently, a new generation of mixed octadecylsilane (ODS) bonded phase called Charge Surface Hybrid (CSH) was developed to improve the peak symmetry in a low ionic strength mobile phase by realizing a first coating with charged compounds [22]. Alternatively, Pesek and coworkers modified the silica structure before the final bonding step by forming a monolayer of SiH groups on the surface [23].

In addition, a second treatment of the silica surface is commonly used to reduce the number of residual silanols after the first attachment of the main ligand [24]. This end-capping involves the bonding of a smaller organosilane such as hexamethyl-disilazane, trimethylsilyl-imidazole or trimethyl-chlorosilane. Another strategy based on the blockage of the remaining silanol groups during the chromatographic analyses was proposed by Reta and Carr [25], who added divalent metals and amines in the mobile phase as silanol blocking agents. Alternatively, Hill [26] and Vervoort et al. [27] used triethylamine and longer hydrocarbon tertiary amines to block the activity of the silanols.

Lastly, another method consists of controlling the silanol population before any derivatization or chromatographic analyses. Halfpenny et al. [28] proposed to use ultraviolet laser radiation to dehydroxylate the surface with controlled irradiance. This dehydroxylation can also be achieved by a thermal treatment of the silica surface [29,30]. Three types of silanols are present on the silica surface; the vicinal silanols that interact through hydrogen bonds, the geminal silanols for which two hydroxyl groups are linked to the same silicon atom and finally, the isolated single silanols. It is established that the type of silanol differs on the silica surface depending on the temperature. Indeed, temperature treatments transform silanols into more hydrophobic siloxane bridges by dehydroxylation [31]. Some authors used the thermal process to selectively rehydroxylate the silica surface for better homogeneity [32,33] and may include an acid treatment [34]; Boudreau and Cooper [35] described a dehydroxylation without rehydroxylation. Different stages can be distinguished during a thermal treatment. At a temperature lower than 400 °C, the dehydration occurs as multilayers of water physically adsorbed on the silica surface are removed. The siloxane bonds formed are unstable, and the silanols can be restored by exposure to water. However, above 400 °C, the siloxane bonds are much more stable, such that even after 2500 column volumes, no rehydroxylation was noticed by Sunseri et al. [36]. Van der Voort and Vansant [30] as well as Zhuravlev [37] also closely studied the surface chemistry of amorphous silica and noticed that between 190 and 400 °C, the first silanols to disappear were the vicinal silanols, favored by the hydrogen bond already created that facilitates the departure of the water molecules. This process is readily reversible upon the introduction of an excess of water, and the complete rehydroxylation takes place by splitting of the weakened

strained siloxane bridges. Then, geminal silanols are totally removed at 400 °C, and the amount of vicinal silanols decreases from 0.8 to 0.2 $\mu\text{mole m}^{-2}$ between 200 °C and 800 °C; finally, the isolated single silanol amount is maximized from 400 °C. Those remain at the surface at higher heating temperatures (1 $\mu\text{mole m}^{-2}$ at 800 °C) [30], where shrinkage and sintering of the silica matrix is noticed [37]. It is necessary to heat to 1200 °C to achieve the complete removal of all silanol groups (only siloxane bridges), but the surface fusion forms a solid network that is chromatographically unusable [36].

Different thermal treatments have already been applied to totally porous silica gels. Maws and Engelhardt showed the influence of the type of silanols on the selectivity of the stationary phase [38], and the ability to reduce the residual silanols was reported by Sunseri et al. [36]. El Rassi and Gonnet [39] found that the most convenient phase for the analysis of apolar solutes was the bonded 300–400 °C pretreated silicas, which presented the maximum coverage. On the contrary, the most suitable phase for the analysis of polar solutes was the bonded 600 °C pretreated silicas, which presented the minimum concentration of hydroxyl groups.

To our knowledge, the present study is the first detailed study of the effect of thermal pretreatments on superficially porous silica particles. Starting from the same superficially porous silica batch, the aim of this work is to control the type of silanol groups on the silica surface before applying the C₁₈ grafting under microwave irradiations, as previously described [40]. Each step was followed by DRIFT, and the degree of coverage was determined by elemental analysis. The type and relative abundance of silanol groups, as well as the covalent bonding of the C₁₈-chains to the different silicon atoms were determined by ²⁹Si CP/MAS and HPDEC solid state NMR, as well as ¹³C, ¹H solid state NMR. The general chromatographic properties of the columns packed with the C₁₈-thermally pretreated SPP silica were studied via the Tanaka test [41]. In addition, the modified [42] and simplified Veuthey test [43] was performed to study the residual silanol activity toward basic solutes in detail and to determine whether a thermal treatment is to be favored for a better base-deactivation of the final SPP silica stationary phases. Starting from the same SPP silica batch, functionalized with the same organosilane, the effect of thermal pretreatment on the final stationary phases was investigated in terms of selectivity and hydrophobicity.

2. Experimental

2.1. Chemicals

The SPP silica particles were provided by Interchim (Montluçon, France). Their specific surface area, nominal particle diameter and pore diameter were 126 m² g⁻¹, 2.6 μm and 90 Å, respectively. Bis(dimethylamino)(dimethyl)octadecylsilane (ODMAS), bis(dimethylamino)(trimethyl)silane (DATS) and bis(dimethylamino)dimethylsilane (BMMS) were obtained from ABCR (Karlsruhe, Germany). Toluene, benzylamine (B), phenol (P), caffeine (C) and uracil were supplied by Sigma-Aldrich (Saint-Quentin Fallavier, France). Butylbenzene (BB), triphenylene (T), *o*-terphenyl (O) were purchased from Alfa Aesar (Schiltigheim, France). Procainamide hydrochloride, pyridine, anhydrous quinine and L-nicotine were purchased from Acros Organics (Geel, Belgium) and penbutolol hydrochloride by Dr. Ehrenstorfer GmbH (Augsburg, Germany). Sodium nitrate was supplied by Carlo Erba (Val-de-Reuil, France). Chlorprocaine hydrochloride was supplied by BASF Orgamol Pharma (Saint-Vulbas, France). Carvedilol was supplied by TCI (Tokyo, Japan). Methanol, acetonitrile and pentylbenzene (PB) were purchased from VWR (Fontenay-sous-Bois, France). For the chromatographic tests, all solvents were of HPLC grade. The columns (4.6 mm \times 50 mm \times 2.6 μm) were

packed by Interchim and were compared to various commercial SPP silica columns with different chemistries: Halo C18 (4.6 mm × 50 mm × 2.7 μm), Phenyl-Hexyl (4.6 mm × 100 mm × 2.7 μm), RP-Amide (4.6 mm × 100 mm × 2.7 μm) from Advanced Materials Technology (Wilmington, DE, USA); Accucore C18 (4.6 mm × 50 mm × 2.6 μm), Accucore C30 (4.6 mm × 100 mm × 2.6 μm), Accucore aQ (4.6 mm × 100 mm × 2.6 μm) from Thermo Fisher Scientific (Courtaboeuf, France); Poroshell 120 EC-C18 (4.6 mm × 50 mm × 2.7 μm) from Agilent-Technologies-France (Courtaboeuf, France); Kinetex EVO C18 (4.6 mm × 150 mm × 5 μm) from Phenomenex (Torrance, CA, USA); and ACE C18 (4.6 mm × 150 mm × 5 μm) from Advanced Chromatography Technologies (Aberdeen, Scotland).

2.2. Apparatus

Thermal treatments were performed using a Navertherm oven (Aubervilliers, France) operating from 20 to 1100 °C.

The syntheses were performed in a CEM Discover microwave reactor (Buckingham, UK) operating at 2450 MHz. The power delivery system was adjusted during the reaction, with a maximum of 300 W. The instrument was monitored with a touchscreen control panel.

SEM images were obtained using a JEOL JCM 5000 NeoScope (München, Germany) operating at an accelerating voltage of 15 kV. The magnifications were approximately 440× and 20,000×. The powder samples were stabilized on analyzing plots using conductive adhesives; they were subsequently coated with gold using a NeoCoater MP-19020NCTR (München, Germany) to reduce charge accumulation during the observations.

The granulometry was measured by a Mastersizer 2000 (Malvern Instruments Ltd, United Kingdom) at a data acquisition rate of 1 kHz, with a maximum red light source of 4 mW He-Ne at 632.8 nm and a maximum blue light source of 0.3 mW LED at 470 nm. The range of particle size measurements was 0.02–2000 μm. The SPP silica was in suspension in acetonitrile for each measurement. The suspension was sonicated for 2 min before measurement.

The determination of the specific surface area of bare silica and of the thermally pretreated materials was achieved by nitrogen adsorption with the BET method on a Quantachrome Nova series (Odelzhausen, Germany) with a 10 mTorr vacuum.

Elemental analysis by the conventional combustion method was performed using a Flash 2000 organic elemental analyzer from Thermo Fisher Scientific (Courtaboeuf, France).

The DRIFT spectra were obtained using a PerkinElmer Spectrum 100 (Norwalk, CT, USA). The sample consisted of a mixture of SPP silica and potassium bromide (KBr, 10% (m/m)) placed in a 2 mm diameter cup. The spectra, which consisted of 64 scans, were acquired at a resolution of 2 cm⁻¹ and were referenced against pure KBr over the range 4000–450 cm⁻¹.

NMR measurements were carried out with a Bruker (Wissembourg, France) Avance III 400 spectrometer equipped with a 4 mm MAS probe. For ¹H MAS (Magic Angle Spinning) experiments, sample spinning was executed at 10 kHz. ¹H 90° pulse and recycle delay times were 5.6 μs and 5 s, respectively. ²⁹Si HPDEC (High Power Decoupling) and CP (Cross Polarization) experiments were executed under MAS at 5 kHz. For ²⁹Si HPDEC experiments, ²⁹Si 90° pulse and recycle delay times were 2.5 μs and 20 s, respectively. ²⁹Si CPMAS experiments were recorded with a contact time of 8 ms and a repetition time of 15 s. All chemical shifts were referenced externally to Octakis(trimethylsiloxy)silsesquioxane (Q8M8).

The chromatographic measurements were performed with a liquid chromatograph from Dionex/ThermoFisher (Courtaboeuf, France), which consisted of a P680 pump, an injection valve (ASI-100 automated sample injector) equipped with a 20 μL injection

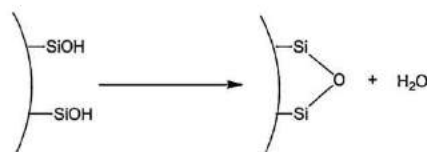


Fig. 1. Dehydroxylation of the silica surface.

loop, and a model UVD 340U diode-array detector (DAD). The column temperature was controlled with a TCC-100 thermostat-controlled column compartment. The data were collected on a computer using the Chromeleon software from Dionex/ThermoFisher (Courtaboeuf, France).

2.3. Procedures

2.3.1. Thermal treatments (Fig. 1)

Three portions of 5 g of SPP silica were heated [39] separately at 400 °C, 900 °C, and 1100 °C. The temperature set was reached after 5–10 min and maintained for 5 h without specific atmosphere. Then, the silica was slowly cooled to room temperature by stopping the oven.

2.3.2. ODMAS grafting (Fig. 2)

The grafting was achieved under microwave irradiation according to the grafting procedure previously developed in our laboratory [40]. A mass of 5 g of activated SPP silica, 50 mL of toluene and 5.75 g of ODMAS were placed in a 100 mL Pyrex vessel, and the mixture was reacted for 30 min. The reactor was cooled to room temperature, and the excess reagent was removed by rinsing with 50 mL of toluene, 50 mL of tetrahydrofuran and 50 mL of acetonitrile. After filtration, the SPP silica was dried at 110 °C for 12 h under vacuum. For the phases end-capped, 2.4 mL of the end-capping reagent was added with 50 mL of toluene. The mixture was reacted for 30 min. The reactor was cooled to room temperature, and the excess reagent was removed by rinsing with 50 mL of toluene, 50 mL of tetrahydrofuran and 50 mL of acetonitrile. After filtration, the SPP silica was dried at 110 °C for 12 h under vacuum.

2.3.3. Silica dissolution experiments

In a 500 mL three-necked round-bottom flask equipped with a mechanical stirrer, 100 mg of silica were added to a solution composed of 250 mL of acetonitrile–0.25 M phosphate buffer (pH 7.0), 20:80 (v/v). The temperature of the mixture was set at 60 °C with stirring for 20 h. The silica was filtered, washed with water, and dried at 110 °C for at least 12 h under vacuum. The same process was applied to the bare SPP silica, the bare porous silica, and the 900 °C pretreated SPP silica.

2.4. Chromatographic procedures

2.4.1. Tanaka test procedure

The Tanaka test was performed as described in the literature [41]. Each target solute was injected three times, with a standard deviation less than 1% for the retention time values.

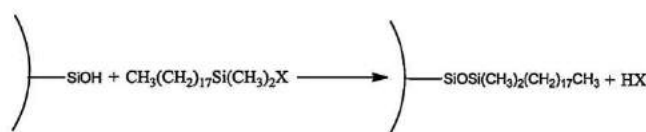
The retention factors (*k*) were calculated using Eq. (1):

$$k = \frac{(t_r - t_0)}{t_0} \quad (1)$$

where *t*₀ is the retention time of uracil, taken as the dead time, as recommended.

The selectivity factors (*α*) were calculated using Eq. (2):

$$\alpha_{a,b} = \frac{k_a}{k_b} \quad (2)$$

Fig. 2. Silanization with ODMAS (X=(N(CH₃)₂)).

where k_a and k_b are the retention factors for solutes a and b , respectively.

The six parameters considered in the Tanaka test and the mobile phases used are described in Table 2. The columns were compared to commercially available columns with different SPP silica chemistries from different manufacturers. The results are presented in radar plots to magnify the small differences between some parameters and to differentiate between each modified SPP silica.

2.4.2. Veuthey test procedure

The simplified Veuthey test is especially useful to evaluate the performance of each stationary phase for the analysis of basic solutes and to classify the chromatographic supports. This method is one way to investigate in detail the silanol activity depending on the thermal pretreatment performed before the functionalization. According to the simplified Veuthey test [43], a set of seven solutes with different physico-chemical properties was injected (acetonitrile-0.0375 M phosphate buffer (pH 7.0), 40:60 (v/v)). As two previously described probes, i.e., methadone and fentanyl, were not easily available, they were substituted by carvedilol and penbutolol hydrochloride to simplify the test [42]. The temperature was set at 30 °C in the oven without pre-heating the mobile phase. The solutes were detected at 215 nm, and the injection volume was 5 μ L. Each target solute was injected three times with standard deviations of less than 1% for the retention time values and the asymmetry factors.

The retention factor was calculated using Eq. (1) with NaNO₃ as the dead time, as recommended. The asymmetry factor was calculated using Eq. (3):

$$As = \frac{1}{2} \times \left(1 + \frac{B}{A} \right) \quad (3)$$

where A and B were half-width before and after the apex, evaluated at 5% of the peak height using the Chromeleon software.

2.4.3. Data analysis

The efficiency (N) values were calculated by the Chromeleon software using Eq. (4):

$$N = 5.54 \times \left(\frac{t_r}{w_{1/2}} \right)^2 \quad (4)$$

Where t_r and $w_{1/2}$ are the retention time and width of the peak at half height, respectively.

Principal Component Analysis (PCA) and Hierarchical Cluster Analysis (HCA) were performed using XLStat 2014.3.05 software (Addinsoft, New York, NY, USA). For HCA, Ward's method was used to cluster the normalized data, and the Euclidean distance defined the distance between two clusters.

3. Results and discussion

3.1. Characterization of the SPP silica surface before functionalization

According to the SEM images, the sphericity was considerable and the distribution was homogeneous. The diameter was found to be approximately 2.6–2.7 μ m for the non-treated SPP silica and remained the same after a 400 °C (data not shown) and a 900 °C thermal pretreatment (Fig. 3a). However, after a thermal pretreatment at 1100 °C, a sintering and shrinkage of the SPP silica matrix was noticed as the diameter decreased to 2.1–2.3 μ m (Fig. 3b). Complementary to the microscopic observations, granulometric measurements were achieved to furnish a size distribution of the overall sample of SPP silica. Thus, the three curves obtained for SPP silica (untreated, 400 °C-pretreated, and 900 °C-pretreated) in acetonitrile were identical and totally stackable, they showed that the distribution is very homogeneous (Fig. 4, in blue). Moreover, the distribution of particle sizes was narrow, centered on 2.6 μ m for the bare silica, as well as for the 400 °C and 900 °C pretreated SPP silica. The shrinkage and sintering of the matrix for the SPP silica pretreated at 1100 °C was confirmed; the size distribution was wider because of aggregation (Fig. 4, in red).

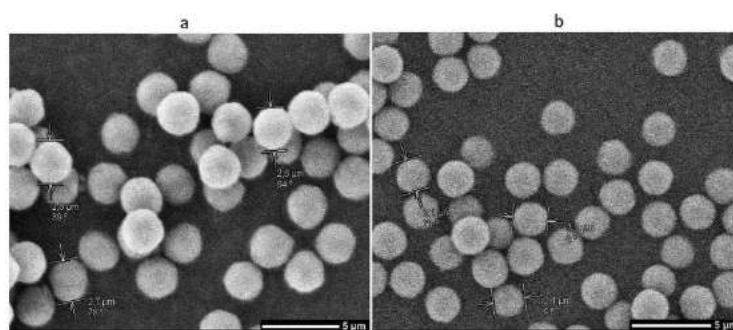


Fig. 3. SEM pictures of 900 °C-pretreated SPP silica (a) and 1100 °C-pretreated SPP silica (b).

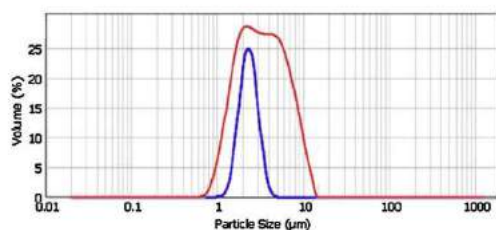


Fig. 4. Granulometric curves of silica (superimposition of the untreated, 400 °C-pretreated, and 900 °C-pretreated) (in blue) and after the thermal treatment at 1100 °C (in red). (For interpretation of the references to colour in this figure legend, the reader is referred to the web version of this article.)

After these morphological characterizations, the specific surface area was measured using the BET method. The values obtained for the bare SPP silica ($126 \text{ m}^2 \text{ g}^{-1}$), as for the 400 °C ($120 \text{ m}^2 \text{ g}^{-1}$) and 900 °C ($116 \text{ m}^2 \text{ g}^{-1}$) pretreated SPP silica were close together and confirmed that up to 900 °C, thermal treatment did not produce noticeable morphological changes. However, after the 1100 °C-pretreatment, the specific surface area drastically decreased to $1 \text{ m}^2 \text{ g}^{-1}$. These results are in contrast to the results obtained for totally porous silica. Indeed, Zhuravlev [37] observed a progressive sintering and shrinkage between 400 and 900 °C in vacuo, and Sunseri [36] noticed that temperatures above 800 °C led to sintering and chromatographically useless silica.

These data suggested that the “solid core” morphology associated with the “porous shell” (core-shell particle) improved the thermal stability compare to the totally porous silica. Consequently, higher thermal pretreatment can be applied (up to 900 °C) before functionalization without destruction of the SPP silica matrix.

3.2. Characterization after functionalization

The elemental analysis was used to determine the grafting rate using Eq. (5):

$$\tau (\mu\text{mol m}^{-2}) = \frac{10^6 \times p_c}{[10^2 \times M_c \times n_c - p_c \times (M_w - 1)] \times S_{\text{BET}}} \quad (5)$$

where p_c is the carbon percentage by weight of the bonded material, M_c is the atomic weight of carbon, M_w is the molecular weight of the grafted molecule, n_c is the total number of carbon atoms in the bonded organic group, and S_{BET} is the specific surface area ($\text{m}^2 \text{ g}^{-1}$ of silica).

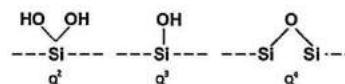


Fig. 6. NMR signal identification.

The maximum coverage was observed for the SPP silica previously treated from ambient temperature to 400 °C (Table 1), and above this temperature, coverage decreased progressively with the thermal pretreatment temperature, until the absence of grafting was observed for the SPP silica treated at 1100 °C. Indeed, it was reported [30,37] that the total silanol group concentration decreased progressively by increasing the temperature and that the concentration of isolated silanol groups was maximized at 400 °C when the vicinal groups were no longer present.

DRIFT spectroscopy is a useful tool to study chemically modified surfaces by the determination of the specific vibrational bands. Compared to the bare SPP silica (Fig. 5a), the progressive decrease of the silanol stretching bands between $3700\text{--}3200 \text{ cm}^{-1}$ was noticed, until the complete disappearance for the 1100 °C calcined SPP silica. Strong stretching bands in the $3000\text{--}2800 \text{ cm}^{-1}$ region as well as weak deformation bands in the $1350\text{--}1550 \text{ cm}^{-1}$ region appeared and clearly indicated the bonding of the alkyl chain (see Fig. 5b). More precisely, for the SPP silica treated at 900 °C before grafting, bands appeared as follows: at 2947 cm^{-1} and 2852 cm^{-1} , the anti-symmetrical stretching band of methyl groups and the symmetrical stretching band of methylene groups, respectively; and at approximately $2870\text{--}2930 \text{ cm}^{-1}$, the symmetrical stretching band of methyl groups and the anti-symmetrical stretching band of methylene groups. The stretching band near 3660 cm^{-1} (Fig. 5b) was attributed to the isolated silanols which remained ungrafted during the silanization process.

In addition, ^{29}Si solid state NMR spectroscopy is useful to study the chemically modified surfaces by determination of the chemical shifts of the species linked to the silicon atoms. All thermally pretreated bare SPP silica, as well as the C_{18} -thermally pretreated SPP silica, were analyzed by ^{29}Si CP/MAS (Cross Polarization with Magic Angle Spinning) and ^{29}Si HPDEC (High Power Decoupling) NMR. The ^{29}Si CP/MAS measurements allowed a good characterization with an appropriate signal to noise ratio for the 400 °C thermally pretreated SPP silica. After pretreatment at 900 °C and 1100 °C, the sensitivity of the ^{29}Si CP/MAS measurements decreased. In these samples, there are probably fewer protons in proximity to the silicon atoms, and the Hartmann–Hahn match could not be efficiently achieved. Consequently, the ^{29}Si HPDEC spectra were used.

According to reports in the literature [44] (Fig. 6), the ^{29}Si CP/MAS spectrum of the bare SPP silica (Fig. 7a) showed main

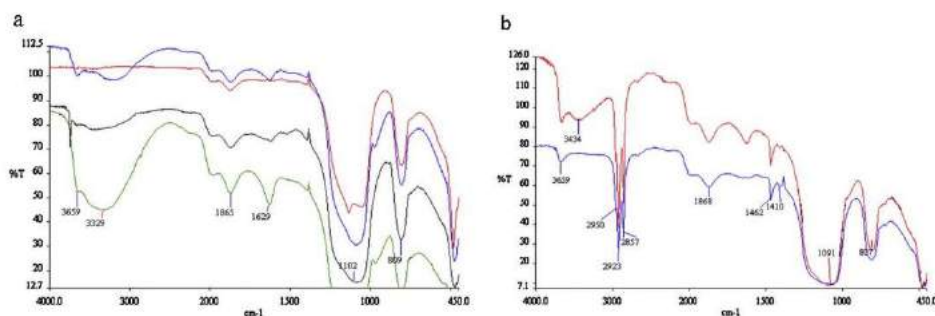


Fig. 5. (a) DRIFT comparison of SPP silica before the thermal treatment (green) and thermally treated at 400 °C (blue), 900 °C (black) and 1100 °C (red) (b) DRIFT of the 900 °C C18 EC MW SPP silica (blue), and the 400 °C C18 EC MW SPP silica (red). (For interpretation of the references to colour in this figure legend, the reader is referred to the web version of this article.)

Table 1
Grafting rates of chemically modified SPP silica under microwave irradiations.

Type of synthesis	End-capping reagent	%C	Thermal treatment (°C)	Grafting rate ($\mu\text{mol m}^{-2}$)	N ^a
C18 MW SPP	–	9.5	–	3.6	12600
C18 EC MW SPP	BMMS	9.5	–	3.6	12100
400 C18 MW SPP	–	9.1	400	3.6	12800
400 C18 EC MW SPP	BMMS	9.3	400	3.7	12500
900 C18 MW SPP	–	7.7	900	3.1	12000
900 C18 EC MW SPP	DATS	7.9	900	3.2	11500
1100 C18 MW SPP	–	0.0	1100	0.0	–

With MW = MicroWave, EC = End-Capping, BMMS = bis-(dimethylamino)dimethylsilane, DATS = dimethylaminotrimethylsilane, SPP = superficially porous particle.

^a Calculated with fluorene CH₂CN-H₂O 70:30 (v/v), 23°C, 254 nm, values rounded to the nearest 100.

resonances at –100 ppm, and –110 ppm, corresponding to isolated silanol Q₃ and siloxane Q₄ groups, respectively (Fig. 6). A small signal at about –90 ppm, characteristic of geminal silanol Q₂ groups, was also observed. ²⁹Si NMR spectra of the thermally pretreated bare SPP silica demonstrated that depending on the thermal treatment, the silanol/siloxane group population was not the same. For the 400°C thermally pretreated SPP silica, the Q₂, Q₃ and Q₄ signals were distinguished by the ²⁹Si CP/MAS measurements (Fig. 7b). After pretreatment at 900°C, the ²⁹Si HPDEC spectrum revealed two peaks: the Q₄ signal (–110 ppm) and the Q₃ signal (–100 ppm) (Fig. 7c). No Q₂ signal was detected, which confirmed

that the geminal silanols were either in very low concentration or entirely removed at this temperature. For the 1100°C thermally pretreated SPP silica, only the siloxane groups (–110 ppm) were clearly detected (Fig. 7d) in the ²⁹Si HPDEC spectrum. Even if, due to the low number of protons, the spectrum is not well resolved, it confirmed that the silanol population was totally removed at this temperature, which was in accordance with the infrared spectroscopy measurements.

After the derivatization of each thermally pretreated SPP silica, ¹H MAS, ²⁹Si and ¹³C CP/MAS and ²⁹Si HPDEC NMR spectra confirmed (see below for a full description) the C₁₈ grafting for the

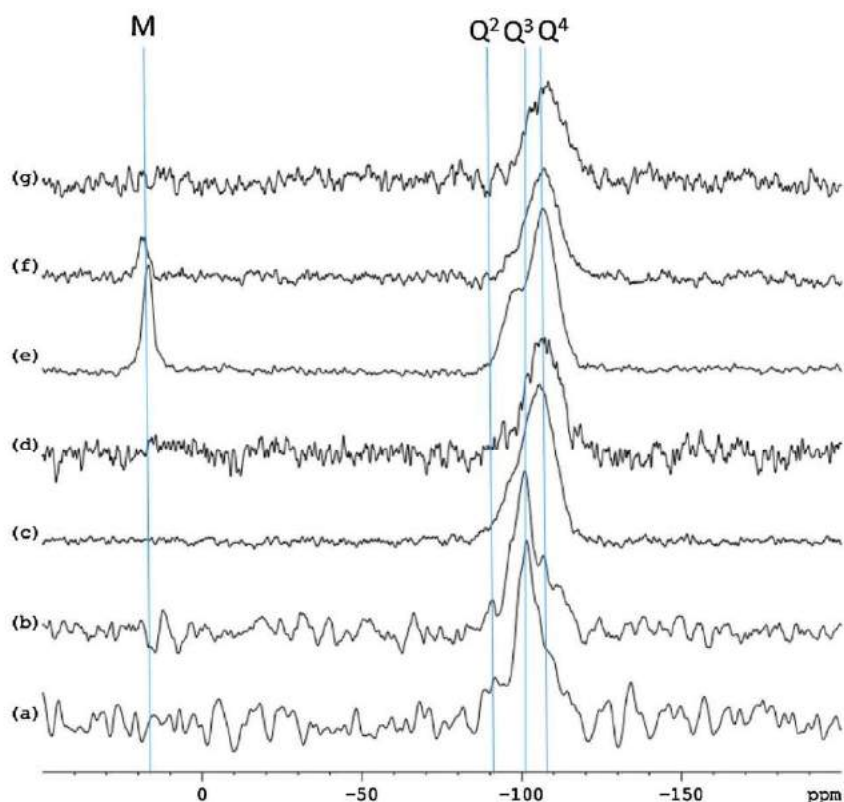


Fig. 7. ²⁹Si NMR spectra of untreated and thermally pretreated bare SPP silica. Q₂ geminal silanols, Q₃ isolated silanols, Q₄ siloxane groups. (a) ²⁹Si CP/MAS spectrum of untreated bare SPP silica, (b) ²⁹Si CP/MAS spectrum of 400°C-pretreated bare SPP silica, (c) ²⁹Si HPDEC spectrum of 900°C-pretreated bare SPP silica, (d) ²⁹Si HPDEC spectrum of 1100°C-pretreated bare SPP silica, (e) ²⁹Si CP/MAS spectrum of 400 C18 MW SPP silica, (f) ²⁹Si HPDEC spectrum of 900 C18 MW SPP silica, (g) ²⁹Si HPDEC spectrum of 1100 C18 MW SPP silica.

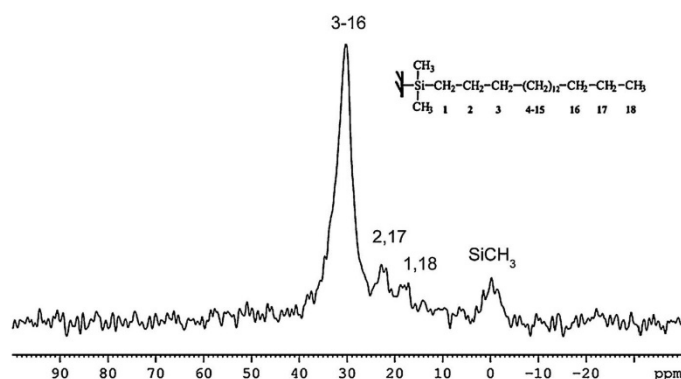


Fig. 8. ^{13}C CP-MAS spectrum of 400 C18 MW SPP silica.

400 °C as well as for the 900 °C thermally pretreated SPP silica. The ^{13}C MAS NMR spectrum was a first confirmation of the grafting of the C_{18} chain (Fig. 8). The peak at 0 ppm was assigned to the methyl groups directly linked to the silicon atom; another peak at approximately 30 ppm corresponded to the methylene units 3–16; and carbons 1, 18 and 2, 17 are associated with peaks at approximately 20 ppm and 25 ppm, respectively.

In the ^{29}Si NMR spectra, the peak at 13 ppm corresponding to the Si–C bond (M groups) confirmed the grafting for the 400 °C as well as for the 900 °C-pretreated SPP silica (Fig. 7e and f). This signal was not observed for the 1100 °C thermally pretreated SPP silica (Fig. 7g). As previously concluded by the elemental analysis and DRIFT measurements, the SPP silica thermally pretreated at 1100 °C was not grafted. The geminal silanol (Q_2) peak at –90 ppm detected for the 400 °C thermally pretreated bare SPP silica completely disappeared, whereas the Q_3 peak at –100 ppm was greatly reduced. These data suggested that the geminal silanols were the most reactive on the surface, which was in accordance with the results presented by Sunseri et al. [36].

The comparison to the ^1H MAS NMR spectra presented in Fig. 9 warrants additional comment. The resolution was sufficient to clearly distinguish the different signals associated with the (CH_2) units (1.2 ppm) and the methyl terminal groups (0.7 ppm). According to Pursch et al. [44], the changes in resolution of the spectra are dependent of the coverage. The high loading of the C_{18} -400 °C pretreated SPP silica led to restricted motions of the alkyl chains and stronger dipolar interactions, which resulted in line broadening in the ^1H MAS NMR spectrum (Fig. 9a). In contrast, the peaks of the C_{18} -900 °C pretreated SPP silica were narrower, due to a lower coverage (Fig. 9b), which was in accordance with the elemental analysis results.

3.3. Chromatographic studies

Two columns were packed with each type of C_{18} -bonded pretreated SPP silica (no pretreatment, 400 °C, 900 °C, 1100 °C), and two columns were packed for each end-capped C_{18} -bonded pretreated SPP silica (no pretreatment, 400 °C, 900 °C, 1100 °C). These columns were tested with probe solutes (uracil, naphthalene fluorene) in $\text{CH}_3\text{CN}-\text{H}_2\text{O}$, 70:30 (v/v), to evaluate their retention behavior and to determine their efficiency (Table 1 for the average values). Three intermediate temperatures (450, 525, and 600 °C) were applied to the SPP silica from the same batch without the C_{18} functionalization. Polar solutes were tested (Table S1) to characterize the evolution of the retention factor and asymmetry factor

with the thermal treatment. The trend was the same: the higher the temperature of the thermal treatment, the higher the retention of the columns but also the higher the asymmetry factors (a discussion with the Tanaka test and Veuthey test is included in the following sections). As expected, for the column packed with the SPP silica thermally pretreated at 1100 °C, no retention was obtained as a result of an absence of C_{18} coverage (data not shown). For the other columns, all of the results were very similar for the two columns of each type, so we decided to perform the Tanaka test and the Veuthey test on one column of each type. We chose SPP silica commercial columns of various functionalities and with similar physical characteristics (particle size, specific surface area, porosity) to compare the chromatographic properties of columns packed with our SPP silica stationary phases. The specifications are available in Table S2. All values reported in the following section correspond to the average value for three injections of each probe.

3.3.1. Tanaka test

The Tanaka test is commonly used in the literature to study the general chromatographic behavior of C_{18} stationary phases. The retention factor k_{PB} describes the hydrophobic retention measured using the retention of pentylbenzene. The highest values were obtained for the C_{18} -900 °C pretreated phases (namely 900 C18 MW SPP and 900 C18 EC MW SPP), despite a lower specific surface area and a lower grafting rate due to the reduced amount of silanol groups still present after the thermal pretreatment (Table 2). Moreover, this result demonstrated that the numerous siloxane bridges resulting from the dehydroxylation of the silanol groups play a role due to their hydrophobicity and polarizability. An illustration of the powerful resolution of this specific phase (900 C18 EC MW SPP) is presented in Fig. 10 with the separation of electron-rich hydrophobic solutes of high concern. The baseline resolution of the 18 standard PAHs was achieved in less than 48 min.

Hydrophobic selectivity, $\alpha_{\text{PB/BB}}$, is the selectivity between pentylbenzene and butylbenzene. It reflects the ability of the phase to separate compounds that differ by only a single methylene group. Only non-end-capped phases were considered to estimate the effect of pretreatment without any contribution of the end-capping ligand. The selectivity was similar regardless of whether the thermal pretreatment was applied (from 1.54 for the non-treated SPP silica to 1.50 for the 900 °C pretreated SPP silica). Indeed, this parameter is dependent of the surface coverage and the nature of the ligand, which was in each case an octadecyl group.

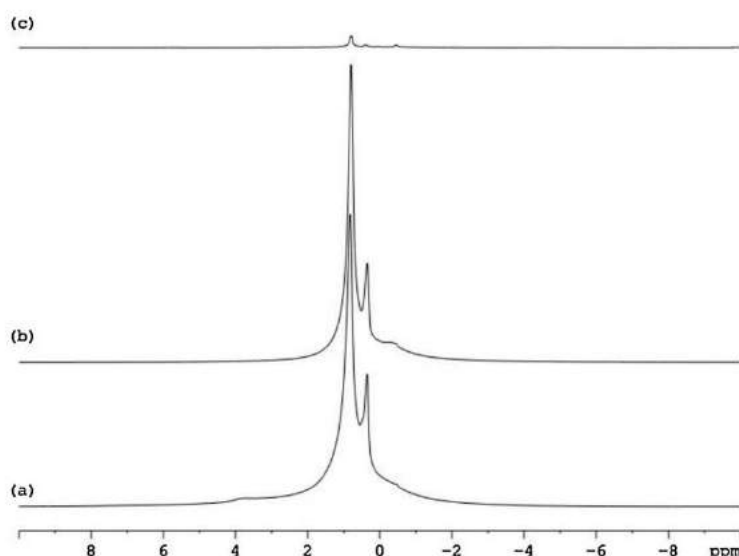


Fig. 9. ^1H NMR spectra of grafted silica (a) 400 C18 MW SPP silica, (b) 900 C18 MW silica, (c) 1100 C18 MW SPP silica.

Shape selectivity, $\alpha_{\text{T/O}}$, describes the ability of the phase to discriminate between planar structures (triphenylene) and those with greater hydrodynamic volume (*o*-terphenyl). This parameter is dependent on the silane functionality and the surface coverage. For our stationary phases, the highest values were obtained for the C₁₈-400 °C pretreated phase (400 C18 MW SPP and 400 C18 EC MW SPP), which was in accordance with the literature data [36,39] obtained for porous material.

Hydrogen bonding capacity, $\alpha_{\text{C/P}}$, describes the column's ability to interact through hydrogen bonds with a polar solute. The necessity of end-capping was evaluated considering this factor, a significant decrease of this factor was noticed for the end-capped-C₁₈-non pretreated (C18 EC MW) as for the end-capped-C₁₈-thermally pretreated (400 C18 EC MW SPP and 900 C18 EC MW SPP) (Table 2) compare to their equivalent non-end-capped

(C18 MW SPP, 400 C18 MW SPP and 900 C18 MW SPP). From this point of view, the 400 C18 EC MW SPP was the best.

Total ion-exchange capacity at pH 7.6, $^{7.6}\alpha_{\text{B/P}}$, reflects the total silanol activity of the column, affecting the peak shape and the selectivity for polar and ionizable analytes. The importance of end-capping was also demonstrated considering this factor; for the C18 MW SPP, the value decreased from 0.49 to 0.30 after end-capping (C18 EC MW SPP); for the 400 C18 MW SPP, from 0.37 to 0.30 after end-capping (400 C18 EC MW SPP), and for the 900 C18 MW SPP, from 0.84 to 0.68 after end-capping (900 C18 EC MW SPP). Performing a pretreatment at 900 °C reduced the amount of silanols, and may favor the accessibility of solutes to residual silanols. Moreover, as the amount of metal impurities was not impacted by the thermal treatment, this led to a lower silanol/metal ratio and the acidic residual silanols (single free silanols) activated by the metals

Table 2
Values obtained in Tanaka test for the stationary phases studied.

Stationary phase	k_{PB}	$\alpha_{\text{PB/BB}}$	$\alpha_{\text{T/O}}$	$\alpha_{\text{C/P}}$	$^{2.7}\alpha_{\text{B/P}}$	$^{7.6}\alpha_{\text{B/P}}$	%C	S_{DET} ($\text{m}^2 \text{g}^{-1}$)
C18 MW SPP	5.31	1.54	1.65	0.52	0.03	0.49	9.5	126
C18 EC MW SPP	5.24	1.51	1.50	0.43	0.06	0.30	7.7	126
400 C18 MW SPP	4.69	1.55	1.74	0.54	0.06	0.37	9.1	120
400 C18 EC MW SPP	4.53	1.53	1.74	0.37	0.05	0.30	9.3	120
900 C18 MW SPP	5.93	1.50	1.60	0.60	0.08	0.84	7.7	116
900 C18 EC MW SPP	5.34	1.51	1.55	0.52	0.05	0.68	7.9	116
Halo C18	5.16	1.53	1.46	0.35	0.04	0.20	7.7	150
Poroshell 120 ES-C18	4.30	1.51	1.33	0.36	0.06	0.11	8.0	130
Accucore C18	3.85	1.51	1.70	0.30	0.04	0.11	9.0	130
ACE C18	5.86	1.50	1.59	0.41	0.07	0.24	15.5	300
Kinetex EVO C18	3.65	1.48	1.32	0.46	0.06	0.21	12.0	200
Halo Phenyl hexyl	2.41	1.38	1.16	0.85	0.06	0.25	7.1	150
Halo RP Amide	3.62	1.47	1.88	0.20	0.02	0.20	8.2	150
Accucore aQ	4.47	1.49	2.25	0.40	0.08	0.61	9.0	130
Accucore C30	3.31	1.52	1.89	0.58	0.07	0.24	5.0	130

With PB - pentylbenzene, BB - butylbenzene, T - triphenylene, O - *o*-terphenyl, C - caffeine, B - benzylamine, P - phenol. Chromatographic conditions: CH₃OH-H₂O 80:20 (v/v) for the determination of hydrophobicity (k_{PB}), amount of alkyl chains ($\alpha_{\text{PB/BB}}$), and steric selectivity ($\alpha_{\text{T/O}}$); CH₃OH-H₂O 30:70 (v/v) for the determination of hydrogen bonding capacity ($\alpha_{\text{C/P}}$) and CH₃OH-phosphate buffer (0.02 M) 30:70 (v/v) for the determination of ion exchange capacity $^{2.7}\alpha_{\text{B/P}}$ and $^{7.6}\alpha_{\text{B/P}}$, 30 °C, 254 nm.

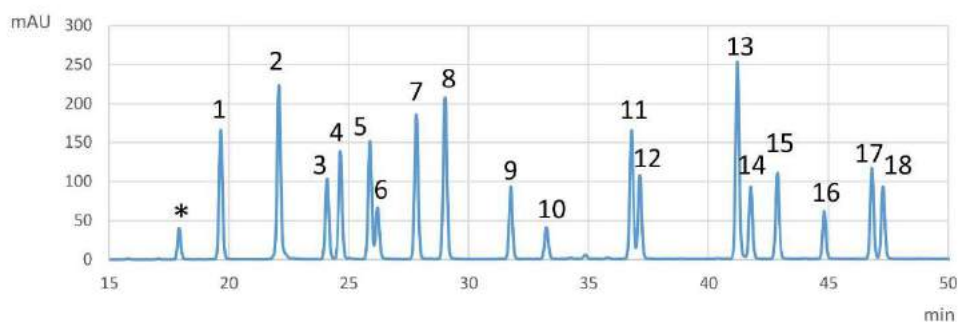


Fig. 10. Chromatogram obtained on 900 C18 EC MW superficially porous phase, 250×4.6 mm, $F=1$ mL/min, 5 min at 50/50 (v/v) $\text{CH}_3\text{CN}/\text{H}_2\text{O}$ to 100% CH_3CN in 50 min, 254 nm, 22 °C. (*) Impurity, (1) Naphthalene, (2) Acenaphthylene, (3) 1-Methylnaphthalene, (4) 2-Methylnaphthalene, (5) Acenaphthene, (6) Fluorene, (7) Phenanthrene, (8) Anthracene, (9) Fluoranthene, (10) Pyrene, (11) Chrysene, (12) Benz(a)anthracene, (13) Benzo(b)fluoranthene, (14) Benzo(k)fluoranthene, (15) Benzo(a)pyrene, (16) Dibenzo(a,h)anthracene, (17) Benzo(g,h,i)perylene, (18) Indeno(1,2,3-cd)pyrene.

could interact strongly by ion interaction with the benzylamine protonated at this pH. Indeed, for the 900 C18 MW SPP and 900 C18 EC MW SPP, a higher value was obtained (0.84) than for the other pretreated phases.

3.3.2. Multivariate data analyses: HCA and PCA of the Veuthey test results

According to the modified Veuthey test, the chromatographic parameters (k and A_s) were calculated for a mobile phase composed of phosphate buffer (0.0375 M, pH 7) and acetonitrile, (60/40, v/v). A set of 7 solutes was tested, representing 4 groups: large polar molecules (procainamide, quinine), large apolar molecules (carvedilol, penbutolol), small polar molecules (nicotine, pyridine) and an intermediate one (chloroprocaine). Under these conditions, the residual silanols and the basic solutes were mostly charged. Consequently, high asymmetry values could be obtained as a result of strong ion interactions. Considering this wide range of physico-chemical properties, different types of interactions between the molecules and the stationary phases could occur, providing a better understanding of the support characteristics. The more data collected, the more relevant the statistical representation of the overall information. So, we considered the retention factors and the asymmetry factors for all of the columns tested (various thermal pretreatment, C_{18} -functionalization under microwave irradiation, and C_{18} -functionalization under conventional heating). The chromatographic properties were independent from the heating source used for the syntheses, as for each C_{18} -pretreated SPP silica, the corresponding columns were gathered (see the explanation of the score plots below). The grafting rates of the supplementary columns are provided in Table S3, and the values for the Tanaka test and Veuthey test are given in Tables S4 and S5, respectively.

The Principal Component Analysis (PCA) was useful to provide a better understanding of the repartition of the columns in a single projected space. The data were normalized (centered and reduced) to give equal significance to each. The score plots are shown in Fig. 11a, and we note that the first two principal components together account for more than 93% of the total variance. Consequently, this representation contained a significant amount of the total information and was amenable to interpretation. For a better understanding of the position of the stationary phases in the score plots in Fig. 11a, it was necessary to take into account the loading plots in Fig. 11b. Firstly, we note that the mean vector of the retention factor is located in the bottom right, or near the abscissa axis. On the contrary, the asymmetry factor vector is located in the top right with an angle approximately 45°. This indicates that

the further toward the right a phase is located, more important the retention is, whatever its position on the ordinate axis. The higher it is, the more it provides high asymmetry values for the analysis of basic solutes in these chromatographic conditions. This was the case for our non-end-capped phases and particularly for the phases pretreated at 900 °C before grafting (900 C18 MW SPP, 900 C18 EC MW SPP), as already noticed with the high value of ion exchange capacity for the Tanaka test. The other supports presented chemistries better adapted to the analysis of basic solutes as they were located on the opposite side of the asymmetry vector. Interestingly, the RP amide phase containing a polar embedded group in the hydrocarbonated chain was not necessarily better than the Poroshell 120 ES-C18 or our 400 C18 EC MW SPP (Table 3). Secondly, the retention factors were located in the same direction and were generally well represented. This signified that the supports in this direction provided high retention for the analysis of basic solutes in these chromatographic conditions. The phases pretreated at 900 °C exhibited a particular behavior in terms of retention capacity (see Table 3 for the Veuthey test and Tanaka test values), despite a lower grafting rate. Actually, as the temperature pretreatment increased, the amount of silanol decreased to the benefit of the formation of siloxane bridges, which are more hydrophobic than the silanol groups. However, these phases also exhibited the highest asymmetry factors. Indeed, at 900 °C, only the isolated silanols remained, which are known to be the most acidic [45], and could interact strongly by hydrogen bonds and ionic interactions, depending on the pH conditions of the analysis. Moreover, the silica contains traces of metal ions left from the manufacturing process, which activates the silanols, making them highly acidic. This phenomenon could be exacerbated if the metal/silanol ratio increases (lower silanol population), leading to higher retention and tailing peaks for the basic solutes. Another interesting result was the location of the C30 phase, at the opposite side of the hydrophobicity vector. This phase did not exhibit as high retentions compared to the C_{18} phases, but exhibited a relatively high value of the asymmetry factor (see the values of the Tanaka test and Veuthey test in Tables 2 and 3, respectively).

Complementary to PCA, which furnishes a global view of all columns, the Hierarchical Component Analysis (HCA) allows for defining clusters of columns that exhibit similar behavior with respect to the Veuthey test. This is a method of grouping objects (here stationary phases) by similarity, which is evaluated by a measurement of distance between pairs of samples. The output is a dendrogram, where the phases separated by a small distance are close to one another and joined by short lines, whereas the most

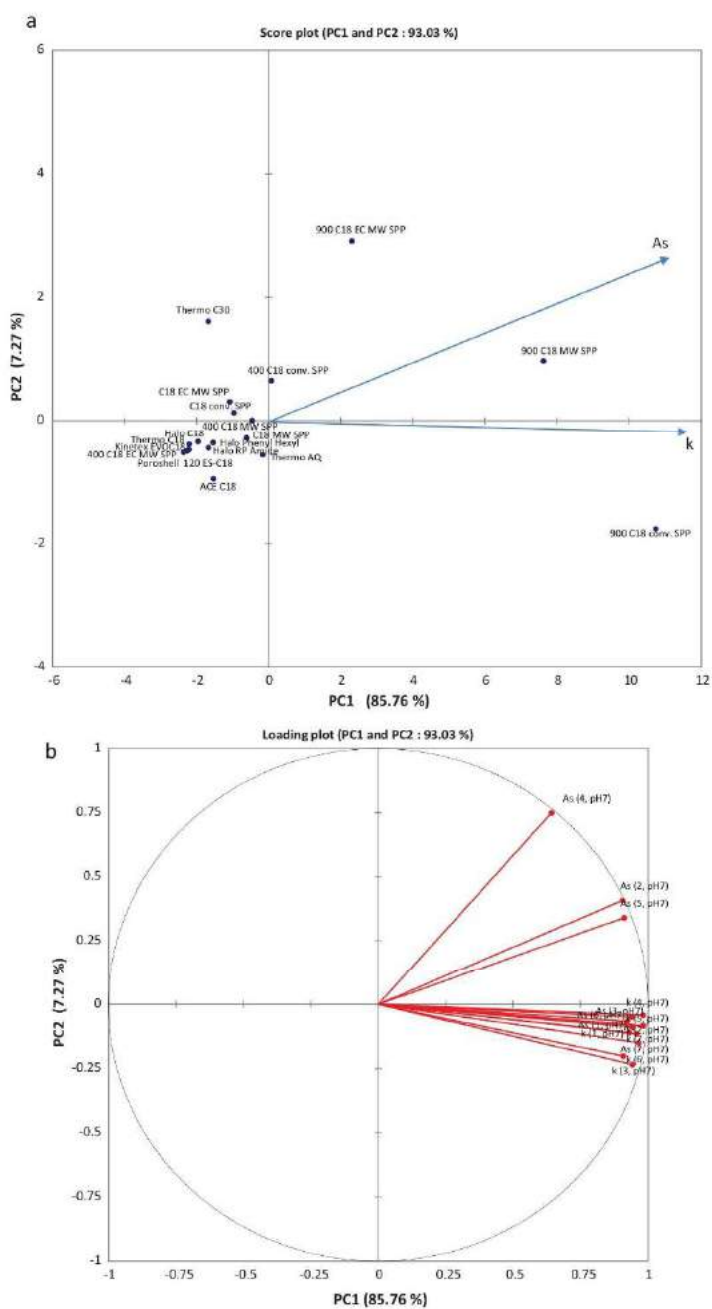


Fig. 11. Principal component analysis based on normalized retention factor and asymmetry factor for the solutes in Table 3. Chromatographic conditions: acetonitrile-pH 7.0, 0.0375 M phosphate buffer 40:60, v/v, 30 °C, 215 nm. (a) Score plot and (b) loading plot.

Table 3Values of the stationary phases for the Veuthey test. Chromatographic conditions: CH₃CN-phosphate buffer pH7, 0.0375 M 60:40 (v/v), 30 °C, 215 nm.

Stationary phase	k (1)	k (2)	k (3)	k (4)	k (5)	k (6)	k (7)	As (1)	As (2)	As (3)	As (4)	As (5)	As (6)	As (7)
C18 MW SPP	1.97	0.69	1.65	2.87	0.55	0.59	0.07	2.74	3.17	4.80	3.21	1.90	1.57	1.59
C18 EC MW SPP	2.82	0.70	0.66	2.69	0.60	0.51	0.05	2.27	2.58	2.79	4.28	1.85	2.06	1.35
400 C18 MW SPP	2.37	0.62	1.48	2.96	0.56	0.68	0.06	1.92	2.85	4.90	4.24	1.81	2.33	1.41
400 C18 EC MW SPP	1.64	0.36	0.43	2.00	0.37	0.42	0.03	1.19	1.73	2.52	2.32	1.44	1.45	1.46
900 C18 MW SPP	11.81	22.73	3.42	85.23	4.12	0.91	0.63	4.36	9.13	8.70	7.94	3.50	3.53	2.48
900 C18 EC MW SPP	5.44	7.74	1.30	29.66	1.86	0.56	0.31	2.19	8.03	4.66	8.67	3.28	1.75	1.84
Poroshell 120 ES-C18	2.28	0.42	0.29	1.93	0.5	0.32	0.02	1.51	1.65	1.57	1.97	1.57	1.36	1.52
Accucore C18	1.57	0.32	0.32	1.42	0.36	0.35	0.02	1.73	1.78	2.00	2.34	1.58	1.54	1.52
Halo C18	2.12	0.42	0.45	1.89	0.46	0.37	0.04	2.10	1.80	2.43	2.80	1.46	1.68	1.40
Halo Phenyl Hexyl	3.97	0.76	0.43	3.56	0.81	0.42	0.19	1.44	1.83	2.97	3.13	1.49	1.43	1.53
Halo RP Amide	4.75	0.98	0.42	5.57	0.77	0.41	0.11	1.27	1.96	2.37	2.74	1.50	1.42	1.53
Accucore aQ	5.45	2.05	1.21	9.79	1.23	0.67	0.32	1.81	3.19	4.13	3.26	1.65	1.53	1.55
Accucore C30	2.47	0.84	0.23	3.32	0.44	0.26	0.06	2.18	3.40	1.57	6.68	1.55	1.43	1.35
Kinetex EVO C18	2.48	0.65	0.40	2.07	0.56	0.43	0.05	1.57	1.75	1.68	2.53	1.39	1.34	1.40
ACE C18	3.89	0.85	0.69	4.17	0.81	0.6	0.07	1.24	1.59	2.98	2.44	1.20	1.80	1.48

With 1 – Carvedilol, 2 – Quinine, 3 – Nicotine, 4 – Penbutolol, 5 – Chlorprocaine, 6 – Pyridine, 7 – Procainamide.

dissimilar phases are linked by longer lines. After normalization, the HCA calculation was obtained using the Ward aggregation method with Euclidean distances.

As for PCA, the HCA analyses were performed on the integral set of data, and the resulting dendrogram is presented in Fig. 12. It

provided a classification of the 15 SPP silica columns studied, based on the normalized retention factors and asymmetry factors for the 7 solutes of the simplified Veuthey test. In accordance with the above classification in Fig. 12, different groups could be distinguished as the clusters are based on the nature of the stationary phases

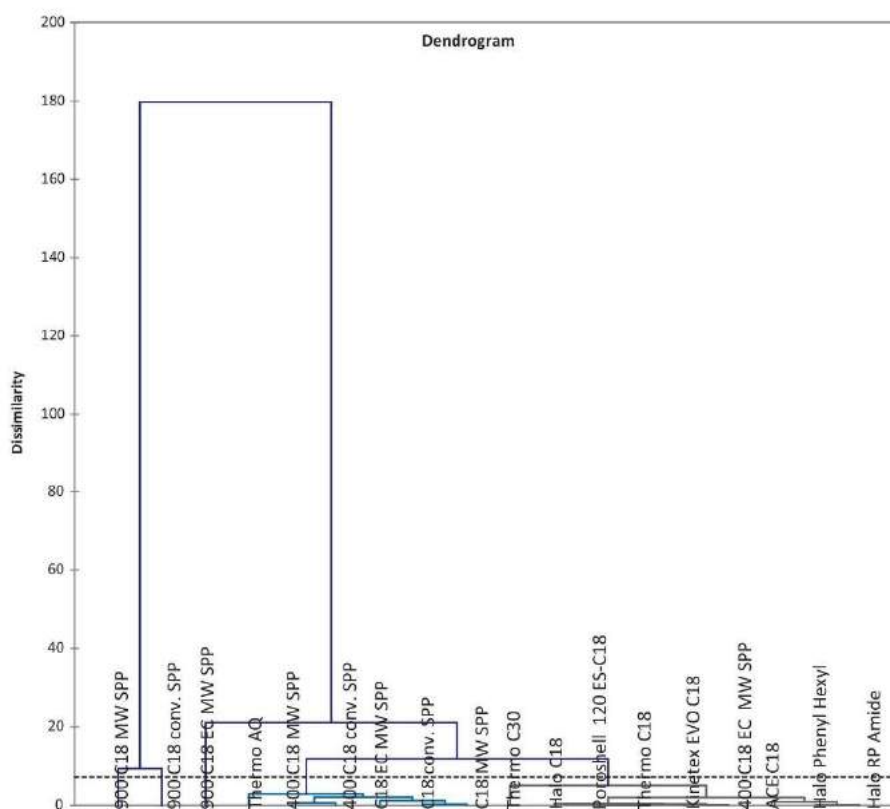


Fig. 12. Hierarchical cluster analysis based on normalized retention factor and asymmetry factor for the solutes in Table 3. Chromatographic conditions: acetonitrile-pH 7.0, 0.0375 M phosphate buffer 40:60, v/v), 30 °C, 215 nm.

and the thermal pretreatment. Although the similarity between the commercially available C₁₈ phases was somewhat expected, the singular position of our C₁₈-900 °C pretreated phases (900 C18 MW SPP, 900 C18 conv. SPP, 900 C18 EC MW SPP) was noticeable. As demonstrated by the Tanaka test and the Veuthey test, the higher the temperature of pretreatment (until 900 °C), the higher the retention of the corresponding C₁₈ phases but also the higher the asymmetry factors. Another interesting fact was the effect of end-capping, as demonstrated for the 400 C18 MW SPP. Indeed, the end-capping put this phase among the C₁₈ commercially available phases, whereas the absence of end-capping made it close to the Accucore aQ phase because of accessible silanols. This was also the case for the 900 C18 EC MW SPP; the end-capping step brought it into the other cluster.

3.3.3. Thermal stability of the stationary phases

As demonstrated by Claessens et al. [46], column degradation is affected by pH, buffer type and concentration but is also strongly affected by temperature. Indeed, the solubility of unmodified silica increases substantially with the temperature. After 20 h (in acetonitrile-phosphate buffer 0.25 M pH 7.0, 20:80 (v/v)), at 60 °C, 49% of the bare porous silica was dissolved. The dissolution was lower for the bare SPP silica (37%) than for the bare porous silica; and even lower for the SPP silica pretreated at 900 °C (27%). Regarding these results, we can assume that the SPP structure of the silica made it less soluble under aggressive conditions at high temperature and that this benefit can be improved by the thermal pretreatment. Consequently, the corresponding functionalized stationary phases can be used at higher temperature to increase efficiency and to improve productivity.

4. Conclusion

Thermal dehydroxylation prior to functionalization can be used to obtain different C₁₈ phases. Depending on the temperature of pretreatment, the silica surface evolved as the silanol groups were progressively removed due to a thermally induced condensation process. DRIFT and NMR experiments confirmed that after dehydration, the vicinal silanols were progressively removed as the temperature increased (until 400 °C), then the geminal silanols (until 900 °C), and finally the complete disappearance of all silanol groups at 1100 °C. The grafting of an octadecyl-chain was successfully performed with a maximum coverage of 3.7 μmol m⁻² for the end-capped-C₁₈-400 °C pretreated SPP silica. The use of chemometric analysis methods allowed the grouping of columns depending on their hydrophobic properties and on their peak asymmetry for the analysis of basic solutes. In general, the non-end-capped phases presented higher peak asymmetry values as residual silanols were still accessible. Alternatively, the non-end-capped phase containing residual accessible silanols was close to the Accucore aQ column. Up to 900 °C, the higher the temperature of pretreatment, the higher the retention of the corresponding C₁₈ phases. The high content of siloxane bridges showing additional hydrophobicity and polarizability made the C₁₈-900 °C pretreated phase efficient for the separation of PAHs isomers with full resolution. However, the residual free acidic silanols led to high asymmetry factors. So, the pure silica (Type B) was not enough to eliminate these secondary interactions. Additional specific treatments have to be performed to remove the metal impurities because that deleterious effect became significant when the ratio of metal to silanol increased. Finally, a wide range of C₁₈ columns could be obtained, depending on the choice of the temperature of pretreatment and of end-capping or not. Although the properties could be different, depending on the process of manufacture and the type of silica, we believe that the general strategy can be applied in all silicas

to obtain different stationary phases based on the same batch of material functionalized with the same C₁₈-reagent. Last, under a high concentration of phosphate buffer and temperature (0.25 M, 60 °C), the 900 °C pretreated SPP silica was more stable to dissolution than the untreated SPP silica, which was itself more stable than the porous silica. The corresponding functionalized stationary phases can be used at higher temperatures, increasing chromatographic efficiency and improving productivity.

As this paper was focalized on the thermodynamic study of these C₁₈-thermally pretreated phases, the evaluation of the kinetic parameters is in progress by determination of the kinetic plots.

Acknowledgments

The authors gratefully acknowledge Emilie Petit and Françoise Ringot for the elemental analysis measurements, and Evelyne Blanchard for some chromatographic studies.

Appendix A. Supplementary data

Supplementary data associated with this article can be found, in the online version, at <http://dx.doi.org/10.1016/j.chroma.2015.09.072>.

References

- [1] J.J. Kirkland, S.A. Schuster, W.L. Johnson, B.E. Boyes, Fused-core particle technology in high-performance liquid chromatography: an overview, *J. Pharm. Anal.* 3 (2013) 303–312.
- [2] L. Li, P.W. Carr, J. Evans, Studies of retention and stability of a horizontally polymerized bonded phase for reversed-phase liquid chromatography, *J. Chromatogr. A* 868 (2000) 153–167.
- [3] M.J. Wirth, H.O. Fatunmbi, Horizontal polymerization of mixed trifunctional silanes on silica: a potential chromatographic stationary phase, *Anal. Chem.* 64 (1992) 2783–2786.
- [4] M.J. Wirth, H.O. Fatunmbi, Horizontal polymerization of mixed trifunctional silanes on silica: 2. Application to chromatographic silica gel, *Anal. Chem.* 65 (1993) 822–826.
- [5] L.C. Sander, S.A. Wise, Synthesis and characterization of polymeric phases for liquid chromatography, *Anal. Chem.* 56 (1984) 504–510.
- [6] L.C. Sander, S.A. Wise, Influence of stationary phase chemistry on shape recognition in liquid chromatography, *Anal. Chem.* 67 (1995) 3284–3292.
- [7] T. Kanda, H. Kutsuna, Y. Ohtsu, M. Yamaguchi, Synthesis of polymer-coated mixed-functional packing materials for direct analysis of drug-containing serum and plasma by high-performance liquid chromatography, *J. Chromatogr. A* 672 (1994) 51–57.
- [8] Y. Ohtsu, Y. Shiojima, T. Okumura, J. Koyama, K. Nakamura, O. Nakata, K. Kimata, N. Tanaka, Performance of polymer-coated silica C18 packing materials prepared from high-purity silica gel: the suppression of undesirable secondary retention processes, *J. Chromatogr. A* 481 (1989) 147–157.
- [9] T. Kanda, O. Shiota, Y. Ohtsu, M. Yamaguchi, Synthesis and characterization of polymer-coated mixed-functional stationary phases with several different hydrophobic groups for direct analysis of biological samples by liquid chromatography, *J. Chromatogr. A* 722 (1996) 115–121.
- [10] S. Kobayashi, I. Tanaka, O. Shiota, T. Kanda, Y. Ohtsu, Synthesis and characterization of a polymer-coated C18 stationary phase with high carbon content for liquid chromatography, *J. Chromatogr. A* 828 (1998) 75–81.
- [11] Y. Ohtsu, H. Fukui, T. Kamia, K. Nakamura, M. Nakano, O. Nakata, Y. Fujiyama, Structures and chromatographic characteristics of capsule-type silica gels coated with hydrophobic polymers in reversed-phase liquid chromatography, *Chromatographia* 24 (1987) 380–384.
- [12] J.J. Kirkland, J.L. Glajch, R.D. Farlee, Synthesis and characterization of highly stable bonded phases for high-performance liquid chromatography column packings, *Anal. Chem.* 61 (1989) 2–11.
- [13] J.J. Kirkland, Development of some stationary phases for reversed-phase high-performance liquid chromatography, *J. Chromatogr. A* 1060 (2004) 9–21.
- [14] A.B. Scholten, J.W. de Haan, H.A. Claessens, L.J.M. van de Ven, C.A.M.G. Cramers, ²⁹Si NMR evidence for the improved chromatographic siloxane bond stability of bulky alkylsilane ligands on a silica surface, *J. Chromatogr. A* 688 (1994) 25–29.
- [15] J.J. Kirkland, J.B. Adams, M.A. van Straten, H.A. Claessens, Bidentate silane stationary phases for reversed-phase high-performance liquid chromatography, *Anal. Chem.* 70 (1998) 4344–4352.
- [16] J.J. Kirkland, M.A. van Straten, H.A. Claessens, Reversed-phase high-performance liquid chromatography of basic compounds at pH 11 with silica-based column packings, *J. Chromatogr. A* 797 (1998) 111–120.
- [17] T.L. Ascab, K.M.R. Kallury, C.A. Szafranski, S.D. Corman, F. Liu, Characterization and high performance liquid chromatographic evaluation of a new

- amide-functionalized reversed phase column, *J. Liq. Chromatogr. Relat. Technol.* 19 (1996) 3049–3073.
- [18] X. Liu, A.V. Bordunov, C.A. Pohl, Preparation and evaluation of a hydrolytically stable amide-embedded stationary phase, *J. Chromatogr. A* 1119 (2006) 128–134.
- [19] J.E. O'Gara, B.A. Alden, T.H. Walter, J.S. Petersen, C.L. Niederlaender, U.D. Neue, Simple preparation of a C8 HPLC stationary phase with an internal polar functional group, *Anal. Chem.* 67 (1995) 3809–3813.
- [20] J.E. O'Gara, D.P. Walsh, B.A. Alden, P. Casellini, T.H. Walter, Systematic study of chromatographic behavior vs alkyl chain length for HPLC bonded phases containing an embedded carbamate group, *Anal. Chem.* 71 (1999) 2992–2997.
- [21] C.R. Silva, L.C.S.F. Jardim, C. Airolidi, Evaluation of the applicability and the stability of a C18 stationary phase containing embedded urea groups, *J. Chromatogr. A* 987 (2003) 139–146.
- [22] I. Nováková, H. Vlčeková, S. Petr, Evaluation of new mixed-mode UHPLC stationary phases and the importance of stationary phase choice when using low ionic-strength mobile phase additives, *Talanta* 93 (2012) 99–105.
- [23] J.J. Pešek, M.T. Matyska, R.J. Yu, Synthesis and characterization of endcapped C18 stationary phases using a silica hydride intermediate, *J. Chromatogr. A* 947 (2002) 195–203.
- [24] D.B. Marshall, C.H. Lochmuller, The effect of end-capping reagent on liquid chromatographic performance, *Anal. Chim. Acta* 142 (1982) 63–72.
- [25] M. Reta, P. Carr, Comparative study of divalent metals and amines as silanol-blocking agents in reversed-phase liquid chromatography, *J. Chromatogr. A* 855 (1999) 121–127.
- [26] D.W. Hill, Evaluation of alkyl bonded silica and solvent phase modifiers for the efficient elution of basic drugs on HPLC, *J. Liq. Chromatogr.* 13 (1990) 3147–3175.
- [27] R.J. Vervoort, M.W. Derksen, A.H. Debets, Monitoring of new silica-based reversed-phase stationary phases for the liquid chromatographic analysis of basic pharmaceuticals using principal components analysis, *J. Chromatogr. A* 765 (1997) 157–168.
- [28] D.R. Halfpenny, D.M. Kane, R.N. Lamb, B. Gong, Surface modification of silica with ultraviolet laser radiation, *Appl. Phys.* A 71 (2000) 147–151.
- [29] J. Nawrocki, The silanol group and its role in liquid chromatography, *J. Chromatogr. A* 779 (1997) 29–71.
- [30] P. Van der Voort, E.F. Vansant, Silylation of the silica surface: a review, *J. Liq. Chromatogr. Relat. Technol.* 19 (1996) 2723–2752.
- [31] K.K. Unger, *Porous Silica*, Elsevier, Amsterdam, 1979.
- [32] J. Kohler, J.J. Kirkland, Improved silica-based column packings for high-performance liquid chromatography, *J. Chromatogr.* 385 (1987) 125–150.
- [33] F. Grossmann, V. Ehwald, C. Du Fresne von Hohenesche, K.K. Unger, Impact of the post-treatment conditions of parent silica on the silanization of n-octadecyl bonded silica packings in reversed-phase high-performance liquid chromatography, *J. Chromatogr. A* 910 (2001) 223–236.
- [34] D. Kumar, K. Schumacher, C. Du Fresne von Hohenesche, M. Grün, K.K. Unger, MCM-41, MCM-48 and related mesoporous adsorbents: their synthesis and characterisation, *Colloids Surf., A* 187–188 (2001) 109–111.
- [35] S.P. Boudreau, W.T. Cooper, Analysis of thermally and chemically modified silica gels by heterogeneous gas-solid chromatography and infrared spectroscopy, *Anal. Chem.* 61 (1989) 41–47.
- [36] J.D. Sunseri, W.T. Cooper, J.G. Dorsey, Reducing residual silanol interactions in reversed-phase liquid chromatography: thermal treatment of silica before derivatization, *J. Chromatogr. A* 1011 (2003) 23–29.
- [37] L.T. Zhuravlev, The surface chemistry of amorphous silica. Zhuravlev model, *Colloids Surf., A* 173 (2000) 1–38.
- [38] M. Maws, H. Engelhardt, Thermal treatment of silica and its influence on chromatographic selectivity, *J. Chromatogr.* 311 (1986) 235–242.
- [39] Z. El Rassi, C. Gonnet, Chemical modification of silica gels after preliminary thermal treatment, *J. Liq. Chromatogr.* 3 (1980) 201–217.
- [40] M. Mignot, A. Tchaplá, O. Mercier, N. Couvrat, S. Tisse, P. Cardinael, V. Peulon-Agasse, High-density octadecyl chemically bonded core-shell silica phases for HPLC: comparison of microwave-assisted and classical synthetic routes, structural characterization and chromatographic evaluation, *Chromatographia* 77 (2014) 1577–1588.
- [41] K. Kimata, K. Iwaguchi, S. Onishi, K. Jinno, R. Elsteén, K. Hosoya, M. Araki, N. Tanaka, Chromatographic characterization of silica C18 packing materials. Correlation between a preparation method and retention behavior of stationary phase, *J. Chromatogr. Sci.* 27 (1989) 721–728.
- [42] C. Lopez, C. Carrara, A. Tchaplá, S. Caldarelli, High-resolution magic angle spinning description of the interaction states and their kinetics among basic solutes and functionalized silica materials, *J. Chromatogr. A* 1321 (2013) 48–55.
- [43] C. Stella, P. Seuret, S. Rudaz, A. Tchaplá, J.Y. Gauvrit, P. Lantéri, J.L. Veuthey, Simplification of a chromatographic test methodology for evaluation of base deactivated supports, *Chromatographia* 56 (2002) 665–671.
- [44] M. Pursch, S. Strohschein, H. Händel, K. Albert, Temperature-dependent behavior of C30 interphases. A solid-state NMR and LC-NMR study, *Anal. Chem.* 68 (1996) 386–393.
- [45] L.R. Snyder, J.J. Kirkland, J.L. Glajch, *The Column*, in *Practical HPLC Method Development*, 2nd ed., John Wiley & Sons, Inc., Hoboken, NJ, USA, 1997.
- [46] H.A. Claessens, M.A. van Straten, J.J. Kirkland, Effect of buffers on silica-based column stability in reversed-phase high-performance liquid chromatography, *J. Chromatogr. A* 728 (1996) 259–270.

With this study, it has been shown that thermal dehydroxylation prior to functionalization can be used to obtain different C18 phases. Depending on the temperature of pretreatment, the silica surface evolved as the silanol groups were progressively removed due to a thermally induced condensation reaction. DRIFT and NMR experiments confirmed that after dehydration, the vicinal silanols were progressively removed as the temperature increased (until 400°C), then the geminal silanols (until 900°C), and finally the complete disappearance of all silanol groups at 1100°C. The grafting of an octadecyl-chain was successfully performed with a maximum coverage of 3.7 $\mu\text{mol}/\text{m}^2$ for the end-capped-C18-400°C pretreated SPP silica. The use of chemometric methods allowed for grouping the columns depending on their hydrophobic properties and on their peak asymmetry for the analysis of basic solutes. In general, the non-end-capped phases presented higher peak asymmetry values as residual silanols were still accessible. Alternatively, the non-end-capped phase containing residual accessible silanols was close to the Accucore aQ column. Up to 900°C, the higher is the temperature of pretreatment, the higher is the retention of the corresponding C18 phases but also the asymmetry factors due to the residual free silanols activity. The high content of siloxane bridges showing additional hydrophobicity and polarizability made the C18-900°C pretreated phase efficient for the separation of PAHs isomers.

An application of the original selectivity of this SP is presented in the next paper (II.2.2).

Finally, a wide range of C18 columns could be obtained, depending on the choice of the temperature of pretreatment and of end-capping or not.

This paper was focused on the thermodynamic study of C18-thermally pretreated phases. The evaluation of the kinetic parameters of pretreated stationary phases without any grafting was done in HILIC mode and is presented later (II.2.3).

II-2-2. Article 3: Use of a high temperature pretreated C18 silica for the separation of phenanthrene/anthracene in a phenanthrene batch

The use of chemometric approaches as data analysis revealed and highlighted the specific behavior of the C18 SP resulting from the functionalization of silica pretreated at 900°C.

Among the column tested, the use of 900°C C18 SP allowed for a complete resolution of many critical pairs of PAHs (e.g. phenanthrene-anthracene), even in a batch of phenanthrene as it is the case here. Indeed, the deal was double: the quantification of the phenanthrene impurities at low concentration in phenanthrene 98%, and the nature of those impurities that are essentially isomers or close structural molecules of the PAHs family.

The quantification of the phenanthrene impurities after purification is presented in Article 3 entitled: "Phenanthrene Purification: Comparison of Zone Melting and Co-Crystallization", published in Chemical Engineering Technology in 2016.

Antoine Burel¹
 Sander J. T. Brugman²
 Mélanie Mignot¹
 Yohann Cartigny¹
 Séverine Tisse¹
 Nicolas Couvrat¹
 Valérie Peulon-Agasse¹
 Pascal Cardinael¹
 Gérard Coquerel¹

¹Normandie Université,
 Laboratoire SMS-EA3233,
 Université Rouen,
 Mont Saint Aignan, France.

²Radboud University, Institute
 for Molecules and Materials,
 Nijmegen, The Netherlands.



Supporting Information
 available online

Phenanthrene Purification: Comparison of Zone Melting and Co-Crystallization

The purification of phenanthrene is a prerequisite before studying its solid-solid phase transition at the molecular scale. Two purification methods, namely, zone melting and co-crystallization with 3,5-dinitrobenzoic acid, were separately studied and compared, in view of reaching ultrapurity which means a purity of >99.9 mol %. An explanation of the relationship between the efficiency of both techniques by using phase diagrams has been attempted. A novel strategy is proposed to optimize phenanthrene ultrapurification based on a combination of the two methods.

Keywords: Co-Crystallization, Phase diagrams, Phenanthrene, Ultrapurification, Zone melting

Received: January 15, 2016; **revised:** February 10, 2016; **accepted:** February 11, 2016

DOI: 10.1002/ceat.201600033

1 Introduction

Chemicals of high purity are required for many applications: preparation of active pharmaceutical ingredients (APIs) [1], polymorphism selection and solid-state design [2, 3], electronic-grade materials [4, 5] or elaboration of analytical standards [6]. Reaching the target purity for one compound generally requires complementary techniques that must be combined in the appropriate order. Among many purification techniques like preparative chromatography [7], phase-separation-based methods, etc., crystallization is one of the most employed techniques to purify chemical species. It offers a large panel of methods that can be combined when appropriate, e.g., solvent-assisted crystallization [8, 9], crystallization from the melt [10] or from the gas phase [11].

One of the most well-known purification methods using crystallization from the molten state is zone melting (ZM) [12]. This technique is widely used to prepare >99.999 % pure silicon [13, 14]. However, it is rarely applied to organic molecules [15] due to their tendency to chemical degradation upon heating. During ZM, a small molten zone is generated by heating a cylindrical sample of a solid to purify, and it is slowly displaced from one extremity of the sample to the other (Fig. 1 a). At every slight translation of the liquid phase, the impurities are displaced according to their equilibrium

partition coefficient k^l , defined by Eq. (1), between the solid recrystallized phase and the parent molten zone.

$$k = C_S/C_L \quad (1)$$

During ZM, an impurity decreasing the melting point of the compound to purify ($k < 1$) is displaced towards the same direction as the molten zone. On the contrary, impurities increasing the melting point ($k > 1$) are displaced towards the opposite direction. Consequently, the number of molten zone passes has to be adapted in order to reach the requested purity in one part of the treated sample. Displacements of the impurities (k values) can be predicted using binary phase diagrams between the compound to purify and the impurities (Fig. 1 b).

Solvent-assisted crystallization techniques are widely applied to purify organic compounds [8–10]. Nevertheless, simple recrystallizations generally lead to limited purifying effects when the compound to purify exhibits a solid solution with the impurities. An alternative to that technique is to add another component to the system, which is able to make a compound (salt, co-crystal, host-guest association, etc.) with the species to purify. In favorable cases, co-crystallization [16–18] can be exclusive: the impurities are not included into the co-crystal lattice and thus remain in the solvent. An improved purifying effect is thus obtained, provided that the target compound can be recovered by a complete removal of the co-crystal former from the isolated co-crystal.

Correspondence: Dr. Yohann Cartigny (yohann.cartigny@univ-rouen.fr), Normandie Université, Laboratoire SMS-EA3233, Université Rouen, 76821, Mont Saint Aignan, France.

1) List of symbols at the end of the paper.

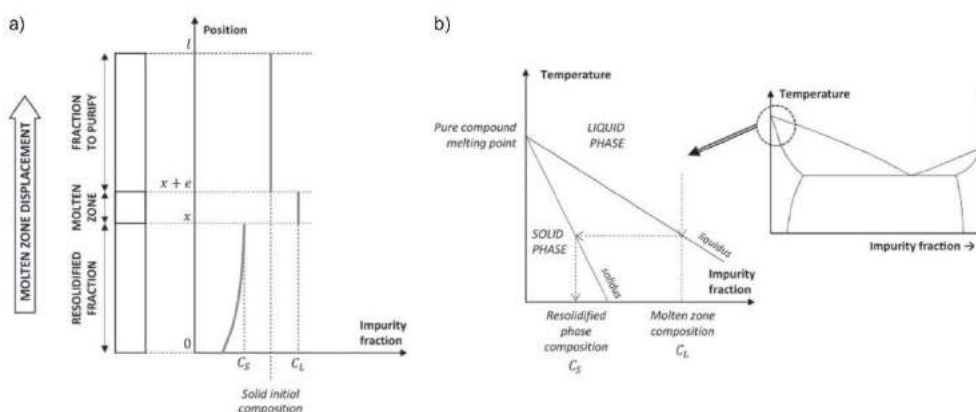


Figure 1. Relationship between ZM and phase diagrams applied on a hypothetical $k < 1$ impurity. (a) General principle of the ZM method; (b) phase diagram between the compound to purify and its impurity.

In this study, the case of phenanthrene (PHEN) molecule is investigated. This polycyclic aromatic hydrocarbon (PAH) exhibits a reversible order-disorder solid-solid phase transition at ca. 65–70 °C [19, 20]. The low-temperature (LT) and high-temperature (HT) phases crystallize in space groups $P2_1$ and $P2_1/c$, respectively. In several studies, the chemical purity of the compound has been highlighted as one major factor affecting the transition temperature [21, 22]. Consequently, ultrapurity (chemical purity > 99.9 mol% [23]) has to be reached to study thoroughly the mechanism of the transition at the molecular scale.

This study investigates the ability of two different purification methods to remove impurities from PHEN. Firstly, ZM has been tested on PHEN, which is possible due to the chemical stability of the molecule in the molten state. Secondly, purification of PHEN by co-crystallization has been attempted.

During preliminary studies, fluorene (FLU), 9,10-dihydroanthracene (9,10-DHA), 9,10-dihydrophenanthrene (9,10-DHP), 1-methylfluorene (1-MeF), dibenzothiophene (DBT), anthracene (ANT), and carbazole (CARB) (see Fig. 2) were identified as major PHEN impurities [21]. The impurity levels can vary according to the supplier and the batches. The existing data related to k values of PHEN impurities imply different behaviors of these impurities during solidification (Tab. 1) [21, 22, 24, 25]. Consequently, opposite impurity displacements are expected during ZM of PHEN. The efficiency of this method in displacing known PHEN impurities is experimentally quantified and discussed on the basis of existing data on phase equilibria mentioned above.

For the purification of PHEN by co-crystallization, a preliminary screening of PHEN co-crystal formers led to the selection of 3,5-dinitrobenzoic acid (3,5-DNBA, Fig. 2i). The PHEN/3,5-DNBA binary phase diagram has been investigated in

Table 1. PHEN impurity partition coefficient values reported in the literature.

Impurity	k value
Fluorene	< 1 (but ~ 1) [21]
Dibenzothiophene	< 1 [21, 24]
Anthracene	> 1 [21]
Carbazole	> 1 [23]

order to characterize the co-crystal in terms of melting point and stoichiometry. In addition, the ability of 3,5-DNBA to co-crystallize with the main impurities of PHEN has been investigated by X-ray powder diffraction (XRPD).

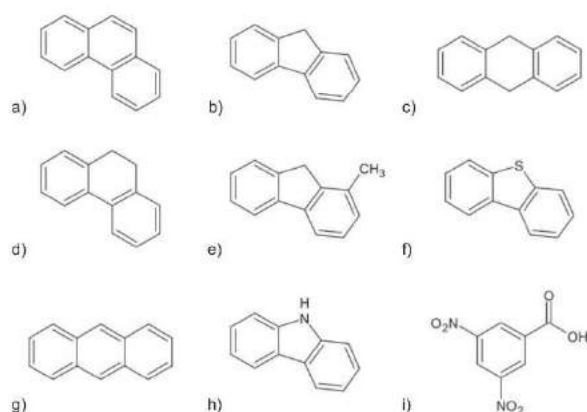


Figure 2. Developed formulae. (a) PHEN; (b) FLU; (c) 9,10-DHA; (d) 9,10-DHP; (e) 1-MeF; (f) DBT; (g) ANT; (h) CARB; (i) 3,5-DNBA.

The purification results of the two methods were discussed in the frame of phase equilibria. The methods were compared in terms of processing time and efficiency of the removal of impurities.

2 Materials and Methods

2.1 Chemicals

Acetone, dichloromethane, chloroform, *n*-heptane, and acetonitrile were obtained from VWR. All solvents were of HPLC grade. Hydrochloric acid (HCl, 37%), sodium hydroxide (NaOH) (98%), naphthalene (99%), and CARB (96%) were purchased from Acros Organics. 1-MeF (98%), 3,5-DNBA (98%), PHEN (98%, used for co-crystallization experiments), FLU (98+%), and DBT (98%) were obtained from AlfaAesar. 9,10-DHA (99%) was from TCI Chemicals; 9,10-DHP (94%), ANT (99%), and PHEN (98%, used for ZM experiments) were purchased from Sigma Aldrich.

2.2 Chromatography

The purifying effect of both techniques was monitored by GC and HPLC. Due to the difficulty to separate PHEN and ANT by GC, a homemade HPLC column was especially designed for this separation. GC was used to estimate FLU, 9,10-DHA, 9,10-DHP, 1-MeF, and DBT traces in PHEN. ANT and CARB contents were determined from HPLC measurements. All the samples were replicated three times. The confidence intervals on the impurity levels were estimated with a 95% confidence level.

2.2.1 Analytical Gas Chromatographic Conditions

GC experiments were performed on a Thermo Finnigan Focus Gas Chromatograph equipped with a split/splitless injector, a flame ionization detector, and a Thermo AI3000 autosampler. A Phenomenex ZB-5 column (30 m × 0.25 mm × 0.25 μm) was selected for separations and helium served as carrier gas with 1.0 mL min⁻¹ constant column outlet flow. The split flow was set at 10 mL min⁻¹. The injector and detector temperatures were set at 300 °C. The column oven temperature was programmed as follows: a first ramp from 70 °C to 100 °C at 10 °C min⁻¹ was applied. Then, the temperature was then held at 100 °C for 5 min and a second 10 °C min⁻¹ ramp was applied up to 150 °C. The oven was maintained at 150 °C for 5 min and a last 10 °C min⁻¹ heating ramp was programmed up to 280 °C. The final temperature was maintained constant during 15 min. The injection volume was set at 1 μL. All the chromatograms were processed using the Thermo ChromCard software (2.4.1 version, Jan. 2007).

The detector calibration was performed according to the internal standard calibration method, using naphthalene as internal standard (ca. 5 ppm). The standard concentration range was 0.5–50 ppm for all impurities. All sample solutions were prepared in 2-mL GC vials, by dissolving ~10 mg of

PHEN in ~2 g of chloroform; ~20 mg of a 550-ppm naphthalene solution in acetonitrile was also added to the sample.

Under these conditions, the following retention times were measured (in minutes): Naphthalene: 11.50, FLU: 23.62, 9,10-DHA: 26.63, 9,10-DHP: 26.98, 1-MeF: 27.27, DBT: 28.25, PHEN: 28.62, ANT: 28.93, CARB: 29.68.

2.2.2 HPLC Column Preparation

A C18-type porous silica column of 250 mm length with 4.6 mm internal diameter and 3 μm particle diameter was packed to perform a part of PHEN analysis. The silica pretreatment and functionalization were achieved according to the procedure developed in our laboratory [26, 27].

2.2.3 Analytical HPLC Conditions

HPLC experiments were performed on a Dionex apparatus, equipped with a P680 pump, an ASI-100 autosampler, a 20-μL injection loop, and a UVD 340U diode array detector. The homemade column as described above was used for separations, applying 1.0 mL min⁻¹ flow rate of an acetonitrile/water 65/35 v/v mobile phase. The column was kept at 30 °C with a TCC-100 thermostat. The solvents were degassed with an on-line degasser. The detection was performed at 234 and 250 nm, using two different acquisition channels.

Detector calibration was performed according to the external standard calibration method, with CARB and ANT standard solution concentrations ranging from ~0.1 to ~2 ppm in a 65/35 v/v acetonitrile/water mixture. CARB and ANT calibration curves were plotted using the data recorded at 234 and 250 nm, respectively.

The sample solutions were prepared by dissolution of ~5 mg of PHEN in ~3 g of acetonitrile. The solutions were then diluted about ten times in an acetonitrile/water 65/35 v/v mixture. Under the sustained conditions, CARB and ANT retention times were found to be 6.95 and 17.95 min, respectively.

2.3 Solid-State Analyses

2.3.1 PHEN/3,5-DNBA Phase Diagram

Mixtures of PHEN/3,5-DNBA of known compositions were dissolved in acetone. The solvent was then evaporated to air. The crystallized powders were manually ground and analyzed by differential scanning calorimetry (DSC) and XRPD.

2.3.2 3,5-DNBA Co-crystals Screening with PHEN Impurities

The ability of major PHEN impurities (FLU, 9,10-DHA, DBT, ANT, and CARB) to co-crystallize with 3,5-DNBA was investigated by preparing ~200 mg of 1:1 stoichiometry physical mixtures that were dissolved in acetone. The solvent was then evaporated to air. The formation of co-crystals was checked by

XRPD, by comparing mixtures XRPD patterns with those of the starting materials.

2.3.3 X-Ray Powder Diffraction

XRPD experiments were performed on a Bruker AXS D5000matic X-Rays diffractometer, using the Cu K α radiation. The 2θ scan range was set between 3° and 30° with a step of 0.04° and a measurement time of 4 s per step.

2.3.4 Differential Scanning Calorimetry

DSC measurements were performed on a Netzsch DSC214 Polyma equipped with an autosampler and an intracooler. The samples (ca. 5–6 mg) were put into closed aluminum pans and submitted to a 5 K min^{-1} heating rate under a 50 mL min^{-1} nitrogen flow. Data were processed using the Netzsch Proteus Thermal Analysis software (version 6.1.0).

2.4 Purification

2.4.1 Purification by Zone Melting

PHEN was pretreated in order to remove some of its inorganic impurities. For this, 10 g of PHEN was dissolved in 50 mL of dichloromethane. Three successive liquid-liquid extractions with 50 mL of a 1 mol L^{-1} aqueous HCl solution were performed. The operation was repeated with a 1 mol L^{-1} aqueous NaOH solution, and eventually with water. The organic phase was then recovered and dichloromethane was evaporated. The obtained powder was dried one night at 50°C . It was then molten in a cylindrical glass tube of 25 cm length and 11 mm internal diameter using a heat gun, to obtain a 9 cm long solid ingot.

The tube was placed in a vertical ZM prototype developed in our laboratory and described in Fig. 3. Fifteen molten zone passes were performed at a 5 mm h^{-1} translational rate, from the bottom to the top parts of the ingot. A 0.21 rad s^{-1} axial rotation speed was set, with a reversal of the rotational direction every π rad. After ZM, the tube was segmented into $\sim 1\text{-cm}$ parts that were analyzed by chromatography.

In the PHEN batch used for this experiment, FLU (0.43 wt %), 9,10-DHA (0.07 %), 1-MeF (0.02 %), DBT (0.58 %), ANT (0.08 %), and CARB (0.05 %) were identified as impurities (see Tab. 2). No additional impurity was detected. The purity of this pretreated commercial PHEN is thus 98.77 wt %.

2.4.2 Purification by Co-Crystallization

Co-crystal formation: 10 g of an equimolar mixture of PHEN/3,5-DNBA, prepared from commercial products, was added to 50 mL of acetone. The system was heated under reflux until a single liquid phase was obtained, and was then cooled down to room temperature under magnetic stirring at 600 rpm for 24 h.

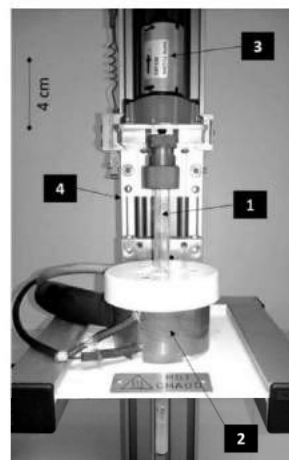


Figure 3. New ZM prototype developed in our laboratory. (1) Glass tube containing the solid to purify; (2) adjustable power annular heater generating the molten zone; (3) autoreverse motor providing glass tube axial rotation to improve the molten zone homogenization; (4) bench allowing glass tube vertical displacement using a step-by-step motor.

A suspension of yellow crystals was obtained. Vacuum filtration was carried out on a $0.45\text{-}\mu\text{m}$ PTFE membrane filter. The crystals were washed with 5 mL of cold (0°C) *n*-heptane. The solid was dried one night at 50°C .

Removal of 3,5-DNBA: 4 g of the solid was put into 100 mL of a 10 wt % NaOH aqueous solution. The system was stirred at 600 rpm for 1 h to dissolve 3,5-DNBA in the aqueous phase by sodium salt formation. A purple solution with a white PHEN suspension was obtained. The suspension was filtered according to the same procedure. The filtered solid was washed with $2 \times 50\text{ mL}$ of the 10 % NaOH solution, and then $4 \times 50\text{ mL}$ of water. It was eventually dried at 50°C for 48 h. Finally, 1.4 g of purified PHEN was obtained.

In the PHEN batch used for this operation, FLU (0.32 wt %), 9,10-DHA (0.43 %), 9,10-DHP (0.02 %), 1-MeF (0.06 %), DBT (0.82 %), ANT (0.28 %), and CARB (0.33 %) were identified as major impurities (see Tab. 3). Some other minor impurities have not been detected and could not be quantified (see Fig. 6). The purity of this PHEN batch is thus at the best 97.75 wt %.

3 Results and Discussion

3.1 Purification by Zone Melting

The impurity contents in the different parts of the treated sample after ZM are given in Tab. 2. The first column entry denotes the position in the treated sample, where 0 represents the starting position of the molten zone (lowest part) and 9 cm its final position (upper part).

Table 2. Impurity content in PHEN before and after ZM, in wt %.

Impurity	FLU	9,10-DHA	1-MeF	DBT	ANT	CARB	Total	
Pretreated commercial PHEN	0.43 ± 0.03	0.065 ± 0.004	0.015 ± 0.002	0.58 ± 0.05	0.084 ± 0.001	0.052 ± 0.002	1.23 ± 0.09	
0–1 cm	0.42 ± 0.02	ND	0.008 ± 0.001	0.18 ± 0.01	0.101 ± 0.004	0.093 ± 0.003	0.80 ± 0.04	
1–2 cm	0.39 ± 0.02	ND	0.007 ± 0.002	0.17 ± 0.01	0.099 ± 0.002	0.090 ± 0.001	0.76 ± 0.04	
2–3 cm	0.41 ± 0.01	ND	0.009 ± 0.003	0.24 ± 0.01	0.083 ± 0.002	0.063 ± 0.001	0.81 ± 0.03	
3–4 cm	0.43 ± 0.02	ND	0.011 ± 0.001	0.33 ± 0.02	0.077 ± 0.001	0.052 ± 0.001	0.90 ± 0.04	
ZM sample part	4–5 cm	0.45 ± 0.01	0.009 ± 0.001	0.014 ± 0.002	0.47 ± 0.01	0.075 ± 0.005	0.044 ± 0.002	1.06 ± 0.03
5–6 cm	0.45 ± 0.02	0.018 ± 0.002	0.016 ± 0.001	0.57 ± 0.02	0.080 ± 0.001	0.036 ± 0.001	1.17 ± 0.03	
6–7.5 cm	0.48 ± 0.03	0.051 ± 0.003	0.020 ± 0.002	0.85 ± 0.05	0.083 ± 0.001	0.028 ± 0.001	1.51 ± 0.09	
7.5–9 cm	0.48 ± 0.01	0.097 ± 0.003	0.025 ± 0.003	1.19 ± 0.03	0.080 ± 0.001	0.019 ± 0.001	1.89 ± 0.05	

ND, not detected.

Considering impurity distributions, various behaviors are observed: (i) no significant effect can be detected for FLU ($k \sim 1$ behavior); (ii) 9,10-DHA, 1-MeF, and DBT exhibit $k < 1$ behaviors as they were displaced towards the same direction as the molten zone; (iii) oppositely, ANT and CARB were dislocated towards the opposite direction, which corresponds to a $k > 1$ behavior. The displacements of FLU, DBT, ANT, and CARB in the ZM sample are consistent with the existing k values of the literature (Tab. 1).

The total impurity content distribution in the treated sample is almost monotonic and increases with the position in the sample from 0.76% in the 1–2 cm part to 1.89% in the upper part. Nevertheless, even if the process exhibited a powerful ability to displace 9,10-DHA and DBT towards the upper part, some other impurities, i.e., ANT and CARB, exhibited antagonist behaviors. Consequently, no ultrapure PHEN was obtained. Further molten zone passes (> 15) are thus required to concentrate the impurities at the extremities of the sample and to access to a purer intermediate part.

Due to the constraints discussed above, ultrapurification of PHEN using ZM requires an appropriate strategy. Different approaches can be employed to tackle this problem:

- (i) Adjusting the ZM parameters, i.e., molten zone translational rate, number of passes, length of the zone, length of the sample; this approach is nevertheless time-consuming due to the number of experiments to perform for process optimization, even using modeling tools.
- (ii) Performing ZM experiments on pre-purified PHEN samples. A pre-purification technique, applied on the starting commercial product, could allow the partial or total removal of some impurities to simplify the ultrapurification by ZM. In this context, co-crystallization can be an interesting complementary method provided that it can remove some impurities.

zation can be an interesting complementary method provided that it can remove some impurities.

3.2 Purification by Co-Crystallization

3.2.1 PHEN/3,5-DNBA Phase Diagram

The XRPD patterns of PHEN/3,5-DNBA mixtures at room temperature are presented in Fig. 4. A 1:1 stoichiometry co-crystal is observed. Between 0 and 50 mol % of 3,5-DNBA, a mixture of the PHEN LT and the co-crystal phases is evidenced. For the upper composition range, a mixture of the co-crystal and 3,5-DNBA phases is observed. No solid solution domain was detected for the PHEN LT, PHEN/3,5-DNBA co-crystal and 3,5-DNBA phases.

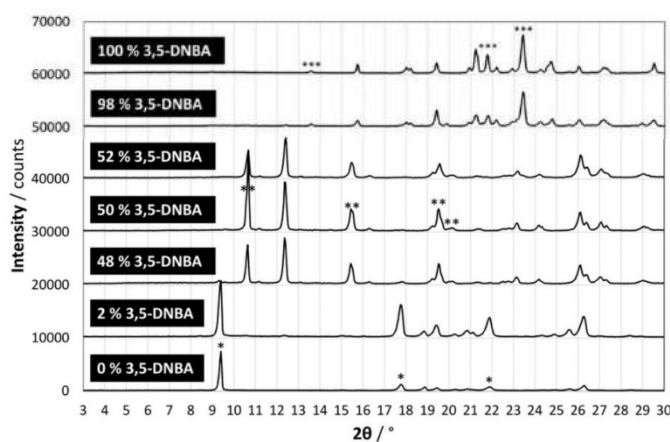


Figure 4. XRPD patterns at room temperature of different PHEN/3,5-DNBA mixtures (compositions in mol %). Ticks: main diffraction peaks associated with * the PHEN LT phase; ** the PHEN/3,5-DNBA co-crystal phase; *** the 3,5-DNBA phase.

The DSC measurements (data not shown) allowed characterizing two eutectic transformations:

- 1) $\langle \text{PHEN HT} \rangle + \langle \text{cc. PHEN/3,5-DNBA} \rangle \rightleftharpoons \text{Liquid}$ at $\sim 97^\circ\text{C}$ in the 0–50 mol % 3,5-DNBA region;
- 2) $\langle \text{cc. PHEN/3,5-DNBA} \rangle + \langle \text{3,5-DNBA} \rangle \rightleftharpoons \text{Liquid}$ at $\sim 188^\circ\text{C}$ in the 50–100 mol % 3,5-DNBA region.

It is worth noting that the accuracy of liquidus points was certainly affected by sublimation of the solid mixtures at high temperatures. In addition, an insufficient resolution between eutectic and liquidus endotherms prevented from determining accurate eutectic compositions from Tammann plots. The thermal events measured with DSC were used to construct the PHEN/3,5-DNBA binary phase diagram in Fig. 5.

3.2.2 Screening of PHEN Impurity Co-Crystals with 3,5-DNBA

The XRPD patterns of FLU/3,5-DNBA, 9,10-DHA/3,5-DNBA, DBT/3,5-DNBA, ANT/3,5-DNBA, and CARB/3,5-DNBA equimolar mixtures are presented in the Supporting Information (Fig.S1). Starting materials patterns were used as references. One can note that new co-crystals were obtained only with FLU, DBT, and CARB. The stoichiometry of these co-crystals is assumed to be 1:1 but further investigations are required for confirmation.

3.2.3 Phenanthrene Purification by Co-Crystallization with 3,5-DNBA

PHEN impurity contents before and after purification by co-crystallization with 3,5-DNBA are given in Tab.3. Normalized GC chromatograms of PHEN samples are presented in Fig. 6. After the recovering of PHEN from the co-crystal, no trace of 3,5-DNBA was detected. The sum of identified impurities contents led us to estimate a commercial PHEN purity of 97.8 wt %, at the best. The co-crystallization-purified PHEN sample purity was approximately 99.5 wt %.

As indicated by these quantifications, the purification experiment provided promising results. Remaining traces of FLU,

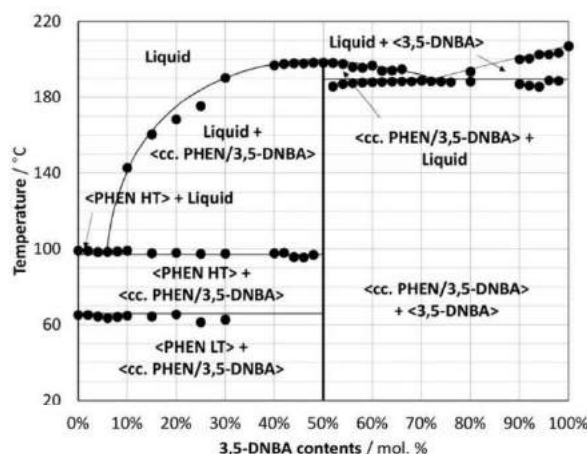


Figure 5. PHEN/3,5-DNBA binary phase diagram determined in this work.

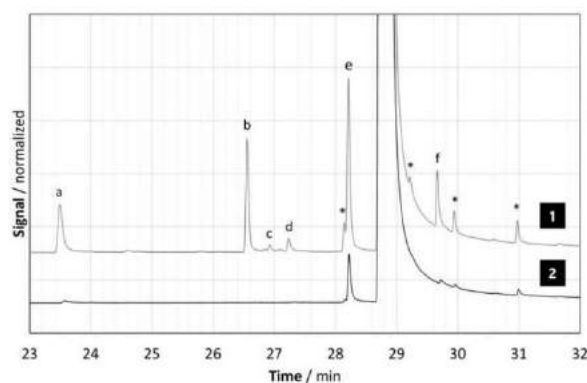


Figure 6. Normalized GC chromatograms with respect to analyzed PHEN amount. (1) Commercial AlfaAesar PHEN; (2) PHEN recovered from PHEN/3,5-DNBA co-crystal. Marks: (a) FLU, (b) 9,10-DHA, (c) 9,10-DHP, (d) 1-MeF, (e) DBT, (f) CARB; *unidentified impurities.

DBT, ANT, and CARB were still observed after the purification treatment, but their contents were significantly reduced. 9,10-DHA, 9,10-DHP, and 1-MeF were no more detected by

Table 3. Impurity contents (in wt %) in PHEN before co-crystallization and after recovering from the co-crystal.

Impurity	FLU	9,10-DHA	9,10-DHP	1-MeF	DBT	ANT	CARB	Total
Commercial PHEN	0.316 ± 0.001	0.426 ± 0.001	0.018 ± 0.001	0.056 ± 0.001	0.824 ± 0.001	0.282 ± 0.002	0.326 ± 0.002	2.25 ± 0.01
PHEN recovered from the co-crystal	0.028 ± 0.001	ND	ND	ND	0.326 ± 0.004	0.073 ± 0.002	0.060 ± 0.001	0.49 ± 0.01

the GC analytical method; detection limits were approximately 0.005–0.01 wt %.

Besides, no absolute correlation could be established between the ability of an impurity to co-crystallize with 3,5-DNBA and its presence in the PHEN/3,5-DNBA co-crystal: (i) FLU, DBT, and CARB are able to co-crystallize with 3,5-DNBA but were not completely removed from PHEN, (ii) 9,10-DHA was totally removed but is unable to form co-crystals with 3,5-DNBA, and (iii) ANT was still detected after purification, while it does not co-crystallize with 3,5-DNBA.

One way to explain the presence of a certain impurity in PHEN after co-crystallization could be related to its ability to make some solid solution with the new PHEN/3,5-DNBA co-crystal phase. This situation can be explained by considering the PHEN/3,5-DNBA/impurity isothermal phase diagrams at room temperature (Fig. 7). The cases where an impurity does not co-crystallize with 3,5-DNBA are considered in Figs. 7a and 7c. The presence of a co-crystal with an impurity of PHEN and the cofomer is represented in Figs. 7b and 7d. The schematic ternary systems of Figs. 7a and 7b both show the existence of PHEN/3,5-DNBA co-crystal solid solutions. In these two cases, traces of impurities should remain in the PHEN/3,5-DNBA co-crystal and their amounts depend on the extent of the co-crystal solid solution in the ternary system. Oppositely, if no PHEN/3,5-DNBA co-crystal solid-solution exists (Figs. 7c and 7d), the impurity should stay in the sol-

vent, regardless the ability of the impurity to co-crystallize or not with 3,5-DNBA. In this case, the obtained co-crystal should be free of impurities.

It can be deduced from the quantification of impurities after co-crystallization that FLU, DBT, ANT, and CARB can be inserted into the PHEN/3,5-DNBA co-crystal lattice. By contrast, no solid solution including 9,10-DHA, 9,10-DHP, and 1-MeF seems to exist. Note that in this approach the effects of each impurity were considered separately but the situation is certainly more complex since the actual order of the thermodynamic system is $2+n$, n being the number of impurities of PHEN.

3.3 Comparison of ZM and Co-Crystallization Applied on PHEN

As explained in the previous paragraphs, under the tested conditions, co-crystallization appeared more suitable to remove impurities from PHEN than ZM. The best global purity obtained by ZM was approximately 99.2 wt %, whereas 99.5 wt % was obtained after co-crystallization. An interesting difference between the two methods is the ability of co-crystallization to remove FLU from PHEN, whereas inadequate phase equilibria between both compounds prevented an efficient removal of FLU by ZM.

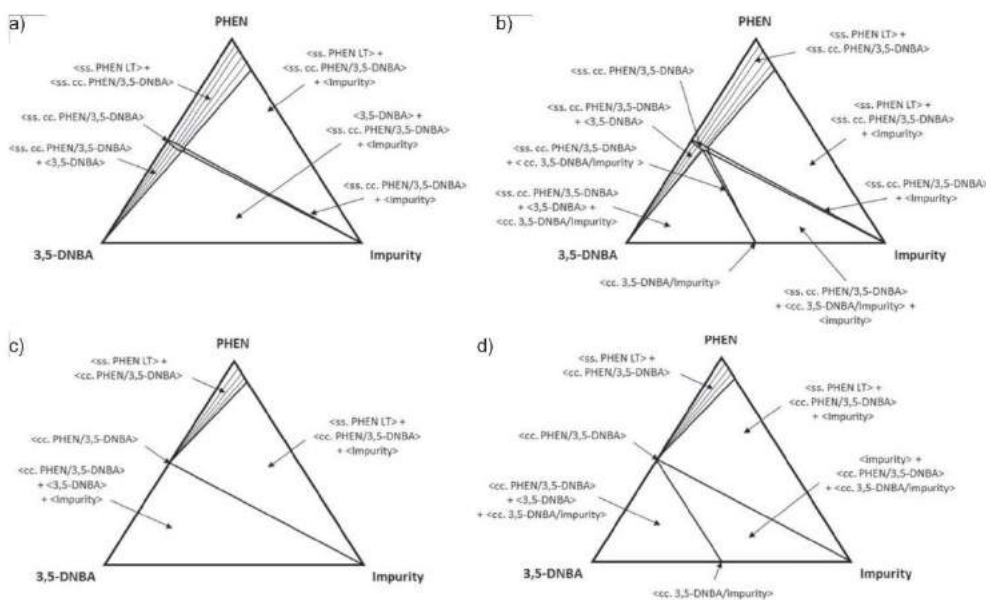


Figure 7. Hypothetical isothermal phase diagrams between PHEN, 3,5-DNBA, and any considered impurity. (a) With a PHEN/3,5-DNBA co-crystal solid solution and no co-crystal between 3,5-DNBA and the impurity; (b) with a PHEN/3,5-DNBA co-crystal solid solution and a co-crystal between 3,5-DNBA and the impurity; (c) with a PHEN/3,5-DNBA co-crystal without solid solution and no co-crystal between 3,5-DNBA and the impurity; (d) with a PHEN/3,5-DNBA co-crystal without solid solution and a co-crystal between 3,5-DNBA and the impurity.

In addition, the purest part of the ZM PHEN sample corresponds to only ~ 11 % of the initial amount of sample. A better yield was obtained by a single crystallization of the PHEN/3,5-DNBA co-crystal, as the recovered mass of purified PHEN corresponds to ~ 30 % of the initially engaged PHEN mass. Conversely, successive co-crystal recrystallization steps could lead to a complete removal of FLU, DBT, ANT, and CARB.

Finally, the processing time of PHEN purification by ZM was about three times higher than that of co-crystallization. For all these reasons, co-crystallization seems to be an appropriate technique for a first PHEN purification step, whereas ZM could allow the removal of remaining traces after this first purification treatment.

4 Conclusions

ZM and co-crystallization exhibited different abilities to remove PHEN impurities under the tested conditions. ZM has shown a limited purifying effect due to the number of impurities and their antagonist behaviors, i.e., k values greater and lower than 1. Oppositely, co-crystallization served to reduce the amount of every impurity present in PHEN by forming a new crystalline phase. In both cases, the use of phase diagrams helps at understanding the purification efficiency and its limits, e.g., presence of solid solutions. As a result, co-crystallization appears as the most relevant first purification process for PHEN before using other appropriate technique(s) such as ZM or sublimation to achieve ultrapurity.

In future work, purification work on PHEN should be pursued by combining these processes in the right order. Some other PHEN co-crystal formers should be tested to check their selectivity with respect to its impurities. A side challenge of this study is to develop appropriate analytical methods in order to measure low amounts of impurities in PHEN samples close to ultrapurity. In this study, two different chromatographic methods had to be used in order to benefit their different selectivity. All known impurities of PHEN could thus be determined. Nevertheless, measuring the purity of PHEN purity beyond ultrapurity will probably require more sensitive methods, with appropriate detection means. In this context, HPLC with fluorescence detector seems to be a promising tool to reach that aim.

Acknowledgment

The Région Haute-Normandie (France) is acknowledged for Antoine Burel's Ph. D. grant. The European Union is acknowledged for the Erasmus+ grant of Sander Brugman.

The authors have declared no conflict of interest.

Symbols used

C	[%]	impurity concentration
e	[mm]	molten zone thickness
l	[mm]	zone melting sample length

k	[-]	impurity partition coefficient
x	[mm]	molten zone solidification surface position
θ	[°]	X-ray incident beam angle

Sub- and superscripts

L	liquid phase
S	solid phase

Abbreviations

ANT	anthracene
APIs	active pharmaceutical ingredients
CARB	carbazole
cc.	co-crystal
DBT	dibenzothiophene
9,10-DHA	9,10-dihydroanthracene
9,10-DHP	9,10-dihydrophenanthrene
3,5-DNBA	3,5-dinitrobenzoic acid
DSC	differential scanning calorimetry
FLU	fluorene
HT	high-temperature phase
LT	low-temperature phase
1-MeF	1-methylfluorene
PAH	polycyclic aromatic hydrocarbon
PHEN	phenanthrene
ss.	solid solution
XRPD	X-ray powder diffraction
ZM	zone melting

References

- [1] N. G. Anderson, in *Practical Process Research and Development*, 2nd ed., Elsevier, Amsterdam **2012**, 13. DOI: 10.1016/B978-0-12-386537-3.00013-7
- [2] G. Coquerel, *Chem. Eng. Process.* **2006**, 45, 857–862. DOI: 10.1016/j.ccep.2005.10.011
- [3] D. Martins, M. Sanselme, O. Houssin, V. Dupray, M.-N. Petit, D. Pasquier, C. Dioloz, G. Coquerel, *Cryst. Eng. Commun.* **2012**, 14, 2507–2519. DOI: 10.1039/C2CE06537A
- [4] Y. Lu, M. Saka, *Mater. Lett.* **2009**, 63 (27), 2294–2296. DOI: 10.1016/j.matlet.2009.07.055
- [5] H. Becker, I. Bach, M. Holbach, J. Schwaiger, H. Spreitzer, *SID Int. Symp. Digest. Tech. Pap.* **2010**, 41 (1), 39–42. DOI: 10.1889/1.3500471
- [6] W. G. Pfann, H. C. Theuerer, *Anal. Chem.* **1962**, 32 (12), 1574–1578. DOI: 10.1021/ac60168a009
- [7] M. Kasperit, A. Seidel-Morgenstern, in *Liquid Chromatography: Fundamentals and Instrumentation* (Eds: P. R. Haddad, S. Fanali, C. F. Poole, P. J. Schoenmakers, D. K. Lloyd), Elsevier, New York **2013**, 19. DOI: 10.1016/B978-0-12-415807-8.00019-5
- [8] J. H. ter Horst, C. Schmidt, J. Ulrich, in *Handbook of Crystal Growth: Bulk Crystal Growth* (Ed: P. Rudolph), 2nd ed., Elsevier, Amsterdam **2015**, 1317–1349. DOI: 10.1016/B978-0-444-63303-3.00032-8

- [9] G. Coquerel, *Chem. Soc. Rev.* **2014**, *43*, 2286–2300. DOI: 10.1039/C3CS60359H
- [10] J. Ulrich, H. C. Bülow, in *Handbook of Industrial Crystallization* (Ed: A. S. Myers), 2nd ed., Butterworth-Heinemann, Woburn, MA **2002**, 161–179. DOI: 10.1016/B978-075067012-8/50009-4
- [11] C. A. Holden, H. S. Bryant, *Sep. Sci.* **1969**, *4* (1), 1–13. DOI: 10.1080/01496396908052233
- [12] W. G. Pfann, *Solid State Phys.* **1957**, *4*, 423–521. DOI: 10.1016/S0081-1947(08)60158-7
- [13] C. C. Hein, *US Patent 2747971 A*, **1956**.
- [14] P. R. Mei, S. P. Moreira, E. Cardoso, A. D. S. Côrtes, F. C. Marques, *Sol. Energy Mater. Sol. Cells* **2012**, *98*, 233–239. DOI: 10.1016/j.solmat.2011.11.014
- [15] W. R. Wilcox, R. Friedenberg, N. Beck, *Chem. Rev.* **1964**, *64* (2), 187–220. DOI: 10.1021/cr60228a006
- [16] N. A. Meanwell, *Annu. Rep. Med. Chem.* **2008**, *43*, 373–404. DOI: 10.1016/S0065-7743(08)00022-5
- [17] J. W. Steed, *Trends Pharmacol. Sci.* **2013**, *34* (3), 185–193. DOI: 10.1016/j.tips.2012.12.003
- [18] C. Neurohr, M. Marchivie, S. Lecomte, Y. Cartigny, N. Couvrat, M. Sanselme, P. Subra-Paternault, *Cryst. Growth Des.* **2015**, *15* (9), 4616–4626. DOI: 10.1021/acs.cgd.5b00876
- [19] S. Matsumoto, T. Fukuda, *Bull. Chem. Soc. Jpn.* **1967**, *40*, 743–746. DOI: 10.1246/bcsj.40.743
- [20] V. Petricek, I. Cisarová, L. Hummel, J. Kroupa, B. Brezina, *Acta Crystallogr., Sect. B: Struct. Sci.* **1990**, *46*, 830–832. DOI: 10.1107/S0108768190007510
- [21] N. Couvrat, A. Burel, S. Tisse, Y. Cartigny, G. Coquerel, *J. Therm. Anal. Calorim.* **2013**, *112* (1), 293–300. DOI: 10.1007/s10973-012-2746-z
- [22] B. J. McArdle, J. N. Sherwood, *J. Cryst. Growth* **1974**, *22* (3), 193–200. DOI: 10.1016/0022-0248(74)90094-3
- [23] A. König, M. Stepanski, A. Kuszlik, P. Keil, C. Weller, *Chem. Eng. Res. Des.* **2008**, *86* (7), 775–780. DOI: 10.1016/j.cherd.2008.04.002
- [24] M. Brandstätter-Kuhnert, H. Weiß, *Monatsh. Chem.* **1957**, *88* (6), 1007–1016. DOI: 10.1007/BF00906079
- [25] N. Couvrat, Y. Cartigny, S. Tisse, M.-N. Petit, G. Coquerel, in *JEEP 2011*, EDP Sciences, London **2011**. DOI: 10.1051/jeeep/201100006
- [26] M. Mignot, A. Tchaplá, O. Mercier, N. Couvrat, S. Tisse, P. Cardinael, V. Peulon-Agasse, *Chromatographia* **2014**, *77* (23), 1577–1588. DOI: 10.1007/s10337-014-2802-x
- [27] M. Mignot, M. Sebban, A. Tchaplá, O. Mercier, P. Cardinael, V. Peulon-Agasse, *J. Chromatogr. A* **2015**, *1419*, 45–57. DOI: 10.1016/j.chroma.2015.09.072

In this article dedicated to the ultra-purification of phenanthrene, the use of dedicated HPLC column was of primary concern to be able to quantify rigorously the phenanthrene impurities at low concentration in phenanthrene 98%.

Those impurities being essentially isomers or structural molecules close to the PAHs family, the separation required high shape selectivity to obtain full resolution between phenanthrene and its isomer anthracene.

The specificity of the home-made column from silica pretreated at 900°C before C18 grafting (Figure 2) allowed for obtaining quantification of all major impurities of phenanthrene, at very low levels.

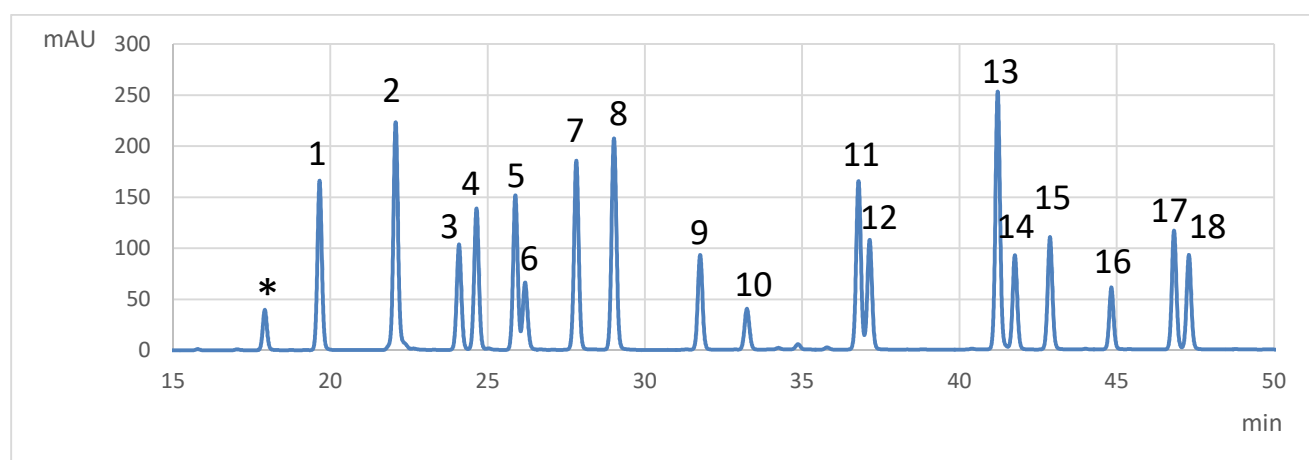


Figure 2: Chromatogram obtained on 900°C C18 home-made column, 250 mm × 4.6 mm × 3 μm, $F = 1\text{ mL/min}$, 5 min at 50/50 (v/v) $\text{CH}_3\text{CN}/\text{H}_2\text{O}$ to 100% CH_3CN in 50 min, 254 nm, 22°C, (*) Impurity, (1) Naphthalene, (2) Acenaphthylene, (3) 1-Methylnaphthalene, (4) 2-Methylnaphthalene, (5) Acenaphthene, (6) Fluorene, (7) Phenanthrene, (8) Anthracene, (9) Fluoranthene, (10) Pyrene, (11) Chrysene, (12) Benz(a)anthracene, (13) Benzo(b)fluoranthene, (14) Benzo(k)fluoranthene, (15) Benzo(a)pyrene, (16) Dibenzo(a,h)anthracene, (17) Benzo(g,h,i)perylene, (18) Indeno(1,2,3-cd)pyrene

It was shown that various C18 SPs can be obtained by varying the surface state of the silica through thermal pretreatment with Article 2, and a concrete use of one C18 SP with silica pretreated at 900°C was presented in Article 3.

The next study was devoted to the possibility of obtaining various SPs from the same silica by varying the temperature of pretreatment. The thermodynamic and especially the kinetic evaluation of the SPs in HILIC mode is the focus of the following part.

II-2-3. Article 4: Use of superficially porous silica particles pretreated at different temperatures in HILIC

The impact of thermal pretreatment on silica and the use of bare silica pretreated at different temperatures in HILIC mode was considered.

This work was achieved in collaboration with the LCAP, University of Geneva, where I spent one month internship under the supervision of Prof. J.L. Veuthey and Dr. D. Guillarme. Evaluating the kinetic performances of SPs with the kinetic plot theory required the use of a dedicated instrumentation with optimized extra-column volumes and capable of supporting very high pressures. A sufficiently retained compound has to be selected to limit the system contributions, in our case cytosine was the probe solute; and at least 10-15 values have to be acquired at various flow rates for suitable fitting. Contrary to Van Deemter plot that corresponds to experimental plate number, the kinetic plot method give access to extrapolated value called the pressure drop limited plate number. By working with one column of a particular length, values can be obtained for other lengths by extrapolation, allowing to have a global evaluation of the column kinetic performances when working at the maximal pressure (600 bars for the SPPs and 1000 bars for the sub-2 μm particles).

The study encompassed the kinetic evaluation of 3 SPs resulting from the pretreatment of bare SPP silica at 3 different temperatures (400°C, 525°C, 900°C). Also, two applications were presented on nucleobases and derivatives, and nicotine and derivatives to demonstrate the potential of such SPs. This work led to the publication entitled "Evaluation of thermally pretreated silica stationary phases under hydrophilic interaction chromatography conditions" in *Journal of Separation Science* in 2016.

Mélanie Mignot¹
 Aurélie Périat²
 Valérie Peulon-Agasse¹
 Pascal Cardinael¹
 Jean-Luc Veuthey²
 Davy Guillarme²

¹Normandie Univ, Laboratoire
 SMS-EA3233, Univ Rouen,
 Mont-Saint-Aignan, France

²School of Pharmaceutical
 Sciences, University of Geneva
 University of Lausanne,
 Geneva, Switzerland

Received January 11, 2016
 Revised February 17, 2016
 Accepted February 17, 2016

Research Article

Evaluation of thermally pretreated silica stationary phases under hydrophilic interaction chromatography conditions

Three novel hydrophilic interaction chromatography columns packed with bare silica 2.6 μm superficially porous particles were evaluated. These stationary phases undergo a different pretreatment temperature (400, 525, and 900°C) that might influence their kinetic performance and thermodynamic properties. In the first instance, we demonstrated that the performance of these columns was inferior to the commercial ones in the low plate count range (10 000 plates), but was more favorable for N values beyond 40 000 plates. Thanks to its high permeability and reasonable flow resistance ($\psi = 695$), together with a minimum reduced heights equivalent to a theoretical plate value of only 2.4, the stationary phase pretreated at 400°C was particularly attractive for $N > 70\,000$ plates with a remarkably low impedance value ($E = 2488$). In a second step, the impact of pretreatment temperature was evaluated using two mixtures of polar substances, namely nucleobases and derivatives, as well as nicotine and derivatives. Retentions and selectivities achieved on the tested stationary phases were appropriate, but selectivity differences were minor when modifying pretreatment temperature from 400 to 525°C. When we increased the pretreatment temperature up to 900°C, the surface chemistry was more seriously modified. Finally, the columns presented a good stability even at high temperature (70°C), especially for the phases pretreated at 400 and 525°C.

Keywords: Hydrophilic interaction chromatography / Kinetic plots / Nicotine derivatives / Pretreatment temperature / Thermal stability
 DOI 10.1002/jssc.201600034



Additional supporting information may be found in the online version of this article at the publisher's web-site

1 Introduction

Even if RPLC is considered as the gold standard in several domains, the analysis of polar/ionizable solutes remains challenging with this chromatographic mode. There have been attempts to improve retention of these solutes, mainly by incorporating a polar embedded group within the bonded ligand, or performing a polar endcapping, to moderate the stationary phase hydrophobicity. Nonetheless, the retention of the most polar substances still remains insufficient. Ion pairing is an interesting solution to analyze any ionizable hydrophilic substances, allowing the use of RP columns.

Correspondence: Dr. Davy Guillarme, School of Pharmaceutical Sciences, University of Geneva, University of Lausanne, Boulevard d'Yvoy 20, 1211 Geneva 4, Switzerland
E-mail: davy.guillarme@unige.ch
Fax: +41 22 379 68 08

Abbreviations: d_p , the particle diameter; E , separation impedance; H , height equivalent to a theoretical plate; h_{min} , minimum reduced height equivalent to a theoretical plate; K_v , column permeability; u_i , mobile phase interstitial linear velocity; ΔP , pressure drop; Φ , flow resistance; η , viscosity

However, the equilibration times may be significantly extended in presence of ion pairing reagents, stationary phase memory effects are critical for repeatability and such strategy is not suitable for MS detection.

Over the years, HILIC has thus been shown as the most promising chromatographic approach for the analysis of hydrophilic/charged/polar compounds [1–5]. In HILIC, the retention mechanism is more complicated than in RPLC, since adsorption, ion exchange, hydrogen bonding, and hydrophilic partitioning between the mobile phase and a water-enriched layer at the surface of the stationary phase, take place together [6–11]. However, HILIC allows achieving orthogonal selectivity [12] and higher ESI-MS sensitivity [13] compared to RPLC. In addition, due to the low viscosity of highly organic HILIC eluents [14], faster separations can be attained, using state-of-the-art columns packed with superficially porous particles. These particles are composed of a solid inner core surrounded by a porous shell, large enough to solve the problem of low capacity of the old pellicular particles proposed in the 1960s [15, 16]. The great success of this new technology started in 2006, with the commercial introduction of sub-3 μm RPLC columns packed with superficially porous particles [17–19]. Gritti and Guiochon described the theoretical

understanding of the kinetic benefits of such particle morphology, compared to fully porous ones [20–23] and HILIC columns packed with superficially porous particles are now commercially available.

Under HILIC conditions, the nature and amount of silanols located at the surface of the stationary phase are particularly important, since they strongly contribute to retention and selectivity. Silanols can be modified by applying, for example, thermal treatments. This strategy was used on porous silica [24–26], but also recently on superficially porous materials [27]. Different silica surface states can be distinguished during a thermal treatment, as reported in [24] on porous silica, treated at different temperatures under vacuum. It was noticed that after the dehydration of the water multilayers physically adsorbed at the silica surface, the first silanols to disappear were vicinal silanols, between 190 and 400°C. Then, geminal silanols were progressively removed upon 400°C and isolated single silanols were the last remaining at the surface at 900°C. The complete removal of all silanol groups (only siloxane bridges) was reached after thermal treatment at 1200°C, but the surface fusion formed a nonporous solid material that was chromatographically unusable [24].

The aim of this work is to evaluate the influence of thermal treatments on columns packed with superficially porous silica-based particles employed in HILIC mode, from a kinetic and thermodynamic point of view. To evaluate kinetic performance, three home-made stationary phases were compared with commercial HILIC materials also made from bare silica particle of different sizes. The thermodynamic aspect was also considered with the fast separation of two mixtures of polar and ionizable solutes, namely nicotine derivatives and nucleobases, nucleosides, and nucleotides.

2 Materials and methods

2.1 Chemical and reagents

Water was obtained from a Mili-Q water purification system from Millipore (Bedford, MA, USA). Acetonitrile (ACN) and formic acid of ULC–MS grade were purchased from Biosolve (Valkenswaard, Netherlands). Ammonium formate buffer 20 mM was prepared by measuring adequate volume of formic acid. The pH was then adjusted to 3.0 with ammonium hydroxide 28% v/v. All nucleobases, nucleotides and nucleosides (i.e. uracil, uridine, adenine, guanosine, adenosine, cytidine, cytosine, and adenosine mono-phosphate; structures reported in Supporting Information Fig. S1) were purchased from Sigma–Aldrich (Steinheim, Germany), while nicotine derivatives (i.e. hydroxycotinine, cotinine, cotinine N-oxide, anatabine, anabasine, normicotine, nicotine, and nicotine N'-oxide; structures reported in Supporting Information Fig. S2) were a kind gift from the Swiss antidoping laboratory (Epalinges, Switzerland). Stock solutions of each individual sample were prepared at 1 mg/mL in an adequate ACN/water proportion to ensure a good dissolution of nucleobases, nucleotides, and nucleosides. Stock solutions of each individual

sample were prepared at 1 mg/mL in pure MeOH for nicotine derivatives. In each case, samples were then diluted in ACN and injected at 50 ppm.

2.2 Instrumentation

The measurements were performed using a Waters Acquity UPLC™ I-Class system (Milford, MA, USA) equipped with a binary solvent delivery pump (maximum flow rate of 2 mL/min and upper pressure limit of 1200 bar), an autosampler and UV detector. The system includes a flow through needle (FTN) injection system with 15 µL needle and a 0.5 µL UV flow-cell. The connection tube between injector and column inlet was 0.003" I.D. and 200 mm long (active preheater included), and the capillary located between the column and detector was 0.004" I.D. and 200 mm long. The overall extra-column volume (V_{ext}) was about 8.5 µL as measured from the injection seat of the autosampler to the detector cell. Data acquisition and instrument control were performed by Empower Pro 2 Software (Waters). Calculation and data transferring were achieved by using a home-made MS Excel template.

The commercial columns employed in this study were Ascentis Express HILIC (50 × 2.1 mm, 2.7 µm) from Supelco (Bellefonte, PA, USA), Acquity bridged ethyl hybrid (BEH) HILIC (50 × 2.1 mm, 1.7 µm) from Waters, Kinetex HILIC (50 × 2.1 mm, 1.3 µm) from Phenomenex (Torrance, USA) and Cortecs HILIC (50 × 2.1 mm, 1.7 µm) from Waters. The column dead times were measured using anthracene as column dead time marker. Temperature was set at 30°C. UV detection was set at 254 nm.

2.3 Preparation of home-made stationary phases

The thermal pretreatment of the superficially porous silica particles were performed as described in a previous work [27]. To briefly summarize, the superficially porous silica particles were heated under atmospheric conditions for 5 h at 400, 525, and 900°C, respectively. Three columns (50 × 2.1 mm, 2.6 µm) were packed by Interchim (Montluçon, France), with each type of pretreated silica particles. The packing quality was evaluated through standard solutes analysis (i.e. tri-*tert*-butylbenzene, diethylphthalate, and dimethylphthalate). Similar chromatographic properties were obtained for three columns of each type of pretreated superficially porous silica particles, so the whole study was only done on one column of each type of pretreated silica (400, 525, and 900°C).

2.4 Evaluation of kinetic performance

In a first instance, the van Deemter curves were plotted for the three HILIC columns pretreated at 400, 525, and 900°C using cytosine at 50 ppm as model compound. For this purpose, experimental plate count values observed at different flow

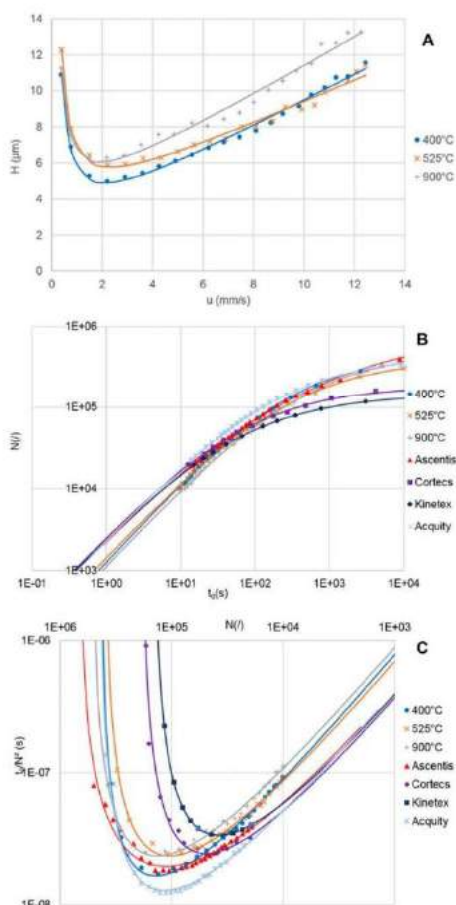


Figure 1. (A) Experimental H - u plots of columns packed with $2.6\ \mu\text{m}$ superficially porous particles pretreated at different temperatures (400, 525, or 900°C). (B) Experimental kinetic plots of N versus t_0 of columns packed with 2.7, 2.6, 1.6, 1.3 superficially porous particles (SPP), and $1.7\ \mu\text{m}$ fully porous particles (FPP). (C) Experimental kinetic plots of t_0/N versus N of columns packed with 2.7, 2.6, 1.6, 1.3 superficially porous particles (SPP), and $1.7\ \mu\text{m}$ fully porous particles (FPP). Experimental conditions: $T = 30^\circ\text{C}$, 96:4 ACN/formate buffer 20 mM pH 3 v/v, UV = 254 nm. Test analyte: cytosine. For the kinetic plots, $\Delta P_{\text{max}} = 600$ bar for the 2.7 and $2.6\ \mu\text{m}$ packings and 1000 bar for the 1.7, 1.6 and $1.3\ \mu\text{m}$ packings.

rates were transformed into height equivalent to a theoretical plate (H) and mobile phase interstitial linear velocity (u_i). Then, the curves were fitted using least square regression model, with the van Deemter equation:

$$H = A + \frac{B}{u_i} + C u_i \quad (1)$$

Where A , B , and C are system constants determined by the magnitude of band broadening due to eddy diffusion, longitudinal diffusion, and resistance to mass transfer, respectively.

The column permeability (K_v) was calculated by measuring the slopes of the experimental pressure drop (ΔP) versus u_i representations, and using Darcy's equation.

$$\Delta P = \frac{\eta L u_i}{K_v} \quad (2)$$

Where L is the column length and η is the mobile phase viscosity.

From the permeability value, the flow resistance (ϕ) can be easily obtained with the following equation:

$$\phi = \frac{d_p^2}{K_v} \quad (3)$$

in which d_p is the particle diameter.

Then, the separation impedance (E) was obtained using the following equation:

$$E = h_{\text{min}}^2 \phi \quad (4)$$

Next to the van Deemter curves, kinetic plots were also constructed, since they are more informative when comparing supports with a different morphology and/or size. Giddings described kinetic plot in the 1960s, but recently Desmet et al. demonstrated the possibility to simplify their construction and improve visualization [28, 29]. In kinetic plot representation, experimental (u_i , H) data are represented as a plot of t_0 versus N , using a scaling value for the pressure drop ΔP and the viscosity η , and making a recombination of all experimentally obtained u_i and H data couples according to Eqs. (5) and (6):

$$N = \frac{\Delta P_{\text{max}}}{\eta} \left(\frac{K_v}{u_i H} \right)_{\text{experimental}} \quad (5)$$

$$t_0 = \frac{\Delta P_{\text{max}}}{\eta} \left(\frac{K_v}{u_i^2} \right)_{\text{experimental}} \quad (6)$$

The advantages of these kinetic plot representations over traditional (u_i , H) curves are that they take into account the flow resistance effect as well as the analysis time needed to produce N plates. As a consequence, every data point on the kinetic plot represents a column that differs in length.

3 Results and discussion

3.1 Impact of pretreatment temperature on kinetic performance

In this study, the impact of thermal treatment on the kinetic performance was investigated for columns packed with bare silica superficially porous type particles ($2.6\ \mu\text{m}$). For this

purpose, van Deemter curves as well as kinetic plots were constructed for three columns pretreated at different temperatures, ranging from 400 to 900°C. Higher pretreatment temperatures were not tested, since it was previously shown that beyond 900°C, the stationary phase was found to be unusable from a chromatographic point of view [24, 27].

Figure 1A shows the van Deemter curves obtained for the three tested columns. To draw reliable conclusions from these representations, the model compound (cytosine) should be sufficiently retained to limit the instrumental contributions to band broadening. In the present study, cytosine had an average retention factor of 9.8, 11.1, and 7.3 for the columns pretreated at 400, 525 and 900°C, respectively. These values were considered for calculating the average column variances, σ_{col}^2 , which were equal to 124, 180, and 88 μL^2 for the columns pretreated at 400, 525, and 900°C, respectively, taking into account the column dimensions.

Experimentally, the instrumental contribution, σ_{ext}^2 of our UHPLC instrument was estimated around 1–2 μL^2 , depending on the mobile phase flow rate [30]. Based on these values, the loss of efficiency attributed to the chromatographic instrument remained always lower than 2% and can be considered as negligible, confirming the reliability of van Deemter curves reported in Fig. 1A.

In RPLC conditions, minimum reduced heights equivalent to a theoretical plate ($h_{\text{min}} = H_{\text{min}}/d_p$) for superficially porous type material have been reported between 1.2 and 1.9 [31]. In this study, experiments were performed under HILIC conditions and therefore, expectations in terms of kinetic performance may be quite different. Indeed, many kinetically slow interactions occur (e.g. H-bond, dipole-dipole, and ionic interactions), which may contribute significantly to band broadening, compared to RPLC conditions with a C material [32]. Therefore, h_{min} of superficially porous type material under HILIC conditions has often been reported as higher than 2 [14]. Using the bare silica columns pretreated at 400, 525, and 900°C, H_{min} values were equal to 4.9, 5.8, and 6.1 μm , respectively. Considering the average diameter of the particles (2.6 μm), h_{min} values were included in the range 1.9–2.3. As reported in Table 1, these values were rather good, particularly for the column pretreated at 400°C, which was much better than other bare silica superficially porous columns, commercially available. The h_{min} values may be attributed to an improved packing quality related to enhanced particle properties (as example, modification of surface roughness), when using pretreatment temperature of 400°C. Increasing the pretreatment temperature has a negative effect on the overall kinetic performance, but results remained acceptable, as shown in Table 1. Optimal linear velocities, u_{opt} were found to be close and included within the range 1.8–2.7 mm/s. Mass transfer resistance (C-term of the van Deemter curve, which corresponds to the right part of the curve) can be graphically compared in Fig. 1A. This parameter is indeed of importance, since the pressure drop observed under HILIC conditions is rather low (low mobile phase viscosity, related to the high proportion of acetonitrile usually employed) and therefore, it is very common to perform experiments in the C-term dom-

inated region. As shown in the figure, C-term values were strictly identical for the columns pretreated at 400 and 900°C, and slightly lower for the column pretreated at 525°C.

To have a fair comparison of the achievable kinetic performance of the different materials, the stationary phase permeabilities (K_p) (which is directly linked to the column pressure drop) have been reported in Table 1 and were generally close, whatever the pretreatment temperature (less than 10% difference).

Then, the information obtained from the van Deemter curves and the permeability values were combined to construct the kinetic plots reported in Fig. 1B ($N = f(t_0)$) and Fig. 1C ($t_0/N^2 = f(N)$), using the methodology described in the experimental section. The three home-made columns were compared between them, but also with other HILIC state-of-the-art columns made of unbonded silica or hybrid silica. In these representations, three superficially porous type columns were considered, namely Kinetex, Cortecs, and Ascentis with particle sizes of 1.3, 1.6, and 2.7 μm , respectively. In addition, a reference column packed with fully porous 1.7 μm particles was also included. It is important to notice that three of the four additional columns were commercial products (i.e. Ascentis, Cortecs, and Acquity), while the Kinetex HILIC 1.3 μm was a prototype, generously given by Phenomenex. The performance of the columns for a given efficiency can be directly compared in Fig. 1B. When considering $N = 10\,000$ plates (usual plate count value in HPLC), the differences between the three home-made HILIC columns were limited, since the required column dead time varied by only 20% (the column offering the highest efficiency also has the worst permeability). The performance of other HILIC columns was better, as the dead time was reduced by almost twofold. The differences of kinetic performance between home-made materials and the other HILIC phases were less pronounced for higher plate count. Indeed, for $N = 30\,000$ plates, the achievable analysis time was comparable for the 400°C, 525°C, Ascentis, Kinetex and Cortecs columns and was in the range of 25–34 s. Only the HILIC column with a pretreatment of 900°C provided lower performance ($t_0 = 41$ s), while the Acquity was the best phase ($t_0 = 20$ s). However, the performance of the Acquity phase may be overestimated since this phase packed with 1.7 μm FPP present a higher porosity than the other SPP phases, and this difference cannot be considered in this kinetic plot representation. These differences can be explained with the help of Fig. 1C. Indeed, in the representation of $t_0/N^2 = f(N)$, the shape of the van Deemter curve is maintained and therefore, it is possible to know whether experiments to attain a certain plate count are conducted in the A, B, or C term dominated region of the van Deemter curves. Due to the very low mobile phase viscosity of HILIC mobile phase, the experiments that allowed us to reach plate count of 10 000 are systematically performed in the C term dominated region since it requires relatively short column length and high flow rate. Experiments performed for generating 30 000 plates are also carried out in the C term region, but much closer to the optimum linear velocity. Because A, B, and C terms contributions

Table 1. Performance characteristics of columns packed with 2.7, 2.6, 1.6, 1.3 μm superficially porous particles (SPP), and 1.7 μm fully porous particles (FPP)

Denomination Provider	Column 400°C Home-made	Column 525°C Home-made	Column 900°C Home-made	Ascentis Sigma	Acquity Waters	Kinetex Phenomenex	Cortecs Waters
Technology	SPP	SPP	SPP	SPP	FPP	SPP	SPP
dp (μm)	2.6	2.6	2.6	2.7	1.7	1.3	1.6
K_v (m^2)	9.73×10^{-15}	9.55×10^{-15}	1.05×10^{-14}	1.35×10^{-14}	5.39×10^{-15}	2.17×10^{-15}	2.64×10^{-15}
Viscosity (Pa.s)	4.1×10^{-4}	4.1×10^{-4}	4.1×10^{-4}	4.0×10^{-4}	4.0×10^{-4}	4.0×10^{-4}	4.0×10^{-4}
h_{min}	1.9	2.2	2.3	2.2	2.4	3.2	2.5
Φ	695	708	644	540	536	779	970
E_{min}	2498	3510	3544	2649	2998	8207	5940
F or N = 10 000 t_0 (s) =	9.0	8.7	10.9	6.0	5.2	5.3	5.2
F or N = 30 000 t_0 (s) =	32.3	34.4	41.1	26.4	20.8	32.3	25.2
F or t_0 = 10s N =	11 000	11 336	9340	14 900	17 300	14 700	16 300

are different between all the tested columns, the kinetic performance ranking of stationary phases may differ depending on the required plate count. The stationary phase pretreated at 900°C appeared as the worst one among the seven HILIC stationary phases, for efficiencies up to 40 000 plates. This behavior can be explained by its low permeability, relatively high h_{min} value and high C term contribution, compared to the other phases. Then, Kinetex and Cortecs phases packed with 1.3 and 1.6 μm , respectively, became the least interesting phases for plate count beyond 40 000 plates, due to their very low permeability. Based on the kinetic plot representation, the columns pretreated at 400 and 525°C had a close behavior up to 20 000 plates (overlaid kinetic plots) and beyond this value, the column pretreated at 400°C clearly outperformed the 525°C. In addition, it is worth mentioning that the column pretreated at 400°C is in second position among the seven tested columns, for $N > 70$ 000 plates, while the Acquity column presented the best kinetic performance from 10 000 to 300 000 plates. The good performance of the 400°C column is related to its high permeability and low flow resistance ($\varphi = 695$), together with h_{min} of only 1.9. In Fig. 1B and C, N values beyond 100 000 plates should be considered with caution, since this plate range is only accessible with very long columns of several meters and extremely low linear velocity, which are not representative from real-life chromatographic experiments. Therefore, such very high N values are not discussed here.

Another interesting figure of merit that can be calculated for the seven HILIC columns at disposal is the separation impedance (E) that describes the compromise between speed, efficiency and pressure. For HPLC columns, impedance values of 3000–5000 are generally observed, and an E value beyond this range could be due to a lack of column efficiency (high h_{min} values) and/or to a high generated pressure drop (high flow resistance values, φ), according to Eq. (4). For the HILIC column pretreated at 400°C, the E value was extremely low (< 2500), confirming the great kinetic performance of this stationary phase, comparable to commercial Ascentis stationary phase ($E = 2649$). The two others home-made HILIC columns also gave very good E values ranging between 3510

and 3544. On the contrary, the two columns packed with the smallest particles sizes (Kinetex and Cortecs) have high E values of 5940 and 8207. For the Cortecs, the flow resistance was particularly high ($\varphi = 970$), while for the Kinetex, the problem came from its high h_{min} value ($h_{\text{min}} = 3.2$).

3.2 Selectivity comparison of the three HILIC columns with different pretreatment

In a second instance, the three HILIC columns pretreated at 400, 525, and 900°C were evaluated for the separation of two mixtures of polar substances.

As a first example, a mixture of several nucleobases, nucleotides, and nucleosides (structures reported in Supporting Information Fig. S1) was analyzed and the corresponding chromatograms are shown in Fig. 2. These compounds were selected since nucleic acids and their analogs are of great interest in pharmaceutical sciences and metabolomics. Due to their high polarity ($\log P$ values ranged from -0.53 for adenine to -5.19 for adenosine monophosphate, as reported in Supporting Information Table S1), these compounds are perfectly adapted to the HILIC mode. After a careful optimization of mobile phase conditions (i.e. gradient profile, mobile phase flow rate, temperature, pH, and buffer), ultra-fast separations were achieved, and all peaks were eluted in less than 1.4 min. Baseline separations were achieved on the columns pretreated at 400 and 525°C, while resolutions between peaks 1 and 2, but also peaks 5 and 6 were not sufficient on the column pretreated at 900°C. Furthermore, peak shapes were highly distorted. This confirms that the surface chemistry of the latter is certainly different from the two other stationary phases. Indeed, it has been previously reported [24, 27] that free silanols may be modified into siloxane bridges at elevated pretreatment temperature, thus reducing the polar character of the stationary phase and its retention under HILIC conditions. On the contrary, the amount and type of silanols (and therefore the surface chemistry) was probably quite similar for columns pretreated at 400 and 525°C, since only a slight

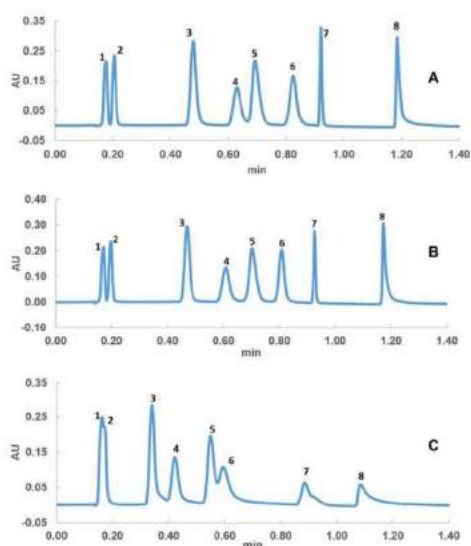


Figure 2. Chromatogram of eight nucleobases, nucleosides, and nucleotides mixture in the different stationary phase at pH = 3, formate buffer 20 mM. Gradient conditions v/v: 95% ACN for 0.5 min, then 50% ACN in 1 min, 50% ACN for 0.5 min, then 95% ACN in 0.1 min, at 1 mL/min, $T = 30^{\circ}\text{C}$, UV = 254 nm. Order of elution: Uracil (1), uridine (2), adenine (3), guanosine (4), adenosine (5), cytidine (6), cytosine (7), AMP (8). (A) Column 400°C , SPP, $2.6\ \mu\text{m}$, (B) Column 525°C , SPP, $2.6\ \mu\text{m}$, (C) Column 900°C , SPP, $2.6\ \mu\text{m}$.

modification of the selectivity was monitored between peaks 4 and 5, in Fig. 2A and B.

A mixture of nicotine and its derivatives (structures reported in Supporting Information Fig. S2) was also analyzed on the HILIC columns with different pretreatment conditions. Again, the selected compounds were quite polar (log P values between -1.05 and 1.22 , as shown in Supporting Information Table S2), and therefore hardly retained on C_{18} material under RPLC conditions. Nicotine has not yet been classified as performance-enhancing drug, but this should happen rapidly [33]. Therefore, it will be soon required to develop an analytical method for the determination of nicotine and some of its metabolites, since monitoring of the latter allows improving detection windows capabilities in urine on many occasions. After optimizing the analytical conditions, the eight nicotine derivatives were not fully resolved, but the separation was promising, taking into account that it has been carried out on a 50 mm column length, with an analysis time of less than 2 min. Obviously, this separation could be significantly improved thanks to the use of a longer column and an extended gradient time, but this is out of the scope of the present paper. Here, the retention was not modified between the columns pretreated at 400 and 525°C , and only a minor change of selectivity was observed between peaks 1 and 2

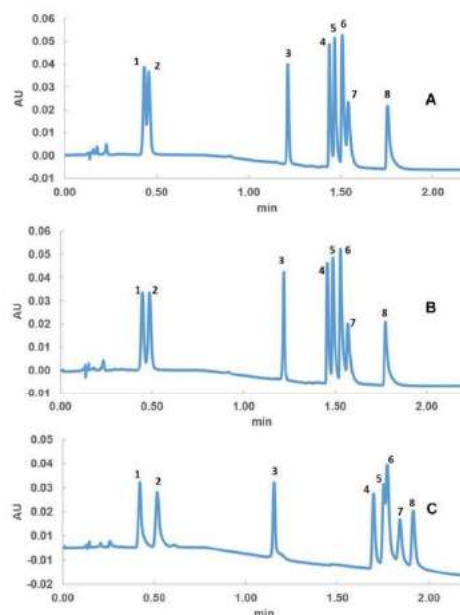


Figure 3. Chromatogram of 8 nicotine derivatives mixture in the different stationary phases at pH = 3, formate buffer 20 mM. Gradient conditions v/v: 95% ACN for 0.5 min, then 50% ACN in 1.75 min, 50% ACN for 0.25 min, then 95% ACN in 0.05 min, at 1 mL/min, $T = 30^{\circ}\text{C}$, UV = 254 nm. Order of elution: Hydroxycotinine (1), cotinine (2), cotinine N-oxide (3), anatabine (4), anabasine (5), nornicotine (6), nicotine (7), nicotine N'-oxide (8). (A) Column 400°C , SPP, $2.6\ \mu\text{m}$, (B) Column 525°C , SPP, $2.6\ \mu\text{m}$, (C) Column 900°C , SPP, $2.6\ \mu\text{m}$.

(Fig. 3A and B), corresponding to cotinine and hydroxycotinine (most basic substances among the eight tested nicotine derivatives, with $\text{p}K_{\text{a}}$ of 4.79). With the column pretreated at 900°C (Fig. 3C), the modification of selectivity was again much more pronounced and, cotinine and hydroxycotinine were fully resolved. With this 900°C column, only anabasine and nornicotine were not resolved. In addition, peaks were much sharper than in Fig. 2C, which could probably be explained by some differences in physicochemical properties of these two series of compounds and also modifications of surface chemistry between the columns pretreated at 400 – 525 and 900°C .

3.3 Thermal stability of the home-made HILIC columns

Preliminary studies of stability under aggressive conditions at elevated temperature were conducted ex-situ for various silica batches [27]. Bare porous silica particles were less stable than core-shell ones. An extensive evaluation of the HILIC

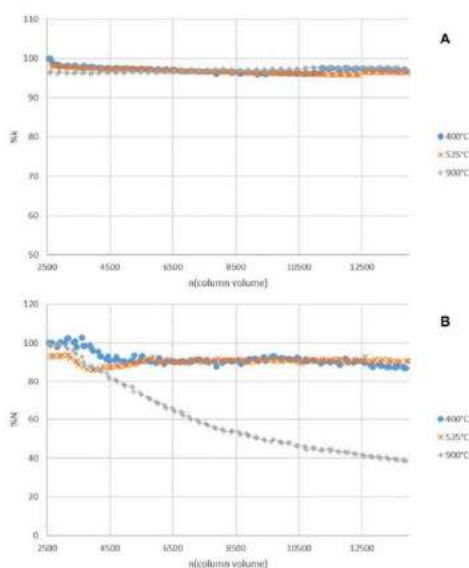


Figure 4. Experimental % k versus $N_{\text{column volume}}$ (A) and % N versus $N_{\text{column volume}}$ (B) plots obtained for columns packed with 2.6 μm superficially porous particles pretreated at different temperatures (400, 525, or 900°C). Experimental conditions: $T = 70^\circ\text{C}$, 95:5 ACN/acetate buffer 20 mM pH6 v/v, UV = 254 nm. Test analyte: cytosine.

columns made of bare core-shell particles pretreated at different temperatures was experimentally conducted at 70°C , 95:5 ACN/acetate buffer 20 mM pH 6 v/v, $k = f(V_{\text{col}})$ and $N = f(V_{\text{col}})$ plots (Fig. 4A and B, respectively), in relative percentages, showed that retentions remained very stable, even after percolating more than 14 000 column volumes. Interestingly, only a slight decrease of efficiencies was noticed for the 400 and 525°C pretreated stationary phases after this extended period of time, while the 900°C pretreated column showed an important loss of efficiency (symmetrical broadening of the peak). This proves that only columns pretreated at 400 and 525°C may be suitable for operation at elevated temperature.

4 Concluding remarks

As shown in this work, the pretreatment temperature of the stationary phase may be a parameter for tuning kinetic and thermodynamic performance as well as stability. To evaluate its impact, three HILIC columns packed with bare silica 2.6 μm superficially porous particles and pretreated at 400, 525, and 900°C were synthesized. First, the kinetic performance of these stationary phases was compared between them and also with other state-of-the-art HILIC materials made from bare silica. h_{min} values ranged between 1.9 and

2.3 for the three home-made stationary phases, while h_{min} was between 2.2 and 3.2 on the four other HILIC materials. However, due to their low permeability, the performance of the three home-made columns was inferior to the commercial ones in the low plate count range (10 000 plates), but was more favorable for N values beyond 40 000 plates, as illustrated in the kinetic plot representations. The HILIC column pretreated at 400°C became particularly attractive for high plate count ($N > 70\,000$ plates), due to its low flow resistance ($\varphi = 695$), together with h_{min} of only 2.4.

Except kinetic performance, the thermodynamic behavior of the three prototype stationary phases was evaluated through the analysis of two mixtures of polar compounds, nucleobases and derivatives as well as nicotine and derivatives. It is expected that the pretreatment temperature modifies the nature of silanols (amount and acidity) at the surface of the column. For the phases pretreated at 400 and 525°C, only minor modifications of selectivity and retention were observed, while changes were much more pronounced with the phase pretreated at 900°C. This shows that selectivity of bare silica phase under HILIC conditions can be simply modified by tuning the pretreatment temperature. However, the phase pretreated at 900°C provided poor peak shape for nucleobases, nucleotides and nucleosides, while peaks corresponding to nicotine derivatives were much more symmetrical. This behavior could be related to the number of H-bond donor groups on the analytes, which was much larger for nucleobases derivatives. Nevertheless, before drawing reliable conclusions, there is a need to perform additional experiments with a larger set of compounds and such study is currently under progress in our laboratory.

Last but not least, the pretreated phases showed a good stability under aggressive conditions (70°C) as the retention remained constant after more than 14 000 column volumes, and the efficiency was still good for the stationary phases pretreated at 400 and 525°C.

The authors wish to thank Dr. Tivadar Farkas from Phenomenex (Torrance, CA, USA) for providing the Kinetex HILIC 1.3 μm prototype column employed in this study. Dr. Raul Nicoli from the Swiss antidoping laboratory (Epalinges, Switzerland) is also acknowledged for the gift of stock solutions of nicotine derivatives.

The authors have declared no conflict of interest.

5 References

- [1] McCalley, D. V., Is hydrophilic interaction chromatography with silica columns a viable alternative to reversed-phase liquid chromatography for the analysis of ionisable compounds? *J. Chromatogr. A* 2007, 1171, 46–55.
- [2] Buszewski, B., Noga, S., Hydrophilic interaction liquid chromatography (HILIC)—a powerful separation technique. *Anal. Bioanal. Chem.* 2012, 402, 231–247.
- [3] Ruta, J., Rudaz, S., McCalley, D. V., Veuthey, J., Guillelme, D., A systematic investigation of the effect of

- sample diluent on peak shape in hydrophilic interaction liquid chromatography. *J. Chromatogr. A* 2010, **1217**, 8230–8240.
- [4] Janders, P., Stationary and mobile phases in hydrophilic interaction chromatography: a review. *Anal. Chim. Acta* 2011, **692**, 1–25.
- [5] Greco, G., Letzel, T., Main interactions and influences of the chromatographic parameters in HILIC separations. *J. Chromatogr. Sci.* 2013, **51**, 684–693.
- [6] Hemstrom, P., Irgum, K., Hydrophilic interaction chromatography. *J. Sep. Sci.* 2006, **29**, 1784–1821.
- [7] McCalley, D. V., Neue, U. D., Estimation of the extent of the water-rich layer associated with the silica surface in hydrophilic interaction chromatography. *J. Chromatogr. A* 2008, **1192**, 225–229.
- [8] Gika, H., Theodoridis, G., Mattivi, F., Vrhovsek, U., Pappalouisi, A., Hydrophilic interaction ultra performance liquid chromatography retention prediction under gradient elution. *Anal. Bioanal. Chem.* 2012, **404**, 701–709.
- [9] Periat, A., Debrus, B., Rudaz, S., Guillaume, D., Screening of the most relevant parameters for method development in ultra-high performance hydrophilic interaction chromatography. *J. Chromatogr. A* 2013, **1282**, 72–83.
- [10] Tyteca, E., Périat, A., Rudaz, S., Desmet, G., Guillaume, D., Retention modeling and method development in hydrophilic interaction chromatography. *J. Chromatogr. A* 2014, **1337**, 116–127.
- [11] Gritti, F., Holtzel, A., Tallarek, U., Guiochon, G., The relative importance of the adsorption and partitioning mechanisms in hydrophilic interaction liquid chromatography. *J. Chromatogr. A* 2015, **1376**, 112–125.
- [12] Ruta, J., Boccard, J., Cabooter, D., Rudaz, S., Desmet, G., Veuthey, J. L., Guillaume, D., Method development for pharmaceuticals: some solutions for tuning selectivity in reversed phase and hydrophilic interaction liquid chromatography. *J. Pharm. Biomed. Anal.* 2012, **63**, 95–105.
- [13] Periat, A., Boccard, J., Veuthey, J. L., Rudaz, S., Guillaume, D., Systematic comparison of sensitivity between hydrophilic interaction liquid chromatography and reversed phase liquid chromatography coupled with mass spectrometry. *J. Chromatogr. A* 2013, **1312**, 49–57.
- [14] Chauve, B., Guillaume, D., Cleon, P., Veuthey, J. L., Evaluation of various HILIC materials for the fast separation of polar compounds. *J. Sep. Sci.* 2010, **33**, 752–764.
- [15] Horvath, C., Preiss, B. A., Lipsky, S. R., Fast liquid chromatography: an investigation of operating parameters and the separation of nucleotides on pellicular ion exchangers. *Anal. Chem.* 1967, **39**, 1422–1428.
- [16] Horvath, C., Lipsky, S. R., Column design in high-pressure liquid chromatography. *J. Chromatogr. Sci.* 1969, **7**, 109–116.
- [17] Gritti, F., Cavazzini, A., Marchetti, N., Guiochon, G., Comparison between the efficiencies of columns packed with fully and partially porous C 18-bonded silica materials. *J. Chromatogr. A* 2007, **1157**, 289–303.
- [18] Fekete, S., Oláh, E., Fekete, J., Fast liquid chromatography: the domination of core-shell and very fine particles. *J. Chromatogr. A* 2012, **1228**, 57–71.
- [19] Fekete, S., Fekete, J., Ganzler, K., Shell and small particles; evaluation of new column technology. *J. Pharm. Biomed. Anal.* 2009, **49**, 64–71.
- [20] Guiochon, G., Gritti, F., Shell particles, trials, tribulations and triumphs. *J. Chromatogr. A* 2011, **1218**, 1915–1938.
- [21] Guiochon, G., Gritti, F., Repeatability of the efficiency of columns packed with sub-3- μm core-shell particles: part I. 2.6- μm Kinetex-C(18) particles in 4.6mm and 2.1mm \times 100mm column formats. *J. Chromatogr. A* 2012, **1252**, 31–44.
- [22] Gritti, F., Guiochon, G., Repeatability of the efficiency of columns packed with sub-3- μm core-shell particles: part II. 2.7 μm Halo-ES-Peptide-C18 particles in 4.6mm and 2.1mm \times 100mm column formats. *J. Chromatogr. A* 2012, **1252**, 45–55.
- [23] Gritti, F., Guiochon, G., Repeatability of the efficiency of columns packed with sub-3- μm core-shell particles: part III. 2.7- μm Poroshell 120 EC-C18 particles in 4.6mm and 2.1mm \times 100mm column formats. *J. Chromatogr. A* 2012, **1252**, 56–66.
- [24] Sunseri, J. D., Cooper, W. T., Dorsey, J. G., Reducing residual silanol interactions in reversed-phase liquid chromatography. Thermal treatment of silica before derivatization. *J. Chromatogr. A* 2003, **1011**, 23–29.
- [25] Van der Voort, P., Vansant, E. F., Silylation of the silica surface: a review. *J. Liq. Chromatogr. Relat. Technol.* 1996, **19**, 2723–2752.
- [26] Zhuravlev, L. T., The surface chemistry of amorphous silica. *Zhuravlev model. Colloids Surf. A* 2000, **173**, 1–38.
- [27] Mignot, M., Sebban, M., Tchaplal, A., Mercier, O., Cardinael, P., Peulon-Agasse V., Thermal pretreatments of superficially porous silica particles for high-performance liquid chromatography: surface control, structural characterization and chromatographic evaluation. *J. Chromatogr. A* 2015, **1419**, 45–57.
- [28] Desmet, G., Clicq, D., Gzil, P., Geometry-independent plate height representation methods for the direct comparison of the kinetic performance of LC supports with a different size or morphology. *Anal. Chem.* 2005, **77**, 4058–4070.
- [29] Desmet, G., Gzil, P., Nguyen, D., Guillaume, D., Rudaz, S., Veuthey, J. L., Vervoort, N., Torok, G., Cabooter, D., Clicq, D., Practical constraints in the kinetic plot representation of chromatographic performance data: theory and application to experimental data. *Anal. Chem.* 2006, **78**, 2150–2162.
- [30] Fekete, S., Kohler, I., Rudaz, S., Guillaume, D., Importance of instrumentation for fast liquid chromatography in pharmaceutical analysis. *J. Pharm. Biomed. Anal.* 2014, **87**, 105–119.
- [31] Fekete, S., Dong, M. W., Guillaume, D., Superficially porous particles: perspectives, practices, and trends. *LC-GC Europe* 2014, **27**, 312–323.
- [32] Grand-Guillaume Perrenoud, A., Farrell, W. P., Aurigemma, C. M., Aurigemma, N. C., Fekete, S., Guillaume, D., Evaluation of stationary phases packed with superficially porous particles for the analysis of pharmaceutical compounds using supercritical fluid chromatography. *J. Chromatogr. A* 2014, **1360**, 275–287.
- [33] *The 2015 Prohibited List*, World Anti-Doping Agency, Montreal, 2015.

This study demonstrated that the pretreatment temperature can be a parameter for tuning kinetic and thermodynamic performance as well as stability of the stationary phases.

In terms of kinetic evaluation, due to their low permeability the performance of the three home-made columns (pretreatment at 400, 525, and 900°C) was inferior to the commercial ones in the low plate count range (10,000 plates), but was more favorable for N values beyond 40,000 plates. Also, the HILIC column pretreated at 400°C became particularly attractive for high plate count ($N > 70,000$ plates), due to its low flow resistance ($\varphi = 695$), together with h_{\min} value of only 2.4.

Except the kinetic performances, the thermodynamic behavior of the three home-made stationary phases was evaluated through the analysis of two mixtures of polar compounds, nucleobases and derivatives as well as nicotine and derivatives. For the phases pretreated at 400 and 525°C, only minor modifications of selectivity and retention were observed, while changes were much more pronounced with the phase pretreated at 900°C. This shows that selectivity of bare silica phase under HILIC conditions can be simply modified by tuning the pretreatment temperature. However, the phase pretreated at 900°C provided poor peak shape for nucleobases, nucleotides and nucleosides, while peaks corresponding to nicotine derivatives were much more symmetrical. This behavior could be related to the number of H-bond donor groups on the analytes, which was much larger for nucleobases derivatives. Nevertheless, due to the diversity of interactions involved in HILIC conditions, it is still difficult to predict the behavior of a stationary phase for which the silica surface has been modified by temperature, with respect to the analysis of a certain class of compounds.

Last but not least, the pretreated phases showed a good thermal stability (at 70°C) as the retention remained constant after more than 14,000 column volumes, and the efficiency was still good for the stationary phases pretreated at 400 and 525°C.



CHAPTER III

Non-conventional multimodal
stationary phases

Introduction

In the first part of this thesis, different types of C18 SPs have been developed depending on the thermal treatment applied before functionalization, and depending on the end-capping step.

This part is dedicated to the development of an original SP containing an alkyl chain (spacer), a polar embedded group (amide), and an aromatic group (anthracenic group). Such selector has been grafted on FPP and on SPP, under conventional heating and under microwave irradiations.

A full characterization of the modified FPP and SPP is presented, but an important part of the work was dedicated to the molecular modeling. The potential of DFT to better understand the chromatographic properties of those multimodal stationary phases was highlighted with a collaboration with Dr. Vincent Tognetti (Equipe Analyse et Modélisation, COBRA) (III.1). At the writing time of this manuscript, such study entitled: "New anthracenyl polar embedded stationary phases with enhanced aromatic selectivity: a combined experimental and theoretical study" has been submitted for publication in *Journal of Chromatography, A*.

Finally, the last part concerned the synthesis of calix[6]arene derivatives achieved (III.2) under the supervision of Prof. Ivan Jabin (LCO, Université Libre de Bruxelles). Those macrocycles contain one carboxylic acid function that allows for grafting onto SPPs, following the synthesis way adopted previously (III.1). The aim was to obtain stationary phases presenting shape selectivity and containing a cavity capable of inclusion of some solutes. The calix[6]arene derivatives were characterized (NMR, MS, IR) before further grafting onto silica particles.

The preliminary studies were done on calix[6]arene derivatives synthesized by Jabin's team, and which contain six carboxylic acid functions. The grafting onto SPP was achieved, and an evaluation of the chromatographic properties of the SPs is presented in the following part.

III-1. Article 5: New polar embedded aromatic stationary phases

New anthracenyl polar embedded stationary phases with enhanced aromatic selectivity: a combined experimental and theoretical study

Mélanie Mignot¹, Benjamin Schammé¹, Vincent Tognetti², Laurent Joubert², Alain Tchaplá³, Olivier Mercier⁴, Pascal Cardinael¹, Valérie Peulon-Agasse^{1*}

¹Normandie Univ., Laboratoire SMS-EA3233, Univ. Rouen, F-76821, Mont Saint Aignan, France

²Normandie Univ., COBRA, UMR 6014 & FR 3038, Univ. Rouen, INSA Rouen, CNRS, 1 rue Tesnière, F-76821 Mont-Saint-Aignan Cedex, France

³Lip(Sys)²- LETIAM[§], Univ. Paris-Sud, Université Paris-Saclay, IUT d'Orsay, Plateau de Moulon F-91400 Orsay, France.

[§](FKA EA4041 Groupe de Chimie Analytique de Paris-Sud)

⁴Interchim R & D, 211 bis avenue JF Kennedy, BP 1140, 03100 Montluçon, France

*corresponding author: valerie.agasse@univ-rouen.fr

Abstract

New polar embedded aromatic stationary phases of different functionalities (mono- and trifunctional) were synthesized to determine the impact of the functionality on the retention process and the selectivity towards aromatic compounds. A full experimental characterization was performed using a combination of techniques (elemental analysis, thermogravimetric measurements, infrared spectroscopy and solid-state NMR) to differentiate unambiguously the mono- and trifunctional structures. Commercially available columns with either an aromatic group or a polar embedded group were compared to the new stationary phases. The latter presented enhanced affinity for polycyclic aromatic hydrocarbons (PAH) structures compared to alkylbenzenes, especially when using methanol instead of acetonitrile as the organic modifier. The structures of the ligands, as well as the chromatographic results and the origin of the selectivity, were theoretically explained by density functional theory calculations.

Keywords: high-performance liquid chromatography, aromatic stationary phase, molecular modeling, polar embedded group, steric selectivity, functional density theory

1. Introduction

Stationary phases used in high-performance liquid chromatography (HPLC) are generally prepared by organosilanization with different types of silane reagents, leading to covalent linkage of ligands to the silanol groups at the silica surface[1,2]. The characteristics (density, molecular structure, conformation, mobility and distribution of the ligands) of the bonded phase are of crucial interest as they can affect the chromatographic properties, such as retention[3,4].

Monomeric bonded phases are in most cases obtained by monofunctional organosilanes, and polymeric bonded materials result from functionalization with polyfunctional organosilanes[5]. Monomeric phases improve the mass transfer capability, whereas polymeric structures present better selectivity towards

non-flexible molecules and are favored for the separation of polycyclic aromatic hydrocarbons (PAHs)[6–10].

C18 stationary phases are the most widely used phases in reversed-phase liquid chromatography (RPLC) because of their versatility and their good performance in terms of selectivity, efficiency, and resolution. When a high aqueous content in the mobile phase is required, polar end-capping can be achieved enhancing the wetting of the C18 stationary phase. Another type of reversed stationary phase is aromatic phases. Their popularity can be explained by their great specificity for aromatic solutes, presumably due to π - π interactions[10–15], making them especially interesting for the separation of aromatic compounds, such as PAHs. Many aromatic silica-based stationary phases have been developed in recent few years, and many are commercially available, such as phenyl-3-propyl, phenyl-6-hexyl, propyl-3-N-urea N'-2-picolinyl (PPUTM), ethyl-2-pyridine, ethyl-4-pyridine, butyl-2-3-4-5-6-pentafluoro-phenyl-bonded silica, and polymeric materials, such as polystyrene-divinylbenzene.

On these phases, specific effects due to π - π interactions are superimposed on the hydrocarbonaceous predominant effect, leading to subtle modification of the selectivity compared to pure alkyl bonded silicas. Elsewhere, the comparison of the eluent strength of the mobile phase calculated from the methylene selectivity on propyl-3-phenyl bonded silica showed that over the complete range of compositions, the mixtures with acetonitrile are more effective eluents than the corresponding ones with methanol as the organic modifier, which is not true on C18 bonded silicas[16]. It was demonstrated that the pure hydrophobic effect (measured by the methylene selectivity) on the phenyl-3-propyl bonded phase is three to four times weaker than on a C18 bonded phase, which could drastically affect the separation on this class of bonded silica[15]. A close examination of the methylene selectivity of all types of these ended single aromatic ring alkyl bonded stationary phases leads to the same conclusion[17], excepted for two poly-aromatic phases (i.e., biphenyl and 1-pyrenyl, for which the methylene selectivity is higher than the mean of the C18 grafts). Nevertheless, new aromatic phases are continuously designed for specific separation challenges.

In particular, the separation of aromatic-substituted isomers and critical PAH isomers is often targeted[18–20]. These developments have led to the commercialization of aromatic groups at the end of different alkyl chain length bonded silica, such as N-9(methyl-anthracene)-amino[21], 1-pyrenyl (PYETM), 2-naphthyl (π NAPTM), biphenyl, pentabromobenzyloxy and nitrophenyl alkyl bonded silicas, at which 1-1' diphenyl-methyl bonded silicas must be added. Among these aromatic bonded silicas, two poly-aromatic biphenyl and 1-pyrenyl present methylene selectivity greater than the mean of C18 grafts. A silanol-free pseudo-aromatic stationary phase, porous graphitic carbon (PGC), showed interesting chromatographic properties similar to those obtained on the PYE or fullerene phases[22–24]. Some other authors demonstrated that the PGC phase was very different from conventional non-polar phases (e.g., C18, C30) especially for the polar solute retention[25]. However, these phases are not widespread because their use is not straightforward. They are mainly used as an alternative to conventional stationary phases (e.g., C18, C8, phenylhexyl) when the separation cannot be achieved or when looking for a second dimension stationary phase in bi-dimensional chromatography[26].

Despite their selectivity, aromatic stationary phases have some disadvantages, and polar solute retention can be too low. The introduction of a polar group into the structure of the ligand led to what are now called polar embedded stationary phases. Until now, these phases were developed in combination with alkyl stationary phases[27–34]. Embedding a polar functional group[35,36] (e.g., a carbamate[37], amide, urea, quaternary ammonium, sulfamide, ether oxide, ester) into a bonded alkyl chain reduces the peak tailing for basic analytes and has unique selectivity for certain classes of analyte, such as phenols[38], stereochemically rigid isomers, and endocrine disruptor solutes in the Engelhardt polar selectivity test[39]. Finally, their methylene selectivity is slightly lower than the mean of C18 grafts. Recently, a new multifunctional stationary phase combining both an embedded group (1-glycero 3-propyl) and an aromatic group (1-aminoanthracene) bonded on bridged ethylene hybrid silica (BEH™ technology) was commercialized by Waters.

Polar-embeddeed group (PEG) poly-aromatic stationary phases can offer various types of interaction. The need for a precise determination of their 3D structure is necessary to understand their chromatographic behavior. This can be achieved theoretically by using molecular modeling tools, such as molecular mechanics, or semi-empirical methods, which have already been used to elucidate the structures of conventional stationary phases. In this paper, we rely on density functional theory (DFT)[40], which improves upon the classic solute modeling and docking[41–46] approaches by introducing a full quantum description of the system. Hence, one of the purposes of this paper is to propose and assess a robust DFT-based computational protocol to model the 3D structure and to better understand the experimental results.

In summary, this article describes the synthesis and the complete characterization of a new generation of polar embedded aromatic stationary phases. It reports the use of DFT to precisely elucidate the 3D ligand structure and to rationalize their chromatographic properties. More precisely, the mono- and trifunctional versions of the new polar embedded aromatic stationary phase are reported by amidation with 9-anthracenecarboxylic acid onto amino-functionalized silica to afford the desired amide-functionalized aromatic stationary phases under microwave irradiation as developed in our laboratory[47,48] (Experimental section in the Supporting information). Then, a deep characterization was performed to differentiate the mono- and trifunctional version by a combination of analytical techniques (microscopy, elemental analysis, thermogravimetry, infrared spectroscopy, ¹H, ¹³C, ²⁹Si CP/MAS NMR available in the Supporting information).

Finally, a theoretical study by DFT is conducted to determine the conformation of the ligands grafted onto the silica surface and to study the influence of the organic modifier of the mobile phase. In addition, the chromatographic properties of these new stationary phases includes the evaluation of their selectivity towards the homologous series of alkylbenzenes as well as different congeners of PAHs. These solutes are indeed good probes to investigate the aromatic and shape selectivity.

2. Experimental section

2.1 Materials and reagents

The silica particles were provided by Interchim (Montluçon, France). For the porous material, its specific surface area, nominal particle diameter and pore diameter were 425 m²/g, 3 μm and 100 Å, respectively. For the superficially porous material, its specific surface area, nominal particle diameter and pore diameter were 126 m²/g, 2.6 μm and 90 Å, respectively. 4-Aminobutyldimethylmethoxysilane (ABDMS) and 4-aminobutyltriethoxysilane (ABTS) were obtained by Fluorochem (Hadfield, United Kingdom). Bis(dimethylamino)(trimethyl)silane (DATS) was purchased from ABCR (Karlsruhe, Germany). Toluene, (benzotriazol-1-yloxy)tripyrrolidinophosphonium hexafluorophosphate (PyBOP), N,N-diisopropylethylamine (DIPEA), 9-anthracenecarboxylic acid, anthracene, naphthalene, benzene and ethylbenzene were supplied by Sigma-Aldrich (Saint-Quentin Fallavier, France). Dimethylformamide and dichloromethane were purchased from VWR (Fontenay-sous-Bois, France). Alkylbenzenes (from pentylbenzene to dodecylbenzene), naphthalene, *p*-terphenyl and *m*-terphenyl were obtained from TCI (Tokyo, Japan). Butylbenzene, triphenylene, and *o*-terphenyl were purchased from Alfa Aesar (Schiltigheim, France), and propylbenzene was from Acros Organics (Geel, Belgium). For the chromatographic tests, all solvents were of HPLC grade.

Elemental analysis was performed by the conventional combustion method using a Flash 2000 organic elemental analyzer from ThermoFisher (Waltham, MA, USA). Elemental analysis was used to determine the percentage of carbon, nitrogen, and hydrogen. The standard deviation for carbon percentages was 0.5%. The calculation of the bonded ligand coverage density was performed using the Berendsen equation.

DRIFT spectra were obtained using a PerkinElmer (Norwalk, CT, USA) Spectrum 100. The sample consisted of a mixture of silica with potassium bromide (10% (*m/m*)) placed in a 2 mm diameter cup. The spectra, which consisted of 64 scans, were acquired at a resolution of 2 cm⁻¹ and were referenced against pure KBr over the range of 4000-450 cm⁻¹.

²⁹Si CP/MAS NMR measurements were conducted with an AVANCE III 500 WB spectrometer equipped with a 4 mm double H/X probe (Bruker, Wissembourg, France). Magic-angle spinning was executed at 10 kHz, and 10240 scans were collected for each sample (²⁹Si and ¹³C). The ¹H 90° pulse was 2.85 μs, and the contact times were 3 ms and 5 ms for ¹³C and ²⁹Si, respectively, with a repetition time of 5 s. All chemical shifts were referenced to trimethylsilane.

The chromatographic measurements were performed with a liquid chromatograph from Dionex/ThermoFisher (Sunnyvale, CA, USA), which consisted of a P680 pump, an injection valve (ASI-100 automated sample injector) equipped with a 20 μL injection loop, and a UVD 340U diode-array detector (DAD). The column temperature was set to 30°C and was controlled with a TCC-100 thermostated column compartment at 1 mL/min. The data were collected on a computer using

Chromleon software. Stock solutions were prepared in acetonitrile and in methanol at 1 g/L. The dead time was measured from the disruption of the baseline of the chromatogram due to the unretained sample solvent.

2.2 Synthesis of the stationary phases

The synthesis steps (Scheme S1) were performed under microwave irradiation in our laboratory. The first step corresponded to the modification of bare silica to aminosilica by the addition of a spacer group (butyl) containing a terminal amino function. The second step was amidation between 9-anthracenecarboxylic acid and aminosilica to afford the final stationary phase. The complete protocol is available in Supporting Information.

3. Results and discussion

3.1 Surface chemistry of the mono- and tri-PEG-anthra

The physical properties of the silica particles are summarized in Table 1.

To investigate the influence of the support material, the monofunctional version was formed both on fully porous and on superficially porous supports. In addition, the influence of the tridimensional structure was studied by synthesizing bonded silica from mono- and trifunctional reagents on fully porous particles.

Column name	Particle diameter (μm)	Surface area (m ² /g)	Pore size (Å)	Carbon load (%)	Coverage density (μmoles/m ²)	Ligand (R) --Si -R	Silica type	Column dimensions (L _c × d _c × d _p) (mm × mm × μm)
*mono-PEG-anthra	2.6	126	90	5.2	1.9	(CH ₂) ₄ NHCO-9-C ₁₄ H ₉	SPP	50 × 4.6 × 2.6
*mono-PEG-anthra (1)	3.0	425	100	13.2	1.6	(CH ₂) ₄ NHCO-9-C ₁₄ H ₉	FPP	50 × 4.6 × 3.0
**mono-PEG-anthra (2)	3.0	425	100	17.6	2.3	(CH ₂) ₄ NHCO-9-C ₁₄ H ₉	FPP	250 × 4.6 × 3.0
**tri-PEG-anthra	3.0	425	100	18.0	-	(CH ₂) ₄ NHCO-9-C ₁₄ H ₉	FPP	250 × 4.6 × 3.0
HALO™ Phenyl-hexyl	2.7	135	90	7.4***	3.4***	(CH ₂) ₆ -C ₆ H ₅	SPP	100 × 4.6 × 2.7

HALO™ C18	2.7	135	90	7.7***	3.5***	C ₁₈ H ₃₇	SPP	50 × 4.6 × 2.7
HALO™ RP- amide	2.7	135	90	8.2***	3.0***	(CH ₂) ₃ NHCO- C ₁₅ H ₃₁	SPP	100 × 4.6 × 2.7

SPP= Superficially Porous Particles, FPP= Fully Porous Particles

*Synthesis performed under conventional heating **Synthesis performed under microwave irradiation

***Manufacturer data

Table 1: Summary of the column characteristics with the corresponding column packing

A deep characterization of the homemade stationary phases is provided in Supplementary information. The calculation of the bonded ligand coverage density was performed using the Berendsen equation[49]. Syntheses under microwave irradiation were successfully achieved, leading to 2.3 $\mu\text{mol}/\text{m}^2$ on the monofunctional porous material. The grafting rates were lower under conventional heating: 1.6 $\mu\text{mol}/\text{m}^2$ for the monofunctional version on porous material and 1.9 $\mu\text{mol}/\text{m}^2$ on the superficially porous material. A further discussion about the coverage density is provided in Supplementary information.

The results were consistent with the thermogravimetric data as the weight loss observed between 200 and 600°C was associated with the loss of the organic groups attached to the surface. In addition, the bonding of the ligand was confirmed by infrared spectroscopy with the appearance of the vibrational bands of the ligand groups. Additionally, solid-state NMR differentiated the mono- and trifunctional structure by unambiguous identification of specific chemical shifts as presented in Table 2. Discussions about the experimental results, as well as the thermogravimetric curves (Figure S1), and the IR (Figure S2) and NMR spectra (Figure S3) are available in Supplementary information.

Column	Silica type	δQ_3 (ppm)	δQ_4 (ppm)	δM (ppm)	δT_2 (ppm)	δT_3 (ppm)
*mono-PEG-anthra	SPP	-101.9	-110.4	11.5	-	-
*mono-PEG-anthra (1)	FPP	-102.1	-110.6	11.7-6.5	-	-
**mono-PEG-anthra (2)	FPP	-102.2	-110.7	11.8	-	-
**tri-PEG-anthra	FPP	-102.6	-111.0	11.4	-59.0	-66.0

Table 2: ²⁹Si NMR signal attribution for the mono- and trifunctional stationary phases

3.2 RPLC studies- Homologous series of alkylbenzenes and PAHs

Regarding the chemical structure of the homemade stationary phases, multiple types of interaction (dipole-dipole, hydrogen-bond, π - π and hydrophobic interactions) have to be considered, which can expand the applicability.

Considering previous works[11,14–16,31,50–54] on the characterization of aromatic bonded phases, the probes selected for this study were a homologous series of alkylbenzenes ($1 \leq n_c \leq 12$), a mixture of

linear PAHs naphthalene, anthracene and naphthacene ; and with the nonlinear PAH triphenylene added and the aromatics isomers *o*-, *m*- and *p*-terphenyl. The retention and selectivity factors are reported in Table S1. In addition, a deep discussion about energetic aspects relative to the functionality and the selectivity towards the probes is provided in Supporting Information and in Table S2.

The following discussion is based on the values recorded using acetonitrile as the organic modifier, but the same conclusions can be drawn from those obtained with methanol as the organic modifier, with an enhancement of the trends. Another feature of interest is that in terms of thermodynamics, there was no influence of the silica material type (SPP and FPP).

The plots of $\log k$ versus $\log P_{o/w}$ for HALO™ C18, HALO™ RP-amide, HALO™ Phenylhexyl, *mono-PEG-anthra (FPP) and **tri-PEG-anthra (FPP) are presented in Figure S4. The HALO™ C18 and HALO™ RP-amide stationary phases did not present particular selectivity towards PAHs compared to alkylbenzenes (Figure S4a and b), and there was no significant difference between the plots of $\log k$ versus $\log P_{o/w}$ for PAHs and alkylbenzenes.

The same trend was found regardless of the organic modifier (ACN or MeOH). The slopes (Table 3) were in the range of 0.209-0.268 for methanol as the organic modifier and 0.235-0.286 for acetonitrile as the organic modifier. HALO™ Phenylhexyl (Figure S4c) presented the same selectivity for the two classes of solutes (similar slope), the latter being largely affected by the organic modifier type because the plots of $\log k$ versus $\log P_{o/w}$ were not superimposable (0.342 and 0.351 for the alkylbenzenes and PAHs, respectively, with methanol; 0.242 and 0.233 for the alkylbenzenes and PAHs, respectively, in acetonitrile). Conversely, our stationary phases (*mono- and **tri-PEG-anthra (FPP)) showed higher selectivity for the PAH structures. For PAHs in acetonitrile, the slope of the plots of $\log k$ versus $\log P_{o/w}$ was higher (0.176) than for alkylbenzenes (0.131), especially when using an organic modifier without π -electrons, such as methanol (0.171 and 0.284 for alkylbenzenes and PAHs, respectively) (Figure S4d and e).

When using a π -selective stationary phase to separate the aromatic solutes, solvents that contain π -electrons, such as acetonitrile, may have a detrimental effect on the separation. These solvents interfere with the π - π interactions and decrease or potentially cancel the stationary phase aromatic selectivity [10,13,16,55,56]. The use of methanol may prevent the π - π interaction competition between the stationary phase and the solvent, favoring the establishment of π - π interactions between the stationary phase and the solutes. Tri-PEG-anthra presented the highest selectivity of 0.135 and 0.253 for alkylbenzenes and PAHs, respectively, in acetonitrile. The latter trend was enhanced when using methanol: 0.179 and 0.399 for the alkylbenzenes and PAHs, respectively.

Stationary phase	MeOH		ACN		MeOH	ACN
	Slope (alkylbenzenes)	Slope (PAHs)	Slope (alkylbenzenes)	Slope (PAHs)	Δ slope (PAHs-alkylbenzenes)	Δ slope (PAHs-alkylbenzenes)
HALO™ C18	0.258	0.268	0.286	0.243	0.010	0.042
r ²	0.997	0.982	0.997	0.987		
HALO™ RP-amide	0.209	0.250	0.240	0.235	0.041	0.005
r ²	0.996	0.981	0.996	0.987		
HALO™ Phenylhexyl	0.342	0.351	0.242	0.233	0.009	0.009
r ²	0.995	0.994	0.997	0.992		
*Mono-PEG-anthra (1)	0.171	0.284	0.131	0.176	0.114	0.045
r ²	0.998	0.993	0.997	0.988		
**Tri-PEG-anthra	0.179	0.399	0.135	0.253	0.220	0.119
r ²	0.997	0.991	0.996	0.984		

Table 3: Slopes of the plots of log k and log P_{o/w} for alkylbenzenes (from benzene to dodecylbenzene) and PAHs (from benzene to naphthacene).

The hydrophobic selectivity, $\alpha_{\text{pentylbenzene/butylbenzene}}$, is the selectivity between pentylbenzene and butylbenzene; it reflects the ability of the phase to separate compounds that differ by only a single methylene group. For our stationary phases containing a short spacer alkyl chain (butyl), it was not surprising to obtain low $\alpha_{\text{pentylbenzene/butylbenzene}}$ values. Nevertheless, they presented similar hydrophobic selectivities of approximately 1.20, regardless of the functionality (mono or tri) and the silica type (SPP or FPP).

The aromatic selectivity describes the capacity of a stationary phase to undergo aromatic interactions with aromatic solutes. Lindner *et al.*[14,51] and Euerby *et al.*[52] suggested an evaluation of the selectivity factor between *n*-pentylbenzene and *o*-terphenyl. As shown in Table S1, $\alpha_{\text{pentylbenzene}/o\text{-terphenyl}} > 1$ for “C18-type stationary phases” (HALO™ C18 and HALO™ RP-amide), meaning that *o*-terphenyl is eluted before *n*-pentylbenzene. In contrast, for stationary phases containing aromatic groups (PH, mono-PEG-anthra and tri-PEG-anthra), *o*-terphenyl, which has a higher number of aromatic rings than pentylbenzene, is more retained, so $\alpha_{\text{pentylbenzene}/o\text{-terphenyl}} < 1$. Moreover, this parameter depends on

the functionality of the stationary phase: $\alpha_{\text{pentylbenzene}/o\text{-terphenyl}} = 0.86$ for mono-PEG-anthra and $\alpha_{\text{pentylbenzene}/o\text{-terphenyl}} = 0.67$ for tri-PEG-anthra.

This is an interesting feature, which may be explained by the cumulative effect of the tri-aromatic units. DFT showed that the more stable conformation between the ligand and the solutes was the T-shape conformation (see below). The higher is the number of aromatic units in the solute structure, the stronger are the interactions with the tri-aromatic units of the ligand.

To evaluate the planarity recognition ability of the stationary phases, we selected the molecules proposed by Tanaka *et al.*[11] and Jinno *et al.*[57], who introduced *o*-terphenyl and triphenylene as probes. The selectivity of triphenylene and *o*-terphenyl is influenced by the spacer length and the functionality of the ligand. Both probes have comparable size (length-to-width ratio) and the same number of carbons and π -electrons but differ in the molecular planarity of their structures. Triphenylene is planar, whereas *o*-terphenyl is twisted out-of-plane, so their separation factor is a good indicator of the selectivity for molecular-planarity[31].

Stationary phases with $\alpha_{\text{triphenylene}/o\text{-terphenyl}} > 3$ have enhanced shape selectivity, whereas stationary phases with $\alpha_{\text{triphenylene}/o\text{-terphenyl}} < 2$ have low shape recognition ability[53]. Although the two compositions of mobile phases used to compare the stationary phases are different: 90/10 MeOH/water (% *v/v*) for both HALO™ C18 and HALO™ RP-amide and 70/30 (% *v/v*) for all five aromatic phases, the following conclusions can be drawn. Considering that the retention of triphenylene is the same on HALO™ RP-amide and mono-PEG-anthra (SPP), it could be observed that, in these isoelutropic conditions, the selectivity for molecular planarity is slightly higher on mono-PEG-anthra (SPP) than on HALO™ RP-amide (2.35 instead of 2.0). The molecular planarity selectivity values for mono-PEG-anthra (SPP) and tri-PEG-anthra (FPP) under the same mobile phase composition conditions shows that it is greatly enhanced on the tri-PEG-anthra stationary phase (3.16 instead of 2.35), which may be explained by the greater rigidity of the tri-PEG-anthra (FPP) phase. With acetonitrile as the organic modifier, although the two compositions of mobile phases used to compare stationary phases are different, the retentions of triphenylene are similar on HALO™ RP-amide and mono-PEG-anthra (SPP). The molecular planarity selectivity is higher on HALO™ RP-amide than on mono-PEG-anthra (SPP) (1.72 compared to 1.4). Comparison of the molecular planarity selectivity values for mono-PEG-anthra (SPP) and tri-PEG-anthra (FPP) obtained under the same mobile phase composition conditions indicates that it is enhanced on the tri-PEG-anthra stationary phase (1.85 compared to 1.40). The final effect is much less important than when using methanol as the organic modifier due to competing π - π interactions between aromatic solutes, acetonitrile and the aromatic stationary phase[10,13,16,55,56]. The difference in mobility of the graft in acetonitrile with respect to methanol should also be taken into account.

3.3 Theoretical modeling

Because the use of quantum chemistry calculations is rare in the chromatography community and because this paper is also intended for a wide audience in analytical chemistry, we believe it is

informative to provide a brief review of their use to cast light on the physicochemical features that may drive the separation process. From a methodological aspect, a theoretical study can be divided into three successive steps: the selection of the computational protocol, the computation itself, and subsequent data processing. Details are provided in the Supplementary information and allow, through a comparative literature survey, for understanding the upgrade of the proposed protocol.

Based on these points, our specifications are the following: a quantum description of the trifunctional phase and of its interactions with aromatic molecules, which includes solvent effects and which describes π -stacking in a reliable way. To this aim, we consider the gas phase, implicit solvent [through the polarizable continuum model (PCM)], and hybrid implicit-explicit [explicit microsolvation consisting of two solvent molecules immersed in PCM that can form hydrogen bonds with the phase, perturbing the internal H-bonds network] calculations on a system including a silica surface ($\text{Si}_3\text{O}_7\text{H}_5$ moiety) that will be allowed to relax during the geometric optimization performed with a modern exchange-correlation functional. However, the fact that the silica bulk could restrain some of these moves will not be considered.

As this paper is not purely theoretical, we have chosen to restrain our discussion to the sole energetic features. Other quantities, such as structural and advanced electronic properties and vibrational data (although infrared spectra could for instance be generated by our approach), will be scrutinized in a forthcoming theoretical paper. However, some important concepts must be clarified. When dealing with the interaction between molecules M_1 and M_2 , different energies can be evaluated: the first is the DFT “*binding energy*” defined by Eq 1:

$$E_{M_1\dots M_2}^{bind} = E^{DFT}(M_1\dots M_2) - E_{M_1}^{DFT}(M_1) - E_{M_2}^{DFT}(M_2), \quad \text{Eq 1}$$

where the DFT energies of molecules M_1 and M_2 are evaluated at the geometries that M_1 and M_2 adopt in the optimized $M_1\dots M_2$ complex. When these two energies are calculated on the optimized free A and B molecules, one evaluates the “*complexation energy*” in Eq 2 (the fragments might never adopt an arrangement close to their most stable conformation during the separation process, making in some cases this reference state irrelevant):

$$E_{M_1\dots M_2}^{compl} = E^{DFT}(M_1\dots M_2) - E_{M_1}^{DFT}(M_1) - E_{M_2}^{DFT}(M_2). \quad \text{Eq 2}$$

The difference between $E_{M_1\dots M_2}^{bind}$ and $E_{M_1\dots M_2}^{compl}$ is the “*deformation energy*” of M_1 and M_2 , $E_{M_1\dots M_2}^{deform}$, that is required to form the stable complex. Adding the vibrational zero-point energy (ZPE) to Eq 3 provides the “*complexation Gibbs energy at 0 K*”:

$$\Delta G_{M_1\dots M_2}^{compl\ 0K} = E^{DFT+ZPE}(M_1\dots M_2) - E_{M_1}^{DFT+ZPE}(M_1) - E_{M_2}^{DFT+ZPE}(M_2). \quad \text{Eq 3}$$

Using standard formulas from statistical thermodynamics, one can evaluate the temperature and entropy contributions at 298.15 K under atmospheric pressure (standard conditions), affording the “*standard Gibbs complexation energy*” in Eq 4:

$$\Delta G_{M_1\dots M_2}^{\circ\ compl} = G_{M_1\dots M_2}^{\circ}(M_1\dots M_2) - G_{M_1}^{\circ}(M_1) - G_{M_2}^{\circ}(M_2). \quad \text{Eq 4}$$

We define the “*thermal contribution to complexation*”, $\Delta G_{M_1 \dots M_2}^{therm}$, as the difference between $\Delta G_{M_1 \dots M_2}^{comp}$ and $\Delta G_{M_1 \dots M_2}^{comp/0K}$. It is an important quantity since temperature can have a significant impact on selectivity. Because our thermodynamic corrections are based on the quantum harmonic oscillator model, our static approach cannot define “*binding Gibbs energies*”. However, the binding energy in Eq 1 can be further explored, as it can be exactly split into two physical counterparts (Eq 5) within the interaction quantum atoms (IQA) framework[58–60]:

$$E_{M_1 \dots M_2}^{bind} = \underbrace{\sum_{atoms A \in M_1} \sum_{atoms B \in M_2} E_{AB}^{int}}_{E_{M_1 \dots M_2}^{int}} + \Delta E_{intra}. \quad \text{Eq 5}$$

The first right-hand side term corresponds to the sum of the interaction energy between each atom in M_1 with each atom in M_2 , while the second describes the energy reorganization inside each fragment (e.g., the energetic (de)stabilization of each atom within the fragment—a contribution that cannot be described by usual force fields—and the variation of the bond strengths inside each moiety upon complex formation; see refs[61] and[62] for a detailed discussion). These interactions are mainly noncovalent, so they can be divided into (“classical”) electrostatic, $E_{M_1 \dots M_2}^{elec}$, and “*dispersion contribution*”, $E_{M_1 \dots M_2}^{disp}$. At the smallest approximation order, $E_{M_1 \dots M_2}^{elec}$ is given by the “*point-charge contribution*”, while $E_{M_1 \dots M_2}^{disp}$ can be evaluated from Grimme’s D2 pair-potential scheme, according to the following equations (Eq 6) (in atomic units):

$$\left\{ \begin{array}{l} E_{M_1 \dots M_2}^{pc} = \sum_{A \in M_1} \sum_{B \in M_2} \frac{q_A q_B}{R_{AB}} \\ E_{M_1 \dots M_2}^{disp} \approx - \sum_{A \in M_1} \sum_{B \in M_2} f_{AB} \frac{C_6^A C_6^B}{R_{AB}^6} \end{array} \right. \quad \text{Eq 6}$$

Henceforth, the interaction process between two moieties will be described by six “imbricated” energetic descriptors: $E_{M_1 \dots M_2}^{pc}$, $E_{M_1 \dots M_2}^{disp}$, $E_{M_1 \dots M_2}^{bind}$, $E_{M_1 \dots M_2}^{deform}$, $\Delta G_{M_1 \dots M_2}^{therm}$, $\Delta G_{M_1 \dots M_2}^{comp}$, which will be computed for three environment models (gas phase, PCM, hybrid). Both their magnitude (which enables us to determine the interaction nature) and their variation within a given compound family are of interest and are potentially not equivalent. For instance, one of these energy components could be of high magnitude but relatively constant in the dataset, so that it will account for coordination but not for discrimination. Conversely, if one small quantity varies significantly from one compound to the other, it will provide less insight into the *interaction nature* but may be valuable to explain *selectivity*. In this paper, we attempt to find the energy components that correlate the most to the experimental $\log(k)$ values.

Figure 1 shows the largest systems under consideration (174 atoms), where one can identify two explicit methanol molecules (a) and two acetonitrile ones (b) in their optimized geometries.

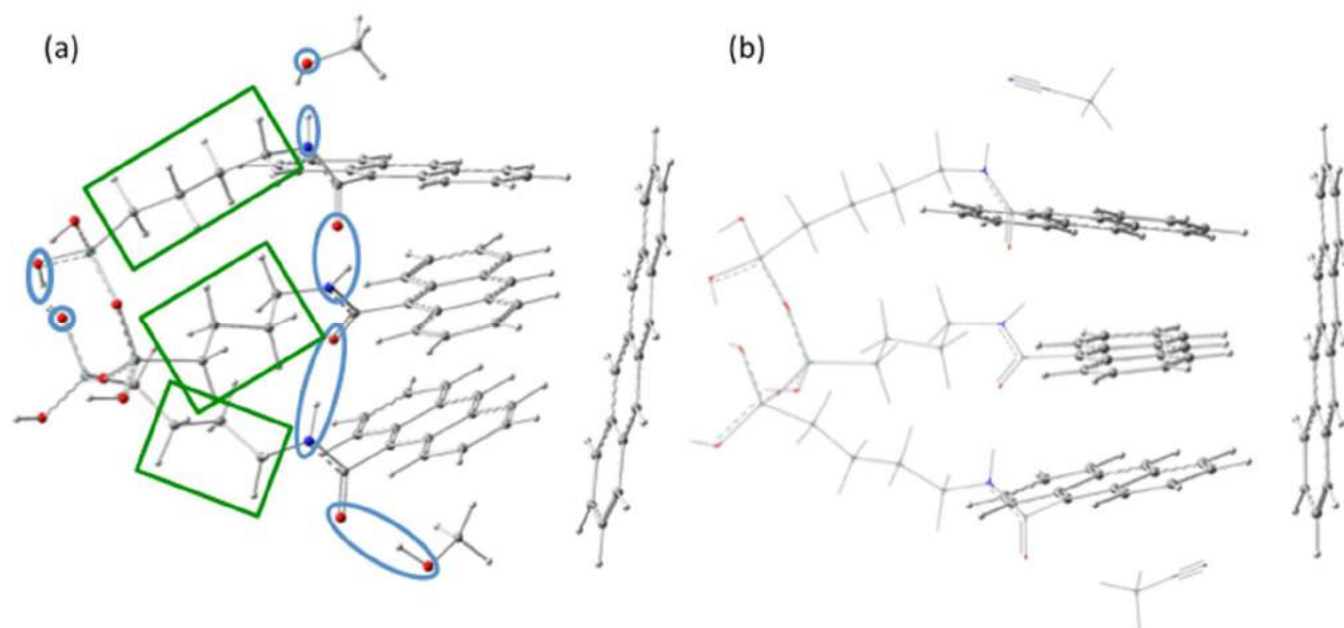


Figure 1: (a). View of the optimized structure for the interaction between naphthacene and the trifunctional stationary phase with two explicit methanol molecules immersed in a methanol implicit continuum. Atoms circled in blue are described by the 6-311++G(d,p) basis set, those in green by STO-3G, and the remaining by 6-31G(d). (b). View of the optimized structure for the interaction between naphthacene and the trifunctional phase with two explicit acetonitrile molecules immersed in an acetonitrile implicit continuum. Atoms shown as balls and sticks are treated at the MP2 level (high-level layer), while atoms in the wireframe format are described by DFT (low-level layer). Color code: H in white, C in grey, N in blue, O in red, and Si in turquoise.

We first focus on the benzene interaction with the stationary phase. Table 4 shows the values for the energy components presented above.

Entry	Phase	Solvent	$E_{M_1 \dots M_2}^{pc}$	$E_{M_1 \dots M_2}^{disp}$	$E_{M_1 \dots M_2}^{bind}$	$E_{M_1 \dots M_2}^{deform}$	$\Delta G_{M_1 \dots M_2}^{therm}$	$\Delta G_{M_1 \dots M_2}^{comp}$
1	tri-PEG-anthra	None	-0.50	-14.39	-8.15	0.24	5.18	-1.73
2	tri-PEG-anthra	PCM MeOH	-0.43	-14.70	-8.03	0.28	5.73	-1.16
3	tri-PEG-anthra	PCM ACN	-0.43	-14.70	-8.03	0.28	5.75	-1.14
4	tri-PEG-anthra	PCM MeOH + 2 MeOH	0.50	-14.88	-8.01	0.28	5.34	-1.33
5	tri-PEG-anthra	PCM ACN + 2 ACN	-0.59	-15.00	-8.14	0.32	5.25	-1.34

Table 4: Energy decomposition for the interaction between the selected functional phases and the benzene molecules at the B97-D DFT level of theory with various solvent models. All values in kcal/mol.

The comparison of entries 1 and 2 in Table 4 shows that the gas phase and solvent models produce significantly different results (particularly for $\Delta G_{M_1 \dots M_2}^{therm}$ and $\Delta G_{M_1 \dots M_2}^{comp}$). However, as shown by entries 2 and 3, the implicit solvent calculations could not differentiate methanol from acetonitrile because the energies were almost identical. This is not surprising since the two solvents have very similar PCM parameters ($\epsilon_r = 35.7$ for CH_3CN and 32.6 for CH_3OH) and since the C_6 coefficients in Eq 6 are solvent-independent. Accordingly, the difference in the absolute SCF energy of the optimized trifunctional phase in the two PCM solvents was 0.1 kcal/mol, which explains why the relative energies are almost the same. Therefore, explicit solvent molecules should be considered and are expected to produce slightly different results since the H...O hydrogen bonds in methanol and the H...N hydrogen bonds in acetonitrile were present. This was corroborated by entries 4 and 5, although the differences remained small.

As expected, the highest energy contribution stems from dispersion (approximately -15.0 kcal/mol). Let us recall that there are several van der Waals geometries for adducts built on aromatic cycles. For instance, for the benzene dimer[63], the two main categories are parallel (the most stable being called “displaced”, where the two cycles are not exactly on top of each other) and T-shaped[64]. As shown in the top of Figure 2, benzene interacts in a T-shaped fashion with the trifunctional phase. This can be explained by the fact that the intramolecular hydrogen bonds inside the stationary phase preclude the intercalation of benzene between two anthracyl groups. This does not occur for the monofunctional phase (which is saturated with hydroxyl groups). As depicted in the lower part of Figure 2b, benzene “slipped” but was not fully parallel to the anthracyl group because one methanol solvent molecule hindered the corresponding face.

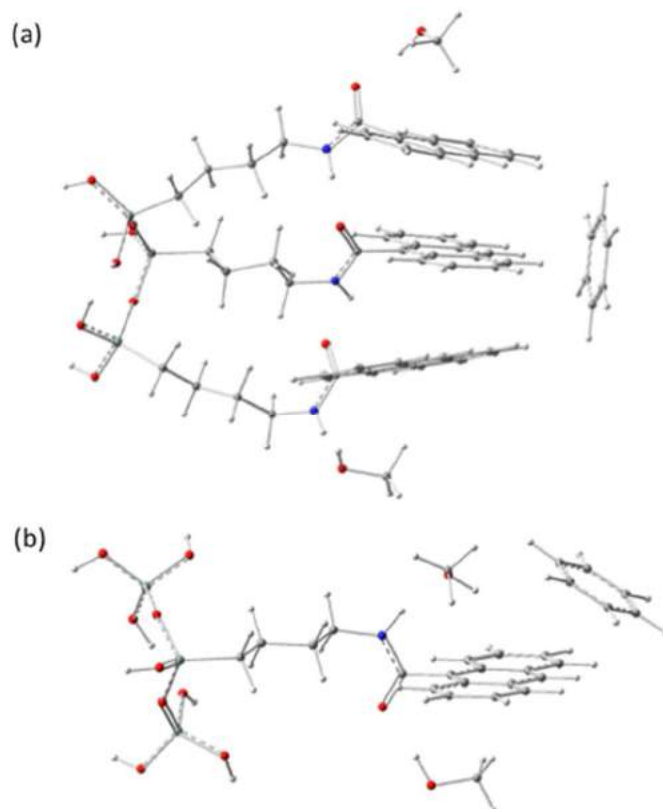


Figure 2: (a). View of the optimized structure of the interaction between benzene and the trifunctional stationary phase with two explicit methanol molecules immersed in a methanol implicit continuum. (b). View of the optimized structure for the interaction between benzene and the monofunctional phase with two explicit methanol molecules immersed in a methanol implicit continuum. Color code: H in white, C in grey, N in blue, O in red, and Si in turquoise.

Having established the required level of theory, we focus on the C_6H_5-R alkylbenzene series with $R=H, CH_3, C_2H_5, C_3H_7,$ and C_4H_9 ; the results are presented in Table 5. The modeling is not realistic for longer alkyl chains because the C_6H_5-R molecule would be larger than the phase width, meaning that it could significantly interact with another trifunctional moiety. This effect can be modeled using a periodic approach that assumes homogeneous grafting (with high coverage) on the silica surface, an assumption that is arguable from the experimental point of view. On the other hand, the explicit quantum treatment of a second trifunctional fragment is precluded by the associated computational cost. We will consider polycyclic aromatic molecules, such as naphthalene, anthracene, and naphthacene. The results are presented in Table 5.

System	Solvent	$E_{M_1...M_2}^{pc}$	$E_{M_1...M_2}^{disp}$	$E_{M_1...M_2}^{bind}$	$E_{M_1...M_2}^{deform}$	$\Delta G_{M_1...M_2}^{therm}$	$\Delta G_{M_1...M_2}^{compl}$	Log(k)
C_6H_5-R (alkylbenzenes)								
R= CH_3	PCM CH_3OH + 2 CH_3OH	-0.58	-16.56	-8.69	0.37	6.34	-0.66	-0.15
R= C_2H_5	PCM CH_3OH + 2 CH_3OH	-0.72	-16.93	-8.70	0.34	5.77	-1.48	-0.07
R= C_3H_7	PCM CH_3OH + 2 CH_3OH	-0.76	-17.14	-8.60	0.31	3.34	-4.01	0.03
R= C_4H_9	PCM CH_3OH + 2 CH_3OH	-0.66	-17.19	-8.38	0.28	3.47	-3.80	0.13
R= CH_3	PCM CH_3CN + 2 CH_3CN	-1.23	-16.26	-9.10	0.60	6.24	-1.16	0.06
R= C_2H_5	PCM CH_3CN + 2 CH_3CN	-1.36	-17.33	-9.23	0.50	4.37	-3.59	0.13
R= C_3H_7	PCM CH_3CN + 2 CH_3CN	-1.46	-17.88	-9.55	0.70	5.75	-2.19	0.21
R= C_4H_9	PCM CH_3CN + 2 CH_3CN	-1.52	-17.92	-9.37	0.69	6.29	-1.39	0.29
Polycyclic (PAHs)								
Naphthalene	PCM CH_3OH + 2 CH_3OH	-0.55	-18.81	-9.52	0.31	5.76	-2.34	0.15
Anthracene	PCM CH_3OH + 2 CH_3OH	-0.75	-20.62	-10.31	0.60	5.66	-2.92	0.62
Naphthacene	PCM CH_3OH + 2 CH_3OH	-0.58	-26.47	-12.54	2.01	4.73	-5.08	1.14
Naphthalene	PCM CH_3CN + 2 CH_3CN	-1.09	-17.20	-8.98	0.53	5.12	-2.42	0.23

Anthracene	PCM CH ₃ CN + 2 CH ₃ CN	-1.57	-22.06	-11.49	0.80	6.12	-4.36	0.52
Naphthacene	PCM CH ₃ CN + 2 CH ₃ CN	-1.68	-25.60	-12.37	0.91	6.21	-4.12	0.89

Table 5: Energy decomposition for the interaction between the trifunctional phase and C₆H₅-R and polycyclic aromatic molecules at the B97-D DFT level of theory. All values in kcal/mol

We found that the electrostatic point-charge contribution was always stabilizing (all values are negative) but very low in absolute value in all cases, less than 0.8 kcal/mol for methanol and less than 1.6 kcal/mol for acetonitrile (with roughly $E_{M_1...M_2}^{pc, CH_3CN} \approx 2 E_{M_1...M_2}^{pc, CH_3OH}$). The variation was not monotonic with respect

to the alkyl chain length in the first case. As a consequence, $E_{M_1...M_2}^{bind}$, $\Delta G_{M_1...M_2}^{therm}$, and $\Delta G_{M_1...M_2}^{comp}$ were not monotonic in methanol, in contrast to the increasing $\log(k)$ values. Moreover, the deformation energy was almost constant and negligible (less than 0.4 kcal/mol), so only the dispersion contribution (always increasing due to the cumulative effect of the C₆-pair potentials) followed the experimental trend for both solvents. The same conclusions (non-monotonic variations of several energy components, dispersion contribution of approximately -20 kcal/mol, binding energies of -10 kcal/mol) could be drawn for the polycyclic (naphthalene, anthracene, naphthacene) aromatic compounds. As expected, the increase of the dispersion contribution was enhanced with respect to the alkylbenzene cases since 6-membered rings have stronger van der Waals interactions than alkyl chains.

One can now consider whether this semi-quantitative analysis can be used for prediction. We considered all the 16 $\log(k)$ values reported in Table S1 a,b: 8 values in methanol solvent (the trifunctional phase interacting with benzene, methylbenzene, ethylbenzene, propylbenzene, butylbenzene, naphthalene, anthracene and naphthacene) and the corresponding 8 values with acetonitrile as the organic modifier. Linear regression between these values and the 6 energy components was investigated, providing the following coefficient of determination (R^2) values: 0.18 ($E_{M_1...M_2}^{pc}$), 0.91 ($E_{M_1...M_2}^{disp}$), 0.89 ($E_{M_1...M_2}^{bind}$), 0.73 ($E_{M_1...M_2}^{deform}$), 0.01 ($\Delta G_{M_1...M_2}^{therm}$), 0.52 and ($\Delta G_{M_1...M_2}^{comp}$). The fact that dispersion showed the highest correlation follows from our previous statements.

One may wonder whether better models can be built using more degrees of freedom. To this aim, we investigated bilinear regressions using $E_{M_1...M_2}^{disp}$ and one of the other components. The highest R^2 value (0.93) was obtained with $E_{M_1...M_2}^{deform}$. Similarly, the best bilinear regression with $E_{M_1...M_2}^{bind}$ involved $\Delta G_{M_1...M_2}^{therm}$, with $R^2 = 0.92$. We also considered nonlinear fitting (polynomial, logarithmic, exponential) based on $E_{M_1...M_2}^{disp}$, but no significant improvement was obtained with only a few parameters. Therefore, we decided to use the best monoliner regression (with the energy in kcal/mol):

$$\log(k) = -1.73 - 0.11 E_{M_1...M_2}^{disp}, \quad \text{Eq 7}$$

which is represented in Figure 3a.

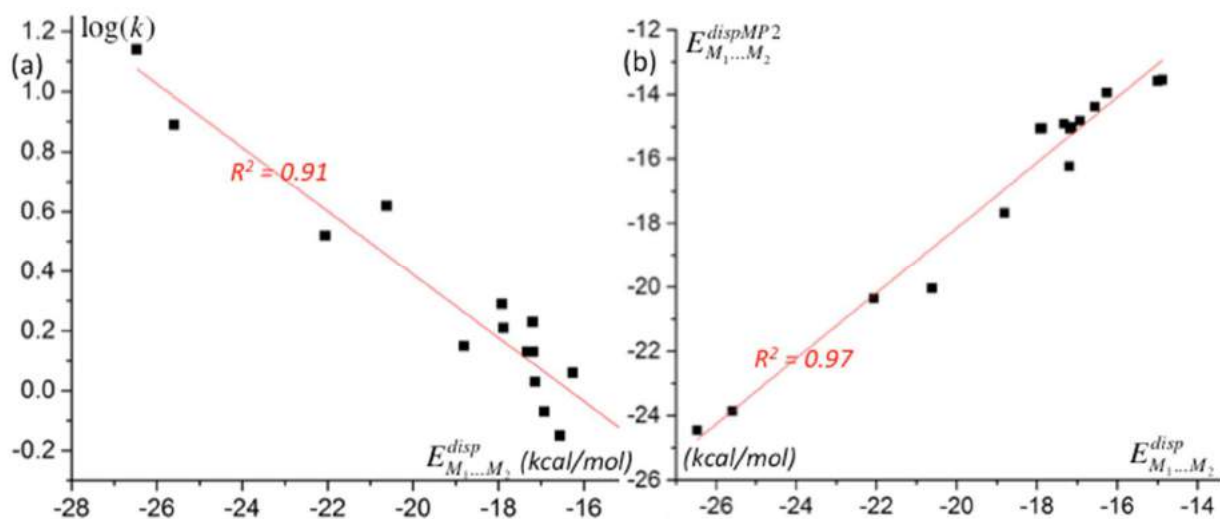


Figure 3: (a). Experimental $\log(k)$ values with respect to the theoretical $E_{M_1 \dots M_2}^{disp}$ values (in kcal/mol).

(b). $E_{M_1 \dots M_2}^{dispMP2}$ values with respect to $E_{M_1 \dots M_2}^{disp}$ (in kcal/mol). The linear regression lines are shown in red.

Thus, as $E_{M_1 \dots M_2}^{disp}$ appeared to be the key to predicting the experimental results, we performed unprecedented post-Hartree-Fock calculations in a QM/QM' fashion (see computational details) to assess the quality of our simple pair-potential model by comparing it to an ab initio approach based on the quantum wave function and not on empirical correction, providing $E_{M_1 \dots M_2}^{dispMP2}$ reference values. We

found a strong linear correlation ($R^2 = 0.97$) between $E_{M_1 \dots M_2}^{disp}$ and $E_{M_1 \dots M_2}^{dispMP2}$ (see Figure 3b). This benchmark validated the chosen Grimme-type simple approach to the dispersion interaction energy contribution. It also proved that no significant improvement could be expected from higher (and much more time-consuming) levels of theory. In a way, the performance of our quite simple model is actually quite surprising. It was based on an optimized static structure. However, the retention time is intrinsically a dynamic (kinetic) parameter. The fact that it can be approached quite successfully by static DFT calculations was not a priori obvious.

Two other remarks about this model are in order. The first is that it does not involve temperature dependence. This means that new regression parameters should be determined if $\log(k)$ is measured at a different temperature. The second is related to the solvent issue. While the differences between

methanol and acetonitrile in the $E_{M_1 \dots M_2}^{disp}$ values remained small within the alkylbenzene family, a significant difference was observed for the largest system: -26.47 kcal/mol for methanol compare to -25.60 kcal/mol for acetonitrile, which could explain why the retention was more intense in the first case.

Furthermore, the $E_{M_1 \dots M_2}^{disp}$ gap between anthracene and naphthalene was larger in methanol (-5.9 kcal/mol) than in acetonitrile (-3.54 kcal/mol), which is another clue to understand the enhanced selectivity for PAHs. However, one should remain cautious with such a simple analysis since it is not fully valid for the smallest molecules, for which the solvent effects are too subtle to be rationalized by such a simple model.

Finally, it is sometimes useful to have a graphical representation of the involved interactions. In the case of van der Waals complexes, this can be achieved using the popular noncovalent index (NCI)[65,66], as represented in Figure 4a. The green layers are characteristic of dispersion interactions and were found to be present inside the stationary phase between the anthracyl groups and in the interaction region between the mobile and the stationary phases, revealing the clear T-shape fashion. This figure also shows that the naphthacene moiety is slightly corrugated, accounting for the non-negligible deformation energy observed in this case. This energy loss is then compensated by a higher absolute dispersion interaction contribution.

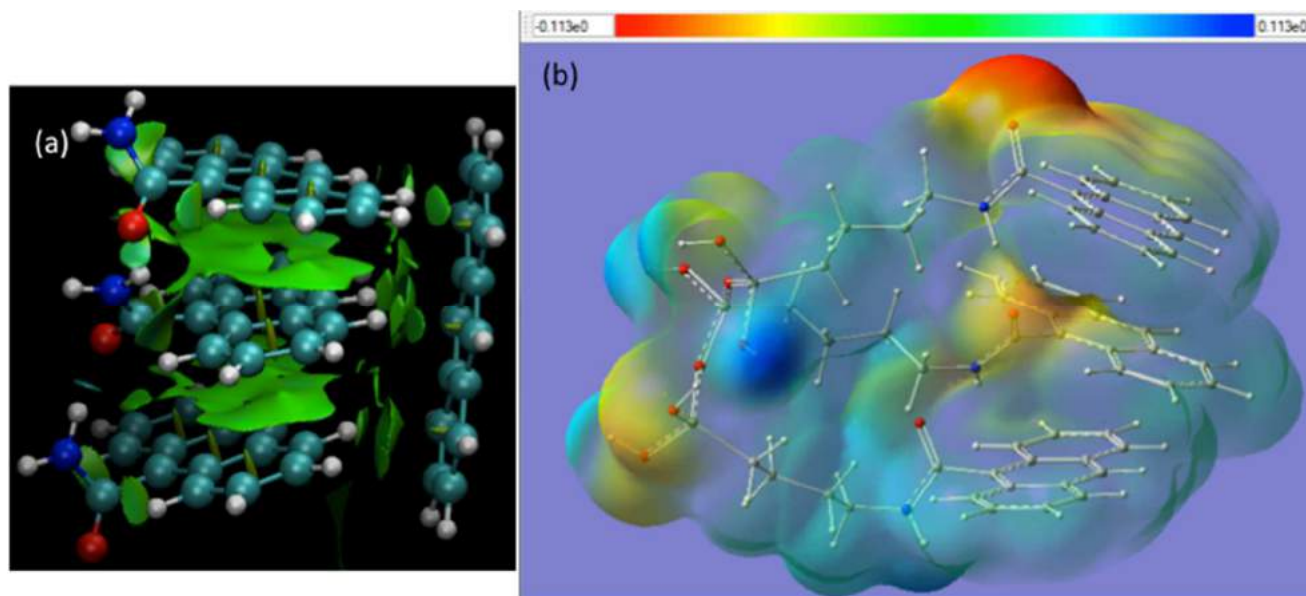


Figure 4: (a). NCI plot: selected reduced density gradient isosurface ($s=0.5$ a.u.) showing noncovalent interactions. (b). View of the molecular electrostatic potential mapped on the 0.001 isodensity surfaces. Atomic units and a color code (red: negative, blue: positive values) are used.

If interested in charged analytes, it would be more relevant to analyze the molecular electrostatic potential. Because it is linked to the local polarity of the molecule, it has already been used to locate the lipophilic/lipophobic or hydrophilic/hydrophobic regions. For the trifunctional phase, it is represented in Figure 4b, which shows that it is anisotropic. Let us recall that zones with negative (positive) values are prone to bind cationic (anionic) species. Interestingly, the two faces of the trifunctional phase are not equivalent: the right upper part is negative (blue-orange color), while the right bottom part is positive (green-blue color). From this viewpoint, this system exhibits an interesting “*Janus character*”.

4. Conclusion

The present paper describes the synthesis and the complete characterization of polar embedded aromatic stationary phases. Solid-state NMR differentiated the mono- and trifunctional structure by unambiguous identification of specific chemical shifts. A modern functional/basis set combination was used to accurately describe the structure of the trifunctional phase. The overall structure (silanol and alkyl chain and PEG and aromatic units) was considered using the ONIOM formalism and by rigorously selecting the layers. With the structure elucidated, the impact of structural modifications inside the stationary phase skeleton on the separation behavior was investigated through a parallel evaluation of the

experimental data, such as the retention (k) and separation factors (α) for PAHs and alkylbenzenes. For the first time, the experimental data coupled with the DFT results indicated that the new polar embedded aromatic stationary phases presented a particular ability to recognize aromatic solutes.

Additionally, the solvent effect was taken into account. Because of the similar constant permittivity of acetonitrile and methanol, the PCM approach could not explain the better selectivity for PAH homologues than alkylbenzenes and the enhancement of this trend when using methanol instead of acetonitrile as the organic modifier. The latter was partly solved for the largest molecules by an explicit solvation model for acetonitrile and methanol.

From a chromatographic point of view, the combination of aromatic and polar embedded groups (mono-PEG-anthra and tri-PEG-anthra) led to stationary phases with hydrophobic properties and aromatic selectivity that could be modulated by adjusting the organic modifier type. In contrast to the functionality of the ligand, which impacts the chromatographic behavior, the silica type has no influence on the thermodynamic properties.

The DFT results match the chromatographic results, providing a better understanding of the interaction mechanisms and highlighting the importance of the multimodal character of the designed stationary phases: alkyl spacers for interactions with hydrophobic solutes, amide embedded groups for dipole-dipole and hydrogen-bond interactions, and aromatic terminal groups for π - π interactions.

Acknowledgments

The authors would like to gratefully acknowledge the high-performance computing facility (CRIANN) funded by the Region Haute Normandie. We also thank Gwendal Petillon, Matthieu Genermont and Françoise Ringot for their assistance with the chromatographic measurements.

References

- [1] H. Qiu, X. Liang, M. Sun, S. Jiang, Development of silica-based stationary phases for high-performance liquid chromatography, *Anal. Bioanal. Chem.* 399 (2011) 3307–3322. doi:10.1007/s00216-010-4611-x.
- [2] J.J. Kirkland, Development of some stationary phases for reversed-phase HPLC, *J. Chromatogr. A.* 1060 (2004) 9–21. doi:10.1016/j.chroma.2004.10.057.
- [3] A.A. Kazarian, M.R. Taylor, P.R. Haddad, P.N. Nesterenko, B. Paull, Ion-exchange and hydrophobic interactions affecting selectivity for neutral and charged solutes on three structurally similar agglomerated ion-exchange and mixed-mode stationary phases, *Anal. Chim. Acta.* 803 (2013) 143–153. doi:10.1016/j.aca.2013.03.063.
- [4] C. Meyer, U. Skogsberg, N. Welsch, K. Albert, Nuclear magnetic resonance and high-performance liquid chromatographic evaluation of polymer-based stationary phases immobilized on silica, *Anal. Bioanal. Chem.* 382 (2004) 679–690. doi:10.1007/s00216-004-2752-5.
- [5] H. Ohta, Y. Saito, N. Nagae, J.J. Pesek, M.T. Matyska, K. Jinno, Fullerenes separation with monomeric type C30 stationary phase in high-performance liquid chromatography, *J. Chromatogr. A.* 883 (2000) 55–66. doi:10.1016/S0021-9673(00)00376-9.
- [6] S.A. Wise, L.C. Sander, W.E. May, Determination of polycyclic aromatic hydrocarbons by liquid chromatography, *J. Chromatogr. A.* 642 (1993) 329–349. doi:10.1016/0021-9673(93)80097-R.
- [7] S.A. Wise, L.C. Sander, R. Lapouyade, P. Garrigues, Anomalous behavior of selected methyl-substituted polycyclic aromatic hydrocarbons in reversed-phase liquid chromatography, *J. Chromatogr. A.* 514 (1990) 111–122. doi:10.1016/S0021-9673(01)89383-3.

- [8] C.A. Rimmer, L.C. Sander, S.A. Wise, Selectivity of long chain stationary phases in reversed phase liquid chromatography, *Anal. Bioanal. Chem.* 382 (2005) 698–707. doi:10.1007/s00216-004-2858-9.
- [9] L.C. Sander, K.E. Sharpless, N.E. Craft, S.A. Wise, Development of engineered stationary phases for the separation of carotenoid isomers, *Anal. Chem.* 66 (1994) 1667–1674.
- [10] A. Tchaplá, S. Héron, E. Lesellier, H. Colin, The Retention Process in Reversed-Phase Liquid Chromatography: General view of molecular interaction mechanisms in reversed-phase liquid chromatography, *J. Chromatogr. A.* 656 (1993) 81–112. doi:10.1016/0021-9673(93)80799-E.
- [11] N. Tanaka, Y. Tokuda, K. Iwaguchi, M. Araki, Effect of stationary phase structure on retention and selectivity in reversed-phase liquid chromatography, *J. Chromatogr. A.* 239 (1982) 761–772. doi:10.1016/S0021-9673(00)82036-1.
- [12] J.L.E. Reubsæet, R. Vieskar, Characterisation of π – π interactions which determine retention of aromatic compounds in reversed-phase liquid chromatography, *J. Chromatogr. A.* 841 (1999) 147–154. doi:10.1016/S0021-9673(99)00253-8.
- [13] D.H. Marchand, K. Croes, J.W. Dolan, L.R. Snyder, R.A. Henry, K.M.R. Kallury, S. Waite, P.W. Carr, Column selectivity in reversed-phase liquid chromatography: VIII. Phenylalkyl and fluoro-substituted columns, *J. Chromatogr. A.* 1062 (2005) 65–78. doi:10.1016/j.chroma.2004.11.014.
- [14] J. Horak, N.M. Maier, W. Lindner, Investigations on the chromatographic behavior of hybrid reversed-phase materials containing electron donor–acceptor systems: II. Contribution of π – π aromatic interactions, *J. Chromatogr. A.* 1045 (2004) 43–58. doi:10.1016/j.chroma.2004.05.096.
- [15] S. Héron, A. Tchaplá, Retention mechanism in reversed-phase liquid chromatography: specific effects of propiophenyl and multifunctional (cyanopropyl-octadecyl) bonded silicas, *J. Chromatogr. A.* 725 (1996) 205–218. doi:10.1016/0021-9673(95)00990-6.
- [16] S. Héron, A. Tchaplá, Validity of a notion of eluent force taking into account the nature of the graft on silica in aqueous and non-aqueous liquid chromatography, *Analisis.* 8 (1997) 257–262.
- [17] A. Tchaplá, D. Charbonneau, B. Chabot, C. Couplier, M. de Person, D. Desquaires, S. Héron, Corrélation de Cinq Tests Généraux Représentée par ACP et CAH pour la Caractérisation des Phases Stationnaires de CLHP, LCGC En Français. (2008) 25–30.
- [18] K. Kimata, K. Hosoya, H. Kuroki, N. Tanaka, J.R. Barr, P.C. McClure, D.G. Patterson, E. Jakobsson, A. Bergman, Selectivity of electron-donor- and electron-acceptor-bonded silica packing materials for hydrophobic environmental contaminants in polar and non-polar eluents, *J. Chromatogr. A.* 786 (1997) 237–248. doi:10.1016/S0021-9673(97)00597-9.
- [19] W. Wielandt, A. Ellwanger, K. Albert, E. Lindner, n-Alkyl fluorenyl phases in chromatography: I. Synthesis and characterization, *J. Chromatogr. A.* 805 (1998) 71–83. doi:10.1016/S0021-9673(98)00014-4.
- [20] R. Brindle, K. Albert, Stationary phases with chemically bonded fluorene ligands: A new approach for environmental analysis of π -electron containing solutes, *J. Chromatogr. A.* 757 (1997) 3–20. doi:10.1016/S0021-9673(96)00682-6.
- [21] M. Verzele, N.V. de Velde, Anthracene silica gel, a new polycyclic-aromatic-bonded stationary phase for HPLC, *Chromatographia.* 20 (1985) 239–241. doi:10.1007/BF02259695.
- [22] N. Tanaka, T. Tanigawa, K. Kimata, K. Hosoya, T. Arai, Selectivity of carbon packing materials in comparison with octadecylsilyl- and pyrenylethylsilylsilica gels in reversed-phase liquid chromatography, *J. Chromatogr. A.* 549 (1991) 29–41. doi:10.1016/S0021-9673(00)91416-X.
- [23] E. Grimvall, A. Colmsjö, K. Wrangskog, C. Östman, M. Eriksson, Quantitative Structure—Retention Relationships for Polychlorinated Biphenyls and Chlorobenzenes on Selected Normal-Phase Liquid Chromatographic Stationary Phases, *J. Chromatogr. Sci.* 35 (1997) 63–70. doi:10.1093/chromsci/35.2.63.
- [24] J.W. Grate, M.H. Abraham, C.M. Du, R.A. McGill, W.J. Shuely, Examination of Vapor Sorption by Fullerene, Fullerene-Coated Surface Acoustic Wave Sensors, Graphite, and Low-Polarity Polymers Using Linear Solvation Energy Relationships, *Langmuir.* 11 (1995) 2125–2130. doi:10.1021/la00006a046.
- [25] B. Kaur, *LC-GC Int.* 3 (n.d.) 41–48.
- [26] W. Nowik, M. Bonose-Crosnier de Bellaistre, A. Tchaplá, S. Héron, Separation of 9,10-anthraquinone derivatives: Evaluation of functionalised stationary phases in reversed phase mode, *J. Chromatogr. A.* 1218 (2011) 3636–3647. doi:10.1016/j.chroma.2011.04.012.

- [27] M. Zhang, J. Chen, A.K. Mallik, H. Qiu, S. Jiang, H. Ihara, Preparation and chromatographic evaluation of new branch-type diamide-embedded octadecyl stationary phase with enhanced shape selectivity, *Anal. Chim. Acta.* 833 (2014) 48–55. doi:10.1016/j.aca.2014.05.011.
- [28] Y. Li, L. Xu, T. Chen, X. Liu, Z. Xu, H. Zhang, Carbon nanoparticles from corn stalk soot and its novel application as stationary phase of hydrophilic interaction chromatography and per aqueous liquid chromatography, *Anal. Chim. Acta.* 726 (2012) 102–108. doi:10.1016/j.aca.2012.03.032.
- [29] N.S. Wilson, J. Gilroy, J.W. Dolan, L.R. Snyder, Column selectivity in reversed-phase liquid chromatography: VI. Columns with embedded or end-capping polar groups, *J. Chromatogr. A.* 1026 (2004) 91–100. doi:10.1016/j.chroma.2003.11.041.
- [30] X. Liu, A.V. Bordunov, C.A. Pohl, Preparation and evaluation of a hydrolytically stable amide-embedded stationary phase, *J. Chromatogr. A.* 1119 (2006) 128–134. doi:10.1016/j.chroma.2005.11.086.
- [31] M.M. Rahman, M. Takafuji, H.R. Ansarian, H. Ihara, Molecular Shape Selectivity through Multiple Carbonyl- π Interactions with Noncrystalline Solid Phase for RP-HPLC, *Anal. Chem.* 77 (2005) 6671–6681. doi:10.1021/ac050851v.
- [32] J.O. Omamogho, E.M. Stack, A. Santalad, S. Srijaranai, J.D. Glennon, H. Yamen, K. Albert, Retention and selectivity properties of carbamate pesticides on novel polar-embedded stationary phases, *Anal. Bioanal. Chem.* 397 (2010) 2513–2524. doi:10.1007/s00216-010-3816-3.
- [33] C.R. Silva, I.C.S.F. Jardim, C. Airoidi, New generation of sterically protected C 18 stationary phases containing embedded urea groups for use in high-performance liquid chromatography, *J. Chromatogr. A.* 987 (2003) 127–138.
- [34] M. Zhang, X. Liang, S. Jiang, H. Qiu, Preparation and applications of surface-confined ionic-liquid stationary phases for liquid chromatography, *TrAC Trends Anal. Chem.* 53 (2014) 60–72. doi:10.1016/j.trac.2013.09.011.
- [35] C. Stella, S. Rudaz, J.-L. Veuthey, A. Tchaplá, Silica and other materials as supports in liquid chromatography. Chromatographic tests and their importance for evaluating these supports. Part I, *Chromatographia.* 53 (2001) S113–S131. doi:10.1007/BF02490318.
- [36] C. Stella, S. Rudaz, J.-L. Veuthey, A. Tchaplá, Silica and other materials as supports in liquid chromatography. Chromatographic tests and their importance for evaluating these supports. Part II, *Chromatographia.* 53 (n.d.) S132–S140. doi:10.1007/BF02490319.
- [37] J.E. O’Gara, B.A. Alden, T.H. Walter, J.S. Petersen, C.L. Niederlaender, U.D. Neue, Simple preparation of a C8 HPLC stationary phase with an internal polar functional group, *Anal. Chem.* 67 (1995) 3809–3813.
- [38] U.D. Neue, J.E. O’Gara, A. Méndez, Selectivity in reversed-phase separations: Influence of the stationary phase, *J. Chromatogr. A.* 1127 (2006) 161–174. doi:10.1016/j.chroma.2006.06.006.
- [39] H. Engelhardt, R. Grüner, M. Scherer, The polar selectivities of non-polar reversed phases, *Chromatographia.* 53 (2001) S154–S161. doi:10.1007/BF02490322.
- [40] R.G. Parr, W. Yang, *Density-functional theory of atoms and molecules*, Oxford University Press, New York, 1989.
- [41] S. Ma, H.-W. Tsui, E. Spinelli, C.A. Busacca, E.I. Franses, N.-H.L. Wang, L. Wu, H. Lee, C. Senanayake, N. Yee, N. Gonella, K. Fandrick, N. Grinberg, Insights into chromatographic enantiomeric separation of allenes on cellulose carbamate stationary phase, *J. Chromatogr. A.* 1362 (2014) 119–128. doi:10.1016/j.chroma.2014.08.032.
- [42] H.-W. Tsui, E.I. Franses, N.-H.L. Wang, Effect of alcohol aggregation on the retention factors of chiral solutes with an amylose-based sorbent: Modeling and implications for the adsorption mechanism, *J. Chromatogr. A.* 1328 (2014) 52–65. doi:10.1016/j.chroma.2013.12.078.
- [43] P. Peluso, V. Mamane, E. Aubert, S. Cossu, Insights into the impact of shape and electronic properties on the enantioseparation of polyhalogenated 4,4'-bipyridines on polysaccharide-type selectors. Evidence of stereoselective halogen bonding interactions, *J. Chromatogr. A.* 1345 (2014) 182–192. doi:10.1016/j.chroma.2014.04.040.
- [44] P. Peluso, V. Mamane, E. Aubert, S. Cossu, High-performance liquid chromatography enantioseparation of atropisomeric 4,4'-bipyridines on polysaccharide-type chiral stationary phases: Impact of substituents and electronic properties, *J. Chromatogr. A.* 1251 (2012) 91–100. doi:10.1016/j.chroma.2012.06.035.

- [45] M. Szalaniec, A. Dudzik, M. Pawul, B. Kozik, Quantitative structure enantioselective retention relationship for high-performance liquid chromatography chiral separation of 1-phenylethanol derivatives, *J. Chromatogr. A.* 1216 (2009) 6224–6235. doi:10.1016/j.chroma.2009.07.002.
- [46] Y. Yamada, K. Ohyama, G. Onodera, M. Kuriyama, N. Kishikawa, N. Kuroda, Molecular-shape selectivity by naphthalimido-modified silica stationary phases: Insight into the substituents effect of naphthalene on shape recognition and π - π interactions via electrostatic potential, *J. Chromatogr. A.* 1425 (2015) 173–179. doi:10.1016/j.chroma.2015.11.030.
- [47] M. Mignot, A. Tchaplá, O. Mercier, N. Couvrat, S. Tisse, P. Cardinael, V. Peulon-Agasse, High-Density Octadecyl Chemically Bonded Core-Shell Silica Phases for HPLC: Comparison of Microwave-Assisted and Classical Synthetic Routes, Structural Characterization and Chromatographic Evaluation, *Chromatographia.* 77 (2014) 1577–1588. doi:10.1007/s10337-014-2802-x.
- [48] M. Mignot, M. Sebban, A. Tchaplá, O. Mercier, P. Cardinael, V. Peulon-Agasse, Thermal pretreatments of superficially porous silica particles for high-performance liquid chromatography: Surface control, structural characterization and chromatographic evaluation, *J. Chromatogr. A.* 1419 (2015) 45–57. doi:10.1016/j.chroma.2015.09.072.
- [49] G.E. Berendsen, L. De Galan, Role of the chain length of chemically bonded phases and the retention mechanism in reversed-phase liquid chromatography, *J. Chromatogr. A.* 196 (1980) 21–37. doi:10.1016/S0021-9673(00)80356-8.
- [50] K. Kimata, K. Iwaguchi, S. Onishi, K. Jinno, R. Eksteen, K. Hosoya, M. Araki, N. Tanaka, Chromatographic Characterization of Silica C18 Packing Materials. Correlation between a Preparation Method and Retention Behavior of Stationary Phase, *J. Chromatogr. Sci.* 27 (1989) 721–728.
- [51] J. Horak, W. Lindner, Investigations on the chromatographic behavior of hybrid reversed-phase materials containing electron donor-acceptor systems: I. Contribution of sulfur-aromatic interactions, *J. Chromatogr. A.* 1043 (2004) 177–194. doi:10.1016/j.chroma.2004.05.095.
- [52] M.R. Euerby, P. Petersson, W. Campbell, W. Roe, Chromatographic classification and comparison of commercially available reversed-phase liquid chromatographic columns containing phenyl moieties using principal component analysis, *J. Chromatogr. A.* 1154 (2007) 138–151. doi:10.1016/j.chroma.2007.03.119.
- [53] R.E. Majors, C.A. Rimmer, K.A. Lippa, L.C. Sander, *Chromatogr. Online.* (2008).
- [54] K. Jinno, C. Okumura, M. Taniguchi, Y.-L. Chen, Molecular shape recognition of polycyclic aromatic hydrocarbons with various alkyl diphenyl bonded phases in microcolumn liquid chromatography, *Chromatographia.* 44 (1997) 613–618. doi:10.1007/BF02466664.
- [55] K. Croes, A. Steffens, D.H. Marchand, L.R. Snyder, Relevance of π - π and dipole-dipole interactions for retention on cyano and phenyl columns in reversed-phase liquid chromatography, *J. Chromatogr. A.* 1098 (2005) 123–130. doi:10.1016/j.chroma.2005.08.090.
- [56] P.G. Stevenson, S. Kayillo, G.R. Dennis, R.A. Shalliker, Effects of π - π Interactions on the Separation of PAHs on Phenyl-Type Stationary Phases, *J. Liq. Chromatogr. Relat. Technol.* 31 (2007) 324–347. doi:10.1080/10826070701780607.
- [57] K. Jinno, K. Yamamoto, H. Nagashima, T. Ueda, K. Itoh, Silicas chemically bonded with multidentate phenyl groups as stationary phases in reversed-phase liquid chromatography used for non-planarity recognition of polycyclic aromatic hydrocarbons, *J. Chromatogr. A.* 517 (1990) 193–207. doi:10.1016/S0021-9673(01)95721-8.
- [58] M.A. Blanco, A. Martín Pendás, E. Francisco, Interacting Quantum Atoms: A Correlated Energy Decomposition Scheme Based on the Quantum Theory of Atoms in Molecules, *J. Chem. Theory Comput.* 1 (2005) 1096–1109. doi:10.1021/ct0501093.
- [59] E. Francisco, A. Martín Pendás, M.A. Blanco, A Molecular Energy Decomposition Scheme for Atoms in Molecules, *J. Chem. Theory Comput.* 2 (2006) 90–102. doi:10.1021/ct0502209.
- [60] V. Tognetti, L. Joubert, Density functional theory and Bader's atoms-in-molecules theory: towards a vivid dialogue, *Phys. Chem. Chem. Phys.* 16 (2014) 14539–14550. doi:10.1039/C3CP55526G.
- [61] O.A. Syzgantseva, V. Tognetti, L. Joubert, On the Physical Nature of Halogen Bonds: A QTAIM Study, *J. Phys. Chem. A.* 117 (2013) 8969–8980. doi:10.1021/jp4059774.
- [62] V. Tognetti, L. Joubert, Following Halogen Bonds Formation with Bader's Atoms-in-Molecules Theory, in: R. Chauvin, C. Lepetit, B. Silvi, E. Alikhani (Eds.), *Appl. Topol. Methods Mol.*

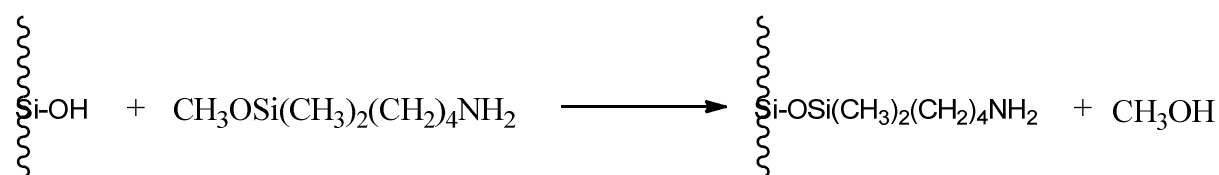
- Chem., Springer International Publishing, 2016: pp. 435–459. http://link.springer.com/chapter/10.1007/978-3-319-29022-5_16 (accessed July 15, 2016).
- [63] M. Pitoňák, P. Neogrady, J. Řezáč, P. Jurečka, M. Urban, P. Hobza, Benzene Dimer: High-Level Wave Function and Density Functional Theory Calculations, *J. Chem. Theory Comput.* 4 (2008) 1829–1834. doi:10.1021/ct800229h.
- [64] R.A. DiStasio Jr., G. von Helden, R.P. Steele, M. Head-Gordon, On the T-shaped structures of the benzene dimer, *Chem. Phys. Lett.* 437 (2007) 277–283. doi:10.1016/j.cplett.2007.02.034.
- [65] E.R. Johnson, S. Keinan, P. Mori-Sánchez, J. Contreras-García, A.J. Cohen, W. Yang, Revealing Noncovalent Interactions, *J. Am. Chem. Soc.* 132 (2010) 6498–6506. doi:10.1021/ja100936w.
- [66] J. Contreras-García, E.R. Johnson, S. Keinan, R. Chaudret, J.-P. Piquemal, D.N. Beratan, W. Yang, NCIPLOT: A Program for Plotting Noncovalent Interaction Regions, *J. Chem. Theory Comput.* 7 (2011) 625–632. doi:10.1021/ct100641a.

Supporting Information

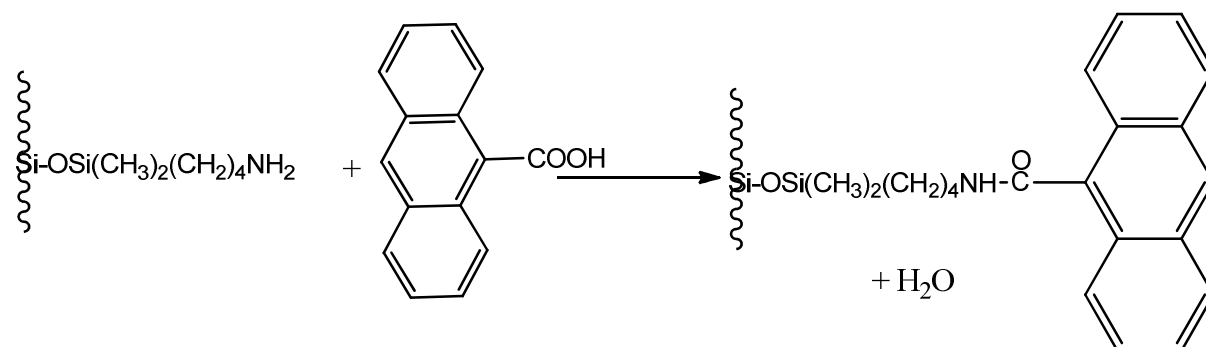
Synthesis of the stationary phases

The synthesis steps (Scheme S1) were performed under microwave irradiation in our laboratory. The first step corresponded to the modification of bare silica to aminosilica by the addition of a spacer group (butyl) containing a terminal amino function. The second step was amidation between 9-anthracenecarboxylic acid and aminosilica to afford the final stationary phase. Three grams of the silica and 2.8 g of ABDMS (or 4.3 g of ABTS) were added to 80 mL of anhydrous toluene in a 150 mL Pyrex vessel, and the mixture reacted for 60 min at reflux. The reactor was cooled to room temperature, and the excess reagent was removed by rinsing with toluene, tetrahydrofuran and acetonitrile. After filtration, the silica was dried at 110°C for 12 h under vacuum. Amidation was achieved by adding 0.51 g of 9-anthracenecarboxylic acid, 1.43 g of PyBOP and 600 μ L of DIPEA in 80 mL of anhydrous toluene in a 150 mL Pyrex vessel, and the mixture reacted for 60 min at reflux. The reactor was cooled to room temperature, and the excess reagent was removed by rinsing with toluene, tetrahydrofuran and acetonitrile. After filtration, the silica was dried at 110°C for 12 h under vacuum. The final stationary phases were end-capped with 1.2 mL of bis(dimethylamino)(trimethyl)silane following the same procedure.

a



b



Scheme S1: Aminobutyldimethylmethoxysilane grafting onto the silica surface (a). Simplified representation of acid coupling onto aminosilica (b).

In reality, PyBOP is used as a coupling reagent with DIPEA as the base. Finally, end-capping with DATS leads to the final stationary phase.

The columns (250 mm \times 3 μ m \times 4.6 mm), (50 mm \times 2.6 μ m \times 4.6 mm) and (50 mm \times 3 μ m \times 4.6 mm) were packed by Interchim and were compared to various commercial columns with different chemistries: HALOTM C18 (50 mm \times 2.7 μ m \times 4.6 mm), HALOTM Phenyl-Hexyl (100 mm \times 2.7 μ m \times 4.6 mm), and HALOTM RP-amide (100 mm \times 2.7 μ m \times 4.6 mm) from Advanced Materials Technology (Wilmington, DE, USA).

Data analysis

The calculation of the bonded ligand coverage density was performed using the Berendsen equation (Eq 1).

$$\tau = \frac{10^6 \times p_c}{[1200 n_c - p_c \times (M_w - n_x)] \times S_{BET}} \quad \text{Eq 1}$$

where τ is the coverage density ($\mu\text{mol}/\text{m}^2$), p_c is the percent of carbon (%), n_c is the number of carbon atoms in the ligand, M_w is the molar mass of the ligand, n_x is the number of functional groups in the reactive group of the silane, and S_{BET} is the specific surface area (m^2/g).

The efficiency (N) values were calculated by Chromeleon software using Eq 2:

$$N = 5.54 \times \left(\frac{t_r}{\omega_{1/2}} \right)^2 \quad \text{Eq 2}$$

where t_r and $\omega_{1/2}$ are the retention time and the width of the peak at half height, respectively.

The retention factors (k) were calculated using Eq 3:

$$k = \frac{t_r - t_0}{t_0} \quad \text{Eq 3}$$

where t_0 is the dead time.

The selectivity factors (α) were calculated using Eq 4:

$$\alpha_{1,2} = \frac{k_2}{k_1} \quad \text{Eq 4}$$

where k_1 and k_2 are the retention factors of the first and second eluted solutes, respectively.

Characterization of the bonded silicas

To investigate the influence of the support material, the monofunctional version was formed both on fully porous and on superficially porous supports. In addition, the influence of the tridimensional structure was studied by synthesizing bonded silica from mono- and trifunctional reagents on fully porous particles.

A previous study comparing the impact of the grafting synthesis mode (microwave or conventional heating)[1] demonstrated that there is no influence on the grafting of the C18 reagent onto the silica surface. A significant grafting rate difference was found for the syntheses performed here, where a better loading was obtained when the syntheses were performed under microwave irradiation. This result may be explained by the higher polarity of the aminosilica compared to the bare silica. Additionally, the reagents involved in this synthesis reaction (9-anthracenecarboxylic acid and coupling reagents) were more polar than the C18 reagents, leading to a more efficient grafting under microwave irradiation.

Under microwave irradiation the grafting rate of the trifunctional synthesis process was similar to the monofunctional synthesis process ($\tau = 18\%$ compared to $\tau = 17.6\%$, with a standard deviation of 0.5%).

In the first step of the synthesis (from bare silica to aminosilica), %N was similar for the mono- and trifunctional processes. Consequently, there was an equivalent amount of amino functionality available for the following derivatization with 9-anthracenecarboxylic acid. However, for the trifunctional structures, it was necessary to consider the way the polymerization occurred. Depending on the water content and the chemical nature of the leaving groups, different structures can be obtained for the same functionalized silica as a result of vertical or horizontal polymerization. In contrast to the C18 structure, where hydrophobic repulsion affects the hydrophobic chain repartition, in our case, π - π interactions may occur between the aromatic units, favoring the high grafting level of the amino functions. This may be the case for the trifunctional structure, where a pre-association exists due to the proximity of each amino group previously linked onto the silica surface, as revealed by the DFT optimizations (see below).

Moreover, compared to the more commonly used propyl spacer group, the choice of a butyl spacer group may offer a better accessibility of the terminal amino groups, leading to an enhanced grafting rate.

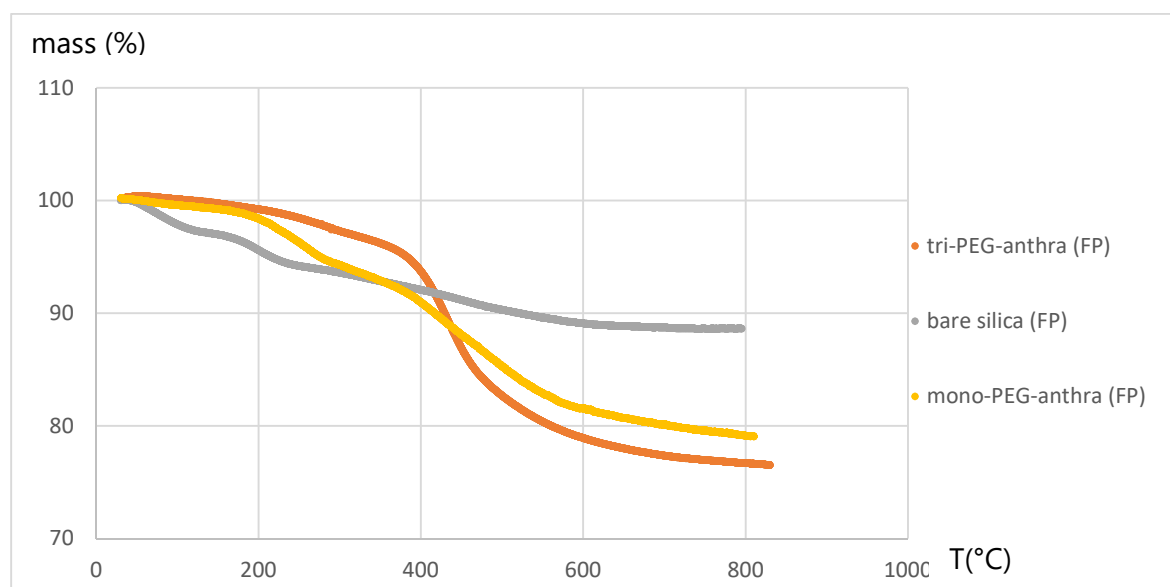


Figure S1: Thermogravimetric curves obtained for unmodified silica, mono-PEG-anthra (FPP) and tri-PEG-anthra (FPP).

Thermogravimetry can be used to determine the surface coverage of the chemically modified silica[2] because the weight loss observed between 200 and 600°C is associated with the loss of the organic groups attached to the surface[3]. Figure S1 shows the thermogravimetric curves for the bare porous silica and the functionalized porous silica under conventional heating. For bare silica, the mass loss is due to the loss of adsorbed water and the condensation of the silanol groups at temperatures higher than 250°C[4]. Above 400°C, the mass loss was higher for the mono-PEG-anthra due to the loss

of organic moieties. For the two PEG anthracenyl-bonded fully porous silicas, although their % carbon is the same, their thermogravimetric mass loss curves are different. Bonded silica functionalized with the trifunctional silane remained more stable up to 400°C. The tri-PEG-anthra presented the highest mass loss (approximately 24% from 200 to 800°C, 21% for the mono-PEG-anthra), which indicates a different spatial arrangement for the two synthesized PEG anthracenyl-bonded fully porous silicas.

Diffuse reflectance infrared spectroscopy is a good tool for the characterization of the ligand ratio on mixed bonded stationary phases and for qualitative confirmation of the bonding of silica[5]. For bare silica (Figure S2a), Si-O asymmetric stretching can be observed as a strong peak at 1082 cm⁻¹, Si-O symmetric stretching from the SiO₄ tetrahedral structure is observed at 801 cm⁻¹, and the Si-O-Si stretching band is observed at 1874 cm⁻¹. The bending vibration band at 1630 cm⁻¹ corresponds to the OH bending vibration of physically adsorbed water. The broad absorption band in the region of 3600 to 3300 cm⁻¹ is due to the stretching of the hydroxyl group of physically adsorbed water and the hydrogen-bonded Si-OH groups.

The spectra of the new stationary phases presented additional bands compared to bare silica. In this work, the butyl-4-amino group was first introduced onto the silica surface. The (Si)-methyl and methylene bands (asymmetric and symmetric C-H stretching bands at 2956, 2923 and 2857 cm⁻¹, bending vibration bands of the CH₂ and CH₃ groups at 1480 cm⁻¹) corresponded to the butyl chain and confirmed the grafting onto the surface of the silica. Furthermore, the shoulders at 3370 cm⁻¹ and 3300 cm⁻¹ on the broad band in the region of 3000-3600 cm⁻¹ corresponded to the stretching band vibration of NH₂, the bands at 1680 and 1600 cm⁻¹ corresponded to NH₂ group bending in the plane vibrational band (Figure S2b) and the shoulder at 850 cm⁻¹ on the 792 cm⁻¹ band corresponded to the bending out-of-plane vibration band of the NH₂ group. After coupling with 9-anthracenecarboxylic acid, the major feature of the spectrum of mono-PEG-anthra (Figure S2c) was the appearance of the band at 3100 cm⁻¹ (stretching vibration band of aromatic CH) and the doublet bands at 850 cm⁻¹ and 740 cm⁻¹ assigned to the out-of-plane bending of the anthracenic C-H at 1450 cm⁻¹. The stretching of the C-C anthracenic ring band was observed, but the superimposition of the different bands in this spectral region led to poor resolution of different the absorption bands and made their precise attribution difficult. Thus, the two broad bands at 1660 cm⁻¹ and 1550 cm⁻¹ were attributed to the CO-NHR amide group, and the shoulder at 3300 cm⁻¹ was attributed to the stretching band vibration of the secondary NH band.

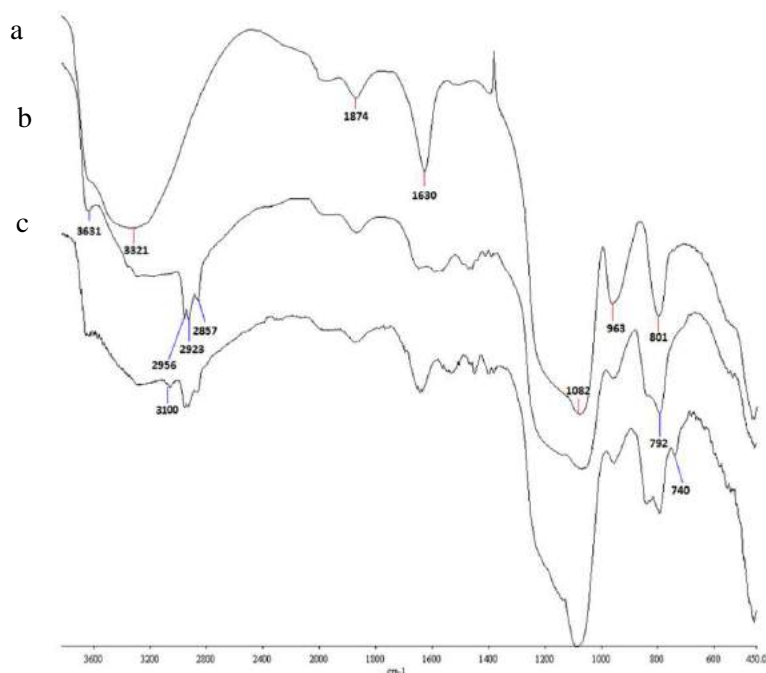


Figure S2: DR-FT-IR spectra of (a) bare silica, (b) butyl-4-amino-silica, (c) butyl-4-amino-silica coupled with 9-anthracene carboxylic acid.

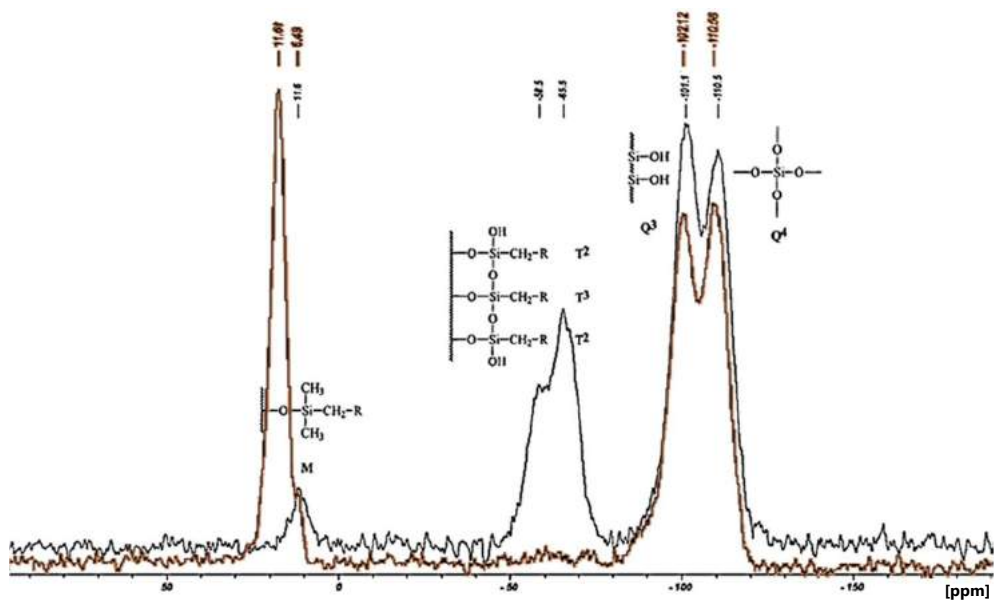
The NMR spectra provided valuable information about the silica surface and chemical bonding. The species found on the surface, described as Q^n and T^n species, are related to the number of oxygens (mono, di, tri or tetra-oxo) bound to the silicon atom[6]. The solid-state ^{29}Si CP/MAS NMR spectra of the tri-PEG-anthra presented two signals (Figure S3a) at -101 ppm (Q_3), and at -110 ppm (Q_4), which corresponded to free hydroxyl groups and siloxane groups, respectively[7]. No evident signal corresponding to geminal silanol at -91 ppm (Q_2) was observed. An additional chemical shift near +12 ppm (M) was ascribed to the final end-capping ligand (O-Si-CH_3)₃ linkage. The ^{29}Si CP-MAS NMR spectra confirmed that a ligand was bonded onto the silica surface. For tri-PEG-anthra, the resulting NMR spectrum presented another set of signals at -58 ppm (T_2) and -65 ppm (T_3), which corresponded to the trifunctional Si-O-Si linkage and the bifunctional Si-O-Si linkage, respectively[6]. The three mono-PEG-anthra did not present these T_2 and T_3 signals, which is consistent with their monomeric structure. Because the mono-PEG-anthra FPP and tri-PEG-anthra FPP stationary phases have the same carbon load, ^{29}Si CP-MAS NMR was especially useful to differentiate the molecular structures of these two bonded phases.

The ^1H MAS NMR spectrum presented in Figure S3b deserves additional discussion. The $(\text{CH}_3)_3$ units of the end-capping ligand were detected at 0.2 ppm, the CH_2 units of the alkyl chain (indicated as a, b, c, and d in Figure S3c) gave the following signals: b+c: 1.2 ppm, a: 1.8 ppm and d: 3.5 ppm, with the anthracenic protons from 5.1 to 6.2 ppm and the amide proton at 2.3 ppm.

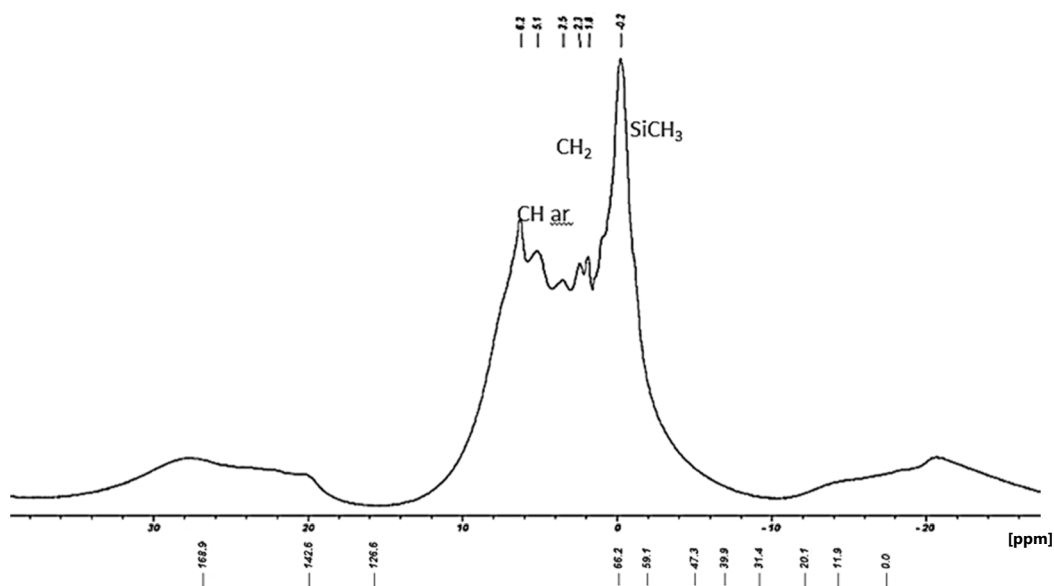
The ^{13}C MAS NMR spectrum provided further confirmation of the grafting. The peak at 0 ppm was ascribed to the methyl groups of the end-capping ligand, which were directly linked to the silicon atom. Another set of peaks (from 10 to 50 ppm) corresponded to the methylene of the alkyl chains (indicated as a, b, c, and d in Figure S3c). The aromatic carbons were between 120 and 150 ppm, and the carbonyl group was at 169 ppm. These attributions were performed based on those previously

reported for the structural characterization of a similar PEG alkyl bonded silica (i.e., 3-propyl-N-urea-N'-octadecyl bonded silica)[8].

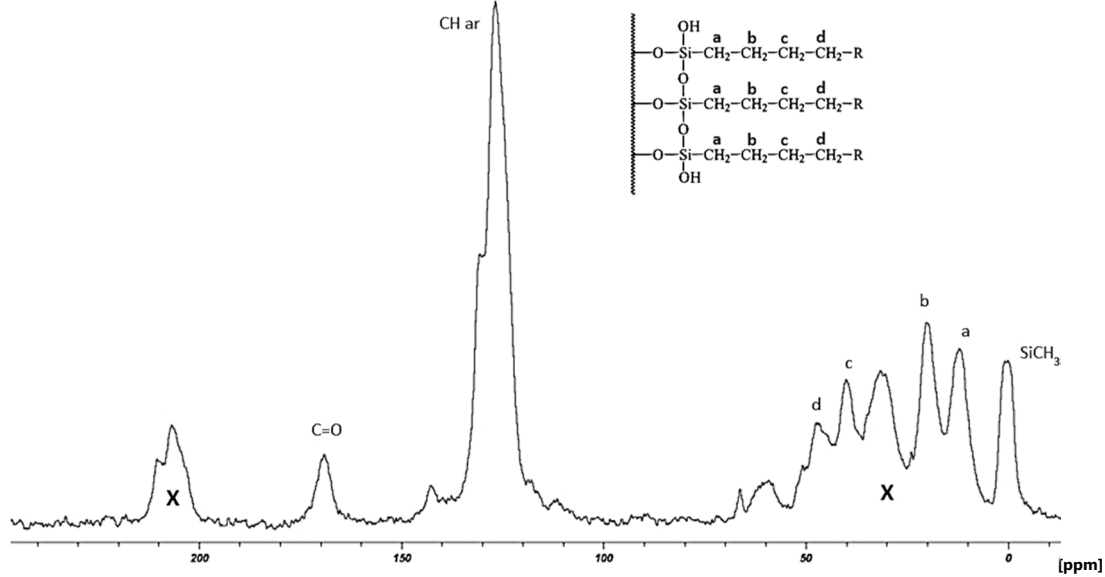
a



b



c



X: Additional cross-labeled peaks corresponded to the rotation bands of the peak at 126 ppm (separated by 10,000 Hz, which corresponds to the rotation speed of the sample).

Figure S3: NMR spectra of 4-aminobutylsilica coupled with 9-anthracene carboxylic acid and end-capped, (a) ^{29}Si CP/MAS (in red, **mono-PEG-anthra and in dark, **tri-PEG-anthra), (b) ^1H NMR, (c) ^{13}C CP/MAS.

For the ^1H and ^{13}C CP/MAS NMR, the spectra of all the synthesized stationary phases were similar.

RPLC studies

The quality of the column packing was evaluated by calculating the efficiency and the tailing factor on the naphthalene peak ($\text{CH}_3\text{CN}-\text{H}_2\text{O}$ 70/30, v/v). For all homemade columns, the efficiencies were comparable (150,000 plates per meter) and the tailing factors were approximately 1.10.

(a) ACN as organic modifier	HALO TM C18	HALO TM RP-amide	HALO TM PH	*mono-PEG-anthra (SPP)	*mono-PEG-anthra (FPP) (1)	**tri-PEG-anthra (FPP)	Log $P_{o/w}$
$k_{(\text{benzene})}$	0.31	0.27	1.07	0.43	0.69	0.95	2.10
$k_{(\text{methylbenzene})}$	0.45	0.38	1.40	0.52	0.81	1.15	2.73
$k_{(\text{ethylbenzene})}$	0.61	0.48	1.88	0.59	0.94	1.36	3.15
$k_{(\text{propylbenzene})}$	0.88	0.65	2.56	0.71	1.12	1.62	3.69
$k_{(\text{butylbenzene})}$	1.25	0.88	3.51	0.85	1.32	1.93	4.40
$k_{(\text{pentylbenzene})}$	1.78	1.18	4.78	1.02	1.56	2.30	4.90
$k_{(\text{hexylbenzene})}$	2.55	1.60	6.53	1.22	1.84	2.73	5.52
$k_{(\text{heptylbenzene})}$	3.68	2.17	8.92	1.47	2.17	3.22	6.10
$k_{(\text{octylbenzene})}$	5.30	2.96	12.10	1.76	2.56	3.84	6.30
$k_{(\text{nonylbenzene})}$	7.65	4.03	16.38	2.13	3.01	4.59	7.10
$k_{(\text{decylbenzene})}$	11.03	5.51	22.18	2.57	3.56	5.27	7.35
$k_{(\text{undecylbenzene})}$	15.99	7.53	29.83	3.23	4.21	6.21	8.14
$k_{(\text{dodecylbenzene})}$	23.10	10.34	40.11	3.95	4.94	7.20	8.80
$k_{(\text{naphthalene})}$	0.54	0.48	1.94	0.66	1.06	1.70	3.55
$k_{(\text{anthracene})}$	1.05	0.92	3.74	1.11	1.70	3.30	4.50
$k_{(\text{naphthacene})}$	2.26	1.92	7.28	1.94	2.95	7.70	5.76
$k_{(o\text{-terphenyl})}$	1.22	0.89	5.73	1.17	1.82	3.45	6.00
$k_{(m\text{-terphenyl})}$	1.41	1.08	6.67	1.35	2.10	4.58	6.02
$k_{(p\text{-terphenyl})}$	1.57	1.18	6.83	1.45	2.28	5.16	6.03
$k_{(\text{triphenylene})}$	1.68	1.52	6.12	1.64	2.63	6.39	5.91

Chapter III. Non-conventional multimodal stationary phases

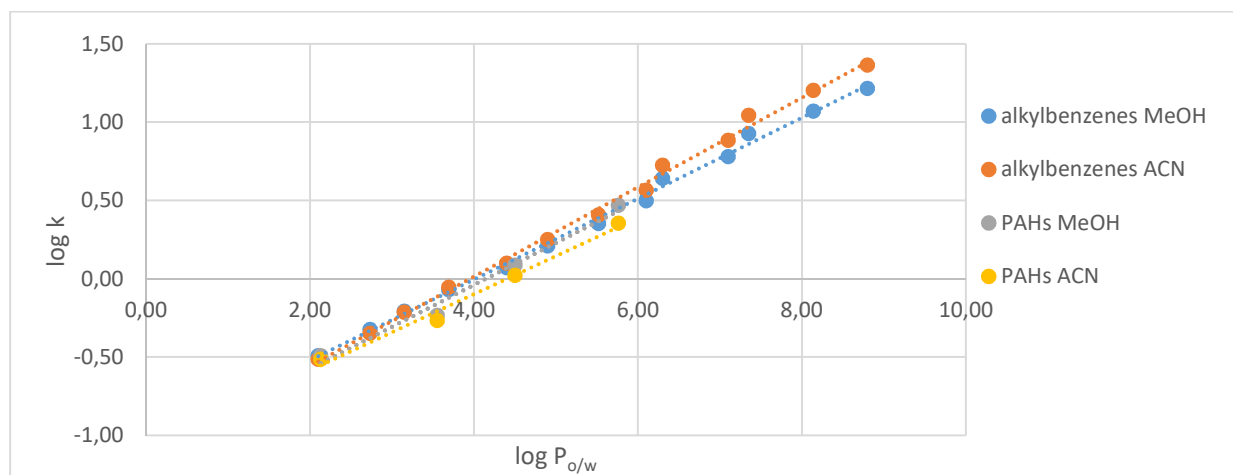
$\alpha_{(\text{triphenylene}/o\text{-terphenyl})}$	1.38	1.72	1.07	1.40	1.45	1.85	
$\alpha_{(\text{pentybenzene}/o\text{-terphenyl})}$	1.46	1.33	0.83	0.87	0.86	0.67	
$\alpha_{(\text{pentybenzene}/\text{butylbenzene})}$	1.42	1.34	1.36	1.20	1.18	1.19	

(b) MeOH as organic modifier	HALO TM C18	HALO TM RP-amide	HALO TM PH	*mono-PEG-anthra (SPP)	*mono-PEG-anthra (FPP) (1)	**tri-PEG-anthra (FPP)	Log P _{o/w}
k _(benzene)	0.32	0.31	0.93	0.15	0.28	0.53	2.10
k _(methylbenzene)	0.47	0.41	1.43	0.21	0.37	0.71	2.73
k _(ethylbenzene)	0.62	0.51	2.11	0.26	0.44	0.86	3.15
k _(propylbenzene)	0.85	0.65	3.21	0.33	0.54	1.06	3.69
k _(butylbenzene)	1.18	0.84	4.97	0.42	0.69	1.34	4.40
k _(pentybenzene)	1.62	1.09	7.59	0.54	0.85	1.68	4.90
k _(hexylbenzene)	2.25	1.43	11.54	0.70	1.04	2.09	5.52
k _(heptylbenzene)	3.14	1.87	17.91	0.89	1.32	2.67	6.10
k _(octylbenzene)	4.37	2.44	27.32	1.19	1.61	3.32	6.30
k _(nonylbenzene)	6.03	3.20	42.37	1.43	2.01	4.20	7.10
k _(decylbenzene)	8.43	4.20	65.49	1.90	2.46	5.19	7.35
k _(undecylbenzene)	11.73	5.50	-	2.52	3.01	6.51	8.14
k _(dodecylbenzene)	16.42	7.29	-	3.43	3.88	8.02	8.80
k _(naphthalene)	0.58	0.53	2.37	0.37	0.59	1.40	3.55
k _(anthracene)	1.22	1.07	6.29	0.87	1.27	4.13	4.50
k _(naphthacene)	2.94	2.39	16.61	2.38	2.95	13.86	5.76
k _(o-terphenyl)	1.30	0.95	12.40	0.83	1.22	3.68	6.00
k _(m-terphenyl)	1.85	1.42	17.63	1.32	1.77	6.85	6.02
k _(p-terphenyl)	2.06	1.52	16.80	1.36	1.88	7.56	6.03
k _(triphenylene)	2.09	1.91	13.22	1.94	2.60	11.64	5.91
$\alpha_{(\text{triphenylene}/o\text{-terphenyl})}$	1.61	2.00	1.07	2.35	2.14	3.16	
$\alpha_{(\text{pentybenzene}/o\text{-terphenyl})}$	1.25	1.15	0.61	0.66	0.70	0.46	
$\alpha_{(\text{pentybenzene}/\text{butylbenzene})}$	1.38	1.29	1.53	1.28	1.22	1.25	

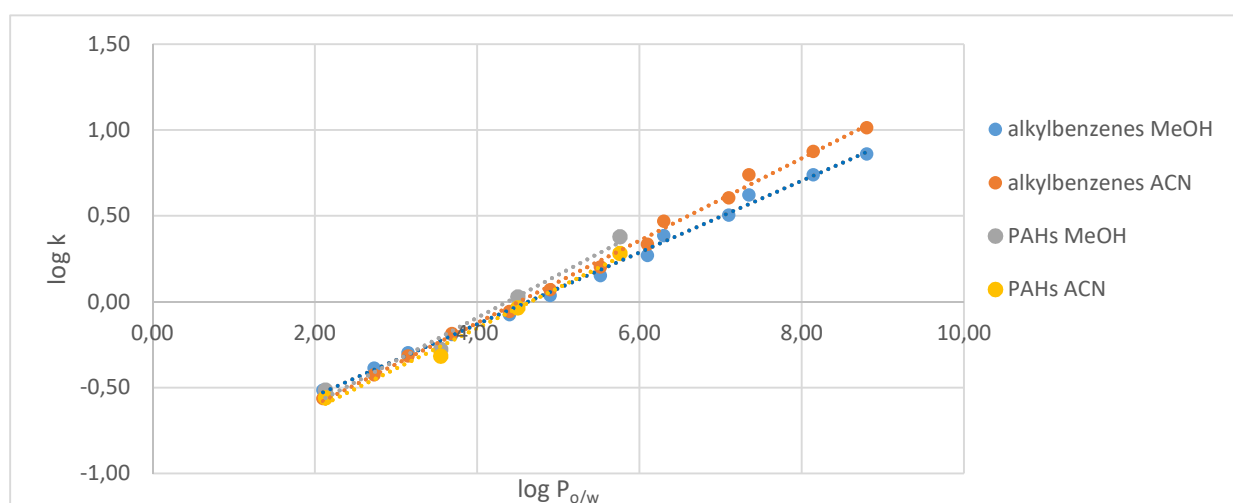
Table S1: Retention and selectivity factors of alkylbenzenes, PAHs, and terphenyl isomers for the commercial and the homemade stationary phases for a mobile phase composed of (a) ACN/H₂O or (b) MeOH/H₂O. Mobile phase with ACN: 85% in water for HALOTM C18 and HALOTM RP-amide, 60% in water for the HALOTM PH, *mono-PEG-anthra (SPP as well as FPP (1)) and **tri-PEG-anthra (FPP). Mobile phase with MeOH: 90% in water for HALOTM C18 and HALOTM RP-amide and 70% in water

for the HALO™ PH, *mono-PEG-anthra (SPP as well as FPP (1)) and **tri-PEG-anthra (FPP). UV: 254 nm, T = 30°C, F = 1 mL/min.

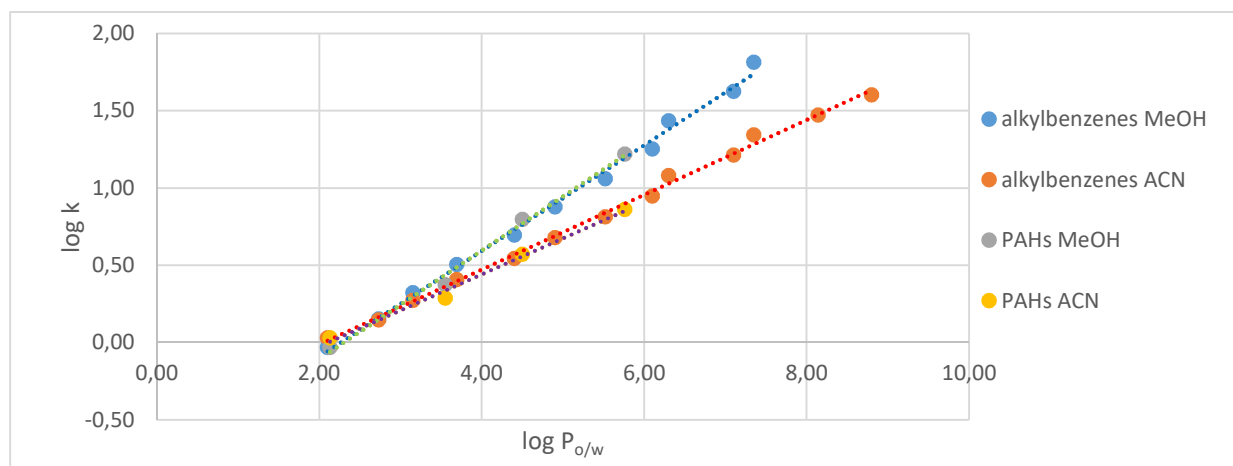
a



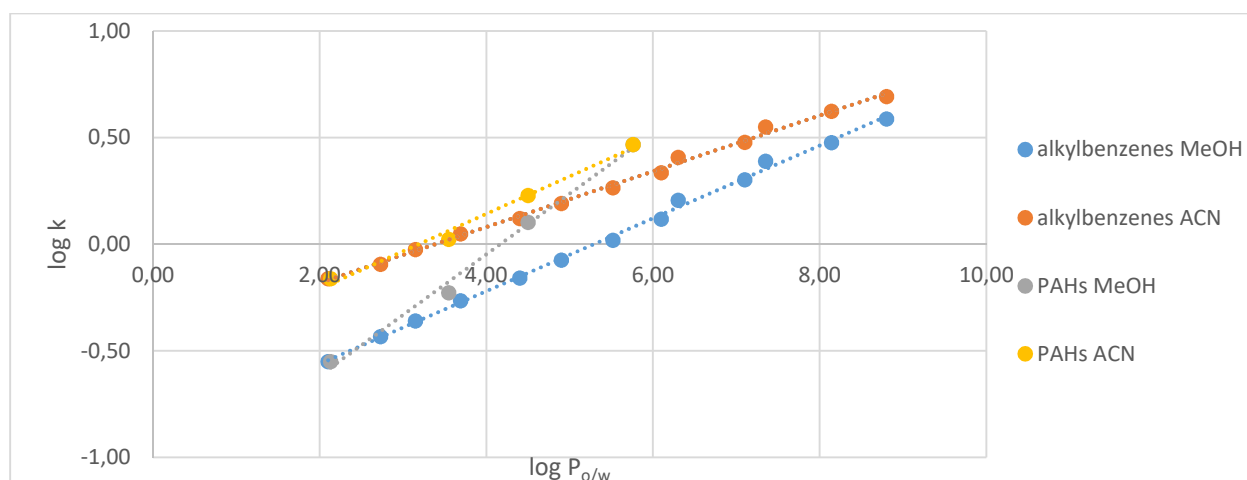
b



c



d



e

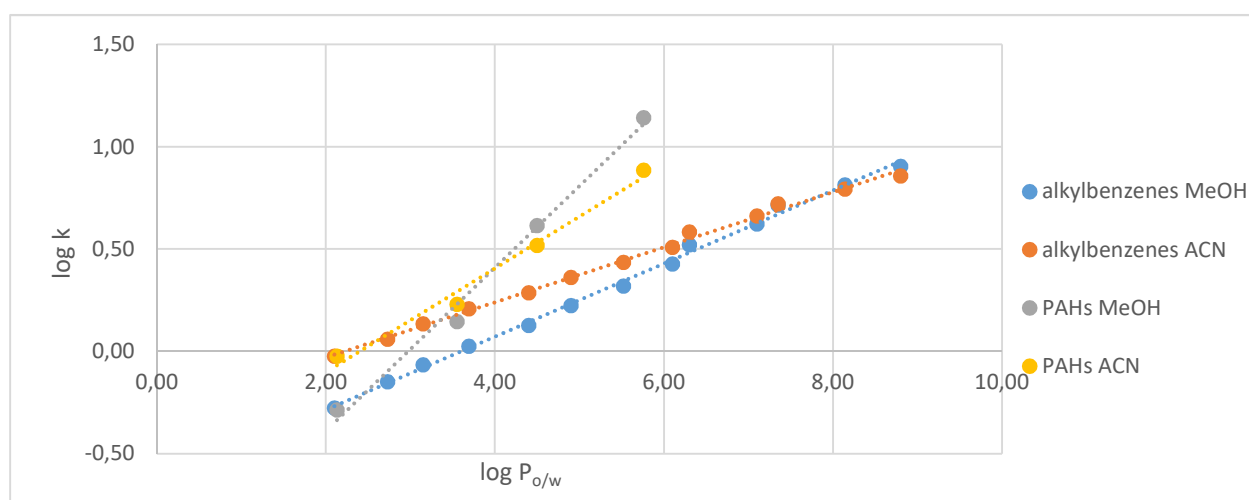


Figure S4: Plots of $\log k$ and $\log P_{o/w}$ for HALO™ C18 (a), HALO™ RP-amide (b), HALO™ PH (c), *mono-PEG-antra (FPP) (d), and **tri-PEG-anthra (FPP) (e). Solutes: alkylbenzenes from benzene to dodecylbenzene and PAHs from benzene to naphthacene. Mobile phase with ACN: 85% in water (a and b) and 60% (v/v) in water (c, d, e). Mobile phase with MeOH: 90% (v/v) in water (a and b) and 70% (v/v) in water (c, d, e). UV: 254 nm, T = 30°C, F = 1 mL/min. These conditions were selected to allow suitable retention of the probe solutes on all stationary phases.

Energetic aspects

To compare the energetics of the chromatographic phenomenon, either by using the same stationary phase with two different mobile phase compositions or two different stationary phases with the same mobile phase, it is convenient to plot the logarithms of the retention factors of a set of solutes under condition A versus the logarithms of the retention factors of the same set of solutes under condition B[9]. When the set of solutes includes a homologous series in the plots, the homologues should fall on a straight line, which is the ratio of the methylene selectivity under each condition[10]. As previously reported, a linear correlation of $\ln k_A$ vs $\ln k_B$ with unit slope indicates a homo-energetic process that is characteristic of an identical retention mechanism under the conditions A and B. This was observed for two C18 bonded silicas with the same mobile phase composition.

A linear correlation with a slope different from unity indicates a similar but not identical retention mechanism and is termed homeo-energetic. This was reported for two different bonded silicas with the same mobile phase composition or for the same stationary phase and two different mobile phase compositions (differing either by the nature of the organic modifier or the % content of water). The absence of a correlation indicates a hetero-energetic process and a mixed or different retention mechanism[10]. This was typically the case when comparing mono-PEG-anthra to tri-PEG-anthra. The results of this study are reported on Table S2.

The behavior of alkylbenzenes on all the PEG-anthra stationary phases was perfectly linear ($r^2 > 0.9984$, with all the experimental plots are randomly distributed along the regression line). No break was observed in the range $1 \leq n_C \leq 12$, independent of the nature of the organic modifier (ACN or MeOH), as was previously reported on C18 bonded silicas with a more extended range of solute ($1 \leq n_C \leq 18$). For the phenyl-3-propyl bonded silica[11], the ratio of the slopes of the curves $\ln k$ vs n_C with methanol and acetonitrile on the same stationary phase was always greater than 1 for the four aromatic bonded phases (from top to bottom in Table S2: 1.39, 1.38, 1.31, 1.33). The thermodynamic process is homeo-energetic, and the molecular structure of the stationary phase is similar for each of these phases, independent of the nature of the organic modifier (ACN or MeOH). If we compare mono-PEG-anthra to tri-PEG-anthra, ratios of 1.05 with methanol and 1.03 with acetonitrile are obtained. The energetic process is homo-energetic, and there is no difference in the chromatographic process on these two phases with solutes that are able to adopt different conformations.

$$HP = \frac{\alpha-1}{\alpha} \times \frac{k_2}{1+k_2} \quad \text{Eq 5}$$

where k_2 is the retention factor of the second eluted solute, and α is the selectivity factor.

However, the hydrophobic potential (HP) (Eq 5) calculated for the pair pentylbenzene/butylbenzene, which characterizes the resolution between two homologues on a stationary phase[12], is the same for the two mono-PEG-anthra but is comparatively increased when tri-PEG-anthra is used, independent of

the nature of the organic modifier. An increase in the separation power of the tri-PEG-anthra was also observed with linear aromatic PAHs, although the behavior of linear aromatic rings is not linear but quadratic. Finally, the selectivity for *m*-terphenyl/*o*-terphenyl is also enhanced on the tri-PEG-anthra compared to the two mono-PEG-anthra, which suggests a small difference in the molecular structure of these two types of phases.

Stationary phase	MeOH	ACN	MeOH			ACN		
	Slope (alkylbenzenes)	Slope (alkylbenzenes)	Quadratic equation (linPAH) a b c			Quadratic equation (linPAH) a b c		
HALO™ C18	0.3259	0.3593	0.0045	0.08	-1.769	0.0033	0.0863	-1.8083
r^2	0.9998	0.9998	1			1		
HALO™ RP-amide	0.2627	0.2627	0.0042	0.07	-1.7478	0.0025	0.1033	-2.0186
r^2	0.9995	0.9995	0.9999			1		
HALO™ Phenylhexyl	0.4254	0.3054	0.0006	0.23	-1.4584	0.0011	0.1336	-0.7764
r^2	0.9999	0.9999	1			0.9999		
*mono-PEG- anthra (SPP)	0.2535	0.1837	0.0016	0.19	-3.0847	0.002	0.0773	-1.3834
r^2	0.9989	0.9984	0.9995			0.9999		
*mono-PEG- anthra (FPP) (1)	0.2155	0.1648	0.0015	0.16	-2.2804	0.0019	0.0751	-0.8883
r^2	0.9996	0.9999	1			0.9999		
**tri-PEG-anthra (FPP)	0.2252	0.1694	0.0037	0.18	-1.861	0.0041	0.0740	-0.6395
r^2	0.9997	0.9994	1			0.9998		

Table S2: Slopes of the plots of $\ln k$ vs n_C for alkylbenzenes (from benzene to dodecylbenzene) and coefficients of the quadratic regression of $\ln k$ vs n_C for linear PAHs (from benzene to naphthalene).

Theoretical modeling

From a methodological aspect, a theoretical study can be divided into three successive steps: the selection of the computational protocol, the computation itself, and subsequent data processing. The first step involves the choice of the model system (which atoms are included) and its components (possible counterions or solvent molecules). The second step requires prior determination of the optimal method with respect to the available computer resources; in practice, it consists of defining the formulas for calculating the relevant energy (e.g., electronic energy, enthalpy, free energy). The third step is related to the extraction of a few pertinent numbers (among the thousands generated by the

computation), called descriptors, which can explain the experimental results and provide guidelines for further experimental improvement.

The size of the model system is not chosen independently of the energy calculation method. Roughly speaking, one can rely on either classical mechanics (the realm of force fields) or quantum chemistry. While full systems can be handled by the first methods, only limited ones (typically hundreds of atoms) can be routinely treated by the latter. However, force fields are generally specialized (for instance, designed for a protein, sugar, or water) and often need to be reparametrized for special cases. The systems we focused on are challenging for force fields since they mix inorganic (silica) and organic fragments. This combination makes quantum chemistry more reliable, to the obvious detriment of computational time.

For this reason, only the end arm of the chromatographic system is generally modeled at the quantum level in the literature[13–19]. Two notable but isolated exceptions are found in a recent work,[20] where the full system was studied, taking advantage of GPU architecture, which requires non-standard technology, and another study[21] where geometries were optimized at the MM3 semi-empirical level of theory, a level that cannot correctly describe the crucial noncovalent interactions of the dispersion type. Therefore, MM3 may produce satisfying results for the silica phase but will not be suitable to investigate its interactions with aromatic compounds.

Neglecting the surface is certainly erroneous in the case of trifunctional phases, where the interactions between the three arms should be geometrically accommodated by the silica and are thus constrained. Moreover, solvent effects are generally not considered (the phase-solute adduct is viewed as a free molecule). Many of the referenced studies reported calculations in the gas phase. Solvent effects are important for practical applications, an issue that we also want to address from a theoretical perspective. The only exceptions we are aware of[15,20] have used an implicit solvation approach. Let us recall that solvent effects can be introduced through an explicit (solvent molecules are described at the atomic level) or implicit (a continuum model[22] mainly accounts for the average electrostatic interaction with the solute) approach. The descriptions can be mixed in a hybrid approach, which is sometimes compulsory to explain subtle conformational differences[23].

For the energy calculation procedure, almost all past studies[13–19,24–26] employed the still popular global hybrid B3LYP exchange-correlation functional. This twenty-three-year-old venerable functional is known to be inaccurate for noncovalent interactions, particularly those stemming from van der Waals dispersion forces[27]. For instance, B3LYP is unable to predict a stable structure for helium, methane, and benzene dimers. This failure, which is now well documented[28], makes it unsuitable when π -stacking is at stake. In addition to the functional issue, a basis set should be cautiously chosen. Quite unexpectedly, the minimal STO-3G basis set is still in use in the chromatography community for describing noncovalent interactions[24–26], but it is too small to produce converged results.

Finally, in the literature, the results are usually rationalized in terms of atomic charges (the use[18] of the Mulliken scheme, while fast, is strongly discouraged since it is not physically motivated and shows spurious basis set convergence) and molecular electrostatic potentials (MEPs). This last tool, which is

meaningful to account for charge-controlled interactions (whereas Fukui functions and their extensions should be used in the case of orbital control)[29] or for noncovalent interactions involving the so-called σ -hole paradigm[30–32], cannot reveal dispersion-controlled interactions because dispersion is a (correlation) non-electrostatic effect. Complementary tools should thus be considered when π -stacking occurs.

Computational details

All calculations were performed using the Gaussian 09 package[33]. The calculations based on density functional theory were performed with the dispersion-corrected B97D exchange-correlation functional,[34] which has two main advantages: it is fast since it does not require the evaluation of non-local exact exchange, and it is designed to correctly account for van der Waals interactions. It was used in conjunction with the following basis set combination, depicted in the left part of Figure 1: atoms involved in hydrogen bonds (these are the two intramolecular bonds involving the amide groups within the trifunctional fragment and the two intermolecular bonds with the solvent) are described by 6-311++G(d,p), while, to save time, the butyl linkers (that have mainly structural and steric effects) are treated by STO-3G. The 6-31G(d) basis set is used for the remaining atoms (a maximum of 2973 primitive Gaussian functions are used to solve the Kohn-Sham equations).

Implicit solvation is described by the conductor polarizable continuum model (CPCM[35], with default parameters), which provides values that are as accurate as more recent implementations (like Gaussian 09's default IEFPCM) for common solvents but is computationally less time-consuming. All structures were fully optimized without symmetry constraints, and the nature of the obtained stationary points was further confirmed by vibrational analyses (only real harmonic frequencies for minima). Standard formulas from statistical mechanics were used to compute the thermodynamic corrections. Because they are based on the ideal gas model, they lead to overestimation of the entropic effects for molecules in solution. To circumvent this drawback, several groups have proposed scaling the obtained values for the rotational and the translational entropies (that are reduced in the condensed phase). In accordance with previous papers and our own experience, we set this scaling factor to 0.65[36–38]. When taken equal to 1.0, the calculated complexation Gibbs energies are positive, indicating that the coordination is endothermic. This is no longer the case when 0.65 is chosen, in agreement with the experimental results. Finally, the binding energies are not corrected from the basis set superposition errors because Boys-Bernardi's counterpoise protocol is not available within PCM.

Point-charge contributions to the electrostatic interaction were evaluated using atomic charges fitted on the electrostatic potential by the ChelpG formalism[39]. Noncovalent index (NCI) analysis was performed using the NCIPLOT software[40] on the self-consistent field electron density (for a simplified system) using default parameters.

Finally, ONIOM-type calculations were conducted within a two-layer QM/QM' approach (see Figure 1b) to estimate the dispersion contribution to the binding energy in a full ab initio way. We defined the high-level layer as the one including the mobile phase and the three anthracyl groups of the stationary

phase, which was described at the second-order Møller-Plesset (MP2) post-HF level of theory with the 6-31G(d) basis set (note that frozen cores were used; despite the small basis set, such calculations required large memory and hard disk space), while the remaining system was treated at the B97D/6-311++G(d,p) DFT level. These QM/QM' calculations were performed in a single-point manner on the geometries optimized at the previous DFT level. As a first approximation, one can assume that the dispersion energy is equal to the second-order perturbation energy. Let us call $E_{M_1...M_2}^{bindMP2}$ the binding energy between the two fragments obtained using the QM/QM' extrapolation, and $E_{M_1...M_2}^{bindHF}$ the energy obtained by replacing the MP2 step with an HF step in the QM/QM' procedure. We then define

$$E_{M_1...M_2}^{dispMP2} \text{ as } E_{M_1...M_2}^{bindMP2} - E_{M_1...M_2}^{bindHF}, \text{ a strategy we used in ref[41]}$$

- [1] M. Mignot, A. Tchaplà, O. Mercier, N. Couvrat, S. Tisse, P. Cardinael, V. Peulon-Agasse, High-Density Octadecyl Chemically Bonded Core-Shell Silica Phases for HPLC: Comparison of Microwave-Assisted and Classical Synthetic Routes, Structural Characterization and Chromatographic Evaluation, *Chromatographia*. 77 (2014) 1577–1588. doi:10.1007/s10337-014-2802-x.
- [2] C.P. Jaroniec, R.K. Gilpin, M. Jaroniec, Comparative studies of chromatographic properties of silica-based amide-bonded phases under hydro-organic conditions, *J. Chromatogr. A*. 797 (1998) 103–110. doi:10.1016/S0021-9673(97)01029-7.
- [3] B. Lumley, T.M. Khong, D. Perrett, The Characterisation of Chemically Bonded Chromatographic Stationary Phases by Thermogravimetry, *Chromatographia*. 60 (2004) 59–62. doi:10.1365/s10337-004-0329-2.
- [4] L.M.L.A. Auler, C.R. Silva, K.E. Collins, C.H. Collins, New stationary phase for anion-exchange chromatography, *J. Chromatogr. A*. 1073 (2005) 147–153. doi:10.1016/j.chroma.2004.10.012.
- [5] S. Héron, A. Tchaplà, A. Charatier, J.-L. Rocca, General method for characterization of the ligand ration on mixed bonded stationary phases by DR/FT-IR spectrometry, *Chim. Oggi*. 10 (1992) 37–42.
- [6] B. Pfeleiderer, K. Albert, E. Bayer, Investigations by ²⁹Si cross-polarization magic angle spinning NMR spectroscopy of reaction pathways of silica gel polyfunctional modification, *J. Chromatogr. A*. 506 (1990) 343–355. doi:10.1016/S0021-9673(01)91590-0.
- [7] M. Pursch, L.C. Sander, K. Albert, Chain Order and Mobility of High-Density C18 Phases by Solid-State NMR Spectroscopy and Liquid Chromatography, *Anal. Chem.* 68 (1996) 4107–4113. doi:10.1021/ac9606113.
- [8] C.R. Silva, S. Bachmann, R.R. Schefer, K. Albert, I.C.S.F. Jardim, C. Airoidi, Preparation of a new C18 stationary phase containing embedded urea groups for use in high-performance liquid chromatography, *J. Chromatogr. A*. 948 (2002) 85–95. doi:10.1016/S0021-9673(01)01263-8.
- [9] W. Melander, J. Stoveken, C. Horváth, Stationary phase effects in reversed-phase chromatography, *J. Chromatogr. A*. 199 (1980) 35–56. doi:10.1016/S0021-9673(01)91360-3.
- [10] S. Héron, A. Tchaplà, Retention mechanism in reversed-phase liquid chromatography: specific effects of propiophenyl and multifunctional (cyanopropyl-octadecyl) bonded silicas, *J. Chromatogr. A*. 725 (1996) 205–218. doi:10.1016/0021-9673(95)00990-6.
- [11] S. Héron, A. Tchaplà, Validity of a notion of eluent force taking into account the nature of the graft on silica in aqueous and non-aqueous liquid chromatography, *Analisis*. 8 (1997) 257–262.
- [12] A. Tchaplà, B. Chabot, D. Charbonneau, D. Desquaires, S. Héron, HPLC 2009- 34th International Symposium on High-Performance Liquid Phase Separation and Related Techniques, (2009).
- [13] R.B. Kasat, C.Y. Chin, K.T. Thomson, E.I. Franses, N.-H.L. Wang, Interpretation of chromatographic retentions of simple solutes with an amylose-based sorbent using infrared spectroscopy and DFT modeling, *Adsorption*. 12 (2006) 405–416. doi:10.1007/s10450-006-0568-7.

- [14] R.B. Kasat, N.-H.L. Wang, E.I. Franses, Experimental probing and modeling of key sorbent–solute interactions of norephedrine enantiomers with polysaccharide-based chiral stationary phases, *J. Chromatogr. A.* 1190 (2008) 110–119. doi:10.1016/j.chroma.2008.02.116.
- [15] M. Szalaniec, A. Dudzik, M. Pawul, B. Kozik, Quantitative structure enantioselective retention relationship for high-performance liquid chromatography chiral separation of 1-phenylethanol derivatives, *J. Chromatogr. A.* 1216 (2009) 6224–6235. doi:10.1016/j.chroma.2009.07.002.
- [16] P. Peluso, V. Mamane, E. Aubert, S. Cossu, High-performance liquid chromatography enantioseparation of atropisomeric 4,4'-bipyridines on polysaccharide-type chiral stationary phases: Impact of substituents and electronic properties, *J. Chromatogr. A.* 1251 (2012) 91–100. doi:10.1016/j.chroma.2012.06.035.
- [17] H.-W. Tsui, E.I. Franses, N.-H.L. Wang, Effect of alcohol aggregation on the retention factors of chiral solutes with an amylose-based sorbent: Modeling and implications for the adsorption mechanism, *J. Chromatogr. A.* 1328 (2014) 52–65. doi:10.1016/j.chroma.2013.12.078.
- [18] S. Ma, H.-W. Tsui, E. Spinelli, C.A. Busacca, E.I. Franses, N.-H.L. Wang, L. Wu, H. Lee, C. Senanayake, N. Yee, N. Gonella, K. Fandrick, N. Grinberg, Insights into chromatographic enantiomeric separation of allenes on cellulose carbamate stationary phase, *J. Chromatogr. A.* 1362 (2014) 119–128. doi:10.1016/j.chroma.2014.08.032.
- [19] Y. Yamada, K. Ohyama, G. Onodera, M. Kuriyama, N. Kishikawa, N. Kuroda, Molecular-shape selectivity by naphthalimido-modified silica stationary phases: Insight into the substituents effect of naphthalene on shape recognition and π – π interactions via electrostatic potential, *J. Chromatogr. A.* 1425 (2015) 173–179. doi:10.1016/j.chroma.2015.11.030.
- [20] M.L. Reyes-Reyes, G. Roa-Morales, R. Melgar-Fernández, H. Reyes-Pérez, L.M. Gómez-Oliván, N. Gonzalez-Rivas, J. Bautista-Renedo, P. Balderas-Hernández, Chiral recognition of abacavir enantiomers by (2-hydroxy)propyl- β -cyclodextrin: UHPLC, NMR and DFT studies, *J. Incl. Phenom. Macrocycl. Chem.* 82 (2015) 373–382. doi:10.1007/s10847-015-0499-6.
- [21] S. Bocian, A. Nowaczyk, B. Buszewski, Synthesis and characterization of ester-bonded stationary phases for liquid chromatography, *Talanta.* 131 (2015) 684–692. doi:10.1016/j.talanta.2014.07.069.
- [22] J. Tomasi, B. Mennucci, R. Cammi, Quantum Mechanical Continuum Solvation Models, *Chem. Rev.* 105 (2005) 2999–3094. doi:10.1021/cr9904009.
- [23] P. Šafář, J. Žůžiová, Š. Marchalín, N. Prónayová, Ľ. Švorc, V. Vrábek, S. Šesták, D. Rendić, V. Tognetti, L. Joubert, A. Daich, Combined Chemical, Biological and Theoretical DFT-QTAIM Study of Potent Glycosidase Inhibitors Based on Quaternary Indolizinium Salts, *Eur. J. Org. Chem.* 2012 (2012) 5498–5514. doi:10.1002/ejoc.201200431.
- [24] W. Zhao, K. Hu, C. Wang, S. Liang, B. Niu, L. He, K. Lu, B. Ye, S. Zhang, New oxo-bridged calix[2]arene[2]triazine stationary phase for high performance liquid chromatography, *J. Chromatogr. A.* 1223 (2012) 72–78. doi:10.1016/j.chroma.2011.12.031.
- [25] A. Yu, D. Peng, K. Hu, A. Cao, J. Chang, Y. Wu, S. Zhang, A new 4-ferrocenylbenzoyl chloride-bonded stationary phase for high performance liquid chromatography, *J. Chromatogr. A.* 1283 (2013) 75–81. doi:10.1016/j.chroma.2013.01.090.
- [26] C. Ding, K. Qu, Y. Li, K. Hu, H. Liu, B. Ye, Y. Wu, S. Zhang, Preparation and characterization of six calixarene bonded stationary phases for high performance liquid chromatography, *J. Chromatogr. A.* 1170 (2007) 73–81. doi:10.1016/j.chroma.2007.09.036.
- [27] I.Y. Zhang, J. Wu, X. Xu, Extending the reliability and applicability of B3LYP, *Chem. Commun.* 46 (2010) 3057–3070. doi:10.1039/C000677G.
- [28] S. Grimme, A. Hansen, J.G. Brandenburg, C. Bannwarth, Dispersion-Corrected Mean-Field Electronic Structure Methods, *Chem. Rev.* 116 (2016) 5105–5154. doi:10.1021/acs.chemrev.5b00533.
- [29] F. Guégan, P. Mignon, V. Tognetti, L. Joubert, C. Morell, Dual descriptor and molecular electrostatic potential: complementary tools for the study of the coordination chemistry of ambiphilic ligands, *Phys. Chem. Chem. Phys.* 16 (2014) 15558–15569. doi:10.1039/C4CP01613K.
- [30] J.S. Murray, P. Lane, P. Politzer, Expansion of the σ -hole concept, *J. Mol. Model.* 15 (2008) 723–729. doi:10.1007/s00894-008-0386-9.
- [31] T. Clark, σ -Holes, *Wiley Interdiscip. Rev. Comput. Mol. Sci.* 3 (2013) 13–20. doi:10.1002/wcms.1113.

- [32] V. Tognetti, L. Joubert, Electron density Laplacian and halogen bonds, *Theor. Chem. Acc.* 134 (2015) 1–10. doi:10.1007/s00214-015-1685-8.
- [33] M.J. Frisch, G.W. Trucks, H.B. Schlegel, G.E. Scuseria, M.A. Robb, J.R. Cheeseman, G. Scalmani, V. Barone, B. Mennucci, G.A. Petersson, H. Nakatsuji, M. Caricato, X. Li, H.P. Hratchian, A.F. Izmaylov, J. Bloino, G. Zheng, J.L. Sonnenberg, M. Hada, M. Ehara, K. Toyota, R. Fukuda, J. Hasegawa, M. Ishida, T. Nakajima, Y. Honda, O. Kitao, H. Nakai, T. Vreven, J.A. Montgomery Jr., J.E. Peralta, F. Ogliaro, M.J. Bearpark, J. Heyd, E.N. Brothers, K.N. Kudin, V.N. Staroverov, R. Kobayashi, J. Normand, K. Raghavachari, A.P. Rendell, J.C. Burant, S.S. Iyengar, J. Tomasi, M. Cossi, N. Rega, N.J. Millam, M. Klene, J.E. Knox, J.B. Cross, V. Bakken, C. Adamo, J. Jaramillo, R. Gomperts, R.E. Stratmann, O. Yazyev, A.J. Austin, R. Cammi, C. Pomelli, J.W. Ochterski, R.L. Martin, K. Morokuma, V.G. Zakrzewski, G.A. Voth, P. Salvador, J.J. Dannenberg, S. Dapprich, A.D. Daniels, Ö. Farkas, J.B. Foresman, J.V. Ortiz, J. Cioslowski, D.J. Fox, Gaussian 09, Gaussian, Inc., Wallingford, CT, USA, 2009.
- [34] S. Grimme, Semiempirical GGA-type density functional constructed with a long-range dispersion correction, *J. Comput. Chem.* 27 (2006) 1787–1799. doi:10.1002/jcc.20495.
- [35] V. Barone, M. Cossi, Quantum Calculation of Molecular Energies and Energy Gradients in Solution by a Conductor Solvent Model, *J. Phys. Chem. A.* 102 (1998) 1995–2001. doi:10.1021/jp9716997.
- [36] P. Chen, B.A. Dougan, X. Zhang, Y.-D. Wu, Z.-L. Xue, Reactions of a tungsten alkylidyne complex with mono-dentate phosphines: Thermodynamic and theoretical studies, *Polyhedron.* 58 (2013) 30–38. doi:10.1016/j.poly.2012.07.042.
- [37] L.-A. Jouanno, V. Tognetti, L. Joubert, C. Sabot, P.-Y. Renard, Thermally Controlled Decarboxylative [4 + 2] Cycloaddition between Alkoxyoxazoles and Acrylic Acid: Expedient Access to 3-Hydroxypyridines, *Org. Lett.* 15 (2013) 2530–2533. doi:10.1021/ol4010195.
- [38] L.-A. Jouanno, V. Di Mascio, V. Tognetti, L. Joubert, C. Sabot, P.-Y. Renard, Metal-Free Decarboxylative Hetero-Diels–Alder Synthesis of 3-Hydroxypyridines: A Rapid Access to *N*-Fused Bicyclic Hydroxypiperidine Scaffolds, *J. Org. Chem.* 79 (2014) 1303–1319. doi:10.1021/jo402729a.
- [39] C.M. Breneman, K.B. Wiberg, Determining atom-centered monopoles from molecular electrostatic potentials. The need for high sampling density in formamide conformational analysis, *J. Comput. Chem.* 11 (1990) 361–373. doi:10.1002/jcc.540110311.
- [40] NCI, (n.d.). <http://www.lct.jussieu.fr/pagesperso/contrera/nciplot.html> (accessed July 19, 2016).
- [41] V. Tognetti, L. Joubert, Unraveling charge transfer processes with the quantum theory of atoms-in-molecules, *Theor. Chem. Acc.* 135 (2016) 1–13. doi:10.1007/s00214-016-1873-1.

Additionally to C18 SPs, polar embedded aromatic stationary phases have been synthesized onto FPP and SPP (Figure 1). The modified particles have been fully characterized through various and complementary physico-chemical techniques. Especially, Solid-state NMR differentiated the mono- and trifunctional structure by unambiguous identification of specific chemical shifts.

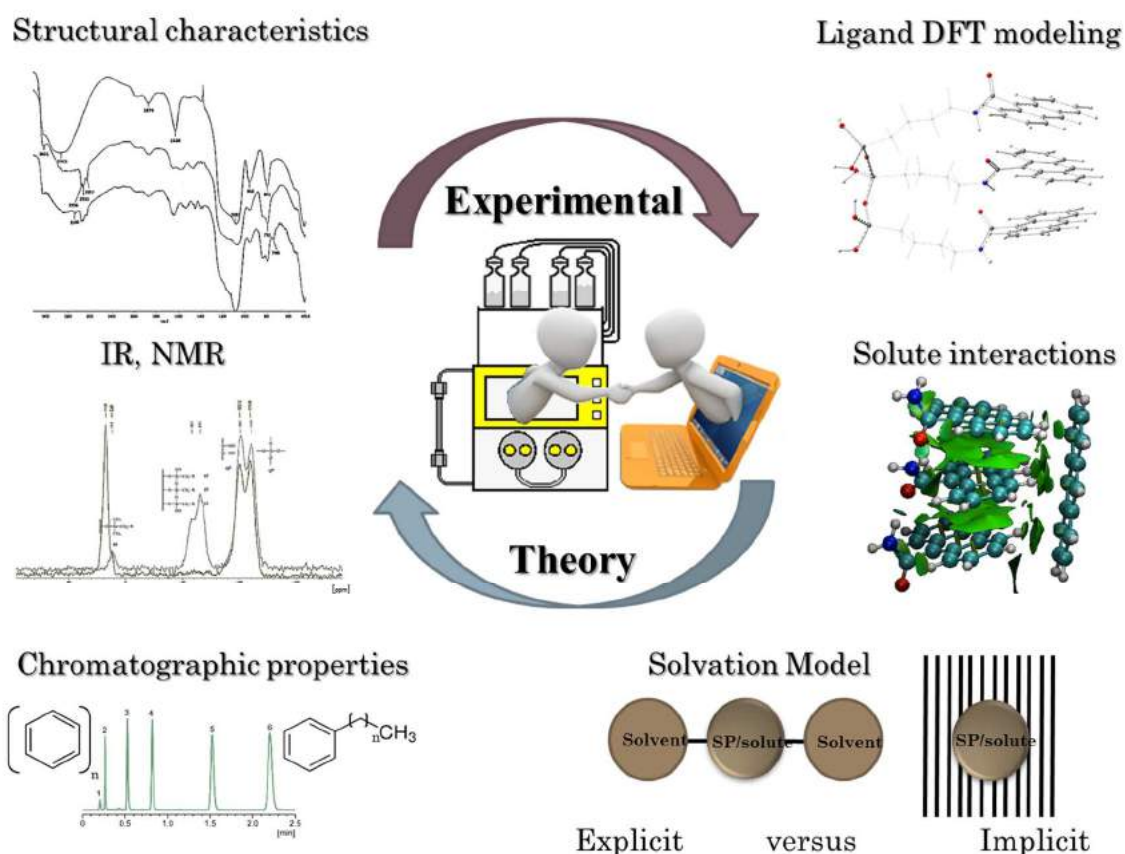


Figure 1: Schematic representation of the synthesis, characterization, and modeling of new polar embedded stationary phases

An important part of this work is dedicated to the potential of DFT to better understand the chromatographic properties of those multimodal stationary phases. A modern functional/basis set combination was used to accurately describe the structure of the trifunctional phase. The overall structure (silanol and alkyl chain and PEG and aromatic units) was considered using the ONIOM formalism and by rigorously selecting the layers. With the structure elucidated, the impact of structural modifications inside the stationary phase skeleton on the separation behavior was investigated through a parallel evaluation of the experimental data, such as the retention (k) and separation factors (α) for PAHs and alkylbenzenes. For the first time, the

experimental data coupled with the DFT results indicated that the new polar embedded aromatic stationary phases presented a particular ability to recognize aromatic solutes.

Additionally, the solvent effect was taken into account. Because of the similar constant permittivity of acetonitrile and methanol, the PCM approach could not explain the better selectivity for PAH homologues than alkylbenzenes and the enhancement of this trend when using methanol instead of acetonitrile as the organic modifier. The latter was partly solved for the largest molecules by an explicit solvation model for acetonitrile and methanol.

From a chromatographic point of view, the combination of aromatic and polar embedded groups (mono-PEG-anthra and tri-PEG-anthra) led to stationary phases with hydrophobic properties and aromatic selectivity that could be modulated by adjusting the organic modifier type. In contrast to the functionality of the ligand, which impacts the chromatographic behavior, the silica type has no influence on the thermodynamic properties.

The DFT results match the chromatographic results, providing a better understanding of the interaction mechanisms and highlighting the importance of the multimodal character of the designed stationary phases: alkyl spacers for interactions with hydrophobic solutes, amide embedded groups for dipole-dipole and hydrogen-bond interactions, and aromatic terminal groups for π - π interactions.

III-2. Calix[6]arene derivative synthesis

In a view to elaborate original stationary phases containing a cavity capable of inclusion of some solutes and/or presenting shape selectivity, we selected calix[6]arene as basic structure. The second part of my internship was achieved in the LCO laboratory, University of Brussels, under the supervision of Prof. I. Jabin for 2 months. This team is mainly focused on the synthesis and the study of new molecular receptors derived from calix[6]arenes, capable of including guest organic molecules. They worked on the rigidification of those host macrocycles to force them adopting a cone conformation that is more favorable for inclusion. Some ways have been developed, such as the formation of covalent bridges¹⁻⁹, the coordination with metals¹⁰ or by self-assembling¹¹⁻¹⁵. I had to synthesize, purify, and characterize three calix[6]arene derivatives, whose choice is explained in the following part. Firstly, a brief overview and generalities about calixarene are proposed (III.2.1). Then, the synthesis of the calix[6]arene derivatives is presented (III.2.2) with the experimental part in appendices. Then, the functionalization of SPP with two calix[6]arene derivatives and the characterization is given (III.2.3). The last part (III.2.4) gathers the results of the preliminary studies about the evaluation of the stationary phases based on those calix[6]arene derivatives.

III-2-1. Calix[n]arene derivative overview

The following section is dedicated to a brief review of the calixarene derivatives used in HPLC, with a particular focus on calix[6]arene derivatives containing a terminal carboxylic acid function. More information can be found on the recent reviews^{16,17}.

General calix[6]arene synthesis and structures are presented in Figure 2^{18,19}. Those macrocycles present a lower rim containing hydroxyl groups that can be functionalized, and an upper rim typically substituted by tert-butyl groups.

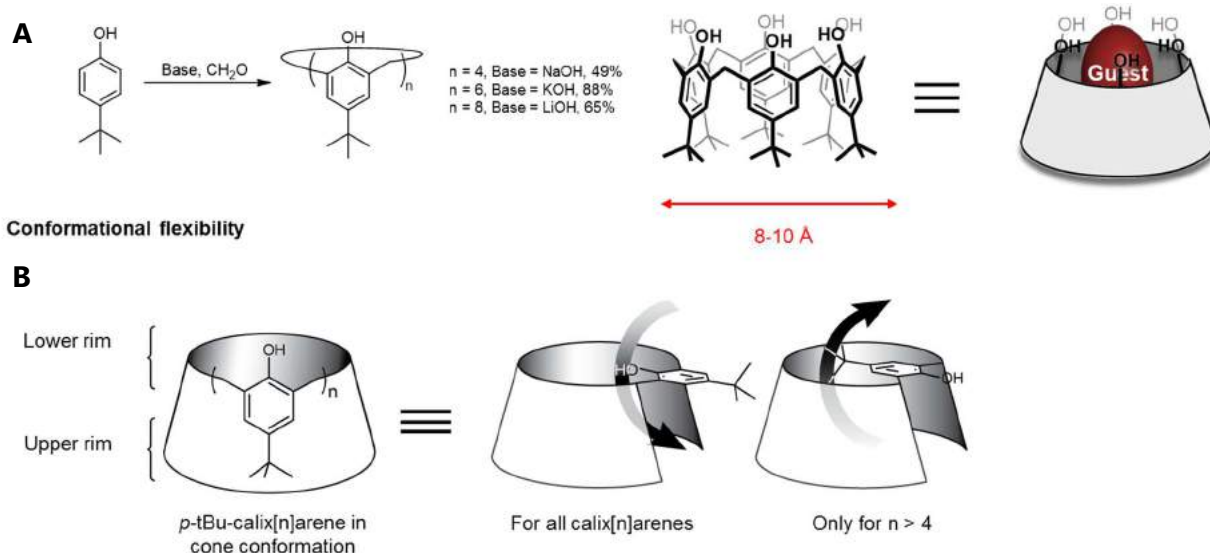
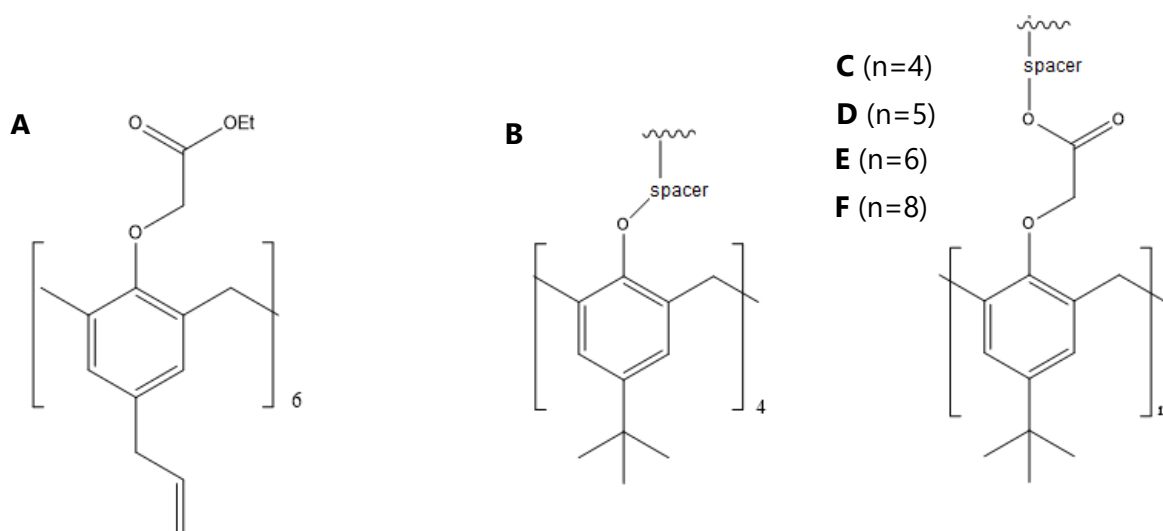


Figure 2: Synthesis of calix[n]arenes (**A**) and representation of their conformations (**B**)

Calix[6]arene derivatives have gained interest in HPLC as selectors to separate neutral and ionic solutes. The derivatives could be grafted onto the silica surface, or can be added in the mobile phase. However, as calixarenes contained many chromophore groups that interfere the solute detection under UV, they were mainly used as immobilized in the SP^{16,17}.

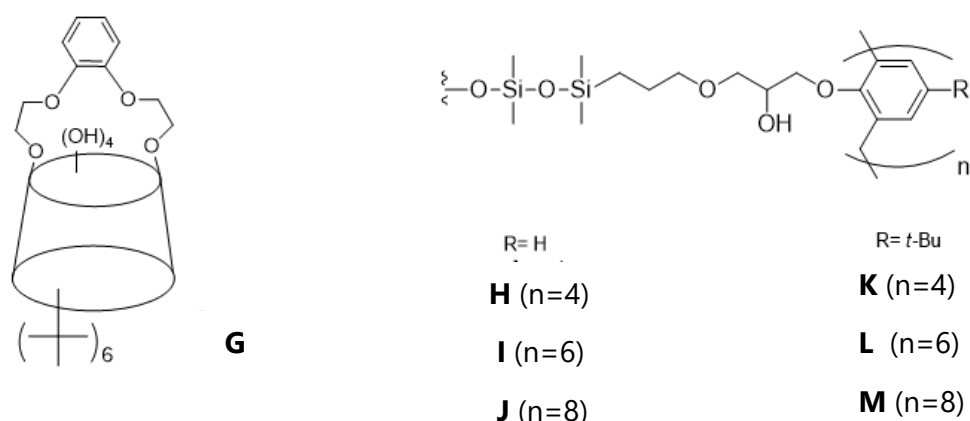
III-2-1-1. Cavity size effect

The cavity size effect has been studied in 1993 by Glennon *et al.*²⁰ The **A** compound (Figure 3) was particularly used to separate alkaline chloride salts and alkaline earth metals. Additionally, a *p*-tBu-calix[4]arene **B** derivative was used for the separation of nitroaniline regioisomers, nucleic bases, nucleosides and cis/trans proline isomers. Some similar derivatives containing carboxylic acid functions that have been attached with a spacer group (**C-F**, Figure 3), were studied for the methyluracil and oestradiol isomer separation. Those new SPs presented a reversed-phase behavior, with a selectivity dependent of the cavity size^{21,22}.

Figure 3: Representation of calixarenes **A-F**

III-2-1-2. Size effect

Another interesting feature is the impact of the structure flexibility on the recognition mechanism. In 2004, Li *et al.*²³ published the preparation and the characterization of a *p-tBu*-calix[6]arene derivative, **G** (Figure 4) grafted onto the silica surface via an epoxide terminal function. The use of crown ether allowed to decrease the flexibility of the calix[6]arene and to improve the PAHs and azo-PAHs recognition. However, the fixed conformation seemed to be unfavorable to the alkylbenzene recognition: the introduction of an ether bridge partially modified the hydrophobicity and the calixarene selectivity. In 2007, Ding *et al.*²⁴ grafted 3 derivatives of calix[n]arene **H-J** (n=4, 6, 8) and 3 derivatives of *p-tBu*-calix[n]arene **K-M** (n=4, 6, 8) onto a silica modified by an epoxide group (Figure 4). The behavior of those SPs was evaluated by the PAHs analysis, and aromatic isomers and acrylate of E- and Z-ethyl 3-(4-acetylphenyl) isomers. The mechanisms of retention were mainly π - π interactions, H-bonds and the formation of inclusion complexes.

Figure 4: Representation of calix[6]arenes **G-M**

III-2-1-3. *p*-*t*Butyl- and carboxylic acid substituted calix[6]arene derivatives

A *p*-*t*Butyl-calix[6]arene (**N**, Figure 5) derivative grafted onto the silica surface with a spacer was achieved by Xu *et al.*²⁵ in 1998. This SP allowed for improving the separation of substituted benzene regioisomers, of PAHs, and some nucleosides.

The SPs based on *p*-*t*Butyl-calix[6]arene containing carboxylic acid functions (**O**, Figure 5) presented a reversed-phase behavior. The selectivity was higher than that obtained on a C18 column, and the mechanisms include hydrophobic interactions, dipolar interactions and inclusion complex formation²⁶.

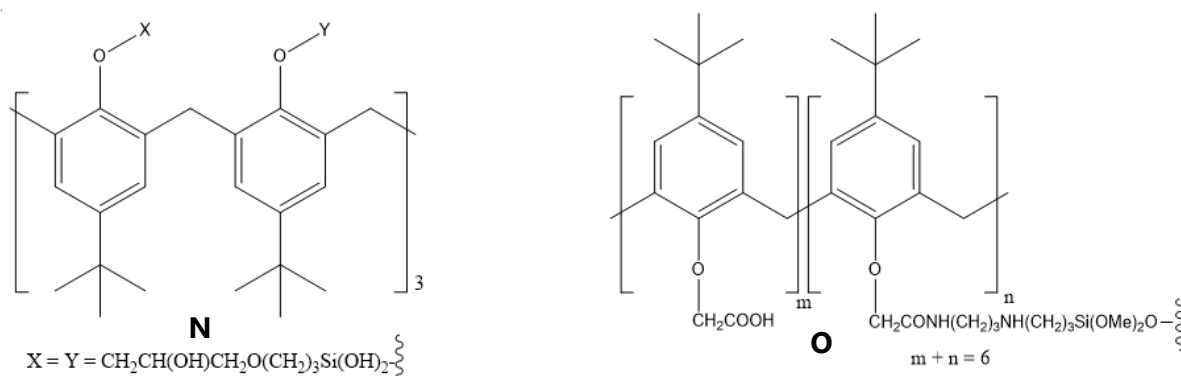


Figure 5: Representation of calixarenes **N** and **O**

III-2-1-4. Evaluation of commercial calix[*n*]arene derivatives

In order to elaborate a prediction model, Schneider and Jira²⁷ analyzed 31 solutes of various molecular structures using different mobile phase compositions. Seven commercial Caltrex® SPs were studied: 6 based on calixarenes **P-U** and the last one a non-polar C18 (Figure 6). The authors demonstrated that the retention, especially for polar compounds, depended on the organic modifier and its amount in the MP.

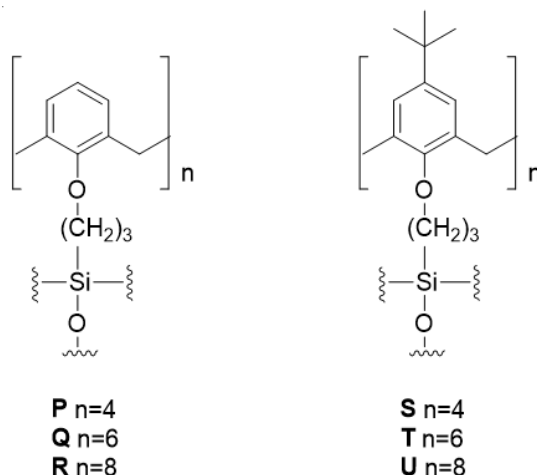


Figure 6: Representation of the Caltrex® phases

III-2-2. Calix[6]arene derivative synthesis

During the second part of my internship in the LCO laboratory, University of Brussels, under the supervision of Prof. I. Jabin, three calix[6]arene derivatives have been synthesized.

In order to better control the calixarene grafting onto silica particles, the monofunctionalization was chosen. To bring some rigidity, the starting calix[6]arene derivative contained *p*-*t*Bu functions at the upper rim. Moreover, the grafting procedure of silica particles through an amide linkage having already been developed for the synthesis of new polar embedded aromatic SPs (III.1), the same strategy was applied here. Consequently, the requirement was to have only one carboxylic acid function for the coupling with amino silica functions. Starting from the *p*-*t*Bu-calix[6]arene-tri-methyl ($X_6\text{Me}_3\text{H}_3$), three new calix[6]arene derivatives have been synthesized during this work, following the synthesis route described in Figure 7.

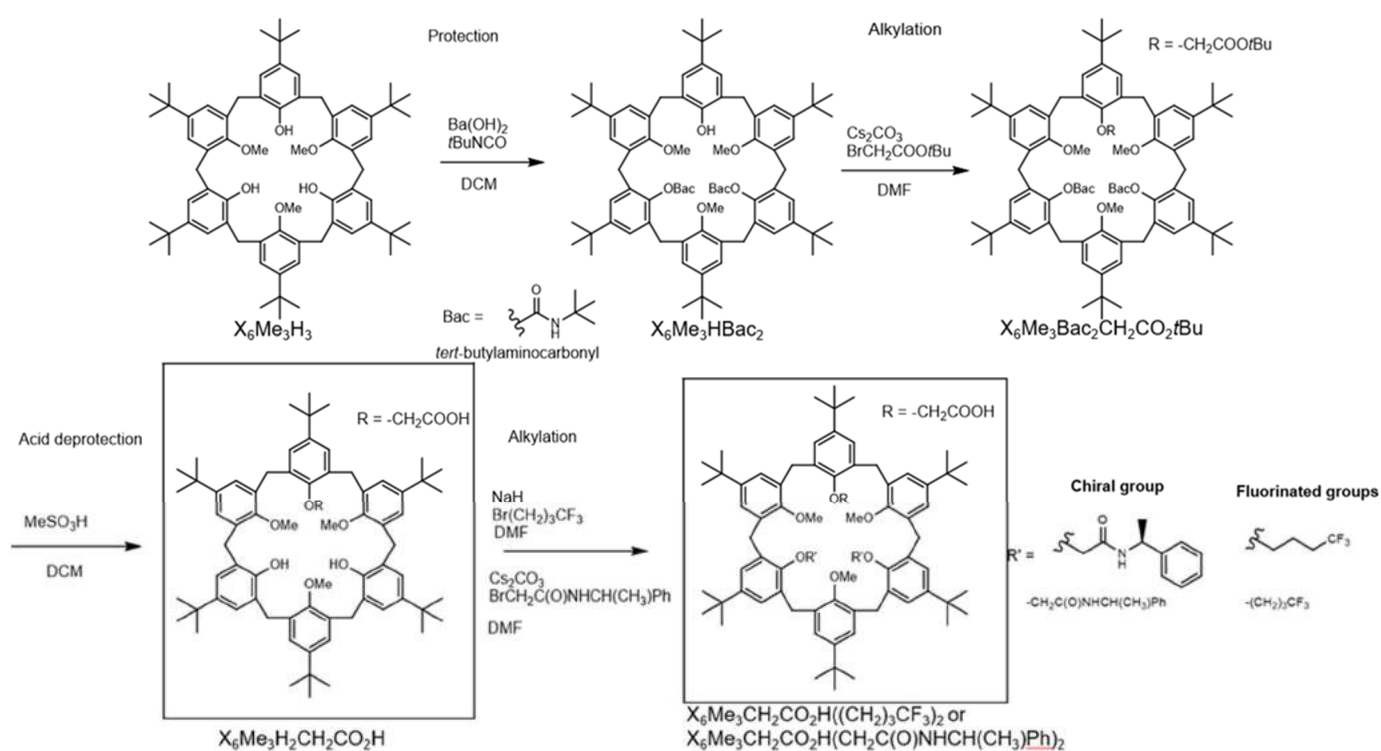


Figure 7: Synthesis route for the calix[6]arene derivatives developed during this work

The bacation procedure developed by Lavendomme *et al.*²⁸ was used to selectively functionalize the calix[6]arene in 4 steps. First, two hydroxyl groups were protected for a selective alkylation of the third one. After deprotection and hydrolysis of the ester group, three different derivatives could be obtained. The *p*-*t*Bu-calix[6]arene-mono-acid was obtained when the hydroxyl groups are non-further functionalized.

Also, two other calix[6]arene derivatives were obtained by alkylation of the two hydroxyl groups. First, the aim was to enhance the hydrophobic character without adding sterically hindered groups, so fluorinated groups were selected and led to the calix[6]arene derivative ($X_6\text{Me}_3\text{CH}_2\text{CO}_2\text{H}((\text{CH}_2)_3\text{CF}_3)_2$). Additionally, alkylation of the two hydroxyl groups with a chiral reagent containing a bromine as leaving group led to the chiral calix[6]arene derivative ($X_6\text{Me}_3\text{CH}_2\text{CO}_2\text{H}(\text{CH}_2\text{C}(\text{O})\text{NHCH}(\text{CH}_3)\text{Ph})_2$).

The characterization of the final products was achieved by NMR, HR-MS, IR and melting point measurements. The reactions were followed by NMR and MS.

The NMR spectra of such macrocycles-especially when non-symmetric structures are obtained after functionalization- can be extremely complicated. Such precise determination is out of the scope of this work, but 1D and 2D NMR (Figure 8) were used to ensure a “just enough” precision level to confirm the structure of the required final calix[6]arene derivative.

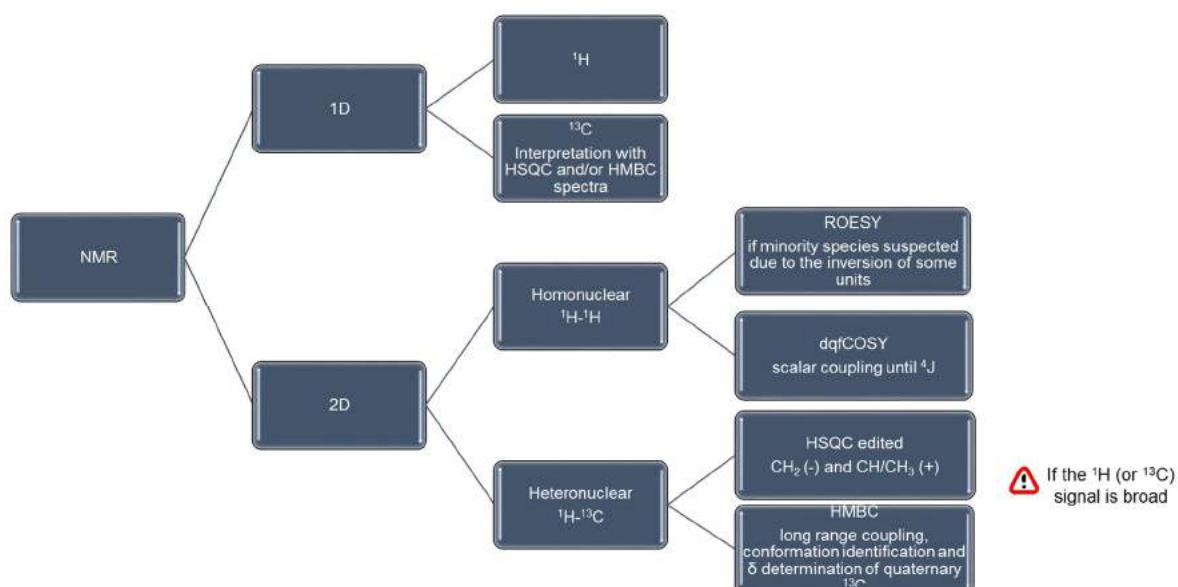


Figure 8: Scheme of the NMR strategy for the calix[6]arene derivatives structure determination

The experimental part of the syntheses is presented in Appendices.

Due to time restriction, the grafting of those derivatives onto silica particles has not yet been achieved, but the bonding of 2 calix[6]arene derivatives provided by the I. Jabin's team and possessing 6 carboxylic acid functions was achieved with Adeline Clergé during her Master 2 internship. Such study is reported on the following part.

III-2-3. Grafting rates of the calix[6]arene derivatives

The structures of the two calix[6]arene-hexa-acid derivatives grafted onto silica particles are presented in Figure 9. The calix[6]arene derivative **C** was the “flexible version” of the **A** calix[6]arene derivative. Indeed, *p*-*t*Butyl groups generate steric hindrance that limit the number of conformations. Also, **B** was taken as the “precursor” of those *p*-*t*Bu-calix[6]arene derivatives to study the cavity effect.

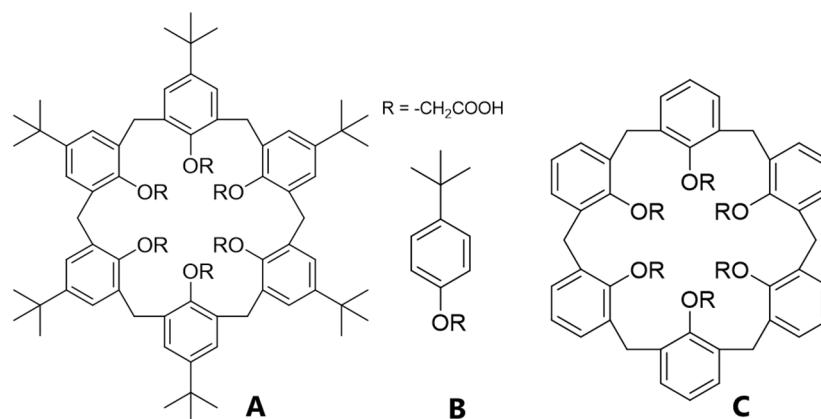


Figure 9: Structures of the *tert*-butylphenoxyacid (**B**) and of the calix[6]arene-hexa-acid derivatives (**A**, **C**)

The bonding of silica particles was achieved in 3 steps:

- Functionalization of bare silica into aminosilica with a butyl spacer group
- Coupling of the amino moieties with the acid functions of the calix[6]arene
- End-capping
-

To compare those new SPs, a C18 SP was prepared on the same silica batch, as well as a *tert*-butylphenoxyamide SP that corresponds to the basic unit of the calix[6]arenes studied (**B**, Figure 9).

The graftings were done on FPP and on SPP, excepted for the calix[6]arene derivatives due to the restricted amount of such costly final molecules. The grafting rates are presented in Table 1.

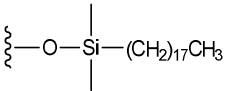
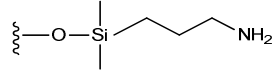
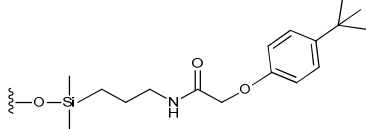
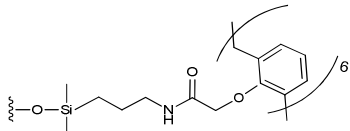
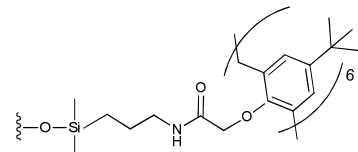
Columns	Structure	Grafting rate on FPP ($\mu\text{mol.m}^{-2}$)	Grafting rate on SPP ($\mu\text{mol.m}^{-2}$)
C18		3.8	3.3
Amino		2.6	2.9
<i>t</i>-butylphenoxyamide + End-capping		2.4	2.1
Calix[6]arene hexa-acid		-	0.7
Calix[6]arene hexa-acid <i>t</i>-Bu		-	0.5

Table 1: Grafting rates for the functionalizations achieved on FPP and SPP

It has to be noticed that the grafting rates were similar whatever the silica support (FPP or SPP) used. The grafting rates for the calixarene derivative were lower as such macromolecules can generate steric hindrance limiting the access to the amino moieties onto the silica surface. However, the grafting rates obtained were comparable to those reported in literature. For instance, in 2016 Hu *et al.*²⁹ obtained $0.56 \mu\text{mol.m}^{-2}$ for the grafting of a calix[4]arene ionic liquid derivative. Also, the grafting rate was lower for the derivative containing *t*-Butyl functions due to the steric hindrance of the *t*-Butyl groups.

III-2-4. Evaluation of stationary phases based on calix[6]arene derivatives

III-2-4-1. LSER model

To evaluate the chromatographic properties of the SPs, the Linear Solvation Energy Relationship (LSER) model was used, as presented in section (I.6.1.6). This model allowed for obtaining the contribution of the different types of interaction involved in the retention mechanisms according to Equation 1:

$$\log k = c + eE + sS + aA + bB + vV \quad \text{Equation 1}$$

E is the excess molar refraction (calculated from the refractive index of the molecule) and expresses polarizability contributions from n and p electrons; S is the solute dipolarity/polarizability; A and B are the solute overall hydrogen-bond acidity (donating ability) and basicity (accepting ability); and V is the McGowan characteristic volume. Model coefficient c is a system constant or the model intercept term.

The terms E, S, A, B, and V are solute-dependent molecular descriptors. Each descriptor is deliberately included in the LSER equation to account for a specific intermolecular interaction. Lower case letters represent the coefficients of the model or system constants, related to the complementary effect of the phases (solute, SP, MP) on these interactions.

Such analysis requires the selection of a solute range possessing various physico-chemical properties that can describe adequately the diversity of the possible interactions during the chromatographic process. It has to be noticed that the relevance of the description depends on the quality of the set probes selected to take into account all types -as possible- of interactions that can occur. Table 2 presents the LSER molecular descriptors for the 80 probes selected.

Solutes	Formula	E	S	A	B	V
Benzene	C_6H_6	0.61	0.52	0.00	0.14	0.72
Toluene	C_7H_8	0.60	0.52	0.00	0.14	0.86
Ethylbenzene	C_8H_{10}	0.61	0.51	0.00	0.15	1.00
Propylbenzene	C_9H_{12}	0.60	0.50	0.00	0.15	1.14
Butylbenzene	$C_{10}H_{14}$	0.60	0.51	0.00	0.15	1.28
Pentylbenzene	$C_{11}H_{16}$	0.60	0.51	0.00	0.15	1.42
Hexylbenzene	$C_{12}H_{18}$	0.59	0.50	0.00	0.15	1.56
Heptylbenzene	$C_{13}H_{20}$	0.58	0.48	0.00	0.15	1.70
Octylbenzene	$C_{14}H_{22}$	0.58	0.48	0.00	0.15	1.84
Nonylbenzene	$C_{15}H_{24}$	0.58	0.48	0.00	0.15	1.98
Decylbenzene	$C_{16}H_{26}$	0.58	0.47	0.00	0.15	2.13
Undecylbenzene	$C_{17}H_{28}$	0.58	0.47	0.00	0.15	2.27
Dodecylbenzene	$C_{18}H_{30}$	0.57	0.47	0.00	0.15	2.41
Cumene	C_9H_{12}	0.60	0.49	0.00	0.16	1.14
Naphthalene	$C_{10}H_8$	1.34	0.92	0.00	0.20	1.09
Aniline	C_6H_7N	0.96	0.96	0.26	0.41	0.82
N-methylaniline	C_7H_9N	0.95	0.90	0.17	0.43	0.96

<i>N,N</i>-dimethylaniline	C ₈ H ₁₁ N	0.96	0.81	0.00	0.41	1.10
Benzylamine	C ₇ H ₉ N	0.83	0.77	0.15	0.72	0.96
Pyridine	C ₅ H ₅ N	0.63	0.84	0.00	0.52	0.68
Benzamide	C ₇ H ₇ NO	0.99	1.50	0.49	0.67	0.98
<i>p</i>-toluenesulfonamide	C ₇ H ₉ NO ₂ S	1.10	1.55	0.55	0.87	1.24
Caffeine	C ₈ H ₁₀ N ₄ O ₂	1.50	1.72	0.00	1.28	1.36
Theophylline	C ₇ H ₈ N ₄ O ₂	1.50	1.60	0.54	1.34	1.22
Nicotinamide	C ₆ H ₆ N ₂ O	1.01	1.09	0.63	1.00	0.93
Carbazole	C ₁₂ H ₉ N	1.79	2.01	0.18	0.08	1.32
Quinoline	C ₉ H ₇ N	1.27	0.97	0.00	0.54	1.04
1-naphtylamine	C ₁₀ H ₉ N	1.67	1.26	0.20	0.57	1.19
<i>o</i>-toluidine	C ₇ H ₉ N	0.97	0.92	0.23	0.45	0.96
<i>p</i>-toluidine	C ₇ H ₉ N	0.92	0.95	0.23	0.45	0.96
<i>m</i>-toluidine	C ₇ H ₉ N	0.95	0.95	0.23	0.45	0.96
Benzoic acid	C ₇ H ₆ O ₂	0.73	0.90	0.59	0.40	0.93
Benzyl alcohol	C ₇ H ₈ O	0.80	0.87	0.39	0.56	0.92
Acetophenone	C ₈ H ₈ O	0.82	1.01	0.00	0.48	1.01
Nitrobenzene	C ₆ H ₅ NO ₂	0.87	1.11	0.00	0.28	0.89
Chlorobenzene	C ₆ H ₅ Cl	0.72	0.65	0.00	0.07	0.84
Benzophenone	C ₁₃ H ₁₀ O	1.45	1.50	0.00	0.50	1.48
Phenol	C ₆ H ₆ O	0.81	0.89	0.60	0.30	0.78
Resorcinol	C ₆ H ₆ O ₂	0.98	1.00	1.09	0.52	0.83
Hydroquinone	C ₆ H ₆ O ₂	1.06	1.27	1.06	0.57	0.83
Pyrogallol	C ₆ H ₆ O ₃	1.17	1.35	1.35	0.62	0.89
<i>B</i>-naphthol	C ₁₀ H ₈ O	1.52	1.08	0.61	0.40	1.14
<i>o</i>-xylene	C ₈ H ₁₀	0.66	0.56	0.00	0.16	1.00
<i>p</i>-xylene	C ₈ H ₁₀	0.61	0.52	0.00	0.16	1.00
<i>m</i>-xylene	C ₈ H ₁₀	0.62	0.52	0.00	0.16	1.00
<i>o</i>-cresol	C ₇ H ₈ O	0.84	0.86	0.52	0.30	0.92
<i>m</i>-cresol	C ₇ H ₈ O	0.82	0.88	0.57	0.34	0.92
<i>p</i>-cresol	C ₇ H ₈ O	0.82	0.87	0.57	0.31	0.92
2,4-dimethylphenol	C ₈ H ₁₀ O	0.84	0.80	0.53	0.39	1.06
2,6-dimethylphenol	C ₈ H ₁₀ O	0.86	0.79	0.39	0.39	1.06
<i>p</i>-isopropylphenol	C ₉ H ₁₂ O	0.79	0.89	0.55	0.38	1.20
<i>o</i>-chlorophenol	C ₆ H ₅ ClO	0.85	0.88	0.32	0.31	0.90

<i>m</i>-chlorophenol	C ₆ H ₅ ClO	0.91	1.06	0.69	0.15	0.90
<i>p</i>-chlorophenol	C ₆ H ₅ ClO	0.92	1.08	0.67	0.20	0.90
<i>o</i>-nitrophenol	C ₆ H ₅ NO ₃	1.02	1.05	0.05	0.37	0.95
<i>m</i>-nitrophenol	C ₆ H ₅ NO ₃	1.05	1.57	0.79	0.23	0.95
<i>p</i>-nitrophenol	C ₆ H ₅ NO ₃	1.07	1.72	0.82	0.26	0.95
Methyl benzoate	C ₈ H ₈ O ₂	0.73	0.85	0.00	0.46	1.07
Ethyl benzoate	C ₉ H ₁₀ O ₂	0.69	0.85	0.00	0.46	1.21
Propyl benzoate	C ₁₀ H ₁₂ O ₂	0.68	0.80	0.00	0.46	1.35
Butyl benzoate	C ₁₁ H ₁₄ O ₂	0.67	0.80	0.00	0.46	1.50
Methylparabene	C ₈ H ₈ O ₃	0.90	1.37	0.69	0.45	1.13
Propylparabene	C ₁₀ H ₁₂ O ₃	0.86	1.35	0.69	0.45	1.41
Biphenyle	C ₁₂ H ₁₀	1.36	0.99	0.00	0.26	1.32
Fluorene	C ₁₃ H ₁₀	1.59	1.06	0.00	0.25	1.36
Phenanthrene	C ₁₄ H ₁₀	2.06	1.29	0.00	0.29	1.45
Anthracene	C ₁₄ H ₁₀	2.29	1.34	0.00	0.28	1.45
9-methylanthracene	C ₁₅ H ₁₂	2.02	1.28	0.00	0.23	1.60
Fluoranthene	C ₁₆ H ₁₀	2.60	1.52	0.00	0.25	1.58
Triphenylene	C ₁₈ H ₁₂	2.71	1.66	0.00	0.29	1.82
<i>o</i>-terphenyl	C ₁₈ H ₁₄	2.00	1.18	0.00	0.30	1.93
<i>p</i>-terphenyl	C ₁₈ H ₁₄	2.04	1.48	0.00	0.30	1.93
Salicylic acid	C ₇ H ₆ O ₃	0.89	0.84	0.71	0.38	0.99
Paracetamol	C ₈ H ₉ NO ₂	1.06	1.63	1.04	0.86	1.17
Quinine	C ₂₀ H ₂₄ N ₂ O ₂	2.47	1.23	0.37	1.97	2.55
2-pentanone	C ₅ H ₁₀ O	0.14	0.68	0.00	0.51	0.83
3-pentanone	C ₅ H ₁₀ O	0.15	0.66	0.00	0.51	0.83
Citral	C ₁₀ H ₁₆ O	0.49	0.84	0.00	0.50	1.45
<i>B</i>-ionone	C ₁₃ H ₂₀ O	0.88	0.90	0.00	0.50	1.76
Geraniol	C ₁₀ H ₁₈ O	0.51	0.63	0.39	0.66	1.49

Table 2: LSER molecular descriptors for the 80 probes³⁰

Few studies used LSER to investigate the chromatographic properties of calixarene based SP used in HPLC. An exception is the study published in 2006³¹, in which the retention characteristics of *p*-tert-butylcalix[4]arene-bonded and three other silica-based phases have been elucidated using LSER. The retention of solutes on all the silica-based phases were dominated by two factors: the solute size and hydrogen bond acceptor basicity. But, for *p*-tert-butylcalix[4]arene-bonded phase, the main factor governing retention was the solute size.

Contrary to the common RP-SPs, the s coefficient was small but positive, as the r coefficient that traduced greater π - π interactions. In general, the LSER results and interpretations suggested that, on the for p -tert-butylcalix[4]arene-bonded phase, the retention mechanism was mainly partitioning.

To compare our SPs, the logarithm of the retention factors were represented according to the logarithm of retention factors of the C18 SP. Values grouped along the linear regression line (R^2 close to 1), indicate that the retention factors are similar on the two SPs, so that the interactions involved were of similar nature. Additionally, the slopes gave information on the interaction mechanisms involved (homogeneous vs different).

As illustrated in Figure 10, $R^2=0.8893$ and the slope is 0.4175 for the logarithms of the retention factors for the t -butylphenoxyamide and C18 SP, respectively.

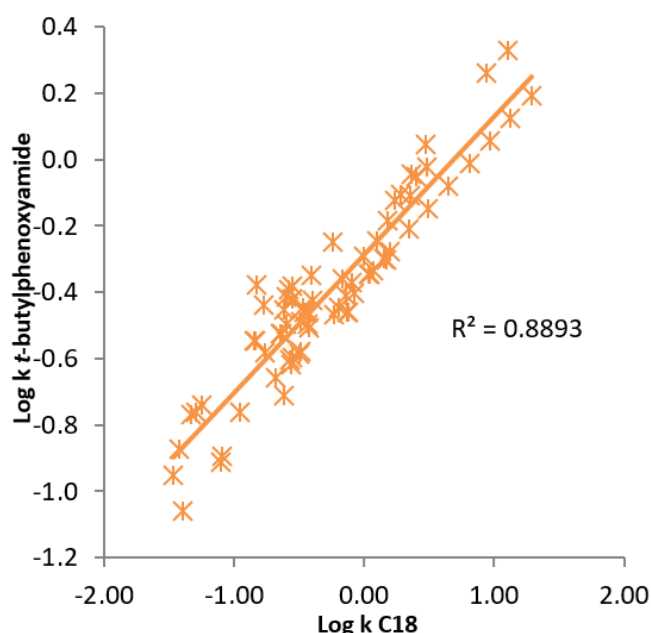


Figure 10: Representation of the correlation between the logarithms of the retention factors for the t -butylphenoxyamide and C18 columns respectively. Analytical conditions: $150 \times 2.1 \text{ mm} \times 3.0 \mu\text{m}$ (FPP), ACN/H₂O 80/20 (v/v) 0.20 mL/min, 30°C, $\lambda = 254 \text{ nm}$ or 210 nm for non-aromatic solutes.

For the calix[6]arene hexa-acid SP that did not possess t -butyl groups exhibiting hydrophobicity, the slope was lower (0.3746). Additionally, the correlation coefficient was the lowest and points were more scattered (Figure 11, **A**). On the contrary, the calix[6]arene hexa-acid t -Bu presented a behavior closer to that of the C18 SP ($R^2 = 0.8727$ and a slope of 0.4162 in Figure 11, **B**). Furthermore, the t -butyl groups generate steric hindrance that limit the number of conformations, and so modify the establishment of interactions such as the formation of inclusion complexes¹⁷ (host-guest).

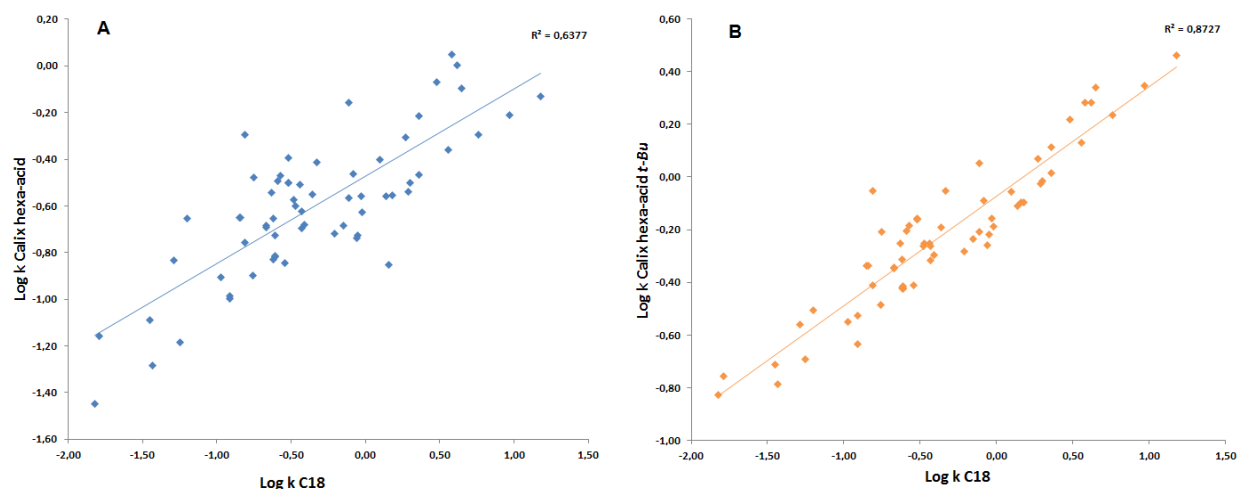


Figure 11: **(A)** Representation of the correlation between the logarithms of the retention factors for the Calix hexa-acid and C18 SP, respectively and **(B)** for the Calix hexa-acid t-Bu and C18 SP, respectively. Analytical conditions: 50 × 2.1 mm × 2.6 μm (SPP), ACN/H₂O 60/40 (v/v), 0.08 mL/min for the Calix hexa-acid and Calix hexa-acid t-Bu columns. 50 × 2.1 mm × 2.6 μm (SPP), ACN/H₂O 80/20 (v/v), 0.08 mL/min for C18 column, 30°C, λ = 254 nm or 210 nm for non-aromatic solutes.

Additionally, West *et al.*³⁰ identified flexibility and globularity as two important properties for enantioselective chromatography, which were not included in the Abraham descriptors E, S, A, B and V. Flexibility is important for chiral resolution because flexible molecules have more conformers, thus more ways for intermolecular interactions. Globularity can be related to steric constraints to insertion into the SP. For that purpose, they added two terms, f and g, to take into account flexibility and globularity.

As calixarenes are macrocycles possessing a cavity, we also used the extensive model proposed³⁰ without significant improvements of the retention description. Consequently, only the Abraham terms are presented in Table 3.

Stationary Phase	c	e	s	a	b	v	n	R ² _{adj}	F	Pr > F
C18	-0.552 <i>0.119</i>	0.285 <i>0.088</i>	-0.687 <i>0.129</i>	-0.406 <i>0.104</i>	-0.672 <i>0.100</i>	0.861 <i>0.078</i>	77	0.864	97.25	< 0.0001
t-butylphenoxyamide	-0.684 <i>0.047</i>	0.114 <i>0.036</i>	-0.136 <i>0.055</i>	0.035 <i>0.039</i>	-0.656 <i>0.050</i>	0.451 <i>0.031</i>	76	0.901	138.21	< 0.0001
Calix hexa-acid	-1.063 <i>0.051</i>	0.201 <i>0.039</i>	-0.020 <i>0.059</i>	0.096 <i>0.043</i>	-0.953 <i>0.054</i>	0.559 <i>0.033</i>	74	0.931	196.86	< 0.0001
Calix hexa-acid t-Bu	-0.658 <i>0.051</i>	0.076 <i>0.038</i>	-0.129 <i>0.058</i>	0.029 <i>0.043</i>	-0.796 <i>0.053</i>	0.719 <i>0.033</i>	73	0.943	240.45	< 0.0001

Table 3: Coefficients values obtained for the LSER model of each stationary phase, with n the number of solutes, R²_{adj} the adjusted correlation coefficients, F the statistics of the Fisher test, Pr > F the probability for the Fisher test and the italic values the confidence limits at 95%.

An adjusted coefficient value R^2_{adj} close to 1 showed that the different coefficients bring a significant contribution to the model. In this study, the values ranged from 0.864 to 0.943, validating the choice of solutes. This was also confirmed by the Fisher test, as the probabilities associated to each F were lower than 0.0001, meaning that the probability to be wrong was inferior to 0.01%.

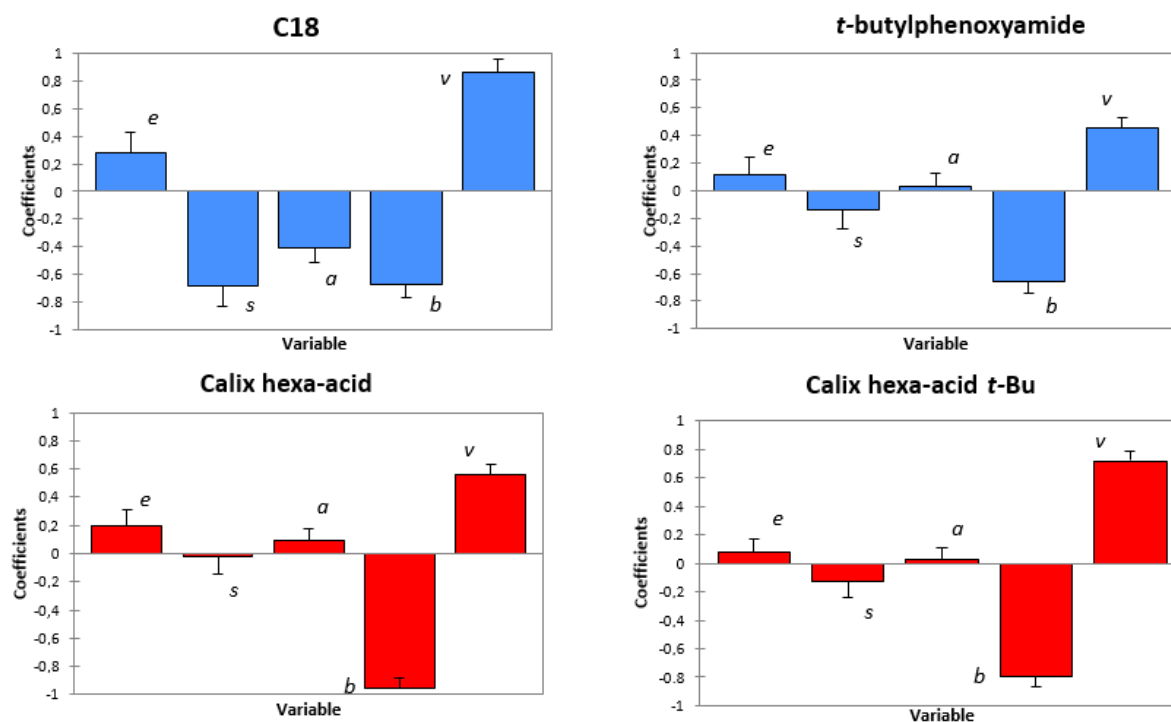


Figure 12: Representation of the system constants from the multiple linear regression of Equation 1. Analytical conditions: $50 \times 2.1 \text{ mm} \times 2.6 \mu\text{m}$ (SPP), ACN/H₂O 60/40 (v/v) for the Calix hexa-acid and Calix hexa-acid t-Bu columns, 0.08 mL/min, 30°C, 254 nm or 210 nm for non aromatic solutes. $150 \times 2.1 \text{ mm} \times 3.0 \mu\text{m}$ (FPP) ACN/H₂O 80/20 (v/v) for C18 column and the t-butylphenoxyamide column, 0.20 mL/min, 30°C, 254 nm or 210 nm for non-aromatic solutes.

Each coefficient represents the difference, for a specific type of interaction, between the solute-SP interactions and solute-MP interactions. A coefficient close to 0 signifies that the interaction with the solute is of the same order as the SP-MP interactions.

In general, b and v were the most important coefficients, which is consistent with the chemical nature of the SPs. Also, in RPLC the mobile phase is more polar than the stationary phase. The b coefficient was negative for all the SPs suggesting a better ability of the MP to elaborate hydrogen bonds than the SP (Figure 12).

Conversely, the v coefficient relating the hydrophobic selectivity was positive for all the SPs, meaning that the interactions solute-SP were stronger than those SP-MP. So, the higher v value was obtained for the C18 SP. Also, the calix hexa-acid t-Bu containing t-butyl groups that reinforces its hydrophobic character, the v coefficient was higher than for the calix hexa-acid.

However, this value was lower for the SPs containing an amide group because it favored the incorporation of solvent molecules and decreased the hydrophobicity of the SPs. Therefore, the formation of cavity became more complicated and lead to a decrease of the v term³². The a coefficient was important only for the C18 SP. This negative value indicates that the SP does not interact via hydrogen-bonds for acidic solutes, which is consistent with the nature of the SP. The negative sign signifies that the polar solutes interact preferentially with the MP that is more polarizable than the SP. Also, the C18 SP is the less polarizable than the 3 others. Finally, the e coefficient was positive but less significant for all the SPs. However, this value was lower for the SPs that contained aromatic cycles, which can be due to acetonitrile adsorption that decreased the specific π - π interactions.

III-2-4-2. Symmetry evaluation

To evaluate the ability of the different SPs to provide thin and gaussian peaks, the symmetry factors were calculated according to Equation 2³³ and are gathered in Table 4 and represented in Figure 13.

$$d(TF; 1) = \sqrt{\sigma_{TF}^2 + (\overline{TF} - 1)^2} \quad \text{Equation 2}$$

With \overline{TF} , the average symmetry factors and σ_{TF} , the standard deviation of the symmetry factors average.

The parameter $d(TF;1)$ takes into account the gap existing between the tailing factor of each compound from the studied set and the perfect symmetry (value 1). The lower this value, the more satisfying the stationary phase is. With this parameter, a classification of stationary phases according to their symmetry factor can be made.

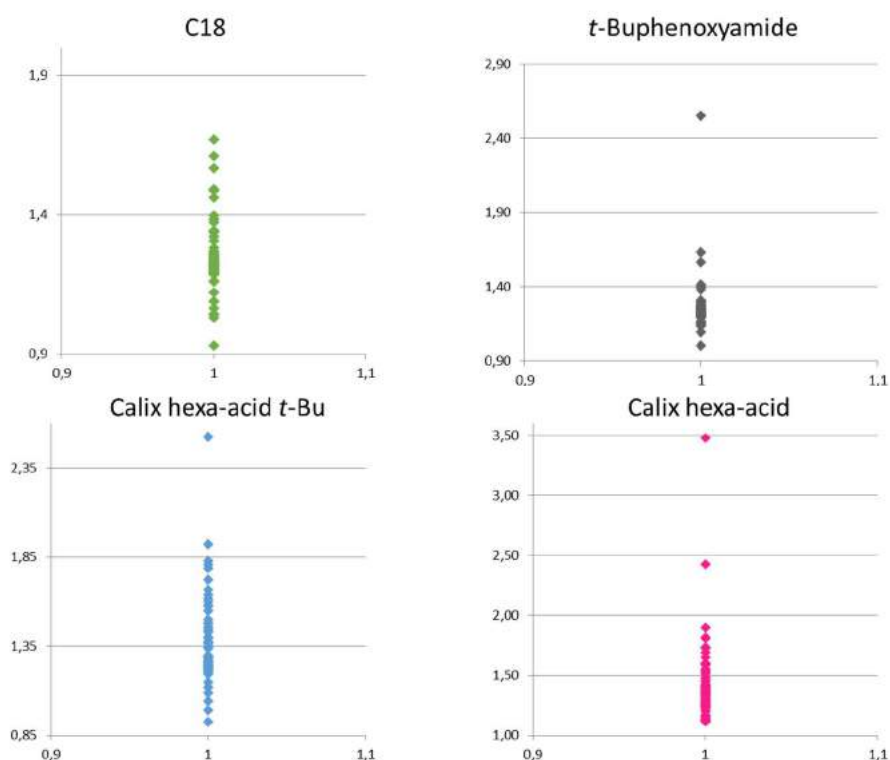


Figure 13: Scattergrams of the different SPs

Stationary phase	\overline{TF}	σ_{TF}	d(TF;1)
C18	1.221	0.186	0.289
<i>t</i> -butylphenoxyamide	1.261	0.177	0.316
Calix hexa-acid	1.429	0.327	0.540
Calix hexa-acid <i>t</i> -Bu	1.370	0.244	0.441

Table 4: Symmetry parameters of the studied columns. Analytical conditions: $50 \times 2.1 \text{ mm} \times 2.6 \mu\text{m}$ (SPP), ACN/H₂O 60/40 (v/v) the Calix hexa-acid and Calix hexa-acid *t*-Bu columns, 0.08 mL/min, 30°C, 254 nm or 210 nm for non-aromatic solutes. $150 \times 2.1 \text{ mm} \times 3.0 \mu\text{m}$ (FPP) ACN/H₂O 80/20 (v/v) for C18 column and the *t*-butylphenoxyamide column, 0.20 mL/min, 30°C, 254 nm or 210 nm for non-aromatic solutes.

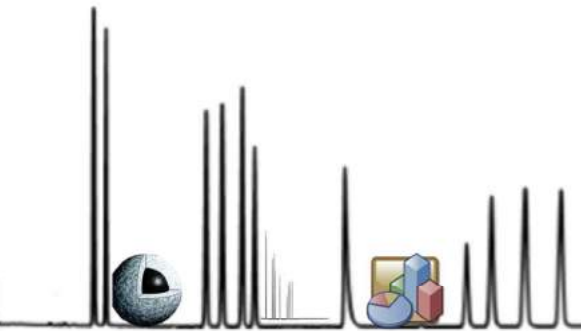
The C18 and *t*-butylphenoxyamide SPs presented the best average symmetry factors. Higher values (around 1.4) were obtained for the calixarene based SPs, due to adsorption phenomena causing peak tailing. The latter being attributed to hydrogen bond interactions between the polar solutes and residual silanols and /or acid functions of the selector and/or ion interactions depending the pH with amino functions. Especially, the most important distortions (tailing peaks) were noticed for bases such as aniline derivatives, or solutes such as pyrogallol that contain hydroxyl groups.

It has to be noticed that the calix[6]arene derivatives grafted here onto aminosilica particles contained six carboxylic acid functions. No univocal analysis allowed for a precise

determination of the number of linkage point to aminosilica per calixarene unit. Consequently, several carboxylic acid units must be free and depending on the pH, ion exchange with the basic solutes can occur. The pH effect has not been studied yet, but is one of the prospects of this study.

III-3. References

- (1) Jabin, I.; Reinaud, O. *J. Org. Chem.* **2003**, *68* (9), 3416–3419.
- (2) Darbost, U.; Giorgi, M.; Reinaud, O.; Jabin, I. *J. Org. Chem.* **2004**, *69* (15), 4879–4884.
- (3) Zeng, X.; Hucher, N.; Reinaud, O.; Jabin, I. *J. Org. Chem.* **2004**, *69* (20), 6886–6889.
- (4) Garrier, E.; Gac, S. L.; Jabin, I. *Tetrahedron Asymmetry* **2005**, *16* (23), 3767–3771.
- (5) Le Gac, S.; Zeng, X.; Reinaud, O.; Jabin, I. *J. Org. Chem.* **2005**, *70* (4), 1204–1210.
- (6) Zeng, X.; Coquière, D.; Alenda, A.; Garrier, E.; Prangé, T.; Li, Y.; Reinaud, O.; Jabin, I. *Chem. – Eur. J.* **2006**, *12* (24), 6393–6402.
- (7) Le Gac, S.; Zeng, X.; Girardot, C.; Jabin, I. *J. Org. Chem.* **2006**, *71* (24), 9233–9236.
- (8) Ménand, M.; Jabin, I. *Org. Lett.* **2009**, *11* (3), 673–676.
- (9) Lascaux, A.; Gac, S. L.; Wouters, J.; Luhmer, M.; Jabin, I. *Org. Biomol. Chem.* **2010**, *8* (20), 4607–4616.
- (10) Hamon, M.; Ménand, M.; Le Gac, S.; Luhmer, M.; Dalla, V.; Jabin, I. *J. Org. Chem.* **2008**, *73* (18), 7067–7071.
- (11) Darbost, U.; Giorgi, M.; Hucher, N.; * I. J.; * O. R. *Supramol. Chem.* **2005**, *17* (3), 243–250.
- (12) Darbost, U.; Zeng, X.; Giorgi, M.; Jabin, I. *J. Org. Chem.* **2005**, *70* (25), 10552–10560.
- (13) Le Gac, S.; Marrot, J.; Reinaud, O.; Jabin, I. *Angew. Chem. Int. Ed.* **2006**, *45* (19), 3123–3126.
- (14) Le Gac, S.; Luhmer, M.; Reinaud, O.; Jabin, I. *Tetrahedron* **2007**, *63* (44), 10721–10730.
- (15) Gac, S. L.; Picron, J.-F.; Reinaud, O.; Jabin, I. *Org. Biomol. Chem.* **2011**, *9* (7), 2387–2396.
- (16) Mokhtari, B.; Pourabdollah, K.; Dalali, N. *J. Incl. Phenom. Macrocycl. Chem.* **2010**, *69* (1–2), 1–55.
- (17) Delahousse, G.; Lavendomme, R.; Jabin, I.; Peulon-Agasse, V.; Cardinael, P. *Curr. Org. Chem.* **2016**, 2237–2249.
- (18) Gutsche, C. D. *Calixarene revisited*, Royal Society of Chemistry.; Cambridge, 1998.
- (19) Gutsche, C. D.; Dhawan, B.; No, K. H.; Muthukrishnan, R. *J. Am. Chem. Soc.* **1981**, *103* (13), 3782–3792.
- (20) Glennon, J. D.; O'Connor, K.; Srijaranai, S.; Manley, K.; Harris, S. J.; McKervey, M. A. *Anal. Lett.* **1993**, *26* (1), 153–162.
- (21) Gebauer, S.; Friebe, S.; Gübitz, G.; Krauss, G.-J. *J. Chromatogr. Sci.* **1998**, *36* (8), 383–387.
- (22) Gebauer, S.; Friebe, S.; Scherer, G.; Gübitz, G.; Krauss, G.-J. *J. Chromatogr. Sci.* **1998**, *36* (8), 388–394.
- (23) Li, L.-S.; Da, S.-L.; Feng, Y.-Q.; Liu, M. *J. Chromatogr. A* **2004**, *1040* (1), 53–61.
- (24) Ding, C.; Qu, K.; Li, Y.; Hu, K.; Liu, H.; Ye, B.; Wu, Y.; Zhang, S. *J. Chromatogr. A* **2007**, *1170* (1–2), 73–81.
- (25) Xu, W.; Li, J.-S.; Feng, Y.-Q.; Da, S.-L.; Chen, Y.-Y.; Xiao, X.-Z. *Chromatographia* **48** (3–4), 245–250.
- (26) Xiao, Y.-X.; Xiao, X.-Z.; Feng, Y.-Q.; Wang, Z.-H.; Da, S.-L. *Talanta* **2002**, *56* (6), 1141–1151.
- (27) Schneider, C.; Jira, T. *J. Chromatogr. A* **2009**, *1216* (35), 6285–6294.
- (28) Lavendomme, R.; Zahim, S.; De Leener, G.; Inthasot, A.; Mattiuzzi, A.; Luhmer, M.; Reinaud, O.; Jabin, I. *Asian J. Org. Chem.* **2015**, *4* (8), 710–722.
- (29) Hu, K.; Zhang, W.; Yang, H.; Cui, Y.; Zhang, J.; Zhao, W.; Yu, A.; Zhang, S. *Talanta* **2016**, *152*, 392–400.
- (30) West, C.; Zhang, Y.; Morin-Allory, L. *J. Chromatogr. A* **2011**, *1218* (15), 2019–2032.
- (31) Huai, Q. Y.; Zuo, Y. M. *J. Liq. Chromatogr. Relat. Technol.* **2006**, *29* (6), 801–814.
- (32) Vitha, M.; Carr, P. W. *J. Chromatogr. A* **2006**, *1126* (1–2), 143–194.
- (33) Bonose-Crosnier de Bellaistre, M.; Nowik, W.; Tchaplá, A.; Héron, S.; *J. Chromatogr. A* **2011**, *1218*, 778–786.

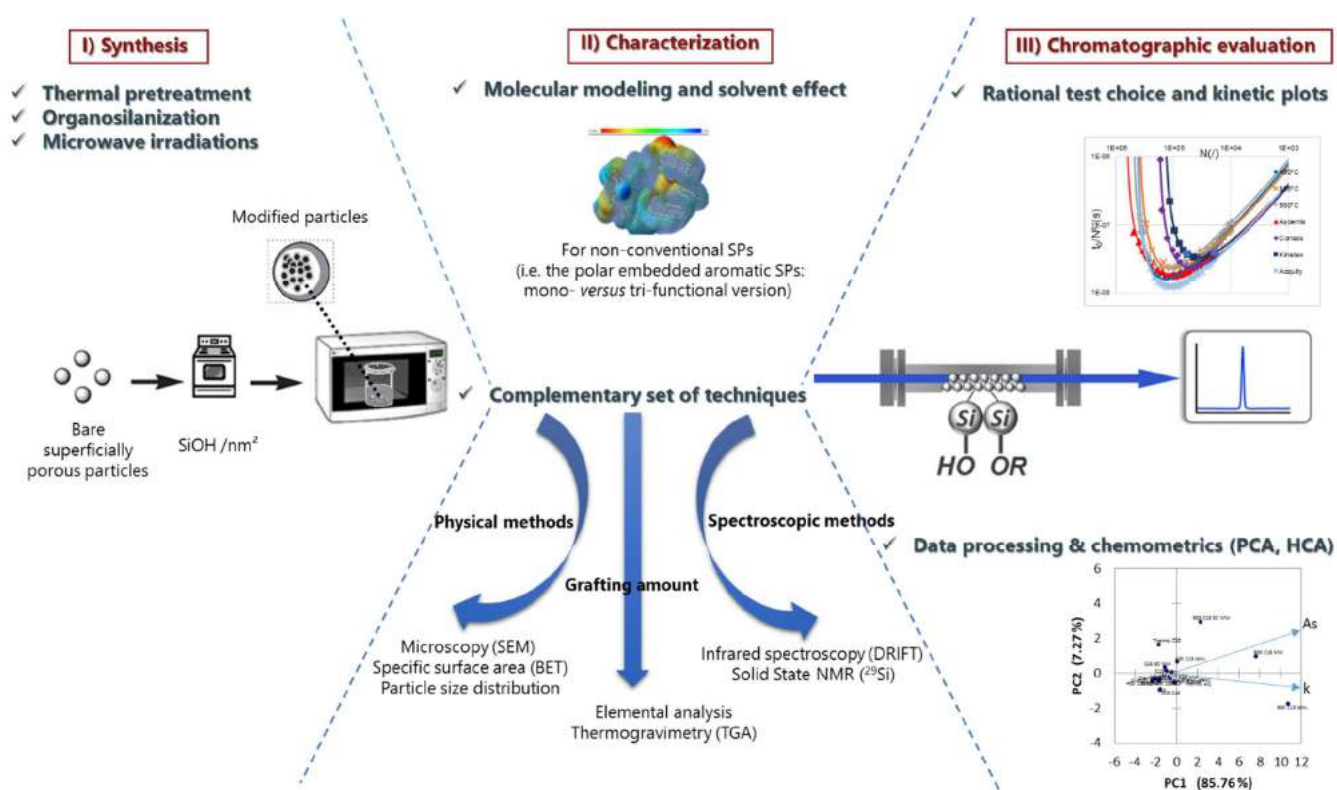


Conclusion
&
prospects



The final purpose of this thesis was to develop a wide range of SPs covering a wide panel of selectivity. These various SPs are presently used with promising results and original selectivity in the analysis of various matrices in the field of healthcare (doping issue, Hospital of Geneva), of environment (analysis of polycyclic aromatic hydrocarbons) and of heritage (Collaboration with the Centre de Recherche et de Restauration des Musées de France on the anthraquinone derivatives analysis).

This research work was articulated around three main topics summarized in the representation below: the pretreatment and the functionalization of the superficially porous particles, the complete characterization of the modified silicas by a complementary set of techniques, and finally the performance evaluation of the packed columns. Especially, the kinetic performances were evaluated by use of the kinetic plots and various tests were used to study the retention mechanisms and the interactions involved during the chromatographic process, depending on the type of Stationary Phase (SP).



Summary of the development and the evaluation of the stationary phases

The first part of this work was devoted to the development of a fast, robust, and efficient grafting method on superficially porous particles. Organosilanization under microwave irradiations allowed to obtain stationary phases exhibiting as good chromatographic performances as those prepared under the conventional synthetic process, but ten times faster (Article 1 (II.1.1)).

After having adjusted the experimental protocol of C18 grafting, we demonstrated that different C18 stationary phases can be obtained from the same silica batch, functionalized with the same grafting procedure, by adjusting the pretreatment temperature (Article 2 (II.2.1)). Chemometric approaches such as HCA were considered to group the columns by family and to make a comparison between the home-made SPs and the commercial ones. In particular, the specific behavior of the C18-900°C pretreated phase was highlighted in Article 3 (II.2.2) for the resolution of PAHs isomers.

Another set of columns for HILIC mode was obtained only by adjusting the pretreatment temperature of silica (400, 525, and 900°C). The kinetic performances by means of kinetic plots, and the thermodynamic properties of the three novel columns were evaluated during an internship with Prof. Jean-Luc Veuthey and Dr. Davy Guillarme, LCAP, Université de Genève, and led to Article 4 (II.2.3).

In addition to C18 and HILIC SPs, two new polar embedded stationary phases were synthesized and solid state NMR allowed to differentiate the mono- from the trifunctional structures by unambiguous identification of the specific chemical shifts (Article 5 (III.1)). The collaboration with the quantum chemist Dr. V. Tognetti allowed for modeling the overall structure (silanol + alkyl chain + PEG + aromatic units) with a modern functional/basis set combination and considering the solvent effect.

In view of obtaining shape selectivity SPs, original ligands based on calix[6]arene derivatives have been synthesized during the second part of the internship with Prof. Ivan Jabin, LCO, Université Libre de Bruxelles (III.2). Each one was fully characterized by NMR, mass spectrometry, and infrared spectroscopy. Those macrocycles contain one carboxylic acid function that allows for grafting onto SPPs.

As a perspective, the complete study of the chromatographic properties of the SPs based on calix[6]arene derivatives possessing only one acidic function has to be performed. As the three derivatives synthesized during my internship (*p*-*t*Bu-calix[6]arene-tri-methyl-mono-acid, *p*-*t*Bu-calix[6]arene-di(propyltrifluoromethyl)tri-methyl-mono-acid and *p*-*t*Bu-calix[6]arene-di(chiral substituent)-tri-methyl-mono-acid) are available at the hundred milligram scale, it is necessary to develop capillary column (150 × 0.3 mm) packing.

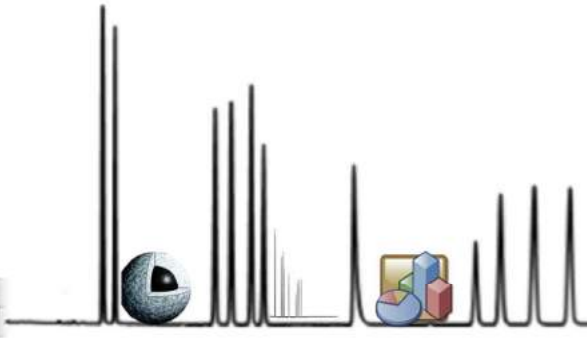
Having a comprehensive view of the functionalization of SPP, we could now envisage to graft simultaneously two ligands to obtain mixed-mode phases. Those SPs and the original ones

developed during my thesis could improve the separation of biomolecules, or be used in a second dimension for comprehensive 2D-LC.

Last but not least, it seemed important for me to add my personal conclusion as a part of the final conclusion, because work is not only theoretical and fundamental research, but also social and personal meetings around it. I've been largely involved in the various aspects of my project because my supervisors let me solve scientific issues, tune it in new ways, and present the results in different congresses. I finally consider my thesis as a multimodal challenge: doing a PhD is managing a project, dealing with the unknown and the complexity, and adapting itself. It is also supervising trainees, setting up collaborations, and developing complicity with colleagues, which finally make days at lab' good days.

But my PhD also upset a part of my personal life, and maybe the first knowledge was about myself.

Because long walks start with one step.



Appendices

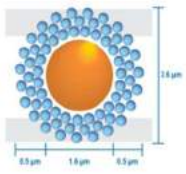


1. Collaborations

1.1 Interchim R&D

One part of this thesis was achieved in collaboration with Interchim R&D.

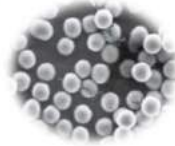
They developed a wide range of stationary phases that allow for working in different HPLC modes: RP, HILIC, and Aqueous Normal Phase (Figure 1).



Uptisphere® CS Evolution™ 2.6µm

Mono-disperse superficially porous silica particles

Identification & Quantification, efficient & fast,
of small molecules of (U)HPLC



Maximum Operational Surface Technology (MOST)

$\begin{array}{c} \text{CH}_3 \\ \\ \text{O}-\text{Si}-\text{CH}_3 \\ \\ \text{CH}_3 \\ \\ \text{O}-\text{Si}-\text{C}_{18}\text{H}_{37} \\ \\ \text{CH}_3 \end{array}$	<p style="text-align: center;">C18-HB Selectivity — Uptisphere® CS Evolution™ — Capacity Productivity</p>	$\begin{array}{c} \text{P} \\ \\ \text{O} \\ \\ \text{OH} \\ \\ \text{CH}_3 \\ \\ \text{O}-\text{Si}-\text{C}_{18}\text{H}_{37} \\ \\ \text{CH}_3 \end{array}$	<p style="text-align: center;">C18-AQ Selectivity — Uptisphere® CS Evolution™ — Capacity Productivity</p>
$\begin{array}{c} \text{CH}_3 \\ \\ \text{O}-\text{Si}-\text{CH}_3 \\ \\ \text{CH}_3 \\ \\ \text{OH} \\ \\ \text{O}-\text{Si}-\text{C}_{18}\text{H}_{37} \\ \\ \text{CH}_3 \end{array}$	<p style="text-align: center;">C18 Selectivity — Uptisphere® CS Evolution™ — Capacity Productivity</p>	$\begin{array}{c} \text{O} \\ \diagup \quad \diagdown \\ \text{R} \\ \\ \text{O} \\ \\ \text{O}-\text{Si}-\text{C}_{18}\text{H}_{37} \\ \\ \text{CH}_3 \end{array}$	<p style="text-align: center;">C18-RP Selectivity — Uptisphere® CS Evolution™ — Capacity Productivity</p>
$\begin{array}{c} \text{CH}_3 \\ \\ \text{O}-\text{Si}-\text{CH}_3 \\ \\ \text{OH} \\ \\ \text{O}-\text{Si}-\text{C}_{18}\text{H}_{37} \\ \\ \text{CH}_3 \end{array}$	<p style="text-align: center;">Hilic-HIT Selectivity — Uptisphere® CS Evolution™ — Capacity Productivity</p>	$\begin{array}{c} \text{CH}_3 \\ \\ \text{O}-\text{Si}-\text{C}_{18}\text{H}_{37} \\ \\ \text{CH}_3 \\ \\ \text{OH} \\ \\ \text{O}-\text{Si}-\text{CH}_2-\text{CH}_2-\text{O}-\text{P}(=\text{O})(\text{O}^-)-\text{O}^- \end{array}$	<p style="text-align: center;">RP/SCX Selectivity — Uptisphere® CS Evolution™ — Capacity Productivity</p>
$\begin{array}{c} \text{O}-\text{H} \\ \\ \text{O}-\text{H} \end{array}$	<p style="text-align: center;">MVP Selectivity — Uptisphere® CS Evolution™ — Capacity Productivity</p>	$\begin{array}{c} \text{OH} \\ \\ \text{O}-\text{Si}-\text{CH}_2-\text{CH}_2-\text{P}(=\text{O})(\text{O}^-)-\text{O}^- \end{array}$	<p style="text-align: center;">MVP Selectivity — Uptisphere® CS Evolution™ — Capacity Productivity</p>

Interchim – 211 bis Av. J.F.Kennedy – BP1140 – BPO3103 Montluçon Cedex – Tel 33(0)4 70 03 88 55 – Fax 33(0)4 70 03 82 60 – interchim@interchim.com – ITM-2015/09/19-C/P




Figure 1: Page of the Interchim commercial book

1.2. Application note for PerkinElmer

The application note is presented as submitted to PerkinElmer. The aim was here to help the consumer in choosing a column adapted to its need.

Insights in column selection and characterization

The main goal of this paper is to guide the scientists through the development of their methods, whether when changing a column for a similar one from another supplier or when looking for a column with another selectivity.

The first part reports the fundamentals of chromatography, explaining why selectivity is a key parameter. Followed by the physical properties of the columns (dimensions, pore/particle sizes...) and the chemistries available, with a focus on the C18 stationary phases. Finally, as there is no universal test to deal with the chromatographic properties, an overview of the most common tests is furnished. Indeed, the same denomination can hide non-equivalent stationary phases as different pre- or/and post-treatments may have been done, affecting the chromatographic properties of the stationary phases.

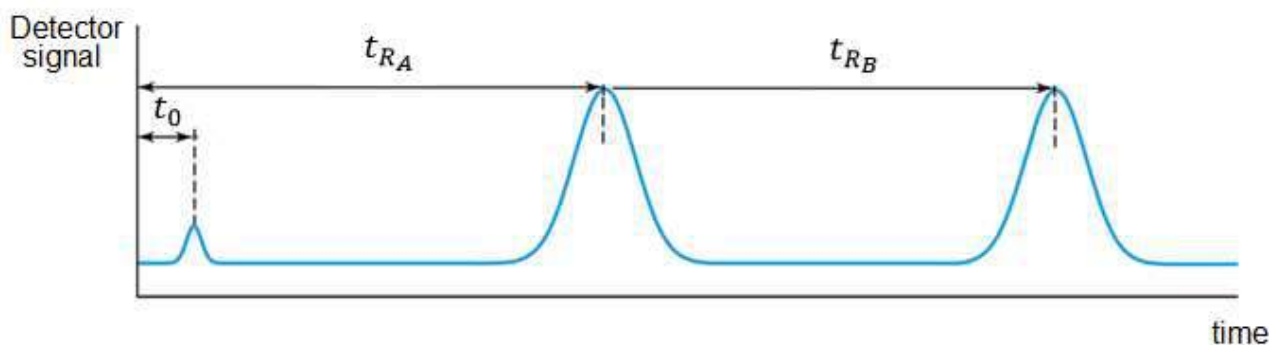
Chromatography fundamentals

- Retention factor

The retention factor (k) described in Equation 1 is a thermodynamic parameter, independent of some key variable factors including flow rate variations and column dimensions. Because of this, it is a useful parameter when comparing the retention of various solutes obtained using different HPLC systems in isocratic mode.

$$k_A = \frac{t_{R_A} - t_0}{t_0} \quad \text{Equation 1}$$

With t_{R_A} the retention time of the analyte A, and t_0 the dead time.



Chromatographers like keeping retention factor values between 2 and 10 for optimized separations. The most effective and convenient way to alter the retention factor is to adjust the solvent strength of the mobile phase, typically modifying the amount of organic solvent in the mobile phase mixture.

- Selectivity factor

The selectivity factor (α) described in Equation 2 is another thermodynamic parameter, and corresponds to the ability of the chromatographic system to distinguish two successive eluted components.

$$\alpha_{A,B} = \frac{k_B}{k_A} \quad \text{Equation 2}$$

The selectivity starts at one for co-eluted compounds, and then high values indicate good separating power. This factor depends on the system analyte- mobile phase- stationary phase for a given analysis temperature; and all these parameters may be altered to optimize or change the HPLC separation. Altering the system selectivity is a good strategy to optimize the resolution since small changes in selectivity can lead to large changes in resolution.

For a specific application with a specific column, various changes in the mobile phase can be envisaged to change the selectivity:

- Water content to change the solvent strength
- Organic modifiers to change the type of interactions
- pH value, which alters the degree of ionization of some analytes effecting their hydrophobicity
- Solvent additives

The temperature has also to be considered as it alters drastically the selectivity for some pairs of analytes.

Finally, last but not least: one of the most efficient way to change the selectivity is to change the stationary phase for another chemistry or material "molecular" structure.

- Efficiency

The efficiency of a peak is a kinetic parameter measuring the dispersion of the analyte band during the path through the HPLC system and column. This dispersion depends on the system analyte- mobile phase- stationary phase for a given analysis temperature. The chromatographic parameter reflecting the column performance is the number of plates (N) and is described on the following equation:

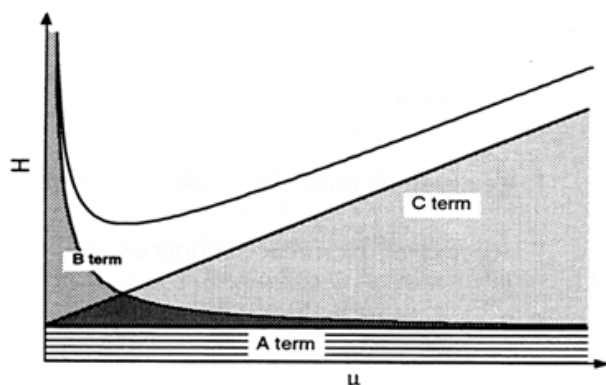
$$N = 5.54 \times \left(\frac{t_R}{W_{1/2}} \right)^2 = \frac{L}{H} \quad \text{Equation 3}$$

With $W_{1/2}$ the half-height peak width, H the height equivalent to a theoretical plate, and L the column length.

The model proposed by Martin and Synge relies on the separation of the column into plates. Each plate represents the distance over which the analyte achieves one equilibration between the stationary phase and the mobile phase. Consequently, the more plates available, the more possible equilibria, and so the better the quality of the separation.

Many factors contribute to the peak broadening, but considering an optimized system with negligible extra-column volume; the biggest contribution comes from the column itself. The quality of the column packing, as well as the length of the column but also both the particle size dispersion and dimension, play an important role in the overall efficiency.

The diffusion of analytes through the column is represented by the Van Deemter curve. The effect of the mobile phase velocity on the height equivalent to a theoretical plate (H) is linked to the efficiency and the column length by the equation:



$$H = A + \frac{B}{\mu} + C \times \mu \quad \text{Equation 4}$$

A-factor is the convective dispersion or streamline-splitting (eddy-diffusion) parameter, related to channeling through a non-ideal packing. It can be minimized by packing columns homogeneously with silica

particles of controlled particle size. The nature and the size of the particles also impacts the efficiency: superficially porous particles instead of totally porous particles but also the smaller the particles, the higher the efficiency.

B-factor is the longitudinal molecular diffusion coefficient of the eluting analytes in the longitudinal direction. It can be minimized by working at higher flow rates, by using lower inner-diameter tubing and connections and using organic modifier of lower viscosity.

C-factor is the resistance to the mass transfer of the analyte in the immobilized mobile phase and in the stationary phase. It can be minimized by using particles of a smaller diameter, superficially porous instead of totally porous particles, working with a lower flow rate and finally at a higher temperature.

- Resolution

Obtaining an optimum resolution in a minimum of time is a challenge for chromatographers. Indeed, a value of 1.5 or more between two peaks of approximately same magnitude ensures a convenient baseline separation. As demonstrated by the fundamental Equation 5, the resolution (R_s) is affected by three important parameters: selectivity, efficiency, and retention.

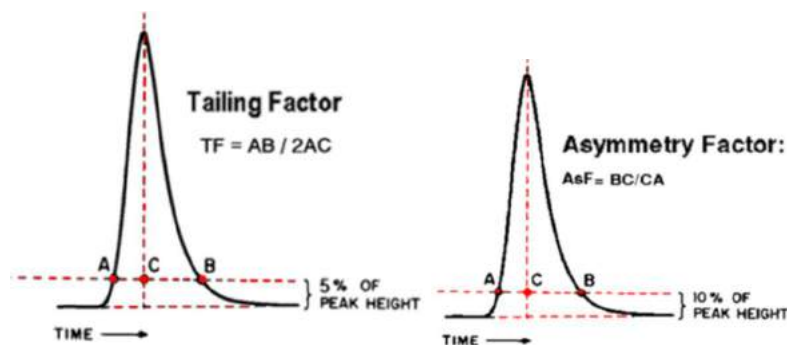
$$R_{s_{A,B}} = \frac{\sqrt{N_B}}{4} \times \frac{\alpha_{A,B} - 1}{\alpha_{A,B}} \times \frac{k_B}{k_B + 1} \quad \text{Equation 5}$$

- Peak asymmetry

Ideally, all chromatographic peaks would be symmetrical (Gaussian). However, due to the effects of instrument extra-volumes, adsorptive effects of the stationary phase and the quality

of the column packing, peaks are often distorted. Asymmetrical peaks lead to a loss of resolution making the quantification tricky. The asymmetry factor is estimated at 10% of the peak height. The tailing factor is estimated at 5% of the peak height. These two parameters are calculated according to the Equation 6.

$$As = \frac{BC}{AC} \text{ and } TF = \frac{AB}{2AC} \quad \text{Equation 6}$$



Standard limits are set for peak asymmetry. A AsF value between 1-1.05 ($1 < TF < 1.033$) is considered as excellent, and up to 1.5 (corresponding to $TF = 1.33$) the chromatography is deemed acceptable.

Columns/mobile phases...When chemistry meets silica

- Pore Size Dimensions

The choice of pore size is of crucial interest when developing a method for a class of compounds. Selecting a column based on silica particles with small or standard pore sizes (around 60 to 120 Å) to analyze large molecules (over 3000 g.mol⁻¹) will result in size exclusion. So far, columns packed with 300 Å pore size particles are recommended for biomolecule analysis.

- Particle Size Dimensions

The typical particle size for HPLC columns is 5 µm or 3 µm, but smaller diameter is now common in method development. If high-speed or higher resolution analyses are required, columns containing 1.8 µm and 2-3 µm particles can be used. Shorter columns with these particles can produce faster separations. But longer columns are required for higher efficiency. Longer columns packed with smaller particles highly improve the global efficiency, but also dramatically increase back-pressure, making this procedure only possible on UHPLC instrumentation.

- Column Dimensions

Choosing the dimensions of the columns is also essential and has extremely changed in the past few years. While 4.6 mm id was largely used in method development, smaller 3.0 mm id or 2.1 mm id columns tend to be more and more common, due to the lower solvent use and the better MS detectors compatibility.

The choice of the length of the columns depends on the need of resolution, and so, on the efficiency: shorter 50, 75 or 100 mm long columns ensure fast analyses with a low solvent consumption. Longer columns (150 or 250 mm) are used when more resolution is needed or when 3 and 5 μm particles are used. We have to find a balance between the efficiency we want and what the system can handle. The columns packed with smaller particles are much more efficient, but cause important back-pressure. The following table allows us to find which combination of parameters can be used to obtain an equivalent efficiency.

Length (mm)	Efficiency for columns packed with particles of (μm)			Analysis time saving
	5.0	3.5	1.8	
150	12,500	21,000	35,000	-
100	8,500	14,000	23,250	33 %
75	6,000	10,500	17,500	50 %
50	4,200	7,000	12,000	67 %

Table 1: Effect of the dimensions of the columns and of the totally porous particles on the efficiency

- pH and Mobile Phase: Solvent-strength selectivity and solvent-type selectivity

Once the column has been selected, the mobile phase choice conditions the separation, it is therefore important to control the nature and the amount of the organic modifier.

Acetonitrile and methanol are the most commonly used organic modifiers. However, selectivity differences and sample retention will vary significantly among mobile phases containing acetonitrile, methanol, and tetrahydrofuran. The choice is determined also by the solubility of the sample and the need of a UV detection at certain wavelengths (e.g., methanol not suitable at 200 nm).

The pH and ionic strength of the aqueous portion of the mobile phase are important parameters to control in order to develop robust methods that are not sensitive to small variations in conditions. This is particularly the case with ionic compounds for which the retention is highly affected by pH. A pH between 2 and 4 is generally a great starting choice to stabilize the retention and the resolution of typical weak acids. For basic solutes a pH value between 7 and 8 is often chosen, but implicates to use inevitably buffered aqueous solution.

Stationary phase chemistries

Most of the time, the base material is high purity silica (Type B) with totally porous particles. The content of the metal impurities has to be as low as possible to avoid strong interactions caused by coordinated metal in the silica matrix or metals adjacent to the surface. From a chromatographic point of view the strongly interacting sites considerably broaden the chromatographic band since they interact much more than "normal" adsorption centers².

Different silica qualities are available. One of the main contaminants is metal ions and these ionic groups form great ion-exchange sites for ionized acids, giving badly tailing peaks for acidic solutes. Moreover, if the metals are adjacent to silanol groups, they withdrew electrons from the adjacent silanol and enhance its ionization, especially at high pH. These activated silanols act as cation-exchange sites for ionized bases, leading to strong retention and badly tailing peaks for basic solutes. These low-purity silicas correspond to Type-A, also named acidic silicas today.

Many efforts have been done to enhance the purity of the silica material and the homogeneity of the particles. Today, the most commonly used is the Type-B silica, based on high purity-low metal content, spherical shape with narrow pore size distribution and high mechanical strength. As for the Type-A silica, the silanol groups can be functionalized, providing a wide range of column chemistries (e.g. C18, C8, CN...).

The Type-C silica support is structurally different as the surface is populated with silicon-hydride groups (-Si-H groups) which are very stable and relatively non-polar. It still has all the advantages of Type-B silica but also other advantages. It can be used for 3 different modes of HPLC and sometimes two at the same time, improving the selectivity power. In Type-C columns with a right choice of mobile phase, polar and non-polar compounds can be separated in the same isocratic run.

- Reversed-phase chemistries

The presence of silanol groups onto the silica surface allows for the functionalization, and various chemistries have been developed offering a wide range of columns.

Polymer materials present a wide range of pH stability and unique separation performances; but monomeric phases are more extensively used as it ensures a better reproducibility of the functionalized silica batch products.

A great part of method development begins with octyl (C8) or more frequently octadecyl (C18) stationary phases and the recommended starting column choice is C18 RP, as it presents high hydrophobic properties and low amount of residual silanols thanks to an effective end-capping step. Therefore, it provides excellent peak shape and can be used over the pH range 2-9, accommodating most typical LC and LC/MS mobile phases.

If the solutes are more polar or need to be analyzed with water as mobile phase, the C18 AQ is a good alternative as the polar groups incorporated in the stationary phase structure allow the analysis in 100% water without the collapse of the bonded chains.

² J. Nawrocki, Debbie L. Moir, W. Szczepaniak, *Chromatographia*, 28, (1989) 147

If the separation is not optimal on these columns, CN and Phenyl columns may offer significant differences in selectivity from straight-chain alkyl phases to effect the separation.

Generally, the separation of larger solutes such as proteins is more efficient on short-chain reversed-phase columns (C3, C4, CN, C8); while peptides and small molecules are better separated on longer-chain columns (C18). However, there are many cases in which this conventional method does not apply. It is better to begin with a phase of median hydrophobicity (e.g., C8), and change to a more hydrophobic phase or a more hydrophilic phase depending on the results obtained, and the solubility of the sample.

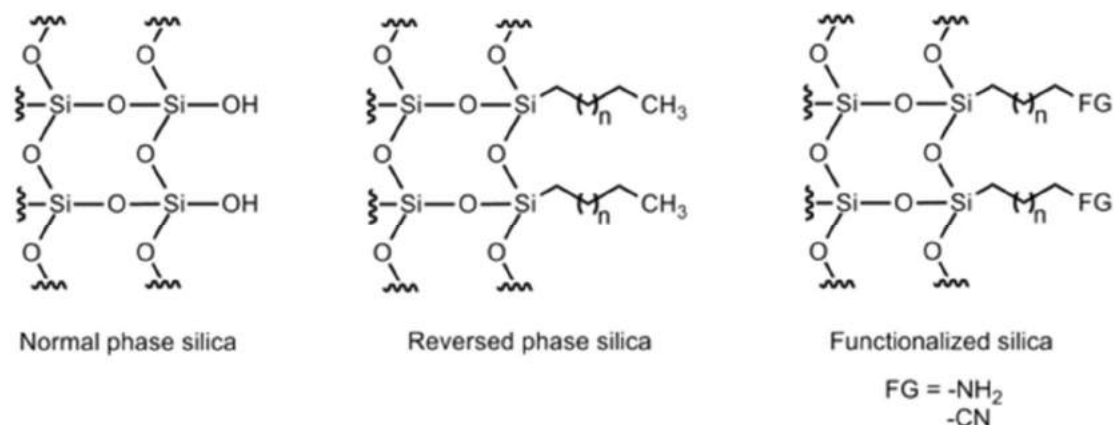


Figure 1: Structural representation of some stationary phase chemistries³

Characterization of C18 phases-Chromatographic tests

All manufacturers are willing to divulge the functionality, the bonding technology, or the composition of their column chemistries. For these reasons, columns similarly called, for example C18, possess different chromatographic properties justifying the need for classification.

Replacing a column with an identical or with a totally different one can be challenging. Some basic data as the specific surface area (in m².g⁻¹), the particle diameter (in μm), the content of metal impurities and the carbon load (in %) may be specified. From these data, the bonding density can be calculated (in mol.m⁻²) with the Equation 7:

$$\tau (\mu\text{mol} \cdot \text{m}^{-2}) = \frac{10^6 \times p_c}{[10^2 \times M_c \times n_c - p_c \times (M_w - 1)] \times S_{BET}} \quad \text{Equation 7}$$

³ http://www.ochemonline.com/Running_a_flash_column

Where p_c is the carbon percentage per weight of the bonded material, M_c the atomic weight of carbon, M_w the molecular weight of the grafted molecule, n_c the total number of carbon atoms in the bonded organic group, and S_{BET} the specific surface area ($\text{m}^2 \cdot \text{g}^{-1}$ of silica). But as the carbon percentage includes both the bonded chains and the silanol end-capping groups, this value is more or less indicative.

Chromatographic measurements can be achieved to complete these data, and various tests have been developed with some similarities in between. Generally, the evaluation relies on the determination of the hydrophobicity (also called hydrophobic selectivity), the shape selectivity (also called steric selectivity), the hydrogen bond capacity (also called silanol activity), the ion exchange capacity, and finally the metal content impurities. Chromatographic data based on the chromatographic peaks are also obtained considering the asymmetry and the number of theoretical plates. To summarize, standard chromatographic values of interest are mainly the retention factor (k), the selectivity factor between appropriate solutes, and the peak asymmetry factor (AsF).

Even if different chromatographic tests have been developed to characterize LC stationary phases, none of these tests provides an exhaustive view of the potential power of separation of a stationary phase relatively to all compound families to analyze. Multiple goals are involved in the characterization of columns. First, obtaining a quantitative understanding of the specific characteristics of a column that impacts the selectivity of a separation. This is helpful to rationalize the selection of a suitable stationary phase for a particular analysis, or for the selection of an alternative column when the first one did not result in a successful separation. Moreover, having a better knowledge of what differentiates one stationary phase from another is useful for the screening in method development; when it is beneficial to maximize the differences between the columns and the mobile phases. Finally, one can be interested in understanding the interactions between the solutes, the mobile phase and the stationary phase driving the separation.

Several reviews as the one proposed by Neue⁴ are interested in the stationary phase characterization. A significant work was achieved by Snyder *et al.*, who characterized a huge number of columns and demonstrated the usefulness of a ranking scale Tanaka test is a widely used test for the characterization in reversed-phase liquid chromatography, especially C18. Analytes are easily commercially available, and not costly. Even if it does not assess properly all the properties of stationary phases, it has the advantage of being the most generally used to compare them. It allows for a minimal evaluation of separation of ionisable compounds. Tchaplal test based on the analysis of polymethylphenols partially evaluates the hydrophobic selectivity. Sander and Wise test furnishes a partial and complementary evaluation of the steric selectivity. Engelhardt *et al.* test partially evaluates the polar selectivity, while Lesellier and Tchaplal classification are interested in polar and steric selectivity. Finally, a more specific test

⁴ U. D. Neue, *J. Sep. Sci.* 30, 2007, 1611

for evaluating stationary phases for analysis of basic compound has been proposed by Stella, Rudaz and Veuthey.

In 2002, Visky *et al.* reported 36 different tests evaluating these properties, but other tests have been elaborated by Neue and Layne.

Silica bonded with hydrophobic chains as C18 or C8 can establish dispersion interactions with analytes. The hydrophobicity depends on the chain length, the bonding density and the specific surface area of silica. For high-density bonded silica, the pore diameter may be an additional parameter.

The hydrophobic selectivity consists in determining the retention variation caused by the addition of a methylene group in the analyte structure.

The shape selectivity evaluates the ability of the stationary phase to differentiate analytes having a same elemental composition but a different three-dimensional structure or configuration, as it is the case for isomers. When the planarity or the stretched configuration of the molecule is affected, the penetration in the stationary phase may differ. The true structure of the bonded chain impacts the steric selectivity, especially the nature of stationary phase (monomeric or polymeric), the length of the alkyl chain (C8 to C30), and the nature of the organic modifier and the temperature. Also, the higher the bonding density, the more probable to have size exclusion.

The silanol activity includes the hydrogen bonding between acidic and basic solutes and neutral silanol groups, and ionic interactions between ionized basic solutes and ionized silanol groups. This parameter is directly linked to the amount and to the nature of available silanols, especially their acidic character, which is determining for the pH range of ionization. Indeed, different types of silanol exist onto the silica surface (single, geminal, and vicinal), showing different activities. It has to be noticed that the purity of silica is also of interest, as the presence of metallic impurities tends to increase the silanol acidity, and consequently, the secondary interactions not suitable for the peak symmetry.

Finally, to compare the stationary phases, different parameters can be used, and different representations are proposed. If one property is taken into account, an histogram is enough; if two properties are considered, a two-dimensional plot is used; and finally five or six properties can be displayed in an histogram or a radar plot as presented above.

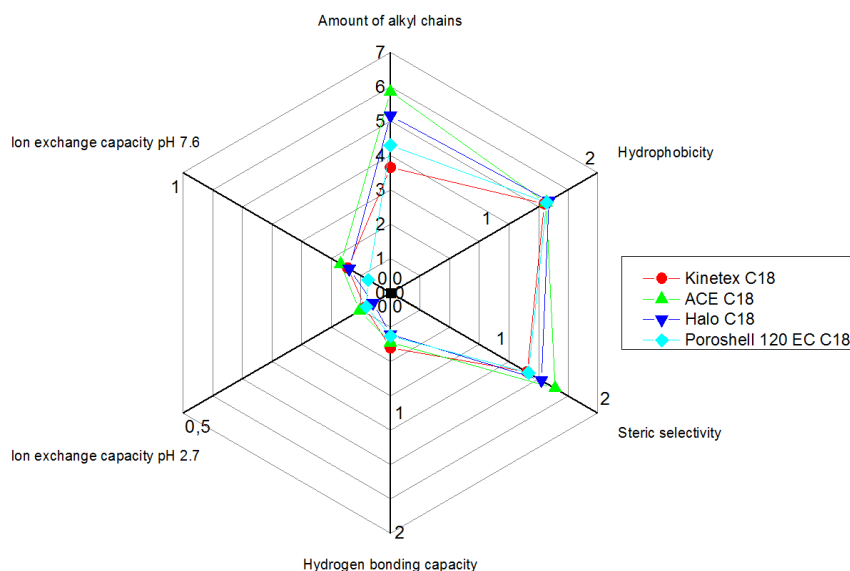


Figure 2: Radar plots of 4 C18-core-shell columns for the Tanaka test

The values of each parameter for each column are displaced along a graduated axis in order to make the comparison easier.

Chemometrics

Chemometric tools can be used to meet the need of classification and produce comparisons between the columns. Among the different approaches, Principal Component Analysis (PCA) is used to assess the chromatographic similarity/dissimilarity of a range of columns. The stationary phases initially spreading in a multi-dimensional space (due to the number of parameters used for the comparison) are displayed in a two- or three-dimensional space and often different groups can be differentiated.

Such method may introduce a loss of information when reducing the data from a multidimensional space to a limited number of significant axes. Moreover, the selection of relevant criteria, those without correlation, is not so simple. More complex models involving thermodynamic approaches are also useful such as the linear solvation energy relationship (LSER), the Abraham solvation descriptors *Poole and Poole*, and the model of Snyder *et al.* These models can produce more precise information to understand the types and the relative strength of the chemical interactions that control retention and selectivity. However, the results of such models are sometimes difficult to interpret, especially when the analytes and the analytical conditions used are different.

For these reasons, the following part is focused on PCA.

Principal component analysis

With this new representation, columns close to each other (in the score plots) present similar chromatographic characteristics regarding the parameters considered (here retention and

asymmetry factors) to define the PCA. On the contrary, the one located in another portion of the scores plot exhibit different properties.

A concrete example is presented on the following part. The variables taken into account are the retention factor (k) and the asymmetry factor (A_s) for solutes numbered from 1 to 7. The conditions of analysis, as well as the solutes chosen correspond to those of the Veuthey test, particularly useful to characterize the chromatographic properties of a stationary phase toward basic solutes.

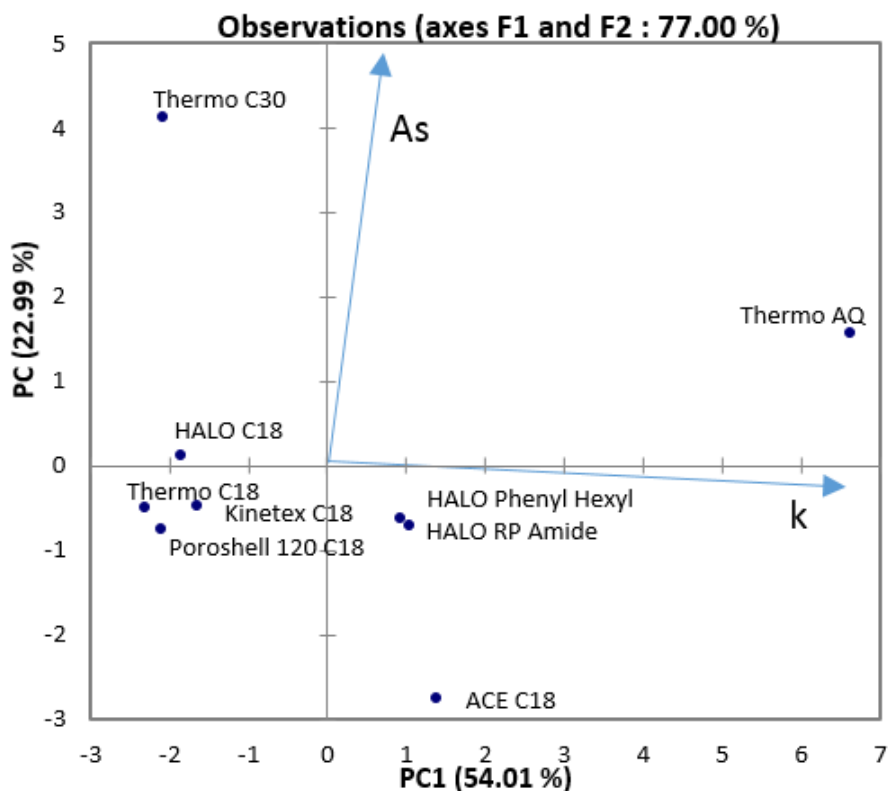


Figure 3: Score plots of some core-shell columns for the Veuthey test at pH 7. The solutes are numbered from 1 to 7. In blue the vectors corresponding to the parameters taken into account for the PCA (retention factor k , asymmetry factor A_s).

The calculation of the principal components which are linear combination of the initial values preserves 77% of the total information, ensuring an amenable interpretation.

Here, the C18 are clustered together except the ACE C18 (Figure 3). They are located at the opposite direction of the vectors of retention factors (Figure 3), meaning that the solutes analyzed in these conditions do not develop important interactions with the stationary phases as they do not present high k values.

The Thermo AQ is particularly suitable for the analysis of basic solutes as those used for the Veuthey test. Indeed, it is located in the direction of the retention factor vectors, and far from the asymmetry vectors (Figure 3). It means that this column present interesting retention properties, without a too strong distortion of the peak symmetry.

The Thermo C30 is also isolated and located in the vector direction of the asymmetry factor. The column is not suitable for the analysis of these types of solute as it does not present interesting retention and high peak asymmetry.

About the database

If you are used to perform your analyses with a given column, have developed all your analytical method on it, and are satisfied with this one... Of course you will not want to change! That's why PerkinElmer developed a user friendly interface called One Source® HPLC Column, available directly from the internet, and which allow you to find the equivalent column to the one you are familiar with. By completing the brand, the bonding, the particle size, the column dimensions and the supplier you are used with, you will get the equivalent in our database. And it can be even faster if you have the column part number, just enter it and it is enough to find in our system the corresponding column.

Conclusion

Depending on the application (molecular weight and solubility of the analytes), the separation mode differs and the corresponding columns also.

If it is important to minimize the extra-column volumes of any HPLC instrument, the column itself remains the most important part of any HPLC system as it is where the separation takes place.

Among all the columns available on the market, it can be quite difficult to define the one that will be the most adapted to your needs. This user guide gave some basic notions to help doing the right choice, and after the column has been selected, finding the PerkinElmer's equivalent with our user friendly interface One Source® HPLC Column.

1.3. Article 6: DFT in pharmaceutical products

I was associated to this last article that presents the study of Schammé *et al.*, in collaboration with Dr. Vincent Tognetti. It is entitled "Molecular relaxations in supercooled liquid and glassy states of amorphous quinidine: dielectric spectroscopy and density functional theory approaches", and was published in Journal of Physical Chemistry in 2016.

Molecular Relaxations in Supercooled Liquid and Glassy States of Amorphous Quinidine: Dielectric Spectroscopy and Density Functional Theory Approaches

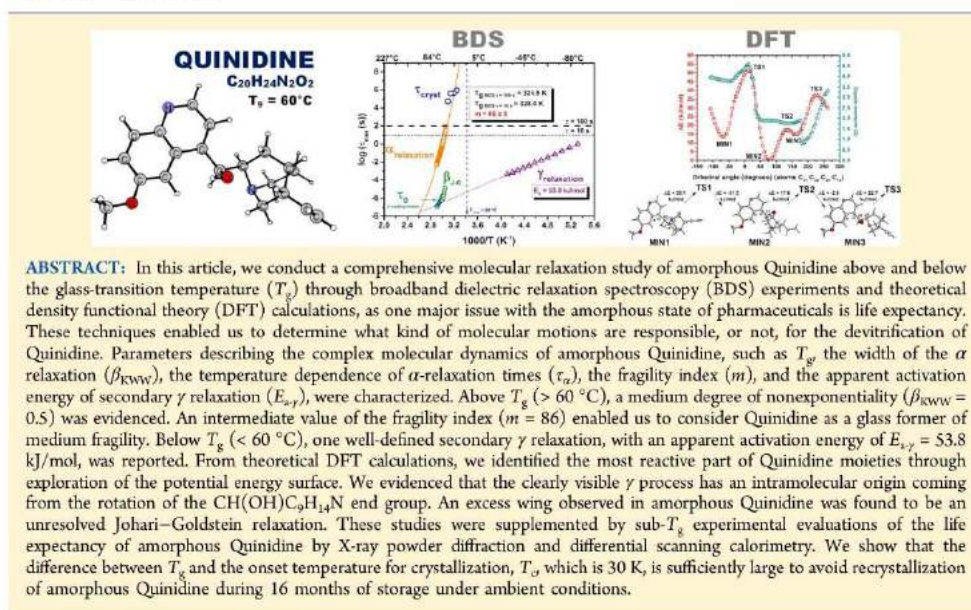
Benjamin Schammé,^{†,‡} Mélanie Mignot,[‡] Nicolas Couvrat,[†] Vincent Tognetti,[§] Laurent Joubert,[§] Valérie Dupray,^{*,†} Laurent Delbreilh,^{*,‡} Eric Dargent,[‡] and Gérard Coquerel[‡]

[†]Normandie Univ, Laboratoire SMS - EA3233, Univ Rouen, F-76821 Mont Saint Aignan, France

[‡]AMME-LECAP EA 4528 International Lab, Avenue de l'Université, BP12, Normandie Univ, Université de Rouen Normandie, 76801 St Etienne du Rouvray, France

[§]COBRA UMR 6014 and FR 3038, Normandie Univ, Université de Rouen, INSA Rouen, CNRS, F-76821 Mont Saint Aignan, Cedex, France

Supporting Information



1. INTRODUCTION

Improvement of drug solubility is one of the most prominent aspects of drug development processes.^{1–3} Although numerous strategies exist for the bioavailability enhancement of drugs, a significant number of active pharmaceutical ingredients (APIs) exhibit poor water solubility, according to the Biopharmaceutics Classification System.^{4,5} In light of this, solubility enhancement approaches have been addressed on the basis of chemical and physical modifications. Preparing poorly soluble drugs in the amorphous state is of particular interest, as it has been demonstrated that amorphous APIs can result in significant

improvements in the dissolution rate and bioavailability with reference to the crystallized solid.⁶

However, the inherent “out-of-equilibrium state” of amorphous materials is reflected by excess entropy, enthalpy, and free energy compared to those of crystalline forms.⁷ Amorphous APIs are prone to conversion to a more thermodynamically stable state.⁸ Crystallization processes may

Received: April 27, 2016

Revised: June 20, 2016

Published: July 8, 2016

take place over the time of storage and use of the product, leading to decreased physical stability as well as loss of the benefits arising from the amorphous state. Several works over the last decade have highlighted that molecular mobility could be a factor accounting for the life expectancy of amorphous APIs^{7,9–12} as well as the crystallization phenomenon.^{13,14} The most commonly adopted approach to assess the stability of amorphous pharmaceuticals is estimation of the gap between the glass-transition temperature (T_g) and storage temperature. It is recognized that storage well below T_g (usually 50 K) could prevent crystallization and ensure a physically stable drug during the shelf life.¹⁵ Storage conditions could also be defined in terms of Kauzmann temperature T_K .¹⁶ This hypothetical temperature is often considered as an indicator of reliable storage conditions, at which the degree of molecular mobility approaches zero. Most recently, a prediction of crystallization was proposed to be the difference between T_g and the onset temperature for crystallization (T_c).¹⁷

Several complementary techniques have been used to assess the molecular mobility of amorphous pharmaceuticals below and above T_g , notably through DSC (enthalpy recovery^{18,19}) and NMR spectroscopy experiments (spin–lattice relaxation time²⁰). Additionally, broadband dielectric spectroscopy (BDS) has proven to be a valuable and highly sensitive technique for monitoring the molecular dynamics (MD) of amorphous APIs.^{21–25} This approach allows thorough monitoring, over a wide range of temperatures and frequencies, of relaxation processes occurring below and above T_g .²⁶ Above the T_g in the supercooled liquid state, pharmaceuticals exhibit a more or less pronounced primary or structural relaxation process (α relaxation hereafter), arising from cooperative motion of molecules. On decreasing the temperature below T_g into the glassy state, the α -relaxation process becomes increasingly slow and often longer than the experimental observation time scale.²⁷ Thus, fast local motions of individual molecules or parts of molecules may occur, designated as secondary relaxation processes (β , γ , δ relaxations).²⁸

The main objective of this work is to provide a clear picture of molecular relaxations of the amorphous state, as one major issue of the amorphous state is physical instability (i.e., life expectancy). For this purpose, we focused our attention toward a model compound, Quinidine. Cinchona alkaloids (i.e., quinine, quinidine, cinchonine, and cinchonidine) are compounds with antimalarial properties found in the bark of Cinchona trees. Among these, Quinidine, which has been shown to have an increasingly important role owing to its medical use against malaria at the beginning of the 17th century,²⁹ is also used as an antiarrhythmic active pharmaceutical. Cinchona alkaloids have recently been investigated by Raman vibrational analysis³⁰ and jet-cooled spectroscopy.³¹ Besides, the physicochemical properties of these compounds as a function of peripheral groups were also considered.³² With regard to the amorphous state, previous investigations from Johari et al. have led to the identification of the distribution of diffusion times in terms of structural relaxation.^{23,33} However, until now, no study has been conducted on Quinidine to obtain a deeper experimental and theoretical understanding on both the MD in the supercooled and glassy states and on its life expectancy under standard conditions of use.

With the aim of characterizing the molecular mobility of amorphous Quinidine (in the supercooled and glassy states), we report herein our investigation using BDS and temperature-modulated differential scanning calorimetry (TMDSC) to

obtain relevant information on the molecular motions from the glass to the liquid state of Quinidine. Our investigations are supplemented by theoretical calculations within the framework of density functional theory (DFT). We show that exploration of the potential energy surface (PES) allows to ascertain activation barriers of secondary processes (with the identification of relevant transition states (TS)) and a deeper comprehension of the most reactive part of molecular moieties. Finally, we attempt to draw a tendency among long-term stability in the amorphous form, molecular origin of secondary relaxation, and molecular mobility in the supercooled and glassy states of Quinidine to determine what kind of molecular motions can be responsible, or not, for devitrification of Quinidine.

2. MATERIALS AND METHODS

2.1. Materials. Quinidine ($C_{20}H_{24}N_2O_2$, $M_w = 324.43$ g/mol) as a crystalline white powder was purchased from Sigma-Aldrich (purity $\geq 98\%$). No impurity was detected under high-performance liquid chromatography-sustained conditions. The compound was consequently used without prepurification. An X-ray diffractogram of commercial Quinidine was recorded and revealed a completely anhydrous crystalline form, in agreement with the Cambridge Structural Database (CSD-BOMDUC)³⁴ (see Figure S1, Supporting Information). The developed formula of Quinidine is shown in Figure 1.

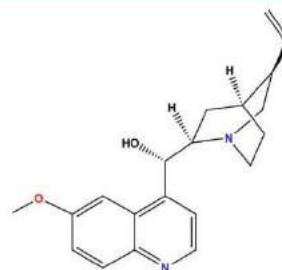


Figure 1. Developed formula of the Quinidine molecule.

2.2. TMDSC. The thermodynamic properties of Quinidine were investigated by the TMDSC technique. Calorimetric measurements were performed on a Q100 DSC instrument (TA Instruments) coupled with a liquid-nitrogen cooling system. Temperature and enthalpy calibrations were carried out with both indium and benzophenone standards. Specific heat capacities were measured using sapphire as a reference. Baseline was calibrated from -20 to 200 °C, with an oscillation amplitude of ± 0.080 K, an oscillation period of 60 s, and a heating rate of 0.5 K/min used in the experiments. The samples (5 ± 0.05 mg) were enclosed in sealed hermetic aluminum pans at T_{temp} and the atmosphere was regulated by a nitrogen flow (50 mL/min).

2.3. X-ray Powder Diffraction (XRPD). XRPD analyses were carried out using a D8 diffractometer (Bruker, Germany) equipped with a LynxEye detector. Cu $K\alpha$ radiation ($\lambda = 1.541$ Å) with the tube voltage and amperage set at 40 kV and 40 mA, respectively, was used as the reference configuration. Powder samples were placed on flat frosted glass and analyzed at room temperature, with a step of 0.04° (2θ) and a dwell time of 0.5 s

from 3 to 50° (2 θ). Therefore, XRPD analysis time was 10 min, performed promptly after sample production. For monitoring the recrystallization tendency, amorphous Quinidine was placed on the same flat frosted glass used previously, and XRPD measurements were carried out at specified temperatures and time intervals. The stability of amorphous Quinidine represents the onset of crystallization in the amorphous sample. We defined the onset time of crystallization as the appearance of the first crystalline peak in the diffractogram (the limit of detection of crystallinity has been estimated to be 1% of the crystalline amount in amorphous material^{35,36}).

2.4. BDS. Ambient-pressure dielectric permittivity measurements were performed using high-quality interdigitated electrodes (IEs) (BDS1410-20-150) from Novocontrol Technologies (sensor diameter 20 mm, gold-plated copper combs, accuracy in loss factor $\tan \delta = 0.001$). The spacing between the comb fingers is 150 μm and their thickness is 35 μm . Prior to sample deposition, each electrode was calibrated by measuring its respective geometric (empty cell) capacity, C_0 , and substrate capacity, C_{sub} , through measurement of a standard material with known permittivity (B-oil; Vacuubrand). From a general standpoint, it is presumed that the electric field penetrates only in the sample and the substrate by creating two independent capacitors. Thus, the measured total capacity results in³⁷

$$C_m^*(\omega) = C_0(\epsilon_s^*(\omega) + \epsilon_{\text{sub}}^*(\omega)) \quad (1)$$

where $C_m^*(\omega)$ is the complex capacity of the electrode and ϵ_s^* and ϵ_{sub}^* are the complex permittivities of the sample and substrate, respectively.

Measurements were carried out in a frequency range of 10^{-2} – 2×10^6 Hz with an α -A Analyzer from Novocontrol Technologies, allowing measurement of the complex impedance as function of frequency. Nonisothermal dielectric spectra were collected over a wide temperature range from -140 to 100 °C, with appropriate successive steps. Accurate temperature control was implemented using the Quatro system (Novocontrol Technologies), allowing a temperature stability of ± 0.2 °C. Amorphous samples were prepared ex situ by the most common method, that is, the quench cooling technique. A small amount (ca. 200 mg) of the as-received crystalline powder was deposited onto the high-quality IEs, whose efficiency to monitor the MD of amorphous APIs has been proven.^{25,38,39} The temperature was increased above the melting point of the compound ($T_m + 5$ K). It was ensured that the sample material covered the entire surface of the comb microstructure electrode. A totally amorphous compound (i.e., TMDSC analysis confirmed the amorphous character) was ensured by rapid quenching of the electrode to -20 °C ($T_g - 80$ K) before immediate analysis to protect it from atmospheric moisture. For each experiment, a fresh amorphous sample was prepared and calibration performed. Each measurement was repeated ($n \geq 3$ times) to ensure the reliability of the characteristic temperatures and parameters retrieved. A detailed description of the BDS experimental protocol and data fitting can be found in the Supporting Information.

2.5. DFT Calculations. Theoretical calculations for the Quinidine molecule ($\text{C}_{20}\text{H}_{24}\text{N}_2\text{O}_3$) have been carried out within the framework of DFT using the Gaussian 09 package.⁴⁰ The initial geometry was obtained from the crystal structure of Quinidine and was optimized at the $\omega\text{B97XD}^{41}/6\text{-31+G(d)}$ level. Relaxed energy scans on dihedral angles were performed to generate PESs corresponding to relevant rotational motions.

Selected structures were then fully reoptimized with Pople's 6-311++G(2d,2p) basis set. The geometry of the Quinidine dimer was optimized starting from the X-ray structure. The atoms directly involved in the intermolecular O–H...N hydrogen bonds were described by the 6-31++G(d,p) basis set, whereas 6-31+G(d) was used for the other atoms. The corresponding interaction energies were corrected for basis set superposition error using the standard Boys–Bernardi counterpoise method. The nature of all stationary points (TS and minima (MIN)) was further confirmed by vibrational analysis (only real harmonic frequencies for MIN, one imaginary frequency for TS). Solvent effects were taken into account through the polarizable continuum model⁴² in the latest⁴³ implementation of the integral equation formalism.⁴⁴ Quantum theory of atoms-in-molecules (QTAIM) decompositions were achieved using the AIMAll software.⁴⁵

3. RESULTS AND DISCUSSION

3.1. Thermodynamic Properties of Quinidine. To prevent any possible degradation in the calorimetric and dielectric studies, samples of Quinidine were heated to a maximum temperature of $T_m + 5$ K (see Figure S2). Figure 2

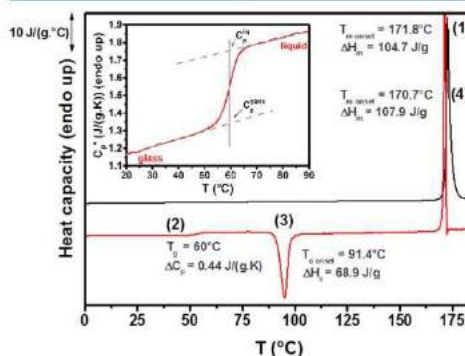


Figure 2. TMDSC measurements of crystalline and amorphous forms of Quinidine. (1) Melting of the commercial stable form, (2) glass-transition region, (3) crystallization of the supercooled melt to the crystalline form, (4) melting of the crystalline form. An oscillation amplitude of ± 0.080 K, an oscillation period of 60 s, and a heating rate of 0.5 K/min were used. The inset shows the in-phase component of the specific complex heat capacity on an enlarged scale.

shows TMDSC thermograms recorded for Quinidine. Upon heating at 20 K/min, this compound exhibits a sharp endothermic event at 171.8 °C ($\Delta H_m = 104.7$ J/g). This event is related to the melting process of the respective commercial stable form. After quenching from the melt, a subsequent TMDSC heating scan at 0.5 K/min (modulation of ± 0.080 K and amplitude of 60 s) from the glassy state reveals a well-defined C_p jump, which signals glass transition at $T_g = 60$ °C ($\Delta C_p = 0.44$ J/(g·K)). An exothermic event is noticed at $T_c = 91.4$ °C ($\Delta H_c = 68.9$ J/g), corresponding to the emerging cold crystallization. At higher temperatures, it is followed by a sharp endothermic event at $T_m = 170.7$ °C ($\Delta H_m = 107.9$ J/g), corresponding to melting of the crystalline form obtained beforehand. It has to be noted that the melting enthalpy of crystalline commercial Quinidine is quasi-identical to that

Table 1. Thermodynamic Properties of Quinidine Obtained from Temperature-Modulated Calorimetry, with a Heating Rate of 0.5 K/min, a Modulation of ± 0.080 K, and an Amplitude of 60 s⁴⁹

T_g (K)	$\Delta C_p(T_g)$ (J/(g K))	T_m (K)	ΔH_m (J/g) (initial crystal)	T_c (K)	ΔH_c (J/g)	T_m (K)	ΔH_m (J/g) (after recryst)
333	0.44	444.9	104.7	364.5	68.9	443.8	107.9
	$C_p^{cryst}(T_g)$ (J/(g K))		$C_p^{liq}(T_g)$ (J/(g K))		$C_p^{cryst}(T_g)$ (J/(g K))		$C_p^{liq}(T_g)$ (J/(g K))
	1.329		1.339				1.752

^aValues of T_c and T_m were taken at onset.

obtained from recrystallization from the amorphous state. Therefore, Quinidine can be fully amorphized by melt-quenching. Characteristic parameters, such as values of heat capacity C_p for crystalline (C_p^{cryst}), amorphous (C_p^{liq}), and liquid (C_p^{liquid}) states taken at T_g (= 60 °C), were extracted. The thermodynamic properties of Quinidine are reported in Table 1.

3.2. Kinetic Stability. From a structural point of view, XRPD measurements support the above DSC results. As illustrated in Figure 3 (middle red XRPD), the XRPD pattern

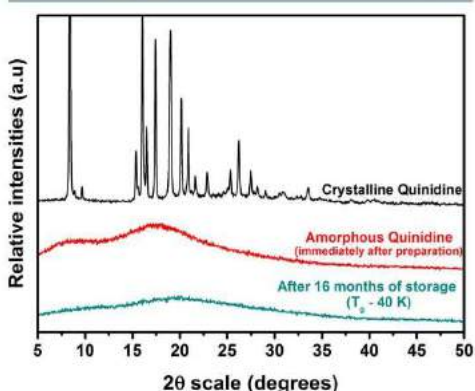


Figure 3. X-ray diffraction patterns of quinidine recorded at room temperature: crystalline (top XRPD), amorphous (middle XRPD) and amorphous sample after 16 months of storage in standard conditions (bottom XRPD).

recorded immediately after melt-quenching is defined by a very broad halo, whereas crystalline samples exhibit well-defined sharp Bragg peaks (top black XRPD). The disordered signature after vitrification confirms that Quinidine prepared by melt-quenching is indeed amorphous (additional DSC analysis confirms this behavior by displaying the same signal as that in Figure 2 (second run) and characteristic temperatures, data not shown). Moreover (bottom blue XRPD), the diffractogram of amorphous Quinidine remains unchanged during our investigation, that is, the sample was still amorphous after 16 months of storage at 20 °C (under a phosphorus pentoxide atmosphere; at room temperature T_g 40 K; atmospheric pressure). DSC analysis of the same sample supports the outcome of XRPD (see Figure S3).

3.3. MD of Quinidine. Understanding the time scales and temperature dependencies of the molecular mobilities of amorphous APIs is of crucial importance as stability evaluation over time to ensure no changes in the physicochemical properties of the final product must be considered. Therefore,

to investigate relaxation dynamics of amorphous Quinidine, dielectric measurements were carried out over a wide range of temperatures and frequencies.

3.3.1. Supercooled Liquid State ($T > T_g$). Figure 4 displays real and imaginary parts of the complex dielectric permittivity

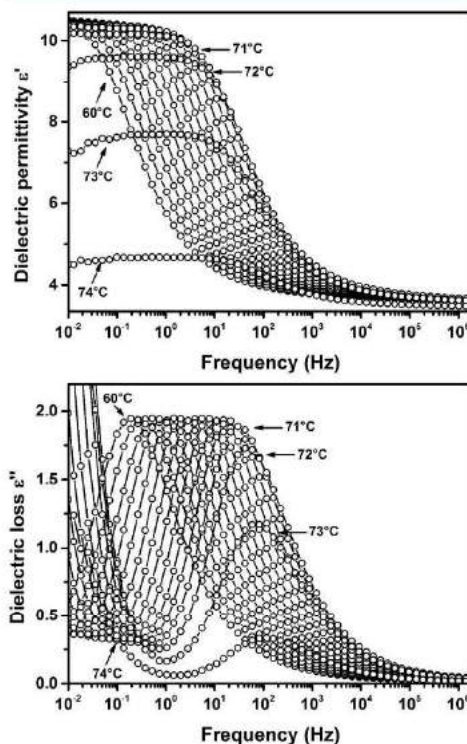


Figure 4. Real (ϵ') and imaginary (ϵ'') parts of the complex dielectric permittivity vs frequency of Quinidine in the supercooled liquid state at temperatures from 60 to 74 °C ($T > T_g$), with an increment of 1 °C.

spectra of Quinidine in the supercooled liquid state (above T_g at temperatures from 60 to 74 °C, with an increment of 0.5 °C; for the sake of clarity, we have chosen to show only steps of 1 °C). First, on ϵ'' at low frequencies, conductivity is observed, which can be ascribed to motion and diffusion of ions and charges in the sample. Toward higher frequencies, a structural relaxation process associated with dynamic glass transition is clearly discernible and was labeled α relaxation.

Relaxation times show a curved temperature dependence when plotted as a function of $1000/T$ (Figure 5). These data

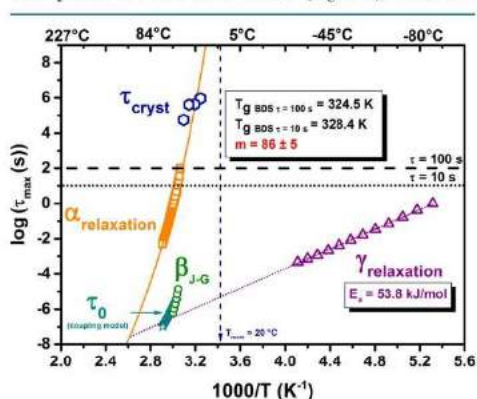


Figure 5. Relaxation map of melt-quenched Quinidine. The temperature dependence of structural α -relaxation times is illustrated by open orange squares. Solid orange lines are the VTF fits to the experimental data. Temperature dependence of the secondary γ -relaxation is illustrated by open purple triangles and was fitted by the Arrhenius equation. Open blue stars are primitive relaxation times τ_0 of the coupling model, calculated with $\beta_{KWW} = 0.5$ at temperatures close to T_g . Open green circles are relaxation times β_{J-G} obtained from the HN fit of the excess wing. Open dark blue hexagons show the temperature dependence of crystallization times τ_{cryst} below T_g .

can be fitted by the Vogel–Tammann–Fulcher (VTF)^{46–48} equation characterizing cooperative glassy dynamics. Upon further heating, the cold-crystallization process of Quinidine can be ascertained. At $T > 71$ °C, the amplitudes of both dielectric permittivity ϵ' and dielectric loss ϵ'' begin to decline with increasing temperature. This behavior is typical of a crystallization process. Indeed, as crystallization proceeds, the number of relaxing molecules decreases, causing progressive weakening of dielectric strength $\Delta\epsilon$ of the α process. Dielectric strength could be defined from the generalized form of Debye theory by Onsager, Fröhlich, and Kirkwood⁴⁹ as

$$\Delta\epsilon = \frac{1}{3\epsilon_0} g_K F \frac{\mu^2 N}{k_B T V} \quad (2)$$

where ϵ_0 is the dielectric permittivity of vacuum, μ is the mean dipole moment of a moving unit in vacuum, g_K is the Kirkwood correlation factor, and F is the Onsager factor (equal to 1). The N/V ratio represents the density of dipoles involved in the relaxation process. Therefore, dielectric strength $\Delta\epsilon$ decreases in the same manner as factor N/V , due to the emergence of cold crystallization of Quinidine (temperature dependence of the fit parameters, $\Delta\epsilon$, α_{HN} , and β_{HN} can be seen in Figures S4 and S5). In the probed temperature range, exponents α_{HN} and β_{HN} have nearly constant values of 0.85 and 0.5, respectively.

A representative relaxation map of the dielectric loss spectra of structural and secondary relaxations of Quinidine is presented in Figure 5. From the estimated parameters of VTF fit (Table 2), T_g can be conveniently determined at dielectric relaxation time $\tau_\alpha = 100$ s. The value of T_g for Quinidine was found to be 51.5 °C (324.5 K), determined at $\tau_\alpha = 100$ s. This value is slightly lower compared to that obtained from TMDSC measurements but is in accordance with that found by Johari et al. ($T_g = 326$ K).²³ However, by comparing the value of T_g for $\tau_\alpha = 10$ s, corresponding to the equivalent frequency of the TMDSC analysis, a value of 55.2 °C (328.4 K) is found. The T_g obtained from TMDSC, that is, $T_g = 60$ °C, will be used throughout the article.

Exploitation of the fragility concept as a classification of glass-forming APIs on the basis of differences in dynamics and also as a possible criterion for life-expectancy changes has met a growing interest in recent years.^{7,50,51} This characteristic feature of the MD of glass-forming liquids was reliably determined from VTF fitting parameters and denoted as kinetic fragility m (also referred to as steepness index). This parameter can be ascertained according to Angell et al.⁵²

$$m = \frac{d \log \tau_\alpha}{d(1/T)} \Big|_{T=T_g} \quad (3)$$

Small values of the fragility parameter indicate an Arrhenius-like temperature dependence (“strong” supercooled liquids), where $\log \tau_\alpha(T)$ is linear in the T_g/T range. When the dependence of $\log \tau_\alpha(T)$ deviates strongly from the linear variation and thus from the Arrhenius pattern, glass-forming liquids are denoted as “fragile”. In this classification, polymers are often classified with relatively high fragility values as PVC⁵³ ($m = 191$), PC⁵⁴ ($m = 170$), PHBV⁵⁵ ($m = 106$), or PVAC⁵⁶ ($m = 90$). Kunal et al.⁵⁷ highlighted that the packing efficiency of the amorphous chain in the glassy state and chain flexibility are the main parameters influencing the fragility index. Moreover, with reference to the classification of pharmaceutical glass formers, studies have shown that small organic molecules are more likely to exhibit m values <40 for strong glass formers, whereas fragile glass formers have m values >75 .⁵⁸ Here, fragility calculation of Quinidine according to the Böhmer calculation⁵⁹ has given an m value of 86 ± 5 . This value is close to that obtained for other amorphous pharmaceuticals examined lately, such as telmisartan⁶⁰ ($m = 87$), indomethacin ($m = 83$),⁶¹ or verapamil hydrochloride ($m = 88$).⁶² Thus, amorphous Quinidine can be classified as a glass-former API of medium fragility.⁶³ One should note that quantification of the fragility index (and thus of relaxation time) could be sometimes subject to misinterpretation.⁶⁴

Moreover, in a complementary manner to the long-term stability measurement at room temperature (T_g , 40 K), sub- T_g experiments have been conducted at various selected temperatures (T_g): 10, 15, 20, and 25 K, through XRPD monitoring. Crystallization onset times (τ_{cryst}) have been plotted in Figure 5 and compared to both structural and secondary relaxation times. Here, we could detect in this temperature range a similar trend between τ_{cryst} times and the extrapolation of the VTF

Table 2. Estimated Parameters of the VTF Fit Obtained for Amorphous Quinidine

	α process					
	T_g ($\tau = 100$ s) (K)	T_g ($\tau = 10$ s) (K)	m ($\tau = 100$ s)	D	τ_0 (s)	T_g (K)
Quinidine	324.5 ± 1	328.4 ± 1	86 ± 5	14.1	-18.7	252

trend of α -relaxation times, indicating a possible correlation between molecular mobility of structural relaxation and crystallization tendency.

Furthermore, it has been shown that the distribution of molecular motions, described by the β_{KWW} parameter, could be a consistent parameter in the life expectancy of amorphous pharmaceuticals. A narrow distribution of structural relaxation, that is, high values of β_{KWW} , would indicate a small propensity of amorphous API to crystallize. On the other hand, a larger distribution of α -relaxation times could suggest faster localized molecular motions, leading to a greater inclination toward crystal nucleation.⁶⁵ For this purpose, to verify the relevance of this parameter in our system, we applied the one-sided Fourier transform of the Kohlrausch–Williams–Watts (KWW) function.⁶⁶ In the temperature range investigated, stretching parameter β_{KWW} remains constant, with the mean value of 0.5. This is consistent with the value of $\beta_{KWW} = 0.520$ found by Johari et al.²³ It is an indication that the distribution of relaxation times in the supercooled liquid state of Quinidine is asymmetric and much broader than that in a classical Debye-type process ($\beta_{KWW} = 1$). Furthermore, it has been recognized from the Alvarez–Alegria–Colmenero equation⁶⁷ that Havriliak–Negami (HN) parameters are linked to stretch exponent β_{KWW} . Therefore, using $\alpha_{HN} = 0.85$ and $\beta_{HN} = 0.5$ determined previously, we obtained $\beta_{KWW} = 0.5$, which is in good agreement with the experimental value found in the analyzed temperature range. As suggested by Shamblin et al.,⁶⁵ the ability of amorphous pharmaceuticals to crystallize might be correlated to the asymmetric distribution of relaxation time (i.e., β_{KWW}). Thus, the stability of amorphous APIs would decrease as the value of β_{KWW} decreases. We found that the β_{KWW} value of Quinidine lies within the range of β_{KWW} values obtained for other pharmaceutical systems, such as aspirin ($\beta_{KWW} = 0.42$)⁶⁸ or ibuprofen ($\beta_{KWW} = 0.52$).²⁴ Hence, one could say that Quinidine is characterized by a medium degree of non-exponentiality⁶⁹ and an intermediate distribution of α -relaxation times. However, it should be recalled in this context that there are exceptions to the above theory and that the expected correlation between the tendency to crystallize and β_{KWW} is not fulfilled by all APIs.^{70,71} As a matter of fact, Adrijanowicz et al.⁶² demonstrated in the case of amorphous verapamil hydrochloride, which exhibits a value of $\beta_{KWW} = 0.61$, that this glass former did not show any tendency toward crystallization during their measurements. On the other hand, Knapik et al.¹¹ showed that amorphous Ezetimibe during its storage at room temperature ($T_g = 38$ K) starts to recrystallize after 14 days, even with a value of $\beta_{KWW} = 0.7$.

From the analysis of a so-called masterplot (Figure 6), a reliable complementary visualization of stretching parameter β_{KWW} was conducted. It is based on horizontal shifting of the spectra taken at various temperatures (from 62 to 72 °C, with an increment of 2 °C) to superimpose them onto a reference spectrum (at 62 °C). This special procedure enables to ascertain whether temperature plays an active role in the shape of the structural relaxation that would have resulted with different relaxation times depending on the temperature. With β_{KWW} equal to 0.5 for Quinidine, temperature has a very weak influence on the shape of the structural process, as all spectra recorded were totally superimposed nearby T_g . Moreover, it can be seen that experimental data deviate from the KWW trend at higher frequencies. In this instance, a so-called excess wing emerges on the high-frequency side of the α process. Deviation of the KWW fit toward an excess wing, which was postulated by

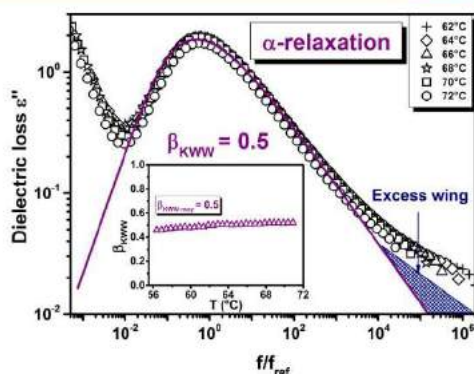


Figure 6. Masterplot of Quinidine in the supercooled liquid (from 62 to 72 °C). The purple full line corresponds to the KWW fit of the structural relaxation peak at 62 °C. The reference spectrum is located at 62 °C. The inset shows stretching parameter β_{KWW} as function of temperature.

Ngai⁷² and confirmed experimentally by other scientists,^{73–75} arises from the high-frequency flank of the secondary relaxation process covered by the dominant structural relaxation. Therefore, among faster and local (inter- or intramolecular) molecular mechanisms affiliated to secondary relaxations, another relaxation, namely, Johari–Goldstein (JG) β relaxation,^{72,76–78} has been considered as a potential precursor of cooperative structural relaxations.

3.3.2. Glassy State ($<T_g$). Figure 7 presents the frequency evolution of dielectric permittivity ϵ'' at various temperatures

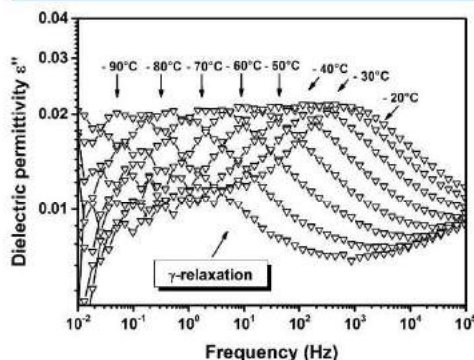


Figure 7. Dielectric loss spectra of Quinidine taken below T_g from -90 to -20 °C, with a 10 °C step size, exhibiting the γ -relaxation occurring in the glassy state of Quinidine.

for Quinidine heated from the amorphous state. The secondary relaxation in amorphous Quinidine was found to shift toward lower frequencies upon cooling, reflecting a supposed decrease in the molecular mobility. This distinct secondary relaxation was fitted using one HN relaxation function.

The activation energy for this secondary process was found to be $E_a = 53.8$ kJ/mol. According to the latest research on

amorphous pharmaceuticals, there has been growing recognition that the high activation-energy barrier (typically, $E_a > 50$ kJ/mol) for secondary relaxation processes may be related to motions involving the whole molecule or conformational motions within it, whereas low values ($E_a < 50$ kJ/mol) could be linked to intramolecular motions.^{30,79} For instance, Grzybowska et al.⁸⁰ have underlined several secondary relaxations in amorphous Celecoxib. They determined that the β process was characterized by a large activation-energy value ($E_{a,\beta} = 80$ kJ/mol), whereas the γ and δ processes had smaller values ($E_{a,\gamma} = 51$ kJ/mol and $E_{a,\delta} = 21$ kJ/mol). β -process relaxation was classified as a JG relaxation, indicating motions involving the whole molecule, whereas the faster γ and δ processes have been ascribed to intramolecular motions of side groups of Celecoxib. Therefore, in light of these facts, the intermediate value of activation energy found for our secondary relaxation process indicates that secondary relaxation may arise from motions of small parts of the Quinidine molecule. This is why in the following sections the present secondary relaxation process will be called γ process.

To definitively confirm the nature of this secondary relaxation in amorphous Quinidine, the extended-coupling model prediction proposed by Ngai was applied.^{72,81} This model predicts a correlation between the relaxation time of JG secondary relaxation (τ_{JG}) and that of primitive relaxation (τ_0), which corresponds to the relaxation times of the hidden secondary process.⁸² As already mentioned, knowing whether a secondary relaxation is a JG relaxation is particularly relevant to the question of MD of amorphous pharmaceuticals.^{62,83} For some years now, the JG β -relaxation has been believed to be the precursor of α relaxation and has been associated with rotation of the entire molecule.⁶⁹

It is clearly observed in the relaxation map in Figure 5 that the dependence of primitive relaxation times $\tau_0(T)$ did not agree with the dependence of relaxation times of the secondary γ relaxation. However, as mentioned above, one cannot exclude the possibility of a hidden relaxation process under the excess wing found close to the structural relaxation. Indeed, the extent of γ -relaxation times tend to overlap the primitive relaxation times (τ_0) at $\log \tau_{\max} = -6.71$ s. Actually, using the representative masterplot of Quinidine in the glassy state in Figure 8, an inspection of the primitive relaxation frequency ($f_0 = 1/2\pi\tau_0 = 124 \times 10^3$ Hz, with $\tau_0 = 0.128 \times 10^{-5}$ s) determined at $T_g = 60$ °C indicates that f_0 lies within a range of frequencies close to the α relaxation in the excess wing. Relaxation times obtained from the HN fit of this excess wing showed that relaxation times from the excess wing (denoted β_{J-G}) and from the coupling model (τ_0) lie in nearly the same dependence range. This procedure confirms that the high-frequency flank of the structural relaxation is a JG β relaxation⁷⁸ and supports the fact that the γ process appears to have an intramolecular origin.

Moreover, as measurement of molecular mobility in the glassy state could be particularly complex, the masterplot approach can be used and extended to the region below T_g to evaluate the time scale of structural relaxation in the glassy state.^{70,84} We were careful to select temperatures adequately close to T_g , at which evolution of the glassy system toward equilibrium is fast. The predicted relaxation times below T_g are displayed in Figure 5. It can be observed that the masterplot prediction follows the VTF trend over a temperature range from $T_g (= 60$ °C) to just below $T_g (= 53$ °C). The extrapolation of this trend shows that the time scale of

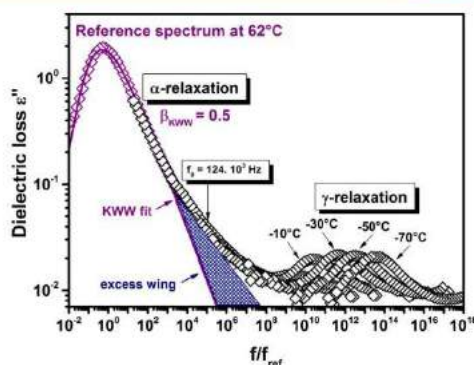


Figure 8. Masterplot of Quinidine in the glassy state, obtained by horizontally shifting several spectra (from 50 to -70 °C) to superimpose the spectrum at 62 °C. The purple full line corresponds to the KWW fit of the structural relaxation peak at 62 °C, with $\beta_{KWW} = 0.5$. The reference spectrum is located at 62 °C.

structural relaxation at room temperature will likely exceed years.

3.4. Origin of the Secondary γ Relaxation in Amorphous Quinidine. Although the value of activation energy of the γ relaxation could be experimentally obtained by dielectric measurements, no evidence of the relevant part of the molecular moieties involved in the transition can be directly inferred. Indeed, the origin of secondary relaxations remains elusive, as no straightforward answer could be obtained until now. Indeed, secondary relaxations may arise from complex intramolecular changes involving more than one moiety or can also be related to a JG process, which is not the case here. As discussed earlier, dielectric measurements can provide valuable information, allowing accurate description of the MD of secondary relaxations occurring below T_g . In recent years, there has been a growing interest in theoretical conformational calculations or MD simulations to unravel the physical nature of the transition at the atomic level,^{85,86} sometimes combined with experimental studies.^{87,88,11} In line with this synergetic approach, additional information is sought to reveal the origin of secondary processes through exploitation of calculated energy barriers and dipole moments when appropriate selected flexible end groups are relaxing.

Kaminski et al.⁸⁹ highlighted in an amorphous equimolar mixture of D-glucose and D-fructose that torsion motions of monosugar units through the glycosidic bond could be responsible of the β relaxation. In the same manner, Włodarczyk et al.⁹⁰ performed studies on β relaxation in amorphous D-maltose and found, after comparison of experimental and theoretical activation energies, that movement of monosugar units around glycosidic linkages could be related to this relaxation process. Likewise, Grzybowska et al.⁸⁰ evidenced possible interconversion pathways of the amorphous Celecoxib molecule and postulated that γ relaxation originates from the rotation of the pH-SO₂NH₂ group of Celecoxib. Moreover, Hensel-Bielowka et al.⁹¹ showed in an amorphous protic ionic conductor that the mechanism of secondary relaxation originates from conformational changes in the dimethylamine group. All of these theoretical data were compared to the experimental dielectric results and found to

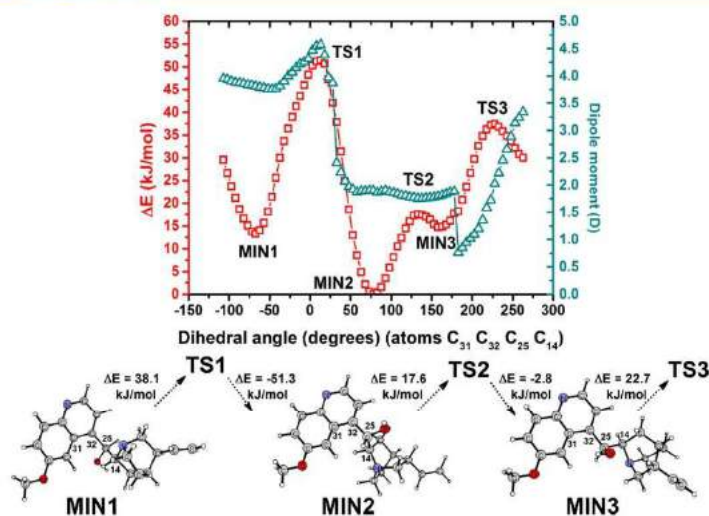


Figure 9. Visualization of variations in the self-consistent field energy (ΔE) and magnitude of the dipole moment during rotation of the $\text{CH(OH)C}_9\text{H}_{14}\text{N}$ group (atoms C_{31} , C_{32} , C_{25} , C_{14}) with DFT at the $\omega\text{B97XD}/6\text{-31+G(d)}$ level in the gas phase. The conformational interconversions during movement of a part of the molecular moiety are also displayed, as well as the calculated energy barriers.

be in relative good agreement (considering the experimental uncertainty). However, these calculations were not performed by taking into account the mean electrostatic behavior taking place in the molten state (i.e., closer to the amorphous state). Thus, we aimed to use the polarizable continuum model to meet our experimental work as closely as possible. Therefore, in a complementary manner to the experimental dielectric study, theoretical calculations in the gas phase and in a solvent environment could allow clarification of the origin of the secondary γ relaxation in amorphous Quinidine.

From this perspective, we first explored the PES in the gas phase through relaxed geometry scans of selected coordinates. With the ωB97XD functional, we chose to first use an intermediate basis set, 6-31+G(d). After clarification of activation barriers with the identification of relevant MIN and TS, we selected a higher level of theory, with the 6-311++G(2d,2p) basis set. Starting from the optimized structure, the dihedral angle was continuously changed by a constant step of 5° in the whole range of 360° , enabling accurate sampling. At the frozen value of the corresponding angle, the rest of the molecule was optimized (i.e., relaxed scan procedure) and the energy as well as molecular dipole moment was calculated.

Exploration of the PES related to the rotation of the $\text{CH(OH)C}_9\text{H}_{14}\text{N}$ group proved that conformational interconversions through three MIN and three TS (Figure 9) are feasible. Moreover, one can have access to the molecular dipole moment as a function of the torsional dihedral angle. Interestingly enough, each energy is linked to a more or less important change in the dipole moment, especially among MIN1/TS1, TS1/MIN2, and MIN3/TS3.

For amorphous Quinidine, the activation energy of the γ relaxation, found experimentally from dielectric measurements, $E_{\gamma, \gamma}$ is 53.8 kJ/mol, in very good agreement with the highest energy barrier concerning the rotation of the $\text{CH(OH)C}_9\text{H}_{14}\text{N}$ end group obtained from theoretical calculations. Indeed, the

highest energy barrier between conformers MIN1 and MIN2 (through TS1) was found to correspond to an energy difference of 51.3 kJ/mol (pathway A). However, another pathway affording MIN2 from MIN1 has been determined: it consists of a two-step mechanism (whereas pathway A corresponds to a single elementary step) through instable intermediate MIN3, which can either reform MIN2 via TS2 (almost no barrier) or evolve into MIN2 through TS3, the overall energy barrier being equal to 37.5 kJ/mol (pathway B). Rotation of the $\text{CH(OH)C}_9\text{H}_{14}\text{N}$ group substituent is connected to a large dipole moment fluctuation from 4.5 to 1.9 D for pathway A (TS1 to MIN2). On the contrary, very small variations in the dipole moment are observed for pathway B (MIN2 to TS3), with a change of 1.9–2.2 D. Therefore, only pathway A could be observed by means of dielectric spectroscopy, as it is highly sensitive to changes in the dipole moment.

Its origin can be traced using Bader's atoms-in-molecules theory (QTAIM),^{92,93} which allows for exact decomposition (eq S3) of molecular dipole moments, $\vec{\mu}^{\text{mol}}$, into atomic components, which can in turn be expressed as the sum of interatomic charge transfer ($\vec{\mu}^{\text{inter}}$) and intra-atomic polarization ($\vec{\mu}^{\text{pol}}$) components.^{92–95} We found that $\vec{\mu}^{\text{inter}}$ is 84% higher in MIN1 than that in MIN2 (4.65 vs 2.53D), whereas $\vec{\mu}^{\text{pol}}$ is only 43% higher in MIN1 than that in MIN2 (2.92 vs 2.04D). The competition between these two contributions can be measured by efficiency factor $\varepsilon = \cos(\vec{\mu}^{\text{pol}}, \vec{\mu}^{\text{inter}})$, which is equal to -1 when the two vectors are strictly opposite (leading to full "counterpolarization") and $+1$ when they have complete cumulative effects. In general,^{94,95} ε is negative, a property that is verified for MIN1 and MIN2, the first conformation being less unfavorable (ε is equal to -0.61 for MIN1 and -0.68 for MIN2). Such values indicate that the higher dipole moment in MIN1 is due to the predominance of interatomic charge transfer over electronic polarization, whereas, quite counter-intuitively, the charge transfer amount (eq S4) between the

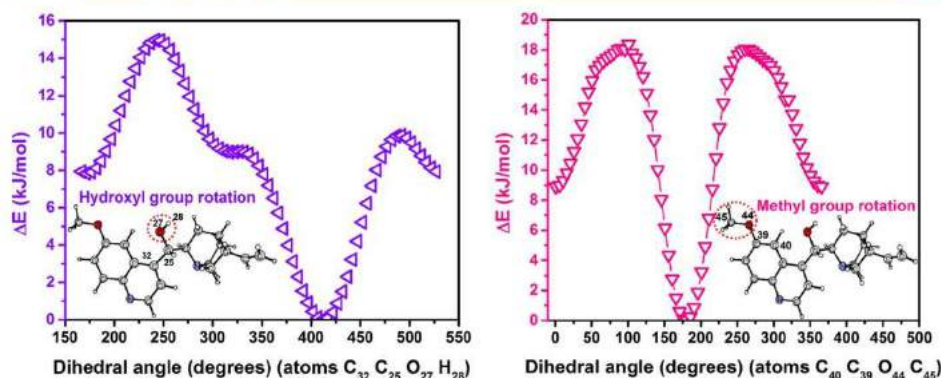


Figure 10. Visualization of changes in the energy (ΔE) during rotation of the hydroxyl group (atoms C_{32} , C_{25} , O_{27} , H_{28}) (left panel) and methyl group (atoms C_{40} , C_{39} , O_{44} , C_{45}) (right panel) with DFT at the ω B97XD/6-31+G(d) level in the gas phase.

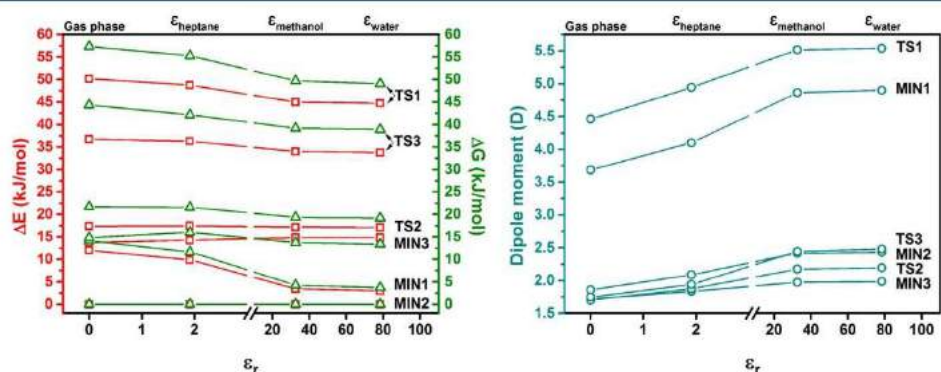


Figure 11. Plot of energy (ΔE) and Gibbs free energy (ΔG^\ddagger) (left) and dipole moment (D) (right) as functions of solvent environment (ϵ_r) at the ω B97XD/6-31+G(2d,2p) level. Please note the break in the x axis.

vinylquinuclidin and methoxyquinolinyl methanol moieties is slightly lower (0.028 vs 0.060e) in MIN1.

Such a decomposition is actually impossible with force fields where atomic charges are generally kept fixed along the whole simulation; thus, the variations in dipole moments in molecular mechanics (MM) calculations are only due to structural changes. Furthermore, the atomic charges defined in a given force field result from fitting on reference molecules that are different from the studied ones. The transferability of common force field parameters to our studied molecules certainly deserves to be studied, but this is clearly outside the scope of the present article.

From another methodological point of view, a closer look at the conformational interconversion in Quinidine between 150 and 200° shows a sudden change in the dipole moment, dropping from 1.88D (at 177.9°) to 0.77D (at 182.9°) (see Figure S6). Despite this, the energy variation is almost continuous (1.4 kJ/mol). Upon careful examination of the conformational interconversion, we can clearly see a conformational change in the hydroxyl group, which is very polar. Obviously, such a “jump” is an artifact of the static approach

that we used, whereas reorientation of the hydroxyl group is expected to occur more smoothly within a dynamic representation.

In the approach of examining all conformations and possible interconversion pathways of the Quinidine molecule to identify its secondary relaxation, it was verified that the rotation of other flexible groups did not lead to activation-energy values corresponding to the secondary relaxation. In fact, for rotation of the hydroxyl group as well as of the methyl group, lower values were found (in the order of 16 and 20 kJ/mol, respectively), with respect to the value of 50 kJ/mol for the secondary process (Figures 10 and 11).

As activation barriers were clarified by identification of relevant MIN and TS, we selected energy calculations at a higher level of theory to refine our estimates. Therefore, we used the same functional ω B97XD but with the 6-311++G(2d,2p) basis set. Calculations were performed in the gas phase, as performed previously, and also in three solvents with distinct values of dielectric constants to cover an electrostatic range of environments as large as possible. For that purpose, we selected heptane ($\epsilon_{\text{heptane}} = 1.9$), methanol ($\epsilon_{\text{methanol}} = 32.6$),

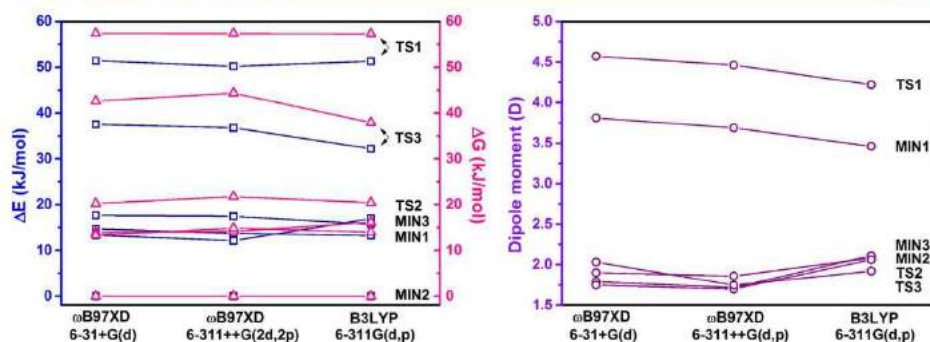


Figure 12. Plot of energy (ΔE) and Gibbs free energy (ΔG^\ddagger) (left) and dipole moment (D) (right) in the gas phase as a function of selected functional and basis sets.

and water ($\epsilon_{\text{water}} = 78.4$). Finally, to assess the relevance of thermodynamic factors, standard Gibbs free energy (ΔG^\ddagger) was retrieved. Figure 11 displays variations in energy (ΔE), Gibbs free energy (ΔG^\ddagger), and dipole moment (D) as functions of solvent environment for the three obtained MIN and TS (see Table S1 for numerical values).

For the MIN as well as TS (Figure 11, left panel), comparison between values of ΔE and ΔG^\ddagger suggests that activation barriers are only very slightly affected by the solvent environment, as the values are almost similar. Moreover, temperature does not have a significant influence on energy barriers, as comparable values for ΔE and ΔG^\ddagger were obtained. This is not surprising, as the transition is intramolecular and thus entropy variations are expected to be small. Finally, we note an intuitive increase in the dipole moment with solvent polarity (Figure 11, right panel). It is worth noting that, experimentally, the dielectric constant range is not as extended as that in the above theoretical calculations (i.e., up to $\epsilon = 78.4$). Indeed, in the temperature and frequency range applied in this work, the dielectric constant of our amorphous Quinidine would only have values of $1 \leq \epsilon_{\text{amorphous Quinidine}} \leq 2$, thus giving rise to almost no modification in activation barrier values with different environments (according to Figure 11).

Finally, we have chosen to compare the functional and basis sets used in this work (i.e., ω B97XD/6-31+G(d) and ω B97XD/6-311++G(2d,2p)) with those most popularly used in the literature. Regardless of the functional and basis sets, we note that the obtained energy barriers for ΔE and ΔG^\ddagger have identical values, except a small decrease for TS3 with B3LYP/6-311G(d,p) (Figure 12, left panel). Let us recall that the global hybrid B3LYP functional, albeit still popular, is actually less "modern" than the dispersion-corrected range-separated hybrid ω B97XD functional. More specifically, ω B97XD has the correct asymptotic behavior (far from the nuclei) of the exchange potential ($v_x(\vec{r}) \approx -1/r$), contrary to B3LYP ($v_x(\vec{r}) \approx -0.20/r$). This feature is actually known to be important for accurate computation of activation barriers. Moreover, B3LYP is unable to describe dispersion (London interaction) effects.

However, one may argue that these last ones are not so important in intramolecular cases. Nevertheless, here, we wanted to design a computational protocol that can be also applied to intermolecular interactions. As a preliminary result, we optimized quinidine dimer ω B97X-D, obtaining an

interaction energy equal to -17.0 kcal/mol. Interestingly, the contribution of Grimme's correction (which provides a crude estimate of the interaction energy due to dispersion) amounts to -7.7 kcal/mol. This number explains why B3LYP predicts a significantly lower (in absolute value) interaction energy (-7.7 kcal/mol for a single-point calculation). As expected, dipole moments (Figure 12, right panel) are more sensitive to the basis set compared to that of activation energies, thus showing limited variation.

Therefore, from the above DFT calculations, we have highlighted that the well-resolved secondary relaxation occurring in glassy Quinidine appears to have an intramolecular origin coming from the rotation of the $\text{CH}(\text{OH})\text{C}_9\text{H}_{14}\text{N}$ end group. This is supported by a comprehensive dielectric relaxation study on Quinaldine (i.e., 2-methylquinoline), which corresponds to the rigid and planar parts of Quinidine.⁹⁶ This study evidenced that Quinaldine displays a lower T_g ($= -93$ °C) and fragility ($m = 76 \pm 6$) but a higher β_{KWW} (0.72). Moreover, it provides evidence that no resolved secondary relaxation is observed in Quinaldine.⁹⁷ It is therefore clear that the flexible part, $\text{CH}(\text{OH})\text{C}_9\text{H}_{14}\text{N}$, of the Quinidine molecule appears to generate the secondary γ relaxation detected. However, one should keep in mind that our static DFT calculations, consistent with those in the literature, were made on an individual molecule; thus, they cannot fully unravel the possible cooperative effects of several molecules on this intramolecular isomerization. Note, however, that the molecule is not "fully" isolated, as it is immersed in a polarizable continuum that implicitly includes the average electrostatic effects of the environment.

It is fair to add that collective effects can be described by calculations of MM. As MM can be used to simulate much more long-time dynamics simulations than those from ab initio quantum dynamics, it also offers a powerful way for determining the frequency-dependent dielectric spectrum through the fluctuation–dissipation theorem. From all points discussed above, it is obvious that both approaches (DFT and MM MD) have their advantages and drawbacks: A synergetic DFT/MM approach would be highly desirable.

4. CONCLUSIONS

Herein, we studied the molecular mobility of an amorphous API, Quinidine, in both the supercooled and glassy states. Using different experimental (BDS and TMDSC) and

theoretical (DFT) techniques, we established descriptions of the different molecular motions from the glass to the liquid state of Quinidine. It was shown that the dielectric analysis was suitable to analyze amorphous Quinidine, allowing (1) direct visualization of the structural relaxation associated with the dynamic glass transition, (2) precise determination of significant parameters to retrieve (T_g , m , β_{KW} , etc.), and (3) observation of a secondary relaxation process well below T_g at which localized motions persist. Above T_g in the supercooled liquid state, dielectric spectra show a medium degree of nonexponentiality ($\beta_{\text{KW}} = 0.5$). The temperature dependence of relaxation times diverges from linearity, which was quantified by a relatively high value of the fragility index ($m = 86$), enabling consideration of Quinidine as an intermediately fragile glass former. Below T_g in the glassy state, the relaxation times of the secondary γ relaxation present an Arrhenius temperature dependence, which gives us an apparent activation energy equal to 53.8 kJ/mol. An unresolved JG β relaxation was also identified in the excess wing observed in amorphous Quinidine. From theoretical DFT calculations, we have highlighted that the well-resolved γ process appears to have an intramolecular origin coming from the rotation of the CH(OH)C₉H₁₄N end group. All obtained theoretical data were compared to experimental dielectric results and found to be in very good agreement, considering the experimental uncertainty. Furthermore, experimental evaluation of the life expectancy of Quinidine in the glassy state has shown that the sample was still amorphous after 16 months of storage at 20 °C. Sub- T_g crystallization experiments have shown a similar trend between τ_{cryst} times and the α -relaxation times, indicating a possible correlation between molecular mobility of structural relaxation and crystallization tendency. Thus, the difference between T_g and the onset temperature for crystallization, T_o , which is 30 K, is sufficiently large to avoid, so far in our study, recrystallization of amorphous Quinidine during more than 1 year of storage under ambient conditions. In conclusion, the relatively high value of T_g indicates the possibility of preparing an oral dosage form of Quinidine that is completely amorphous under standard conditions.

■ ASSOCIATED CONTENT

Supporting Information

The Supporting Information is available free of charge on the ACS Publications website at DOI: 10.1021/acs.jpcb.6b04242.

Experimental and calculated XRPD patterns of crystalline Quinidine; thermogravimetric analysis of the as-received crystalline Quinidine; DSC thermograms of amorphous Quinidine, measured immediately after preparation and after 16 months of storage at 20 °C (T_g , 40 °C), dielectric strength $\Delta\epsilon$ parameter of the HN relaxation function as a function of temperature, symmetric and asymmetric broadening parameters of the HN relaxation function as a function of temperature; visualization of energy, dipole changes, and conformational interconversions before and after the sharp decrease in the dipole moment during the rotation of the CH(OH)C₉H₁₄N group; and finally, the energy (ΔE), Gibbs free energy (ΔG^\ddagger), and dipole moment (D) for the three obtained MIN and TS with and without solvent at the ω B97XD/6-311++G(2d,2p) level. Detailed descriptions of the BDS experimental protocols and data fitting and QTAIM

decomposition of molecular dipole moments are also provided (PDF)
3D rotatable image of conformational interconversions during movement of the flexible part of the molecule (XYZ)

■ AUTHOR INFORMATION

Corresponding Authors

*E-mail: valerie.dupray@univ-rouen.fr. Tel: +33 2 32 39 90 82 (V.D.).

*E-mail: laurent.delbreilh@univ-rouen.fr. Tel: +33 2 32 95 50 84 (L.D.).

Notes

The authors declare no competing financial interest.

■ ACKNOWLEDGMENTS

The Region Haute Normandie is acknowledged for financial support to B.S. via E.D. No. 351 (SPMII). V.T. and L.J. thank the FEDER program and LABEX SynOrg for support. V.T. thanks the Centre National de la Recherche Scientifique (CNRS) for a half-time "délégation". The authors would like also to acknowledge the high-performance computing facility (CRIANN) funded by the Region Haute Normandie.

■ REFERENCES

- (1) Serajuddin, A. T. M. Solid Dispersion of Poorly Water-Soluble Drugs: Early Promises, Subsequent Problems, and Recent Breakthroughs. *J. Pharm. Sci.* **1999**, *88*, 1058–1066.
- (2) Leuner, C.; Dressman, J. Improving Drug Solubility for Oral Delivery Using Solid Dispersions. *Eur. J. Pharm. Biopharm.* **2000**, *50*, 47–60.
- (3) Vasconcelos, T.; Sarmiento, B.; Costa, P. Solid Dispersions as Strategy to Improve Oral Bioavailability of Poor Water Soluble Drugs. *Drug Discovery Today* **2007**, *12*, 1068–1075.
- (4) Amidon, G. L.; Lennernäs, H.; Shah, V. P.; Crison, J. R. A Theoretical Basis for a Biopharmaceutical Drug Classification: The Correlation of in Vitro Drug Product Dissolution and in Vivo Bioavailability. *Pharm. Res.* **1995**, *12*, 413–420.
- (5) Williams, H. D.; Trevaskis, N. L.; Charman, S. A.; Shanker, R. M.; Charman, W. N.; Pouton, C. W.; Porter, C. J. H. Strategies to Address Low Drug Solubility in Discovery and Development. *Pharmacol. Rev.* **2013**, *65*, 315–499.
- (6) Babu, N. J.; Nangia, A. Solubility Advantage of Amorphous Drugs and Pharmaceutical Cocrystals. *Cryst. Growth Des.* **2011**, *11*, 2662–2679.
- (7) Zhou, D.; Zhang, G. G. Z.; Law, D.; Grant, D. J. W.; Schmitt, E. A. Physical Stability of Amorphous Pharmaceuticals: Importance of Configurational Thermodynamic Quantities and Molecular Mobility. *J. Pharm. Sci.* **2002**, *91*, 1863–1872.
- (8) Schammé, B.; Couvrat, N.; Malpeli, P.; Dudognon, E.; Delbreilh, L.; Dupray, V.; Dargent, É.; Coquerel, G. Transformation of an Active Pharmaceutical Ingredient upon High-Energy Milling: A Process-Induced Disorder in Bidotymol. *Int. J. Pharm.* **2016**, *499*, 67–73.
- (9) Aso, Y.; Yoshioka, S.; Kojima, S. Relationship between the Crystallization Rates of Amorphous Nifedipine, Phenobarbital, and Flopropione, and Their Molecular Mobility as Measured by Their Enthalpy Relaxation and ¹H NMR Relaxation Times. *J. Pharm. Sci.* **2000**, *89*, 408–416.
- (10) Bhugra, C.; Pikal, M. J. Role of Thermodynamic, Molecular, and Kinetic Factors in Crystallization from the Amorphous State. *J. Pharm. Sci.* **2008**, *97*, 1329–1349.
- (11) Knapik, J.; Wojnarowska, Z.; Grzybowska, K.; Hawelek, L.; Sawicki, W.; Włodarski, K.; Markowski, J.; Paluch, M. Physical Stability of the Amorphous Anticholesterol Agent (Ezetimibe): The Role of Molecular Mobility. *Mol. Pharmaceutics* **2014**, *11*, 4280–4290.

- (12) Schammé, B.; Couvrat, N.; Malpeli, P.; Delbreilh, L.; Dupray, V.; Dargent, É.; Coquerel, G. Crystallization Kinetics and Molecular Mobility of an Amorphous Active Pharmaceutical Ingredient: A Case Study with Bicyclotymol. *Int. J. Pharm.* **2015**, *490*, 248–257.
- (13) Yoshioka, M.; Hancock, B. C.; Zografi, G. Crystallization of Indomethacin from the Amorphous State below and above Its Glass Transition Temperature. *J. Pharm. Sci.* **1994**, *83*, 1700–1705.
- (14) Sun, Y.; Zhu, L.; Wu, T.; Cai, T.; Gunn, E. M.; Yu, L. Stability of Amorphous Pharmaceutical Solids: Crystal Growth Mechanisms and Effect of Polymer Additives. *AAPS J.* **2012**, *14*, 380–388.
- (15) Capen, R.; Christopher, D.; Forenzo, P.; Ireland, C.; Liu, O.; Lyapustina, S.; O'Neill, J.; Patterson, N.; Quinlan, M.; Sandell, D.; et al. On the Shelf Life of Pharmaceutical Products. *AAPS PharmSciTech* **2012**, *13*, 911–918.
- (16) Kauzmann, W. The Nature of the Glassy State and the Behavior of Liquids at Low Temperatures. *Chem. Rev.* **1948**, *43*, 219–256.
- (17) Chen, L.; Okuda, T.; Lu, X.-Y.; Chan, H.-K. Amorphous Powders for Inhalation Drug Delivery. *Adv. Drug Delivery Rev.* **2016**, *100*, 102–115.
- (18) Hancock, B. C.; Shamblin, S. L. Molecular Mobility of Amorphous Pharmaceuticals Determined Using Differential Scanning Calorimetry. *Thermochim. Acta* **2001**, *380*, 95–107.
- (19) Sánchez, M. S.; Touzé, Y.; Saiter, A.; Saiter, J. M.; Ribelles, J. L. G. Influence of the Chemical Structure on the Kinetics of the Structural Relaxation Process of Acrylate and Methacrylate Polymer Networks. *Colloid Polym. Sci.* **2004**, *283*, 711–720.
- (20) Nunes, T. G.; Viciosa, M. T.; Correia, N. T.; Danède, F.; Nunes, R. G.; Diogo, H. P. A Stable Amorphous Statin: Solid-State NMR and Dielectric Studies on Dynamic Heterogeneity of Simvastatin. *Mol. Pharmaceutics* **2014**, *11*, 727–737.
- (21) Alié, J.; Menegotto, J.; Cardon, P.; Duplaa, H.; Caron, A.; Lacabanne, C.; Bauer, M. Dielectric Study of the Molecular Mobility and the Isothermal Crystallization Kinetics of an Amorphous Pharmaceutical Drug Substance. *J. Pharm. Sci.* **2004**, *93*, 218–233.
- (22) Carpentier, L.; Decressain, R.; De Gussemé, A.; Neves, C.; Descamps, M. Molecular Mobility in Glass Forming Fananserine: A Dielectric, NMR, and TMDSC Investigation. *Pharm. Res.* **2006**, *23*, 798–805.
- (23) Johari, G. P.; Kim, S.; Shanker, R. M. Dielectric Relaxation and Crystallization of Ultraviscous Melt and Glassy States of Aspirin, Ibuprofen, Progesterone, and Quinidine. *J. Pharm. Sci.* **2007**, *96*, 1159–1175.
- (24) Brás, A. R.; Noronha, J. P.; Antunes, A. M. M.; Cardoso, M. M.; Schönhal, A.; Affouard, F.; Dionísio, M.; Correia, N. T. Molecular Motions in Amorphous Ibuprofen As Studied by Broadband Dielectric Spectroscopy. *J. Phys. Chem. B* **2008**, *112*, 11087–11099.
- (25) Danturli, A. K. R.; Amin, A.; Puri, V.; Bansal, A. K. Role of α -Relaxation on Crystallization of Amorphous Celecoxib above T_g Probed by Dielectric Spectroscopy. *Mol. Pharmaceutics* **2011**, *8*, 814–822.
- (26) Dantras, E.; Menegotto, J.; Demont, P.; Lacabanne, C. Dielectric Relaxation in Polymeric Materials. In *Dielectric Materials for Electrical Engineering*; Martínez-Vega, J., Ed.; John Wiley & Sons, Inc., 2013; pp 79–100.
- (27) Angell, C. A.; Ngai, K. L.; McKenna, G. B.; McMillan, P. F.; Martin, S. W. Relaxation in Glassforming Liquids and Amorphous Solids. *J. Appl. Phys.* **2000**, *88*, 3113–3157.
- (28) Bhattacharya, S.; Suryanarayanan, R. Local Mobility in Amorphous Pharmaceuticals—Characterization and Implications on Stability. *J. Pharm. Sci.* **2009**, *98*, 2935–2953.
- (29) Kaufman, T. S.; Ruveda, E. A. The Quest for Quinine: Those Who Won the Battles and Those Who Won the War. *Angew. Chem., Int. Ed.* **2005**, *44*, 854–885.
- (30) Roman, M.; Chruszcz-Lipska, K.; Baranska, M. Vibrational Analysis of Cinchona Alkaloids in the Solid State and Aqueous Solutions. *J. Raman Spectrosc.* **2015**, *46*, 1041–1052.
- (31) Sen, A.; Bouchet, A.; Lepère, V.; Le Barbu-Debus, K.; Scuderi, D.; Puzzi, F.; Zehacker-Rentien, A. Conformational Analysis of Quinine and Its Pseudo Enantiomer Quinidine: A Combined Jet-Cooled Spectroscopy and Vibrational Circular Dichroism Study. *J. Phys. Chem. A* **2012**, *116*, 8334–8344.
- (32) Lai, J.; Ma, Z.; Mink, L.; Mueller, L. J.; Zaera, F. Influence of Peripheral Groups on the Physical and Chemical Behavior of Cinchona Alkaloids. *J. Phys. Chem. B* **2009**, *113*, 11696–11701.
- (33) Johari, G. P.; Kim, S.; Shanker, R. M. Dielectric Study of Equimolar Acetaminophen-Aspirin, Acetaminophen-Quinidine, and Benzoic Acid-Progesterone Molecular Alloys in the Glass and Ultraviscous States and Their Relevance to Solubility and Stability. *J. Pharm. Sci.* **2010**, *99*, 1358–1374.
- (34) Kashino, S.; Haisa, M. Structure of Quinidine, $C_{20}H_{21}N_3O_2$. *Acta Crystallogr., Sect. C: Struct. Chem.* **1983**, *39*, 310–312.
- (35) Suryanarayanan, R.; Rastogi, S. X-Ray Powder Diffractometry. In *Encyclopedia of Pharmaceutical Technology*, 3rd ed.; Taylor & Francis, 2013; pp 4103–4116.
- (36) Sibik, J.; Löbmann, K.; Rades, T.; Zeitler, J. A. Predicting Crystallization of Amorphous Drugs with Terahertz Spectroscopy. *Mol. Pharmaceutics* **2015**, *12*, 3062–3068.
- (37) Dhotel, A.; Chen, Z.; Sun, J.; Youssef, B.; Saiter, J.-M.; Schönhal, A.; Tan, L.; Delbreilh, L. From Monomers to Self-Assembled Monolayers: The Evolution of Molecular Mobility with Structural Confinements. *Soft Matter* **2015**, *11*, 719–731.
- (38) Carpentier, L.; Decressain, R.; Desprez, S. Dynamics of the Amorphous and Crystalline α - γ -Phases of Indomethacin. *J. Phys. Chem. B* **2006**, *110*, 457–464.
- (39) Willart, J.-F.; Carpentier, L.; Danède, F.; Descamps, M. Solid-State Vittrification of Crystalline Griseofulvin by Mechanical Milling. *J. Pharm. Sci.* **2012**, *101*, 1570–1577.
- (40) Frisch, M. J.; Trucks, G. W.; Schlegel, H. B.; Scuseria, G. E.; Robb, M. A.; Cheeseman, J. R.; Scalmani, G.; Barone, V.; Mennucci, B.; Petersson, G. A.; et al. *Gaussian 09*; Gaussian, Inc.: Wallingford, CT, 2009.
- (41) Chai, J.-D.; Head-Gordon, M. Long-Range Corrected Hybrid Density Functionals with Damped Atom–atom Dispersion Corrections. *Phys. Chem. Chem. Phys.* **2008**, *10*, 6615–6620.
- (42) Tomasi, J.; Mennucci, B.; Cammi, R. Quantum Mechanical Continuum Solvation Models. *Chem. Rev.* **2005**, *105*, 2999–3094.
- (43) Scalmani, G.; Frisch, M. J. Continuous Surface Charge Polarizable Continuum Models of Solvation. I. General Formalism. *J. Chem. Phys.* **2010**, *132*, No. 114110, DOI: 10.1063/1.3359469.
- (44) Cancès, E.; Mennucci, B.; Tomasi, J. A New Integral Equation Formalism for the Polarizable Continuum Model: Theoretical Background and Applications to Isotropic and Anisotropic Dielectrics. *J. Chem. Phys.* **1997**, *107*, 3032–3041.
- (45) Keith, T. A. *AIMAll*; TK Gristmill Software: Overland Park, KS, 2016.
- (46) Vogel, H. The Law of the Relation between the Viscosity of Liquids and the Temperature. *Phys. Z.* **1921**, *22*, 645.
- (47) Fulcher, G. S. Analysis of Recent Measurements of the Viscosity of Glasses. *J. Am. Ceram. Soc.* **1925**, *8*, 339–355.
- (48) Tammann, G.; Hesse, W. The Dependence of Viscosity upon the Temperature of Supercooled Liquids. *Z. Anorg. Allg. Chem.* **1926**, *156*, 245–257.
- (49) *Broadband Dielectric Spectroscopy*; Kremer, F., Schönhal, A., Eds.; Springer: Berlin, 2003.
- (50) Adrjanowicz, K.; Kaminski, K.; Włodarczyk, P.; Grzybowska, K.; Tarnacka, M.; Zakowicki, D.; Garbacz, G.; Paluch, M.; Jurga, S. Molecular Dynamics of the Supercooled Pharmaceutical Agent Posaconazole Studied via Differential Scanning Calorimetry and Dielectric and Mechanical Spectroscopies. *Mol. Pharmaceutics* **2013**, *10*, 3934–3945.
- (51) Kawakami, K.; Harada, T.; Yoshihashi, Y.; Yonemochi, E.; Terada, K.; Moriyama, H. Correlation between Glass-Forming Ability and Fragility of Pharmaceutical Compounds. *J. Phys. Chem. B* **2015**, *119*, 4873–4880.
- (52) Angell, C. A. Glass Science and Technology Problems and Prospects for 2004 Spectroscopy Simulation and Scattering, and the Medium Range Order Problem in Glass. *J. Non-Cryst. Solids* **1985**, *73*, 1–17.

- (53) Rijal, B.; Delbreilh, L.; Saiter, A. Dynamic Heterogeneity and Cooperative Length Scale at Dynamic Glass Transition in Glass Forming Liquids. *Macromolecules* **2015**, *48*, 8219–8231.
- (54) Arabeche, K.; Delbreilh, L.; Saiter, J.-M.; Michler, G. H.; Adhikari, R.; Baer, E. Fragility and Molecular Mobility in Micro- and Nano-Layered PC/PMMA Films. *Polymer* **2014**, *55*, 1546–1551.
- (55) Crétois, R.; Delbreilh, L.; Dargent, E.; Follain, N.; Lebrun, L.; Saiter, J. M. Dielectric Relaxations in Polyhydroxyalkanoates/organoclay Nanocomposites. *Eur. Polym. J.* **2013**, *49*, 3434–3444.
- (56) Puente, J. A. S.; Rijal, B.; Delbreilh, L.; Fatyeyeva, K.; Saiter, A.; Dargent, E. Segmental Mobility and Glass Transition of Poly(ethylene-Vinyl Acetate) Copolymers: Is There a Continuum in the Dynamic Glass Transitions from PVAc to PE? *Polymer* **2015**, *76*, 213–219.
- (57) Kunal, K.; Robertson, C. G.; Pawlus, S.; Hahn, S. F.; Sokolov, A. P. Role of Chemical Structure in Fragility of Polymers: A Qualitative Picture. *Macromolecules* **2008**, *41*, 7232–7238.
- (58) Yu, L. Amorphous Pharmaceutical Solids: Preparation, Characterization and Stabilization. *Adv. Drug Delivery Rev.* **2001**, *48*, 27–42.
- (59) Böhmer, R.; Ngai, K. L.; Angell, C. A.; Plazek, D. J. Nonexponential Relaxations in Strong and Fragile Glass Formers. *J. Chem. Phys.* **1993**, *99*, 4201–4209.
- (60) Adrjanowicz, K.; Wojnarowska, Z.; Włodarczyk, P.; Kaminski, K.; Paluch, M.; Mazgalski, J. Molecular Mobility in Liquid and Glassy States of Telmisartan (TEL) Studied by Broadband Dielectric Spectroscopy. *Eur. J. Pharm. Sci.* **2009**, *38*, 395–404.
- (61) Wojnarowska, Z.; Adrjanowicz, K.; Włodarczyk, P.; Kaminska, E.; Kaminski, K.; Grzybowska, K.; Wrzaliak, R.; Paluch, M.; Ngai, K. L. Broadband Dielectric Relaxation Study at Ambient and Elevated Pressure of Molecular Dynamics of Pharmaceutical: Indomethacin. *J. Phys. Chem. B* **2009**, *113*, 12536–12545.
- (62) Adrjanowicz, K.; Kaminski, K.; Paluch, M.; Włodarczyk, P.; Grzybowska, K.; Wojnarowska, Z.; Hawelek, L.; Sawicki, W.; Lepek, P.; Lunio, R. Dielectric Relaxation Studies and Dissolution Behavior of Amorphous Verapamil Hydrochloride. *J. Pharm. Sci.* **2010**, *99*, 828–839.
- (63) Graeser, K. A.; Patterson, J. E.; Zeitler, J. A.; Gordon, K. C.; Rades, T. Correlating Thermodynamic and Kinetic Parameters with Amorphous Stability. *Eur. J. Pharm. Sci.* **2009**, *37*, 492–498.
- (64) Johari, G. P.; Shanker, R. M. On Determining the Relaxation Time of Glass and Amorphous Pharmaceuticals' Stability from Thermodynamic Data. *Thermochim. Acta* **2010**, *511*, 89–95.
- (65) Shamblin, S. L.; Hancock, B. C.; Dupuis, Y.; Pikal, M. J. Interpretation of Relaxation Time Constants for Amorphous Pharmaceutical Systems. *J. Pharm. Sci.* **2000**, *89*, 417–427.
- (66) Williams, G.; Watts, D. C. Non-Symmetrical Dielectric Relaxation Behaviour Arising from a Simple Empirical Decay Function. *Trans. Faraday Soc.* **1970**, *66*, 80–85.
- (67) Alvarez, F.; Alegria, A.; Colmenero, J. Relationship between the Time-Domain Kohlrausch-Williams-Watts and Frequency-Domain Havriliak-Negami Relaxation Functions. *Phys. Rev. B: Condens. Matter Mater. Phys.* **1991**, *44*, 7306–7312.
- (68) Nath, R.; Nowaczyk, A.; Geil, B.; Böhmer, R. 2H NMR Studies of Supercooled and Glassy Aspirin. *J. Non-Cryst. Solids* **2007**, *353*, 3788–3795.
- (69) Rodrigues, A. C.; Viciosa, M. T.; Danède, F.; Affouard, F.; Correia, N. T. Molecular Mobility of Amorphous S-Flurbiprofen: A Dielectric Relaxation Spectroscopy Approach. *Mol. Pharmaceutics* **2014**, *11*, 112–130.
- (70) Grzybowska, K.; Capaccioli, S.; Paluch, M. Recent Developments in the Experimental Investigations of Relaxations in Pharmaceuticals by Dielectric Techniques at Ambient and Elevated Pressure. *Adv. Drug Delivery Rev.* **2016**, *100*, 158–182.
- (71) Kolodziejczyk, K.; Paluch, M.; Grzybowska, K.; Grzybowski, A.; Wojnarowska, Z.; Hawelek, L.; Ziolo, J. D. Relaxation Dynamics and Crystallization Study of Sildenafil in the Liquid and Glassy States. *Mol. Pharmaceutics* **2013**, *10*, 2270–2282.
- (72) Ngai, K. L.; Paluch, M. Classification of Secondary Relaxation in Glass-Formers Based on Dynamic Properties. *J. Chem. Phys.* **2004**, *120*, 857.
- (73) Schneider, U.; Brand, R.; Lunkenheimer, P.; Loidl, A. Excess Wing in the Dielectric Loss of Glass Formers: A Johari-Goldstein β -Relaxation? *Phys. Rev. Lett.* **2000**, *84*, 5560–5563.
- (74) Lunkenheimer, P.; Wehn, R.; Riegger, T.; Loidl, A. Excess Wing in the Dielectric Loss of Glass Formers: Further Evidence for a β -Relaxation. *J. Non-Cryst. Solids* **2002**, *307–310*, 336–344.
- (75) Kessairi, K.; Capaccioli, S.; Prevosto, D.; Lucchesi, M.; Sharifi, S.; Rolla, P. A. Interdependence of Primary and Johari-Goldstein Secondary Relaxations in Glass-Forming Systems. *J. Phys. Chem. B* **2008**, *112*, 4470–4473.
- (76) Johari, G. P.; Goldstein, M. Viscous Liquids and the Glass Transition. II. Secondary Relaxations in Glasses of Rigid Molecules. *J. Chem. Phys.* **1970**, *53*, 2372–2388.
- (77) Johari, G. P.; Goldstein, M. Viscous Liquids and the Glass Transition. III. Secondary Relaxations in Aliphatic Alcohols and Other Nonrigid Molecules. *J. Chem. Phys.* **1971**, *55*, 4245–4252.
- (78) Ngai, K. L.; Lunkenheimer, P.; León, C.; Schneider, U.; Brand, R.; Loidl, A. Nature and Properties of the Johari-Goldstein β -Relaxation in the Equilibrium Liquid State of a Class of Glass-Formers. *J. Chem. Phys.* **2001**, *115*, 1405–1413.
- (79) Tarnacka, M.; Adrjanowicz, K.; Kaminska, E.; Kaminski, K.; Grzybowska, K.; Kolodziejczyk, K.; Włodarczyk, P.; Hawelek, L.; Garbacz, G.; Kocot, A.; et al. Molecular Dynamics of Itraconazole at Ambient and High Pressure. *Phys. Chem. Chem. Phys.* **2013**, *15*, 20742.
- (80) Grzybowska, K.; Paluch, M.; Włodarczyk, P.; Grzybowski, A.; Kaminski, K.; Hawelek, L.; Zakwiecki, D.; Kasprzycka, A.; Jankowska-Sumara, I. Enhancement of Amorphous Celecoxib Stability by Mixing It with Octaacetylmaltose: The Molecular Dynamics Study. *Mol. Pharmaceutics* **2012**, *9*, 894–904.
- (81) Ngai, K. L. An Extended Coupling Model Description of the Evolution of Dynamics with Time in Supercooled Liquids and Ionic Conductors. *J. Phys.: Condens. Matter* **2003**, *15*, S1107.
- (82) Hassine, B. B.; Négrier, P.; Romanini, M.; Barrio, M.; Macovez, R.; Kallel, A.; Mondieig, D.; Tamarit, J. L. Structure and Reorientational Dynamics of 1-F-Adamantane. *Phys. Chem. Chem. Phys.* **2016**, *18*, 10924–10930.
- (83) Wojnarowska, Z.; Swiety-Pospiech, A.; Grzybowska, K.; Hawelek, L.; Paluch, M.; Ngai, K. L. Fundamentals of Ionic Conductivity Relaxation Gained from Study of Procaine Hydrochloride and Procainamide Hydrochloride at Ambient and Elevated Pressure. *J. Chem. Phys.* **2012**, *136*, No. 164507, DOI: 10.1063/1.4705274.
- (84) Grzybowska, K.; Paluch, M.; Grzybowski, A.; Wojnarowska, Z.; Hawelek, L.; Kolodziejczyk, K.; Ngai, K. L. Molecular Dynamics and Physical Stability of Amorphous Anti-Inflammatory Drug: Celecoxib. *J. Phys. Chem. B* **2010**, *114*, 12792–12801.
- (85) Weingärtner, H.; Knocks, A.; Boresch, S.; Höchtel, P.; Steinhauser, O. Dielectric Spectroscopy in Aqueous Solutions of Oligosaccharides: Experiment Meets Simulation. *J. Chem. Phys.* **2001**, *115*, 1463–1472.
- (86) Molinero, V.; Goddard, W. A. Microscopic Mechanism of Water Diffusion in Glucose Glasses. *Phys. Rev. Lett.* **2005**, *95*, No. 045701, DOI: 10.1103/PhysRevLett.95.045701.
- (87) Włodarczyk, P.; Paluch, M.; Wojnarowska, Z.; Hawelek, L.; Kaminski, K.; Pilch, J. Theoretical and Experimental Studies on the Internal Mobility of Two Sulfonylurea Agents: Glibenclamide and Glimperide. *J. Phys.: Condens. Matter* **2011**, *23*, No. 425901, DOI: 10.1088/0953-8984/23/42/425901.
- (88) Wojnarowska, Z.; Grzybowska, K.; Hawelek, L.; Dulski, M.; Wrzaliak, R.; Gruszka, I.; Paluch, M.; Pienkowska, K.; Sawicki, W.; Bujak, P.; et al. Molecular Dynamics, Physical Stability and Solubility Advantage from Amorphous Indapamide Drug. *Mol. Pharmaceutics* **2013**, *10*, 3612–3627.
- (89) Kaminski, K.; Kaminska, E.; Hensel-Bielowka, S.; Chelmecka, E.; Paluch, M.; Ziolo, J.; Włodarczyk, P.; Ngai, K. L. Identification of the

Molecular Motions Responsible for the Slower Secondary (β) Relaxation in Sucrose. *J. Phys. Chem. B* **2008**, *112*, 7662–7668.

(90) Włodarczyk, P.; Kaminski, K.; Adrjanowicz, K.; Wojnarowska, Z.; Czarnota, B.; Paluch, M.; Ziolo, J.; Pilch, J. Identification of the Slower Secondary Relaxation's Nature in Maltose by Means of Theoretical and Dielectric Studies. *J. Chem. Phys.* **2009**, *131*, No. 125103, DOI: 10.1063/1.3224856.

(91) Hensel-Bielowka, S.; Ngai, K. L.; Swiety-Pospiech, A.; Hawelek, L.; Knapik, J.; Sawicki, W.; Paluch, M. On the Molecular Origin of Secondary Relaxations in Amorphous Protic Ionic Conductor Chlorpromazine Hydrochloride — High Pressure Dielectric Studies. *J. Non-Cryst. Solids* **2015**, *407*, 81–87.

(92) Bader, R. F. W. *Atoms in Molecules: A Quantum Theory*; International Series of Monographs on Chemistry; Oxford University Press: New York, 1990.

(93) Popelier, P. L. *Atoms in Molecules: An Introduction*; Pearson Education: Harlow, 2000.

(94) Bader, R. F. W.; Matta, C. F. Atomic Charges Are Measurable Quantum Expectation Values: A Rebuttal of Criticisms of QTAIM Charges. *J. Phys. Chem. A* **2004**, *108*, 8385–8394.

(95) Tognetti, V.; Joubert, L. Unraveling Charge Transfer Processes with the Quantum Theory of Atoms-in-Molecules. *Theor. Chem. Acc.* **2016**, *135*, 124.

(96) Li, X.; Wang, M.; Liu, R.; Ngai, K. L.; Tian, Y.; Wang, L.-M.; Capaccioli, S. Secondary Relaxation Dynamics in Rigid Glass-Forming Molecular Liquids with Related Structures. *J. Chem. Phys.* **2015**, *143*, No. 104505, DOI: 10.1063/1.4930262.

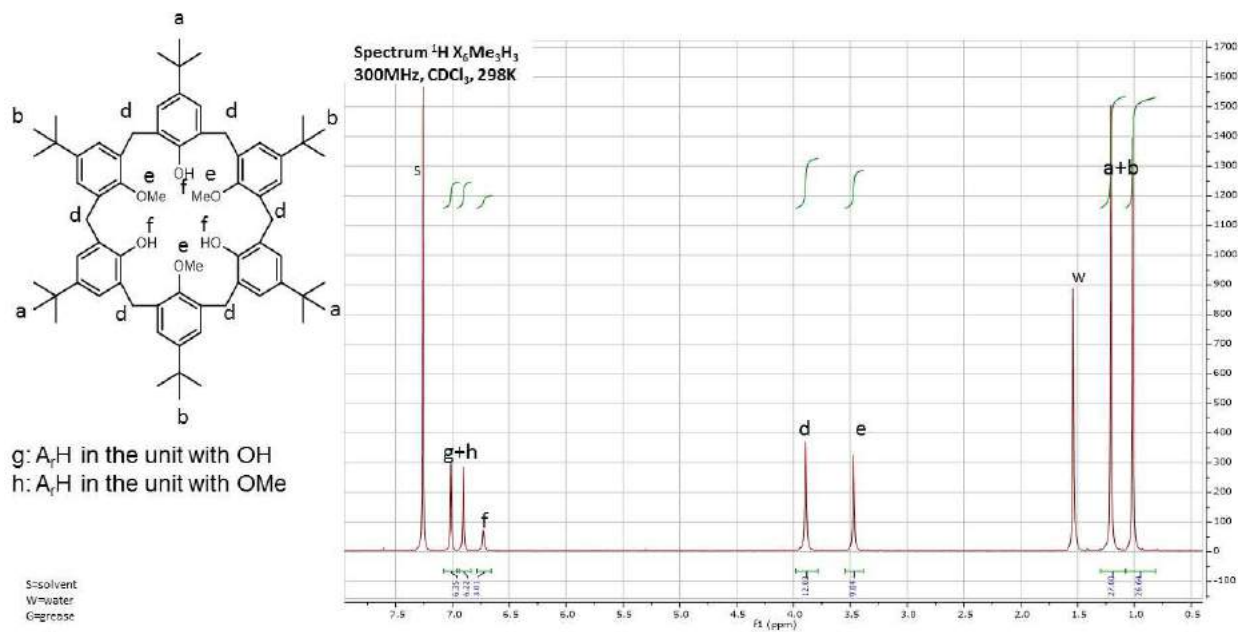
(97) Kahlau, R.; Gnutzmann, T.; Emmerling, F.; Rademann, K.; Rössler, E. A. Quinaldine: Accessing Two Crystalline Polymorphs via the Supercooled Liquid. *J. Chem. Phys.* **2012**, *137*, No. 054505, DOI: 10.1063/1.4738583.

2. Experimental section

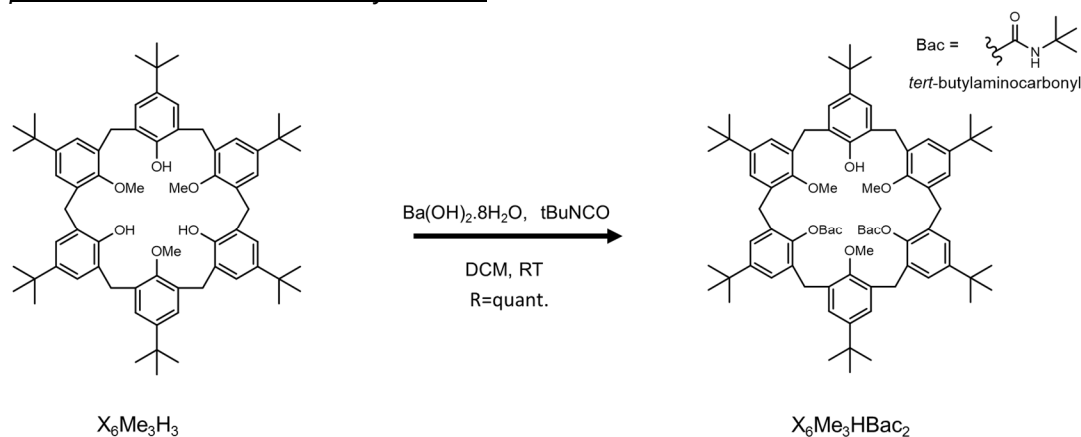
2.1. Calix[6]arene derivative synthesis

For all spectra, w refers to water and s to solvent.

Starting product: *p*-*t*Bu-calix[6]arene-tri-methyl



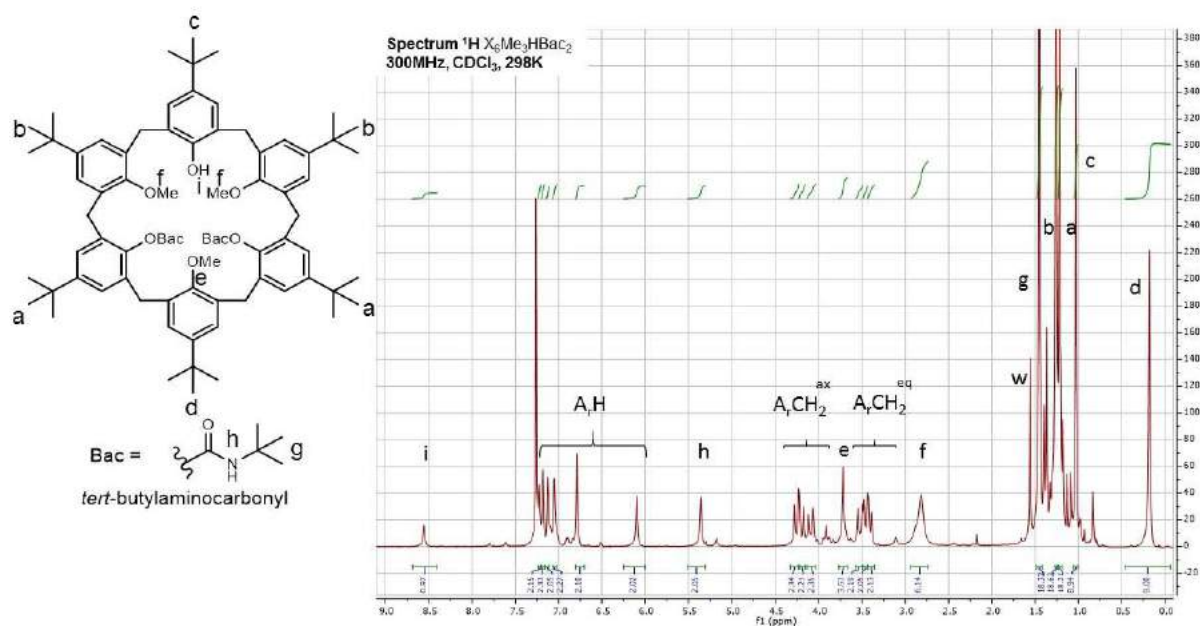
p-*t*Bu-calix[6]arene-tri-methyl-di-Bac



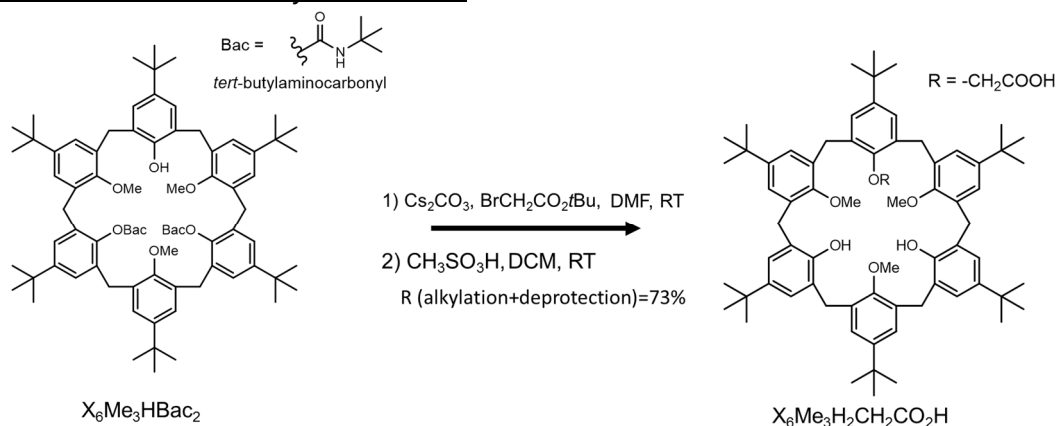
To 1 equivalent of *p*-*t*Bu-calix[6]arene ($\text{X}_6\text{Me}_3\text{H}_3$) in solution in DCM, 2 equivalents of $\text{Ba(OH)}_2 \cdot 8\text{H}_2\text{O}$ and then, 9 equivalents of *tert*-butylisocyanate (*t*BuNCO) were added and let under stirring for 24 hours. Then, a solution of HCl 0.1 M was added and the compound was extracted with DCM, and concentrated under vacuum. After purification under silica gel (DCM/Acetone 98/2 (v/v)), $\text{X}_6\text{Me}_3\text{HBac}_2$ was obtained quantitatively as a white solid.

MS: m/z 1287.73 [$\text{X}_6\text{Me}_3\text{HBac}_2 + t\text{BuNH}_3$]⁺

NMR: See the following spectra for attribution



p-*t*Bu-calix[6]arene-tri-methyl-mono-acid



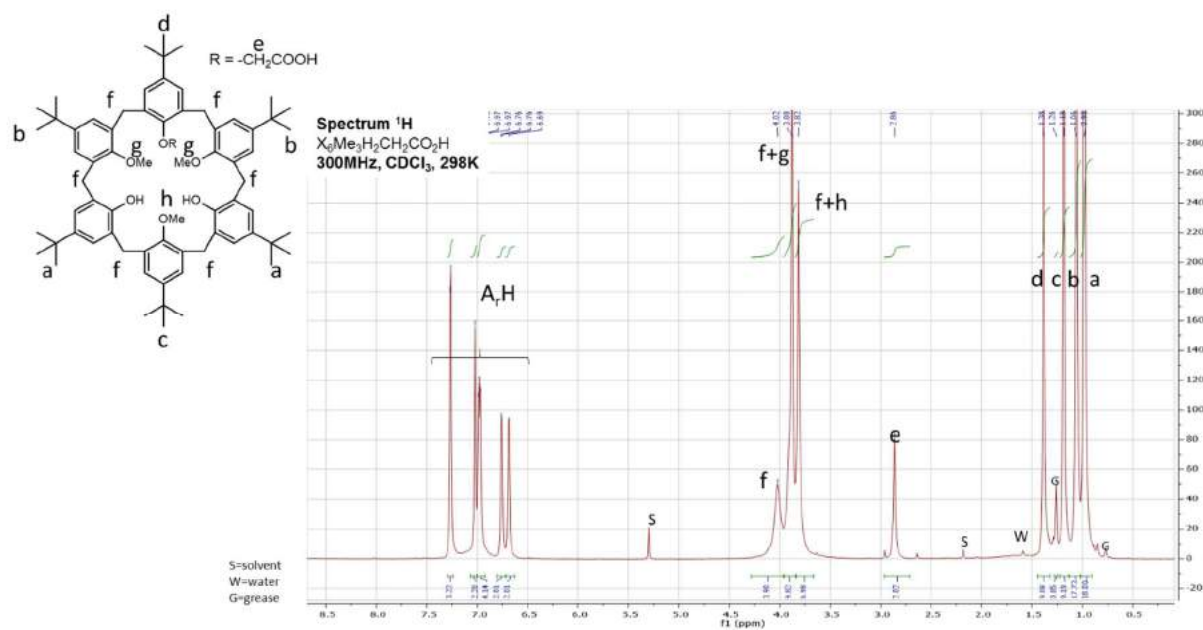
To 1 equivalent of $\text{X}_6\text{Me}_3\text{HBac}_2$ in solution in anhydrous DMF, 1.5 equivalent of anhydrous Cs_2CO_3 were added, with 5 equivalents of $\text{BrCH}_2\text{CO}_2t\text{Bu}$. The mixture reacted under agitation for 4 hours. To quench the reaction, a solution of HCl 0.1 M was added and precipitation of the product was obtained by addition of water. After filtration, successive dissolution in acetone and precipitation by water addition removed the excess of reagent. To the solid previously obtained, 20 equivalents of $\text{CH}_3\text{SO}_3\text{H}$ was added in DCM for 24 hours. The organic phase was washed with water until neutralization. After concentration under vacuum, the product was purified under silica gel (DCM/Acetone from 10% (v/v) to 30%).

MP: 171-172°C (dec.)

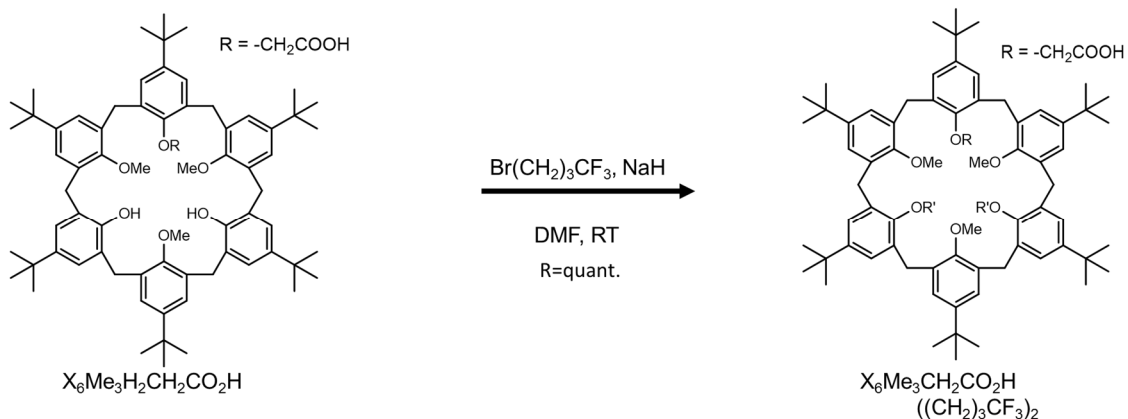
IR: 2956, 1684 cm^{-1}

HR-MS (ESI-TOF): m/z 1073.6931 $[\text{M}+\text{H}]^+$

NMR: See the following spectra for attribution



p-*t*Bu-calix[6]arene-di(propyltrifluoromethyl)tri-methyl-mono-acid



To 1 equivalent of the *p*-*t*Bu-calix[6]arene-mono-acid ($\text{X}_6\text{Me}_3\text{H}_2\text{CH}_2\text{CO}_2\text{H}$), 5 equivalents of NaH were added with 5 equivalents of $\text{Br}(\text{CH}_2)_3\text{CF}_3$ in anhydrous DMF for 4 hours under agitation.

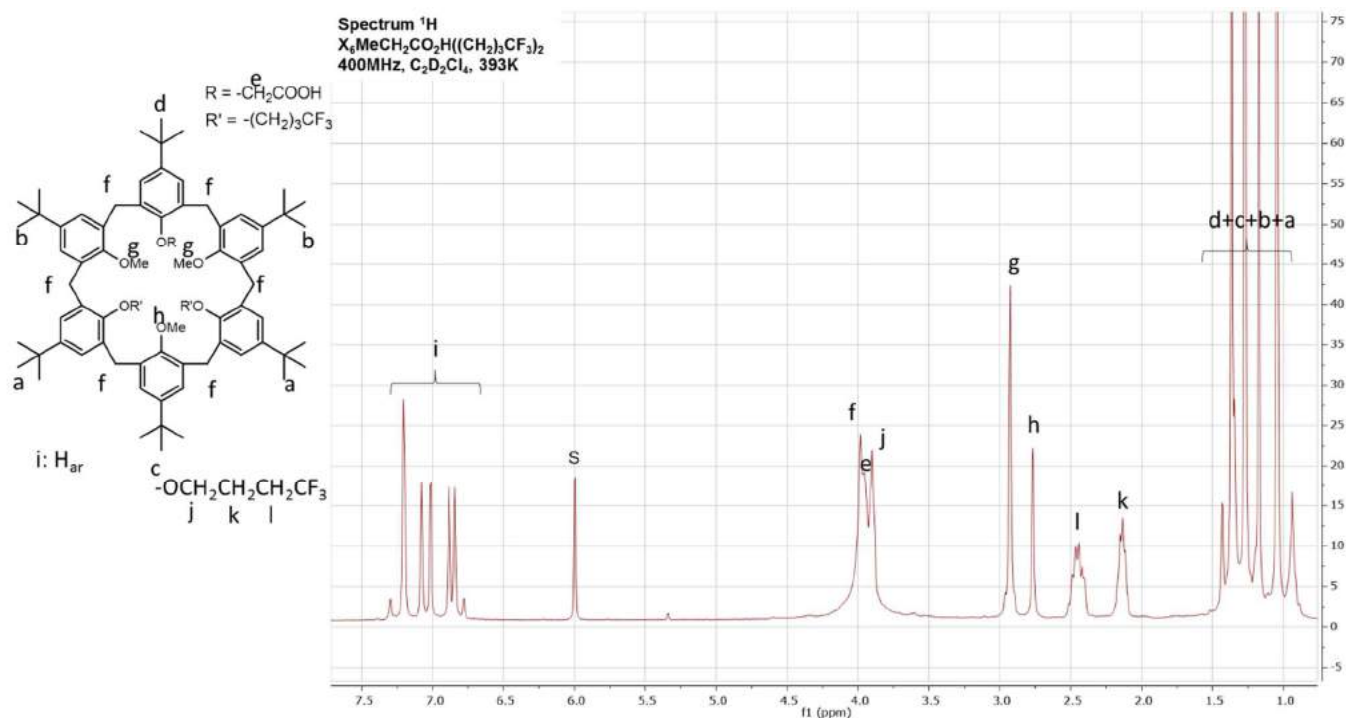
A solution of HCl 0.1 M was added and precipitation of the product was obtained by addition of water. After filtration, the final product was obtained quantitatively.

MP: 156-159°C

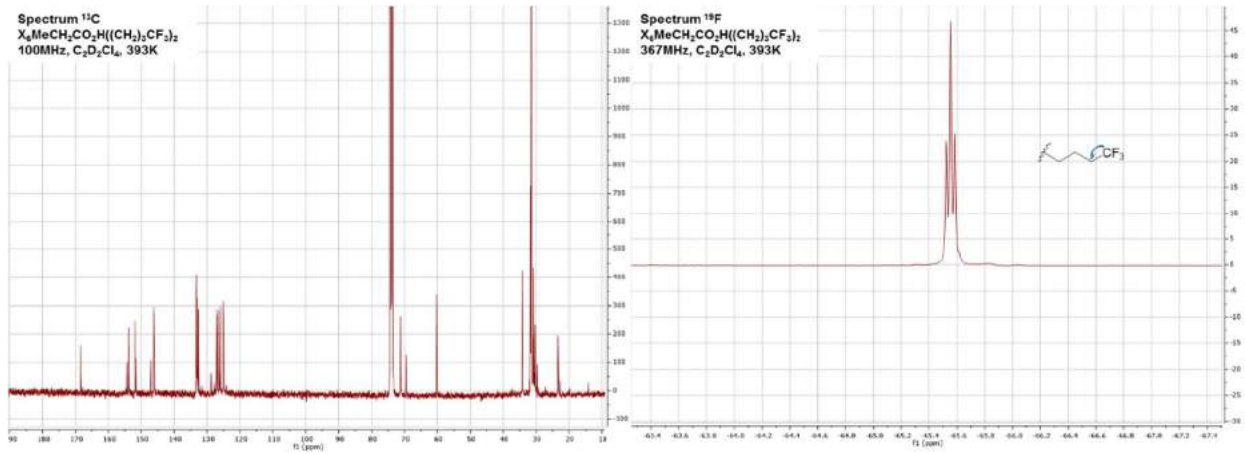
IR: 2951, 1736, 1478, 1245, 1015, 872 cm^{-1}

MS: calcd for $\text{C}_{79}\text{H}_{106}\text{F}_6\text{NO}_8$ $[\text{M} + \text{NH}_4]^+$ m/z 1293.7552, found m/z 1293.7528

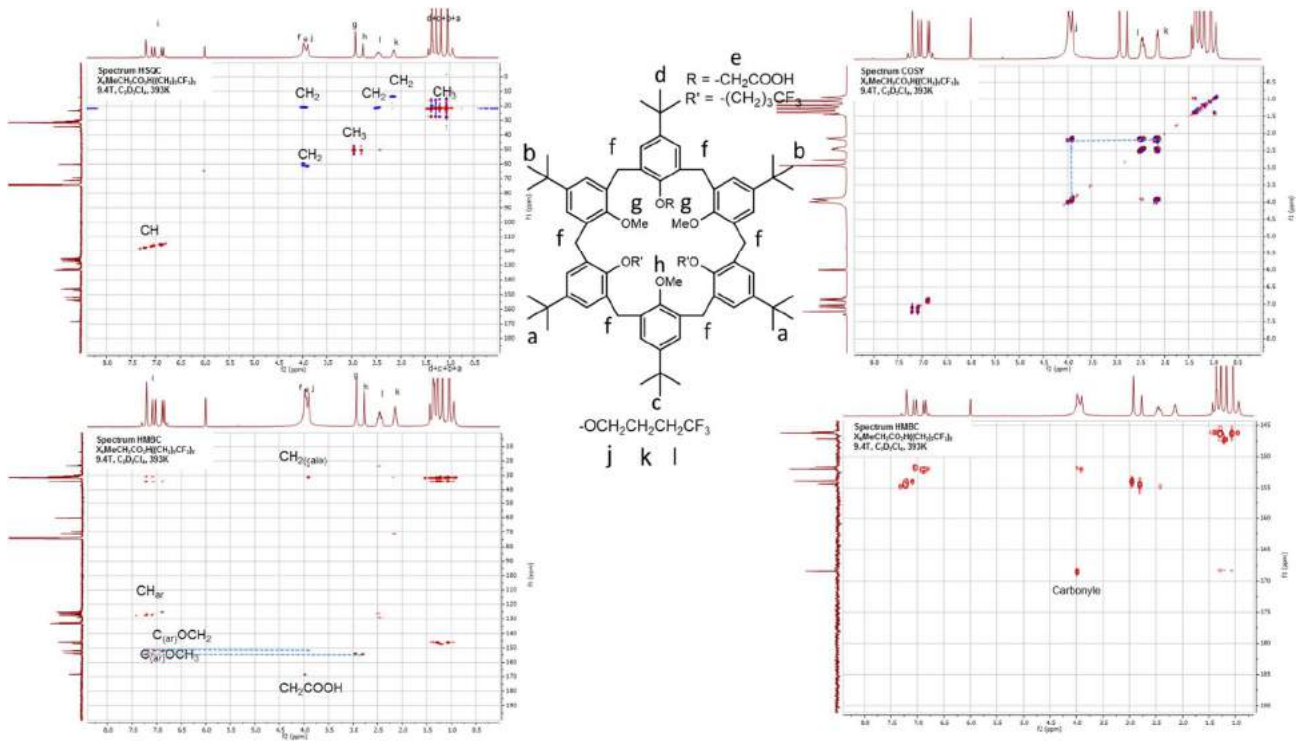
NMR: See the following spectrum for attribution



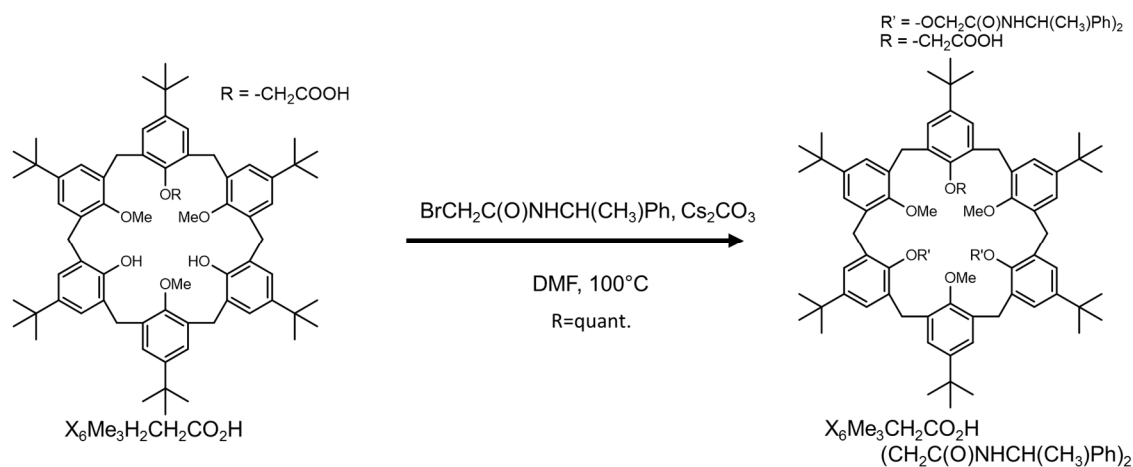
^{13}C , ^{19}F NMR



2D-NMR



p-tBu-calix[6]arene-di(chiral substituant)-tri-methyl-mono-acid



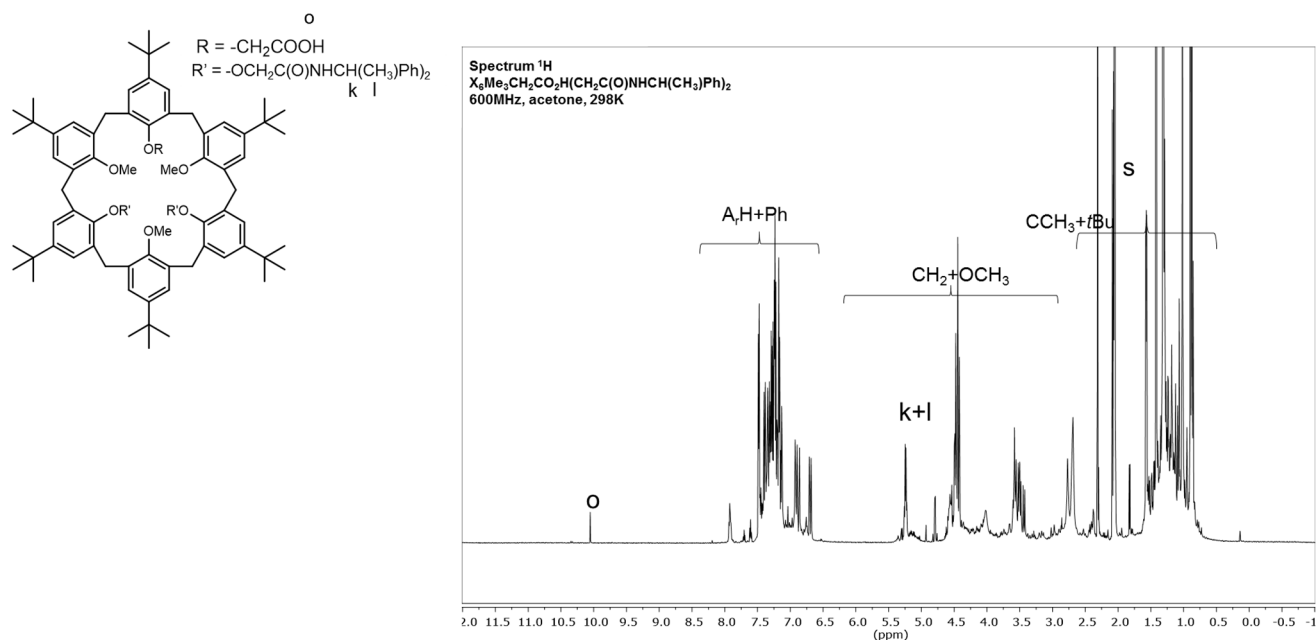
To 1 equivalent of the *p*-tBu-calix[6]arene-mono-acid ($\text{X}_6\text{Me}_3\text{H}_2\text{CH}_2\text{CO}_2\text{H}$), 10 equivalents of Cs_2CO_3 with 10 equivalents of $\text{BrCH}_2\text{C}(\text{O})\text{NHCH}(\text{CH}_3)\text{Ph}$ were added in anhydrous DMF. After 2 days under agitation at 100°C , the mixture was treated with a solution of HCl 0.1 M, and precipitation with water led quantitatively, after filtration, to the final product.

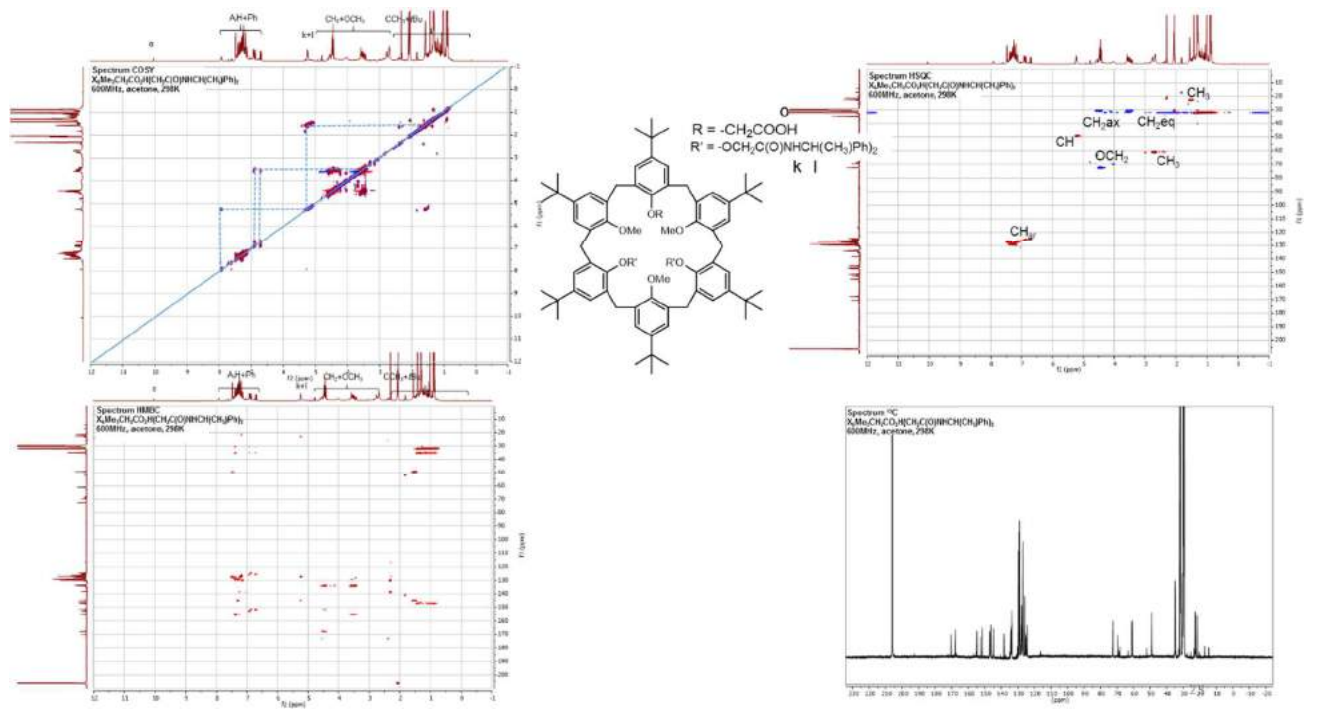
MP: 121-124°C

IR: 3412, 2961, 1668, 1478, 1201, 1116, 872, 696 cm^{-1}

MS: calc for $\text{C}_{91}\text{H}_{115}\text{N}_2\text{O}_{10}$ $[\text{M} + \text{H}]^+$ m/z 1395.8546, found m/z 1395.8557

NMR: See the following spectrum for attribution

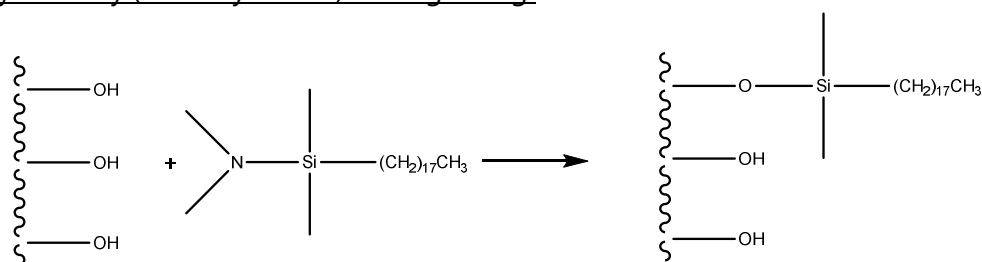




2.2. Calix[6]arene derivative grafting

To compare the new calix[6]arene based SPs, a C18 SP was done on the same silica batch, as well as a tert-butylphenoxyamide SP that corresponds to the basic pattern of the calix[6]arenes studied.

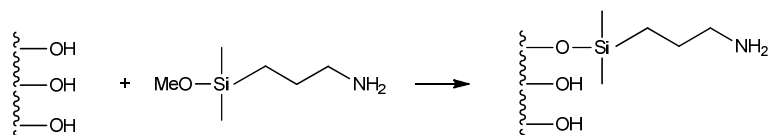
Octadecyldimethyl(dimethylamino)silane grafting



A mass of 2.0 g of FPP silica (*SPP*: 1.0 g) with 20 mL of toluene (*SPP*: 10 mL) were placed into a 100 mL round-bottom flask. After addition of 5.21 g of octadecyldimethyl-(dimethylamino)silane (*SPP*: 2.09 g), the mixture was purged with argon and reacted for 30 min at 110°C. The reactor was cooled to room temperature, and 0.96 mL (*SPP*: 0.48 mL) of N-(trimethylsilyl)dimethylamine was added and reacted at 110°C for 30 min. The reactor was cooled to room temperature and the excess reagent was subsequently removed by rinsing with 10 mL of toluene, 10 mL of tetrahydrofuran and 10 mL of acetonitrile. After filtration, the silica was dried at 110°C for 12 h under vacuum.

IR: $\sigma_{\text{O-H}} = 3653 \text{ cm}^{-1}$, $\sigma_{\text{CH}_3} = 2956 \text{ cm}^{-1}$, $\sigma_{\text{CH}_2} = 2923 \text{ cm}^{-1}$ and 2851 cm^{-1} , $\sigma_{\text{Si-O-Si}} = 1871 \text{ cm}^{-1}$, $\delta_{\text{CH}_2} = 1465 \text{ cm}^{-1}$, $\delta_{\text{CH}_3} = 1410 \text{ cm}^{-1}$, $\sigma_{(\text{Si-O})_{\text{as}}} = 1064 \text{ cm}^{-1}$, $\sigma_{(\text{Si-O})_{\text{sym}}} = 795 \text{ cm}^{-1}$

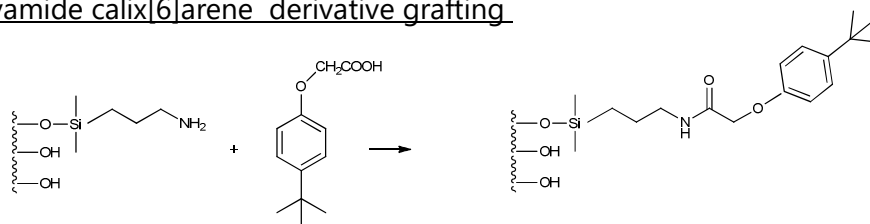
4-aminobutyldimethylmethoxysilane grafting



A mass of 3.0 g of FPP silica (*SPP*: 1.5 g) with 30 mL of toluene (*SPP*: 15 mL) were placed into a 100 mL round-bottom flask. After addition of 3.0 g of 4-aminobutyldimethyl-methoxysilane (*SPP*: 460 mg), the mixture was purged with argon and reacted for 60 min at 110°C. The reactor was cooled to room temperature and the excess reagent was subsequently removed by rinsing with 10 mL of toluene, 10 mL of tetrahydrofuran and 10 mL of acetonitrile. After filtration, the silica was dried at 110°C for 12 h under vacuum.

IR: $\sigma_{\text{O-H}} = 3641 \text{ cm}^{-1}$, $\sigma_{\text{amine}} = 3361 \text{ cm}^{-1}$ and 3305 cm^{-1} , $\sigma_{\text{CH}_3} = 2952 \text{ cm}^{-1}$, $\sigma_{\text{CH}_2} = 2929 \text{ cm}^{-1}$ and 2862 cm^{-1} , $\sigma_{\text{Si-O-Si}} = 1868 \text{ cm}^{-1}$, $\delta_{\text{amine}} = 1600 \text{ cm}^{-1}$, $\delta_{\text{CH}_2} = 1454 \text{ cm}^{-1}$, $\delta_{\text{CH}_3} = 1406 \text{ cm}^{-1}$ and 1393 cm^{-1} , $\sigma_{(\text{Si-O})_{\text{as}}} = 1076 \text{ cm}^{-1}$, $\sigma_{(\text{Si-O})_{\text{sym}}} = 805 \text{ cm}^{-1}$

t-butylphenoxyamide calix[6]arene derivative grafting

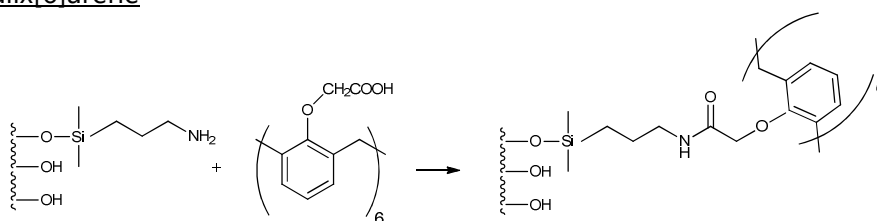


A mass of 3.28 g of FPP aminosilica (*SPP*: 0.5 g) with 20 mL of toluene (*SPP*: 10 mL) were placed into a 100 mL round-bottom flask (solution 1). In an other round-bottom flask (solution 2), 5.77 g of (benzotriazol-1-yloxy)tripyrrolidinophosphonium hexafluorophosphate (*SPP*: 0.89 g), 1.92 g of t-butylphenoxyamide (*SPP*: 0.29 g) and 2.42 mL of N,N-Diisopropylethylamine (*SPP*: 0.37 mL) were mixed with 35 mL of toluene (*SPP*: 15 mL). After mixing of the 2 solutions, the mixture was purged with argon and reacted for 60 min at 110°C. The reactor was cooled to room temperature and the excess reagent was subsequently removed by rinsing with 10 mL of toluene, 10 mL of tetrahydrofuran and 10 mL of acetonitrile. After filtration, the silica was dried at 110°C for 12 h under vacuum.

IR: $\sigma_{\text{O-H}} = 3635 \text{ cm}^{-1}$, $\sigma_{\text{amide}} = 3428 \text{ cm}^{-1}$ and 3310 cm^{-1} , $\sigma_{\text{CH}_3} = 2957 \text{ cm}^{-1}$, $\sigma_{\text{CH}_2} = 2868 \text{ cm}^{-1}$, $\sigma_{\text{Si-O-Si}} = 1871 \text{ cm}^{-1}$, $\sigma_{\text{C=O amide}} = 1661 \text{ cm}^{-1}$, $\sigma_{\text{aromatic cycle}} = 1608 \text{ cm}^{-1}$, $\sigma_{\text{NH-amide}} = 1535 \text{ cm}^{-1}$, $\delta_{\text{CH}_2 + \sigma_{\text{Ar-H}}} = 1443 \text{ cm}^{-1}$, $\sigma_{\text{Ar-H}} = 1412 \text{ cm}^{-1}$, $\delta_{\text{CH}_3} = 1395 \text{ cm}^{-1}$, $\sigma_{(\text{Si-O})_{\text{as}}} = 1146 \text{ cm}^{-1}$, $\sigma_{\text{SiOSi}} = 827 \text{ cm}^{-1}$, $\delta_{\text{Ar-H para disubstituted aromatic cycle}} = 794 \text{ cm}^{-1}$

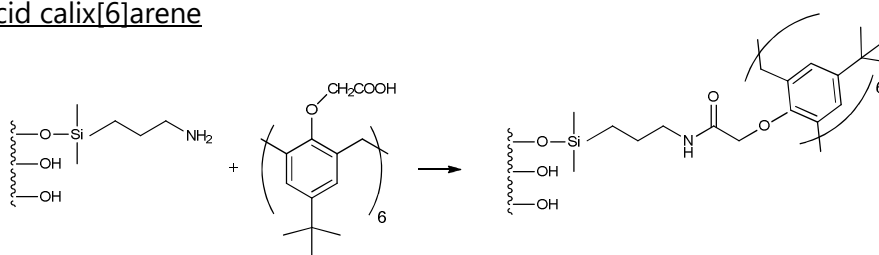
t-butylphenoxyamide end-capping

A mass of 1.5 g of FPP t-butylphenoxyamide silica (*SPP*: 0.44 g) with 15 mL of toluene (*SPP*: 10 mL) were placed into a 100 mL round-bottom flask. Then, 0.72 mL of N-(trimethylsilyl)dimethylamine (*SPP*: 0.24 mL) were added and the solution was purged under argon. After reaction for 30 min at 110°C, the reactor was cooled to room temperature and the excess reagent was subsequently removed by rinsing with 10 mL of toluene, 10 mL of tetrahydrofuran and 10 mL of acetonitrile. After filtration, the silica was dried at 110°C for 12 h under vacuum.

hexa-acid calix[6]arene

In a 50 mL round-bottom flask (solution 1), 0.45 g of aminosilica (already end-capped) was placed in 5 ml of toluene. In another 50 mL round-bottom flask (solution 2), 0.89 g of (benzotriazol-1-yloxy)tripyrrolidinophosphonium hexafluorophosphate, 75 mg of hexa-acid calix[6]arene and 0.37 mL of N,N-Diisopropylethylamine were added with 12 mL of toluene. After stirring, solution 2 was mixed to solution 1, and the mixture was purged with argon and reacted at 110°C for 60 min under microwave irradiations. The reactor was cooled to room temperature and the excess reagent was subsequently removed by rinsing with 10 mL of toluene, 10 mL of tetrahydrofuran and 10 mL of acetonitrile. After filtration, the silica was dried at 110°C for 12 h under vacuum.

IR: $\sigma_{\text{O-H}} = 3659 \text{ cm}^{-1}$, $\sigma_{\text{amide}} = 3417 \text{ cm}^{-1}$, $\sigma_{\text{CH}_3} = 2961 \text{ cm}^{-1}$, $\sigma_{\text{CH}_2} = 2934 \text{ cm}^{-1}$ and 2873 cm^{-1} , $\sigma_{\text{Si-O-Si}} = 1871 \text{ cm}^{-1}$, $\sigma_{\text{C=O amide}} = 1659 \text{ cm}^{-1}$, $\sigma_{\text{NH-amide}} = 1533 \text{ cm}^{-1}$, $\sigma_{(\text{Si-O})_{\text{as}}} = 1100 \text{ cm}^{-1}$, $\sigma_{(\text{Si-O})_{\text{sym}}} = 806 \text{ cm}^{-1}$, $\delta_{\text{Ar-H 1,2,3 trisubstituted aromatic cycle}} = 700 \text{ cm}^{-1}$

t-Bu hexa-acid calix[6]arene

In a 50 mL round-bottom flask (solution 1), 0.42 g of aminosilica (already end-capped) was placed in 5 mL of toluene. In another 50 mL round-bottom flask (solution 2), 0.89 g of (benzotriazol-1-yloxy)tripyrrolidinophosphonium hexafluorophosphate, 95 mg of *t*-Bu-hexa-acid calix[6]arene and 0.37 mL of *N,N*-Diisopropylethylamine were added with 10 mL of toluene. After stirring, solution 2 was mixed to solution 1, and the mixture was purged with argon and reacted at 110°C for 60 min under microwave irradiations. The reactor was cooled to room temperature and the excess reagent was subsequently removed by rinsing with 10 mL of toluene, 10 mL of tetrahydrofuran and 10 mL of acetonitrile. After filtration, the silica was dried at 110°C for 12 h under vacuum.

IR: $\sigma_{\text{O-H}} = 3653 \text{ cm}^{-1}$, $\sigma_{\text{amide}} = 3302 \text{ cm}^{-1}$, $\sigma_{\text{CH}_3} = 2956 \text{ cm}^{-1}$, $\sigma_{\text{CH}_2} = 2906 \text{ cm}^{-1}$ and 2873 cm^{-1} , $\sigma_{\text{Si-O-Si}} = 1873 \text{ cm}^{-1}$, $\sigma_{\text{C=O amide}} = 1668 \text{ cm}^{-1}$, $\sigma_{\text{NH-amide}} = 1533 \text{ cm}^{-1}$, $\delta_{\text{CH}_2} = 1445 \text{ cm}^{-1}$, $\delta_{\text{CH}_2} = 1390 \text{ cm}^{-1}$, $\sigma_{(\text{Si-O})_{\text{as}}} = 1059 \text{ cm}^{-1}$, $\delta_{\text{Ar-H } 1,2,3,5 \text{ tetrasubstituted aromatic cycle}} = 803 \text{ cm}^{-1}$

Infrared spectra

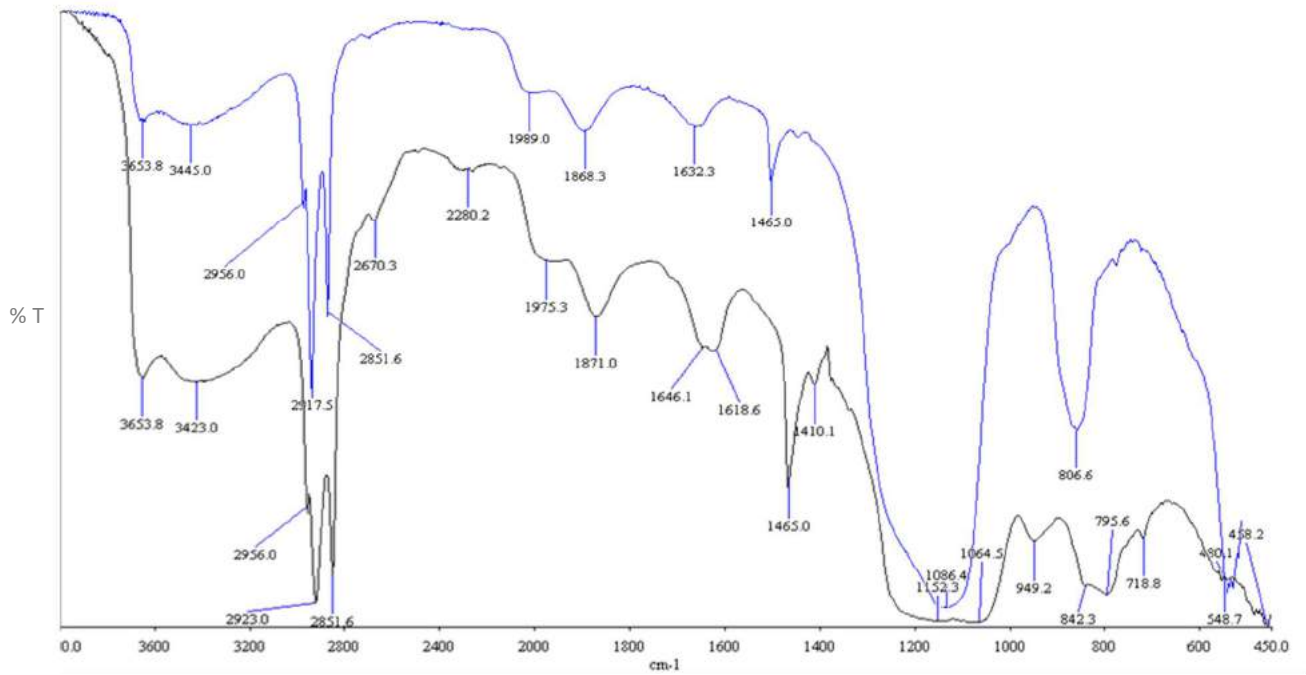


Figure A: IR spectra of the C18 silicas (SPP C18, FPP C18)

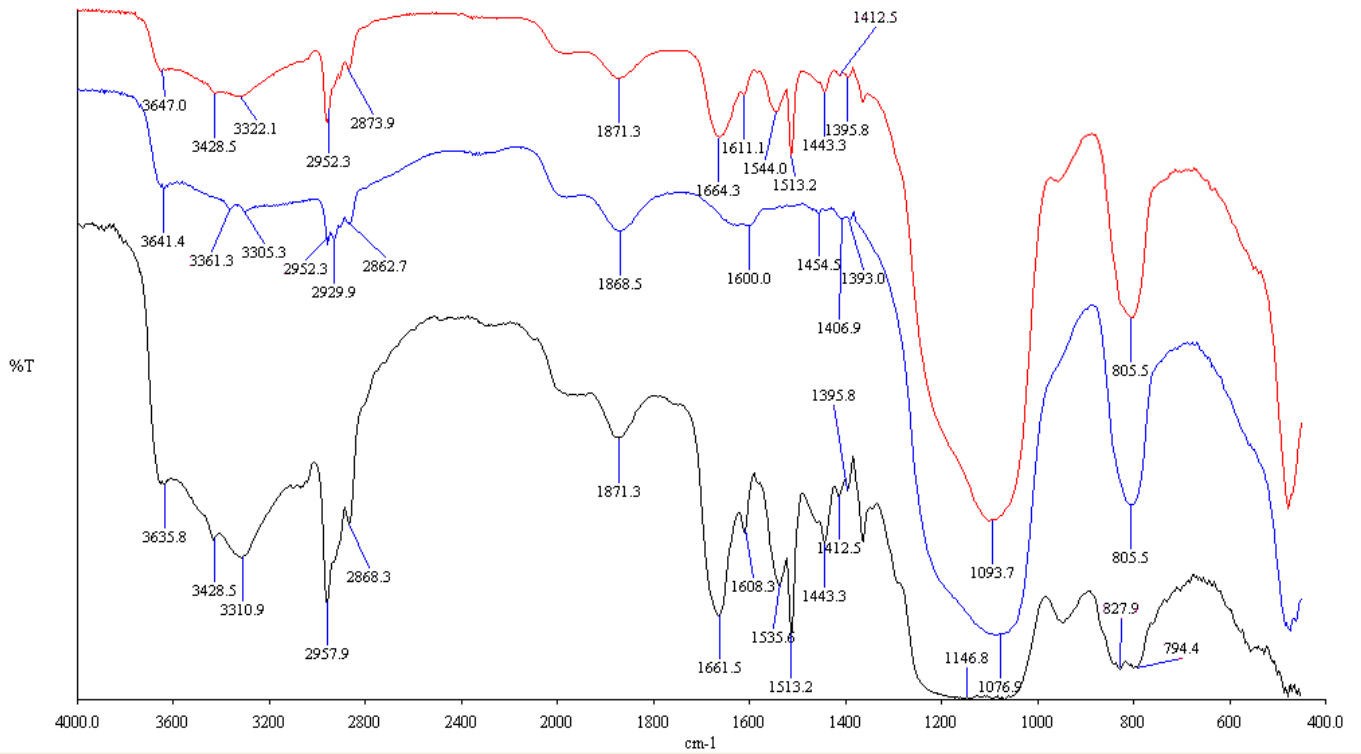


Figure B: IR spectra of SPP amino and SPP t-butylphenoxyamide (SPP Aminosilica, FPP t-butylphenoxyamide, SPP t-butylphenoxyamide)

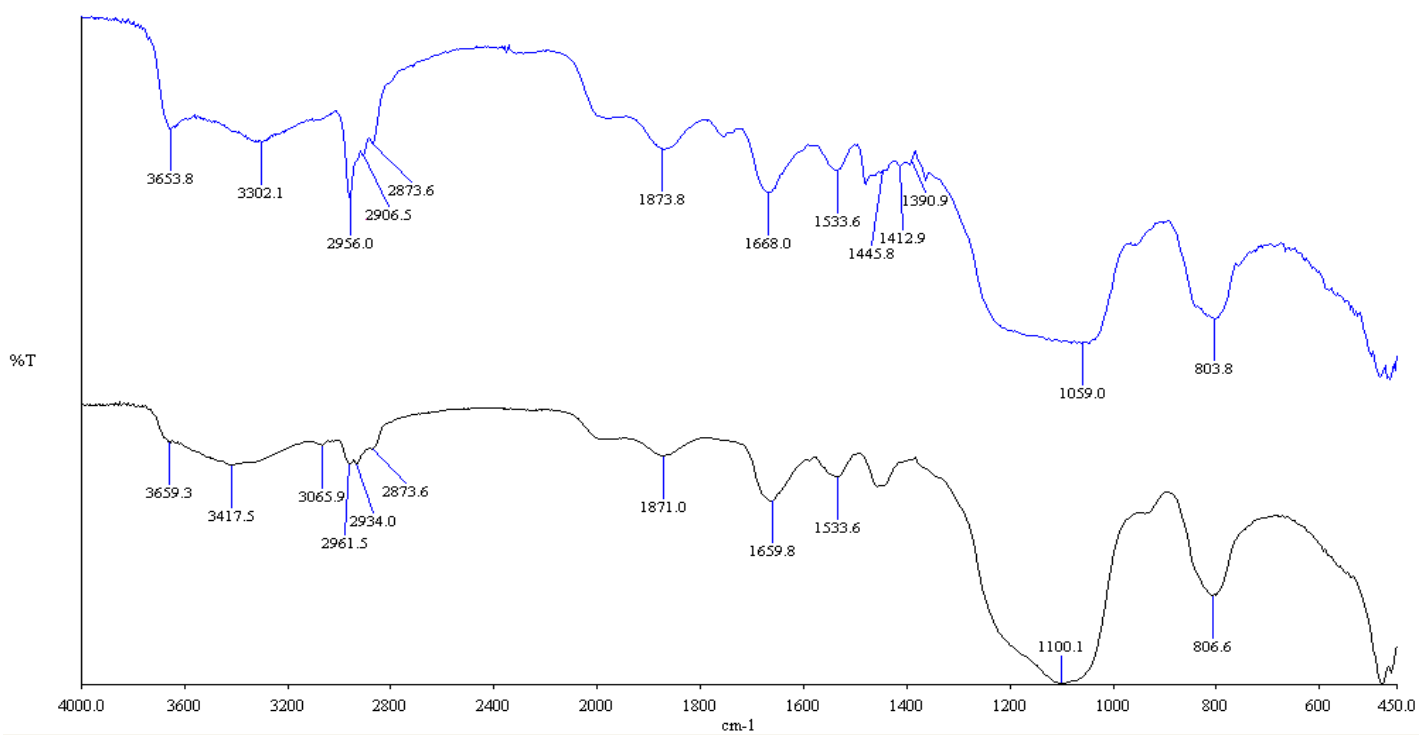


Figure C: IR spectra of SPP hexa-acid Calix[6]arene amino and SPP hexa-acid Calix[6]arene (SPP t-Bu-hexa-acid Calix[6]arene, SPP hexa-acid Calix[6]arene)